# PROCESS INTENSIFICATION: CROSS-CORRUGATED POLYMER FILM COMPACT HEAT EXCHANGER (PFCHE)


Liza Zaheed-Maheswaran BEng (Hons)

Thesis submitted in partial fulfillment for the degree of PhD in Engineering

Process Intensification and Innovation Centre (PIIC)

School of Chemical Engineering and Advanced Materials

University of Newcastle Upon Tyne

May 2003

## Abstract

Until recently, work on compact metallic heat exchangers has sparked interest amongst heat exchanger manufacturers due to its enhanced thermal performance and energy saving benefits in comparison to conventional heat exchangers. Nevertheless, the limitations of these metallic heat exchangers which involve corrosion, weight and cost issues have created the need to develop alternative units.

Much of the initial interest in the development of polymer compact heat exchangers was stimulated by their ability to handle both liquids and gases (single and two phase duties); their resistance to fouling and corrosion and their possible use in humidification and dehumidification duties. But, most importantly, the use of polymers offers substantial weight, volume, space and cost savings which give them a competitive edge over exchangers manufactured from more exotic alloys.

This research focuses on the development and performance investigation of a polymer heat exchanger using thin films (PFCHE). The design incorporates the use of thin 100μm PEEK films, to combat the low thermal conductivity of the polymer and adopts laminar flows to avoid high pressure drops. Performance testing using industrial conditions was carried out for square and spiral PFCHE configurations, leading to the development of design correlations for various fluid systems ($0.7<Pr<192$), tested in the respective units. These correlations have been used in case studies, to develop alternative designs to metallic heat exchangers for suitable applications where weight and cost issues are a primary concern.

Other design aspects of the PFCHE such as the effect of the corrugation angle, surface geometry and the material of construction have also been investigated to obtain a better understanding of the unit and more importantly, to optimise the performance capability and extend its potential. Performance comparisons with compact metallic heat exchangers are also carried out to highlight the advantages of the PFCHE design. In this thesis, scientific contributions in the form of design correlations involving different PFCHE configurations, fluid systems, corrugation angles and the influence of the Pr number have been established.

Tests to investigate the mechanical robustness of the heat exchanger were not carried out as part of this study, as this thesis highlights the thermal performance of the PFCHE. A detailed mechanical testing of the prototype is being considered in collaboration with an industrial partner.

## TABLE OF CONTENTS

# ILLUSTRATIONS AND TABLES

*Illustrations*

*Tables*

## NOMENCLATURE

Roman Letter Symbols

| | | |
|---|---|---|
| $A_{ff}$ or $A_c$ | minimum free flow area | $m^2$ |
| $A_T$ or A | heat transfer area | $m^2$ |
| A | constant in momentum transfer expression | |
| a | specific surface area | $m^2$ |
| a | constant in Jh and f expressions | |
| B | constant in St expression | |
| C | heat transfer capacity, m cp | J/Ks |
| cp | specific heat at constant pressure | J/kgK |
| d | tube diameter | m |
| dA | element of heat transfer area | $m^2$ |
| $d_h$ | hydraulic diameter | m |
| $dP_f$ | friction pressure drop associated with dA | $N/m^2$ |
| E | pumping power | $W/m^2$ |
| E | effectiveness of heat exchanger | |
| F | extension factor | |
| f | friction factor | |
| $f_i$ | fouling coefficient of interior film | $W/m^2K$ |
| $f_o$ | fouling coefficient of exterior film | $W/m^2K$ |
| G | exchanger flow stream mass velocity | $kg/m^2s$ |
| H | height of CPHE corrugation | m |
| h | film heat transfer coefficient | $W/m^2K$ |
| h | channel height | m |
| ID | internal diameter | mm |
| $I_n$ | nth order modified Bessel function | |
| J | number of measured variables | |
| Jh | Colburn factor ($St\ Pr^{2/3}$) | |
| Jh/f | Goodness factor | |
| k | fluid thermal conductivity | W/mK |
| $k_{film}$ | film thermal conductivity | W/mK |
| $k_{tube}$ | tube thermal conductivity | W/mK |
| $k_{wall}$ | wall thermal conductivity | W/mK |
| L | fluid path length | m |
| $L_w$ | channel width | m |

| | | |
|---|---|---|
| $L_s$ | flow length of sheet | m |
| m | mass flow rate | kg/s |
| Nu | Nusselt number ($hd_h/k$) | |
| OD | outer diameter | mm |
| P | pressure | $N/m^2$ |
| P | pitch of CPHE corrugation | m |
| Pe | Peclet number (RePr) | |
| Pr | Prandtl number ($cp\mu/k$) | |
| Q | heat transfer duty | W |
| q | heat flux | $W/m^2$ |
| $R^2$ | coefficient of determination (0 to 1) | |
| Re | Reynolds number ($\rho v d_h/\mu$) | |
| r | experimental result | |
| $r_h$ | hydraulic radius ($4r_h = d_h$) | m |
| St | Stanton number (Nu/RePr) | |
| T | temperature | K |
| $T_g$ | glass transition temperature | K |
| $T_w$ | wall temperature | K |
| t | thickness of polymer film | m |
| $t_p$ | plate thickness | m |
| U | uncertainty | |
| $U_r/r$ | relative uncertainty of result | % |
| $U_{Xi}$ | absolute uncertainty | |
| $U_{Xi}/X_i$ | relative uncertainty of measured variable | % |
| U | overall heat transfer coefficient | $W/m^2K$ |
| Ua | heat transfer capacity for a given matrix | W/K |
| $U\Delta T/\tau V$ | heat flux achieved with pumping power incurred | $\dot{W}/m^2$ |
| v | velocity of fluid | m/s |
| *v* | volumetric flow rate | $m^3/hr$ |
| w | heat capacity ratio ($C_{min}/C_{max}$) | |
| $X_i$ | measured variable | |
| x | constant in Nu expression | |
| x | length of fluid flow in tube | m |
| Z | volumetric heat transfer | $MW/m^3$ |

Greek Letter Symbols

| | | |
|---|---|---|
| $\Lambda$ | plate spacing | m |
| $\Delta P$ | pressure drop | kPa |
| $\Delta T$ | temperature difference | K |
| $\Delta Re$ | range of Re numbers | |
| $\phi$ | viscosity ratio | |
| $\gamma$ | working angle in PFCHE | ($^o$) |
| $\gamma$ | inclination angle in CPHE | ($^o$) |
| $2\gamma$ | corrugation angle in PFCHE | ($^o$) |
| $\eta_o$ | total surface temperature effectiveness | |
| $\mu$ | viscosity of fluid | $Ns/m^2$ |
| $\nu$ | specific volume | $m^3/kg$ |
| $\rho$ | density of fluid | $kg/m^3$ |
| $\theta_i$ | absolute sensitivity coefficient | |
| $\tau$ | wall shear stress | $N/m^2$ |

Subscripts

| | |
|---|---|
| a | air-side |
| c | cold fluid stream |
| cond | conduction |
| conv | convection |
| h | hot fluid stream |
| i | interior |
| L | laminar |
| m | mean conditions |
| max | maximum |
| min | minimum |
| o | exterior |
| T | turbulent |
| w | water-side |

Superscripts

| | |
|---|---|
| b | Reynolds number exponent in Jh and f expressions |
| c | Prandtl number exponent in f expression |
| y | Reynolds number exponent in Nu expression |
| z | Prandtl number exponent in Nu expression |

Abbreviations

| | |
|---|---|
| CFD | Computational fluid dynamics |
| CHE | Compact heat exchanger |
| CPHE | Cross-corrugated plate heat exchanger |
| FGD | Flue gas desulphurisation |
| FI | Flow meter |
| HVAC | Heating Ventilation Air Conditioning |
| LCP | Liquid crystal polymer |
| LMTD | Log mean temperature difference |
| MVR | Mechanical vapour compression |
| NTU | Number of heat transfer units |
| Ni-Cr-Mo | Nickel-chromium-molybdenum alloy (Hastelloy) |
| PC | Polycarbonate |
| PE | Polyethylene |
| PEEK | Poly ether ether ketone |
| PF | Plate fin heat exchanger |
| PFCHE | Polymer film compact heat exchanger |
| P-Frame | Plate frame heat exchanger |
| PI | Process intensification |
| PP | Polypropylene |
| PPO | Polypheynylene oxide |
| PPS | Polyphenylene sulphide |
| PTFE | Polytetrafluoroethylene |
| PVDF | Polyvinylidene fluoride |
| ST | Shell and tube heat exchanger |
| TC | Thermocouple |

## ACKNOWLEDGEMENTS

Special notes of gratitude...

To my ex-personal tutor, Dr. Ming Tham. Thanks Tuan for your words of wisdom, reassurance and for not losing your patience or your humour during my countless whinging sessions. They really, really meant a lot. Also, thanks so much for the glowing reference that enabled me to receive the ORS (Overseas Research Studentship) for the duration of my PhD study.

To the technical staff at the workshop. Special thanks to Mr. Stuart Latimer, Mr. Brian Dourish, Mr. Paul Sterling and Mr. Rob Dixon, for putting together the test rig and for sorting out my lab equipment problems. Your efforts are very much appreciated.

To the industrial collaborators of this project - SERCK Aviation, Honeywell SERCK, Victrex and the Energy Efficiency Best Practice Programme (EEBPP), for their valuable contributions towards this research.

To my friends at the fourth floor (PIIC) office. Thank you all for your friendship and support. You might not think so, but you have helped in many ways. Special thanks to Mileta (my next table neighbour), for tolerating my outbursts on the 'not so good' days, Marija for sharing with me her computer skills, Kamelia for motivating me when things were not going well and the rest of the gang for the much needed coffee breaks.

To my friends outside the department, thanks guys for the moral support and for reminding me that there is more to life than writing a thesis.

Last but not least, to Mum and Dad. Thank you so much for your constant love and encouragement, for listening to my frustrations and then putting things in perspective; especially during the final stages of writing up, and for always telling me that I can and believing that I could.

# CHAPTER 1 - COMPACT HEAT EXCHANGERS IN PROCESS INTENSIFICATION

## 1.0 Introduction

Heat exchangers are devices that enhance or facilitate the flow of heat. Countless examples are found in everyday life. Every living thing is equipped in some way or another with heat exchangers. Mammals have complicated heat exchangers. The primary unit is the lungs, which not only cool the body by saturating the expelled air with water vapour but also serve as complex mass exchangers, taking oxygen from air and carbon dioxide from the blood. The skin acts as a supplementary heat exchanger, changing its character to promote or inhibit the transfer of heat from the body depending on the temperature, humidity and velocity of the air. For reasons only known to God, mammals (with the notable exception of camels) have a specific operating temperature; even a few degrees of variation, up and down, result in severe physiological disturbance. An adequate, well-controlled heat exchange process is therefore vital, literally a matter of life and death.

Industrial heat exchangers are fortunately much less complicated, although the trappings of technological civilisation make them no less vital. Manufactured heat exchangers are found in every facet of life. Boiling water or frying an egg requires a heat exchanger. Refrigerators operate on a vapour-compression cycle using two heat exchangers; one to cool the freezer compartment and the other to transfer to the air, heat from the freezer compartment plus the work required to drive the system. Automobiles are equipped with heat exchangers, known as radiators, and all electrical and electronic equipment must be provided with heat exchangers for cooling. Heating and cooling systems for buildings also involve the use of heat exchangers. Electricity, generated in base-load electric power stations depend on heat exchangers to generate and conduct the steam used to drive the turbine-powered alternators. In addition, oil refineries and chemical processing plants use many different heat exchangers. Last but not least, food processing, baking, brewing, mixing and freezing all involve the use of heat exchangers of one sort or another. Indeed the list for the use of heat exchangers is endless.

This vast range of capacities embraces a diversity of types, shapes, and arrangements of heat exchangers. The majority serve to facilitate the energy transfer between two fluid streams at different temperature levels. Others involve solid mass heating or cooling systems. One example is the convective cooling fins placed on electrical apparatus to dissipate to the ambient air, the heat generated by internal resistance. In food processing, sides of beef are cooled for refrigerated preservation or, conversely, meat and bread are heated for cooking.

It is evident that heat exchangers exist in great numbers and are widely used throughout industry and commerce. They are found in an enormous range of heat transfer capacities. The smallest (<1 W) are included in miniature cryocoolers for infrared thermal imaging, heat seeking missile guidance, or superconducting electronic applications. The largest (>1 GW) are the boilers, condensers, and condenser cooling-water air coolers in base-load electric power stations.

Chemical plants can be thought of as a combination of heat and mass transfer operations. These operations include reactors, separation units, pumps and heat exchangers. Heat exchangers account approximately 14% of the total plant cost (Redman 1988). A large amount of this cost can be attributed to piping and civil works. If the size of the heat exchanger can be reduced, this will inevitably result in a significant cost saving. Metallic compact heat exchangers have been used in the aircraft and automobile industries for a considerable period of time, but their adoption in the process industries has been slow. This is essentially due to the conservative attitude of the engineers who have been involved in the design of chemical plants.

Nevertheless the process plant industry has reached maturity, and is now moving into a new phase of design and creativity, where 'small is beautiful'. Process intensification is a design philosophy directed at radical reduction in process plant size, normally by integrating a number of 'intensified' or enhanced performance unit operations, that could lead to significant energy, capital, environmental and safety benefits. Compact heat exchangers play an important role in achieving this target.

This research focuses on the use of a particular type of compact heat exchanger; a polymer film compact heat exchanger (PFCHE), which incorporates a novel technique of using thin corrugated PEEK (poly ether ether ketone) films to facilitate heat exchange in laminar flows, as an alternative to metallic units.

We begin this chapter with brief introductions to process intensification and compact heat exchangers, to provide a research background and to set the scene for the PFCHE work discussed in this thesis. It is in the area of process intensification that this research concentrates. We will then proceed to give a description of the performance evaluation methods employed for compact heat exchangers. This is necessary, as these methods will be heavily adopted in analysing the experimental results and other design aspects of the PFCHE, in later chapters of this thesis.

Following this, the initial incentive to adopt the PFCHE technology is shown using a comparison study with conventional plate frame and shell and tube metallic heat exchangers, whereby the PFCHE performance is found to be superior. The chapter concludes with a

listing of the aims of the research and an outline for the remainder of this thesis. Before we go any further in discussing the incentive of using PFCHEs in the area of process intensification, we first need to have a basic understanding of what process intensification entails.

## 1.1 Process intensification overview

Process intensification (PI) is a novel concept within Chemical Engineering and can be described as a key for future development in process plants. The aim is to substantially reduce the size of process plants, while maintaining the production objectives. The benefits of process intensification have been widely documented, and it is in this area that this research concentrates.

The virtue of the PI approach will be recognised when it is appreciated that the main plant items involved in the process such as reactors and heat exchangers only contribute around 20% of the cost of a given plant (Ramshaw 1995). The balance is incurred by installation costs, which involve pipe work, structural support, civil engineering and so on. Therefore a major reduction of equipment size, coupled preferably with a high degree of 'telescoping' of equipment function, could generate very significant cost savings by eliminating support structure, expensive column foundations and long pipe runs. These units will be designed to carry out heat and mass transfer operations, or heat transfer and chemical reactions, at the same time, and within the same unit (Cross and Ramshaw 1986). A first step towards reaching this objective is to design more compact units that will carry out a single operation. One such unit is known as the compact heat exchanger (CHE).

While cost reduction was the original target for PI, it quickly became apparent that there were other important benefits, particularly in respect to improved intrinsic safety, reduced environmental impact and energy consumption. Given the anticipated plant volume reductions, the toxic and flammable inventories of intensified plants are correspondingly reduced thereby making a major contribution to intrinsic safety. As has been said by Trevor Kletz, "what you don't have can't leak" (Kletz 1991). Also, if an intensified plant can be reduced to be below the tree line, which is a modest aim, it will not create an eye-sore for the local population.

The main resistance to process intensification is from the conservative nature of process engineers who seem to 'rush to be second', which is understandable considering the present economic situation. It is the safety of using tried and tested equipment which is the barrier to process intensification. If this attitude can be changed, which can only be done by solid proof, then there is nothing to stop the path of intensified plants where the final goal must be, to be able to transport a process in the back of a lorry to where the product is needed.

In accordance with this objective, this thesis investigates the industrial potential of using a novel type of compact heat exchanger namely the Polymer Film Compact Heat Exchanger (PFCHE) towards the development for a new intensified plant for the future. To gain a better appreciation of the benefits in adopting this new design, we must first understand the concept of compact heat exchangers in the process industries and also acquire some knowledge on the current available units in the market.

## 1.2 Introduction to compact heat exchangers

A compact heat exchanger (CHE) is a heat exchanger having a surface area density on any one side greater than 700 $m^2/m^3$ regardless of the structural design for units operating in gas streams, and in excess of 300 $m^2/m^3$ when operating in liquid or two-phase streams (Reay 1999). The most basic CHEs have volumes of less than 50%, of that of a comparable shell and tube heat exchanger, for a given duty. It is highly efficient and more versatile than traditional units. Depending on the type, CHEs can handle up to four or more process streams and can accommodate most operating temperatures and pressures. This enables them to be implemented in complex thermal processing plants. The high surface area densities, reduces substantially the exchanger volume and mass for the same surface area or the same duty. This will also reduce considerably the structural support requirement and associated cost, supporting the aim of process intensification. In the following two sections, we outline the advantages and perceived limitations of compact heat exchangers.

### *1.2.1 Advantages of compact heat exchangers*

- Improved energy efficiency
- Achievement of closer approach temperatures
- Smaller volume and weight for a given duty
- Lower installed cost
- Multi stream and multi pass configurations possible
- Tighter temperature control
- Power savings
- Improved safety
- Radical approach to design

*1.2.2 Perceived limitations of compact heat exchangers*

- Lack of industrial awareness
- Limited choice
- Susceptibility of fouling
- Lack of Codes of Practice
- Increased operational requirements

The description of the major types of compact heat exchangers available in the process industries, along with a summary of the principal applications are given in Appendix A. Next, we consider the performance evaluation methods used in compact heat exchangers.

## 1.3 Performance evaluation methods in compact heat exchangers

A description of the four methods used in evaluating the experimental PFCHE results in this thesis is outlined below. Further explanation will be given in context to the relevant chapters in this thesis (Chapters Four, Five, Seven, Eight and Nine).

*1.3.1 Colburn factor (Jh)*

The Jh factor gives a direct measure of the heat transfer capability of a heat exchange unit, as it is proportional to the heat transfer coefficients that can be achieved. In order to understand the implications of this dimensionless factor on the PFCHE heat transfer, the definition of the Jh factor is outlined below.

$$J = St\,Pr^{2/3} = \left(\frac{Nu}{Re\,Pr}\right)\left(Pr^{2/3}\right) = \frac{h\,d_h\,Pr^{-0.33}}{k\,Re} \qquad (1.1)$$

In this thesis, heat transfer correlations in the form of Jh as a function of Reynolds (Re) number, are developed for different fluid systems in the PFCHE. The Jh correlations play a role in designing PFCHE units for suitable applications currently dominated by metallic heat exchangers. These correlations take the form below.

$$Jh = a\,Re^{b}$$

where a and b are constants depending on the kind of surface and the flow character.

*1.3.2 Friction factor (f)*

Whilst the Jh factor provides a measure of the heat transfer, the friction factor gives an indication of the pressure drop ($\Delta P$) needed to overcome the wall shear stress ($\tau$), generated when a fluid flows along a channel in a heat exchanger. The friction factor can be calculated from the following expression:

$$f = (2\ \Delta P\ d_h) / (4\ \rho\ v^2\ L) \qquad (1.2)$$

or $f = \tau / 0.5\ \rho\ v^2$

= wall shear stress/ velocity head

It is interesting to note that in the design of liquid-to-liquid heat exchangers, accurate knowledge of the friction characteristics of the heat transfer surface is relatively unimportant because of the low power requirement for pumping high-density fluids. For gases, however, because of their lower density, the friction power per unit mass flow rate is much higher. Therefore the friction factors assume an importance equal to that of the heat transfer characteristic. As with the heat transfer shown earlier, friction factor correlations are also developed for the different fluid systems investigated in the PFCHE. Both the Jh and f correlations are known collectively as the design correlations for a heat exchange unit.

The f correlations take a similar form to the Jh correlations, as shown below.

$$f = a\ Re^b$$

Once these two factors are established, we can now look at two methods that incorporate both the heat transfer and pressure drop characteristics to evaluate the overall heat exchanger performance. The methods are disclosed in the next two sections, where we begin with the pumping power before moving on to the goodness factor.

*1.3.3 Pumping power (E)*

The pumping power is the energy required to force the fluid through the heat exchanger matrix. It can be determined by multiplying the wall shear stress ($\tau$) with the fluid velocity (v), as shown in the equation below.

$$E = \tau\ v \qquad (1.3)$$

The wall shear stress is calculated as follows:

$$\tau = 0.5\ f\ \rho\ v^2 \qquad (1.4)$$

An interesting and important feature of the compact heat exchanger surfaces can be demonstrated if the heat transfer coefficient (h) is plotted as a function of the mechanical power expended to overcome fluid friction per unit of surface area. This mechanical power expended is also known as the pumping power (E). The heat transfer coefficient, evaluated for some particular set of fluid properties, is interpreted as the heat transfer rate for a unit of area and for one degree of temperature difference. It can be calculated using the following equation

$$h = \frac{cp\,\mu}{\Pr^{2/3}} \frac{1}{4r_h} \left(St \Pr^{2/3}\right) \mathrm{Re} \qquad (1.5)$$

The equation above can be derived by re-arranging the Colburn definition in equation (1.1), and incorporating the definitions of the Pr number (Pr) and the hydraulic diameter ($d_h$).

where $\Pr = (cp\ \mu)/ k$ (1.6)

$d_h = 4r_h$ (1.7)

We obtain the pumping power equation, by considering the pumping power as the 'friction power per unit area'. Let $dP_f$ be the friction pressure drop associated with the heat transfer area (dA), which gives,

$$E = -\frac{dP_f}{\rho} G A_c \frac{1}{dA} \text{ (loss of mechanical energy due to pressure drop)} \qquad (1.8)$$

Next, we incorporate the equation to calculate the pressure drop in a heat exchanger (ignoring the entrance and exit effects) as shown below.

$$\frac{dP_f}{\rho} = -\frac{-f}{2} \frac{G^2}{\rho^2} \frac{dA}{A_c} \qquad (1.9)$$

By combining and re-arranging equations (1.8) and (1.9) and incorporating the definition for the Reynolds number (Re), we obtain the expression for the pumping power in equation (1.11) below.

where $\mathrm{Re} = (4\ r_h G)/ \mu$ (1.10)

The pumping power expended per unit of surface area, can be readily evaluated as a function of the Re number, the friction factor, and the specified fluid properties from

$$E = \frac{1}{2}\frac{\mu^3}{\rho^2}\left(\frac{1}{4r_h}\right)^3 f\,\mathrm{Re}^3 \qquad (1.11)$$

The pumping power plot (h versus E) can be prepared once the basic convection heat transfer and friction characteristics are known as functions of the Re number. The interesting feature of this plot, is the very wide difference in pumping power expenditure for a given heat flux of different surfaces, or conversely, the smaller difference in heat flux for a given pumping power expenditure. It is well known that the influence of pumping power expenditure is important for the design of gas heat exchangers as it is very easy to expend as much mechanical energy in overcoming friction as is transferred as heat.

In gas flow heat exchangers it is a necessity to minimise pumping power that forces the use of large amounts of surface area. This in turn resulted in the development of more compact heat transfer surfaces, but it is apparent that another way to minimise pumping power is to select surfaces that plot 'high' on a pumping power plot.

A geometry or heat transfer surface that has a basic characteristic of high heat flux relative to the pumping power expenditure will be termed a *'high performance surface'*. It should be first noted that compactness itself leads to high performance. A compact surface has small flow passages, and the heat transfer coefficient is always inversely proportional to the hydraulic diameter of the passage. Thus compact surfaces tend, by their very nature, to have high heat transfer coefficients, which leads to high performance curves on the heat transfer pumping power plot.

Following this, we now consider the second method that adopts both heat transfer and pressure drop characteristics in its evaluation of heat exchanger performance, namely the goodness factor.

### *1.3.4 Goodness factor (Jh/f)*

The goodness factor (Jh/f) provides a direct relationship of the ratio between the Colburn factor (Jh) and the friction factor (f) in a heat exchanger. The Jh/f plot is a presentation of this characteristic as a function of the Re number for different surface geometries. It highlights the thermal efficiency of the surfaces studied and is involved in the surface selection for a heat exchanger. A point that plots high on the graph has a higher thermal efficiency.

The Jh/f plot provides a means of selecting a surface geometry that results in an exchanger of smaller flow area. The Jh/f or St/f value contains the core surface characteristics for a given fluid and is used in the core velocity equation shown below (Kays and London 1984).

$$\frac{V_1^2}{P_1 / \rho_1} \approx \left(\frac{\Delta P}{NTU}\right)_{oneside} \frac{\rho_m}{\rho_1} \frac{St}{f} \eta_o \qquad (1.12)$$

This equation provides a direct relationship of the pressure drop to heat transfer performance. To emphasise this point, consider the following reformulation of the core velocity equation, using the mass velocity (G) as a replacement for velocity ($V_1$).

$$G = \frac{m}{A_c} \approx \left[\frac{P_1}{\upsilon_m} \eta_o \left(\frac{\Delta P / P_1}{NTU}\right)_{side} \left(\frac{St}{f}\right)\right]^{1/2} \qquad (1.13)$$

It is evident that the surface with the higher St/f or Jh/f will have a smaller flow area. Thus a surface flow area 'goodness factor' method of selection is provided by a Jh/f plot. Incidentally, this is why the Jh/f plot is also known as the goodness factor plot.

Apart from a surface flow area goodness factor (Jh/f), a companion goodness factor, namely, a heat transfer surface area (core volume or core mass) goodness factor can also be determined. The equations for the heat transfer coefficient and pumping power, equations (1.5) and (1.11) shown earlier will suffice for this consideration. A surface geometry selection that falls high on the pumping power plot will have the smallest heat transfer area requirement. This is based on a given set of fluid properties (cp, $\mu$, Pr, $\rho$) and a specified hydraulic diameter ($d_h$). The heat transfer surface area goodness factor plot corresponds to the h versus E plot earlier, which incidentally is the pumping power plot. Therefore the heat transfer surface area goodness factor is basically the pumping power loss, outlined in the previous section.

With the knowledge to evaluate the performance of heat exchangers, we can now conduct a comparison study to show the benefits of the PFCHE compared to two conventional metallic heat exchangers. This is shown in the following section.

### 1.4 Comparison of Shell and Tube and Plate Frame heat exchangers with PFCHE

The heat transfer characteristics of the polymer film compact heat exchanger may be compared with that of a typical plate frame and shell and tube exchanger to show the obvious benefits of the PFCHE. The details of the plate frame and shell and tube exchangers, which have been used for a comparative study, are attached in Appendix B and the correlations which have been used to calculate the film coefficients are as follows, Saunders (1988):

Plate frame heat exchanger

$$Nu = h\,d_h/k = Jh\,Pr^{0.33}\,\phi^{0.17} \qquad Re < 500 \qquad (1.14)$$

$$h = Jh\,k\,Pr^{0.33}\,\phi^{0.17}/d_h$$

Tube side coefficient in a shell and tube heat exchanger

$$Nu = h\,d_h/k = 1.86\,(x/\,d_h)^{-1/3}/\,Re^{-1/3}\,\phi^{0.14} \qquad Re < 2000 \qquad (1.15)$$

Polymer film compact heat exchanger (Jachuck and Ramshaw 1992)
(water-water system)

$$Jh = 0.0213\,Re^{-0.263} \qquad Re < 1000 \qquad (1.16)$$

$$h = 0.0213\,Re^{-0.263}\,k\,Re/\,d_h\,Pr^{-0.33}$$

In this comparison study between PFCHE and the conventional metallic units, we investigate the laminar heat transfer film coefficients, friction factor characteristics and the pumping power requirements in a water/water system. Graphs are plotted to aid the comparison for all three aspects. We begin with the study of laminar heat transfer film coefficients.

*1.4.1 Study of laminar heat transfer film coefficients (h)*

Figure 1.1 below shows the laminar heat transfer film coefficients for a typical plate frame and shell and tube heat exchanger, along with those for a PFCHE. It is apparent that the film coefficients achieved by the PFCHE in this flow regime is much higher than both the plate frame and shell and tube exchangers. However, the plate frame and shell and tube exchangers would seldom be operated at such low Re numbers and hence a direct comparison of the above would be misleading. A more significant comparison is to evaluate the respective volumetric heat transfer performances for each unit, while operating at its typical Re number and at a fixed temperature differential of 5$^{o}$C (Jachuck and Ramshaw 1992).

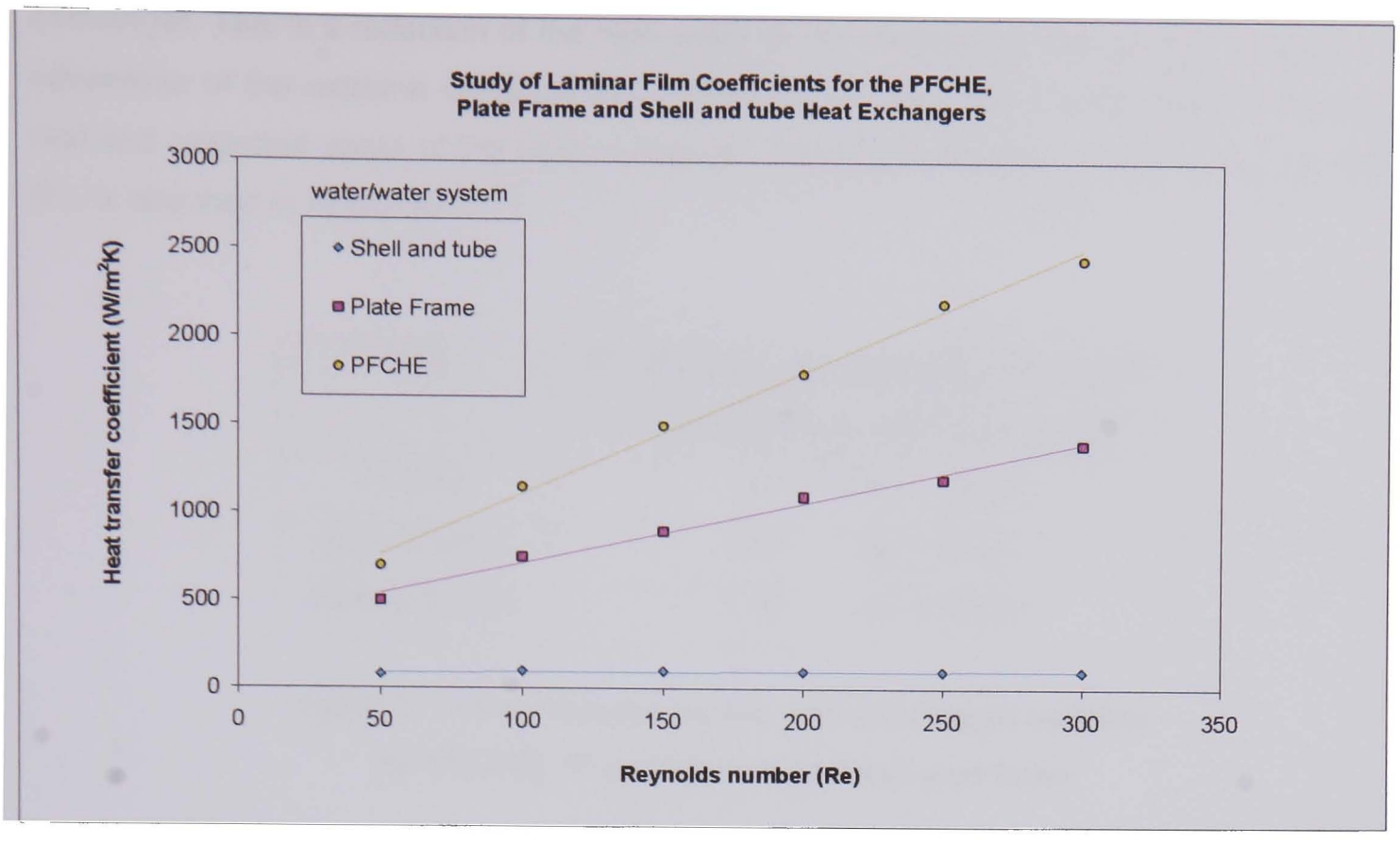


**Figure 1.1 Study of laminar film coefficients for PFCHE, Plate Frame and Shell and Tube**

The ratio between the heat transferred and the volume of the heat exchanger may be defined as follows:

Z = Heat transferred/ volume of the exchanger matrix

= UA $\Delta$T / Effective Matrix Volume

A temperature difference ($\Delta$T) of 5°C has been considered for calculating the heat transferred per unit matrix volume, and the U values for both the plate frame and shell-tube exchangers. The overall heat transfer coefficient (U), which has been used in calculating the Z values for the plate frame, shell and tube and the polymer film heat exchanger respectively are as follows (Jachuck and Ramshaw 1992):

(a) Plate frame at Re = 3000 U = 6000

(b) Shell and tube at Re = 50000 U = 1000

(c) PFCHE at Re = 1000 U = 5000

(Based on the projected area and taking the film resistance into account)

Re of 3000, 50000 and 1000 have been used for the plate frame, shell and tube and PFCHE exchangers respectively, in order to simulate actual operating flow conditions. From Table 1.1 below, it is apparent that $Z_{PFCHE} / Z_{P\text{-}Frame} = 3$ and $Z_{PFCHE} / Z_{ST} = 68.5$, suggesting a significant increase in heat transfer per unit matrix volume for a polymer film compact heat

exchanger. This is a reflection of the high value of the extension factor (F) and highlights the advantage of the extreme compactness of the PFCHE, whereby F is the ratio between the real and projected areas of the heat exchanger. Sample calculations of the extension factor (F), is attached in Appendix C.

| Type | Z= Q(MW) / Effective Matrix Vol. ($m^3$) (For temperature difference of 5°C) |
|---|---|
| PFCHE | 24 Re = 1000 |
| Plate Frame | 7.83 Re = 3000 |
| Shell and tube | 0.35 Re = 50000 |

**Table 1.1 Heat transferred per unit exchanger volume for PFCHE, Plate Frame and Shell and Tube**

So far only the heat transfer performance of the PFCHE has been studied. Hence, to get an overall view of its performance, the resistance offered to the fluid flow by the polymer matrix is next considered in the following section.

*1.4.2 Study of friction factor characteristics (f)*

The relation between the friction factor (f) and the Reynolds number (Re) for the polymer film exchanger is as follows (Jachuck and Ramshaw 1992):

$$f = 14.12\ Re^{-1.06} \qquad Re<1000 \qquad (1.17)$$

In order to compare the pressure drop performance of the PFCHE, the fluid flow characteristics of a plate frame, shell and tube and polymer film compact heat exchanger have been presented, for the following Re numbers:

(a) Plate frame 1000<Re<3500
(b) Shell and tube 2000<Re<55000
(c) PFCHE Re<1000

(The Re range suggests the characteristic flow regimes in which each of the above mentioned heat exchangers are most likely to be used).

The expressions used to calculate the friction factors for the plate frame and the shell and tube exchangers, presented in Figure 1.2 are as follows:

Shell and tube (tube-side): $f = 0.0014 + 0.125\ Re^{-0.32}$ Re>2000 (1.18)

Plate frame: $f = 0.639\ Re^{-0.213}$ Re>500 (1.19)

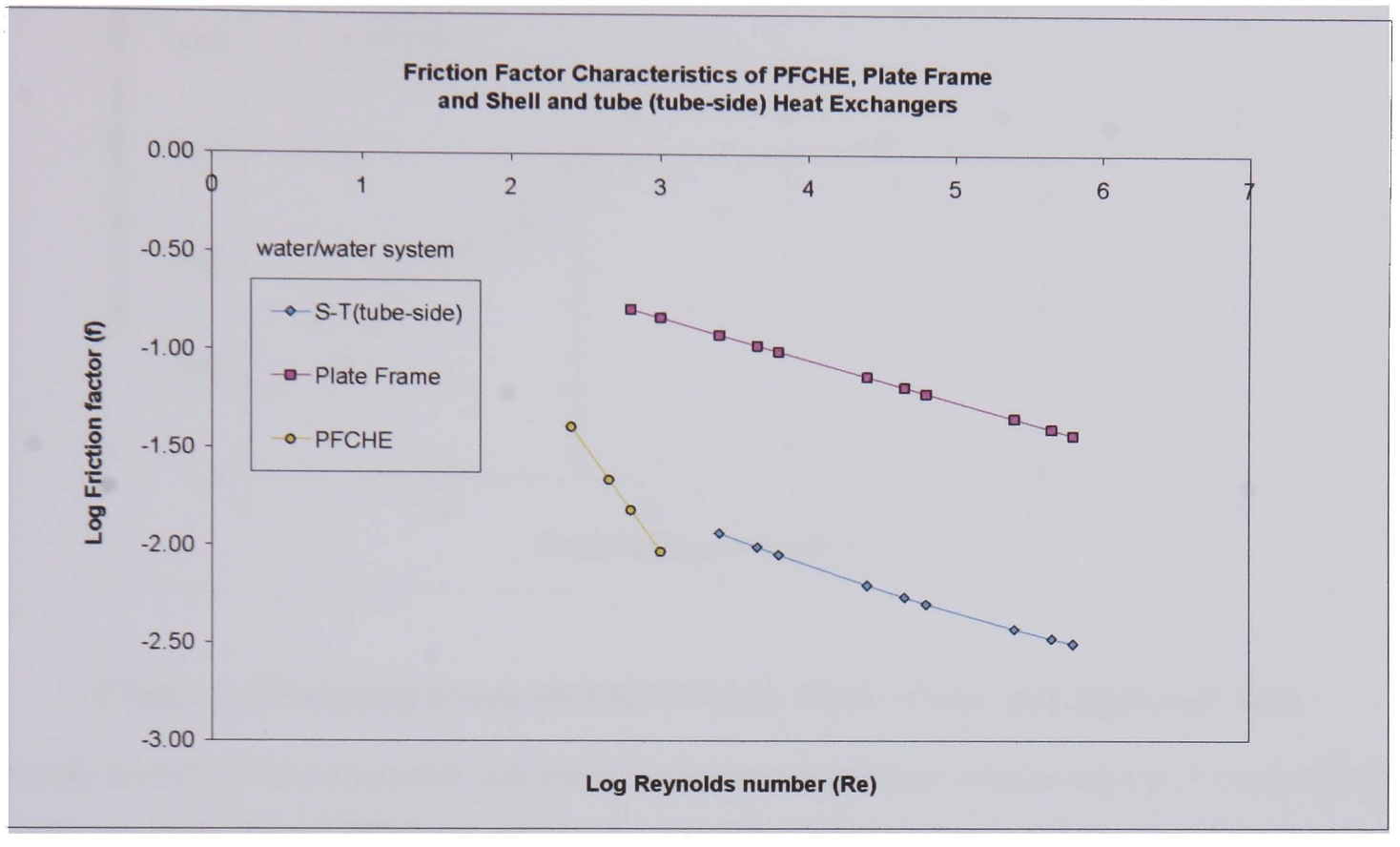


**Figure 1.2 Friction factor characteristics for PFCHE, Plate Frame, Shell and Tube**

From Figure 1.2, it can be concluded that the friction offered by the polymer film compact heat exchanger, is less than the plate frame but more than the shell and tube heat exchanger. The plate frame has the highest friction of the three. However, in order to get a complete picture of the heat exchanger performance, the pumping power necessary to achieve a given heat transfer coefficient, which is of significant design interest, is evaluated in the next section.

*1.4.3 Study of pumping power loss (E)*

In Figure 1.3 below, the heat transfer coefficient based on the projected area is plotted against the pumping power for the PFCHE and also for the plate frame and the shell and tube heat exchangers. For a typical heat transfer coefficient of about 6000 $W/m^2K$, the energy lost due to the fluid flow resistances are as follows:

(a) PFCHE 8.5 $W/m^2$
(b) Plate frame 14 $W/m^2$
(c) Shell and tube (tube-side) 20 $W/m^2$

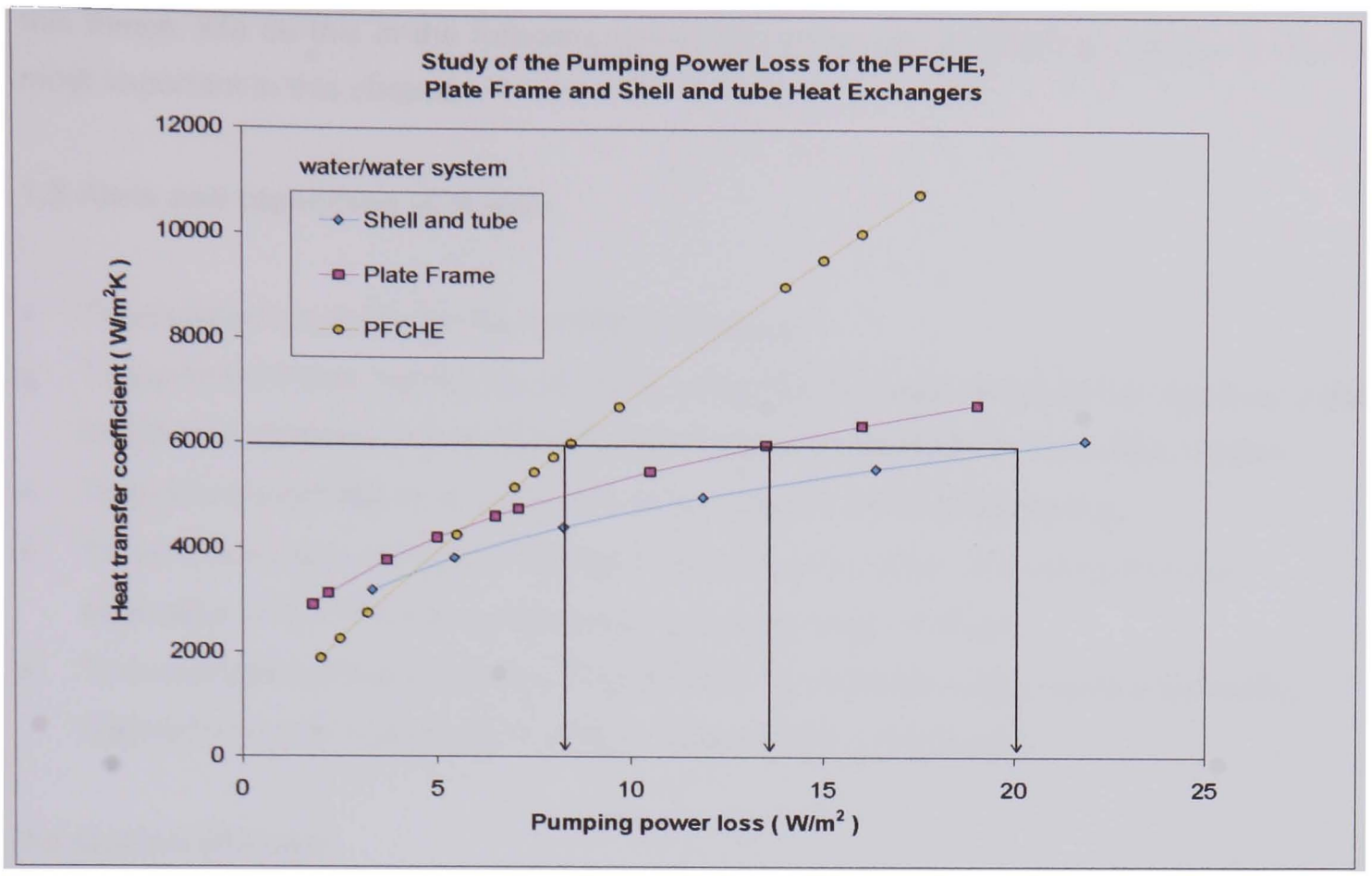


**Figure 1.3 Pumping power plot for PFCHE, Plate Frame and Shell and Tube**

It may therefore be concluded that there could be a significant energy saving, if conventional units are replaced by PFCHEs. However, the plate frame and the polymer film exchangers have their own merits and demerits that should be taken into account before deciding on the type of exchanger to be used.

*1.4.4 Conclusions*

The following conclusions can be drawn from this investigation:

- Thermal performance of the PFCHE has been shown to be very much greater than that of either plate frame or shell and tube exchangers at low Re numbers.
- Thus for typical conditions, the heat transfer per unit volume (Z) of the PFCHE, is a factor of 68 greater than a shell and tube and 3 times more than a plate frame exchanger.
- PFCHE friction factors under typical operating conditions are lower than that of the plate frame exchanger at but higher than the shell and tube.
- For comparable heat transfer, the energy loss through fluid flow resistance in the polymer film exchanger is 60% of that of the plate frame exchanger, and 43% of a typical shell and tube.

Having had a grasp of the research background, an understanding of the heat exchanger performance evaluations and a taste for the incentive for developing the PFCHE technology, we can now establish the aims of the research and provide an outline for the remainder of

this thesis. We do this in the following two remaining sections, which are arguably the two most important in this chapter.

## 1.5 Aims and objectives of thesis

- To establish credibility for the PFCHE technology
- To perform PFCHE testing for different configurations using different fluid systems under industrial conditions and to develop performance correlations for each fluid system
- To present industrial case studies for evaluating the PFCHE technology
- To develop unique design correlations involving Pr number, that will enable the evaluation of the PFCHE performance for a wide range of fluids
- To investigate different aspects of the PFCHE (corrugation angle, surface geometry, material of construction) and its effect on exchanger performance

## 1.6 Outline of thesis

Chapter Two describes the relative merits of using polymers in compact heat exchangers which is followed by details of available polymer compact heat exchanger designs, currently employed in various industrial applications. This chapter then focuses on a particular type of polymer exchanger namely the polymer film compact heat exchanger (PFCHE), which is incidentally the research topic for this thesis. Following this, reasons for adopting the PFCHE design aspects are explained and its advantages are highlighted. The chapter concludes by addressing the potential market for the technology, covering a wide range of applications, based on studies from literature.

Chapter Three outlines a general uncertainty analysis conducted for all the PFCHE experiments mentioned in this thesis. The uncertainty analysis evaluates the reliability of the experimental data by taking into account the accuracy of the equipment involved and shows how the errors propagate when incorporated in data reduction equations to obtain heat transfer (Jh) and friction factor (f) results. Sample calculations for all experiments involving differentiation of the measured variables in the data reduction equations are included. The chapter ends by showing that all the experimental data used to describe the PFCHE heat transfer performance, is within the uncertainty level of 10%.

Chapter Four describes the performance testing on the square PFCHE using six different fluid systems (air/air, water/water and four glycerol-water mixtures/water), in laminar conditions. In the previous chapter, the reliability of the PFCHE experimental data was proven and following this, we proceed to investigate the laminar flow performance characteristics using different fluid systems. Four performance evaluation methods (Jh, f, E and Jh/f) were used to generate the unit's performance evaluation plots. Finally, using these

plots we conclude the chapter with the development of the design correlations for the square PFCHE. These correlations are a major tool in developing alternative heat exchanger designs to metal units.

Chapter Five looks at another PFCHE configuration, that is the spiral PFCHE. Besides testing different fluids, it is also interesting to consider different unit configurations, especially for applications where the square PFCHE is deemed unsuitable. As with the square unit, the performance testing of the spiral PFCHE is carried out using the same performance evaluation methods but using an air/water system. Following this, the design correlations are developed at the end of the chapter.

Chapter Six illustrates the use of the PFCHE design correlations; established in previous chapters, towards developing alternative units for suitable applications dominated by metallic heat exchangers. Five case studies involving a cabin air cooler, filter cooler, two fuel cell heat exchangers and a car radiator are carried out. These alternative designs incorporate correlations for the air/air and water/water systems in the square PFCHE and also the air/water system for the spiral unit. Results show that significant weight and cost savings can be achieved in the aviation, fuel cell transport and automobile industries when employing the alternative PFCHE designs.

Chapter Seven investigates the effect of using different corrugation angles on the square PFCHE performance; a progression towards the work done in previous chapters, involving the use of different fluid systems and configurations in the PFCHE. The performance of the $30^{o}$, $60^{o}$ and $90^{o}$ corrugation angles in an air/air system are studied collectively with the results for the $90^{o}$, obtained from Chapter Four. Performance evaluation methods are then carried out to determine the optimum angle for the square PFCHE. Using the results of each corrugation angle, we conclude this chapter with a PFCHE performance comparison with metallic heat exchangers.

Chapter Eight investigates the effect of Prandtl numbers (Pr) on the square PFCHE performance; using results of the six fluid systems tested in Chapter Four. These dimensionless numbers are used to represent the different fluid properties of each system. Six Pr systems (Pr=0.7, 7, 19, 30, 49 and 192) are studied in five performance evaluation plots (Jh, Nu, f, Jh/f and E). Using regression analysis, the Nu and f plots are used to develop a design model (unique PFCHE design correlations) as a function of both Re and Pr numbers. Once the correlations are established, the chapter ends with a PFCHE performance comparison; involving the Pr number, with data from literature.

Chapter Nine studies the effect of surface geometry and material of construction for the PFCHE. A performance comparison between the sinusoidal corrugations of the PFCHE and

six plate fin geometries (strip, wavy, louvered, perforated, pin and plain) is conducted, using four performance evaluation plots (Jh, f, Jh/f and E), in an air/air system. The similar hydraulic diameters, $d_h \approx$ 2mm of the geometries form the basis of the comparison. Using the results obtained, the strengths and weaknesses of the sinusoidal corrugations are highlighted. Following this, the performance of a PVDF exchanger is compared with the PEEK PFCHE to investigate the effect of using another type of polymer on the PFCHE performance. This is done to enable an alternative polymer to be used in applications where PEEK is deemed unsuitable.

Chapter Ten draws together the results and conclusions from the previous chapters in this thesis. Some future recommendations for the research are also outlined.

## 1.7 Summary

We have seen in this chapter that there is a huge incentive to pursue the research on polymer film compact heat exchangers (PFCHE), due to its superior performance to conventional metallic heat exchangers. Background information on process intensification; the area of which this research concentrates on, plus an insight on compact heat exchangers, as well as its performance evaluation methods are disclosed to provide an initial appreciation for the research topic.

Having seen the potential for this new technology, we proceed in the following chapter to examine the design aspects of the PFCHE. Prior to this, we will consider the merits of using polymers over metals and briefly describe other available polymer heat exchanger designs. Proposed future applications adopting the PFCHE design are outlined at the end of the chapter.

# CHAPTER 2 - LITERATURE REVIEW ON PFCHE

## 2.0 Introduction

In the previous chapter, we introduced the concept of process intensification (PI) and compact heat exchangers (CHEs) in the process industries. We looked briefly at the role of compact heat exchangers in achieving the aim of process intensification and listed the advantages and perceived limitations of these units, from being implemented in industry. This background serves as a stepping-stone towards understanding the benefits of a new type of compact heat exchanger researched in this thesis, namely the polymer film compact heat exchanger (PFCHE).

Following the background on CHEs, we then disclosed four performance evaluation methods (Jh, f, E and Jh/f), which will be frequently adopted for the evaluation of the PFCHE. We concluded the chapter, by showing the initial incentive to adopt the PFCHE technology through a performance comparison with plate frame and shell and tube exchangers, whereby the polymer unit emerged superior. Having laid the background for the research activity plus a glimpse of the incentive offered, we now need to disclose further explanation on the benefits of using polymers over metals, pertaining in particular to the PFCHE design.

Until recently, work on compact metallic heat exchangers has sparked interest amongst heat exchanger manufacturers due to its enhanced thermal performance and energy saving benefits in comparison to conventional heat exchangers. Nevertheless, the limitations of these metallic heat exchangers which involve corrosion, weight and cost issues have created the need to develop alternative units.

Much of the initial interest in the development of polymer compact heat exchangers was stimulated by their ability to handle both liquids and gases (single and two phase duties), their resistance to fouling and corrosion and also their possible use in humidification and dehumidification duties. But, most importantly, the use of polymers offers substantial weight, volume, space and cost savings which give them a competitive edge over exchangers manufactured from more exotic alloys.

In this chapter, we provide a general review on polymer compact heat exchangers. The first section outlines the types of polymers used and their respective characteristics. This is followed by the relative merits of using polymers over metals, leading to a section on the current types of polymer compact heat exchangers available in the process industries. Subsequently, we introduce a recent advancement in the field, which showcases the development of the polymer film compact heat exchanger, highlighting the advantages of its design. We conclude this chapter with a series of future applications for this novel technology.

## 2.1 Types of polymers used in compact heat exchangers

The types of high performance polymers currently used in polymer compact heat exchangers are PVDF (polyvinylidene fluoride), Teflon or PTFE (polytetrafluoroethylene), PP (polypropylene), PE (polyethylene), PC (polycarbonate), PPS (polyphenylene sulphide) and (PPO) polyphenylene oxide.

PVDF can accommodate highly corrosive applications at high temperatures involving appreciable mechanical stress. Its processing temperature is 220°C and it decomposes at 350°C.The service temperature range of PVDF is –1.6°C to 154°C. It swells in ketones, dissolves in polar solvents and is not recommended for use in contact with bases. It is suitable for heat recovery processes involving acids, reducing pollution emissions and flue gas cleaning purposes.

Teflon is well known for its virtual universal chemical inertness and non-stick properties. It is resistant to everything except from molten alkali metals and fluorine. Teflon can withstand temperatures up to 204°C and pressures up to 862 kPa. It is widely used in bromine recovery systems, metal pickling, plating solutions and deionised water heating.

Polypropylene (PP) is rigidly constructed and is only prone to attack by oxidising agents on the tertiary hydrogen. Of the other hydrocarbon polymers, PP has the highest melting point at 165°C. It is non-toxic, non-staining and exhibits excellent corrosion resistance. It has a significant application in mechanical vapour compression (MVR) units.

Polyethylene (PE) is the first of the polyolefins originally prepared some fifty years ago, by the high-pressure polymerisation of ethylene. Its comparatively low density arises from the presence of a small amount of branching, on the carbon chain (on about 2% of the carbon atoms). This results in a more open structure. PE is a most useful and widely used plastic. It is transparent to opaque, robust enough to be virtually unbreakable, and, at the same time, quite flexible. Chemically, PE is unreactive at room temperature although it is slowly attacked by strong oxidising agents and some solvents will cause softening or swelling. It may be used at temperatures of up to 95°C for short periods and at 80°C continuously. PE is ideally suited to a wide range of laboratory apparatus including wash bottles, pipette-washing equipment and tanks.

Polycarbonate (PC) has good chemical resistance to acids but poor resistance to alkalis and solvents. It is resistant to mineral acids, organic acids, greases and oils and dissolves in nitrile, polyamide and hot melt. The melting point of the polymer is 149°C. It has a service temperature range of -4°C to 135°C. Of all the glazing materials on the market today, water-clear, high impact resistant polycarbonate sheets provide the widest range of properties. PC is recognised not only for its clarity, safety, security and energy savings, but also for the design freedom it provides to architects.

Polyphenylene sulphide (PPS) is noted for its exceptional resistance to acid attack. Results of tests in 85% sulphuric acid at 120°C for up to 5000 hours, suggested that PPS is the best performer in acidic conditions compared to Teflon and PVDF.

Polyphenylene oxide (PPO) is similar in chemical composition to polyphenylene ether (PPE), and they are generally treated as equivalents. It has good heat resistance but poor chemical resistance. Nevertheless, the strength, stability and the acceptance of flame-retardants of PPO makes it desirable for machine and appliance housings. The lack of chemical resistance and colour stability means that the latter often have to be painted in these applications. Low water absorption leads to the use of PPO in various water-handling products. Moreover, PPO can also be electroplated.

Having known the types of polymers that can be adopted in compact heat exchangers, we now proceed to evaluate the merits of using polymers over metals in such units. This is shown in the following section.

## 2.2 Relative merits of polymer compact heat exchangers

It has been argued that the use of polymers can cause problems during design and manufacture owing to their low strength, poor creep resistance, relatively poor thermal conductivity and large thermal expansion. Nevertheless, their impressive resistance to chemical attack at moderate temperatures and pressures and also their lower relative cost can offset these factors. The latter is proven mathematically as follows:

PVDF has a thermal conductivity of 0.17 W/mK ,which is 100 to 1000 times lower than that of steels and other metals (Verschaeve 1987). Therefore, it would appear futile to pursue this technology. However, it does present opportunities when the formula for the calculation of the surface of the heat exchanger is examined.

The formula for evaluating the overall heat transfer coefficient through a cylindrical tube is as follows:

$$\frac{1}{U} = \frac{d_i}{2k_{tube}} \ln\frac{d_o}{d_i} + \frac{1}{h_i} + \frac{1}{f_i} + \frac{1}{h_o}\frac{d_i}{d_o} + \frac{1}{f_o}\frac{d_i}{d_o} \qquad (2.1)$$

For the sake of simplicity, the formula that applies only to heat transfer through plane walls is used.

$$\frac{1}{U} = \frac{t}{k_{wall}} + \frac{1}{h_i} + \frac{1}{f_i} + \frac{1}{h_o} + \frac{1}{f_o} \qquad (2.2)$$

For instance, the latter formula is applied in the case of a Ni-Cr-Mo alloy (Hastelloy) using,

$t$ = 1mm

$h_i$ & $h_o$ = 4000 W/m$^2$K

$f_i$& $f_o$ = 4000 W/m$^2$K

$$\frac{1}{U} = \frac{0.001}{8} + \frac{1}{4000} + \frac{1}{4000} + \frac{1}{4000} + \frac{1}{4000} \qquad (2.3)$$

U = 890 W/m$^2$K

In the case of PVDF, by using the same film and fouling coefficients, the equation becomes:

$$\frac{1}{U} = \frac{0.001}{0.17} + \frac{1}{4000} + \frac{1}{4000} + \frac{1}{4000} + \frac{1}{4000} \qquad (2.4)$$

U = 145 W/m$^2$K

Thus, the ratio of the overall heat transfer coefficients is 890:145 = 1:6

Consequently, the PVDF exchange surface has to be six times larger than one Ni-Cr-Mo alloy.

However, if we consider PVDF and Ni-Cr-Mo tubes of the same diameter and same thickness, which is correct in practice, the weight ratio of the exchange unit surface is expressed by the ratio of the densities.

Weight of 1m$^2$ of Ni-Cr-Mo = 8.9

Weight of 1m$^2$ of PVDF = 1.78

$\approx 5$

Moreover, if we introduce the price of materials in the form of tubes, then the price of materials for the essential part of the exchanger is shown by the following ratio:

$$\frac{\text{Price of exchanger Ni-Cr-Mo}}{\text{Price of exchanger PVDF}} = \frac{1}{6} \times \frac{5}{1} \times \frac{3000}{1000} = 2.5$$

1:6 = ratio of exchanger surfaces

5:1 = ratio of weights of unit surface

3000:1000 = ratio of tube prices

This means that if all other conditions remain equal, a tube bundle of Ni-Cr-Mo alloy will cost 2.5 times as much as one PVDF bundle. The price difference that exists is significant enough to recommend the development of PVDF heat exchangers. This quantitative assessment shows the benefits of adopting polymers over metals in compact heat exchangers.

In addition, it should be noted that the polymers adopted in compact heat exchangers have suitably high glass transition temperatures ($T_g$), which ensures good durability without property degradation. For example, the glass transition temperature for PEEK and PVDF are 157°C and 160°C respectively. Basically the $T_g$ is the temperature at which the polymer experiences a transition from a solid to a liquid state. If a polymer is heated, the kinetic energy of the molecule increases. Motion is still restricted however, to short range vibrations and rotations so long as the polymer retains its glasslike structure. As the temperature is increased further, there comes a point where a decisive change takes place; the polymer loses its glasslike properties and assumes those more commonly identified with a rubber. The temperature at which this takes place is called the glass transition temperature ($T_g$). If heating is continued, the polymer will eventually lose its elastomeric properties (ability to stretch and retract rapidly) and melt to a flowable liquid. A polymer can serve as a useful alternative material to metal, as along as its glass transition temperature is appropriately higher than the temperature of its intended work environment. For example, a plastic used in manufacturing coffee which has a glass transition temperature above the temperature of hot coffee is deemed suitable.

Polymer compact heat exchanger technologies are very advanced. However, the use of polymers in industrial heat exchangers has remained a niche market for some time. Their acceptance in the process industries is not yet widespread. The reasons for this are the lack of awareness of polymer compact heat exchanger benefits and the absence of reliable design methods, along with investigations under actual operating conditions. Perhaps industrial applications are limited only by the imagination of process designers, particularly as these materials are increasingly used in pumps, valves and other plant ancillaries.

Bearing in mind the merits supporting the use of polymers as an alternative to metal units, we now look at the three major categories of polymer compact heat exchangers that are available in industry. They are the polymer plate heat exchangers, heat exchanger coils and shell and tube heat exchangers.

## 2.3 Classification of polymer compact heat exchangers

### *2.3.1 Plate heat exchangers*

The DIABON 100 plate heat exchanger *(Sigri and Alfa Laval)* is made of the new DIABON composite material, a fluoroplastic PVDF bonded graphite. It is used in the flue gas cleaning

process which results in fumes bringing 700 to 1000 ppm(volume) of $SO_2$ and 7 to 10 ppm(volume) of $SO_3$ with a 1% sulphur content, burnt in 11% of excess air (Tayler 1988).

The ENKA compact heat exchanger *(Solvay)* introduced the use of hollow fibre PVDF heat exchangers. It was mainly designed for heat recovery combined with condensation of hazardous vapours from corrosive exhausts and stack gases, as well as for depollution units and desulphurisation processes (Maquet 1988).

Polymer plate compact heat exchangers are also used in liquid-liquid applications *(Ciat).* This company developed the first of such heat exchangers in France. The design uses plastic netting between plates to enhance heat transfer, but is otherwise similar to metal designs (Tayler 1988). A large unit would have a surface area of around 100 $m^2$ for a maximum flow of 200 $m^3/h$. At 60°C, the maximum operating pressure is 2 bar.

The Channelplate heat exchanger *(Akzo Nobel)* is used in gas-liquid applications (Tayler 1988). For instance, in cooling flue gases, air from dryers and other process exhausts. It is also used in dehumidifying polluted gas streams and cooling corrosive liquids.

The tube plate heat exchanger *(George Fischer)* is used for heat transfer between corrosive fluids. It is constructed from PVDF and PP. It is suitable for high purity deionised water, other high purity fluids and condensation of aggressive vapours (George Fischer 1999).

A competitive plate heat exchanger (*IndHex AB),* consists of several layers of polypropylene twin-wall sheets welded together to form an air-tight heat exchanger core (IndhexAB 2000). It is compatible with the sophisticated in-house developed software to optimise the heat exchanger. The design alternatives are cross flow heat exchanger cores, counter flow heat exchanger cores, cores with framework or cores with housing.

A polymer plate heat exchanger *(Recupair)* made from polycarbonate was aimed principally at HVAC (Heating Ventilation Air Conditioning) applications and swimming pool heat recovery markets. Identical in design to aluminium plate units, the plastic version can operate at up to 80°C. The maximum differential pressure is 1 kPa (Tayler 1988).

*GE Plastics* developed a plate heat exchanger from polyphenylene oxide (PPO) for condensation purposes in a gas-fired boiler (Tayler 1988). The heat exchanger is part of its total energy control package. Exhaust gases from a gas-fired boiler are used to preheat the fresh air supply. The corrosion resistance of the unit allows it to work in condensing mode.

Work has also been conducted in developing similar condensing heat exchangers for larger boilers at the *Institute Francais du Petrole* (Reay 2000). The heat exchanger is operated in the flue gases from a boiler burning No. 2 heavy fuel oil (corrosive and with particulates). The polymer selected is polyphenylene sulphide (PPS). An overall heat transfer coefficient value of 40 $W/m^2K$ was achieved, with condensation on one side and preheating air on the other. Other uses for

variants of the condensing heat exchanger were in boilers for apartment blocks and malt kiln heat recovery.

Polymer exchangers have great potential in lower temperature areas. An example being the *Nordwest-deutsche Kraftwerke* power station in Wilhelmhaven, Germany (Reay 2000), which has plastic elements on the cold side of its fuel gas cleaning plant regenerative reheat system. Despite wet contact with chlorides and sulphur oxides, which produces a highly acidic environment for 10000 hours, no degradation was reported in the material supplied by *GE Plastics* other than some age-hardening.

Gas liquid heat exchangers made from PP *(Powell Duffryn)* have principal applications that include heat recovery for corrosive effluents. It is primarily an economiser. Available in a range of sizes; the most interesting feature is the incorporation of 1.5 mm diameter water channels in the plates, which form the heat transfer area on the gas side. The unit is limited to 65°C on the water-side and requires fibre-reinforced material in the polysulphone resin, if the pressure exceeds 1.5 bar. Headers and components may be fabricated in PVC, PP or metal (Tayler 1988).

A polymer heat exchanger *(Akzo Nobel)* made from a mixture of PVDF and PP was developed to act as an evaporator in mechanical vapour recompression (MVR) units (Tayler 1988).

Another plate heat exchanger made from the same mixture of polymers; PVDF and PP, *(Novelerg)* is used intensively in heating and ventilating systems such as car radiators. It is a form of constructed prototype plate exchanger using 60 plates measuring 45cm x 45cm. The unit transfers 26.4 kW and operates successfully at 75°C with 6.5 bar differential pressure (Reay 2000).

An additional plate heat exchanger worthy of interest is the *Dutch LEVEL* unit. This unit has a triangular flow path cross-section, not far removed from the PFCHE concept, but it operates in counterflow in one variant. A compactness of up to 1000 $m^2/m^3$ is claimed. The polymer unit can be used as a recuperator for dryers (Reay 2000).

Polymer plate heat exchangers are also used as air conditioners at *Ficom Pty Ltd.* in Australia (Australian Energy News 1998). Such plate heat exchangers are capable of reducing energy needs for air-conditioning, by using exhaust air to condition intake air without physical mixing. The use of plate heat exchangers allows considerable increases in ventilation rates (up to 100% fresh air) without significant increases in energy consumption and cost.

A heat exchanger having plastic channels is manufactured by stacking plates with intermediate spacer members (Alander 1995). This invention relates to a method of manufacturing heat exchangers for counter flow, cross flow or parallel flow. The channel plates are extruded from a plastic material preferably polypropylene, although any other material with corresponding properties may be used. The material must utilise the stress induced in the plates during their

extrusion. The channel plates comprise of two outer walls that are interconnected by a plurality of intermediate walls. The end portions of the intermediate walls are melted along a predetermined length, whilst the end portions of the outer walls of each channel plate are bent away from one another. This is done such that the edges of the outer walls will from integrated unities with the edges of the adjacent end portions, which are situated next to the channel plates. Prior to solidification of the resultant joins, these may be flattened out with the aid of a roller. According to the invention, the spaces defined by the outer walls of the channel plates may be filled with plastic particles, which form an integrated unity with the end portions of the channel plates.

Next we have a crosscurrent heat exchanger made up of a stack of joined, parallel flow web polymer plates and a hollow chamber for flow across them, situated between each two successive web plates. This unit has been designed by Emmerich (1990). The cover layers of successive polymer web plates are sloped toward one another at their ends over the hollow chamber that is enclosed between them. These web plates are joined tightly to one another over the entire width. Extrudable plastics that can be used for this design are PE, PP, PVC, polystyrene or polymethyl methacrylate. PC and polysulfone plastics are useful for operating temperatures above 100°C to approximately 120°C. Polyphenylene oxides, polyether imides or polyether sulfones, for example, can be used for operating temperatures up to 150°C. Suitable dimensions of the web plates are as follows: a length of 500 to 3000 mm, a width of 300 to 2000 mm and a thickness of 33 to 30 mm, but these dimensions are not critical.

A new concept for a liquid-liquid plate heat exchanger has been studied by Deronzier and Bertolini (1997) using thermoplastic polymers. Considering their advantages, polymers called LCP `liquid crystal polymers', have been developed in the laboratory from a base formulation of pure LCP (SPER1) to improved formulations (SPER12), using fillers such as silica powder, glass and carbon fibres. A fully aromatic structure (SPER12FA) and a modified fully aromatic structure (SPER12IA) were also developed and synthesised. Corrosion and mechanical tests in the laboratory with a selected LCP (SPER12IA) have shown a relatively low chemical resistance and high mechanical resistance in comparison with commercial LCP Vectra.

To conclude this section on polymer plate heat exchangers, we consider a process for producing heat exchangers by forming plastic plates using a plasma deep drawing technique. This process has been developed by Eberhard (2000). The plates are placed on top of each other and hollow chambers are formed between them. Air can pass through the chambers, which act as heat exchangers. In the following section, we look into some of the polymer heat exchanger coils that are currently being used in industry.

*2.3.2 Heat exchanger coils*

PVDF coils *(Solvay)* used as cooling and heating coils for aggressive fluids in tanks, were built very easily. PVDF's high mechanical performance characteristics make heating coils appropriate for vapour of up to 145°C.These coils resist particularly well to water-hammering (Therme-America 1988).

The tankcoil heat exchanger *(Du Pont)* is used for the elimination of acid cooling downtime. It is the first *Du Pont* tankcoil heat exchanger in Europe. Each tankcoil provides a heat transfer area of 116 $m^2$. The acid inlet temperature is 100°C and the acid outlet from the coolers is maintained at 72°C. Inlet cooling water is at 23°C and outlet water is at 40°C (DuPont 1988).

Tankcoils *(AMETEK),* on the other hand are typically used for cooling of dryer tower and absorber acids in sulphuric acid manufacturing plants. These Teflon units are the largest immersion coils. They are ideal for handling high heat loads in corrosive environments (AMETEK 1988).

Reactor coils *(Du Pont)* were developed to solve metal pickling and pickling acid recovery problems. The R500 Reactor coil, used in pickling acid recovery operation has Teflon tubing (DuPont 1988).

Reactor coils *(AMETEK)* are typically used for crystallisation in corrosive liquids including the removal of Glauger's salt (sodium sulphate decahydrate) from rayon spin baths, removal of salt in purification of 50% caustic and the separation of $FeSO_4$ from spent pickle liquor (AMETEK 1988).

Slimline coils *(Du Pont) i.e.* immersion coils of different 'U' configurations are used for heating and maintaining 10% sulphuric acid at up to 90°C. Based on the successful pickling applications, these units are now considered for use as a replacement for the existing cooling system in crystallisation tanks. In addition, Teflon heat exchangers are not fouled with ferrous sulphate, able to work continuously, require minimum maintenance, and can fit into existing crystalliser tanks (DuPont 1988).

Slimline coils *(AMETEK)* are used in a variety of services in the metal processing industry. The design is increasingly used for steel pickling. Slimlines are less than 127 mm wide and permit mounting close to the sides of the acid tank (AMETEK 1988).

Supercoils *(AMETEK)* are used for heating and cooling in essentially all plating and metal finishing solutions (AMETEK 1988). In particular, they are used in electroplating, electroforming and electroless plating baths plus acidic and alkaline solutions for etching, chemical milling, anodising, cleaning, stripping, electropolishing and similar operations. Supercoils are multi-braided, flexible coils of only 89 mm thick, which can be fitted into almost any tank configuration.

Minicoils *(AMETEK)* are well suited to the electronics industry for etching, precious metal plating, and also in the deionised water rinse tanks used in the production of wafers, microcircuits and

connectors. Minicoils are available as single or dual units (AMETEK 1988). Teflon FEP tubing is laced to support sheets. In addition to single and dual minicoils, *AMETEK* offers twelve additional models designed specifically for plating baths.

Coils made from PVDF and PP *(Rekuperator)* have a significant application for plastic heat exchangers, as the evaporator in mechanical vapour compression (MVR) units (Tayler 1988).

Immersion coils from Teflon *(Fluorotherm)* are used for heating and cooling chemically aggressive fluids. They feature corrosion resistant and ultrapure fluoropolymer immersion heat exchangers. They are unsurpassed in chemical resistance due to their fluoropolymer construction and are superior to other exotic metals, alloys, glass and graphite (Fluorotherm 2000). The next two applications considered in this section involve the use of plastic tubes or pipes.

Plastic tube-type heat exchanger structures are made with partially crystallised and partially aromatic polyamides of high glass transition temperature (Doshi 2000). The structures are then annealed to further crystallise the polyamides, causing shrinkage and building up residual tensile stresses. These stresses counteract the swelling caused by water absorption and temperature rise during use of the heat exchanger, and keep the structures dimensionally stable. The present invention provides a tube for use in a heat exchanger, which is made from thermoplastic composition. The polyamide has a glass transition temperature of 65°C or higher. This design involves a process for manufacturing a tube-type plastic heat exchanger, in which curving and bending of the tubes can occur in service environments. By adopting this design, pickup or loss of moisture and thermal expansion caused by the bending and curving is prevented.

Finally to end this section, we consider a plastic heat exchanger used for condensation purposes. The heat exchanger is positioned in a gas-fired hot air furnace and has a ceramic pipe forming an initial portion of a fluid flow path through the heat exchanger (Holowczak 1997). The ceramic pipe receives the combustion gases from a primary heat exchanger and reduces the temperature of the combustion gases to below a certain temperature. A polymer-based structure is connected to the ceramic pipe and forms the remaining portion of the fluid flow path through the heat exchanger. The geometry and orientation of the ceramic pipe is selected so that the certain temperature of the combustion gases exiting the ceramic pipe is less than the softening temperature of the polymer-based structure. The resultant heat exchanger combines the high temperature and corrosion resistance of ceramic materials with the low cost and high corrosion resistance of polymer materials. As a result, a low cost heat exchanger can be produced which can withstand both the high temperatures of the combustion gases as well as the corrosive properties of the condensates from the combustion gases.

In the next section, we consider the last of three categories for the polymer compact heat exchangers, currently adopted in industry. This category involves the different types of shell and tube polymer heat exchangers available in the market.

### 2.3.3 *Shell and tube polymer heat exchangers*

Small size PVDF industrial exchangers *(Solvay)* have been developed to cool down an aqueous solution of HCl at 35% concentration. They consist of an exchanger with four series of standard elements. Each element has a nominal diameter of 100mm and a length of 4m. The shell is ordinary steel and contains 22 PVDF tubes with diameters 12.0mm to 10.4mm.

U-tube *(Solvay)* heat exchangers are used for recovering acids and reducing pollution emissions. The use of PVDF tubes improves the efficiency of condensers by decreasing the absolute pressure of the operating vacuum.

U-tube *(Therme-America)* was developed for the production of manganese dioxide, used to manufacture dry alkaline batteries. It features chemical inertness in the presence of highly corrosive sulphuric environments. The temperature ranges from 90°C to 100°C for the electrolyte, and 130°C for the steam at a pressure of 3 bar (Therme-America 1988).

The ECOFUME system *(SAG)* associated with *Flakt(B)* developed a new PVDF heat exchanger technology designed to work below the acid dew point in flue gases from fossil oil combustion. The system consists of a whole set of gas-liquid heat exchangers and regulators allowing it to work above and below the sulphuric acid dew point (Maquet 1988).

*GEA (Germany)* developed the ECOGAVO and ECONOX systems for flue gas cleaning and depollution units. GEA recently claimed to be the largest manufacturer of waste heat recovery systems in the world. Certainly some of the largest heat exchangers within this category are in power station plants, in particular those where flue gas desulphurisation (FGD) processes exist (Maquet 1988).

In the ECOGAVO system, at first the heat exchanger module battery recovers the heat from hot, untreated gas, in a calorific fluid. The fluid is pumped to the second heat exchanger module battery, to reheat the cleaned gas coming from the fuel gas unit, prior to evacuating it to the stack. Due to the temperature service where the uncleaned flue gas temperature is greater than 160°C and the calorific fluid temperature is between 135°C to 140°C, PFA is used for the untreated gas heat exchanger. PVDF is used to reheat the cleaned gas to 75°C.

In the ECONOX system, the process is similar to the ECOGAVO system with an additional component. This component combines four batteries of heat exchanger modules. The PVDF heat exchanger is placed after fuel gas cleaning takes place and coupled with a steel heat exchanger, which is installed after depollution has taken place and before evacuation to the stack.

PVDF shell and tube heat exchangers *(ECOPOL)* were used as an early application for space heating from a solvent laden exhaust gas stream. This has been developed by (*Neu)* in France. The tube material comes in a roll. This is cut to length and may be attached to collars on-site by

heat shrinking. Tubes have a diameter of 32mm. The use of very thin, 100μm wall thicknesses achieved overall heat transfer coefficients close to those of metal exchangers (ECOPOL 1999).

Teflon shell and tube heat exchangers *(Fluorotherm)* are designed for applications where chemical inertness to aggressive fluids is critical. Their applications include semi-conductor, biotechnology (ultrapure), environmental, laboratory and products finishing industries. Units are designed with efficient heat transfer as the primary aim (Fluorotherm 2000).

Teflon shell and tube heat exchangers *(Du Pont)* are used for sulphuric acid cooling. *Olin Corporation (McIntosh, Alabama)* has found that two Du Pont shell and tube heat exchangers have been highly successful in cooling sulphuric acid under their chlorine drying towers. The heat exchanger contains 230 tubes (0.6cm OD x 0.5cm ID) of Teflon inside a carbon steel shell (DuPont 1990).

Teflon shell and tube heat exchangers *(Du Pont)* were also developed to solve tube failure problems in bromine recovery systems. *Great Lakes Chemical Corporation (Indiana)* experienced costly maintenance and downtime problems with metallic heat exchangers in bromine recovery systems (Schubert 1988).

Another use of Teflon shell and tube heat exchangers *(Du Pont),* are to help copper manufacturers reduce costs and improve sulphuric acid production, as experienced by *Inspiration Copper Globe (Arizona)* which had a water balance problem (AMETEK 1990).

Teflon shell and tube heat exchangers *(AMETEK)* are used for heating, cooling and condensing chemically aggressive process streams *i.e.* sulphuric, hydrofluoric, nitric, hydrochloric and other acids, caustic and other alkalis, halogenated compounds, salt solutions and organic compounds. They are also used for pickling, plating solutions and deionised water heating, where using a Teflon immersion coil is not possible (AMETEK 1990).

Calorplast *(George Fischer)* gas or liquid heat exchangers are designed specifically for condensing and/or reheating highly corrosive gas streams. Manufactured from tough, impact-resistant PVDF or PP, these exchangers are capable of handling gas stream temperatures of up to 138°C (George Fischer 1999).

PP and PVDF shell and tube heat exchangers *(Eta Process Plant Limited)* were developed for external heat transfer between highly corrosive fluids. These units are particularly suitable for high-purity media such as deionised water, and also as a condenser for flows of up to approximately 500 $m^3/h$ (Ferreira 2000). The gas liquid heat exchanger is used for heating and cooling corrosive gases with condensation. The exchanger tubing consists of interchangeable removable modules. The heat exchange surface is 6mm (OD) smooth wall tubing with 12mm clearance between the tube rows.

Shell and tube heat exchangers *(Placon)* are used for heat recovery processes from aggressive waste air; for example in electroplating, the chemical industry and in the electronics industry. They are also used for cooling aggressive waste gases, upstream of scrubbers and subsequent heating; for instance in drying processes or in chemical metal treatments. These units can act as condensers in the chemical and pharmaceutical industries for drying processes (Placon 1996).

A high density polyethylene (HDPE) shell and tube heat exchanger *(Chem Resist)*, has been developed for use in the chemical, pharmaceutical, electronics (ultra-pure liquids), metal finishing and seawater processing industries (Chem-Resist 1990).

The following specification discloses an air-to-air, polymeric heat exchanger having a housing and a core that is removable. The core is mounted within the housing (Huebner 1988). The housing includes four generally identical units, which are secured to one another, and a top and a bottom, which are secured to the duct units. The core includes a pair of end walls and a plurality of tubes extending between, and opening through, the end walls. Each end wall includes a plurality of tubular projections or pockets extending from the end wall in a common direction. Opposite ends of the tubes are secured within the tubular pockets in the opposite walls. A method of constructing the core includes the step of severing the tubular projections, after the tubes are positioned. This is done to expose the tube interiors through the end walls. Preferably, the tubular projections are severed using a hot wire to also fuse the tubes within the end walls.

Finally we have a heat exchanger in the form of a comfort heat exchanger, which includes two manifold elements adapted to receive and discharge fluids and a plurality of tube units transversely located between the manifolds (Fletcher 1992). Each tube unit is connected to substantially rigid end elements that fit into the manifolds. The tubes are orientated and expanded to approximately their original diameter. The heat exchanger is to be fabricated from polymer, especially polyamide compositions. The tube units are intended to be manufactured using injection molding techniques, and then subjected to orientation and expansion steps. The heat exchangers are particularly intended for use as comfort heat exchangers in automobiles, for the heating and air-conditioning systems.

Following the descriptions of the three main categories for polymer compact heat exchangers, we now describe a new novel compact heat exchanger design, incorporating thin (100μm) corrugated polymer films. The unit is known as the Polymer Film Compact Heat Exchanger (PFCHE).

## 2.4 Recent advances: Polymer Film Compact Heat Exchangers (PFCHE)

As mentioned before, the vast majority of presently available and commercially used heat exchange apparatus are made of metals such as stainless steel. The use of metals for forming a heat exchange apparatus, provides certain significant disadvantages including being heavy and costly. Since metals are good conductors of heat, the atmosphere surrounding the heat

exchanger provides either a source of unwanted heat to a coolant fluid or an unwanted extractor of heat from a heating fluid used in the heat exchanger. In addition, the use of metals when processing corrosive fluids is quite limited, and generally results in the required use of specialised, expensive metals. Also, most metals are easily wet with liquids, which in turn promote their interaction with the liquid such as chemical reactions and fouling of the metal.

Bearing all this in mind, it is desirable to find an alternative material of construction for the heat exchange apparatus, which can address these shortcomings and also acquire high heat exchange efficiencies and is easily fabricated. This is where the use of polymers comes into play. In accordance to this need and in order to further enhance the thermal performance of existing polymer compact heat exchangers, thin polymer films are adopted in a new design as opposed to the more conventional shell and tube, plate or coil configurations.

In current designs, the wall thickness can only be decreased to a range of 0.5 to 1mm without affecting the mechanical strength of the polymers. However, the use of polymer films of approximately 100 μm thick is possible and this will subsequently promote a better thermal performance. In order to minimise the thermal resistance offered by polymeric materials, a polymer film compact heat exchanger using 100μm thick polymer films has been developed by *PIIC (Process Intensification & Innovation Centre),* at Newcastle University. The presence of corrugations on the films also aids towards heat transfer enhancement, as it encourages more mixing of the fluid flow.

PEEK (poly ether ether ketone) was chosen for the material of construction, as it has excellent chemical and fatigue resistance. It resists a wide range of organic and inorganic liquids and is only susceptible to concentrated nitric or sulphuric acids (>50% concentration). This superior chemical resistance has allowed it to work effectively as a metal replacement in harsh environments. Moreover, it also exhibits good thermal stability and has a working temperature of about 220°C. Additionally the matrix, constructed of corrugated 100μm PEEK films, is remarkably robust and can withstand a differential pressure of about 10 bar at ambient temperatures (Jachuck 1999). The matrix is made up of many sheets stacked on top of one another, so that the turbulence in the headers can be efficient enough to homogenise the temperature within. An illustration of the arrangement for the corrugated PEEK films in the matrix is shown in Figure 2.1 below.

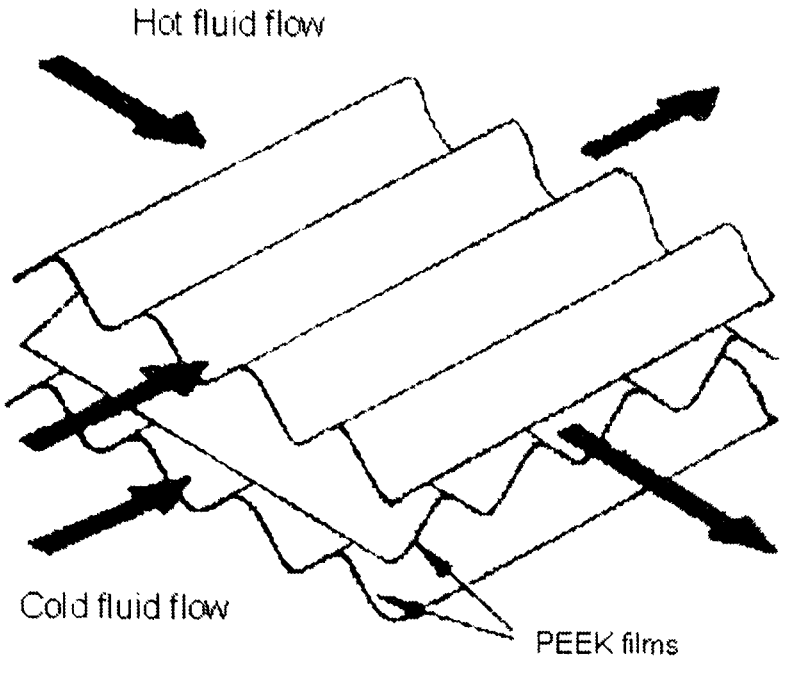


**Figure 2.1 Corrugated PEEK films stacked at 90° angle to each other in the PFCHE**

The PEEK films also have hydrophobic super-smooth surfaces together with a high coefficient of thermal expansion. Therefore, the fouling characteristics of polymer films are intrinsically superior to those of metal with regards to the smooth surface. The thermal expansion, on the other hand, can assist in the 'self-cleaning' capability of the unit but considerations should be given to the level of expansion when installing the unit. The cost of PEEK is around £40-50/kg; more than normal plastics and certainly much more, than common metals. Nevertheless plastic densities are generally much lower than metal densities so material costs remain a small proportion of total costs.

The analytic reasoning behind the design aspects of the cross-corrugated PFCHE is outlined in the following sections. This involves the reasons for the use of thin films, corrugations, narrow channels and the adoption of laminar flows, which is then followed by studies from literature to support each design aspect. We begin in the following section, with an explanation for the use of thin polymer films.

*2.4.1 Thin Polymer Films*

In order to overcome the low thermal conductivity in polymer compact heat exchangers, thin films or sheets are chosen in preference to tubes, coils or plates. The use of thin films may enhance the thermal performance of heat exchangers. This is shown mathematically below:

The thermal conductivity of PVDF is 0.17 W/mK. It is possible to improve this value by adding certain filters in the production of tubes, but this would be to the detriment of chemical resistance. Hence this is not advisable, as we do not want to alter the basic property of PVDF. Using equation (2.2) earlier, (see page 20) the best way to improve the overall heat transfer coefficient is to modify the material resistance, t/k. Indeed, if we neglect the influence of film and fouling coefficients in the formula for the overall coefficient, we find that for a 1mm thick PVDF wall,

$$\frac{1}{U'} = \frac{0.001}{0.17} \qquad (2.5)$$

U'=170 W/m$^2$K which is higher than U=145 W/m$^2$K, as shown earlier in equation (2.4). Thus, the thickness of the PVDF wall is the principal obstacle to heat transfer. It ought to be noted that this does not apply to metals, as they have high thermal conductivity.

$$\frac{1}{\uparrow U} = \frac{t \downarrow}{k_{film} \uparrow} \qquad (2.6)$$

As the thermal conductivity value is constant, we can only act upon the thickness.

Calculations show that in the case for PVDF:

| Thickness, t (mm) | Overall heat transfer coefficient, U (W/m$^2$K) |
|---|---|
| 1 | 145 |
| 0.9 | 160 |
| 0.8 | 175 |

**Table 2.1 Overall heat transfer coefficient and wall thickness values for a PVDF heat exchanger**

Nevertheless, the wall thickness cannot be reduced beyond the limit of mechanical strength. This is why the 0.8mm wall thickness, in this case has been chosen because the mechanical properties of such PVDF films are still good. However for PEEK, lower thickness can be adopted whilst retaining the mechanical strength, as shown by the 100μm thick films employed in the PFCHE. Having seen the importance of film thickness in polymer heat exchangers, we now proceed to look at some thin fluid and thin material film studies, to provide support for its use in the PFCHE design.

2.4.1.1 Thin fluid and material film studies from literature

Some recent work on thin films highlighting its advantages particularly to heat transfer, are outlined in this section, to support the use of the technology in the PFCHE design.

Computational fluid dynamics (CFD) has been used to study the hydrodynamics and heat transfer of thin film periodic laminar flow by obtaining velocity and temperature fields, for a wavy interface

(Jayanti and Hewitt 1997). Results show that the presence of the sinusoidal waves enhances the heat transfer coefficient across the film, mainly due to the effective thinning of the films used. The effective thinning here corresponds to the experimental observation that upon the onset of wavy flow, the mean film thickness decreases as compared to the film thickness in the wave-free region. This decrease in the effective film thickness, gives rise to an enhancement in the heat transfer coefficient. The work here exhibits the importance of adopting thin films in designs where good heat transfer is a priority.

Thin film technology is also used in a novel high intensity heat pump (Aoune and Ramshaw 1999) to improve its heat transfer performance. The heat pump comprises of a series of discs housed within a sealed rotating envelope. Each disc is irrigated with a thin film of fluid, which is involved in absorption or evaporation functions within the heat pump cycle. Experimental results show that very high heat transfer coefficients, can be achieved using the thin fluid films. This is attributed to the good degree of mixing within the thin films.

Another apparatus using thin film technology has been developed for the measurement of thermal conductivity under steady conditions (Zeng et al. 1996). The apparatus was used to measure the thermal conductivity of silica aerogel. The heat transfer modes in silica aerogel include gas and solid conduction, along with thermal radiation. The apparatus uses a thin (10nm thick), gold film heater that is coated on a polyester sheet. Due to the thin gold film used, a uniform heat generation is achieved in the heater with only a small edge loss of heat.

Prior to this thin film application, an improved horizontal-tube, thin-film evaporator that has a high heat transfer coefficient at low temperatures has been designed (Takada and Drake 1983). When applying this evaporator, it is possible to design a multi-effect distiller with a very large number of effects and a vapour compression distiller with an extremely small compression ratio, thus achieving a considerable reduction in energy consumption in those processes. This lower energy consumption shows the advantage of incorporating the thin fluid films.

Next we consider the desalination of seawater, where heat transfer losses are great. Thin film heat exchangers which nowadays constitute desalination systems are of great interest due to the fact that they feature high intensification of heat transfer, elimination of possibility for scale formation on the surface, essential decrease of equipment corrosion and low temperature head between surface and heated seawater (Slesarenko 2001). This investigation includes the development of a mathematical model of thin film water movement, by heating surfaces. An analysis of regimes of all plant types was made and equations for coefficients of heat transfer and hydrodynamic resistance were derived. The work shows that the adoption of thin film technology in the desalination industry brings several benefits, notably the high heat transfer that can be achieved.

Looking at another angle, the use of thin micro fins in advanced computers is employed to enable efficient cooling technology in microelectronic devices (Go 2001). Advanced computers are facing thermal engineering challenges from both high heat generation, due to rapid performance improvement and the reduction of an available heat removal surface, due to large packaging density. The use of thin micro fins arranged in an array helps to provide heat transfer enhancement in laminar flow, using flow-induced vibration. In this study, thermal resistances are measured to evaluate the thermal performance of the micro fin array heat sink compared to those of a plain-wall heat sink. For an air velocity of 4.4 m/s, the thermal resistance of the micro fin array heat sink is measured to be 4.45 K/W and that of the plain-wall heat sink is 4.69 K/W; indicating a 5.5% cooling enhancement. This shows that the use of thin fins enables the computer to cool down at a faster rate.

Next we have work involving finite element analysis of heat flow in a new class of tunable optical fiber devices. These devices use thin film resistive heaters micro-fabricated on the surface of the fiber (Salamon et al. 2001). The high rate of heat loss from these cylindrical microstructures can be exploited for tuning the optical properties of in-fiber gratings. Approximate one-dimensional analytical calculations capture important aspects of the thermal characteristics of these systems. Comparison with experimental results that were obtained from devices with established designs, validates certain features of the computations, such as the higher rate of heat transfer. This modelling also establishes the suitability of integrated thin-film heaters for several new types of tunable fiber grating devices.

We end this section by considering work by (Tan and Yang 1997). This study investigated the wave nature of heat propagation in a thin film, subjected to a temperature change on both sides by solving the hyperbolic heat conduction equation. It is shown that in transient heat conduction, a heat pulse is transported as a wave, which is attenuated in the thin film, and that heat conduction is extremely significant within a certain range of film thickness and time. When a film of less than a certain film resistance (t/k) is heated on both walls, temperature overshoot occurs within a very short period of time. This temperature overshoot can be used to explain the heat transfer enhancement achieved, when adopting thin films in heat exchange processes.

It can be seen that these studies from literature do support the fact that thin films promote better heat transfer, hence reinforcing its use in the PFCHE design. Following the adoption of thin films, we now go on to consider the advantages of using corrugations on the films.

*2.4.2 Corrugated films*

In addition to the use of thin films, corrugations on the films also promote better thermal performance of the heat exchanger. Without corrugations, the fluid flow into and through a smooth channel takes time to develop the parabolic profile, which is characteristic of laminar flow.

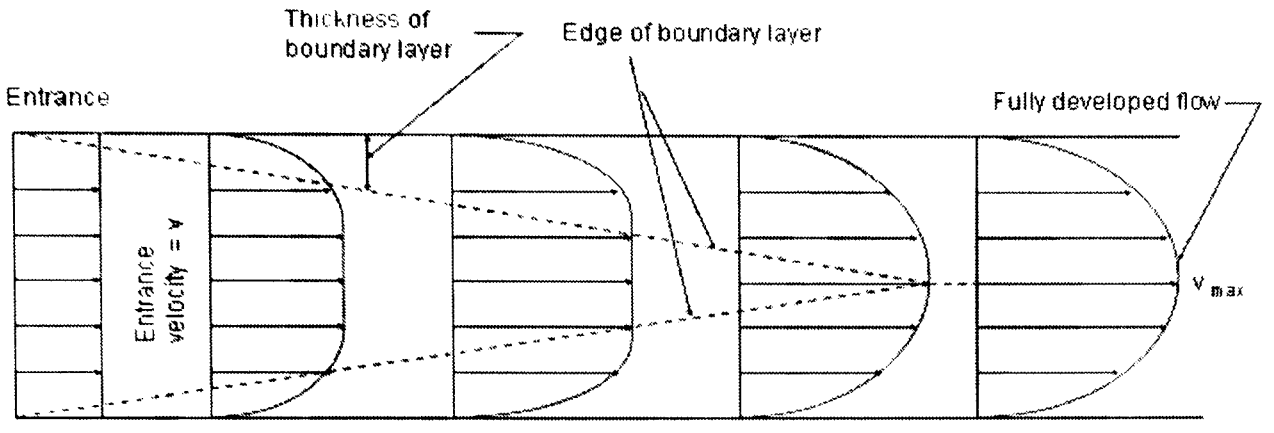


**Figure 2.2 Parabolic profile of laminar flow in a smooth channel**

The corrugated films improve the thermal performance as they break down the boundary layers of the fluid, also known as 'the massaging effect' and hence create more turbulence by breaking up the flow to obtain developing flow. Although the flow is laminar (low Re), it is not streamline but instead exhibits good internal mixing characteristics, which leads to better heat transfer due to the presence of corrugations on the film. The Nusselt number (Nu), which is directly proportional to the heat transfer coefficient, varies along the channel length as illustrated in the following graph, where L is the characteristic length of undeveloped flow.

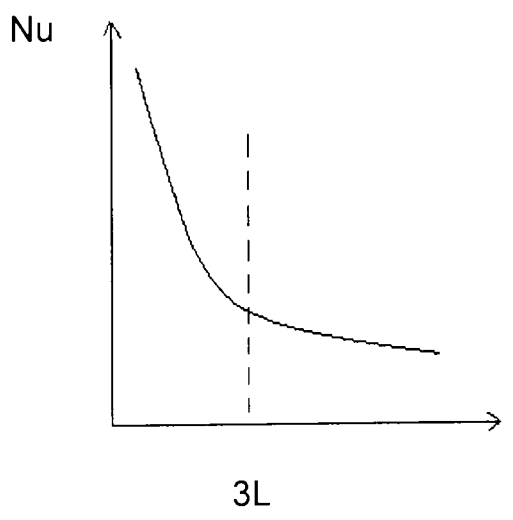


**Figure 2.3 Nusselt number variation with smooth channel length**

From the graph above, in the first few diameters of entry length, the heat transfer performance is higher than further along the channel, where the flow is fully developed. Thus, the corrugated channel design ensures that the flow is repeatedly mixed and then redeveloped to maximise the heat transfer performance. Besides enhancing the thermal performance, the corrugations also provide some rigidity to the films, as well as to the heat exchanger itself. In the following section,

we elaborate further on the developing flow that is achieved along the corrugations, by highlighting its advantages over fully developed flow.

#### 2.4.2.1 Developing flow along corrugated film

In simple terms, developing flow produced by the corrugations generates superior heat transfer than fully developed flow, due to a higher degree of mixing that is achieved. Normally, when a fluid flows into a continuous smooth duct, there is a developing region near the entrance of the duct, where a higher heat transfer coefficient is attained. The energy transfers in the entrance region can be compared to the developing flow in the PFCHE.

The transition to a fully developed condition occurs after the boundary layers forming on the walls meets in the centre of the duct, and the velocity and dimensionless temperature profiles become invariant in the flow direction. A fully developed flow will have a fully developed velocity and temperature profile. A fully developed velocity profile, transfers less heat from a duct wall because of the convective influence of the velocity profile on the temperature profile. A fully developed temperature profile transfers less heat from a duct wall because the gradient of the temperature at the wall is reduced due to the adiabatic centreline boundary condition. Therefore to maximise heat transfer, the developing flow is preferred as the thermal and velocity boundary layers are repeatedly broken down. Next we provide further evidence, on the heat transfer benefits when employing corrugations, by showing similar findings from literature.

#### 2.4.2.2 Corrugation studies from literature

Studies on flow behaviour through corrugations are outlined below, to support the use of the sinusoidal corrugations in the PFCHE, for heat transfer enhancement.

We begin with work conducted by (Sawyers et al. 1998) which states that the heat transfer achieved for a corrugated film is higher than that for flat plates due to the presence of recirculation zones. In this study, the effect of three-dimensional hydrodynamics on laminar heat transfer in corrugated channels is investigated, using a combination of analytical and numerical techniques. The Re range of ($0<Re<250$) is considered to avoid unsteady flows. The recirculation zones are situated at the crests and troughs of the corrugations and are known as the stagnation points of the fluid flow. There is increased advection near each stagnation point, which when combined with the fluid flow in the downstream direction, leads to a larger area-averaged heat transfer coefficient. In the three-dimensional case, the corrugations are sinusoidal in two orthogonal directions. A small mean flow in the transverse direction leads to an increase in the heat transfer by allowing particles to cross between the recirculation zones and the main flow. This study helps to explain why laminar flows in the sinusoidal corrugations of the PFCHE, experiences good heat transfer.

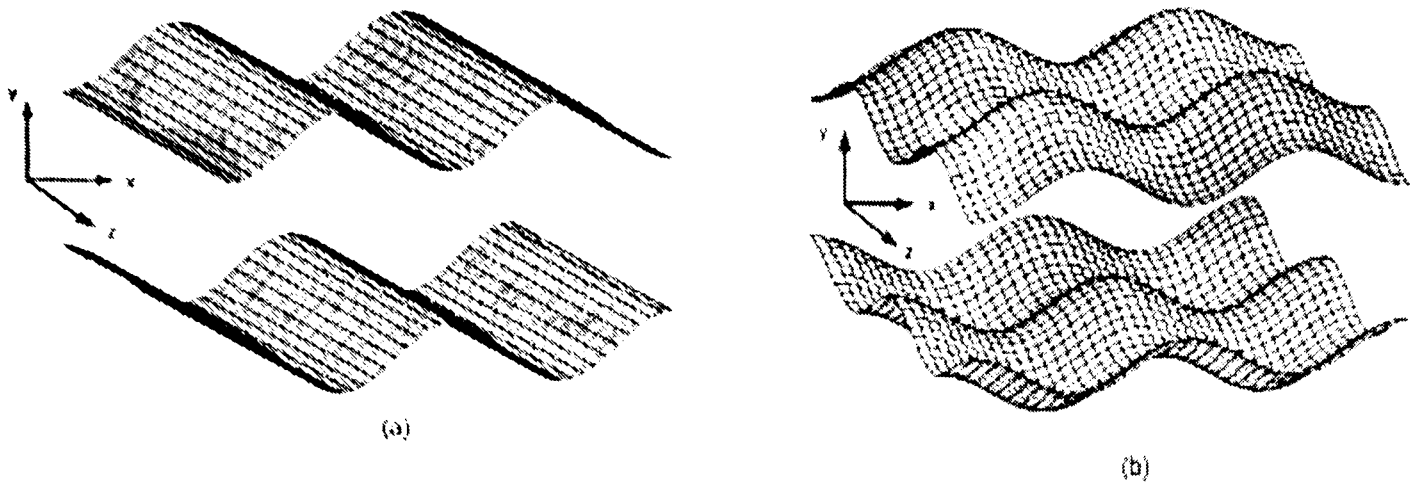

**Figure 2.4 Channels with (a) two-dimensional and (b) three-dimensional corrugations**

In addition to the recirculation zones, when fluid flows through corrugations, the destruction and restarting of the boundary layer causes an increase in heat transfer by producing a boundary layer that is thinner on average, than the uninterrupted boundary layer (Jacobi and Shah 1998). The mixing benefits that are associated with self-sustained unsteadiness are obtained in corrugated passages. For instance, the use of a finely undulated surface can achieve significant augmentations in heat transfer during condensation (Thonon and Mercier 1997). It has been shown that corrugations can promote turbulent equilibrium between the phases and thus contribute to the increase in heat transfer.

Nishimura et al. (1987) has investigated the instability of flow for a sinusoidal wavy channel with a narrow spacing. They describe a rearrangement of dye streaks in the form of off-set fins with a phase shift at each trough, and so conclude the existence of vortices. It can be inferred that the presence of these vortices leads to better heat transfer. At higher Re numbers turbulence appears and an unsteady spiral motion can be noticed instead of the off-set fin pattern.

Apart from flow patterns, heat transfer characteristics in a sinusoidally curved converging-diverging channel have been investigated through accurate numerical solutions (Wang and Vanka 1995). The wavy channel studied, corresponds to the geometry where for Re numbers less than 180, steady laminar flow is observed. Beyond this value, a transition to chaotic flow accompanied by significant increase in heat transfer is observed. This enhancement in the heat transfer results from self-sustaining oscillations, which leads to the destabilisation of the laminar thermal boundary layer.

An application employing sinusoidal corrugations involves a type of plate heat exchanger. The plate heat exchangers in free flow arrangements, consist of channels with curved concave and convex surfaces (sinusoidal wavy ducts in free flow arrangements), which are employed for the enhancement of heat and mass transfer (Gschwind et al. 1999). This geometry is used in food technology for the heat treatment of juices and mashes with fibers.

All of the above studies show that corrugations do significantly increase heat enhancement, due to better mixing of the fluids and the destruction of the boundary layers. This provides further support towards the use of sinusoidal corrugations in the PFCHE design. The next design aspect to consider is the use of narrow channels in the PFCHE design.

*2.4.3 Narrow channels*

Heat transfer performance of a given piece of equipment is normally specified in terms of a Nusselt number (Nu), which is then related to the fluid properties and the Reynolds number (Re). From the definition of Nusselt number (Nu) shown below,

$$Nu = \frac{hL}{k} = \frac{h\Delta T}{k\Delta T / L} \qquad (2.7)$$

we see that it can be regarded as an effectiveness factor. The equation expresses the ratio between the observed convection heat flux, with that generated by conduction over the chosen characteristic length (L).

$$Nu = \frac{heat\ flux\ via\ convection}{heat\ flux\ via\ conduction} = \frac{q_{conv}}{q_{cond}} = \frac{h\Delta T}{k\frac{\Delta T}{L}} = \frac{hL}{k} \qquad (2.8)$$

Hence, large Nu numbers do not necessarily imply good heat transfer performance, if they are associated with large characteristic dimensions. Conversely, narrow channels appear attractive provided they do not bring severe practical problems such as fouling, since:

$$\uparrow h \propto \frac{1}{L\downarrow}$$

Following this, a selected study from literature is next described to provide further backing towards the adoption of narrow channels in the PFCHE design, where its use is shown to reduce resistance to flow.

2.4.3.1 Narrow channel studies from literature

Pfahler et al. (1991) investigated the influence of viscosity on liquid and gas flow through microchannels, with depths ranging from a thousand Angstroms to tens of microns. The small channels were etched in silicon with depths ranging from 0.5 μm to 50 μm. The liquids used were isopropyl alcohol and silicone oil, and the gases were nitrogen and helium. Experimental results showed that the viscosity of fluids, adjacent to the wall surface is consistently smaller than the

bulk value, so the friction factor in microchannels would be smaller than that in macrochannels. This could be due to the difference in the transport properties between the 'wall adjacent layer' and the bulk region. The results indicate that the resistance to fluid motion, or the fluid's apparent viscosity is consistently smaller than that predicted by conventional, incompressible theory (Navier-Stokes equations) and that for liquids the apparent viscosity decreases with decreasing channel depth. After establishing the advantages of incorporating thin films, corrugations and narrow channels in the PFCHE design, we now move on to consider yet another design aspect, which is the adoption of laminar flows. In the following section, a quantitative assessment is used to show the benefits of laminar flow heat transfer, over that achieved in turbulent flows.

### *2.4.4 Laminar flow in PFCHE channels*

The relative merits of laminar flow, as opposed to turbulent flow in the channels are considered by comparing the performance of turbulent flow in large passages, with laminar flow in small passages (Cross and Ramshaw 1986). Three important parameters are used for the comparison. These are the pressure drop ($\Delta P$), the heat transfer capacity of a given matrix (Ua), and the heat flux achieved with the fluid power dissipation incurred ($U\Delta T/\tau v$). Consider the case of thermal resistances distributed equally on the hot and cold sides, and that the wall thermal resistance and fouling resistances are negligible. Here, the overall heat transfer coefficient (U) would be U=h/2. If the film coefficients of both fluids are equal, the heat transfer capacity of a given matrix volume is proportional to Ua, where U=h/2 and a, is the specific surface area.

It is evident from equation (2.9) below, that one way of achieving small units is to operate at high fluid velocities. Unfortunately, the corresponding pressure drop penalty will ultimately limit the extent to which this can be done. Therefore, a second performance criterion ($U\Delta T/\tau v$) is of interest. This compares the heat flux achieved with the fluid power dissipation, or in other words the pumping power incurred. Before we move on to show the relative merits of laminar flow in small channels, we first consider the performance characteristics of turbulent flow in large passages.

Turbulent Flow

Heat transfer with fully developed turbulent flow between smooth parallel plates is correlated by

$$Nu = 0.023\, Re^{0.8}\, Pr^{0.4} = hd_h/k \qquad (2.9)$$

where $Re = \rho v d_h/\mu$ and $Pr = cp\ \mu/k$.

From expression (2.9), the following relations can be concluded

$$h \propto Re^{0.8} \propto v^{0.8} d_h^{-0.2}$$

Thus, an increase in fluid velocity (v) would result in an increase in fluid film coefficient (h) as desired. This, however, would result in an increase in the pressure drop since

$$\Delta P \propto v^2$$

The characteristic dimension is taken as the equivalent hydraulic diameter ($d_h$), where $d_h=2\Delta$, with $\Delta$ being the plate spacing. The wall shear stress ($\tau$) for a smooth plate surface is given by the Blasius relation for $3000<Re<10^5$:

$$\tau/\rho v^2 = 0.04Re^{-0.25} \qquad (2.10)$$

In a given array of plates, the specific surface area (a) depends upon the plate spacing ($\Delta$) and thickness ($t_p$). Taking an arbitrary case where the plate thickness is half the spacing, ($t_p = 0.5\Delta$) we have

$$a = \frac{2}{3}\Delta \qquad (2.11)$$

Hence for turbulent flow,

$$U_T = \frac{h}{2} = \frac{Nuk}{4\Delta_T}$$

$$(Ua)_T = \left(\frac{Nuk}{4\Delta_T}\right)\left(\frac{2}{3}\Delta_T\right)$$

$$(Ua)_T = 6.7x10^{-3} k\left(\frac{\rho}{v}\right)^{0.8} \mathrm{Pr}^{0.4}\left(\frac{v_T^{0.8}}{\Delta_T^{1.2}}\right) \qquad (2.12)$$

and $$\left(\frac{U\Delta T}{\tau v}\right)_T = \left(\frac{Nuk}{4\Delta_T}\right)\left(\frac{\Delta_T}{\tau v}\right)$$

$$\left(\frac{U\Delta T}{\tau v}\right)_T = 0.288\frac{\mathrm{Re}^{1.05}\,\mathrm{Pr}^{0.4}\,k\Delta T}{\rho v_T{}^3 d_h} \qquad (2.13)$$

Next, we consider the performance characteristics for laminar flow in small channels.

Laminar Flow

For constant wall temperature,

$$Nu = 7.6 \qquad (2.14)$$

$$\tau = 6v\mu/\Delta_L \qquad (2.15)$$

The Nusselt number is independent of flow velocity (v). Therefore, v can be kept low to keep $\Delta P$ small and h can be increased, by reducing the channel diameter.

Also for laminar flow,

$$(Ua)_L = \left(\frac{h}{2}\right)\left(\frac{2}{3}\Delta_L\right)$$

$$(Ua)_L = \left(\frac{Nuk}{d_h}\right)\left(\frac{1}{3}\Delta_L\right)$$

$$(Ua)_L = \frac{1.27k}{\Delta_L{}^2} \quad \text{and} \qquad (2.16)$$

$$\left(\frac{U\Delta T}{\tau v}\right)_L = 0.32\,\frac{k\Delta T}{\mu}\,\frac{1}{v_L{}^2} \qquad (2.17)$$

Now comparing the performance corresponding to laminar flow in a fine matrix, with that for turbulent flow in a coarse matrix we have:

$$\frac{(Ua)_L}{(Ua)_T} = 1.9x10^{-2}\left(\frac{\mu}{\rho}\right)^{0.8}\frac{1}{\Pr^{0.4}}\left(\frac{\Delta_T^{1.2}}{\Delta_L^{2}\nu_T^{0.8}}\right) \qquad (2.18)$$

$$\frac{\left(\frac{U\Delta T}{(\tau\nu)_L}\right)}{\left(\frac{U\Delta T}{(\tau\nu)_T}\right)} = 1.1\frac{1}{\Pr^{0.4}}\left(\frac{\nu_T}{\nu_L}\right)^2 \qquad (2.19)$$

Comparing experimental data for water between laminar flow and turbulent flow, we have:

| Description | Laminar | Turbulent |
|---|---|---|
| Plate spacing, $\Delta_L$ or $\Delta_T$ | $3.0 \times 10^{-4}$ m | $3.0 \times 10^{-2}$ m |
| Velocity, $v_L$ or $v_T$ | 0.83 $ms^{-1}$ | 4.2 $ms^{-1}$ |
| Reynolds number (Re) | 833 | $2.1 \times 10^5$ |

**Table 2.2 Experimental data showing the comparison of laminar and turbulent flow**

Using this data and plugging it into equations (2.18) and (2.19), we obtain the following ratios, showing that the heat transfer capacity of a given matrix (Ua), and the heat flux achieved with the fluid power dissipation incurred ($U\Delta T/\tau u$), are higher for laminar flows by a factor of 72 and 13 respectively.

$$\left(\frac{(Ua)_L}{(Ua)_T}\right) = 72 \quad ; \quad \left(\frac{\left(\frac{(U\Delta T)}{\tau\nu}\right)_L}{\left(\frac{(U\Delta T)}{\tau\nu}\right)_T}\right) = 13$$

Clearly a laminar flow strategy has attractions for the design of heat exchangers, which are both compact and efficient, providing that the obvious practical reservations relating to fouling in fine matrices, can be overcome. Note that a minimum velocity of 1 $ms^{-1}$ is usually taken as a guide to avoid silting in turbulent flow. Following this, we may use equations (2.10) and (2.15) to establish the relative stresses, $\tau_L/\tau_T$. As before, we take the example of water flow in a plate matrix with turbulent flow and laminar flow.

It is found that:

$$\left(\frac{\tau_L}{\tau_T}\right) = 9$$

Therefore, laminar flow units should also be resistant to silting under these conditions. This comparison between the performance of laminar and turbulent flows, clearly shows that laminar flows have good potential to be incorporated in heat exchange units, especially in applications where pressure drops are a primary concern.

We now move on to consider some studies from literature, to support the positive results for laminar flow in this quantitative assessment.

#### 2.4.4.1 Laminar flow studies from literature

An example of an application in laminar flow, is in the aerodynamic and thermal design of a new compact laminar flow heat exchanger with stainless-steel micro-tubes for helium refrigerators by Saji et al. (2001). Laminar flow conditions are adopted for the flows of inner and outer tubes to keep a high heat transfer rate and a low-pressure loss. In addition, the adoption of laminar flow decreases the potential for vibration and hence lengthens the life of the facility.

Laminar flow is also adopted in microcell aluminium honeycombs for augmenting heat transfer in compact heat exchangers (Lu 1998). For convective cooling, the overall heat transfer rate increases by about two orders of magnitude, when an open channel is designed with an aluminium honeycomb core. The performance is comparable to that achieved by using open-celled aluminium foams, but attributed to different mechanisms. At low Re numbers (Re<2000), the flow is essentially laminar in the honeycombs, in contrast to the largely turbulent flow in metal foams. This deficiency in fluid dynamics is compensated by the superior surface area density offered by honeycombs over foams. Another advantage of designing heat sinks with honeycombs is the relatively small pressure drop experienced and minimal noise generated by the laminar flow. The results are of relevance for thermal management applications in high power electronics, where compact and highly efficient heat dissipation media are required.

Custom and precision manufacturing methods, now allow novel micro-tube strip type (MTS) exchangers, to operate in the laminar flow regime. This has enabled the recent production of high effectiveness, gas-to-gas cryogenic exchangers, with a factor of four decrease in mass relative to comparable high-performance exchangers (Boman and Doty 2001). The exchangers operate under laminar conditions even at high levels of power and flow, by using hundreds (or thousands) of parallel micro-tubes.

The laminar flow has also applications in the medical world, involving a new hollow fiber membrane oxygenator, in which the gas flows through the fibers and blood flows around the fibers (Karlson et al. 1987). The fibers are microporous polypropylene with a pore size of 0.03 microns. Membrane surface area is 2.0 $m^2$ and the priming volume is 480 ml, including the heat exchangers for oxygen and carbon dioxide transfer. Oxygen transfer is as high as 230 ml/min.

This low prime device transfers large volumes of gas, an efficiency that results from a crossed arrangement of the fibers to break up the laminar flow of the blood around them. This study shows that laminar flow does not only increase heat transfer, but also enhances mass transfer.

A stacked plate chemical reactor employing laminar flow has been developed by Georg et al. (2001). When openings in adjacent plates are properly aligned, a fluid pathway is defined between inlet ports for each chemical reactant and an outlet port for a chemical product. Precise dimensional control of the reactant fluid pathway height, enables stacked laminar flow paths for the reactants to be achieved, allowing efficient and rapid diffusion mixing to occur. The preferred material for the fabrication of the reactor plates is stainless steel, although other materials such as glass or plastic can alternatively be used, provided they are compatible with the selected reactants and the desired product. This study can be used to support the good laminar flow mixing achieved in the PFCHE, which leads to higher heat transfer. Having considered the explanations for the adoption of the main design aspects in the PFCHE, we now move on to investigate the fouling characteristics in the PFCHE.

### *2.4.5 Fouling in PFCHE*

Whilst the heat transfer and pressure drop studies were being performed, in parallel a detail fouling study on the PFCHE was also carried out by El-Bourawi and Ramshaw (1998). The aim of the study was to investigate the particulate fouling rate of the PFCHE and also to develop cleaning methods for the unit. Fouling tests were performed with a particle system comprising several grades of alumina in the range of 0.015 to 88μm. The PFCHE test section was instrumented so that any foulant deposition, taking place within it, could be monitored with the aid of differential pressure sensors installed at the entrance and exit. The sensor outputs were linked to a data logger, which was used to measure and record the pressure readings. The results of such measurements indicated the variation of the fouling deposit with time.

The study involved three foulant removal techniques, which were the flow pulsation technique, intermittent flow stoppage and air bubbling technique. The injection of air bubbles, which rapidly cleared the surface deposits of the particles, was found to be the most effective fouling mitigation technique. This technique was found to be the most effective of those tested, as whenever a stream of air was introduced to the system, a significant pressure drop reduction was achieved. An air flow rate of 0.9 m/s was found to be capable of restoring the pressure drop of the system to the initial value. Lower air flow rates were only able to partially clean the test section. The smoothness and undulating surface geometry of the PEEK sheets, is believed to play an important role in enhancing the particle removal rate and hence improving the fouling characteristics of the PFCHE. It is also of interest to note that fine particles tended to foul the matrix more effectively than the larger particles tested, provided that the latter did not plug the channel entrances.

In the following section, we consider the potential applications for the polymer film compact heat exchanger (PFCHE) in the process industries.

## 2.5 Potential applications for Polymer Film Compact Heat Exchangers

In this section, we show some of the possible applications for the existing PFCHE design based on current available heat exchanger units adopting polymer films.

### *2.5.1 Thin plastic film heat exchangers for absorption chillers*

Gas fired absorption heat pump apparatus; particularly absorption chillers, require the use of large area heat exchanger elements in the absorber and evaporator sections of the heat pump systems. This is important in order to have high coefficients of performance, and also to be efficient and competitive against the more conventional cooling apparatus in current use. However, with increased size, increased weight and cost follows. Accordingly, alternatives to metal construction heat exchanger elements are being sought.

One alternative is the use of plastic films. The heat exchanger is formed by two layers of thin plastic film material, in which flow passages are formed, by placement of seams or welds between the two layers (Lowenstein 1999). The two layers are bonded or sealed together by thermal or ultrasonic welds, to produce a serpentine passage through the heat exchanger. Such heat exchangers would be situated in a working environment; at less than atmospheric pressure in a vacuum vessel, and during operation these units are exposed to a continuous partial vacuum.

### *2.5.2 Plastic film plate heat exchangers for heat recovery*

This invention relates to low cost heat exchangers of the parallel plate type useful for recovery or dissipation of heat energy in buildings. They can also be used for heat recovery in the chemical process, electrical power and other industries. Conventional metallic units have several disadvantages. There are relatively expensive, have complex designs and also high costs are involved for welding, assembly and other aspects of fabrication. Hence, to reduce costs for heat exchangers for domestic and office building use, plastic materials are preferred as an alternative. The plastic film plate type heat exchangers of this invention are designed for operation at low absolute pressures, for example, 1370 kPa up to 2060 kPa maximum (Schnon 1988). They are also used for relatively small differential pressures between the fluids being interchanged.

### *2.5.3 Film heat exchanger as a thermo-compressor evaporator*

This invention is particularly suitable for use in a film evaporator or distillation apparatus, operating in the thermo-compressor principle (Kordelin 1997). Basically, it is an apparatus where

the heat exchanger unit is formed of flat bag-like elements of thin plastic sheets placed against each other. Heat transfer takes place from the vapour condensing inside the elements through the sheet, to the evaporating liquid falling on the outer surfaces of the elements. The vapour, which is introduced into the elements and which releases heat upon condensing, is generated outside the elements. A compressor raises the pressure and the temperature of the vapour, before it is introduced into the elements.

The lower part of the bag ends to a condensate receiver, which is provided with a drainpipe for the condensate. The upper part of the bag has means for introducing the vapour into the bag, and distributing the liquid to be evaporated, onto the outer surface of the bag. It is characteristic that inside the bag, a perforated corrugated plate is fitted in a vertical direction, with its width chosen so that the bag tightens suitably around the corrugated plate. The length (P) of the corrugated plate corresponds to a major portion of the length of the bag. A perforated corrugated plate is also fitted in a horizontal direction against the outer surface of the bag, with its length (P') corresponding to the width of the bag. Here, the use of thin plastic sheets is coupled with the use of metal plates but perhaps, with the PFCHE design, thicker polymer plates can be used to develop an all-plastic heat exchanger.

*2.5.4 Cross-corrugated polymer film exchanger as an evaporator*

A gas and liquid contact apparatus in which gas and liquid flow in cross-flow relationship to one another is disclosed (Thomas 1992). More particularly, this application relates to a self-cleaning gas and liquid contact body that includes an apparatus for concentrating bleed off water. The apparatus is made up of a plurality of plastic corrugated sheets. The corrugations extend at an angle to the edges, and lie alongside each other at points in adjacent sheets. This arrangement forms the flow channels for the gas and liquid. The edges of the sheets, define gas inlet and outlet ports in the contact body. The gas inlet edge has a plurality of rows of channel-shaped notches that will allow the liquid flowing through the contact body, to agglomerate at the notches. The agglomerated liquid will flow downwards along the gas inlet edge of the contact body, to clean the sheet at that gas inlet edge. A collection trough is located along one of the rows, and includes a flange extending into one row of notches, to intercept contaminated water and remove it from the system.

*2.5.5 Thin film polymer heat exchanger as a heater*

The polymer heater specified, is a portable heat generating device in which fuel vapour and an oxygen supply (e.g. air) are directed through channels contained within a thin, flexible and compliant polymer sheet (Welles 2000). Elongated catalytic heat elements, placed strategically within the channels, spontaneously interact with the fuel-air stream liberating heat energy. Means and methods are defined that permit flameless catalytic combustion to be uniformly extended over

the length of each heat element, lowering power density but maintaining the overall power generated. This permits the use of many types of low temperature materials like plastics and polymers in the construction of the heater. For example polymers such as polyimide or PEEK, can be utilised if modified. This can be achieved by lamination, deposition of metal film structures or external attachment of thermal conducting strips on the polymer, which will act to effectively increase the thermal conductivity of the polymer.

The heat generation process starts, by pumping an air stream into a reservoir, which contains a fuel source (e.g. methanol). This action saturates the air stream with fuel vapour. The fuel vapour is mixed with another stream of air to achieve a particular fuel/air ratio and directed into channels within the polymer sheet. Here, it reacts with the catalytic heat elements to produce flameless combustion. The warm exhaust gas is directed to a thermally controlled diverter valve. The valve senses the temperature of the liquid fuel supply and diverts some or all of the warm exhaust gas, as necessary, to heat the fuel and keep its temperature within a specified range. Exhaust by-products are passed into a miniature scrubber module adjacent to the fuel module. The scrubber absorbs any noxious components in the exhaust stream that may occur during start-up or rapid changes in the operating conditions.

### *2.5.6 Polymer heat exchangers in the refrigeration and ventilation industry*

PFCHEs can also be used as condensers employing compact noncircular passages as used with metallic plate heat exchangers in many industrial applications. Their potential benefits include high heat fluxes, small volumes and total lower cost. The suggested application is in the cooling of secondary liquid refrigerants such as chilled-water for process cooling duties. Besides this, they can also be used for heat recovery in the form of warm glycol for defrosting coolers or under-floor heating of cold stores. Next, we briefly consider two applications in the refrigeration and ventilation industry that employ plastic units but not necessarily polymer films.

A small diameter dilution refrigerator especially designed to be used in high magnetic fields has been constructed (Wagner and Frossati 1990). It is completely made of plastic, including the heat exchanger, in order to eliminate eddy current heating. Temperatures of 10 mK have been reached in field tests.

In recent years, passive infiltration of air into greenhouses has been reduced drastically. However, very low air exchange rates can lead to abnormally high levels of humidity that can damage harvests. Hence, farmers have to ventilate. A plastic heat exchanger was designed to be used as a dehumidifier in an effort aimed at reducing heating costs related to ventilation (Rousse et al. 2000). An air-to-air multi-pipe counterflow heat exchanger unit, was installed in a greenhouse used for the experimental cultivation of tomatoes and cucumbers. The first series of tests carried out in a 576 $m^3$ enclosure, demonstrated that average efficiencies of 84% and 78% were obtainable. Latent heat was found to play a major role in the overall heat transfer, contributing

about 40% of the total energy exchanged in some situations. The unit made of plastic, is durable, rust resistant and efficient in the presence of frost and ice. A commercial implementation is now being considered.

### *2.5.7 Polymer heat exchangers in the food industry*

Another possible application for PFCHEs, is for them to act as biocidal heat exchangers (Reay 1999). An organisation called *Interface Inc.* has a patent on a biocidal protective layer for heat exchanger coils, formed by applying a polymeric composition containing an organic water-resistant polymer that has associated with it a biocidal compound, which inhibits corrosion, fouling and biological build-up. This seems like an interesting extension of a polymer, and if it could be added to the surface of a PFCHE, it may open up new market opportunities.

### *2.5.8 Polymer heat exchangers as solar collectors*

This application for the PFCHE, discusses plastic solar collectors for low temperature applications that dominate the market. Benefiting from the rapid progress of polymer technology, manufacturers have been able to solve many of the problems for plastics, when exposed to sunlight, heat, chemicals, and pressure that made them of questionable value in solar heating. Plastics are easy to manufacture, lend themselves to volume production, are lightweight, low in cost and readily available. They are ideal for such low temperature applications such as swimming pool heating where oxidation, corrosion and erosion can be avoided under adverse conditions.

A plastic solar collector that has been developed as an alternative to metal units is the advanced corrugated duct solar collector. The collector (air heater) is constructed of corrugated surfaces similar to those used for compact heat exchangers, with the air flowing normal to the corrugations (Metwally et al. 1997). When the collector was compared to five other conventional designs, it was revealed that the efficiency of the corrugated duct collector increases by a ratio of 15 to 43% over that of the next best conventional design (flow below flat absorber). This new design is economically encouraging as the cost is almost the same, whereas the efficiency is enhanced by about 75% compared to the collector of flow below flat absorber.

Another case in point is the polymer solar energy absorber module. A solar energy absorber module having a molded top sheet of translucent plastic material and a molded bottom sheet of solar absorbing plastic material, bonded together by circular bond indentations in the body has been developed by Smith (1998). The top and bottom sheets are spaced from each other at a distance equal to the diameter of the circular bond. This assembly forms a plurality of convex lens-like elliptical sites for augmentation of solar energy and a plurality of longitudinal tortuous sinusoidal channels that connect to a header at each end of the module. The working fluid flows

through the header and channels. This invention is directed towards providing a simple, inexpensive, durable solar energy absorber adapted to serve low, intermediate and high temperatures. The flexibility in design enables it to provide for low, intermediate and high temperature requirements having the advantage of increased solar collection by means of lens augmentation for the absorber and a wide range of solar acceptance angles.

Besides the absorber designs mentioned above, the low thermal conductivity of polymers has also imposed the need of yet another absorber design. It is composed of a pair of dark, closely spaced parallel plates at the top, of which solar radiation is absorbed, forming a thin channel for the flow of the heat transfer fluid (Tsilingiris 2000). The incorporation of thin channels in this polymer plate absorber design overcomes the polymer's thermal conductivity deficiency. From these designs shown, it can be inferred that there is potential for the use of PFCHEs as solar collectors, as many of its design aspects are employed in current polymer units.

*2.5.9 Thin polymer film heat exchangers in the desalination industry*

A plastic unit performing heat exchange by evaporation and condensation has been adopted in the desalination industry (Perry et al. 1983). It can be used for large-scale operations, such as those used in converting saline or brackish water to pure water. Nevertheless, it is also capable of being used on any application requiring a heat exchanger with operating conditions; within the pressure and temperature capability of the materials of construction.

The apparatus is made up of a plurality of thin film plastic sheets, which are bonded to one another, to form a heat exchange structure. Alternate pairs of sheets are bonded together longitudinally, extending along bond lines. These bond lines are positioned at transverse locations along the width dimensions of the sheets. A second set of alternate pairs of sheets are bonded in the same way, but these bonds are positioned between the first set of longitudinal bond lines mentioned earlier. The first and second alternate pairs of sheets are adjacent to each other. The design mentioned here has similarities with the PFCHE, whereby the flow channels are constructed by stacking alternate pairs of polymer sheets. Hence, it may be inferred that the PFCHE design is feasible for further investigation towards this application.

*2.5.10 Plastic fin heat exchangers in the computer industry*

Currently there is a huge demand for cost-effective thermal control systems for processors in desk-top and lap-top computers, where heat dissipation needs are increasing. The PFCHE design is probably not suitable for this application, however the use of a comformable polymer two-phase sealed heat transfer system might. It is an area worth looking into to extend the PFCHE technology. Lessons can be taken from current available computer thermal control designs, incorporating plastic materials.

In a portable notebook computer, a specially designed heat pipe-based heat exchanger assembly has been used to efficiently dissipate heat from a processor board in the computer's base housing to ambient air surrounding the computer (Moore 2000). The heat exchanger assembly is made up of a graphite fiber-filled outer heat exchanger body which consists of a finned first portion disposed within the base housing, and a second portion disposed within the base housing and thermocoupled to the processor board. The graphite outer heat exchanger body is directly overmolded onto a thermosyphoning heat pipe. The heat pipe has first and second longitudinal portions respectively, which are encapsulated within the first and second outer heat exchanger portions mentioned earlier.

During computer operations, processor heat is conducted to the second heat pipe portions and is transmitted via the balance of the heat pipe, to the finned outer heat exchanger portion for dissipation to ambient air. The exposed fin edges of the first outer heat exchanger, may have a layer of plastic material, suitably placed to serve as a type touch guard structure, for the exposed portion of the heat exchanger.

### *2.5.11 Plastic recuperators in the cryogenic industry*

An investigation on the viability of polymers at cryogenic temperatures shows that certain polymers do exhibit high brittle impact failure at low temperatures. For instance, expanded polystyrene can be used with liquid nitrogen. PEEK, on the other hand, becomes brittle at temperatures below $-10^{o}C$ (Reay 2000). However, such a failure mechanism is unlikely to be encountered by a cryogenic heat exchanger in normal service. Using this as an incentive, we briefly consider two applications of plastics in the cryogenic industry.

A low thermal conductivity support has been described. It is rigid in all three directions and constructed from a taut band of Kapton, a strong plastic film (Gush 1991). The support is compact and readily fabricated.

The experimental performance of the first superfluid Stirling refrigerator (SSR), to use a plastic recuperator is reported by (Patel and Brisson 1998). This unit is a single stage machine, has a total internal volume of 83 $cm^3$, and uses a 3 $cm^3$ Kapton heat exchanger. The refrigerator operates from a high temperature of 1.0 K and using a 1.5% 3He-4He mixture, it achieves a low temperature of 344 mK and delivers net cooling powers of 1.86 mW at 750 mK, 358 μW at 500 mK and 97 μW at 400 mK.

*2.5.12 Panel polymer heat exchangers in the automotive industry*

A panel polymer heat exchanger is invented by Shuster and Cesaroni (1990).The heat exchangers are relatively economical to manufacture and may be used in a variety of end uses, depending on the properties of the polymer composition, including in some instances as heat exchangers in automobiles. This invention relates to heat exchangers, particularly liquid to gas heat exchangers for use in vehicles. The unit is essentially a planar panel having a pair of relatively thin outer walls formed from a composition of a thermoplastic polymer, especially a polyamide. The walls, which have a thickness of less than 0.7 mm, are bonded together to form a labryinth of fluid passages between the walls. The passages extend between the inlet and outlet entrances and occupy a substantial proportion of the area of the panel.

Another variation of the panel polymer heat exchanger is formed from two sheets of thermoplastic polymer, again preferably polyamide (Fletcher 1991). The units may be used in a variety of end-uses, including automotive oil coolers, automotive comfort heaters, refrigerators and industrial uses. Each sheet has a thickness of 0.07 to 0.7 mm, and a plurality of grooves extending at least partially across the width of the sheet. The sheets are superimposed in a face-to-face relationship and bonded together in a fluid tight bond. The headers are situated at opposite ends of the panel, where the grooves form a plurality of fluid flow channels between the inlet and outlet headers.

Next we disclose the latest form of the plastic heat exchanger, for applications in the automotive industry. The multi-panelled heat exchanger is in the form of a radiator for an automobile (Cesaroni 1996). These heat exchangers maybe used in automotive end uses, for example as part of the water and oil cooling systems. In addition, the heat exchangers may also be used in less demanding end uses for example in refrigeration and in comfort heat exchangers. Nevertheless, these units are intended for use in situations where there is a large flow of air and to reduce the generation of noise in such situations.

The preferred material of construction is aliphatic polyamide, particularly nylon 66 and nylon 6. Examples of other thermoplastic polymers that may be used are PE, PP, polyesters, polyetherester, PVC and polyurethane. The exchanger has a plurality of parallel tubes in a spaced apart, side-by-side relationship. The tubes are located between two plastic sheets that envelope and conform to the shape of the tubes, so as to maintain the tubes in the side-by-side relationship. The sheets are bonded together between the parallel tubes. The flow in each end of the tubes is connected to an inlet and outlet manifold. Each panel is wave-like in shape with peaks and troughs extending across the width of the panel. Multi-panelled heat exchangers are formed from individual panel heat exchangers by stacking. These heat exchangers may be manufactured in a versatile and relatively simple manner. Simple moulds and fabrication techniques may be used, including continuous processes using rolls.

*2.5.13 Polymer heat exchanger as a chemical reactor*

Instead of just being involved in heat transfer, the PFCHE can also be adopted as a chemical reactor as an attempt to diversify its functions. This idea is supported by the development of the polymer unit below.

A stacked plate chemical reactor in which simple plates, each incorporating no surface features other that an opening has been developed by Georg et al. (2001).These plates are stacked together and when openings in adjacent plates are properly aligned, a fluid pathway is defined between inlet ports for each chemical reactant and an outlet port for a chemical product. A preferred material for the fabrication of the plates is stainless steel, although other materials such as plastic and glass can alternatively be used, as long as they are compatible with the selected reactants and the desired product. Because the simple plates incorporate no features other than openings, fabrication of such plates are easily achieved. Different reactor designs having additional reactant pathways, more or fewer heat transfer fluid pathways, heat exchangers, mixing chambers, reaction chambers and sensor pathways can readily be achieved by adding or removing plates from the stack. This can also be achieved by changing the pattern and number of openings in the simple plates that are used. The plates can be held in the stack during use, by using pressure exerted on opposite outer plates of the stack, or can be permanently joined.

In one embodiment of the invention, sixteen simple plates are stacked to provide a reactor incorporating three heat transfer fluid pathways, two reactant fluid pathways, one product fluid pathway, multiple mixing chambers, multiple reaction chambers, two reactant pre-treatment heat exchangers, two reaction chamber heat exchangers, and multiple temperature sensor pathways. Precise dimensional control of the reactant fluid pathway height, enables stacked laminar flow paths for the reactants to be achieved, allowing efficient and rapid diffusion mixing to occur.

## 2.6 Summary

In this chapter, we listed out the types of polymers that can be used, as an alternative material of construction to metals in heat exchangers. The relative merits of using polymers over metals were shown through a quantitative comparison, between PVDF and Hastelloy heat exchangers. When incorporating the same tube dimensions, thickness and fluid film coefficients, significant cost savings can be achieved using the PVDF exchanger. The descriptions of the three main categories of polymer compact heat exchangers currently available in industry were then provided to some detail.

Following this, the polymer film compact heat exchanger (PFCHE) design was introduced to address the disadvantages of both metallic and present polymer heat exchangers. Notable design aspects of the unit are the use of thin (100μm) polymer films to address the thermal conductivity

deficiency and the adoption of laminar flows to deal with high-pressure drops. In addition, the presence of corrugations on the films promotes better fluid mixing, which increases the thermal performance of the unit. Due to its excellent thermal, chemical and mechanical stability, PEEK (poly ether ether ketone) is adopted in the PFCHE design. The benefits of the PFCHE design aspects (thin films, corrugations, narrow channels and developing laminar flow) were then highlighted and relevant studies from literature were included to support its use. The chapter concludes with a listing of the potential applications for the PFCHE in the process industries, based on the incentive provided by available polymer exchanger designs, particularly those incorporating thin polymer films.

The purpose of this chapter is to offer further explanation on the motivation for the research and to provide a better appreciation of the technology, prior to discussing the PFCHE experimental work and analysis of the results obtained, which forms the main bulk of this thesis. The objectives of conducting the experimental work are as follows:

- To develop design correlations (Jh and f ) for different PFCHE configurations using different fluid systems under industrial conditions
- To present industrial case studies for evaluating the potential of the PFCHE technology over conventional metallic units
- To develop unique design correlations involving Pr number, that will enable the evaluation of the PFCHE performance for a wide range of fluids
- To investigate different aspects of the PFCHE (corrugation angle, surface geometry, material of construction) and its effect on exchanger performance

In the following chapter, we set out to show the reliability of the PFCHE experimental data; depicted through performance data plots in later chapters. We do this by conducting a general uncertainty analysis on the raw data for all the PFCHE experiments, discussed in this thesis.

# CHAPTER 3 - GENERAL UNCERTAINTY ANALYSIS FOR PFCHE EXPERIMENTS

## 3.0 Introduction

Chapter One disclosed a background on process intensification, the area on which this research topic stems from and briefly showed the initial incentive for employing PFCHEs over conventional metal heat exchangers; with the former having superior performance. Chapter Two introduced the PFCHE design and highlighted the merits of its design aspects.

In this chapter, we use the concept of uncertainty to describe the reliability of the experimental measurements for all the PFCHE experiments, mentioned in this thesis. This is done to support the validity of the data plots that will be shown in later chapters. Uncertainty is an estimate of experimental error and the uncertainty analysis is the analysis of the uncertainties in experimental measurements and results (Coleman 1999).

When using property data or other experimentally determined information in an analytical solution, we should consider how "good" the experimental information is. If the answer or solution must be known within, say, 10% as in the case for the PFCHE experiments, it would make no sense to spend time and money to perform the experiments only to find that the probable amount of error in the results was considerably more than 10%. Uncertainty analysis when used in the initial planning phase of an experiment, can identify such situations and save the experimentalist, much time, money and embarrassment.

In the PFCHE experiments, we have three main data reduction equations (Jh, f and Re), where we need to determine how the results depend on one another. All three equations involve a combination of variables that must be measured or found from tabulated data (as in the case of fluid properties). Experimental measurements are taken for the fluid flow rates, temperatures and pressure drops and the uncertainties allocated for the equipment involved are shown in Tables 3.2a to 3.2i. Once the experimental measurements are recorded, we validate them by incorporating these measurements in data reduction equations to generate heat transfer and friction factor results. The PFCHE experiments are designed and executed to determine the relationship between the non-dimensional groups (Jh, f and Re) and to produce design correlations relating Jh and f with Re by using regression analysis.

To simplify the calculations, the uncertainty analysis presented in this chapter is based only on measured data from experimental equipment and does not include the uncertainty when determining physical property values. The physical properties used in calculating the dimensionless numbers (Jh, f and Re) have been estimated as a function of temperature only.

As shown in Tables 3.2a to 3.2i, the sensitivity of the temperature measurements ranged from ±0.2°C to ±0.05°C; suggesting acceptable errors in the estimation of physical properties used in the calculations. Therefore, it can be assumed that the uncertainty for the physical property data will not have a strong influence on the final experimental results involving the Jh and f factors. In other words, the physical property data used in the PFCHE experiments can be deemed to have sufficient levels of accuracy.

## 3.1 Propagation of uncertainties

Experiments used to characterise the performance of the PFCHE involved the measurements of three variables (temperatures, pressure drops and flow rates) that have equipment uncertainties associated with them. These individual equipment uncertainties propagate through various data reduction equations, the main ones being (Jh, f and Re), to give an experimental result. The uncertainty analysis is performed to evaluate the propagation of these uncertainties, in order to ensure that the final experimental results (Jh and f factors), are within the desired uncertainty level. In the following section, we begin the uncertainty analysis by first considering the different PFCHE experiments investigated in this thesis, followed by a list of the equipment uncertainties involved.

### *3.1.1 Equipment uncertainty*

Before we consider the equipment uncertainties, we first list out all the PFCHE experiments investigated in this thesis and the relevant chapter numbers, in which they have been discussed.

| Configuration | Polymer material and corrugation angle | System | Chapter |
|---|---|---|---|
| Square | PEEK 90° | air/air | 4,6,7 and 8 |
| | PEEK 90° | water/water | 4,6 and 8 |
| | PEEK 90° | 30% glycerol + water/water | 4 and 8 |
| | PEEK 90° | 40% glycerol + water/water | 4 and 8 |
| | PEEK 90° | 50% glycerol + water/water | 4 and 8 |
| | PEEK 90° | 70% glycerol + water/water | 4 and 8 |
| | PEEK 60° | air/air | 7 |
| | PEEK 30° | air/air | 7 |
| | PVDF 90° | air/air | 9 |
| Spiral | PEEK 20° | air/water | 5 and 6 |

**Table 3.1 List of PFCHE experiments**

A list of the equipment involved in the PFCHE experiments, along with the associated uncertainties for the flow rate, temperature and pressure drop measurements are shown in Tables 3.2a to 3.2i below. Table 3.2a to Table 3.2h, relate the uncertainties for the square PFCHE experimental equipment, whilst Table 3.2i shows the uncertainty for the spiral PFCHE. The equipment uncertainties listed in the tables have been obtained from the manufacturers' manual.

3.1.1.1 Square PFCHE experiments

(a) Air/air system (PEEK 90°)

| Measurement | Device | Uncertainty |
|---|---|---|
| Temperature | Platinum resistance thermocouple (PRT) connected to digital recorder | ±0.05°C |
| Flow rate | Nixon rotameter | ±0.5 $m^3$/hr (3-15 $m^3$/hr) |
| Pressure drop | Digital pressure meter (2000 Series manometer) | ±0.1 kPa |

**Table 3.2a Equipment uncertainty for the air/air system**

(b) Water/water system (PEEK 90°) (Jachuck and Ramshaw 1992)

| Measurement | Device | Uncertainty |
|---|---|---|
| Temperature | K-thermocouple connected to digital recorder | ±0.1°C |
| Flow rate | 35S rotameters | ±0.01 $m^3$/hr |
| Pressure drop | Digital manometer | ±0.01 kPa |

**Table 3.2b Equipment uncertainty for the water/water system**

(c) 30% glycerol + water/water system (PEEK 90°) (Melendo 1996)

| Measurement | Device | Uncertainty |
|---|---|---|
| Temperature | K-thermocouple connected to digital recorder | ±0.1°C |
| Flow rate | 24S rotameters | ±0.01 $m^3$/hr |
| Pressure drop | Digital manometer | ±0.01 kPa |

**Table 3.2c Equipment uncertainty for the 30% glycerol + water/water system**

(d) 40% glycerol + water/water system (PEEK 90°) (Melendo 1996)

| Measurement | Device | Uncertainty |
|---|---|---|
| Temperature | K-thermocouple connected to digital recorder | ±0.1°C |
| Flow rate | 24S rotameters | ±0.01 $m^3$/hr |
| Pressure drop | Digital manometer | ±0.01 kPa |

**Table 3.2d Equipment uncertainty for the 40% glycerol + water/water system**

(e) 50% glycerol + water/water system (PEEK 90°) (Melendo 1996)

| Measurement | Device | Uncertainty |
|---|---|---|
| Temperature | K-thermocouple connected to digital recorder | ±0.1°C |
| Flow rate | 24S rotameters | ±0.01 $m^3$/hr |
| Pressure drop | Digital manometer | ±0.01 kPa |

**Table 3.2e Equipment uncertainty for the 50% glycerol + water/water system**

(f) 70% glycerol + water/water system (PEEK 90°) (Melendo 1996)

| Measurement | Device | Uncertainty |
|---|---|---|
| Temperature | K-thermocouple connected to digital recorder | ±0.1°C |
| Flow rate | 24S rotameters | ±0.01 $m^3$/hr |
| Pressure drop | Digital manometer | ±0.01 kPa |

**Table 3.2f Equipment uncertainty for the 70% glycerol+ water/water system**

(g) Air/air system (PEEK 30° and PEEK 60°) (Menes 1997)

| Measurement | Device | Uncertainty |
|---|---|---|
| Temperature | K-thermocouple connected to digital recorder | ±0.1°C |
| Flow rate | Fisher Control 18X rotameter<br>Nixon rotameter | ±0.2 $m^3$/hr (<5 $m^3$/hr)<br>±0.5 $m^3$/hr (>5 $m^3$/hr) |
| Pressure drop | Tubular manometer<br>Digital pressure gauge | ±0.02 kPa (<7 kPa)<br>±0.1 kPa (>7 kPa) |

**Table 3.2g Equipment uncertainty for the 30° and 60° angles in an air/air system**

(h) Air/air system (PVDF 90°) (Walker 1997)

| Measurement | Device | Uncertainty |
|---|---|---|
| Temperature | K-thermocouple connected to digital recorder | ±0.1°C |
| Flow rate | Fisher Control 18X rotameter<br>Nixon rotameter | ±0.2 $m^3$/hr (<5 $m^3$/hr)<br>±0.5 $m^3$/hr (>5 $m^3$/hr) |
| Pressure drop | Digital pressure gauge | ±0.1 kPa |

**Table 3.2h Equipment uncertainty for the PVDF PFCHE in an air/air system**

3.1.1.2 Spiral PFCHE experiment

(i) Air/water system (PEEK 20°)

| Measurement | Device | Uncertainty |
|---|---|---|
| Temperature | Platinum resistance thermocouple (PRT) connected to digital recorder | ±0.05°C |
| Water flow rate<br>Air flow rate | Placon rotameters<br>Nixon rotameters | ±0.1 $cm^3$/min (20-80 $cm^3$/min)<br>±0.5 $m^3$/hr (5-15 $m^3$/hr) |
| Pressure drop | Digital pressure meter (2000 Series manometer) | ±0.1 kPa |

**Table 3.2i Equipment uncertainty for the air/water system**

### 3.2 Method for general uncertainty analysis

Consider a general case in which an experimental result, r is a function of J measured variables ($X_i$).

$$r = r(X_1, X_2, \ldots\ldots X_J) \tag{3.1}$$

Equation (3.1) is the data reduction equation used for determining an experimental result from the measured values of the variables ($X_i$).

The uncertainty (**U**) in the result is given by

$$\mathbf{U}_r^2 = \left(\frac{\partial r}{\partial X_1}\right)^2 \mathbf{U}_{x_1}^2 + \left(\frac{\partial r}{\partial X_2}\right)^2 \mathbf{U}_{x_2}^2 + \ldots\ldots + \left(\frac{\partial r}{\partial X_J}\right)^2 \mathbf{U}_{x_J}^2 \tag{3.2}$$

$\mathbf{U}_{Xi}$ = absolute uncertainties which take into account the uncertainties in the measured variables $X_i$.

Assumptions:

(i) Equation (3.2) is continuous and has continuous derivatives in the domain of interest

(ii) Measured variables $X_i$ are independent of one another

(iii) Uncertainties in the measured variables are independent of one another

If the partial derivatives are defined as 'absolute sensitivity coefficients' so that

$$\theta_i = \frac{\partial r}{\partial X_i} \tag{3.3}$$

Equation (3.2) can be written as

$$\mathbf{U}_r^2 = \sum_{i=1}^{J} \theta_i^{\,2}\ \mathbf{U}_{x_i}^2 \tag{3.4}$$

A non-dimensionalised form of equation (3.2), which is useful in a planning phase of uncertainty analysis, is shown in equation (3.5). To arrive at equation (3.5), we divide both sides of equation (3.2) by $r^2$ and then multiply each term on the right hand side by $(X_i/X_i)^2$, which of course is equal to 1.

$$\frac{\mathbf{U}_r^2}{r^2} = \left(\frac{X_1}{r}\frac{\partial r}{\partial X_1}\right)^2\left(\frac{\mathbf{U}_{X_1}}{X_1}\right)^2 + \left(\frac{X_2}{r}\frac{\partial r}{\partial X_2}\right)^2\left(\frac{\mathbf{U}_{X_2}}{X_2}\right)^2 + \ldots\left(\frac{X_J}{r}\frac{\partial r}{\partial X_J}\right)^2\left(\frac{\mathbf{U}X_J}{X_J}\right)^2 \qquad (3.5)$$

$\mathbf{U}_r/r$ = relative uncertainty of result

$\mathbf{U}_{Xi}/X_i$ = relative uncertainties of each variable. In general, the relative uncertainties will be numbers less than 1.

$\left(\frac{X_i}{r}\frac{\partial r}{\partial X_i}\right)$ = uncertainty magnification factors (UMFs)

The UMFs are the factors in parentheses that multiply the relative uncertainties of the variables. The UMF for a given $X_i$ indicates the influence of the uncertainty in that variable on the uncertainty in the result. A UMF greater than 1 indicates that the influence of the uncertainty in the variable is magnified as it propagates through the data reduction equation into a result. A UMF less than 1 indicates that the influence of the uncertainty in the variable is diminished as it propagates through the data reduction equation into result. Since the UMFs are squared in equation (3.5), their signs are of no importance. Thus, we consider only the absolute values of the UMFs when performing a general uncertainty analysis.

## 3.3 Sample calculations of uncertainty analysis

### *3.3.1 Square PFCHE experiments*

#### 3.3.1.1 Air/air system

a) Heat transfer area (A)

| Measurements | Uncertainty |
|---|---|
| L = 135 mm | ±0.5 |
| w = 135 mm | ±0.5 |

$$A = Lw$$

$$\mathbf{U}_A^2 = \left(\frac{\partial A}{\partial L}\right)^2 \mathbf{U}_L^2 + \left(\frac{\partial A}{\partial w}\right)^2 \mathbf{U}_w^2$$

$$\left(\frac{\mathbf{U}_A}{A}\right)^2 = \left(\frac{1}{A}\frac{\partial A}{\partial L}\right)^2 \mathbf{U}_L^2 + \left(\frac{1}{A}\frac{\partial A}{\partial w}\right)^2 \mathbf{U}_w^2$$

$$\frac{\partial A}{\partial L} = w$$

$$\frac{\partial A}{\partial w} = L$$

$$\frac{1}{A}\frac{\partial A}{\partial L} = \frac{w}{Lw} = \frac{1}{L}$$

$$\frac{1}{A}\frac{\partial A}{\partial w} = \frac{L}{Lw} = \frac{1}{w}$$

$$\left(\frac{\mathbf{U}_A}{A}\right)^2 = \left(\frac{\mathbf{U}_L}{L}\right)^2 + \left(\frac{\mathbf{U}_w}{w}\right)^2$$

$$= \left(\frac{0.5}{135}\right)^2 + \left(\frac{0.5}{135}\right)^2$$

$$\left(\frac{\mathbf{U}_A}{A}\right) = 5.2\ x\ 10^{-3} \quad (0.5\%)$$

(b) Free flow area ($A_{ff}$)

| Measurements | Uncertainty |
|---|---|
| h = 1 mm | ±0.05 |
| w = 135 mm | ±0.5 |

$$A_{ff} = 0.5\ hw$$

$$\mathbf{U}_{Aff}^2 = \left(\frac{\partial A_{ff}}{\partial h}\right)^2 \mathbf{U}_h^2 + \left(\frac{\partial A_{ff}}{\partial w}\right)^2 \mathbf{U}_w^2$$

$$\left(\frac{\mathbf{U}_{A_{ff}}}{A_{ff}}\right)^2 = \left(\frac{1}{A_{ff}}\frac{\partial A_{ff}}{\partial h}\right)^2 \mathbf{U}_h^2 + \left(\frac{1}{A_{ff}}\frac{\partial A_{ff}}{\partial w}\right)^2 \mathbf{U}_w^2$$

$$\frac{\partial A_{ff}}{\partial h} = 0.5w$$

$$\frac{\partial A_{ff}}{\partial w} = 0.5h$$

$$\frac{1}{A_{ff}}\frac{\partial A_{ff}}{\partial h} = \frac{0.5w}{0.5hw} = \frac{1}{h}$$

$$\frac{1}{A_{ff}}\frac{\partial A_{ff}}{\partial w} = \frac{0.5h}{0.5hw} = \frac{1}{w}$$

$$\left(\frac{\mathbf{U}_{A_{ff}}}{A_{ff}}\right)^2 = \left(\frac{\mathbf{U}_h}{h}\right)^2 + \left(\frac{\mathbf{U}_w}{w}\right)^2$$

$$= \left(\frac{0.05}{1}\right)^2 + \left(\frac{0.5}{135}\right)^2$$

$$\frac{\mathbf{U}_{A_{ff}}}{A_{ff}} = 0.05 \quad (5\%)$$

(c) Velocity (v)

| Measurements | Uncertainty |
|---|---|
| $\nu$ = 11 $m^3$/hr | ±0.5 |

$$v = \frac{\nu}{A_{ff}}$$

$$\mathbf{U}_v^2 = \left(\frac{\partial v}{\partial \nu}\right)^2 \mathbf{U}_\nu^2 + \left(\frac{\partial v}{\partial A_{ff}}\right)^2 \mathbf{U}_{A_{ff}}^2$$

$$\left(\frac{\mathbf{U}_v}{v}\right)^2 = \left(\frac{1}{v}\frac{\partial v}{\partial \nu}\right)^2 \mathbf{U}_\nu^2 + \left(\frac{1}{v}\frac{\partial v}{\partial A_{ff}}\right)^2 \mathbf{U}_{A_{ff}}^2$$

$$\frac{\partial v}{\partial \nu} = A_{ff}^{-1}$$

$$\frac{\partial v}{\partial A_{ff}} = -\nu\, A_{ff}^{-2}$$

$$\frac{1}{v}\frac{\partial v}{\partial \nu} = \frac{A_{ff}^{-1}}{\nu A_{ff}^{-1}} = \frac{1}{\nu}$$

$$\frac{1}{v}\frac{\partial v}{\partial A_{ff}} = \frac{-\nu A_{ff}^{-2}}{\nu A_{ff}^{-1}} = -\frac{1}{A_{ff}}$$

$$\left(\frac{\mathbf{U}_v}{v}\right)^2 = \left(\frac{\mathbf{U}_v}{v}\right)^2 + \left(\frac{\mathbf{U}_{A_{ff}}}{A_{ff}}\right)^2$$

$$= \left(\frac{0.5}{11}\right)^2 + (0.05)^2$$

$$\frac{\mathbf{U}v}{v} = 0.06 \quad (6\%)$$

(d) Hydraulic diameter ($d_h$)

$$d_h = \frac{4A_{ff}L}{A} = 4A_{ff}LA^{-1}$$

$$\mathbf{U}_{d_h}^2 = \left(\frac{\partial d_h}{\partial A_{ff}}\right)^2 \mathbf{U}_{A_{ff}}^2 + \left(\frac{\partial d_h}{\partial L}\right)^2 \mathbf{U}_L^2 + \left(\frac{\partial d_h}{\partial A}\right)^2 \mathbf{U}_A^2$$

$$\left(\frac{\mathbf{U}d_h}{d_h}\right)^2 = \left(\frac{1}{d_h}\frac{\partial d_h}{\partial A_{ff}}\right)^2 \mathbf{U}_{A_{ff}}^2 + \left(\frac{1}{d_h}\frac{\partial d_h}{\partial L}\right)^2 \mathbf{U}_L^2 + \left(\frac{1}{d_h}\frac{\partial d_h}{\partial A}\right)^2 \mathbf{U}_A^2$$

$$\frac{1}{d_h}\frac{\partial d_h}{\partial A_{ff}} = \frac{4LA^{-1}}{4A_{ff}LA^{-1}} = \frac{1}{A_{ff}}$$

$$\frac{1}{d_h}\frac{\partial d_h}{\partial L} = \frac{4A_{ff}A^{-1}}{4A_{ff}LA^{-1}} = \frac{1}{L}$$

$$\frac{1}{d_h}\frac{\partial d_h}{\partial A} = \frac{-4A_{ff}LA^{-2}}{4A_{ff}LA^{-1}} = -\frac{1}{A}$$

$$\left(\frac{\mathbf{U}_{d_h}}{d_h}\right)^2 = \left(\frac{\mathbf{U}_{A_{ff}}}{A_{ff}}\right)^2 + \left(\frac{\mathbf{U}_L}{L}\right)^2 + \left(\frac{\mathbf{U}_A}{A}\right)^2$$

$$= (0.05)^2 + \left(\frac{0.5}{135}\right)^2 + (0.005)^2$$

$$\frac{\mathbf{U}_{d_h}}{d_h} = 0.05 \quad (5\%)$$

(e) Reynolds number (Re)

| Measurements | Uncertainty |
|---|---|
| $v$ = 11 $m^3$/hr | ±0.5 |
| ΔT = 8.10 | ±0.05 |

$$\mathrm{Re} = \frac{\rho v d_h}{\mu} = \rho v d_h \mu^{-1}$$

$$\left(\frac{\mathbf{U}_{\mathrm{Re}}}{\mathrm{Re}}\right)^2 = \left(\frac{1}{\mathrm{Re}}\frac{\partial \mathrm{Re}}{\partial v}\right)^2 \mathbf{U}_v^2 + \left(\frac{1}{\mathrm{Re}}\frac{\partial \mathrm{Re}}{\partial d_h}\right)^2 \mathbf{U}_{d_h}^2$$

$$\frac{1}{\mathrm{Re}}\frac{\partial \mathrm{Re}}{\partial v} = \frac{\rho d_h \mu^{-1}}{\rho v d_h \mu^{-1}} = \frac{1}{v}$$

$$\frac{1}{\mathrm{Re}}\frac{\partial \mathrm{Re}}{\partial d_h} = \frac{\rho v \mu^{-1}}{\rho v d_h \mu^{-1}} = \frac{1}{d_h}$$

$$\left(\frac{\mathbf{U}_{\mathrm{Re}}}{\mathrm{Re}}\right)^2 = \left(\frac{\mathbf{U}_v}{v}\right)^2 + \left(\frac{\mathbf{U}_{d_h}}{d_h}\right)^2$$

$$= (0.06)^2 + (0.05)^2$$

$$\frac{\mathbf{U}_{\mathrm{Re}}}{\mathrm{Re}} = 0.07 \quad (7\%)$$

(f) Heat transfer duty (Q)

$$Q = \rho v \, cp \, \Delta T$$

$$\left(\frac{\mathbf{U}_Q}{Q}\right)^2 = \left(\frac{1}{Q}\frac{\partial Q}{\partial v}\right)^2 \mathbf{U}_v^2 + \left(\frac{1}{Q}\frac{\partial Q}{\partial \Delta T}\right)^2 \mathbf{U}_{\Delta T}^2$$

$$\frac{1}{Q}\frac{\partial Q}{\partial v} = \frac{\rho \, cp \, \Delta T}{v \, \rho \, cp \Delta T} = \frac{1}{v}$$

$$\frac{1}{Q}\frac{\partial Q}{\partial \Delta T} = \frac{v\,\rho\,cp}{v\,\rho\,cp\Delta T} = \frac{1}{\Delta T}$$

$$\left(\frac{\mathbf{U}_Q}{Q}\right)^2 = \left(\frac{\mathbf{U}_v}{v}\right)^2 + \left(\frac{\mathbf{U}_{\Delta T}}{\Delta T}\right)^2$$

$$= \left(\frac{0.5}{11}\right)^2 + \left(\frac{0.05}{8.1}\right)^2$$

$$\frac{\mathbf{U}_Q}{Q} = 0.04 \quad (4\%)$$

(g) Heat transfer coefficient (h)

The accuracy of the heat transfer coefficient is dependent on the E-NTU values generated using the E-Bessel equation (Baclic 1978). This equation will be explained further in Chapter Four. The E values are first calculated using the expression ($E=Q_{act}/Q_{max}$) and then fed into the E-Bessel equation to obtain the corresponding NTU values, via the goal seek function in Microsoft Excel. All E values correspond to NTU in a range of values up to 4, where the E-NTU behaviour was very sensitive. Following this, we perform an uncertainty analysis on the overall heat transfer coefficient (U).

$$U = \frac{NTUC_{\min}}{A} = NTUC_{\min}A^{-1}$$

$$\left(\frac{\mathbf{U}_U}{U}\right)^2 = \left(\frac{1}{U}\frac{\partial U}{\partial NTU}\right)^2 \mathbf{U}_{NTU}^2 + \left(\frac{1}{U}\frac{\partial U}{\partial A}\right)^2 \mathbf{U}_A^2$$

$$\frac{1}{U}\frac{\partial U}{\partial NTU} = \frac{C_{\min}A^{-1}}{NTUC_{\min}A^{-1}} = \frac{1}{NTU}$$

$$\frac{1}{U}\frac{\partial U}{\partial A} = \frac{-NTUC_{\min}A^{-2}}{NTUC_{\min}A^{-1}} = -\frac{1}{A}$$

$$\left(\frac{\mathbf{U}_U}{U}\right)^2 = \left(\frac{\mathbf{U}_{NTU}}{NTU}\right)^2 + \left(\frac{\mathbf{U}_A}{A}\right)^2$$

$$= (0.05)^2 + (0.005)^2$$

$$\left(\frac{\mathbf{U}_U}{U}\right) = 0.05 \quad (5\%)$$

Therefore, the relative uncertainty for the heat transfer coefficient is 0.05, as shown below.

$$\left(\frac{\mathbf{U}_h}{h}\right) = 0.05 \quad (5\%)$$

(h) Colburn factor (Jh)

$$Jh = h\,d_h\,\mathrm{Pr}^{-0.33}\,k^{-1}\,\mathrm{Re}^{-1}$$

$$\left(\frac{\mathbf{U}_{Jh}}{Jh}\right)^2 = \left(\frac{1}{Jh}\frac{\partial Jh}{\partial h}\right)^2 \mathbf{U}_h^2 + \left(\frac{1}{Jh}\frac{\partial Jh}{\partial d_h}\right)^2 \mathbf{U}_{d_h}^2 + \left(\frac{1}{Jh}\frac{\partial Jh}{\partial \mathrm{Re}}\right)^2 \mathbf{U}_{\mathrm{Re}}^2$$

$$\frac{1}{Jh}\frac{\partial Jh}{\partial h} = \frac{d_h\,\mathrm{Pr}^{-0.33}\,k^{-1}\,\mathrm{Re}^{-1}}{h\,d_h\,\mathrm{Pr}^{-0.33}\,k^{-1}\,\mathrm{Re}^{-1}} = \frac{1}{h}$$

$$\frac{1}{Jh}\frac{\partial Jh}{\partial d_h} = \frac{h\,\mathrm{Pr}^{-0.33}\,k^{-1}\,\mathrm{Re}^{-1}}{h\,d_h\,\mathrm{Pr}^{-0.33}\,k^{-1}\,\mathrm{Re}^{-1}} = \frac{1}{d_h}$$

$$\frac{1}{Jh}\frac{\partial Jh}{\partial \mathrm{Re}} = \frac{-h\,d_h\,\mathrm{Pr}^{-0.33}\,k^{-1}\,\mathrm{Re}^{-2}}{h\,d_h\,\mathrm{Pr}^{-0.33}\,k^{-1}\,\mathrm{Re}^{-1}} = -\frac{1}{\mathrm{Re}}$$

$$\left(\frac{\mathbf{U}_{Jh}}{Jh}\right)^2 = \left(\frac{\mathbf{U}_h}{h}\right)^2 + \left(\frac{\mathbf{U}_{d_h}}{d_h}\right)^2 + \left(\frac{\mathbf{U}_{\mathrm{Re}}}{\mathrm{Re}}\right)^2$$

$$= (0.05)^2 + (0.05)^2 + (0.07)^2$$

$$\left(\frac{\mathbf{U}_{Jh}}{Jh}\right) = 0.10 \quad (10\%)$$

(i) Friction factor (f)

| Measurements | Uncertainty |
|---|---|
| ΔP = 15 kPa | ±0.1 |
| L = 135 mm | ±0.5 |

$$f = \frac{2\Delta P\, d_h}{4\rho v^2 L} = \frac{1}{2\rho}\Delta P d_h v^{-2} L$$

$$\left(\frac{\mathbf{U}_f}{f}\right)^2 = \left(\frac{1}{f}\frac{\partial f}{\partial \Delta P}\right)^2 \mathbf{U}_{\Delta P}^2 + \left(\frac{1}{f}\frac{\partial f}{\partial v}\right)^2 \mathbf{U}_v^2 + \left(\frac{1}{f}\frac{\partial f}{\partial d_h}\right)^2 \mathbf{U}_{d_h}^2 + \left(\frac{1}{f}\frac{\partial f}{\partial L}\right)^2 \mathbf{U}_L^2$$

$$\frac{1}{f}\frac{\partial f}{\partial \Delta P} = \frac{\frac{1}{2\rho} d_h v^{-2} L}{\frac{1}{2\rho}\Delta P d_h\, v^{-2} L} = \frac{1}{\Delta P}$$

$$\frac{1}{f}\frac{\partial f}{\partial v} = \frac{\frac{1}{2\rho}\Delta P d_h L\, x - 2v^{-3}}{\frac{1}{2\rho}\Delta P d_h\, v^{-2} L} = -\frac{2}{v}$$

$$\frac{1}{f}\frac{\partial f}{\partial d_h} = \frac{\frac{1}{2\rho}\Delta P v^{-2} L}{\frac{1}{2\rho}\Delta P d_h\, v^{-2} L} = \frac{1}{d_h}$$

$$\frac{1}{f}\frac{\partial f}{\partial L} = \frac{\frac{1}{2\rho}\Delta P d_h v^{-2}}{\frac{1}{2\rho}\Delta P d_h\, v^{-2} L} = \frac{1}{L}$$

$$\left(\frac{\mathbf{U}_f}{f}\right)^2 = \left(\frac{\mathbf{U}_{\Delta P}}{\Delta P}\right)^2 + \left(\frac{-2}{v}\right)^2 \mathbf{U}_v^2 + \left(\frac{\mathbf{U}d_h}{d_h}\right)^2 + \left(\frac{\mathbf{U}_L}{L}\right)^2$$

$$= \left(\frac{0.1}{15}\right)^2 + (2\ x 0.06)^2 + (0.05)^2 + \left(\frac{0.5}{135}\right)^2$$

$$\left(\frac{\mathbf{U}_f}{f}\right) = 0.13 \quad (13\%)$$

3.3.1.2 Water/water system

(a) Velocity (v)

| Measurement | Uncertainty |
|---|---|
| $v$ = 0.79 $m^3$/hr | ±0.01 |

$$\left(\frac{\mathbf{U}_v}{v}\right)^2 = \left(\frac{\mathbf{U}_v}{v}\right)^2 + \left(\frac{\mathbf{U}_{A_{ff}}}{A_{ff}}\right)^2$$

$$= \left(\frac{0.01}{0.79}\right)^2 + (0.05)^2$$

$$\left(\frac{\mathbf{U}_v}{v}\right) = 0.05 \quad (5\%)$$

(b) Reynolds number (Re)

$$\left(\frac{\mathbf{U}_{\mathrm{Re}}}{\mathrm{Re}}\right)^2 = \left(\frac{\mathbf{U}_v}{v}\right)^2 + \left(\frac{\mathbf{U}_{d_h}}{d_h}\right)^2$$

$$= (0.05)^2 + (0.05)^2$$

$$\left(\frac{\mathbf{U}_{\mathrm{Re}}}{\mathrm{Re}}\right) = 0.07 \quad (7\%)$$

(c) Colburn factor (Jh)

$$\left(\frac{\mathbf{U}_{Jh}}{Jh}\right)^2 = \left(\frac{\mathbf{U}_h}{h}\right)^2 + \left(\frac{\mathbf{U}_{d_h}}{d_h}\right)^2 + \left(\frac{\mathbf{U}_{\mathrm{Re}}}{\mathrm{Re}}\right)^2$$

$$= (0.05)^2 + (0.05)^2 + (0.07)^2$$

$$\left(\frac{\mathbf{U}_{Jh}}{Jh}\right) = 0.10 \quad (10\%)$$

(d) Friction factor (f)

| Measurement | Uncertainty |
|---|---|
| ΔP= 0.73 kPa | ±0.01 |

$$\left(\frac{\mathbf{U}_f}{f}\right)^2 = \left(\frac{\mathbf{U}_{\Delta P}}{\Delta P}\right)^2 + \left(-\frac{2}{v}\right)^2 \mathbf{U}_v^2 + \left(\frac{\mathbf{U}_{d_h}}{d_h}\right)^2 + \left(\frac{\mathbf{U}_L}{L}\right)^2$$

$$= \left(\frac{0.01}{0.73}\right)^2 + (2x0.05)^2 + (0.05)^2 + \left(\frac{0.5}{135}\right)^2$$

$$\left(\frac{\mathbf{U}_f}{f}\right) = 0.11 \quad (11\%)$$

3.3.1.3 30% glycerol + water/water system

(a) Velocity (v)

| Measurement | Uncertainty |
|---|---|
| $v$ = 0.63 $m^3$/hr | ±0.01 |

$$\left(\frac{\mathbf{U}_v}{v}\right)^2 = \left(\frac{\mathbf{U}_v}{v}\right)^2 + \left(\frac{\mathbf{U}_{A_{ff}}}{A_{ff}}\right)^2$$

$$= \left(\frac{0.01}{0.63}\right)^2 + (0.05)^2$$

$$\left(\frac{\mathbf{U}_v}{v}\right) = 0.05 \quad (5\%)$$

(b) Reynolds number (Re)

$$\left(\frac{\mathbf{U}_{\mathrm{Re}}}{\mathrm{Re}}\right)^2 = \left(\frac{\mathbf{U}_v}{v}\right)^2 + \left(\frac{\mathbf{U}_{d_h}}{d_h}\right)^2$$

$$= (0.05)^2 + (0.05)^2$$

$$\left(\frac{\mathbf{U}_{\mathrm{Re}}}{\mathrm{Re}}\right) = 0.07 \quad (7\%)$$

(c) Colburn factor (Jh)

$$\left(\frac{\mathbf{U}_{Jh}}{Jh}\right)^2 = \left(\frac{\mathbf{U}_h}{h}\right)^2 + \left(\frac{\mathbf{U}_{d_h}}{d_h}\right)^2 + \left(\frac{\mathbf{U}_{\mathrm{Re}}}{\mathrm{Re}}\right)^2$$

$$= (0.05)^2 + (0.05)^2 + (0.07)^2$$

$$\left(\frac{\mathbf{U}_{Jh}}{Jh}\right) = 0.10 \quad (10\%)$$

(d) Friction factor (f)

| Measurement | Uncertainty |
|---|---|
| ΔP = 9.8 kPa | ±0.01 |

$$\left(\frac{\mathbf{U}_f}{f}\right)^2 = \left(\frac{\mathbf{U}_{\Delta P}}{\Delta P}\right)^2 + \left(-\frac{2}{v}\right)^2 \mathbf{U}_v^2 + \left(\frac{\mathbf{U}_{d_h}}{d_h}\right)^2 + \left(\frac{\mathbf{U}_L}{L}\right)^2$$

$$= \left(\frac{0.01}{2.23}\right)^2 + (2x0.05)^2 + (0.05)^2 + \left(\frac{0.5}{135}\right)^2$$

$$\left(\frac{\mathbf{U}_f}{f}\right) = 0.11 \quad (11\%)$$

3.3.1.4 40% glycerol + water/water system

(a) Velocity (v)

| Measurement | Uncertainty |
|---|---|
| $v$ = 0.47 $m^3$/hr | ±0.01 |

$$\left(\frac{\mathbf{U}_v}{v}\right)^2 = \left(\frac{\mathbf{U}_v}{v}\right)^2 + \left(\frac{\mathbf{U}_{A_{ff}}}{A_{ff}}\right)^2$$

$$= \left(\frac{0.01}{0.47}\right)^2 + (0.05)^2$$

$$\left(\frac{\mathbf{U}_v}{v}\right) = 0.05 \quad (5\%)$$

(b) Reynolds number (Re)

$$\left(\frac{\mathbf{U}_{\mathrm{Re}}}{\mathrm{Re}}\right)^2 = \left(\frac{\mathbf{U}_v}{v}\right)^2 + \left(\frac{\mathbf{U}_{d_h}}{d_h}\right)^2$$

$$= (0.05)^2 + (0.05)^2$$

$$\left(\frac{\mathbf{U}_{\mathrm{Re}}}{\mathrm{Re}}\right) = 0.707 \quad (7\%)$$

(c) Colburn factor (Jh)

$$\left(\frac{\mathbf{U}_{Jh}}{Jh}\right)^2 = \left(\frac{\mathbf{U}_h}{h}\right)^2 + \left(\frac{\mathbf{U}_{d_h}}{d_h}\right)^2 + \left(\frac{\mathbf{U}_{\mathrm{Re}}}{\mathrm{Re}}\right)^2$$

$$= (0.05)^2 + (0.05)^2 + (0.07)^2$$

$$\left(\frac{\mathbf{U}_{Jh}}{Jh}\right) = 0.10 \quad (10\%)$$

(d) Friction factor (f)

| Measurement | Uncertainty |
|---|---|
| ΔP = 1.82 kPa | ±0.01 |

$$\left(\frac{\mathbf{U}_f}{f}\right)^2 = \left(\frac{\mathbf{U}_{\Delta P}}{\Delta P}\right)^2 + \left(-\frac{2}{v}\right)^2 \mathbf{U}_v^2 + \left(\frac{\mathbf{U}_{d_h}}{d_h}\right)^2 + \left(\frac{\mathbf{U}_L}{L}\right)^2$$

$$= \left(\frac{0.01}{1.82}\right)^2 + (2x0.05)^2 + (0.05)^2 + \left(\frac{0.5}{135}\right)^2$$

$$\left(\frac{\mathbf{U}_f}{f}\right) = 0.11 \quad (11\%)$$

3.3.1.5 50% glycerol + water/water system

| Measurement | Uncertainty |
|---|---|
| $v$ = 0.43 $m^3$/hr | ±0.01 |

(a) Velocity (v)

$$\left(\frac{\mathbf{U}_v}{v}\right)^2 = \left(\frac{\mathbf{U}_v}{v}\right)^2 + \left(\frac{\mathbf{U}_{A_{ff}}}{A_{ff}}\right)^2$$

$$= \left(\frac{0.01}{0.43}\right)^2 + (0.05)^2$$

$$\left(\frac{\mathbf{U}_v}{v}\right) = 0.05 \quad (5\%)$$

(b) Reynolds number (Re)

$$\left(\frac{\mathbf{U}_{\mathrm{Re}}}{\mathrm{Re}}\right)^2 = \left(\frac{\mathbf{U}_v}{v}\right)^2 + \left(\frac{\mathbf{U}_{d_h}}{d_h}\right)^2$$

$$= (0.05)^2 + (0.05)^2$$

$$\left(\frac{\mathbf{U}_{\mathrm{Re}}}{\mathrm{Re}}\right) = 0.07 \quad (7\%)$$

(c) Colburn factor (Jh)

$$\left(\frac{\mathbf{U}_{Jh}}{Jh}\right)^2 = \left(\frac{\mathbf{U}_h}{h}\right)^2 + \left(\frac{\mathbf{U}_{d_h}}{d_h}\right)^2 + \left(\frac{\mathbf{U}_{\mathrm{Re}}}{\mathrm{Re}}\right)^2$$

$$= (0.05)^2 + (0.05)^2 + (0.07)^2$$

$$\left(\frac{\mathbf{U}_{Jh}}{Jh}\right) = 0.10 \quad (10\%)$$

(d) Friction factor (f)

| Measurement | Uncertainty |
|---|---|
| ΔP = 1.85 kPa | ±0.01 |

$$\left(\frac{\mathbf{U}_f}{f}\right)^2 = \left(\frac{\mathbf{U}_{\Delta P}}{\Delta P}\right)^2 + \left(-\frac{2}{v}\right)^2 \mathbf{U}_v^2 + \left(\frac{\mathbf{U}_{d_h}}{d_h}\right)^2 + \left(\frac{\mathbf{U}_L}{L}\right)^2$$

$$= \left(\frac{0.01}{1.85}\right)^2 + (2 \times 0.05)^2 + (0.05)^2 + \left(\frac{0.5}{0.135}\right)^2$$

$$\left(\frac{\mathbf{U}_f}{f}\right) = 0.12 \quad (12\%)$$

3.3.1.6 70% glycerol + water/water system

| Measurement | Uncertainty |
|---|---|
| $v$ = 0.35 m$^3$/hr | ±0.01 |

(a) Velocity (v)

$$\left(\frac{\mathbf{U}_v}{v}\right)^2 = \left(\frac{\mathbf{U}_v}{\nu}\right)^2 + \left(\frac{\mathbf{U}_{A_{ff}}}{A_{ff}}\right)^2$$

$$= \left(\frac{0.01}{0.35}\right)^2 + (0.05)^2$$

$$\left(\frac{\mathbf{U}_v}{v}\right) = 0.06 \quad (6\%)$$

(b) Reynolds number (Re)

$$\left(\frac{\mathbf{U}_{\mathrm{Re}}}{\mathrm{Re}}\right)^2 = \left(\frac{\mathbf{U}_v}{v}\right)^2 + \left(\frac{\mathbf{U}_{d_h}}{d_h}\right)^2$$

$$= (0.06)^2 + (0.05)^2$$

$$\left(\frac{\mathbf{U}_{\mathrm{Re}}}{\mathrm{Re}}\right) = 0.08 \quad (8\%)$$

(c) Colburn factor (Jh)

$$\left(\frac{\mathbf{U}_{Jh}}{Jh}\right)^2 = \left(\frac{\mathbf{U}_h}{h}\right)^2 + \left(\frac{\mathbf{U}_{d_h}}{d_h}\right)^2 + \left(\frac{\mathbf{U}_{\mathrm{Re}}}{\mathrm{Re}}\right)^2$$

$$= (0.05)^2 + (0.05)^2 + (0.08)^2$$

$$\left(\frac{\mathbf{U}_{Jh}}{Jh}\right) = 0.10 \quad (10\%)$$

(d) Friction factor (f)

| Measurement | Uncertainty |
|---|---|
| ΔP = 46.3 kPa | ±0.01 |

$$\left(\frac{\mathbf{U}_f}{f}\right)^2 = \left(\frac{\mathbf{U}_{\Delta P}}{\Delta P}\right)^2 + \left(-\frac{2}{v}\right)^2 \mathbf{U}_v^2 + \left(\frac{\mathbf{U}_{d_h}}{d_h}\right)^2 + \left(\frac{\mathbf{U}_L}{L}\right)^2$$

$$= \left(\frac{0.01}{46.3}\right)^2 + (2\ x\ 0.06)^2 + (0.05)^2 + \left(\frac{0.5}{0.135}\right)^2$$

$$\left(\frac{\mathbf{U}_f}{f}\right) = 0.12 \quad (12\%)$$

3.3.1.7 Air/air system (30°)

(a) Velocity

| Measurement | Uncertainty |
|---|---|
| $v$ = 6 m$^3$/hr | ±0.5 |

$$\left(\frac{\mathbf{U}_v}{v}\right)^2 = \left(\frac{\mathbf{U}_\nu}{\nu}\right)^2 + \left(\frac{\mathbf{U}_{A_{ff}}}{A_{ff}}\right)^2$$

$$= \left(\frac{0.5}{6}\right)^2 + (0.05)^2$$

$$\left(\frac{\mathbf{U}_v}{v}\right) = 0.09 \quad (9\%)$$

(b) Reynolds number (Re)

$$\left(\frac{\mathbf{U}_{\mathrm{Re}}}{\mathrm{Re}}\right)^2 = \left(\frac{\mathbf{U}_v}{v}\right)^2 + \left(\frac{\mathbf{U}_{d_h}}{d_h}\right)^2$$

$$= (0.09)^2 + (0.05)^2$$

$$\left(\frac{\mathbf{U}_{\mathrm{Re}}}{\mathrm{Re}}\right) = 0.10 \quad (10\%)$$

(c) Colburn factor (Jh)

$$\left(\frac{\mathbf{U}_{Jh}}{Jh}\right)^2 = \left(\frac{\mathbf{U}_h}{h}\right)^2 + \left(\frac{\mathbf{U}_{d_h}}{d_h}\right)^2 + \left(\frac{\mathbf{U}_{\mathrm{Re}}}{\mathrm{Re}}\right)^2$$

$$= (0.05)^2 + (0.05)^2 + (0.1)^2$$

$$\left(\frac{\mathbf{U}_{Jh}}{Jh}\right) = 0.12 \quad (12\%)$$

(d) Friction factor (f)

| Measurement | Uncertainty |
|---|---|
| ΔP = 18.7 kPa | ±0.1 |

$$\left(\frac{\mathbf{U}_f}{f}\right)^2 = \left(\frac{\mathbf{U}_{\Delta P}}{\Delta P}\right)^2 + \left(-\frac{2}{v}\right)^2 \mathbf{U}_v^2 + \left(\frac{\mathbf{U}_{d_h}}{d_h}\right)^2 + \left(\frac{\mathbf{U}_L}{L}\right)^2$$

$$= \left(\frac{0.1}{18.7}\right)^2 + (2\ x\ 0.09)^2 + (0.05)^2 + \left(\frac{0.5}{0.135}\right)^2$$

$$\left(\frac{\mathbf{U}_f}{f}\right) = 0.17 \quad (17\%)$$

3.3.1.8 Air/air system (60°)

(a) Velocity (v)

| Measurement | Uncertainty |
|---|---|
| $v$ = 8.5 $m^3$/hr | ±0.5 |

$$\left(\frac{\mathbf{U}_v}{v}\right)^2 = \left(\frac{\mathbf{U}_v}{v}\right)^2 + \left(\frac{\mathbf{U}_{A_{ff}}}{A_{ff}}\right)^2$$

$$= \left(\frac{0.5}{8.5}\right)^2 + (0.05)^2$$

$$\left(\frac{\mathbf{U}_v}{v}\right) = 0.07 \quad (7\%)$$

(b) Reynolds number (Re)

$$\left(\frac{\mathbf{U}_{\mathrm{Re}}}{\mathrm{Re}}\right)^2 = \left(\frac{\mathbf{U}_v}{v}\right)^2 + \left(\frac{\mathbf{U}_{d_h}}{d_h}\right)^2$$

$$= (0.07)^2 + (0.05)^2$$

$$\left(\frac{\mathbf{U}_{\mathrm{Re}}}{\mathrm{Re}}\right) = 0.08 \quad (8\%)$$

(c) Colburn factor (Jh)

$$\left(\frac{\mathbf{U}_{Jh}}{Jh}\right)^2 = \left(\frac{\mathbf{U}_h}{h}\right)^2 + \left(\frac{\mathbf{U}_{d_h}}{d_h}\right)^2 + \left(\frac{\mathbf{U}_{\mathrm{Re}}}{\mathrm{Re}}\right)^2$$

$$= (0.05)^2 + (0.05)^2 + (0.08)^2$$

$$\left(\frac{\mathbf{U}_{Jh}}{Jh}\right) = 0.11 \quad (11\%)$$

(d) Friction factor (f)

| Measurement | Uncertainty |
|---|---|
| ΔP = 14 kPa | ±0.1 |

$$\left(\frac{\mathbf{U}_f}{f}\right)^2 = \left(\frac{\mathbf{U}_{\Delta P}}{\Delta P}\right)^2 + \left(-\frac{2}{v}\right)^2 \mathbf{U}_v^2 + \left(\frac{\mathbf{U}_{d_h}}{d_h}\right)^2 + \left(\frac{\mathbf{U}_L}{L}\right)^2$$

$$= \left(\frac{0.1}{14}\right)^2 + (2 \times 0.07)^2 + (0.05)^2 + \left(\frac{0.5}{0.135}\right)^2$$

$$\left(\frac{\mathbf{U}_f}{f}\right) = 0.14 \quad (14\%)$$

3.3.1.9 Air/air system (PVDF 90°)

(a) Velocity (v)

| Measurement | Uncertainty |
|---|---|
| $v$ = 8.0 $m^3$/hr | ±0.5 |

$$\left(\frac{\mathbf{U}_v}{v}\right)^2 = \left(\frac{\mathbf{U}_v}{v}\right)^2 + \left(\frac{\mathbf{U}_{A_{ff}}}{A_{ff}}\right)^2$$

$$= \left(\frac{0.5}{8.0}\right)^2 + (0.05)^2$$

$$\left(\frac{\mathbf{U}_v}{v}\right) = 0.08 \quad (8\%)$$

(b) Reynolds number (Re)

$$\left(\frac{\mathbf{U}_{\mathrm{Re}}}{\mathrm{Re}}\right)^2 = \left(\frac{\mathbf{U}_v}{v}\right)^2 + \left(\frac{\mathbf{U}_{d_h}}{d_h}\right)^2$$

$$= (0.08)^2 + (0.05)^2$$

$$\left(\frac{\mathbf{U}_{\mathrm{Re}}}{\mathrm{Re}}\right) = 0.09 \quad (9\%)$$

(c) Colburn factor (Jh)

$$\left(\frac{\mathbf{U}_{Jh}}{Jh}\right)^2 = \left(\frac{\mathbf{U}_h}{h}\right)^2 + \left(\frac{\mathbf{U}_{d_h}}{d_h}\right)^2 + \left(\frac{\mathbf{U}_{\mathrm{Re}}}{\mathrm{Re}}\right)^2$$

$$= (0.05)^2 + (0.05)^2 + (0.09)^2$$

$$\left(\frac{\mathbf{U}_{Jh}}{Jh}\right) = 0.11 \quad (11\%)$$

(d) Friction factor (f)

| Measurement | Uncertainty |
|---|---|
| ΔP = 2 kPa | ±0.1 |

$$\left(\frac{\mathbf{U}_f}{f}\right)^2 = \left(\frac{\mathbf{U}_{\Delta P}}{\Delta P}\right)^2 + \left(-\frac{2}{v}\right)^2 \mathbf{U}_v^2 + \left(\frac{\mathbf{U}_{d_h}}{d_h}\right)^2 + \left(\frac{\mathbf{U}_L}{L}\right)^2$$

$$= \left(\frac{0.1}{2}\right)^2 + (2\ x\ 0.08)^2 + (0.05)^2 + \left(\frac{0.5}{0.135}\right)^2$$

$$\left(\frac{\mathbf{U}_f}{f}\right) = 0.17 \quad (17\%)$$

*3.3.2 Spiral PFCHE experiment*

3.3.2.1 Air/water system (air-side)

| Measurement | Uncertainty |
|---|---|
| L = 210 mm | ±0.5 |
| w = 100 mm | ±0.5 |

(a) Heat transfer area (A)

$$\left(\frac{\mathbf{U}_A}{A}\right)^2 = \left(\frac{\mathbf{U}_L}{L}\right)^2 + \left(\frac{\mathbf{U}_w}{w}\right)^2$$

$$= \left(\frac{0.5}{210}\right)^2 + \left(\frac{0.5}{100}\right)^2$$

$$\left(\frac{\mathbf{U}_A}{A}\right) = 0.005 \quad (0.5\%)$$

(b) Free flow area ($A_{ff}$)

| Measurement | Uncertainty |
|---|---|
| h = 1 mm | ±0.05 |
| L = 210 mm | ±0.5 |

$$\left(\frac{\mathbf{U}_{A_{ff}}}{A_{ff}}\right)^2 = \left(\frac{\mathbf{U}_h}{h}\right)^2 + \left(\frac{\mathbf{U}_L}{L}\right)^2$$

$$= \left(\frac{0.05}{1}\right)^2 + \left(\frac{0.5}{210}\right)^2$$

$$\left(\frac{\mathbf{U}_{A_{ff}}}{A_{ff}}\right) = 0.05 \quad (5\%)$$

(c) Velocity (v)

| Measurement | Uncertainty |
|---|---|
| $v$ = 10 $m^3$/hr | ±0.5 |

$$\left(\frac{\mathbf{U}_v}{v}\right)^2 = \left(\frac{\mathbf{U}_v}{v}\right)^2 + \left(\frac{\mathbf{U}_{A_{ff}}}{A_{ff}}\right)^2$$

$$= \left(\frac{0.5}{10}\right)^2 + (0.05)^2$$

$$\left(\frac{\mathbf{U}_v}{v}\right) = 0.07 \quad (7\%)$$

(d) Hydraulic diameter ($d_h$)

$$\left(\frac{\mathbf{U}_{d_h}}{d_h}\right)^2 = \left(\frac{\mathbf{U}_{A_{ff}}}{A_{ff}}\right)^2 + \left(\frac{\mathbf{U}_w}{w}\right)^2 + \left(\frac{\mathbf{U}_A}{A}\right)^2$$

$$= (0.05)^2 + \left(\frac{0.5}{100}\right)^2 + (0.005)^2$$

$$\left(\frac{\mathbf{U}_{d_h}}{d_h}\right) = 0.05 \quad (5\%)$$

(e) Reynolds number (Re)

$$\left(\frac{\mathbf{U}_{\mathrm{Re}}}{\mathrm{Re}}\right)^2 = \left(\frac{\mathbf{U}_v}{v}\right)^2 + \left(\frac{\mathbf{U}_{d_h}}{d_h}\right)^2$$

$$= (0.07)^2 + (0.05)^2$$

$$\left(\frac{\mathbf{U}_{\mathrm{Re}}}{\mathrm{Re}}\right) = 0.08 \quad (8\%)$$

(f) Colburn factor (Jh)

$$\left(\frac{\mathbf{U}_{Jh}}{Jh}\right)^2 = \left(\frac{\mathbf{U}_h}{h}\right)^2 + \left(\frac{\mathbf{U}_{d_h}}{d_h}\right)^2 + \left(\frac{\mathbf{U}_{\mathrm{Re}}}{\mathrm{Re}}\right)^2$$

$$= (0.05)^2 + (0.05)^2 + (0.08)^2$$

$$\left(\frac{\mathbf{U}_{Jh}}{Jh}\right) = 0.10 \quad (10\%)$$

(g) Friction factor (f)

| Measurement | Uncertainty |
|---|---|
| ΔP = 0.5 kPa | ±0.1 |

$$\left(\frac{\mathbf{U}_f}{f}\right)^2 = \left(\frac{\mathbf{U}_{\Delta P}}{\Delta P}\right)^2 + \left(-\frac{2}{v}\right)^2 \mathbf{U}_v^2 + \left(\frac{\mathbf{U}_{d_h}}{d_h}\right)^2 + \left(\frac{\mathbf{U}_L}{L}\right)^2$$

$$= \left(\frac{0.1}{0.5}\right)^2 + (2\ x\ 0.07)^2 + (0.05)^2 + \left(\frac{0.5}{100}\right)^2$$

$$\left(\frac{\mathbf{U}_f}{f}\right) = 0.14 \quad (14\%)$$

3.3.2.2. Air/water system (water-side)

(a) Free flow area ($A_{ff}$)

| Measurement | Uncertainty |
|---|---|
| d =1 mm | ±0.03 |

$$\left(\frac{\mathbf{U}_{A_{ff}}}{A_{ff}}\right)^2 = \left(2\frac{\mathbf{U}_d}{d}\right)^2$$

$$= (2 x 0.03)^2$$

$$\left(\frac{\mathbf{U}_{A_{ff}}}{A_{ff}}\right) = 0.06 \quad (6\%)$$

(b) Velocity (v)

| Measurement | Uncertainty |
|---|---|
| $v$ = 20 $cm^3$/min | ±0.1 |

$$\left(\frac{\mathbf{U}_v}{v}\right)^2 = \left(\frac{\mathbf{U}_v}{v}\right)^2 + \left(\frac{\mathbf{U}_{A_{ff}}}{A_{ff}}\right)^2$$

$$= \left(\frac{0.1}{20}\right)^2 + (0.06)^2$$

$$\left(\frac{\mathbf{U}_v}{v}\right) = 0.06 \quad (6\%)$$

(c) Hydraulic diameter ($d_h$)

$$\left(\frac{\mathbf{U}_{d_h}}{d_h}\right)^2 = \left(\frac{\mathbf{U}_{A_{ff}}}{A_{ff}}\right)^2 + \left(\frac{\mathbf{U}_L}{L}\right)^2 + \left(\frac{\mathbf{U}_A}{A}\right)^2$$

$$= (0.06)^2 + \left(\frac{0.5}{210}\right)^2 + (0.005)^2$$

$$\left(\frac{\mathbf{U}_{d_h}}{d_h}\right) = 0.06 \quad (6\%)$$

(d) Reynolds number (Re)

$$\left(\frac{\mathbf{U}_{\mathrm{Re}}}{\mathrm{Re}}\right)^2 = \left(\frac{\mathbf{U}_{v}}{v}\right)^2 + \left(\frac{\mathbf{U}_{d_h}}{d_h}\right)^2$$

$$= (0.06)^2 + (0.06)^2$$

$$\left(\frac{\mathbf{U}_{\mathrm{Re}}}{\mathrm{Re}}\right) = 0.08 \quad (8\%)$$

(f) Colburn factor (Jh)

$$\left(\frac{\mathbf{U}_{Jh}}{Jh}\right)^2 = \left(\frac{\mathbf{U}_{h}}{h}\right)^2 + \left(\frac{\mathbf{U}_{d_h}}{d_h}\right)^2 + \left(\frac{\mathbf{U}_{\mathrm{Re}}}{\mathrm{Re}}\right)^2$$

$$= (0.05)^2 + (0.06)^2 + (0.08)^2$$

$$\left(\frac{\mathbf{U}_{Jh}}{Jh}\right) = 0.11 \quad (11\%)$$

### 3.4 Conclusion

The relative uncertainties for the Colburn factors ($\mathbf{U}_{Jh}/Jh$) and friction factors ($\mathbf{U}_f/f$), for all the PFCHE experiments calculated from experimental data are shown in Table 3.3 below.

| Configuration | Polymer material and corrugation angle | System | ($\mathbf{U}_{Jh}/Jh$) (%) | ($\mathbf{U}_f/f$) (%) |
|---|---|---|---|---|
| Square | PEEK 90° | air/air | 10 | 13 |
| | PEEK 90° | water/water | 10 | 11 |
| | PEEK 90° | 30% glycerol-water/water | 10 | 11 |
| | PEEK 90° | 40% glycerol-water/water | 10 | 11 |
| | PEEK 90° | 50% glycerol-water/water | 10 | 12 |
| | PEEK 90° | 70% glycerol-water/water | 10 | 12 |
| | PEEK 60° | air/air | 11 | 14 |
| | PEEK 30° | air/air | 12 | 17 |
| | PVDF 90° | air/air | 11 | 17 |
| Spiral | PEEK 20° | air/water (air-side) | 10 | 14 |
| | PEEK 20° | air/water (water-side) | 11 | n/a |

**Table 3.3 Relative uncertainties for the PFCHE experiments**

Overall, the relative Colburn factor uncertainties are within the target of 10% for both the square and spiral PFCHEs. Nevertheless, the relative friction factor uncertainties do exceed 10%; particularly for the PEEK 30° (Menes 1997) and PVDF 90° (Walker 1997) systems, due to the inherent insensitivity of the flow meters used in the experiment. This can be addressed by using more accurate equipment to measure low flow rates (less than 10 $m^3$/hr) and low pressure drops (less than 2 kPa). For the spiral PFCHE, the relative friction factor uncertainty is at 14% and this can also be addressed by using more accurate equipment for low pressure drops (less than 1 kPa).

### 3.5 Summary

In this chapter, the experimental data for all the PFCHE experiments mentioned in this thesis is first validated using the general uncertainty analysis. This approach is necessary in order to justify the reliability of the measurements recorded and presented in later chapters to investigate the performance of the PFCHE.

The analysis takes into account the equipment uncertainty for each experiment (ten systems in all) and also the propagation of these uncertainties when incorporated into data reduction equations, before arriving at an experimental result. For the PFCHE experiments, there are three main data reduction equations (Jh, f and Re) involved in determining the overall heat transfer and pressure drop result for the unit. By taking on a mathematical approach and performing differential analysis on the measured variables in each data reduction equation, the relative uncertainty of each variable can be calculated and subsequently the relative uncertainties for the Jh and f factors are determined. Overall, it was found that the relative uncertainties for the Jh factors are within the target uncertainty limit of 10%.

Establishing the fact that the experimental data is valid, we now proceed to describe the square PFCHE experiments in the next chapter; involving the air/air, water/water and glycerol-water mixtures/water systems.

# CHAPTER 4 - SQUARE POLYMER FILM COMPACT HEAT EXCHANGER

## 4.0 Introduction

In Chapter Three, the reliability of the experimental data for the PFCHE experiments presented in this thesis was established by carrying out an uncertainty analysis (Coleman 1999). The heat transfer results obtained showed that the uncertainty level was within the target of 10%. Acknowledging this, we now move on to describe the cross-corrugated flow configuration, the test facility and the experimental activity involving a square PFCHE module. Experimental results pertaining to heat transfer and pressure drop characteristics coupled with design correlations in the form of Jh and f factors have been presented in this chapter. In the next chapter, similar details for the spiral configuration will be discussed.

In order to investigate the thermal as well as the pressure drop characteristics of the square PFCHE, six fluid systems namely the air/air, water/water and four thickened water/water systems were conducted. The four thickened water/water systems were made up of 70%(w), 50%(w), 40%(w) and 30%(w) glycerol-water mixtures respectively. The design correlations developed in the form of Jh and f correlations over a range of Re numbers, play a vital role towards producing alternative designs to current metallic heat exchangers, in suitable applications.

We begin the chapter with a description of the experimental test facility and the procedures involved, for each fluid system tested in the square PFCHE.

## 4.1 Experimental apparatus: Design details and test procedure

Using 100 μm corrugated PEEK (poly ether ether ketone) films, which had a corrugation width of 2 mm and corrugation height of 1 mm, a square module was fabricated. Details of the PEEK film and the cross-corrugated configuration have been explained in Chapter Two. The square PFCHE unit consists of a number of corrugated PEEK sheets. The number of sheets used can vary for different fluid systems and range of flow rates tested. The dimensions of the sheets are 13.5 cm by 13.5 cm. The film thickness of the corrugated sheet is approximately 70 μm (100 μm for non-corrugated).The sheets are stacked together, each rotated at $90^{o}$ with respect to the next sheet; creating a cross-corrugated matrix. The stacked sheets are illustrated in Figure 4.1 below.

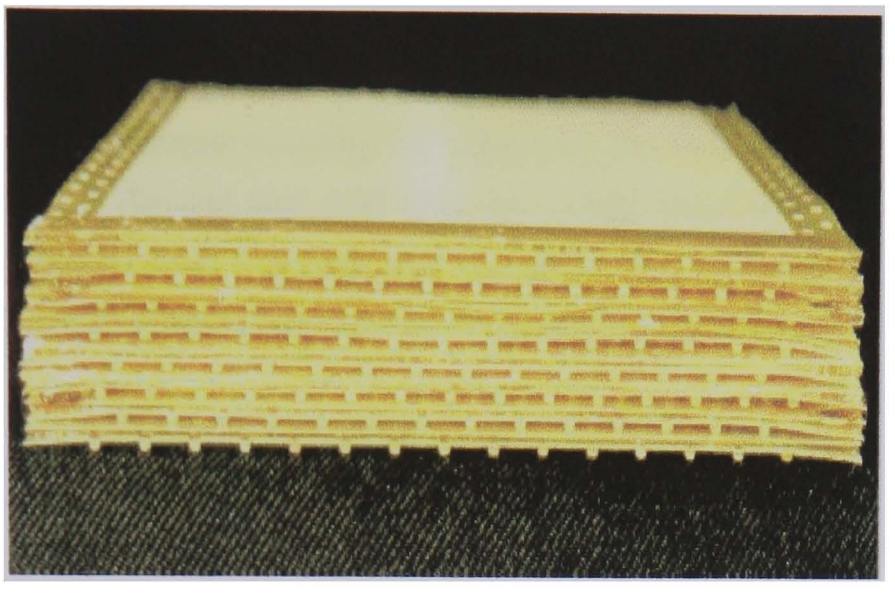

**Figure 4.1 Diagram of stacked PEEK films**

The polymer sheets were arranged in this manner, to ensure that a perfect cross flow was obtained and there was no mixing of the flows (hot and cold streams did not mix as they flowed through the heat exchanger). This was achieved by carefully sealing the edges of the sheets, such that successive sheets formed a cross corrugation. This means that the corrugations cut one another at right angles as they ran along the length of the heat exchanger, compressing several of the above sheets and sealing them to prevent any leakage. Sealing the edge of the sheets created the flow passage for each stream. This was done using a sealant (Araldite AV 119). An illustration of the sealed PEEK films is depicted in Figure 4.2 below.

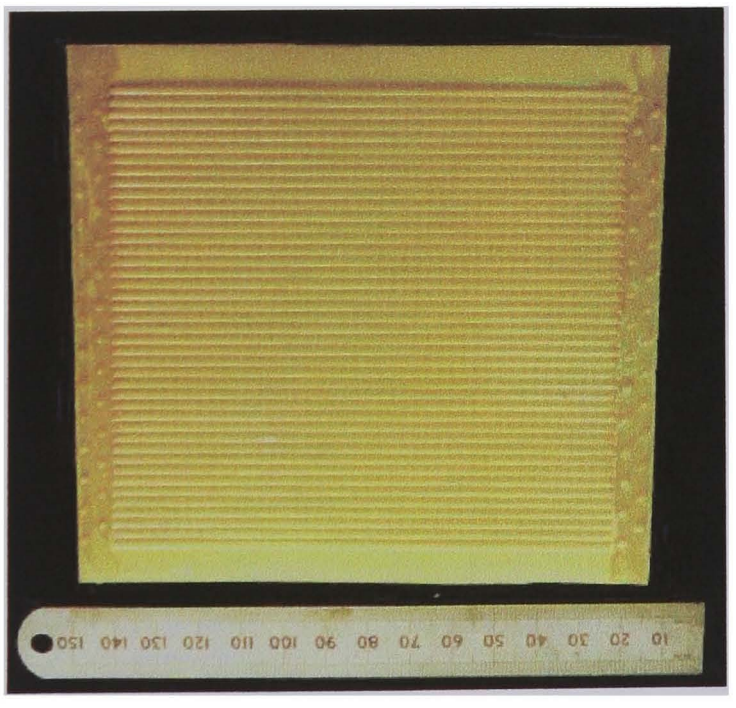

**Figure 4.2 Diagram of sealed PEEK films**

PEEK films are used because they can be easily corrugated and have excellent chemical, mechanical and thermal stability. They have a continuous service temperature of about 220°C, and can withstand a differential pressure of about 1000 kPa. The stacked and compressed films were then placed inside a perspex housing. By doing this, four isolated compartments, one each for the inlet and outlet of the hot and cold streams respectively, were formed. The heat loss through the walls of the perspex housing was negligible. A diagram of the square PFCHE is shown in Figure 4.3 and a schematic version is illustrated in Figure 4.4.

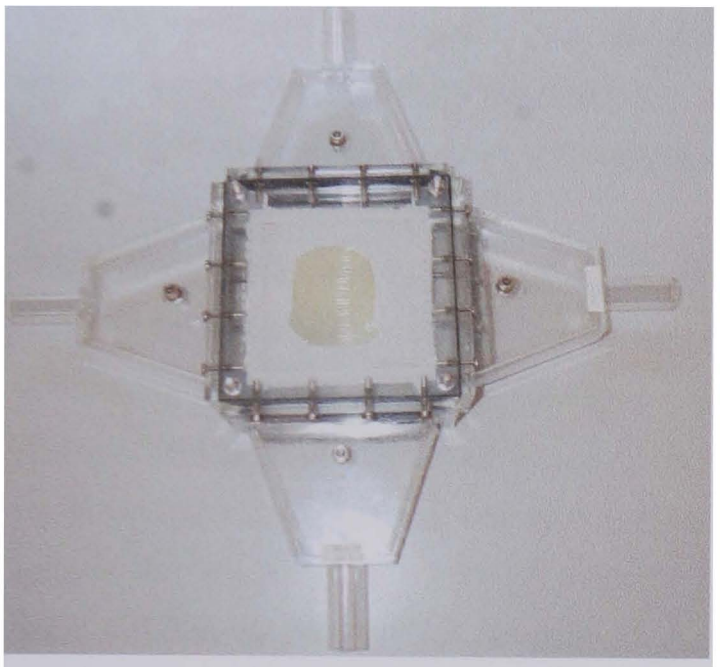

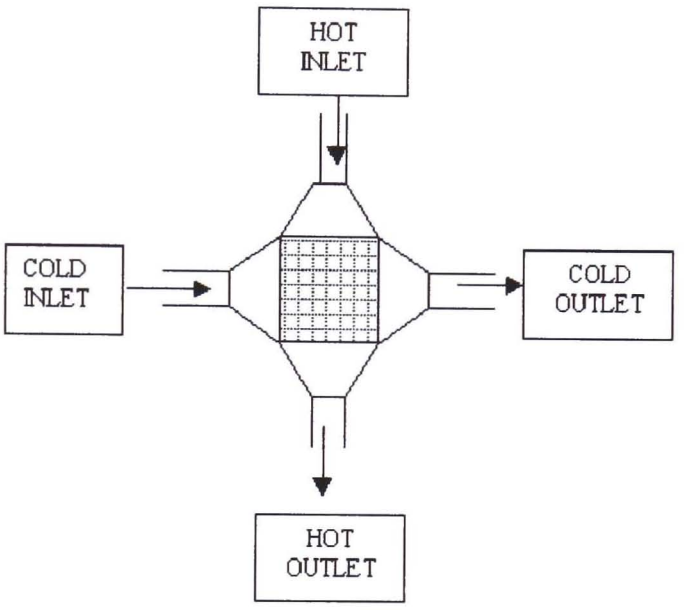


**Figure 4.3 Diagram of the square PFCHE** **Figure 4.4 Schematic of the square PFCHE**

In the next section, we go on to describe the procedures involved in conducting the experiments for the six fluid systems in the square PFCHE. We start with the air/air system, followed by the water/water system and then finally conclude with the glycerol-water mixtures/water systems.

*4.1.1 System: air/air*

For the air/air system, 5 corrugated PEEK sheets were used. Compressed air (275 kPa) from the main supply was used to feed both the hot and cold air streams. An electric heater was used to pre-heat the hot stream. Pipe work was constructed from 20 mm copper tubes and was adequately lagged. Volumetric flow rates were measured using Nixon rotameters (PVDF floats encapsulated with aluminium). Two different types were used having the range of (1-7 $m^3$/hr) and (5-50 $m^3$/hr) respectively. The range of air flow rates tested in this experiment was between 3-15 $m^3$/hr.The temperatures were measured at the inlet and outlet compartment for both streams. Inlet and outlet temperatures were measured using platinum resistance thermocouples (PRTs) having an accuracy of ±0.05°C.

Small holes were drilled in the four headers in which the thermocouples were inserted. At the inlet headers, the thermocouples were placed mid way down the header and as close as possible from the edge of the corrugated sheets, especially on the hot side, to prevent any errors in temperature measurements, arising due to heat losses from the walls of the header. At the outlet headers, the thermocouples were placed mid way down the header but not very close from the edge of the corrugated sheets. The thermocouples were positioned in the middle of the headers to minimise potential error due to the non-homogeneous temperature of the outlet stream. However, with this measurement procedure, the heat balance was not satisfactory for very low flow rates corresponding to Re<500. The turbulence inside the outlet headers was not enough to provide a uniform temperature. At higher flow rates, the air temperature was more uniform due to the better turbulence created.

The pressure drop across the exchanger was measured between the inlet and the outlet of each stream. Two pressure meters (2000 Series Manometer) having a range of 0-700 kPa, were connected to the exchanger by flexible tubes. The accuracy of the unit was ±0.1 kPa. The highest pressure drop recorded between the air streams was 15 kPa. The same procedure was used for each run. Both the hot and cold air streams were first set to the same flow rates. The system is then allowed to run for at least 1-2 hours, without any modification concerning flow rates and the electric heater, in order to achieve steady state. It was assumed that the steady state was established when the four temperatures did not fluctuate more than $\pm 0.05^{o}C$; equal to the thermocouple accuracy. Once the steady state was achieved, the inlet and outlet temperatures were measured using the four thermocouples inserted in the headers. The thermocouples were connected to a voltage display unit, where the conversion used was 0.025 V/ $1^{0}C$. Once all the experimental data were noted (flow rates, temperatures and pressure drops), the procedure was repeated over a range of flow rates, with a maximum of 15 $m^3/hr$. This was set to be the maximum limit in order to prevent any damage to the PFCHE, due to increased pressure drops.

The projected and real heat transfer areas of the unit are 0.05 $m^2$ and 0.1 $m^2$ respectively. The projected heat transfer area is defined as the heat transfer area of the PFCHE, when the corrugated sheets are not stretched. This area is the length multiplied by the width of sheets, multiplied by the number of sheets in the heat exchanger. On the other hand, the real heat transfer area is defined as the heat transfer area of the PFCHE, when the corrugated sheets are stretched. The real heat transfer area is the projected area multiplied by the extension factor (F). The extension factor is the difference between the projected and the real heat transfer area of one sheet. The calculation procedure in determining the extension factor is attached in Appendix C. A simplified flow diagram of the experimental set-up is shown below in Figure 4.5. In the next

section, we consider the experimental procedure for the water/water system in the square PFCHE.

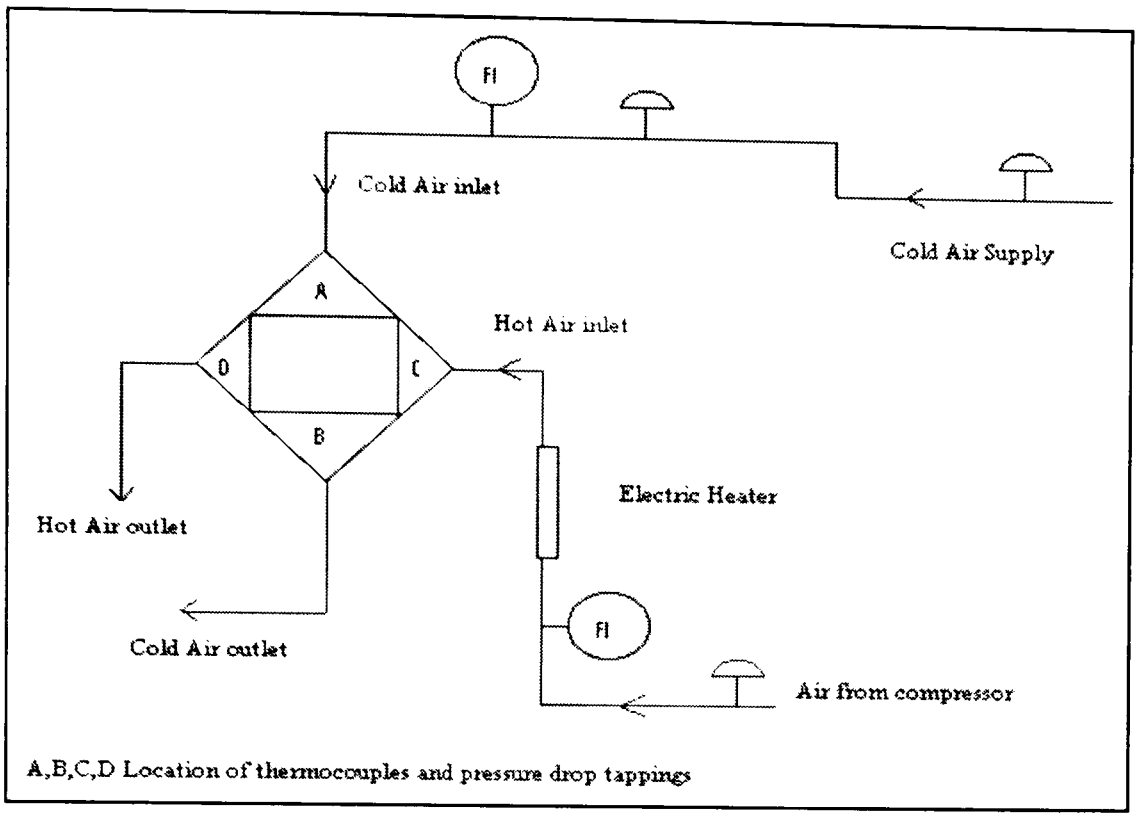


**Figure 4.5 Simplified flow diagram of the square PFCHE experimental set-up for the air/air system**

*4.1.2 System: water/water*

For the water/water system, (Jachuck and Ramshaw 1992) and the thickened water/water systems (Melendo 1996), 44 corrugated PEEK sheets were employed. The water flow rates were measured using '35S' type rotameters. The hot water supply was taken from a reservoir that included both a heater and a temperature controller. Hot water from the reservoir was supplied to the exchanger, by a pump that could develop a 9 m head. Tap water was used to supply the cold water stream. The inlet and outlet temperatures were monitored using thermocouples that were placed mid way down the exchanger stack, in the inlet and outlet chambers. K-type thermocouples were used and were dropped from the top of the chamber, and held in position by a thin glass tube. Temperatures were recorded by a digital recorder, which had an accuracy of $\pm 0.1^{\circ}C$. To measure the pressure drop across the heat exchanger, tappings in the form of glass tubes were taken from the inlet and outlet chambers. These were connected to a digital manometer by means of flexible tubes. The digital manometer had an accuracy of $\pm 0.01$ kPa. Having explained the air/air and water/water systems, we next proceed to describe the experimental procedures for the glycerol-water mixtures/water systems in the square PFCHE.

*4.1.3 System: glycerol-water mixtures/water*

Tests have been carried out with different concentrations of glycerol-water mixtures on one side of the heat exchanger and water on the other side, in order to evaluate the heat exchanger performance when working with more viscous fluids. The glycerol-water mixtures have higher Prandtl numbers (Pr) than the systems previously tested. Four different concentrations of glycerol-water mixtures have been tested corresponding to concentrations of 70%(w), 50%(w), 40%(w) and 30%(w) glycerol. The flow rate of tap water was held constant at about 8.2 l/min and acted as a cooling fluid. The glycerol-water mixture flow was varied depending on the concentration of glycerol, in order to avoid possible damage of the polymer matrix, which could occur when working with very viscous fluids at high flow rates. The glycerol-water mixture flow rates were measured using '24S' type rotameters. Although the flow rates for the runs with the different concentrations of glycerol were similar, there was a significant difference on the range of Re numbers calculated. This is due to the wide variation of viscosity ($\mu$) values for the different mixtures, which exerts a significant impact on the calculated Re number ($Re=\rho v d_h/\mu$). The inlet and outlet temperatures and the pressure drop readings, were measured using the same equipment and technique, as adopted in the water/water system. A simplified flow diagram for the water/water and glycerol-water mixtures/water experiments is shown below.

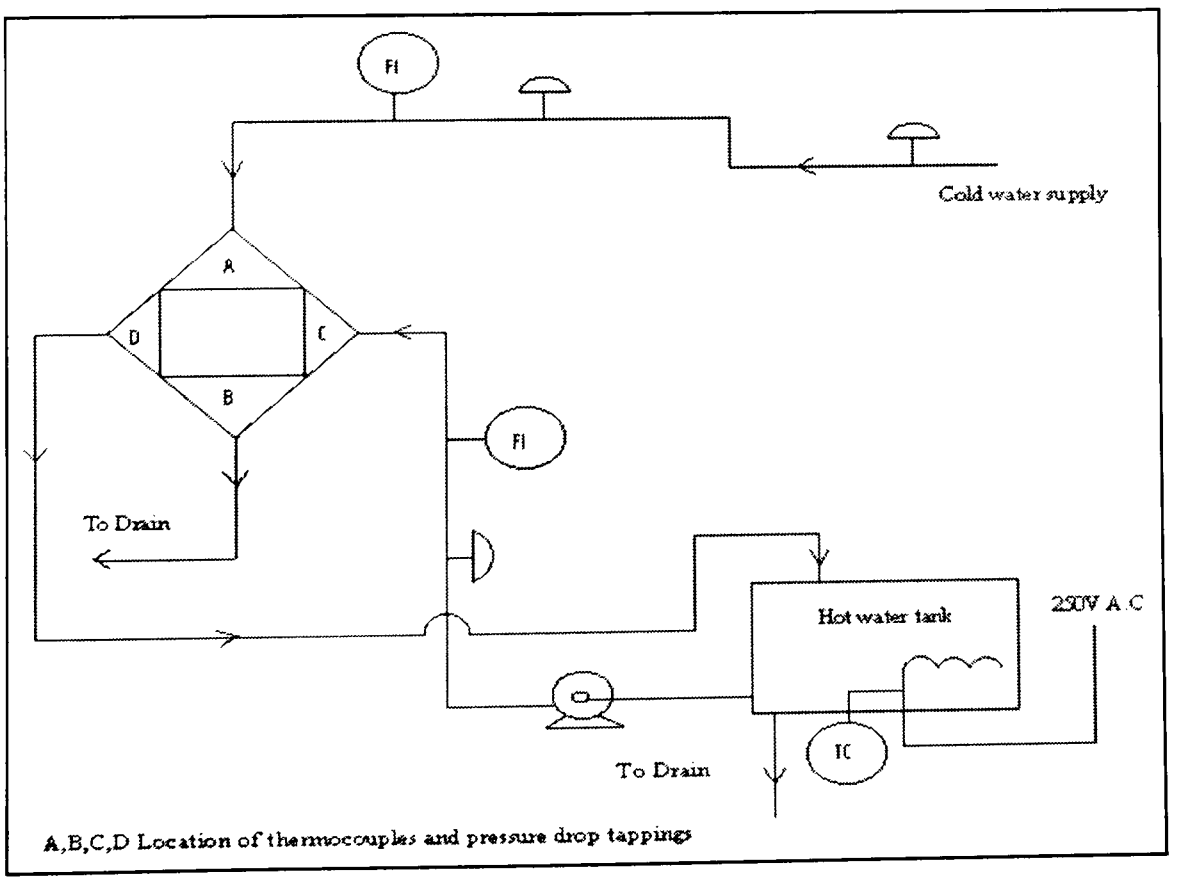


**Figure 4.6 Simplified flow diagram of the square PFCHE experimental set-up for the water/water and glycerol-water mixtures/water systems**

Using the experimental data recorded in the form of temperature differences ($\Delta T$) and pressure drops ($\Delta P$); attached in Appendix D, the heat transfer and pressure drop analysis was carried out using the E-NTU method. The steps involved in obtaining the design correlations (Jh and f) are shown in the following section.

## 4.2 Development of PFCHE design correlations

As the design equations for predicting heat transfer and pressure drop characteristics of heat exchangers are generally presented in the form of Jh (Colburn factor) and f (friction factor) correlations, in this study the experimental results are also summarised by such correlations. The correlations (Jh and f) are expressed as a function of Re numbers as shown below.

$$Jh = St\ Pr^{2/3} = a\ Re^{b} \qquad (4.1)$$

$$f = 2\ \Delta P\ d_h / 4\rho\ v^2 L = a\ Re^{b} \qquad (4.2)$$

where a and b are constants depending on the kind of surface and flow character

The formulae used for the Jh and f correlations above, are the same as outlined in Chapter One. The first step in obtaining the design correlations is to develop Jh and f curves, by plotting the factors against a range of Re numbers. We can only do this, when both factors have been determined using experimental data and then incorporating them in expressions (4.1) and (4.2). Once these plots are established, we then proceed to obtain the expressions for the best fitting curves through the data points using Microsoft Excel. In the next two sections, we attempt to show how the Jh and f factors are calculated, by describing the heat transfer and friction factor calculation procedures for the air/air system in the square PFCHE.

### *4.2.1 Heat transfer calculation procedure*

Using the experimentally recorded temperatures, the thermal effectiveness (E) is first calculated for different flow rates, corresponding to a Re number range of 500<Re<2500.

$$E = Q_{act}/Q_{max} \qquad (4.3)$$

Where $Q_{act}$ = actual heat transfer achieved, either using $Q_h$ or $Q_c$

= (m cp $\Delta$T) for either the hot or cold stream

$Q_{max}$ = maximum heat transfer that can be achieved

= $(m\ cp)_{min}\ \Delta T_{max}$

$(m\ cp)_{min}$ = the minimum heat transfer capacity, either using the hot or cold stream

$\Delta T_{max}$ = $Th_{in} - Tc_{in}$

Once the thermal effectiveness has been determined, the NTU is then determined using the effectiveness expression shown below for a cross-flow heat exchanger where both fluids are unmixed (Baclic 1978).

$$E = 1 - \exp\left[-(w+1)NTU\right]\left[I_o\left(2NTU\sqrt{w}\right) + \sqrt{w}\, I_1\left(2NTU\sqrt{w}\right) - \left(\frac{1-w}{w}\right)\sum_{n=2}^{\infty} w^{n/2}\, I_n\left(2NTU\sqrt{w}\right)\right]$$

When $w = C_{min}/C_{max} = 1$, the expression simplifies to

$$E = 1-\exp(-2\ NTU)\left[I_o(2\ NTU)+I_1(2\ NTU)\right] \qquad (4.4)$$

Where $I_n$ = modified Bessel function (I) of n order

The modified Bessel functions and integer order appearing in the formula are calculated using Microsoft Excel. The NTU is then determined by matching the effectiveness value calculated in equation (4.3) into equation (4.4), using the goal seek function. Following this, the overall heat transfer coefficient (U) was consequently determined using equation (4.5) below.

$$NTU = UA/C_{min} \qquad (4.5)$$

Since the mass flow rates were equal for both air streams, and the corrugated sheets were arranged so that the core was symmetrical about the diagonal of the frame, the heat transfer properties, hydraulic diameter and free flow area were considered to be the same for both streams. Bearing this in mind, the film heat transfer coefficient and the Jh factor were calculated by using the following simplified expressions:

$$1/U = 2/h + t/k_{film} \qquad (4.6)$$

$$Jh = St\ Pr^{2/3} = (h\ d_h\ Pr^{-0.33})/k\ Re \qquad (4.7)$$

Prior to using equation (4.7), the hydraulic diameter was first determined using equation (4.8) below, giving a value of 2 mm. The hydraulic diameter calculation is attached in Appendix C.

$$d_h=( 4 A_{ff} L)/A \qquad (4.8)$$

Once the Jh factors were determined, they were then plotted as a function of Re number. The heat balance errors for the reported data were less than 10%, and all the results were based on the projected heat transfer area. To convert the values of U and h to the equivalent values based on the real heat transfer area, they should be multiplied by F=1.9, where F is the ratio of the real and projected heat transfer areas (see Appendix C). The cross-corrugated exchanger core is rather complicated and the details of flows are really complex. In order to simplify the heat transfer calculations, it was assumed that the heat loss through the walls of the perspex frame (33 mm thick) was negligible, and that the hot and cold air flows did not mix as they flowed through the heat exchanger core. In the following section, we look at how the friction factors (f) are calculated.

### *4.2.2 Friction factor calculation procedure*

Using the experimental pressure drops taken over the same range of air flow rates ($500<Re<2000$) as for the heat transfer, the friction factors were calculated by incorporating the pressure drop values in the expression below.

$$f = (2 \Delta P d_h)/ (4 \rho v^2 L) \qquad (4.9)$$

Apart from the Jh and f factors, the pumping power and goodness factor are also evaluated to enable an accurate prediction of the PFCHE performance, since they involve both heat transfer and pressure drop characteristics. The method for calculating the pumping power is described in the following section.

### *4.2.3 Pumping power calculation procedure*

The energy required to force the fluid through the heat exchanger matrix, known as the pumping power (E) is determined using the equation below.

$$E = \tau \ v \qquad (4.10)$$

The wall shear stress ($\tau$), is calculated using equation (4.11) as follows.

$$\tau = 0.5\, f\, \rho\, v^2 \qquad (4.11)$$

Finally, we consider the steps to evaluate the goodness factor (Jh/f) for the square PFCHE. The goodness factor is the last of the four performance evaluation methods used in the unit.

*4.2.4 Goodness factor calculation procedure*

The goodness factor (Jh/f) provides a measure of the thermal efficiency of the square PFCHE, and can be determined by calculating the ratios of the Jh and f factors previously determined. In the next section, we describe in detail the experimental results for each of the six fluid systems investigated in the square PFCHE. This involves the plots for the four performance evaluation methods (Jh, f, E and Jh/f), outlined in the previous sections.

**4.3 Experimental results**

The details of the 6 different fluid systems tested in the square PFCHE, are shown in Table 4.1.

| System | Pr | Re range | Flow rate ($m^3$/hr) |
|---|---|---|---|
| air/air | 0.7 | 510<Re<2540 | 3-15 |
| water/water | 7 | 87<Re<235 | 0.44-1.17 |
| (30% glycerol + water mixture/water) | 19 | 19<Re<78 | 0.22-0.90 |
| (50% glycerol + water mixture/water) | 30 | 12<Re<44 | 0.20-0.76 |
| (60% glycerol + water mixture/water) | 49 | 8<Re<24 | 0.21-0.66 |
| (70% glycerol + water mixture/water) | 192 | 2<Re<5 | 0.18-0.44 |

**Table 4.1 Details on the six fluid systems tested on the square PFCHE**

The experimental results for the air/air, water/water and four glycerol-water mixtures/water systems in the square PFCHE are disclosed in this section following the order shown above. We begin by describing the results for the air/air system.

*4.3.1 System: air/air*

The experimental results for the air/air system, involves five different plots. These are each explained in turn, following the order listed below.

(i) Colburn factor (Jh)
(ii) Heat balance error (HBE)
(iii) Friction factor (f)
(iv) Pumping power (E)
(v) Goodness factor (Jh/f)

In addition, a section involving a flow visualisation study is also included to show that the PFCHE achieves good mixing in laminar flows due to the presence of developing flow along the corrugations. This consequently leads to heat transfer enhancement for the unit.

4.3.1.1 Colburn factor (Jh)

From Figure 4.7 below, it can be seen that Jh decreases as the Re increases. This trend is expected as shown in equation (4.7), where Jh is inversely proportional to Re. The curve obtained from the experimental values plotted, gives a good fit to the experimental data measured. This is because the Jh experimental values over the entire Re range investigated, does not deviate far from the curve generated. The equation for the best fitting curve was generated using Microsoft Excel. The Jh correlation developed is as follows:

$Jh = 2.0097\ Re^{-0.7644}$ for $510<Re<2540$

Looking at the graph more critically, a slight deviation occurs at Re = 510, 680, 1349, 1517 and 1691, whereby these five data plots do not fall exactly on the curve. This occurrence maybe due to the equipment uncertainty involved, as shown in Chapter Three.

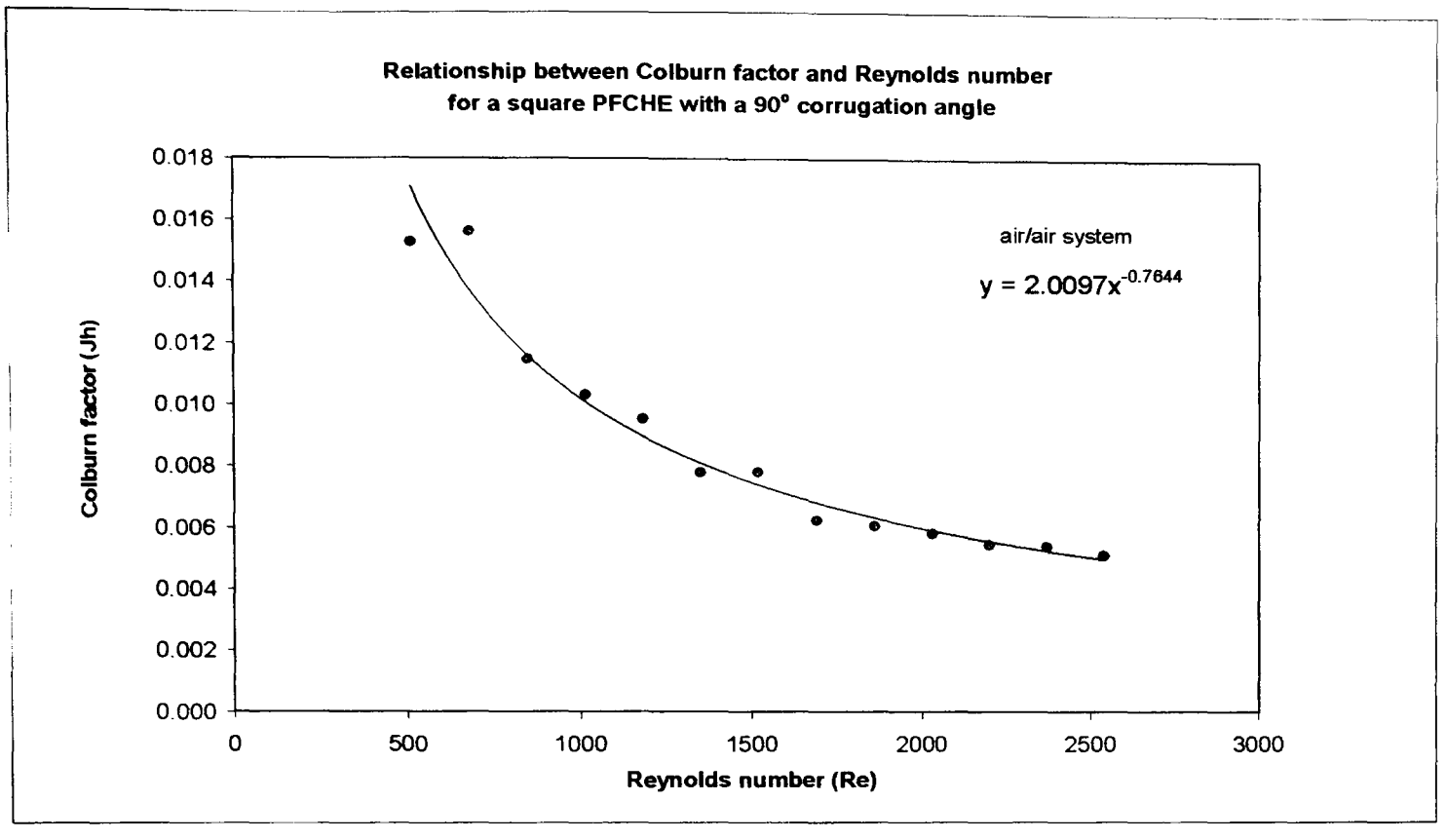


**Figure 4.7 Graph of Colburn factor (Jh) vs. Reynolds number (Re) for a square PFCHE in an air/air system**

The heat balance errors for the range of air flow rates used are investigated in the next section.

4.3.1.2 Heat balance error (HBE)

Figure 4.8 below, shows the heat balance errors for the range of air flow rates tested in the square PFCHE. Overall, it clearly shows that the heat balance errors are within 10% for all air flow rates. Looking closely, it can be noted that the errors exceed 5% for five different Re values, which are similar to the Re values that deviate from the Jh curve earlier.

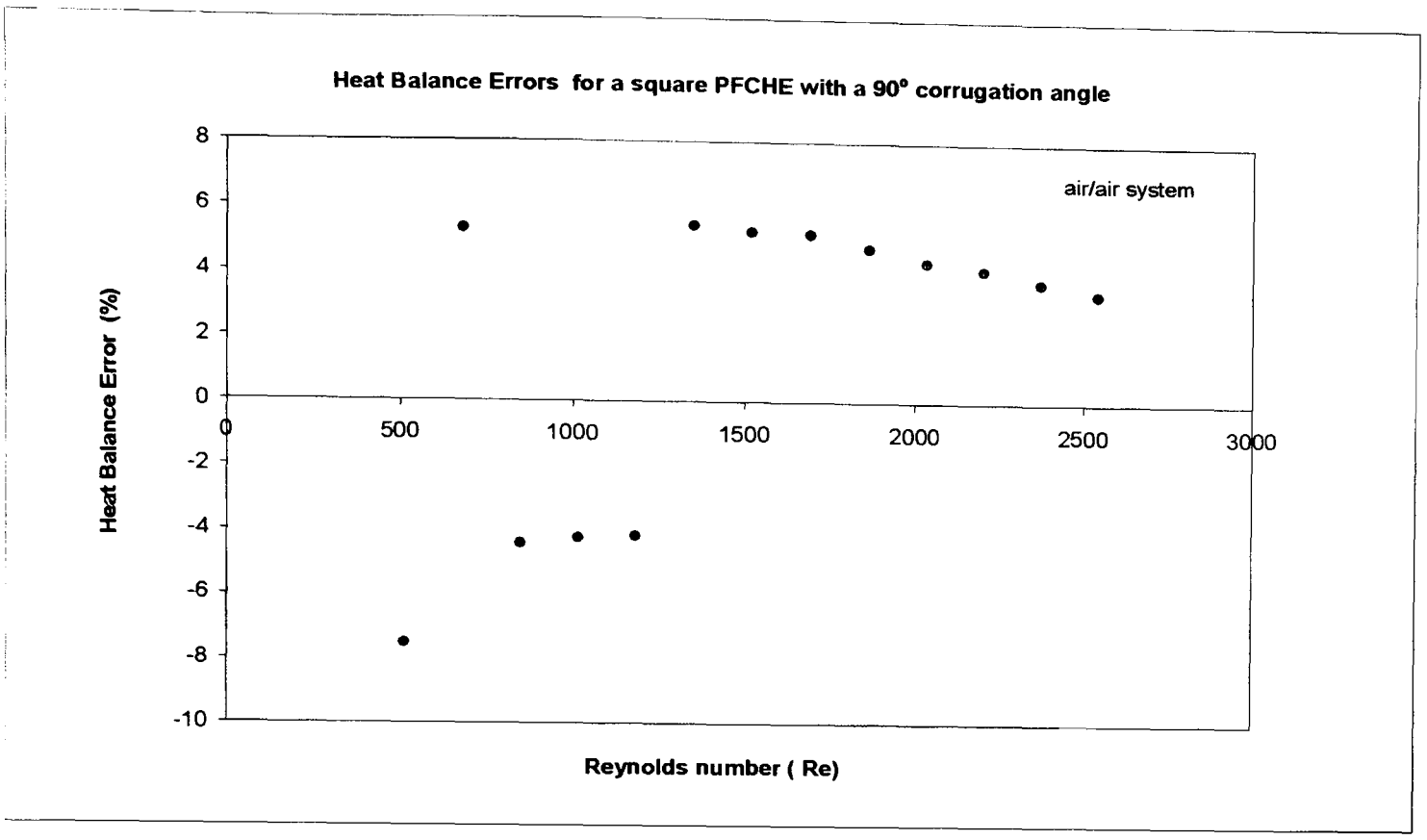


**Figure 4.8 Graph of heat balance error (%) vs. Reynolds number (Re) for a square PFCHE in an air/air system**

These higher heat balance errors will cause an inaccuracy towards the calculation of the heat exchanger effectiveness, which will ultimately lead to less accurate Jh values. However, it should be noted that the deviation of the data points from the Jh curve is caused mainly by equipment uncertainty, which has been discussed in Chapter Three. Next, we consider the friction factor plot.

### 4.3.1 3 Friction factor (f)

From the pressure drops measured for the range of air flow rates tested, the friction factors were calculated and plotted as a function of Re, as shown in Figure 4.9 below. The general trend observed from the graph is that the friction factor decreases as Re increases, thus abiding to the relationship shown in equation (4.9). From this equation, it can be seen that the friction factor is inversely proportional to the square of the fluid velocity (v). Therefore since ($Re = \rho v d_h/\mu$), it is shown through this equation that the friction factor is inversely proportional to the Re number. The best fitting curve for the friction factor data points is generated using Microsoft Excel. The friction factor correlation developed is as follows:

$f = 0.5992\ Re^{-0.1697}$ for $510<Re<2540$

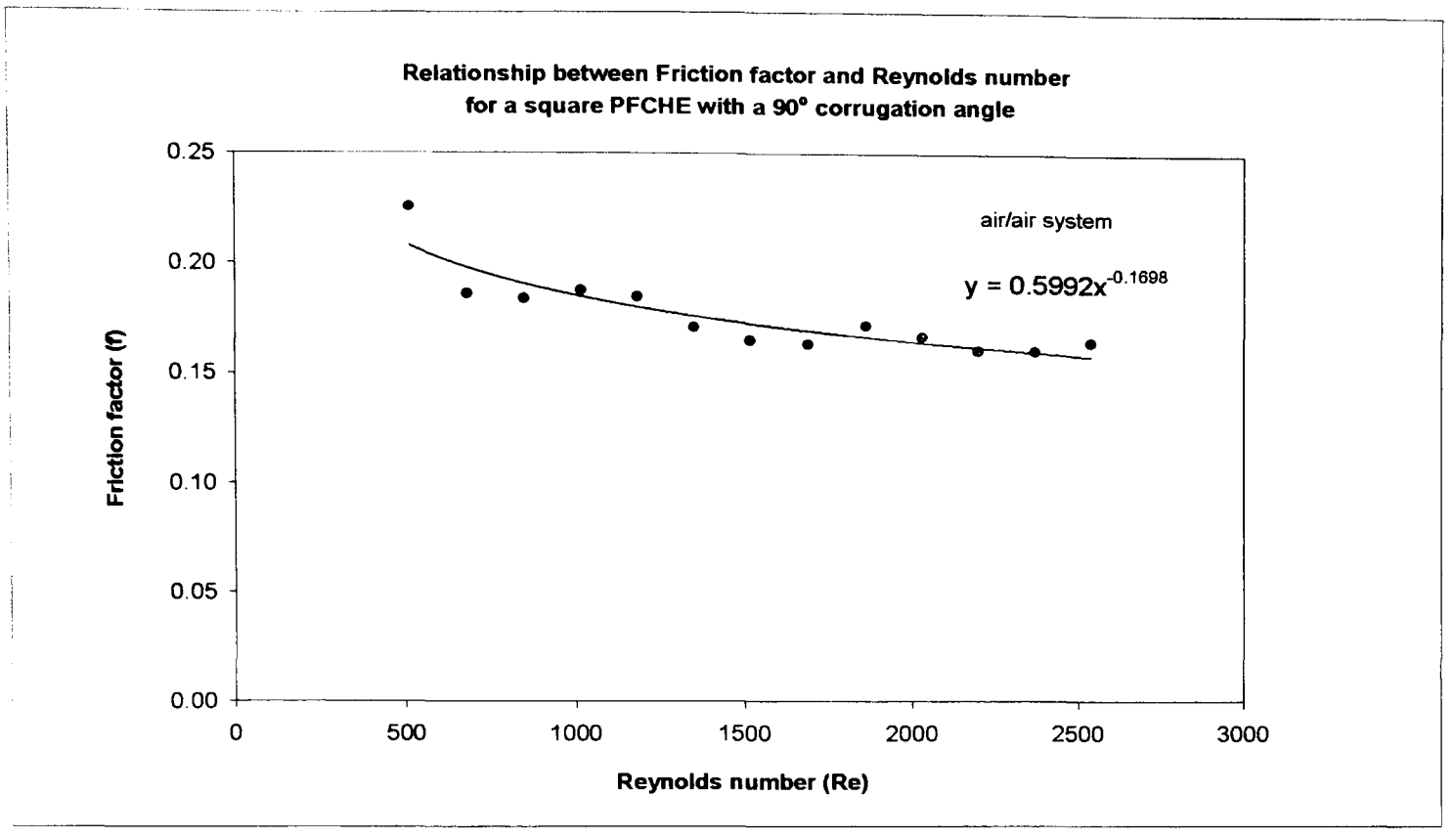


**Figure 4.9 Graph of friction factor (f) vs. Reynolds number (Re) for a square PFCHE in an air/air system**

There is only a small scatter of the friction factor data points from the curve generated, and hence the pressure drop measurements are deemed to be accurate. No apparent outlying points are observed throughout the range of air flow rates tested. In the following section, we proceed to look at the pumping power plot.

4.3.1.4 Pumping power (E)

It is clearly shown from Figure 4.10 below, that the heat transfer coefficient increases with pumping power. This trend is expected as h is proportional to Re, and E is proportional to $Re^3$ as shown in equations (4.12) and (4.13) below. These expressions can be derived from equations (4.7) and (4.10) shown earlier.

$$h = \frac{Jh\,k\,\mathrm{Re}}{d_h\,\mathrm{Pr}^{-0.33}} \qquad (4.12)$$

$$E = 0.5\,\frac{\mu^3}{\rho^2}\,\frac{1}{d_h{}^3}\,\mathrm{Re}^3\,f \qquad (4.13)$$

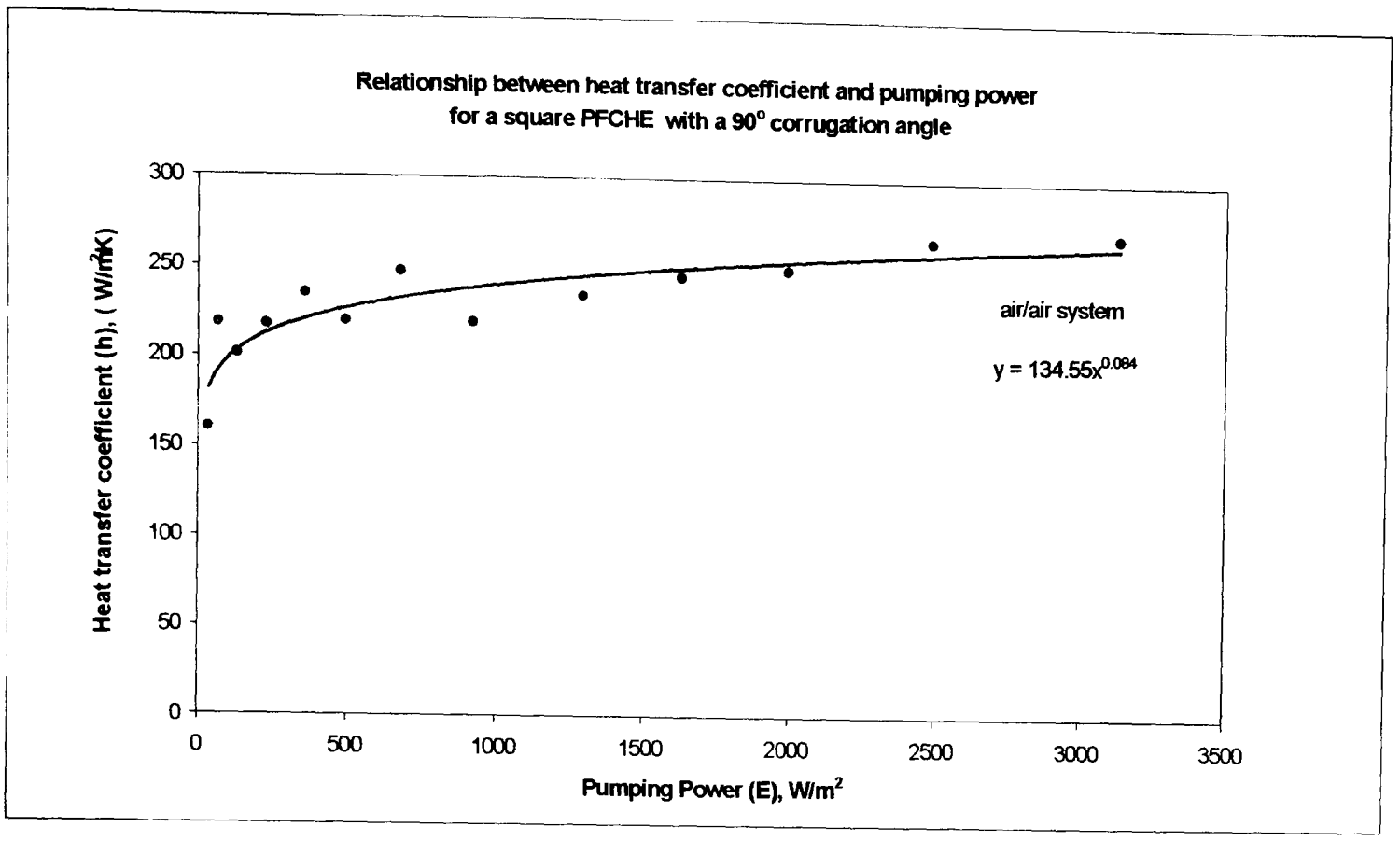


**Figure 4.10 Graph of heat transfer coefficient (h) vs. pumping power (E) for a square PFCHE in an air/air system**

To get an expression relating h and E, we substitute the Jh and f correlations found earlier into equations (4.12) and (4.13) and then combine the equations. The Jh and f correlations for the air/air system are as follows.

$$Jh = 2.0097\ Re^{-0.7644} \qquad (4.14)$$

$$f = 0.5992\ Re^{-0.1698} \qquad (4.15)$$

We then obtain the following expression,

$$h = \frac{6.707\ E\ k^{0.67} cp^{0.33}}{\mu^{0.07} d_h^{0.6}\ \rho^{0.6}\ v^{2.6}} \qquad (4.16)$$

Logically more heat would be transferred from the fluids, when more energy is expended to overcome fluid friction across the heat exchanger. It is evident that higher heat transfer coefficients can be obtained at the expense of higher pumping power losses. However, the heat transfer coefficient value hits a plateau and after that an increase in pumping power would not greatly affect the heat transfer coefficient value. The point at which the plateau occurs is known as the optimum operating point on the h-E curve. From Figure 4.10, it can be seen that the heat

transfer coefficient increases and then gradually levels out. The optimum operating point for the air/air system cannot be accurately established, as the exponential increase does not level out completely at the highest pumping power depicted in the plot. Nevertheless, the heat transfer coefficient is not expected to increase any further beyond a pumping power value of 3500 $W/m^2$.

A design engineer considering the use of a PFCHE, can theoretically use the pumping power plot to determine optimum exchanger performance. However, it should be remembered that the chosen operating point will also depend on other factors such as, for example, maximum allowable pressure drop, desired flow rate, limits imposed by heat exchanger fabrication plus cost of energy and temperature limits. In the next section, we finally consider the last performance evaluation plot for the air/air system, which is the goodness factor plot.

4.3.1.5 Goodness factor (Jh/f)

The goodness factor gives a measure of the thermal efficiency of the heat exchanger. Figure 4.11 below, shows that the thermal efficiency decreases at higher Re numbers. This can be due to the increase in velocity. Although high velocities enhance heat transfer due to the turbulence created, nevertheless a high pressure drop penalty occurs, which leads to high friction factors.

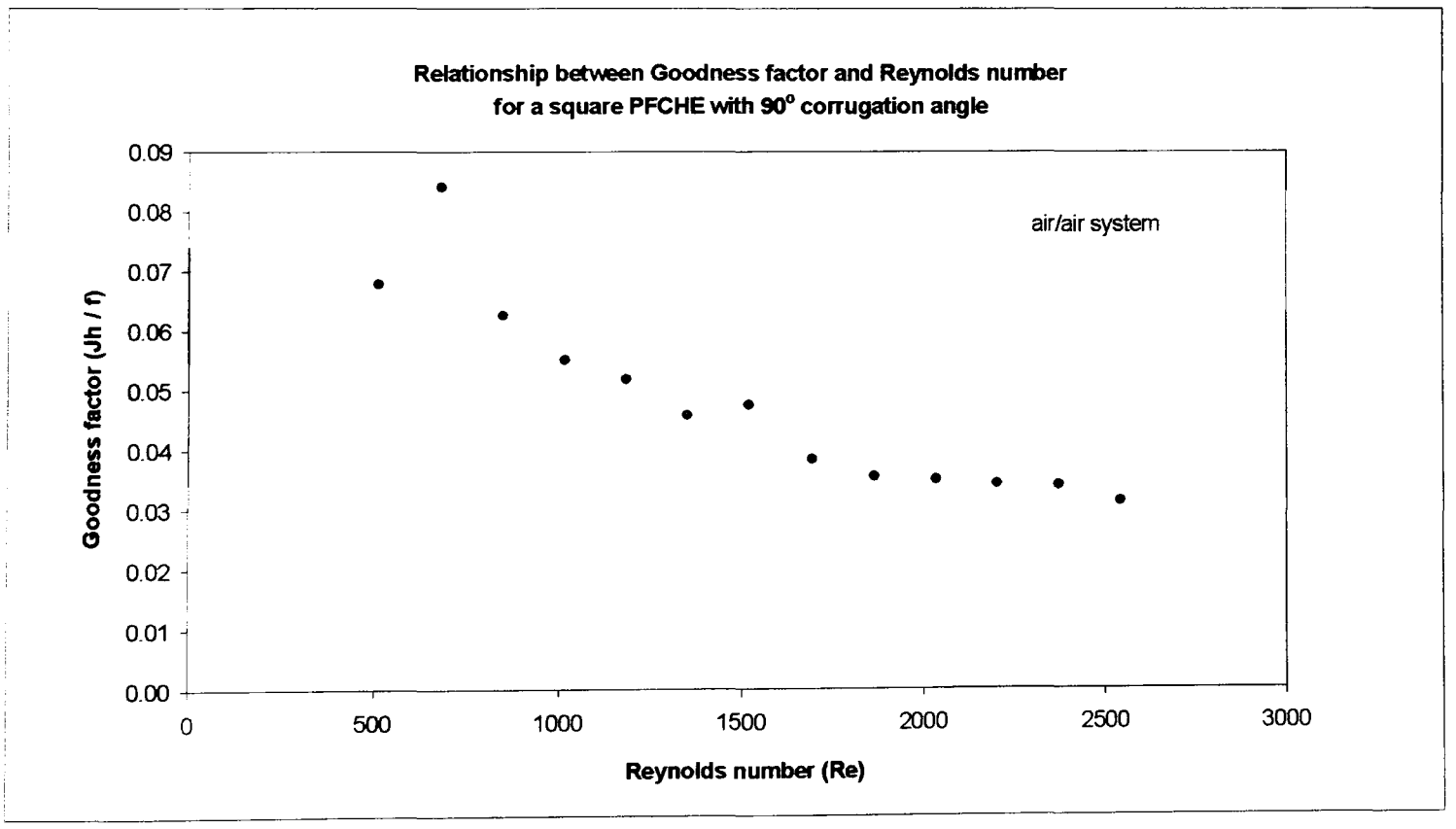


**Figure 4.11 Graph of goodness factor (Jh/f) vs. Reynolds number (Re) for a square PFCHE in an air/air system**

Therefore from the graph above, it can be concluded that at high Re numbers, the friction factors obtained outweighs the heat transfer benefits. Figure 4.11 shows that the thermal efficiency is better at lower Re numbers. This is a special feature achieved by the PFCHE due to its sinusoidal corrugations. The flow boundary layers are broken down as fluid moves across the crests and troughs of the corrugations. This 'massaging effect' on the fluid flow achieves good mixing characteristics comparable to that of turbulent flow. Therefore even at low Re numbers, heat transfer is enhanced. This can be supported by the findings in a flow visualisation study as shown in the following section.

#### 4.3.1.6 Flow visualisation study

A square corrugated glass matrix module is used to replicate the PFCHE, for the flow visualisation experiment. The mixing characteristics observed in this experiment support the fact that good mixing is indeed achieved for all laminar fluid flows in the PFCHE. The unit, as shown in Figure 4.12 below, is made up of two corrugated glass blocks placed 90° to each other and housed in a perspex frame. Methylene blue dye was used as a tracer to study the flow patterns in the module. The mixing patterns between the dye and water flows were observed over a range of laminar flows. Good mixing was indicated by the dispersion of the dye flow in the matrix. In general, faster dispersion occurred at higher Re numbers in the laminar region. This is shown in the schematic diagrams depicted in Figure 4.13.

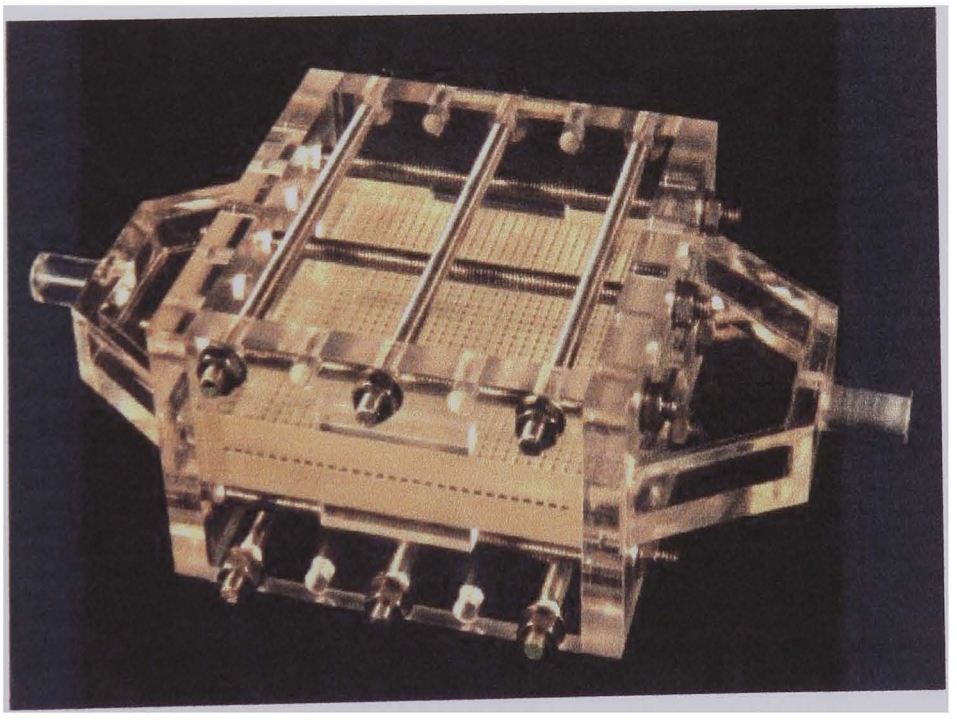

**Figure 4.12 Diagram of glass matrix module**

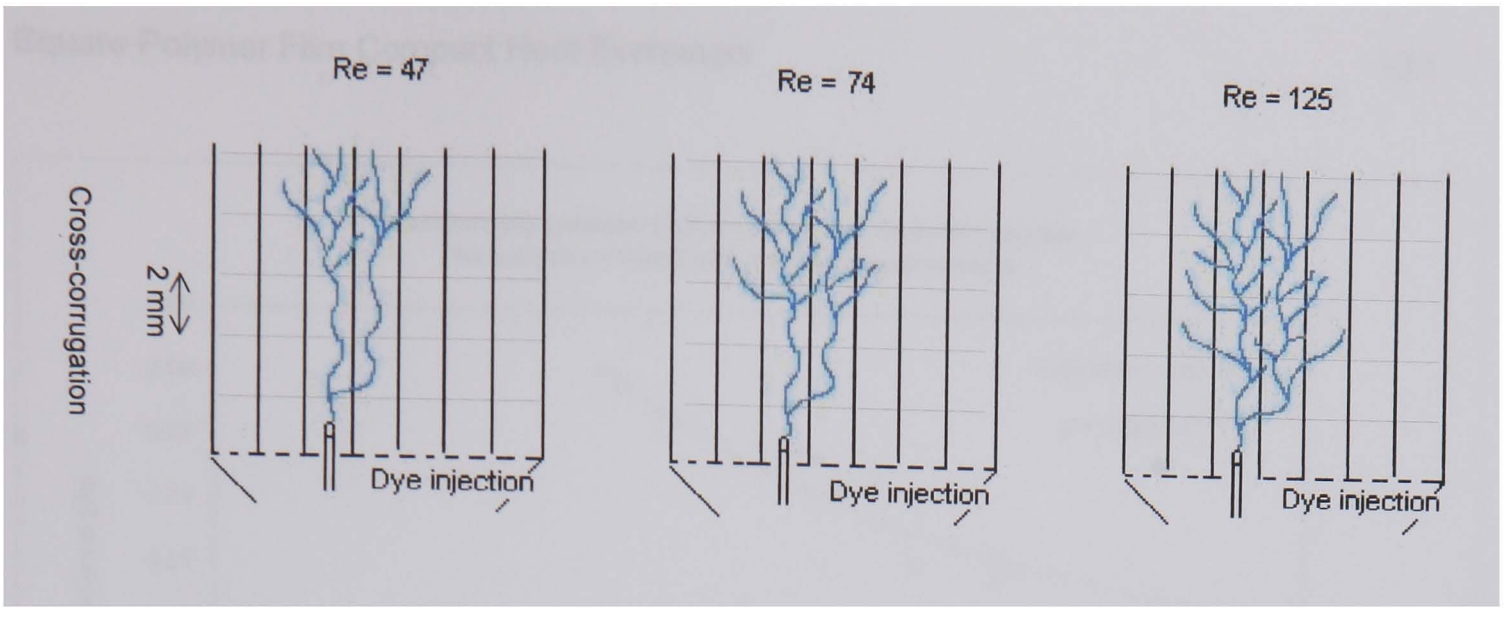


**Figure 4.13 Laminar flow mixing patterns in the glass matrix module**

Using the flow visualisation experiment, a better appreciation of the mixing characteristics for laminar flow in the PFCHE is achieved. The good degree of mixing obtained is associated with the heat transfer capability of the unit. More detailed work showing the good mixing obtained in the glass matrix module has been conducted by Hall et al. (1999). In the following section, we consider the experimental results for the water/water system in the square PFCHE.

*4.3.2 System: water/water*

The experimental results for the water/water system, involves six different plots as shown below.

(i) Colburn factor (Jh)
(ii) Heat balance error (HBE)
(iii) Friction factor (f)
(iv) Pumping power (E)
(v) Goodness factor (Jh/f)
(vi) Heat transfer coefficient (h)

These experimental plots will be explained in the order listed above.

4.3.2.1 Colburn factor (Jh)

From the graph below, the general trend observed is the same as the air/air system in the previous section, whereby Jh decreases as the Re increases. Nevertheless, scatter of data does occur from this proportional trend. The scatter that occurs in the water/water system is more pronounced than the air/air system. This can be due to the higher relative uncertainty at low water flow rates. To overcome this, experimental readings (temperatures and pressure drops) are repeated over the low water flow rates to decrease the errors generated and consequently optimise the accuracy of the Jh correlation developed. The Jh correlation is developed by fitting the best curve through the data points, which is executed using Microsoft Excel.

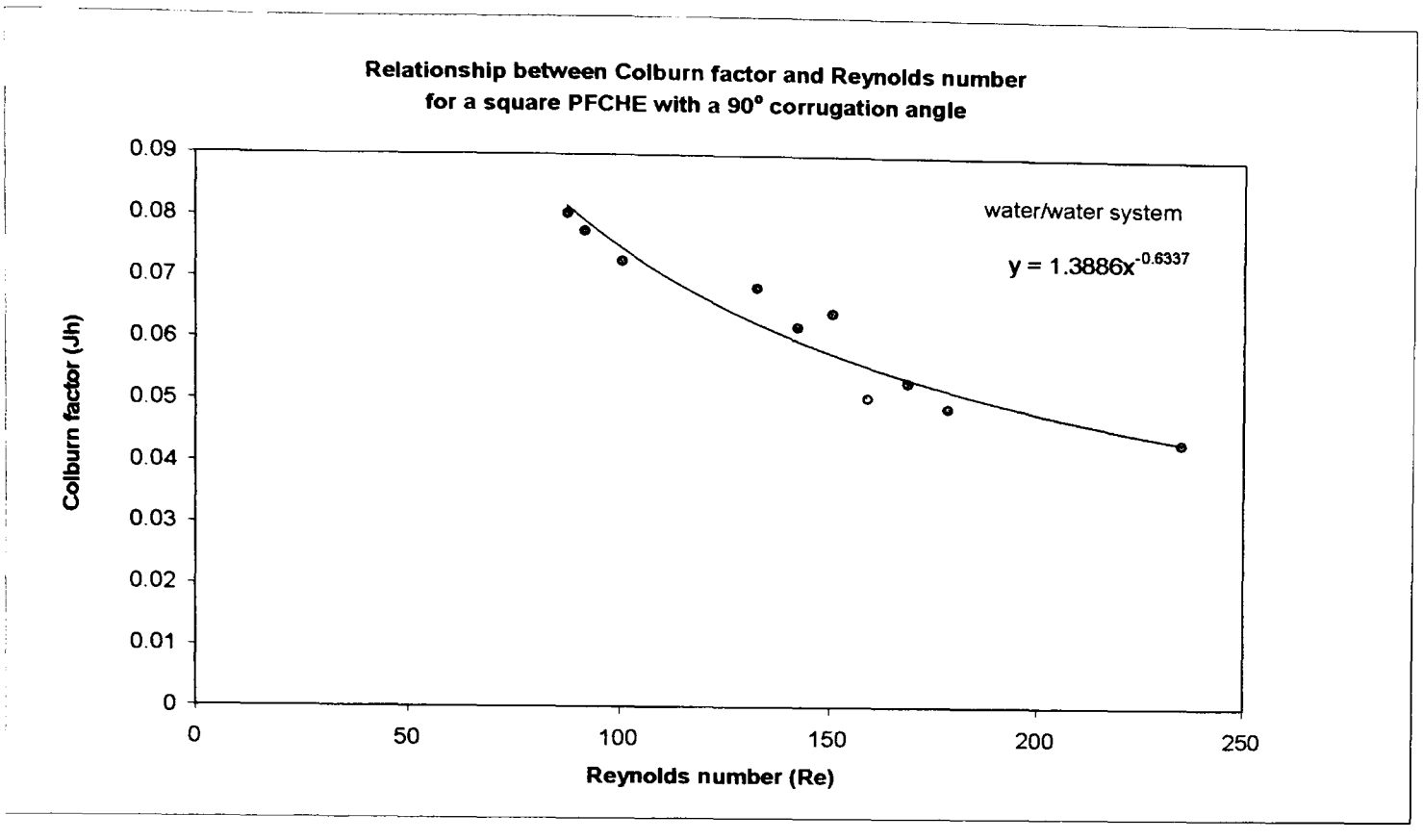


**Figure 4.14 Graph of Colburn factor (Jh) vs. Reynolds number (Re) for a square PFCHE in a water/water system**

The correlation developed is as follows:

$Jh = 1.3886\ Re^{-0.6337}$ for $87<Re<235$

To evaluate the experimental measurements obtained, which is to check whether they can be used towards the development of the Jh curve, a heat balance is conducted. The heat balance errors are calculated from the four inlet and outlet, hot and cold water temperatures, over the range of water flow rates tested. The data points for the Jh curve have heat balance errors less than 10%, which makes them acceptable. This is shown in the following section.

4.3.2.2 Heat balance error (HBE)

From Figure 4.15 below, it can be seen that the water flow rates tested in the PFCHE, have heat balance errors less than 10%. This shows that there is indeed a negligible heat loss from the unit, thus justifying that the Jh correlation generated from the experimental data is acceptable.

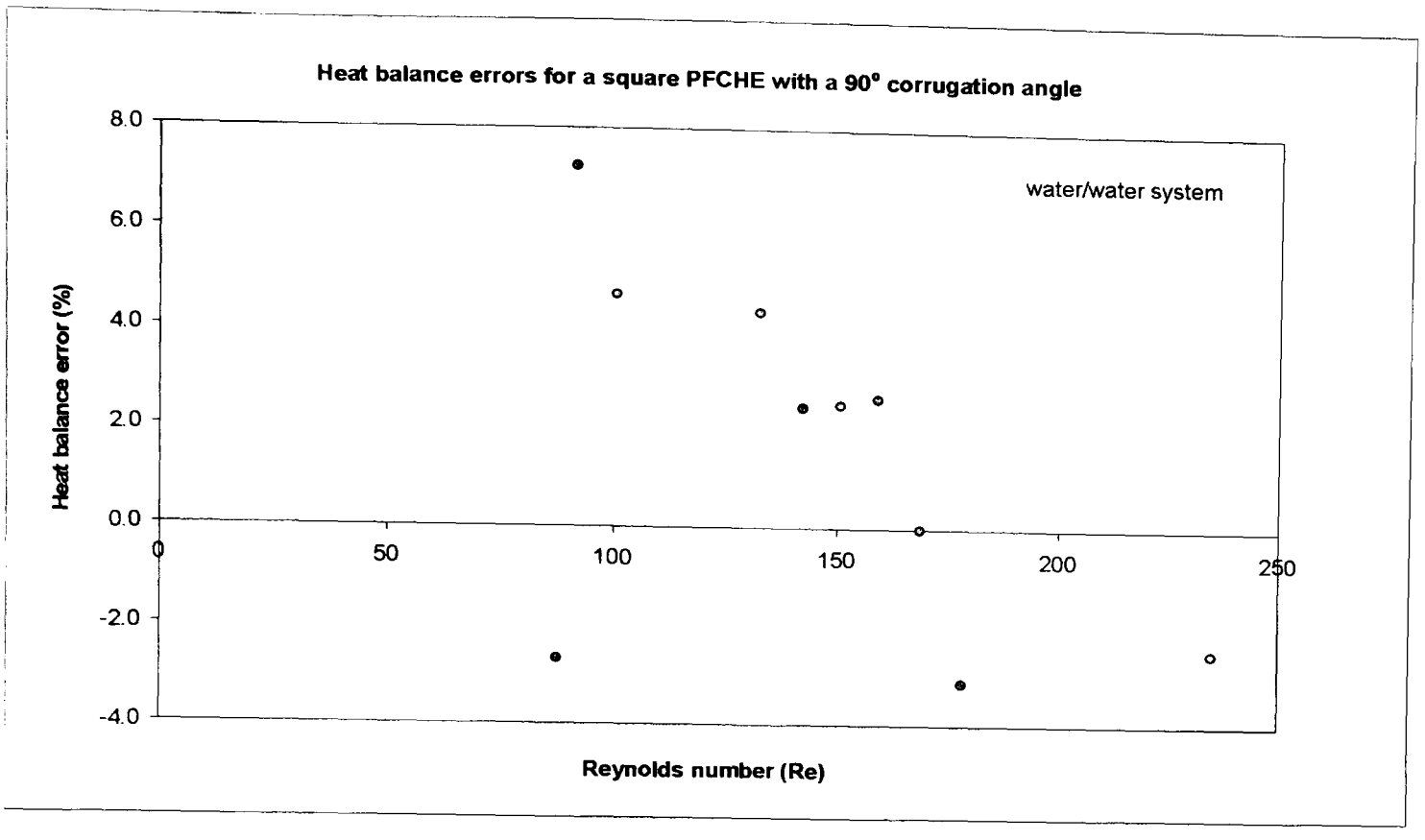


**Figure 4.15 Graph of heat balance error (%) vs. Reynolds number (Re) for a square PFCHE in a water/water system**

We now proceed to explain the friction factor plot.

4.3.2.3 Friction factor (f)

The general trend observed is that the friction factor decreases as the Re increases. This trend is similar to the friction factor plot for the air/air system. Hence, this observation also abides to the friction factor definition, whereby the friction factor is inversely proportional to the velocity and consequently the Re number. The f correlation developed is as follows:

$f = 32.797\ Re^{-0.7192}$ for $87<Re<235$

From Figure 4.16, it can be seen that there is negligible deviation or scatter of data present, which leads to a tight distribution band. Therefore, this indicates that the experimental pressure drops recorded are accurate and can be used towards the calculation of the friction factors. The pressure drops measured, varied between 0.1 to 1.2 kPa over the range of water flow rates tested. Following this, we next consider the pumping power plot for the water/water system.

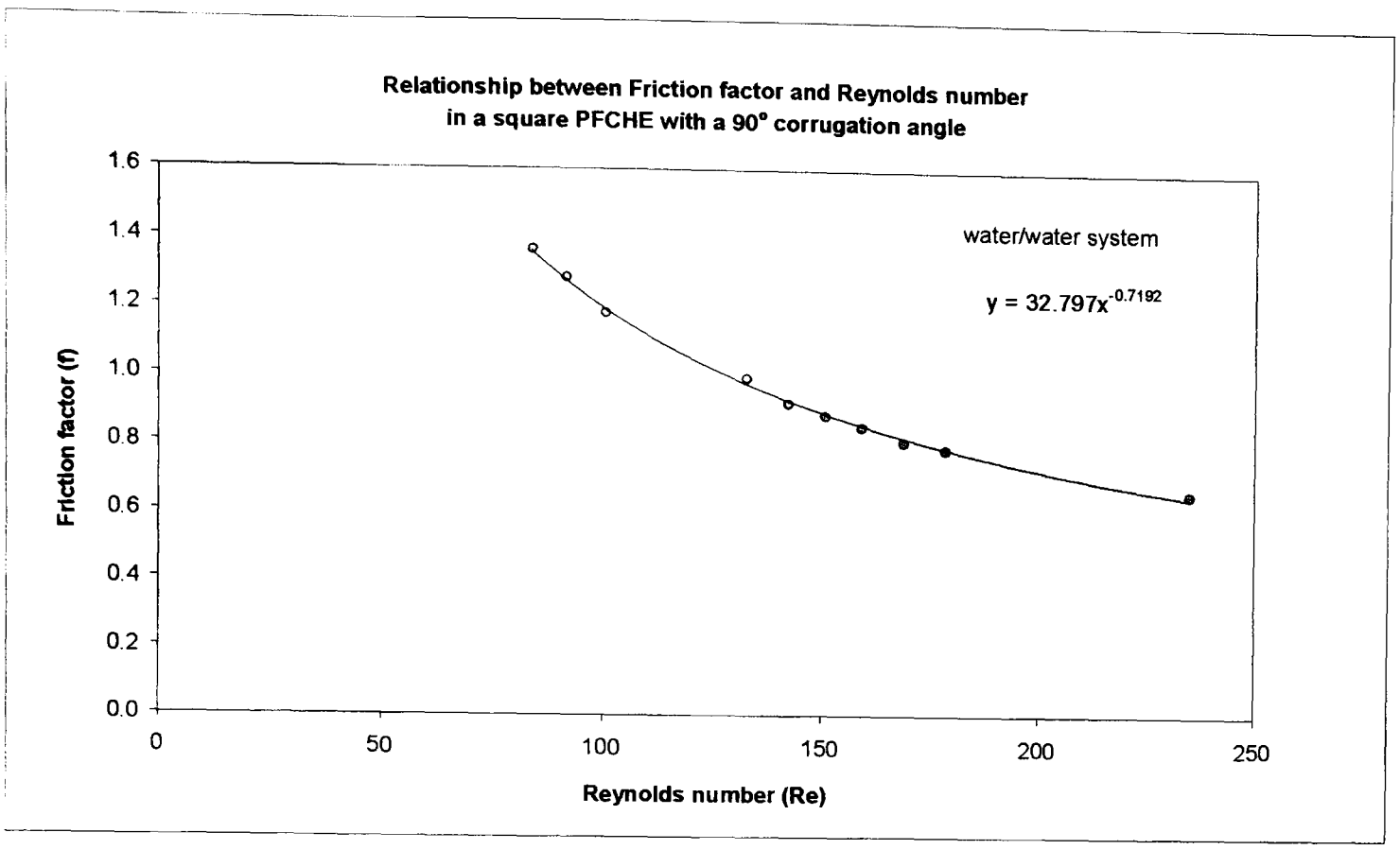


**Figure 4.16 Graph of friction factor (f) vs. Reynolds number (Re) for a square PFCHE in a water/water system**

### 4.3.2.4 Pumping power (E)

As with the Colburn and friction factor plots, the trend for the pumping power plot in a water/ water system is similar to the air/air system. Therefore the relationship between the heat transfer coefficient and the pumping power abides to both the heat transfer coefficient and the pumping power definitions respectively.

Compared to air, the pumping power expended for the water/water system is relatively low, which explains a little why the pressure drop characteristics is considered more important for gas flows compared to other fluids. In water systems, less energy is needed to overcome the friction to fluid flow across the heat exchanger. This can be due to the huge difference in densities between air and water; involved in the pumping power calculation. For a better appreciation of the performance evaluation in the water/water system, we proceed to look at the goodness factor plot.

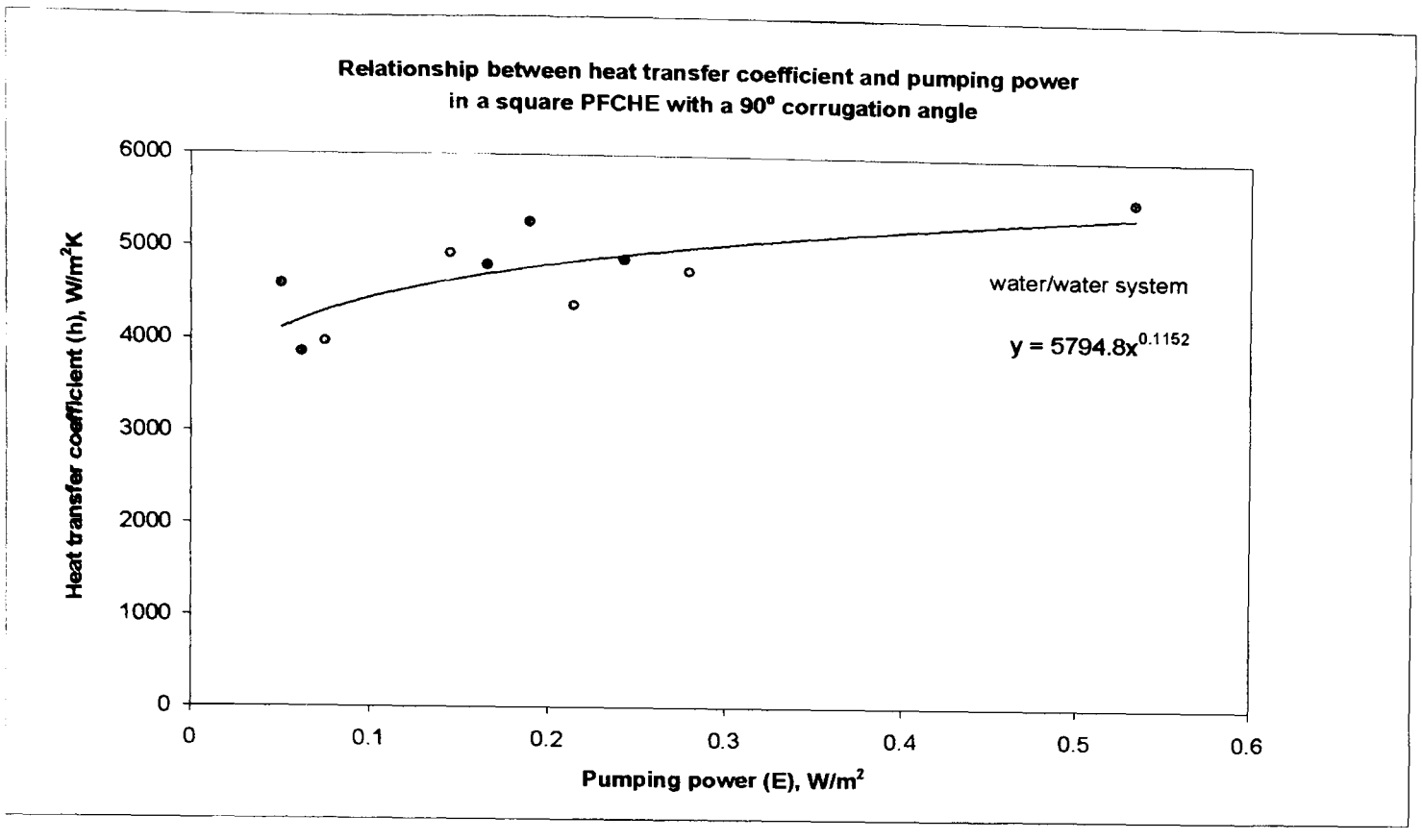


**Figure 4.17 Graph of heat transfer coefficient (h) vs. pumping power (E) for a square PFCHE in a water/water system**

4.3.2.5 Goodness factor (Jh/f)

Unlike the other plots, the goodness factor trend observed for the water/water system differs from the air/air system. For the air/air system, there is a steady decrease in goodness factor with increasing Re number, excluding only the first data point (see Figure 4.11). However for the water/water system, as shown in Figure 4.18 below, the goodness factor fluctuates with Re number, though there is a general decrease over the Re range. This could mean that the thermal efficiency is best at Re numbers where there is developing flow and sufficient mixing. When there is insufficient mixing, the thermal efficiency decreases.

At very low Re numbers, there is insufficient mixing. This explanation agrees with the air/air system, corresponding to the first data point. Low thermal efficiency occurs at low Re, due to insufficient mixing at low fluid velocities, which dampens heat transfer. Low thermal efficiency also occurs at high Re, as shown for the air/air system due to increased pressure drops at high fluid velocities. Hence a compromise between the two opposing effects at high and low Re, has to be reached to achieve high thermal efficiency, which from Figure 4.18 below is located in the intermediate Re range.

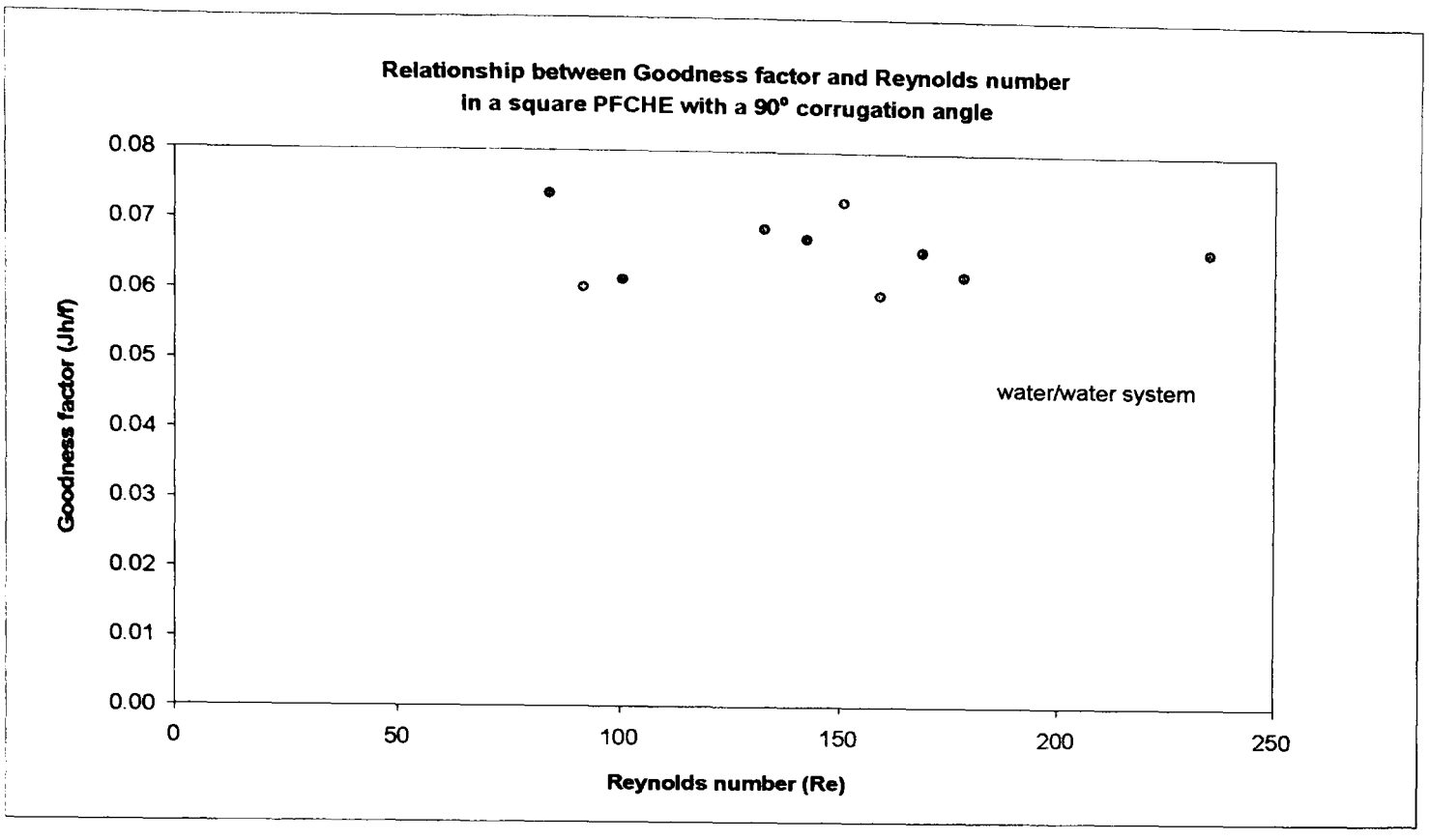


**Figure 4.18 Graph of goodness factor (Jh/f) vs. Reynolds number (Re) for a square PFCHE in a water/water system**

Further tests should be conducted to include higher Re until around 2000, to confirm this deduction. Following this, we next explain the heat transfer coefficient plot for the water/water system.

4.3.2.6 Heat transfer coefficient (h)

This graph was plotted so that a direct correlation, relating the heat transfer coefficient and Re number can be obtained. This correlation will come in useful towards the evaluation of water heat transfer coefficients for the experiments on different glycerol-water mixtures/water systems in the square PFCHE, which will be elaborated later in this chapter. The general trend observed is as expected with the heat transfer coefficients increasing with Re number. This can be seen in equation (4.12) earlier, under the air/air system.

From Figure 4.19, it is shown approximately, that there is an equal amount of scatter above and below the curve generated using Microsoft Excel. The h correlation developed is as follows:

$h = 754.35\ Re^{0.3663}$ for $87<Re<235$

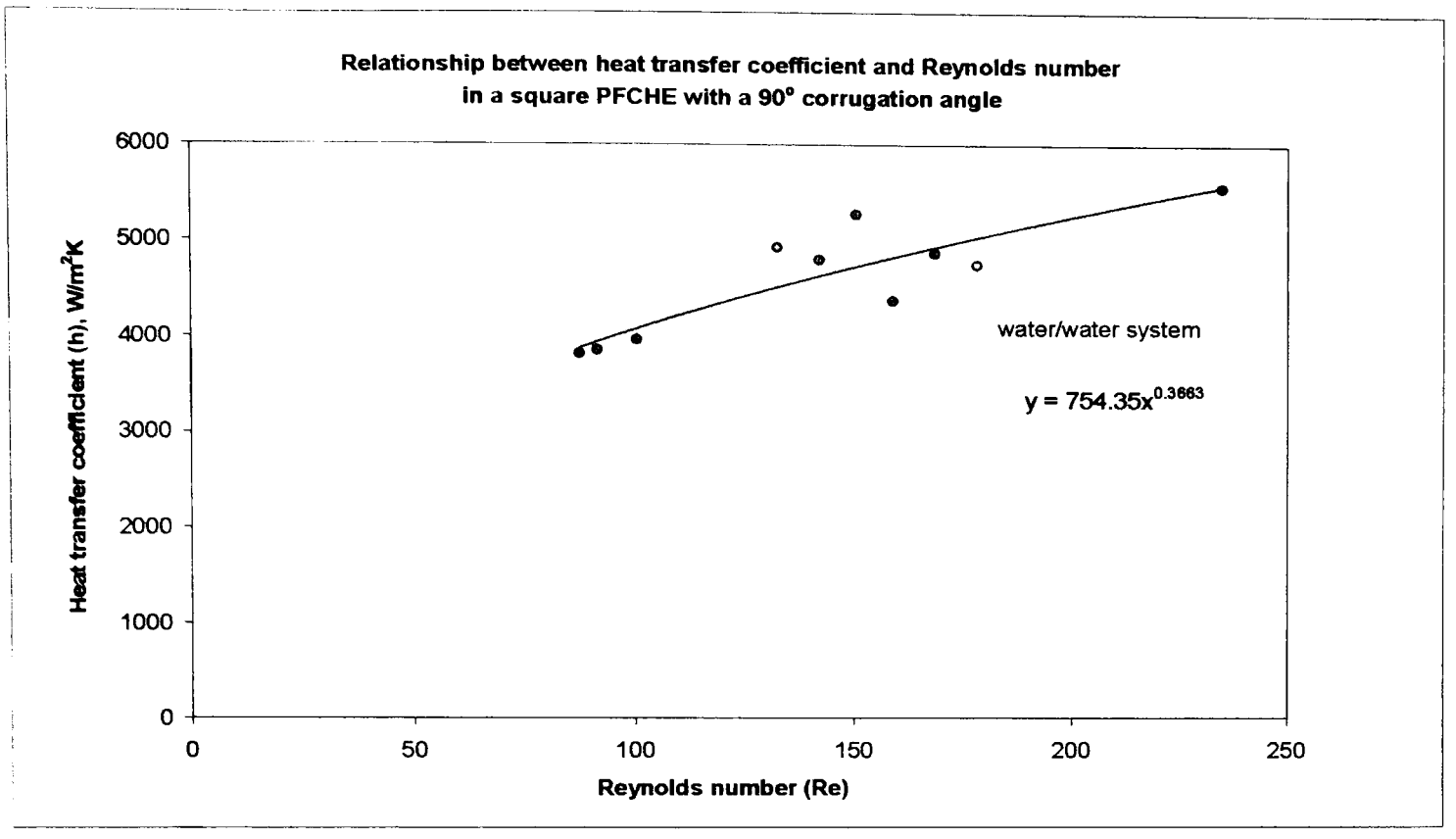


**Figure 4.19 Graph of heat transfer coefficient (h) vs. Reynolds number (Re) for a square PFCHE in a water/water system**

This indicates that the correlation generated takes into account the overall average values of the data points over the Re range specified. Therefore it can be concluded, that the water heat transfer coefficients generated using this correlation for the glycerol-water mixtures/water systems are valid. In the next section, we provide the experimental results for the four glycerol-water mixtures/water systems. We begin with the 30%(w) glycerol mixture followed by the 40%(w), 50%(w) and 70%(w) mixtures respectively.

*4.3.3 System: 30% glycerol-water mixture/water system*

The experimental results for the 30% glycerol-water mixture/water system and also for the 40%, 50% and 70% glycerol mixtures, involve three different plots as shown below.

(i) Colburn factor (Jh)
(ii) Friction factor (f)
(iii) Heat transfer coefficient (h)

These plots will be explained in the order listed above. The pumping power and goodness factor plots will be shown in Chapter Eight, in accordance with evaluating the effect of Pr numbers on the performance in the square PFCHE. The Pr number is a dimensionless factor that represents a group of physical properties for a specified fluid system, whereby ($Pr=cp\mu/k$).

4.3.3.1 Colburn factor (Jh)

From Figure 4.20 shown below, the general trend observed is that the Jh factor decreases with an increase in Re number. Several runs are repeated at the same flow rates to obtain and average and to reduce inaccuracies in the Jh curve plotted. The experimental data fits well with the curve generated with errors less than ±10%.

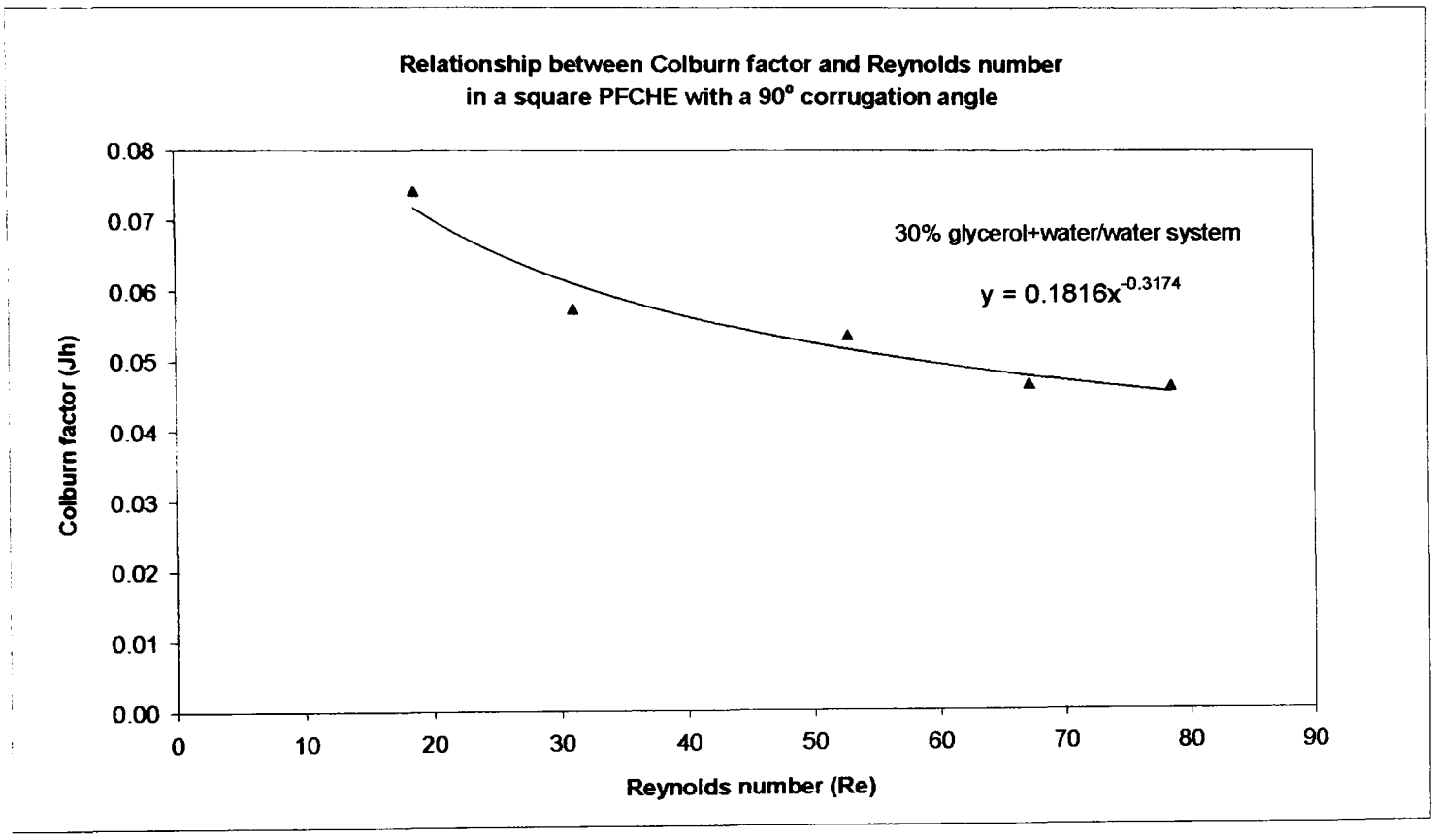


**Figure 4.20 Graph of Colburn factor (Jh) vs. Reynolds number (Re) for a square PFCHE with a 30% glycerol-water mixture/water system**

The heat balance errors calculated for this system are less than 6%. This can be seen in the table of results attached in Appendix D. Therefore, the Jh factors calculated based on experimental temperature readings can be deemed to be accurate. The Jh correlation developed is as follows:

$Jh = 0.1816\ Re^{-0.3174}$ for $19<Re<78$

In the following section, we consider the experimental pressure drop results through the friction factor plot.

### 4.3.3.2 Friction factor (f)

As with the other systems investigated in the square PFCHE, the friction factor decreases with Re number as expected. The curve generated using Microsoft Excel coincides very well with the experimental data, as shown in Figure 4.21 below.

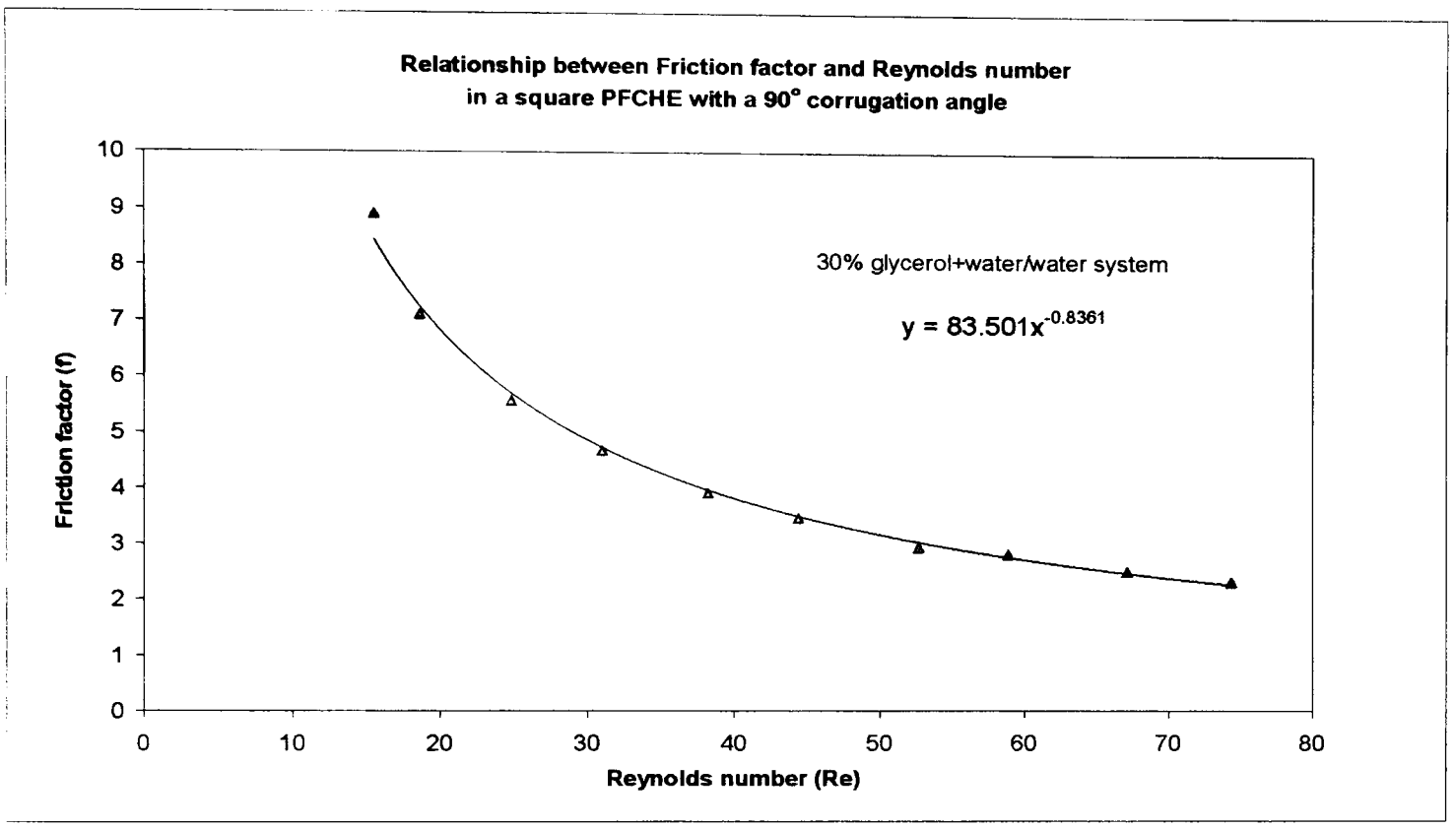


**Figure 4.21 Graph of friction factor (f) vs. Reynolds number (Re) for a square PFCHE in a 30% glycerol-water mixture/water system**

The f correlation developed is as follows:

$f = 83.501\ Re^{-0.8361}$ for $19<Re<78$

As the pressure drops and temperatures are each measured at different flow rates corresponding to different Re numbers (though having the same range), a heat transfer correlation is needed to calculate the heat transferred for the whole range of flow rates tested. Plotting the graph of heat transfer coefficient vs. Re number, generates this correlation. This is shown in the following section.

### 4.3.3.3 Heat transfer coefficient (h)

From Figure 4.22, it can be seen that the heat transfer coefficient increases along with Re number, abiding to equation (4.12). The heat transfer coefficient correlation will help in

determining the heat transfer coefficients at Re numbers where only the pressure drops, and not the temperature measurements are noted.

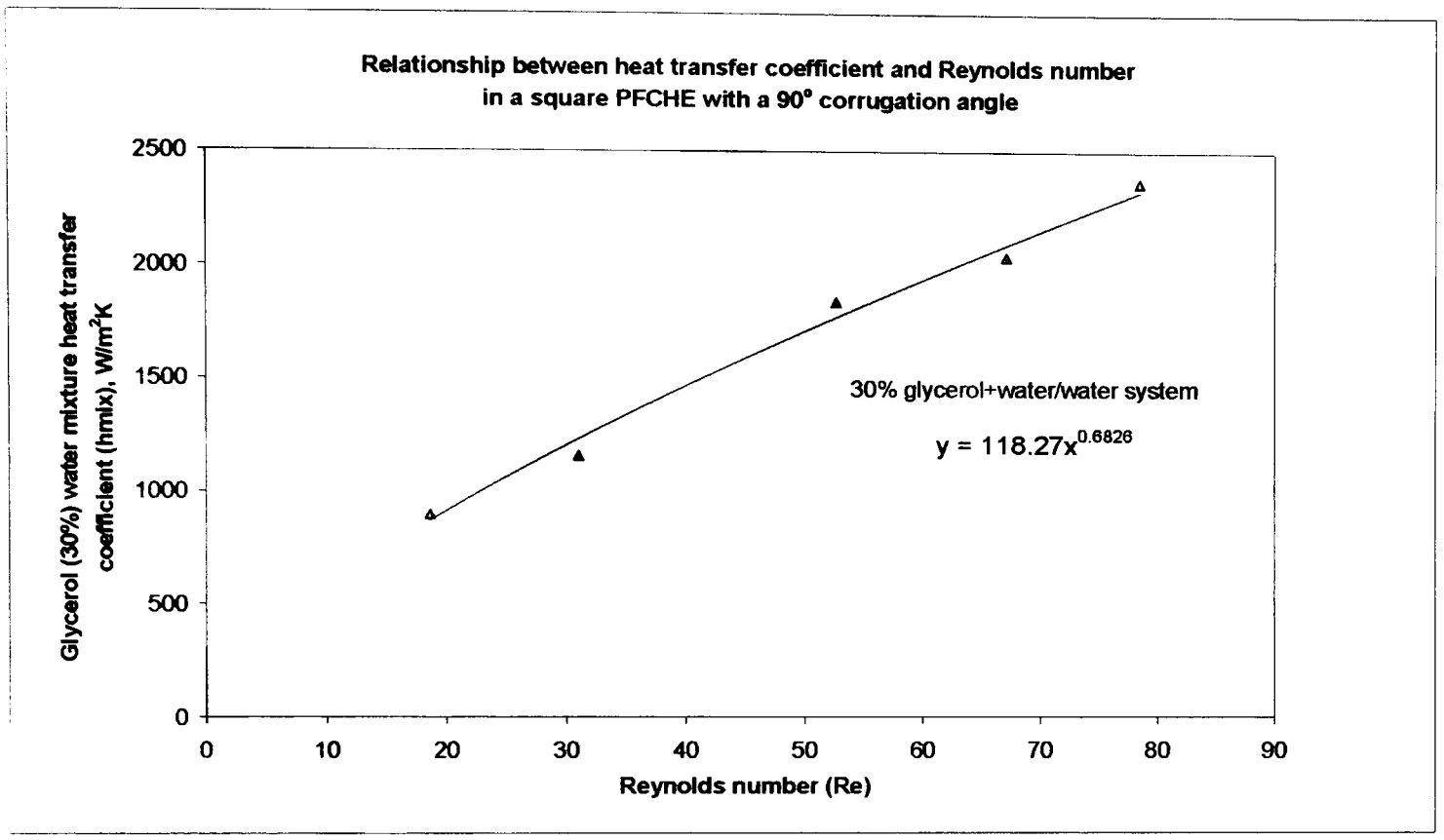


**Figure 4.22 Graph of heat transfer coefficient (h) vs. Reynolds number (Re) for a square PFCHE in a 30% glycerol-water mixture/water system**

Once this is established, the goodness factor and the pumping power at each flow rate can be calculated. The heat transfer correlation developed using Microsoft Excel for the 30% glycerol-water mixture/water system is shown below.

$h = 118.27\ Re^{0.6826}$ for $19<Re<78$

We now move on to consider the next glycerol-water mixture/water system, which involves a 40% glycerol-water mixture.

*4.3.4 System: 40% glycerol-water mixture/water system*

To describe the experimental results for this system, we first consider the Colburn factor plot, followed by the friction factor plot and finally conclude with the heat transfer coefficient plot.

### 4.3.4.1 Colburn factor (Jh)

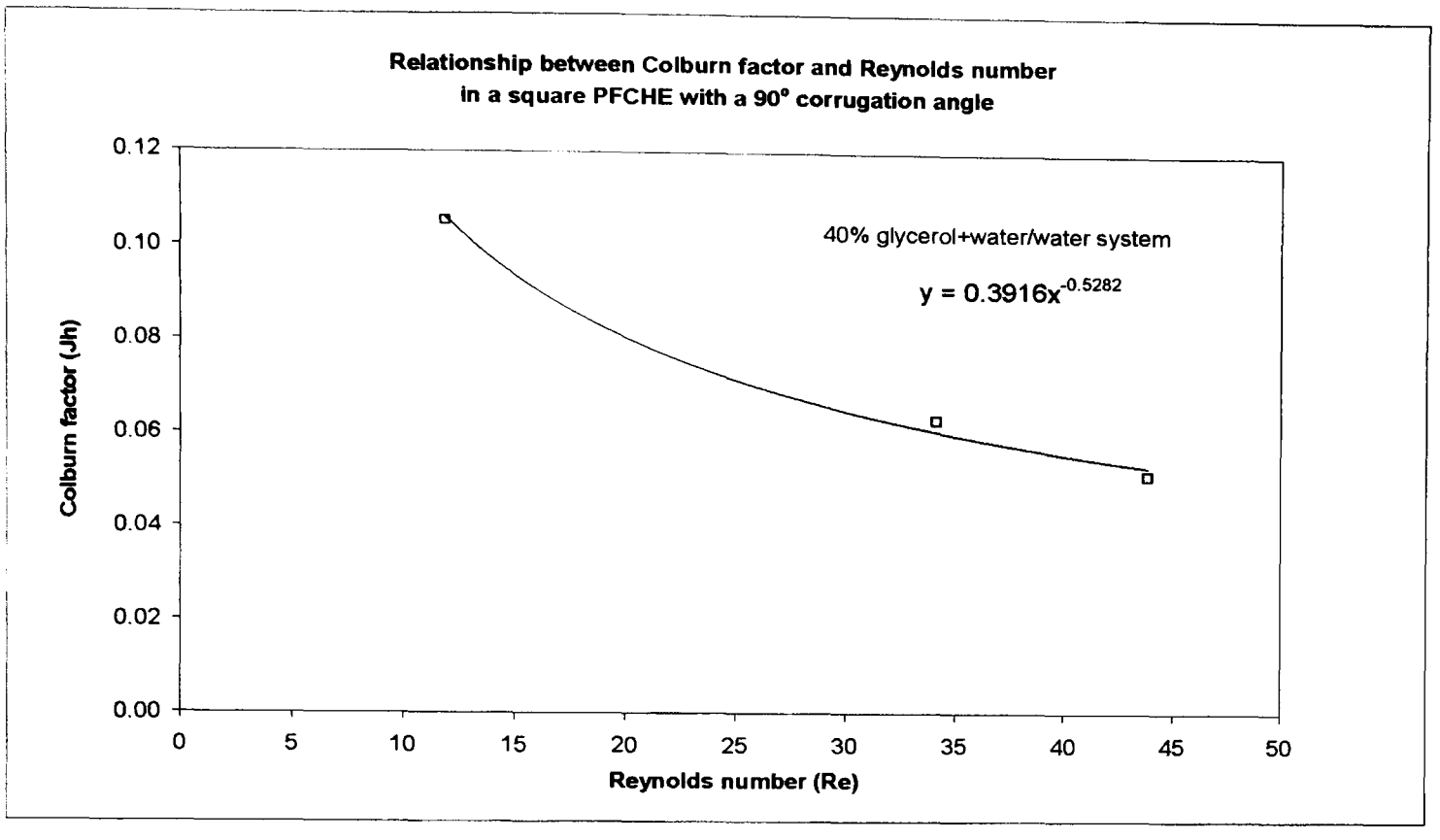


**Figure 4.23 Graph of Colburn factor (Jh) vs. Reynolds number (Re) for a square PFCHE in a 40% glycerol-water mixture/water system**

The Colburn factor trend is the same as the 30% glycerol-water mixture/water system. The range of flow rates tested however is lower, as the 40% mixture is more viscous and therefore it is difficult to obtain temperature readings for higher flow rates. The heat balance calculated for this system is less than 8%; hence the Jh factors calculated have a satisfactory degree of accuracy. The results of the heat balance errors are shown in the table of results, attached in Appendix D. A comparison between the different glycerol mixtures will be explained further in Chapter Eight, where the effects of Pr number on the performance of the square PFCHE is discussed. The best fitting curve through the data points is generated using Microsoft Excel. For the 40% glycerol-water mixture/water system, the Jh correlation developed is as follows:

$Jh = 0.3916\ Re^{-0.5282}$ for $12<Re<44$

### 4.3.4.2 Friction factor (f)

The friction factor trend is similar to the 30% glycerol-water mixture, where the friction factor decreases as the Re number increases. The experimental friction factors coincide well with the curve generated using Microsoft Excel.

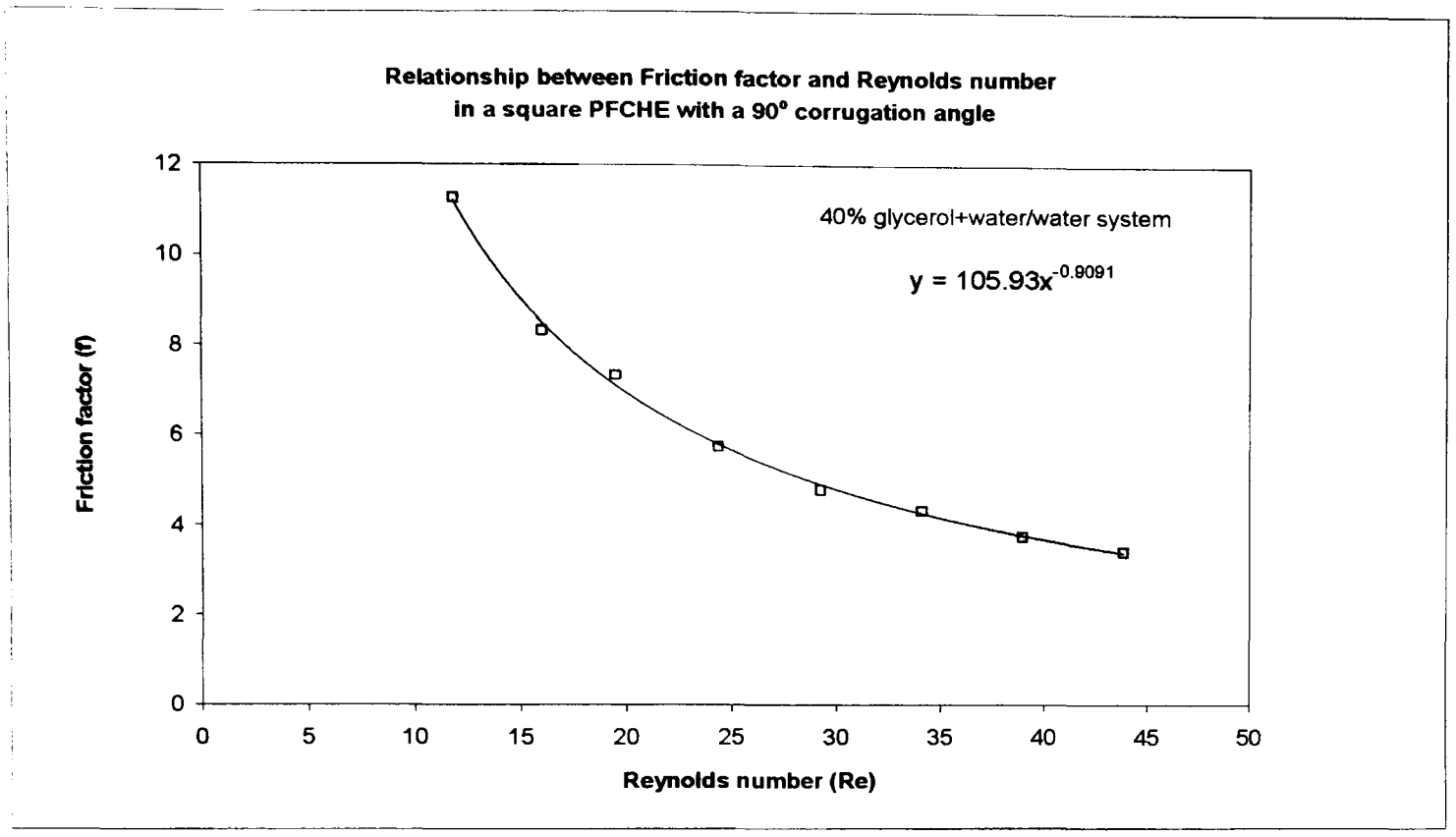


**Figure 4.24 Graph of friction factor (f) vs. Reynolds number (Re) for a square PFCHE in a 40% glycerol-water mixture/water system**

This shows that the pressure drops measured are accurate with very low measurement errors. The friction factor correlation established is as follows:

$f = 105.93\ Re^{-0.9091}$ for $12<Re<44$

4.3.4.3 Heat transfer coefficient (h)

Figure 4.25 below, shows that the heat transfer coefficient increases with Re number. Runs at similar flow rates were repeated to minimise the deviation of experimental data from the curve generated using Microsoft Excel. The heat transfer coefficient correlation generated is shown below:

$h = 274.79\ Re^{0.4636}$ for $12<Re<44$

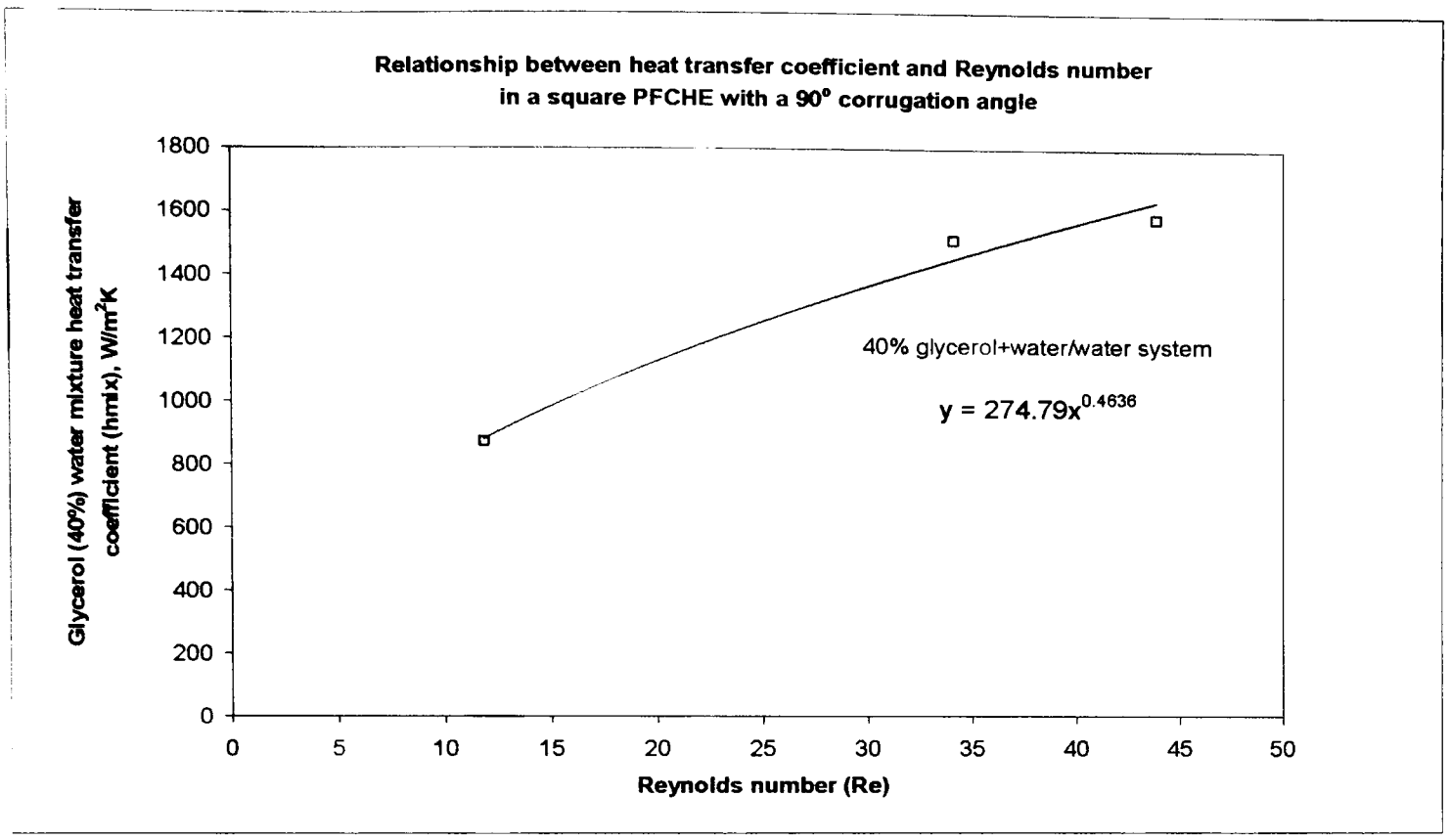


**Figure 4.25 Graph of heat transfer coefficient (h) vs. Reynolds number (Re) for a square PFCHE in a 40% glycerol water- mixture/water system**

In the following section, we consider the experimental results for the 50% glycerol-water mixture/water system.

*4.3.5 System: 50% glycerol-water mixture/water system*

As with the 30% and 40% glycerol mixtures, three experimental plots are considered for this system, namely the Colburn factor, friction factor and the heat transfer coefficient plots. We first describe the Colburn factor plot, before moving on to the friction factor and heat transfer coefficient plots.

4.3.5.1 Colburn factor (Jh)

The general trend observed is the same as the two previous glycerol mixtures, but the Re range is shorter and the values lower. This is due to the increase in viscosity, which prevents high velocities and consequently high Re numbers from being achieved. Due to the fluctuations in fluid flow rates and to minimise the errors in the temperature readings, several runs are repeated at the same flow rates to reduce inaccuracies. The curve through the data points and its corresponding equation are obtained using Microsoft Excel.

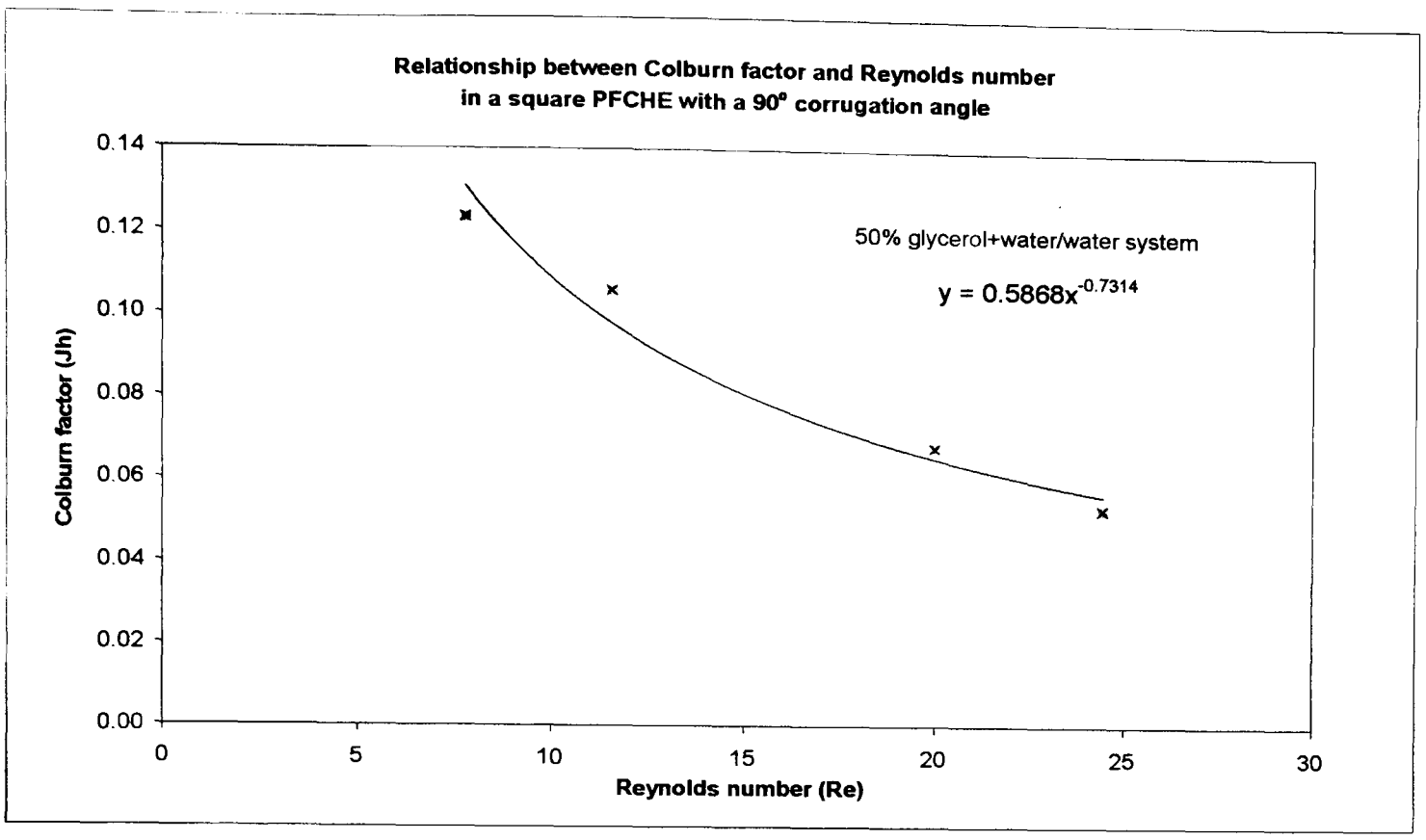


**Figure 4.26 Graph of Colburn factor (Jh) vs. Reynolds number (Re) for a square PFCHE in a 50% glycerol-water mixture/water system**

The Jh correlation developed is as depicted below.

$Jh = 0.5868\ Re^{-0.7314}$ for 8<Re<24

The heat balance errors calculated for this system are in the order of less than 8%, therefore the Jh correlation developed above is deemed acceptable. The results for the heat balance errors calculated are shown in Appendix D.

4.3.5.2 Friction factor (f)

The trend observed is as expected with the friction factor decreasing with increasing Re number. However unlike the 30% and 40% glycerol mixtures, the friction factors do not fall exactly on the curve generated. The slight deviations could be due to measurement errors in reading the pressure drops, as they are generally higher than the previous glycerol mixtures. The friction factor correlation obtained using Microsoft Excel is as follows:

$f = 70.811\ Re^{-0.7701}$ for 8<Re<24

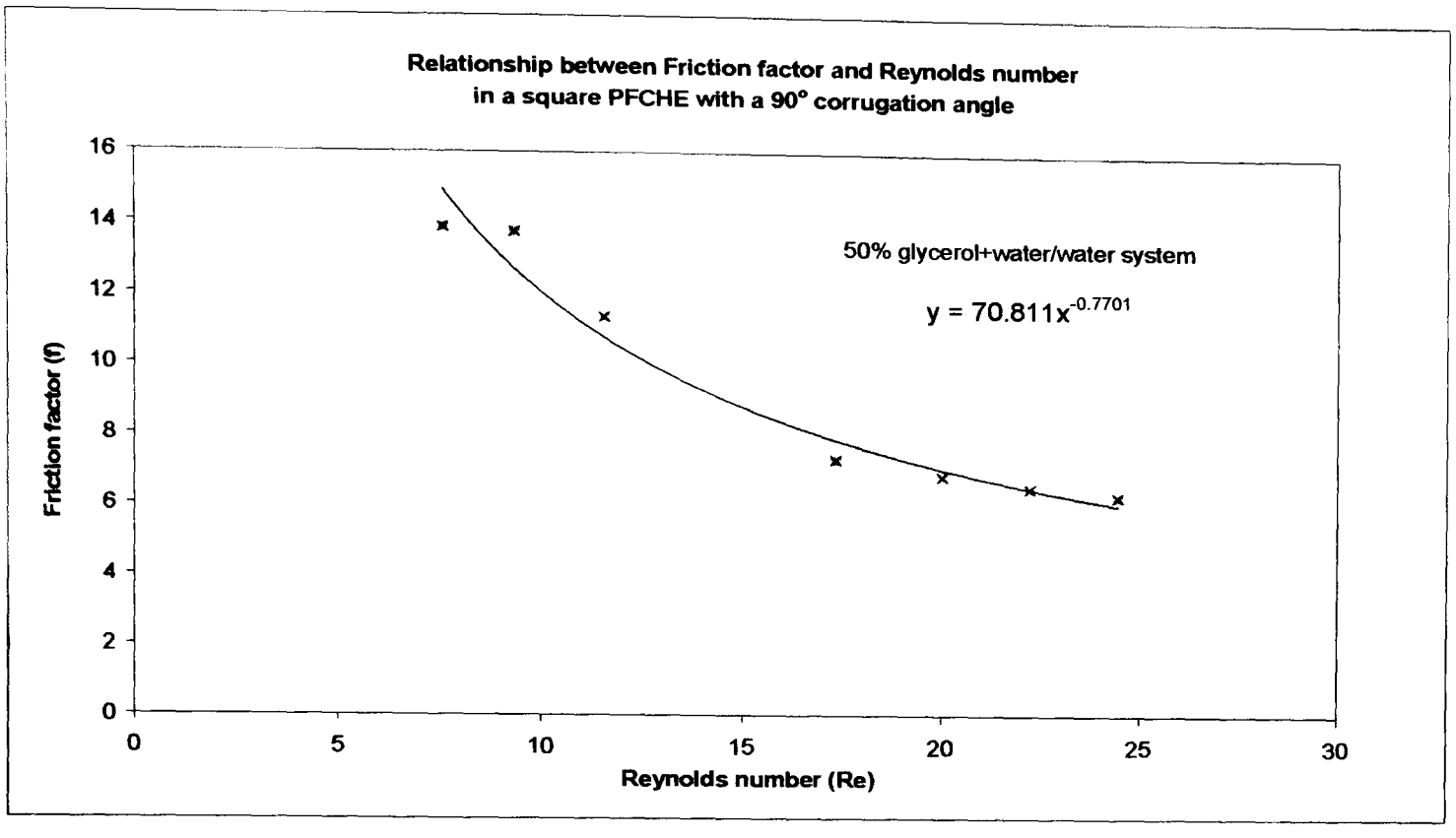


**Figure 4.27 Graph of friction factor (f) vs. Reynolds number (Re) for a square PFCHE in a 50% glycerol-water mixture/water system**

4.3.5.3 Heat transfer coefficient (h)

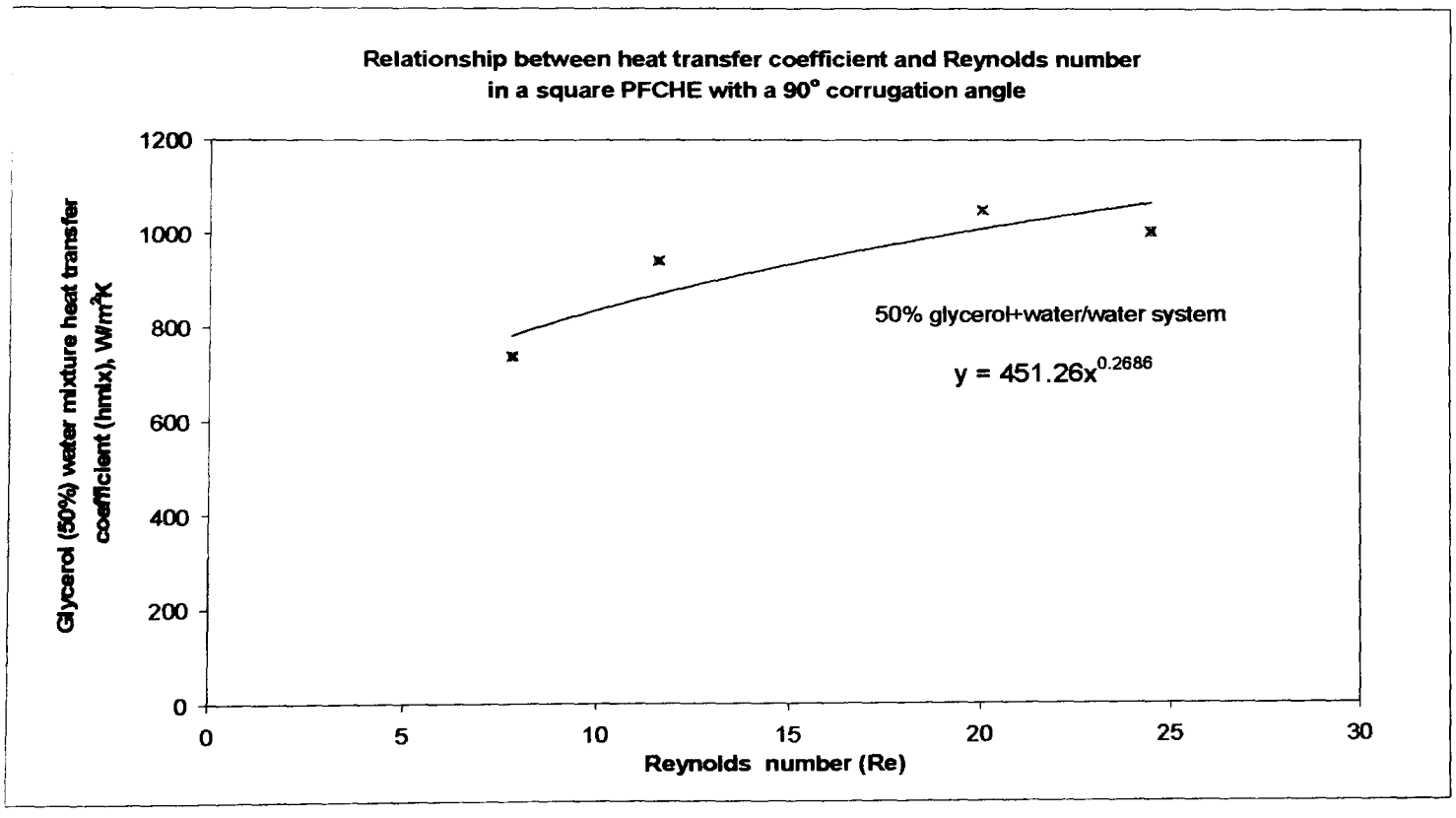


**Figure 4.28 Graph of heat transfer coefficient (h) vs. Reynolds number (Re) for a square PFCHE in a 50% glycerol water-mixture/water system**

As with previous glycerol mixtures, the heat transfer coefficient increases with Re number for a 50% glycerol-water mixture/water system. Temperature and pressure drop readings are repeated at similar fluid flow rates, to reduce the inaccuracies in the correlation developed for the heat transfer coefficient. The correlation developed for the 50% glycerol-water mixture/water system is as follows:

$h = 451.26\ Re^{0.2686}$ for $8<Re<24$

In the next section, we describe the experimental results for the final glycerol-water mixture system investigated in the square PFCHE. It involves a 70% glycerol-water mixture/water system.

### *4.3.6 System: 70% glycerol-water mixture/water system*

The experimental results for this final glycerol-water mixture system, also involves the same three plots as the previous glycerol systems. Below, we provide an explanation for the Colburn factor plot and then the friction factor plot. We finally conclude the experimental results for this system with a description of the heat transfer coefficient plot.

#### 4.3.6.1 Colburn factor (Jh)

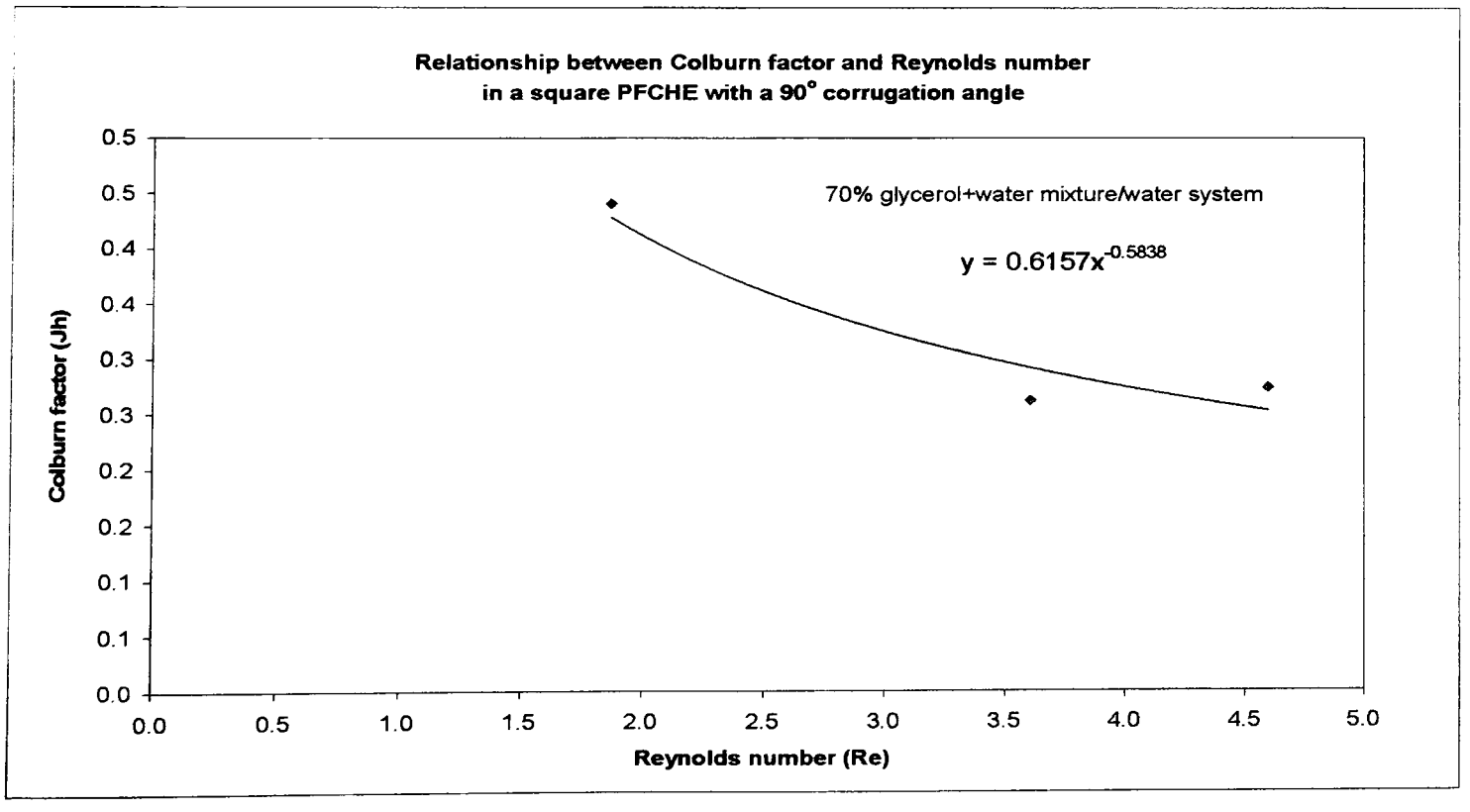


**Figure 4.29 Graph of Colburn factor (Jh) vs. Reynolds number (Re) for a square PFCHE in a 70% glycerol-water mixture/water system**

The general pattern is as expected with the Colburn factor decreasing with increasing Re numbers. It can be observed that the Re range gets shorter and lower in value with increasing percentage in glycerol, for the four different glycerol-water mixtures investigated. This effect on the Re number is mainly due to the higher viscosity experienced by the higher percentage glycerol mixtures, as similar flow rates are used for the 30%, 40% and 50% glycerol mixtures. This increase in viscosity also means that the higher percentage glycerol mixtures have higher Pr numbers. As mentioned before, the effect of Pr numbers on the performance in the square PFCHE will be elaborated further in Chapter Eight.

The heat balance errors generated for this system are less than 5%, showing that the Jh factors calculated have a satisfactory level of accuracy. The heat balance results are attached in Appendix D at the end of this thesis. The Jh correlation developed for the 70% glycerol water mixture/water system is shown below:

$Jh = 0.6157\ Re^{-0.5838}$ for $2<Re<5$

4.3.6.2 Friction factor (f)

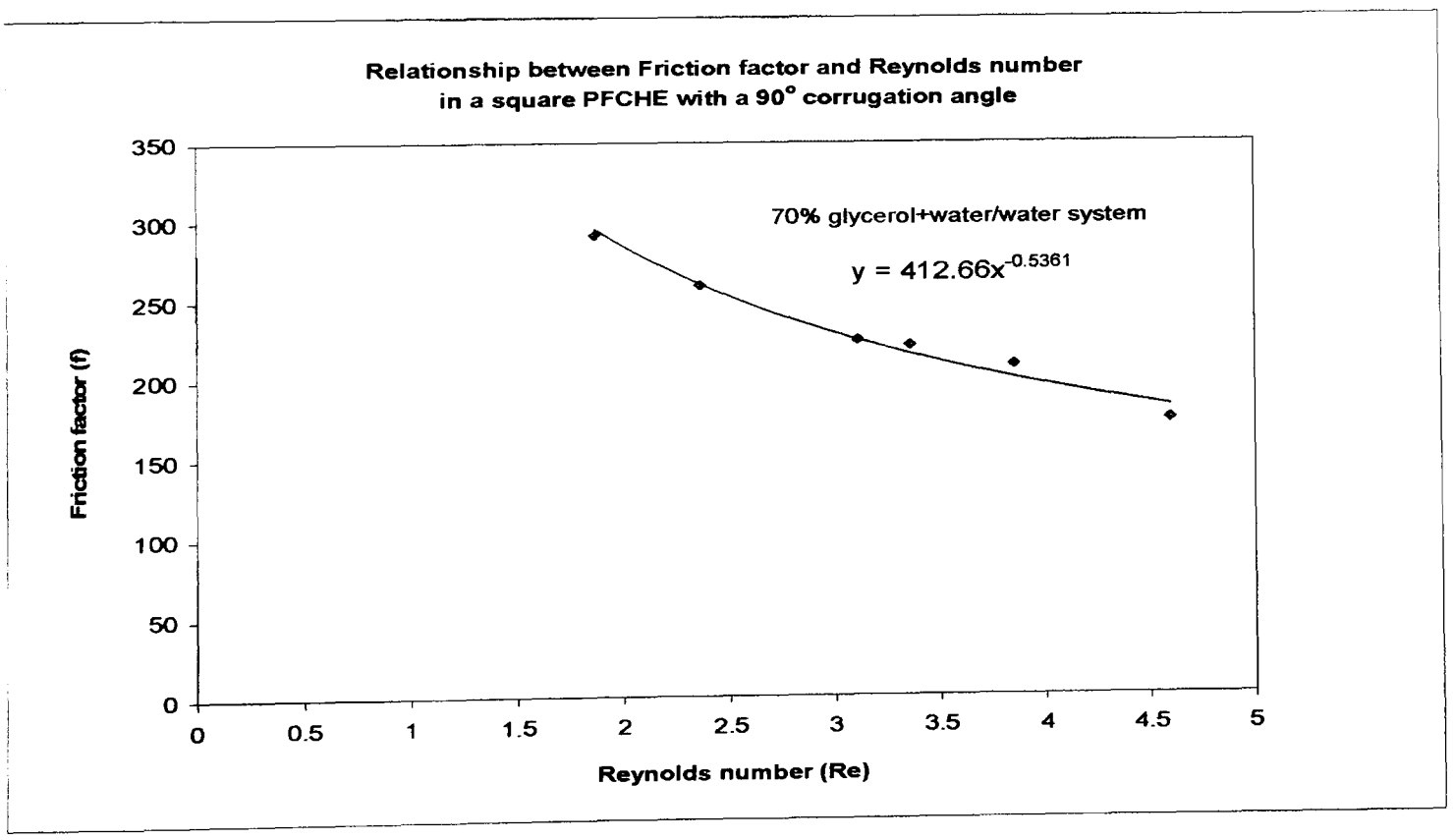


**Figure 4.30 Graph of friction factor (Jh) vs. Reynolds number (Re) for a square PFCHE in a 70% glycerol-water mixture/water system**

As expected, the friction factor decreases with increasing Re number. The friction factors plotted are well distributed along the best fitting curve generated using Microsoft Excel. The friction factors calculated from the pressure drops measured are a factor of 10-15 times higher, than the previous glycerol-water mixtures. This shows that there is a dramatic increase in restriction to fluid flow, from the 50% to 70% glycerol mixtures, which can be due to the large increase in viscosity values. As with the Pr number, the effects of the individual physical properties for the different glycerol mixtures will be explained in Chapter Eight. The friction factor correlation developed for the 70% glycerol-water mixture/water system is as follows:

$f = 412.66\ Re^{-0.5361}$ for 2<Re<5

4.3.6.3 Heat transfer coefficient (h)

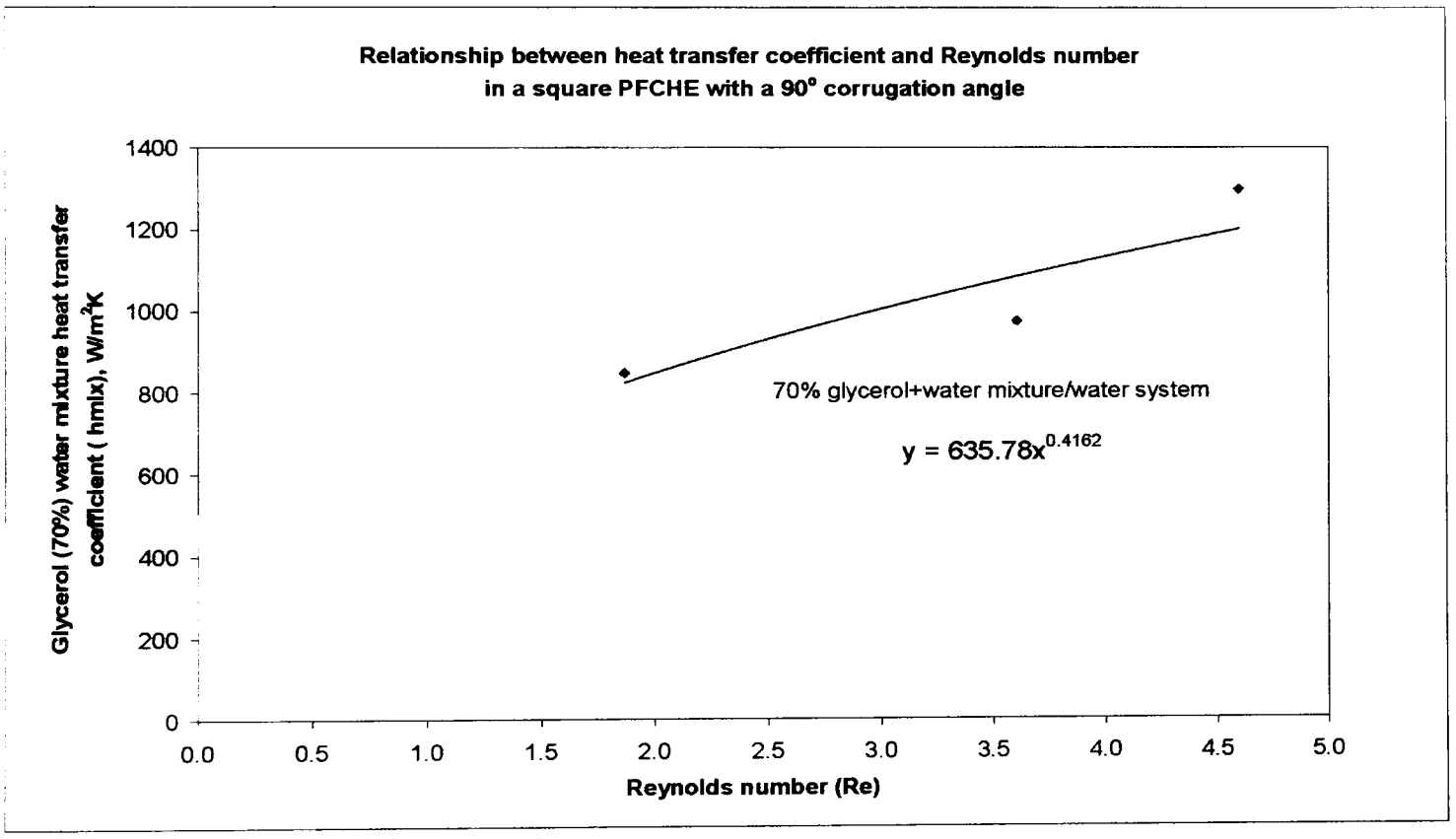


**Figure 4.31 Graph of heat transfer coefficient (h) vs. Reynolds number (Re) for a square PFCHE in a 70% glycerol-water mixture/water system**

As with the other heat transfer coefficient plots, higher coefficients are obtained with increasing Re numbers. The heat transfer coefficient correlation developed using Microsoft Excel is shown below.

$h = 653.78\ Re^{0.4162}$ for 2<Re<5

## 4.4 Conclusion

The design correlations developed for the six fluid systems are tabulated in Table 4.2, which shows the Re range over which the correlation pertains and also the corresponding Pr numbers for each system. For all the six systems investigated, the heat balance errors were low, therefore justifying the use of the experimental data obtained in developing the design correlations.

| Systems | Re | Pr | Jh | f |
|---|---|---|---|---|
| air/air | 510<Re<2540 | 0.7 | $2.0097Re^{-0.7644}$ | $0.5992\ Re^{-0.1697}$ |
| water/water | 87<Re<235 | 7 | $1.3886\ Re^{-0.6337}$ | $32.797\ Re^{-0.7192}$ |
| glycerol(30%)+water mixture/ water | 19<Re<78 | 19 | $0.1816\ Re^{-0.3174}$ | $83.501\ Re^{-0.8361}$ |
| glycerol(40%)+water mixture/ water | 12<Re<44 | 30 | $0.3916\ Re^{-0.5282}$ | $105.93\ Re^{-0.9091}$ |
| glycerol(50%)+water mixture/ water | 8<Re<24 | 49 | $0.5868\ Re^{-0.7314}$ | $70.811\ Re^{-0.7701}$ |
| glycerol(70%)+water mixture/ water | 2<Re<5 | 192 | $0.6157\ Re^{-0.5838}$ | $412.66\ Re^{-0.5361}$ |

**Table 4.2 Design correlations for the square PFCHE**

## 4.5 Summary

This chapter shows the experimental results for the performance testing in the square PFCHE using six different fluid systems (air/air, water/water and four glycerol-water mixtures/water) under laminar conditions. The four glycerol-water mixtures correspond to 30%(w), 40%(w), 50%(w) and 70%(w) concentrations of glycerol respectively. The heat transfer and pressure drop characteristics are investigated using performance evaluation methods and following this, the design correlations (Jh and f) are developed for each fluid system. A design model using regression analysis which incorporates the six different fluid systems investigated (different Pr numbers), will be discussed in Chapter Eight.

In the following chapter, performance testing on another PFCHE configuration is conducted; namely the spiral PFCHE. As with the square PFCHE, the design of the unit is first outlined and then followed by the experimental procedure involving an air/water system. Experimental results are then explained using performance evaluation methods, en route to developing the design correlations for the spiral unit.

# CHAPTER 5 - SPIRAL POLYMER FILM COMPACT HEAT EXCHANGER

## 5.0 Introduction

Chapter Three provided evidence to support the reliability of the experimental data for all the PFCHE experiments described in this thesis. This was achieved by conducting a general uncertainty analysis, which incorporates the equipment uncertainties and also the propagation of these uncertainties in determining the final experimental results (Jh and f factors).

Following this, the square PFCHE was described in Chapter Four and the performance testing results involving six different fluid systems (air/air, water/water and four glycerol-water mixtures/water) in laminar conditions, were outlined. Using the results obtained, the design correlations (Jh and f) were then developed for each fluid system. These design correlations will come in useful when attempting to develop alternative PFCHE units to replace metallic heat exchangers.

As the next progressive step in the research, design correlations involving not only different fluid systems, but also different PFCHE configurations, could be investigated to obtain a wider range of choice when attempting alternative designs to suit a selected application. In this chapter, the spiral PFCHE is investigated. As with the square PFCHE; flow rate, temperature and pressure drop measurements were carried out for evaluating the thermal and hydraulic performance of the unit, en route to developing the design correlations. However unlike the square PFCHE, only one fluid system is investigated, which is an air/water system.

We first look at the advantages of adopting the spiral design, followed by a section on previous work conducted on an early spiral PFCHE. This builds up towards the description of the new improved spiral design investigated in this chapter. We then proceed with the performance calculation procedures, before showing the experimental results obtained. The chapter ends with the development of the spiral design correlations. Before we consider the spiral design concept, an illustration of the spiral PFCHE is shown in Figure 5.1 below. A schematic diagram will be shown in Figure 5.2.

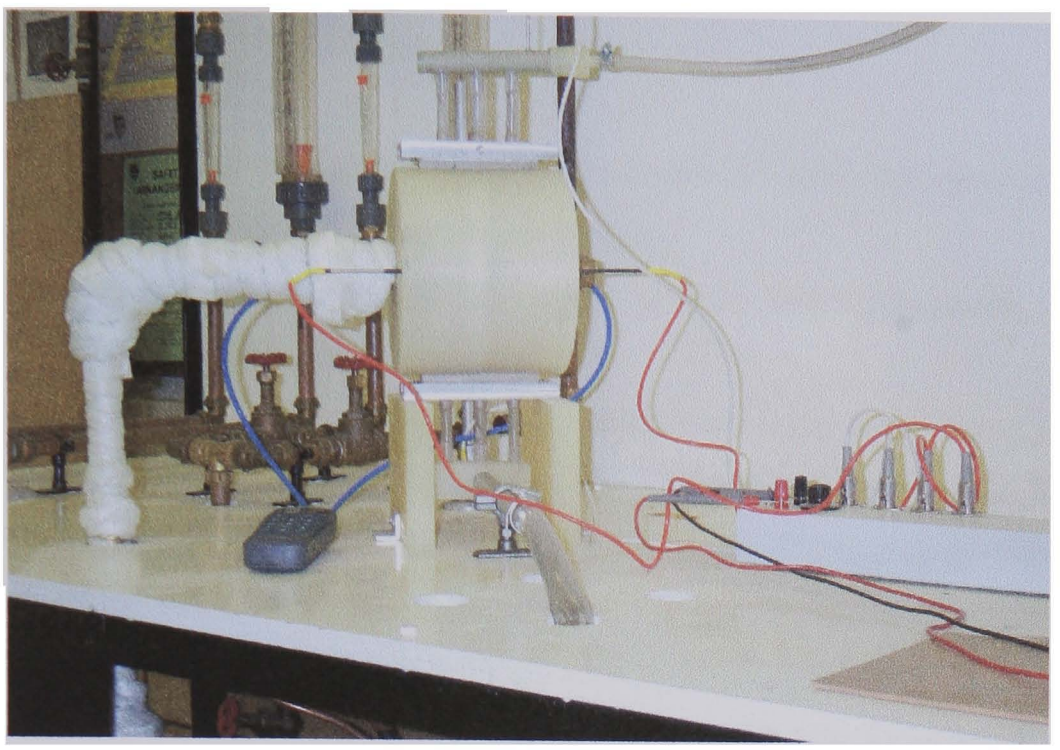

**Figure 5.1 Diagram of the spiral PFCHE**

## 5.1 Spiral design concept

Having proved that the square PFCHE concept worked, the spiral PFCHE was fabricated to address the problem of pressure drop on the gas side for special applications. The gas flow path length in the spiral PFCHE is shorter than that of the fluid flow. The configuration of the unit is such that it allows heat transfer between a large volumetric flow rate of gas and a low volumetric flow rate of liquid. The design is also best suited for minimising the pressure on the liquid, as well as the gas side. This type of configuration is suitable for use as car radiators, air conditioning, as well as water heating for domestic sectors and for waste heat recovery applications.

In these applications, the short gas flow path length is necessary in order to keep a low pressure drop on the gas side. In addition, the compact nature of the heat exchanger is also necessary, as the units would have to fit into a very small space. Although the heat transfer achieved for a given pressure drop is competitive compared with that of more conventional exchangers, it must still be noted that the pressure drop per unit length is comparatively high. This suggests that in order to keep the pressure drop to a minimum, the design of such heat exchangers must incorporate a short path length but a large frontal area.

For a better appreciation of the spiral PFCHE configuration, the advantages of adopting the spiral design in metallic units are outlined in the next section.

*5.1.1 Advantages of the spiral configuration in metallic units*

- Can be used for fluid systems with different volumetric flows (high and low)
- Units have exceptionally high heat transfer rates
- Low fouling tendencies and therefore useful for flows which are heavily fouling, as they result in a self-scrubbing action
- Full access to all heat transfer surfaces for easy inspection, maintenance and cleaning
- High thermal efficiency especially in close temperature approach situations
- Fully countercurrent, LMTD needs no correction factor due to their configuration
- For any given application, the units have higher LMTD than a conventional exchanger and therefore would need less heat transfer area for a given duty
- They consist of two long strips of plate metal, which are wrapped to form a pair of concentric spiral passages through which the fluids flow. In this way, true counter-current flow is maintained at all times
- Produces overall heat transfer coefficient (U) values 120-150% higher than conventional heat exchangers for the same pressure drop, by producing extremely high convective heat transfer coefficients on both sides and minimising the potential for fouling
- Works well in fouling, viscous, slurry and fibrous applications where fouling is expected. The fouling factor is ¼ of that for a shell and tube exchanger
- Configuration allows for thermal expansion without generating high mechanical stresses that can result in mechanical failure
- Coiling action allows the exchanger to be used where the temperature difference between the two streams is very high

It is due to these advantages that the design for the spiral PFCHE was attempted. It was thought to be a good idea to incorporate the advantages of using thin polymer films and the spiral geometry, for applications where the square PFCHE could not be employed. An example of this is in applications having different fluid flow rates. In the following section, the initial spiral PFCHE design is briefly described, before moving on to the current design investigated in this chapter.

*5.1.2 Previous work*

The initial testing of the spiral PFCHE concept for a small range of Re numbers, was carried out by Lyon (1995).The study showed that the unit could perform useful duties and has potential applications in car radiators, domestic heating, heat recovery and air conditioning. The first primary application considered for the design was the car radiator.

Strips of PEEK are woven around a mandrel, which then forms the air path through the spaces between the alternate layers. The air path is very short which leads to low pressure drops on the air-side. The spiral configuration is held together with end caps, directly into which the air-line is directed. The water flow enters and leaves by ports, which are inserted such that all the available heat transfer area is utilised by being in constant contact with both the fluids. The air flow is in total cross flow with the water flow. Silicoset was used to bond the edges of the strips.

The corrugations would ideally be at 90° to each other to achieve the best heat transfer but as this would render the strip unable to bend, therefore a compromise between fabrication and heat transfer was made and the channels formed a chevron pattern at 20°. Spacers (1 cubic mm blobs of Silicoset) were inserted to keep the sheets separated in the middle, thus reducing the pressure drop (reduced path length of water). Spacers also helped in stopping the water channel from 'bowing' when large water flow rates were employed. The spacers could also act as baffles and promote uniform distribution and good mixing characteristics within the water stream.

The water flow used in the actual car radiator is much greater than that used in the test rig. It was necessary, therefore, to redesign the spiral PFCHE to cope with this extra flow rate. The only way to keep down the fluid velocity and also the pressure drop is to increase the free flow area for the fluid. To cope with a reasonable water flow of 50 l/min, the increase has to be significantly large. It was therefore decided to have several water channels in the new unit. This would greatly increase the fluid flow area. In addition, the water flow path length is to be reduced by using sheets bent into an arc and attached to a mandrel, instead of woven round it. This will limit the water pressure drop. No further measures need to be taken to reduce the air flow path length, as the length used generates sufficiently low air pressure drops.

The new spiral PFCHE design adopting these new ideas is described in the following section. The experimental results and design correlations developed in this chapter will be based on this new improved design.

## 5.2 Design details of the spiral PFCHE

A schematic diagram of the spiral PFCHE can be seen in Figure 5.2 below. The spiral PFCHE prototype consists of 6 corrugated PEEK (poly ether ether ketone) sheets and an aluminium core housed in a polypropylene cylindrical shell. The dimensions of the sheets are 24 cm (length) by 11 cm (width). The nominal film thickness is 100 μm.

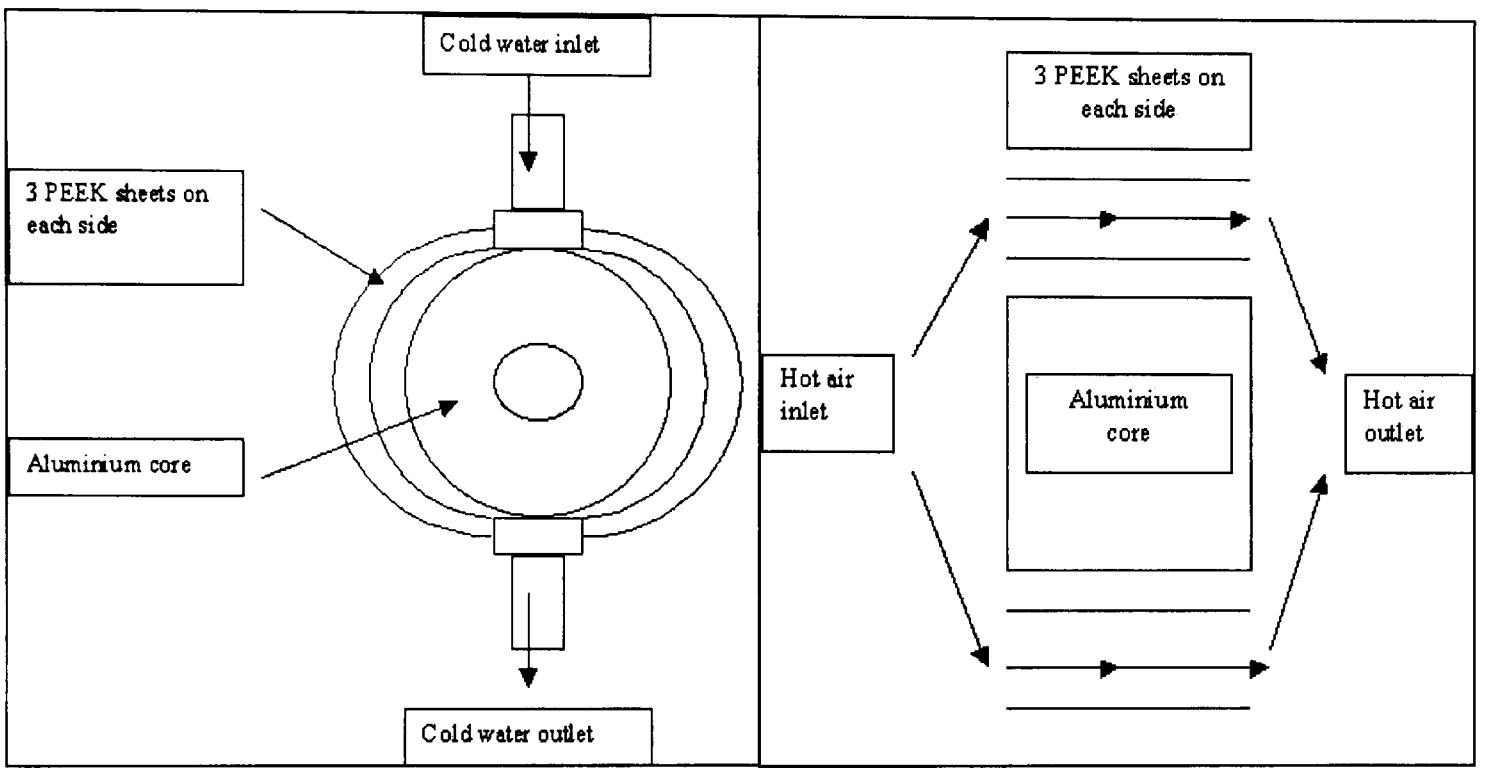


**Figure 5.2 Schematic diagrams of the spiral PFCHE**

There are 3 sheets bent into an arc on each side of the aluminium cylindrical core, creating a spiral configuration. Each sheet has been folded and laser welded on the edges to create the flow passage for the water stream, through a distributor. Therefore, there are six distributors in total. Each distributor (10 cm by 1 cm) is a PEEK strip with 33 (1 mm diameter) holes. They are placed at the top end of each sheet using a sealant (Araldite AV 119). An illustration of the PEEK water distributors is shown in Figure 5.3 below.

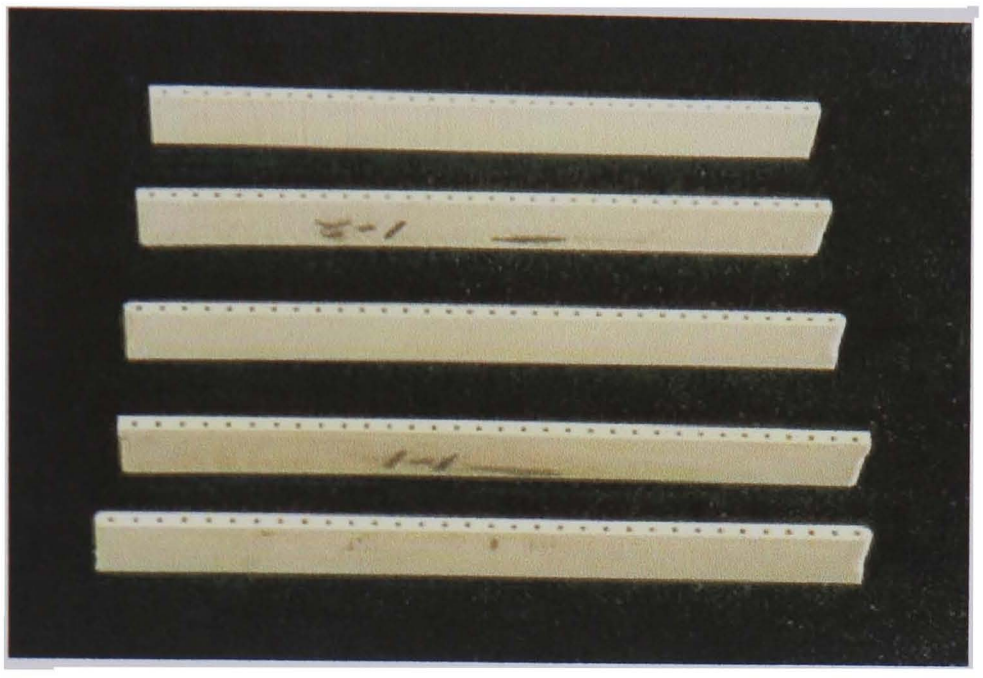

**Figure 5.3 Diagram of PEEK water distributors**

The welded and glued joints are then etched with acid, before the whole assembly is baked in an oven at 140°C.The aluminium cylindrical core is used to withstand these temperatures up to 140°C, otherwise polypropylene can be used to achieve an all polymer unit, such as in the square assembly. By using an aluminium core, the sheets can be removed and re-assembled. This would not be possible if polypropylene is used, as it deforms at high temperatures.

Water flows through the distributor channels along the circumference of the aluminium core, whilst air is passed through the length of the exchanger. The air flow is in total cross flow with the water flow. Compressed air from the main supply at (276 kPa) was used to feed the hot air stream. An electric heater, consisting of an electric heating coil fitted with a variac, was used to warm the cold air, which was then fed to the exchanger core as the hot stream. Pipe work, as short as possible on the hot side to avoid as much as possible heat losses, was constructed using 20 mm copper tubes. The rig was linked to the copper pipe work by 25 mm PVC flexible tubes. The main details of the spiral PFCHE is given in the table below.

| | |
|---|---|
| Projected heat transfer area | 0.08 $m^2$ |
| Real heat transfer area | 0.16 $m^2$ |
| Water flow path length | 0.21 m |
| Water hydraulic diameter | 1.0 mm |
| Air flow path length | 0.1 m |
| Air hydraulic diameter | 2.0 mm |

**Table 5.1 Details of the spiral PFCHE**

In the following section, we describe the experimental procedure for the performance testing in the spiral PFCHE, using an air/water system.

### 5.3 Experimental procedure

The flow rate, temperature and pressure drop measurements were noted for the spiral PFCHE in an air/water system. Water flow rates were fixed while varying the air flow rates. Three sets of runs were investigated; with constant water flow rates at 20, 50 and 80 $cm^3$/min whilst the air flow rates were varied between 5-15 $m^3$/hr, for each constant water flow rate.

The air flow rates were measured using Nixon Rotameters (PVDF floats encapsulated with aluminium), whilst Placon rotameters were used for the water flow rates. The experimental measurements were noted for 33 runs in total; 11 runs in each set. The heater was maintained at a constant variac for all runs conducted. This is to ensure that the temperature readings for the hot air inlet stream in each set of runs were similar.

A pressure meter (2000 Series Manometer) was used to measure the air-side pressure drop. The pressure drop on the water-side was too small to be measured. Higher water flow rates, which could have resulted in measurable pressure drops, could not be used due to leakage problems. The temperatures were measured using platinum resistance thermocouples (PRTs). Four temperatures were measured for the inlet and outlet, hot air and cold water streams respectively. The thermocouples were inserted at the inlet and outlet headers for the water stream and also across the polypropylene casing for the air stream. An illustration of this is shown below.

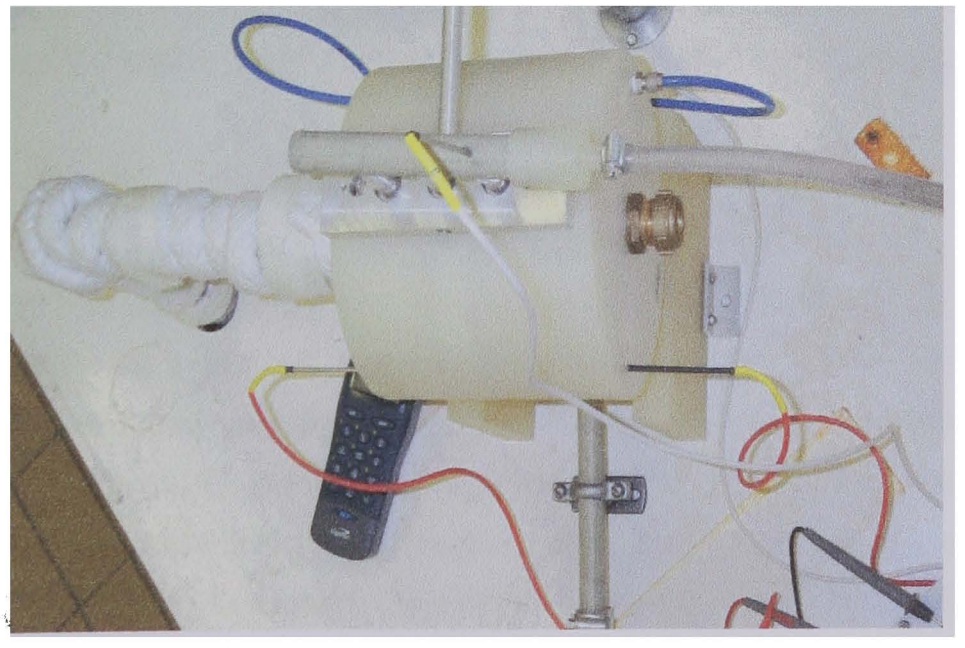

**Figure 5.4 Top view of the spiral PFCHE**

Once steady state conditions were achieved, the experimental measurements were noted. Following this, the heat balance was calculated using the temperatures for the inlet and outlet, hot and cold streams. This heat balance calculation marks the beginning of the performance evaluation for the unit. A simplified flow diagram of the experimental set-up for the spiral PFCHE experiment is shown below.

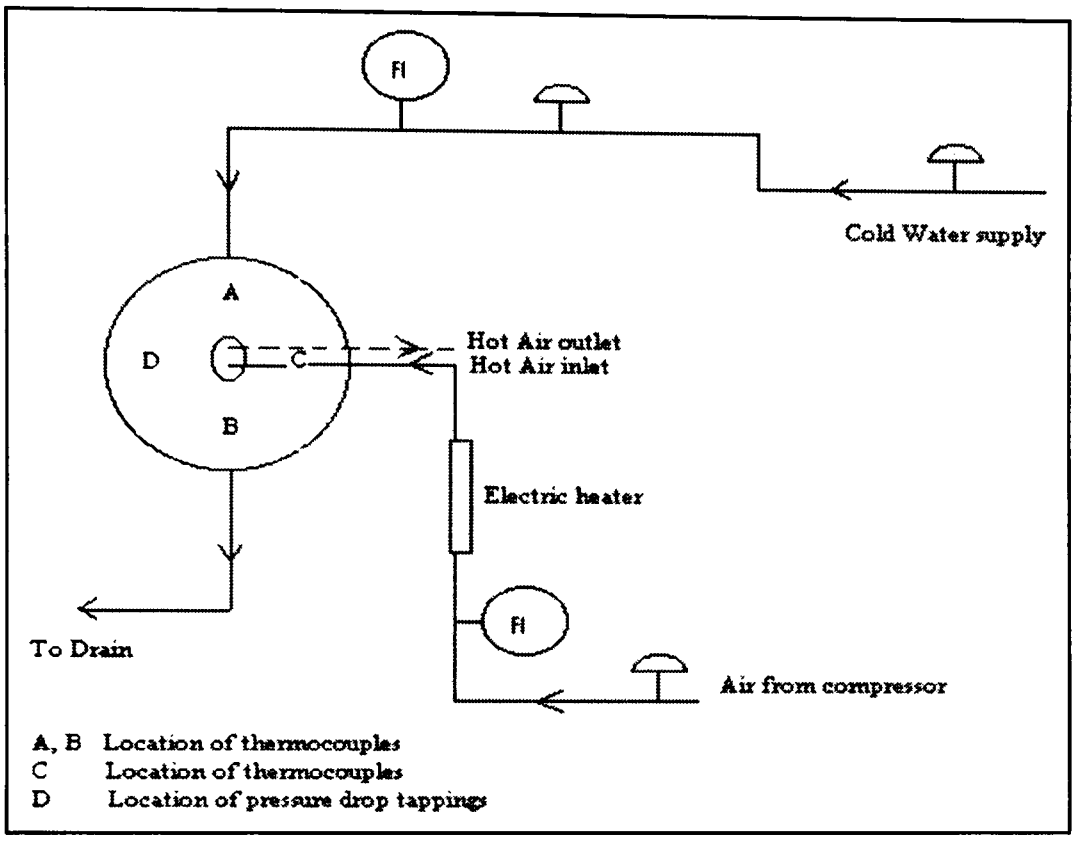


**Figure 5.5 Simplified flow diagram of the spiral PFCHE experimental set-up for the air/water system**

In the next section, we highlight some of the problems encountered while conducting the experiments, before moving on to describe the performance calculations involved.

*5.3.1 Operating problems*

There was a slight leakage on the water-side (a trickling of water flow). This was due to the accumulation of water all along the welded PEEK sheets. Burnt spots were present on the sheets as a result of the laser welding. These burnt spots created vulnerable sites for leaks to occur. Furthermore once glued and etched with acid, the possibilities for leaks were increased. Also at higher water flow rates tested, the situation got worse where the back-pressure of water may have caused the welds to loosen. To overcome this problem, the welding of the sheets needs to be addressed. We now look at the performance calculations conducted, based on the experimental measurements taken for the spiral PFCHE in an air/water system.

## 5.4 Performance calculations for the spiral PFCHE

In general, the performance calculations adopted for the spiral PFCHE are similar to the square PFCHE. Nevertheless, there is a difference in the evaluation of the fluid heat transfer coefficients, as the spiral PFCHE involves heat exchange between two different fluids with different flow rates. In addition, the exchanger is not symmetrical about its diagonal line as in the square PFCHE, therefore the free flow area for both fluids are not the same. This causes the performance calculations for the spiral PFCHE to be more complex than the square PFCHE. The basic differences involved are explained in this section. We first begin with the heat balance calculation.

### *5.4.1 Heat balance error (HBE)*

Unlike the square PFCHE where the heat balance just involves the fluid temperatures, the heat transfer capacity also needs to be considered for the spiral unit, due to the different fluids used. The heat balance errors are determined using the expression below.

$$\text{Heat balance error} = \frac{\text{Difference between the heat transferred in the hot and cold streams}}{\text{Maximum heat transfer value of either two streams}} \quad (5.1)$$

$$= (Q_h - Q_c) / \text{max of either } Q_h \text{ or } Q_c$$

where $Q = m\ cp\ \Delta T = C\ \Delta T$

For the spiral PFCHE, it should be noted that there is a difference in the heat capacity (C) values for each stream, due to the different specific heat capacity (cp) values and flow rates (m) used. Since the water flow rates were fixed for each set of runs, the heat capacity value for the water stream in each set remains constant. However, the air heat capacity values differ as the flow rate varies from one run to the next. The specific heat capacity values for both water and air streams, were calculated as functions of the inlet and outlet temperatures, and tabulated in a spreadsheet using Microsoft Excel. This was done prior to calculating the heat capacity values, en route to performing the heat balance calculation using the expression above.

The next main difference from the square PFCHE, involves the calculation of the fluid heat transfer coefficients, where in the spiral unit each fluid stream has to be considered separately.

*5.4.2 Water heat transfer coefficient ($h_w$)*

The water heat transfer coefficient was determined using the Jh correlation previously developed for the square PFCHE, in a water/water system. Both units adopt the cross-flow arrangement and since the water resistance is small, this approach has been used. The correlation was extrapolated to include the low water flow rates having a Re range of 2.4<Re<8.4. The Jh correlation for the water/water system in the square PFCHE is shown below.

$$Jh_w = 1.3886\ Re^{-0.6337} \qquad \text{for } 87<Re<235 \qquad (5.2)$$

The water heat transfer coefficient ($h_w$) was then determined using the following equation.

$$h_w = (\ Jh\ k\ Re)/(d_h\ Pr^{-0.33}) \qquad (5.3)$$

Once the water heat transfer coefficient was determined, the air heat transfer coefficient ($h_a$) can be evaluated from the overall heat transfer coefficient. Prior to this, the overall heat transfer coefficient (U) is first determined by using the E-NTU method, as employed for the square PFCHE. The calculation for the air heat transfer coefficient is shown in the following section.

*5.4.3 Air heat transfer coefficient ($h_a$)*

Once the water and the overall heat transfer coefficients have been determined, the air heat transfer coefficient ($h_a$) can now be calculated using the expression below.

$$h_a = \left( \frac{1}{\left(\frac{1}{U}\right) - \left(\frac{1}{h_w}\right) - \left(\frac{t}{k_{film}}\right)} \right) \qquad (5.4)$$

Following this, the Colburn factor for the air-side ($Jh_a$) can be calculated using a re-arrangement of equation (5.3). In the next section, we consider the friction factor calculations involved in the spiral PFCHE.

### *5.4.4 Air-side friction factor ($f_a$)*

The pressure drop of the spiral PFCHE is measured on the air-side, over the inlet and outlet air streams. The water-side pressure drops are not measured as the water flow rates tested are relatively low, thus generating low negligible pressure drops. Therefore, only the air pressure drops are noted. The air-side friction factors are determined using the same formula as adopted by the square PFCHE. Once the Jh and f factors have been evaluated, the design correlations for the spiral PFCHE were developed from the Jh and f plots. In the following section, we proceed to explain the experimental results obtained, by using four performance evaluation plots (Jh, f, E and Jh/f). We begin by considering the heat balance errors involved in the unit, for each constant water flow rate tested.

## 5.5 Experimental results

### *5.5.1 Heat balance error (HBE)*

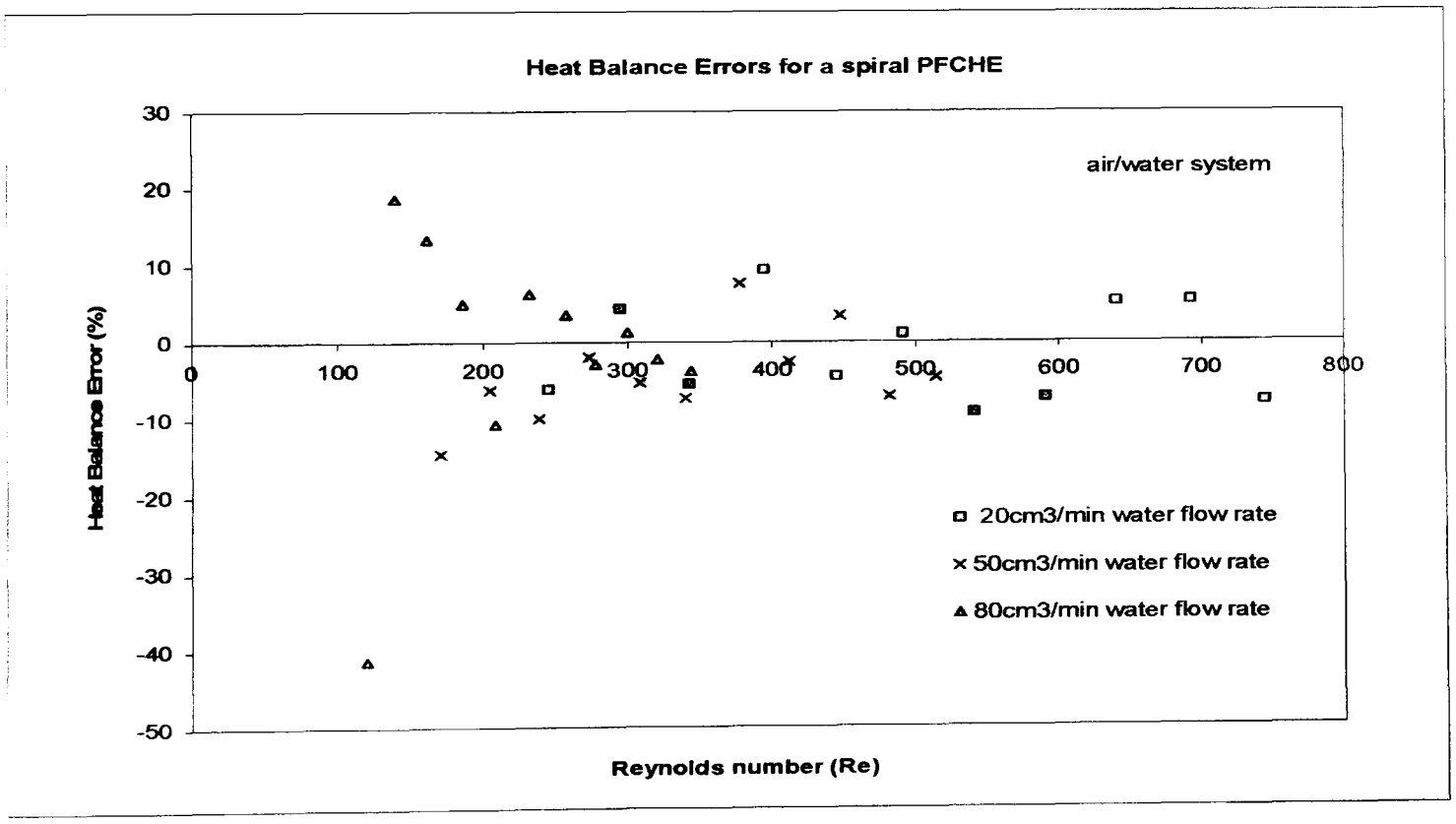


**Figure 5.6 Heat balance errors for a spiral PFCHE with 20, 50 and 80 $cm^3$/min constant water flow rates**

It can be seen from Figure 5.6 that at 20 $cm^3$/min constant water flow rate, there is the least heat loss over the range of Re numbers investigated. The 80 $cm^3$/min system has the highest errors followed by the 50 $cm^3$/min system. This can be due to the fact that leaks occur at higher water

flow rates. It is also interesting to note that the high errors obtained are mostly prominent at low air flows, corresponding to the lower Re numbers as shown in the graph above. At higher Re (550<Re< 700), both the 80 and 50 $cm^3$/min systems can achieve lower heat losses than the 20 $cm^3$/min system. However, this observation is not sufficient to outweigh the overall heat balance evaluation, whereby the 20 $cm^3$/min system has heat balance errors consistently less than 10%. To confirm and support the current findings, further testing at higher Re numbers are needed, along with an improvised design to accommodate higher water flows.

In accordance to this heat balance result, the performance evaluation for the spiral PFCHE was then conducted for the system that gave the least heat losses, namely the 20 $cm^3$/min constant water/air system. This system was chosen to ensure that the design correlations developed would have a broader Re range, with heat balance errors of less than 10%. If the 50 $cm^3$/min or 80 $cm^3$/min constant water systems were used, the design correlations will have a shorter valid Re range and therefore be less useful. In the following section, the heat transfer results for the spiral PFCHE using the 20 $cm^3$/min constant water flow rate with varying air flows between 5-15 $m^3$/hr, are explained. We first consider the Colburn factor plot for the air-side and then move on to the water-side.

### *5.5.2 Air-side Colburn factor ($Jh_a$)*

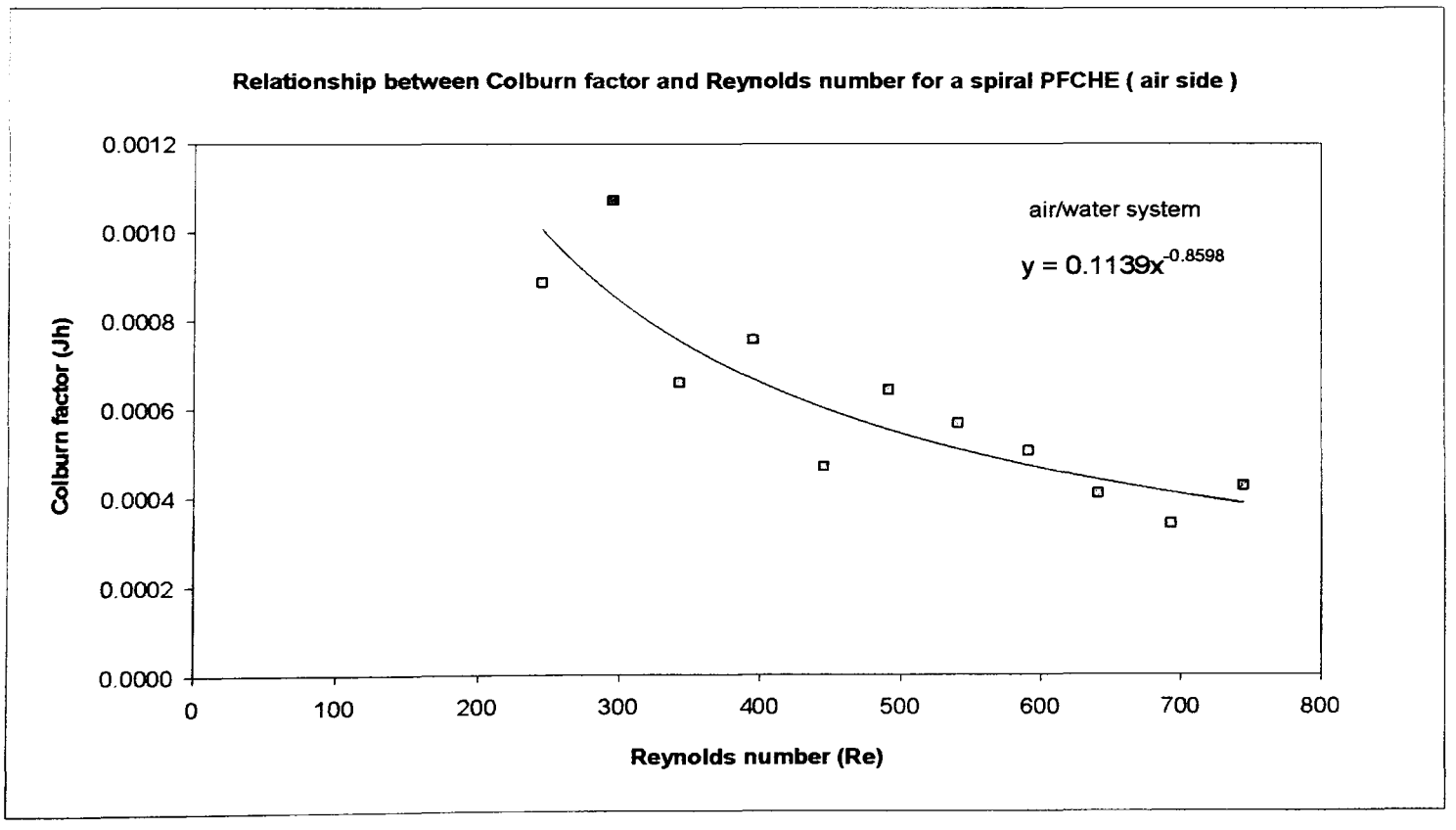


**Figure 5.7 Relationship between Colburn factor (Jh) and Reynolds number (Re) for a spiral PFCHE(air side)**

The general trend observed is the same as the square PFCHE, whereby the Jh decreases with an increase in Re number. An equal scatter is noted above and below the best fitting Jh curve, generated using Microsoft Excel. The deviation between the experimental data points and the curve is approximately ±10%. At higher air flow rates, the relative uncertainty decreases and hence there is better agreement between the experimental data points and the Jh curve obtained. This can be observed from Figure 5.7 above.

The Jh correlation established using Microsoft Excel for the air-side is as follows:

$Jh_a = 0.1139\ Re^{-0.8598}$ for 245<Re<744

We now proceed to develop the Jh correlation for the water-side in the spiral PFCHE.

### *5.5.3 Water-side Colburn factor ($Jh_w$)*

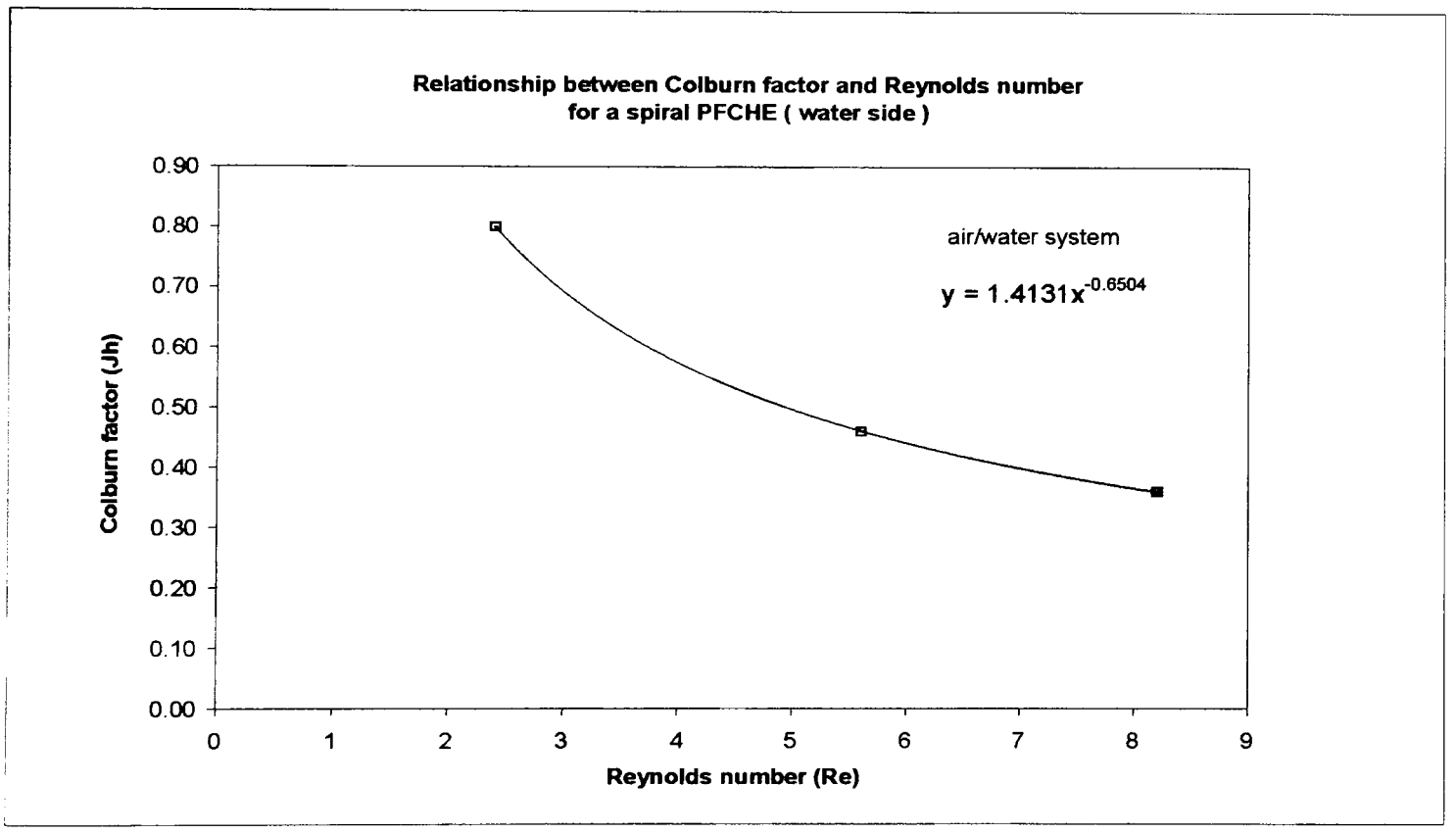


**Figure 5.8 Relationship between Colburn factor (Jh) and Reynolds number (Re) for a spiral PFCHE(water side)**

Similarly for constant air flow rates, the water flow rate was varied and the thermal performance for the water-side was determined, leading to the development of the Jh correlation using Microsoft Excel. The water-side heat transfer coefficient for each water flow rate was determined using the Jh correlation for the square configuration previously developed, in a water/water

system. Three water flow rates were tested at 20 $cm^3$/min, 50 $cm^3$/min and 80 $cm^3$/min respectively. The Jh correlation developed is as follows:

$Jh_w = 1.4131\ Re^{-0.6504}$ for 2.4<Re<8.4

As with the air-side, the Jh decreases with an increase in Re number. Further studies involving higher Re numbers are needed to establish a more useful Jh water correlation, covering a broader Re range in the spiral PFCHE. Once this is developed, a valid comparison between the water heat transfer coefficients in the square and spiral PFCHEs can be conducted, as the water flow rates currently used in the spiral unit are relatively low. This exercise is proposed to show the effect on the water heat transfer coefficients, due to the different PFCHE configurations. Next we will look at the effect of pressure drop in the spiral PFCHE. Note that pressure drop measurements are taken over the air-side, as the water pressure drops are very small and therefore can be ignored.

*5.5.4 Air-side friction factor (f)*

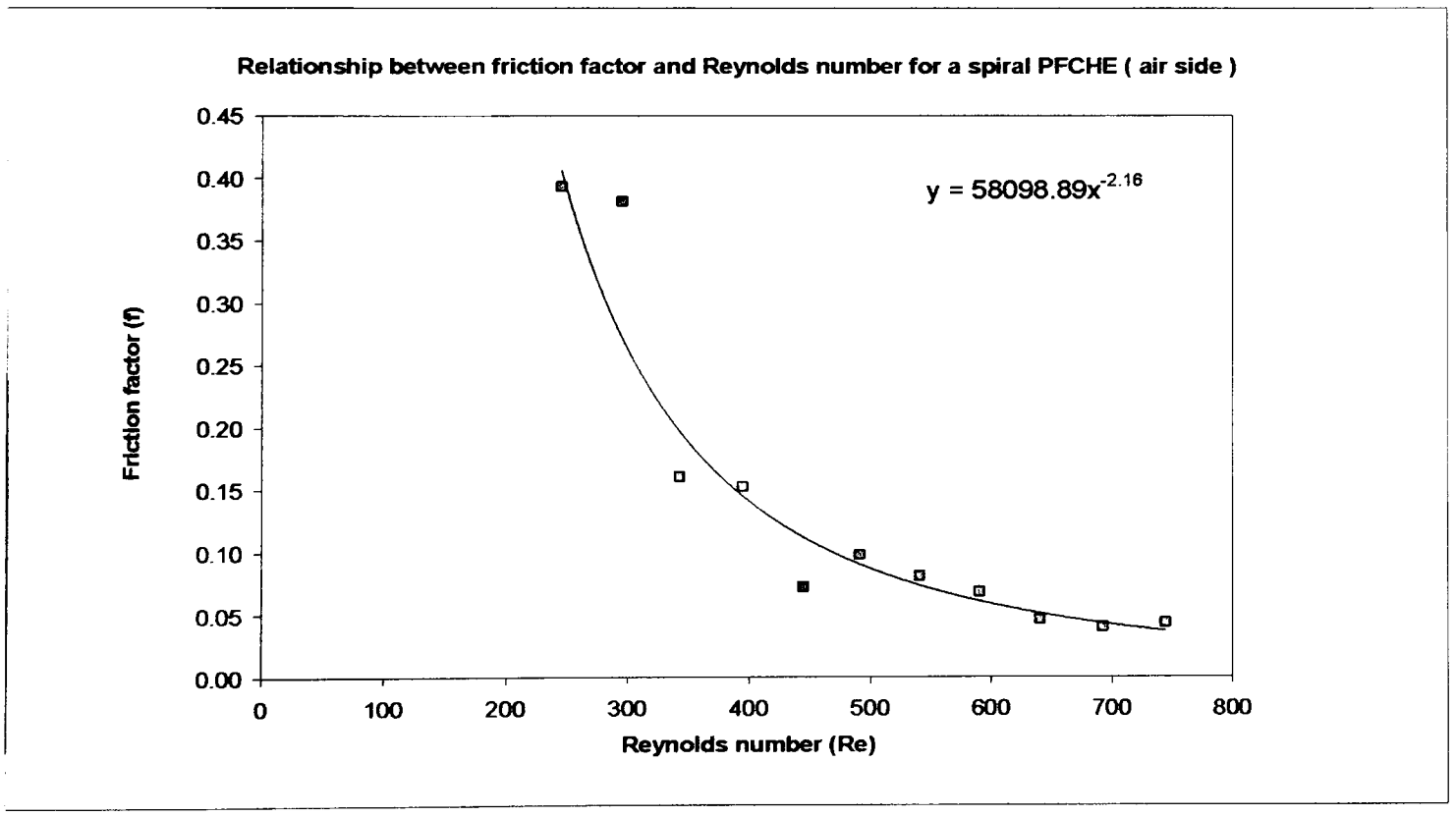


**Figure 5.9 Relationship between friction factor (f) and Reynolds number (Re) for a spiral PFCHE(air side)**

The friction factor decreases with an increase in Re number. There is better agreement between the experimental friction factors calculated and the curve generated using Microsoft Excel,

compared to the Colburn factor plot earlier. This translates into the pressure drop measurements being more accurate than the temperature measurements, as the air flow rates used are the same. Errors generated between the f curve and the experimental data points are approximately ±10%. The friction factor correlation developed is as follows:

$f_a = 58098.89\ Re^{-2.16}$ for 245<Re<744

After considering the Jh and f plots, we now move on to consider the pumping power characteristics of the spiral PFCHE in an air/water system.

### *5.5.5 Pumping power (E)*

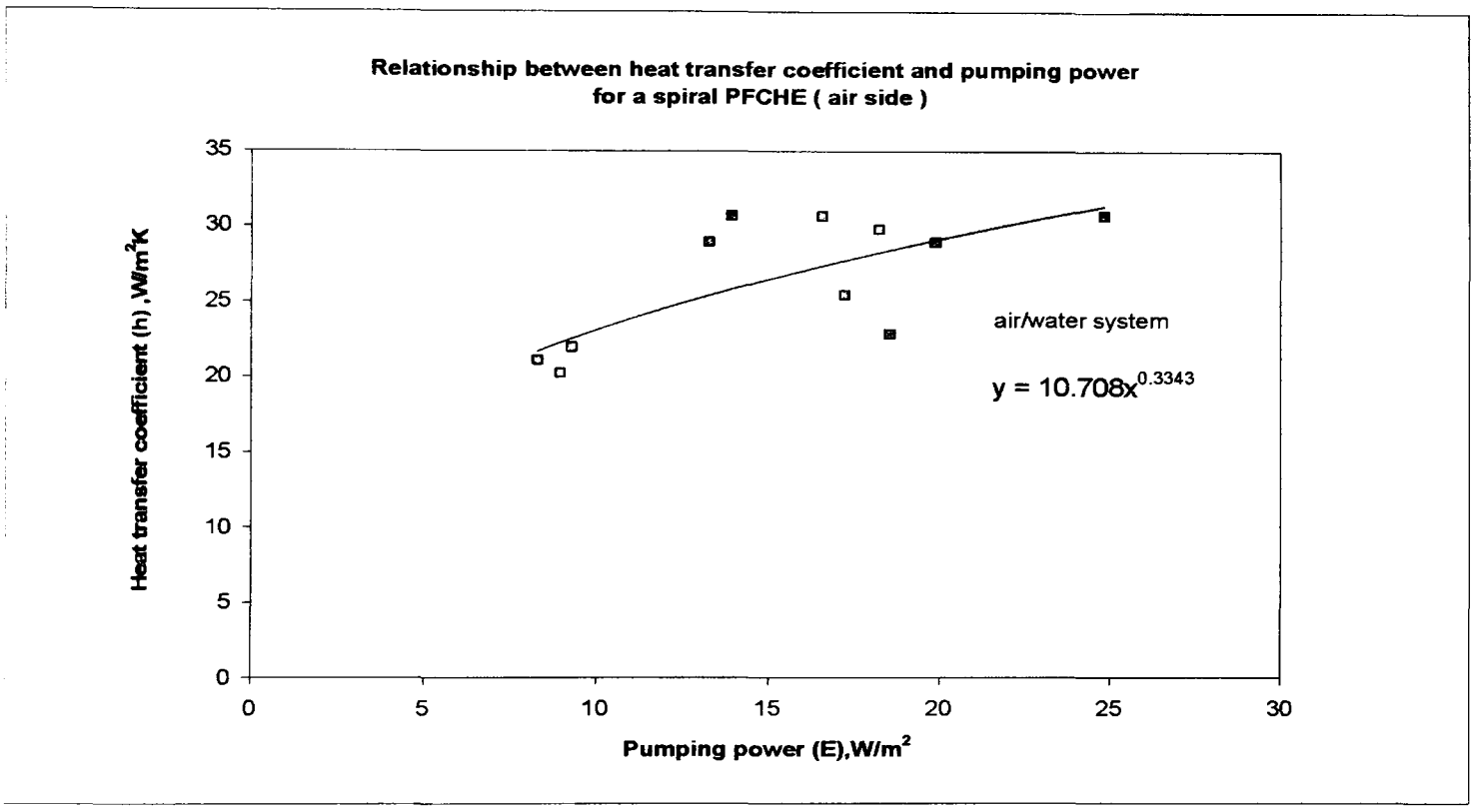


**Figure 5.10 Relationship between heat transfer coefficient (h) and pumping power (E) for a spiral PFCHE(air side)**

The pumping power requirements increase, in order to achieve higher heat transfer coefficients. In the mid-pumping power values plotted, a scatter of data occurs from this overall trend, as shown in Figure 5.10 above. Nevertheless, the scatter is quite well distributed above and below the best fitting curve generated using Microsoft Excel. The errors generated between the curve and experimental data are in the region of ± 10%, with an exception being at E=18 W/m$^2$. The error at this point is in the order of 25%, whereby the corresponding heat transfer coefficient achieved is less than expected. Perhaps at this pumping power value, there should be less

resistance to flow than is currently presented to enable higher heat transfer. Again, this could be due to an inaccuracy in the pressure drop measurement. The pumping power correlation generated using Microsoft Excel is as follows:

$h = 10.708\ Re^{0.3343}$ for $8.3<E<24.8$

In addition to the performance evaluation methods above, we now investigate the air heat transfer coefficients for the spiral PFCHE. Once the water heat transfer coefficients were established, the air heat transfer coefficients for the spiral PFCHE could then be calculated. From this, a comparison between the values obtained for the spiral and square PFCHE could be carried out, as both adopt the same range of air flow rates in the respective units. Therefore, the difference in value could be put down to the difference in the heat exchanger configuration.

Furthermore as shown earlier, the Jh correlation (square PFCHE) for the water/water system was used to calculate the spiral water-side heat transfer coefficients. Therefore, this lends support to the validity of the comparison above.

*5.5.6 Spiral and square PFCHE heat transfer coefficients (h)*

The heat transfer comparison is based on the data obtained for the 90° corrugation angle. However, for the spiral PFCHE configuration the air flow experiences a corrugation angle closer to 60°, when it is bent around the aluminium core. It will be shown in Chapter Seven that at low Re numbers, the thermal performance of the 60° angle is inferior to the 90° angle in the square PFCHE (see Figure 7.4). In accordance to this, when we calculate the heat transfer obtained for the spiral PFCHE at Re=500, we find that it attains 36% of that achieved in the square 60° configuration. At Re=500, the square 60° heat transfer coefficient is obtained by extrapolation. The heat transfer comparison between the spiral and the square PFCHEs is shown in Figure 5.11 below.

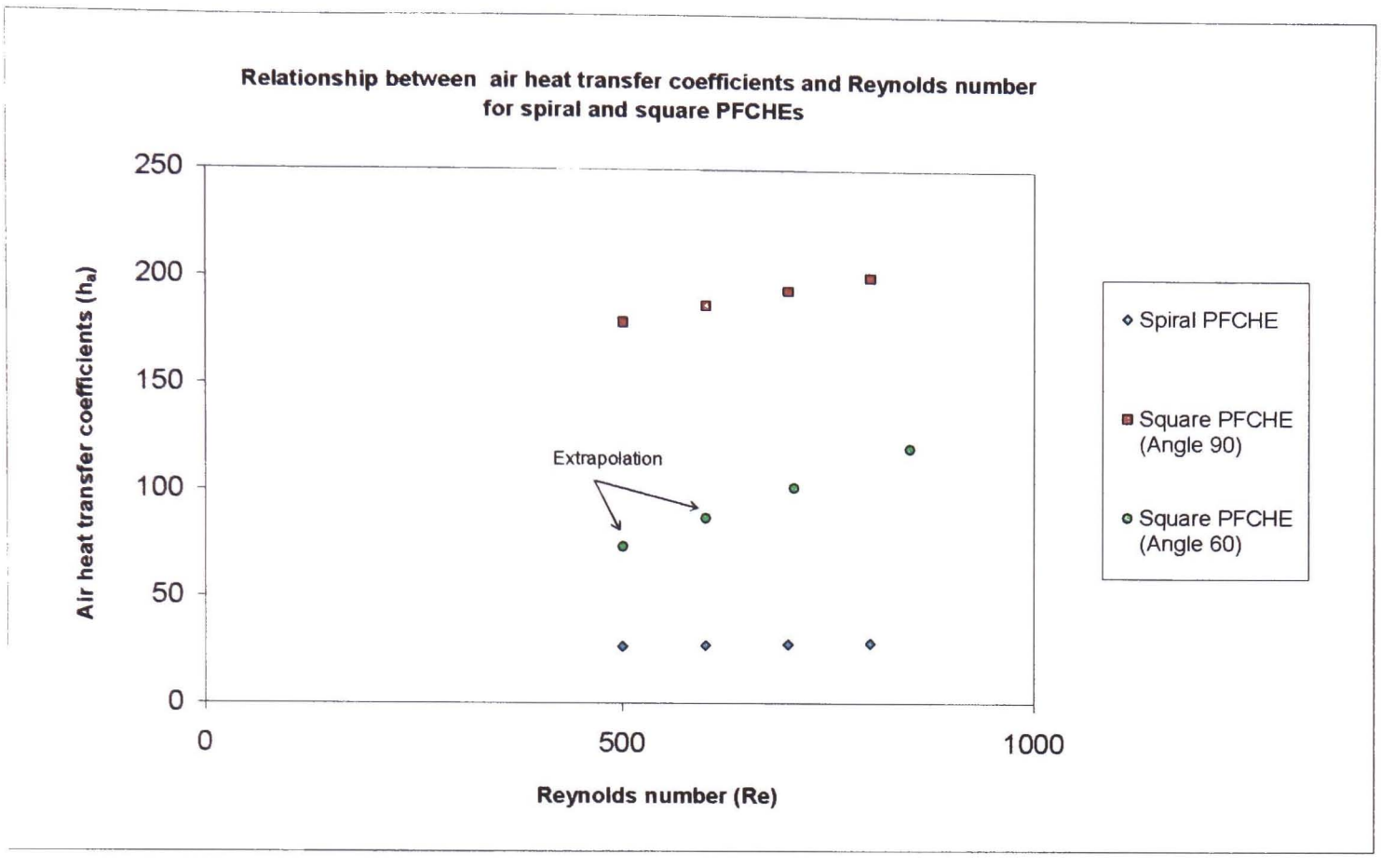


**Figure 5.11 Relationship between heat transfer coefficient (h) and Reynolds number (Re) for the spiral and square PFCHE**

*5.5.7 Spiral and square PFCHE friction factors (f)*

Following the comparison on heat transfer, we next consider the difference in the friction factors achieved for both the spiral and square PFCHEs. As with the heat transfer comparison, the spiral PFCHE is compared with both the square 60° and 90° configurations, with emphasis on the 60° angle. This is shown in Figure 5.12 below.

At Re=500, it is found that the spiral friction factor is 8% of that achieved in the square 60° configuration. Apart from the difference in the corrugation angles, this observation can also be also due to the shorter air flow path length for the spiral unit (see Table 5.3), which causes a lower pressure drop penalty. This result is expected as minimising the pressure loss for the air; as well as the water flow, is the main aim of the spiral design. The liquid pressure loss in the spiral unit is kept low by using a small volumetric liquid flow rate.

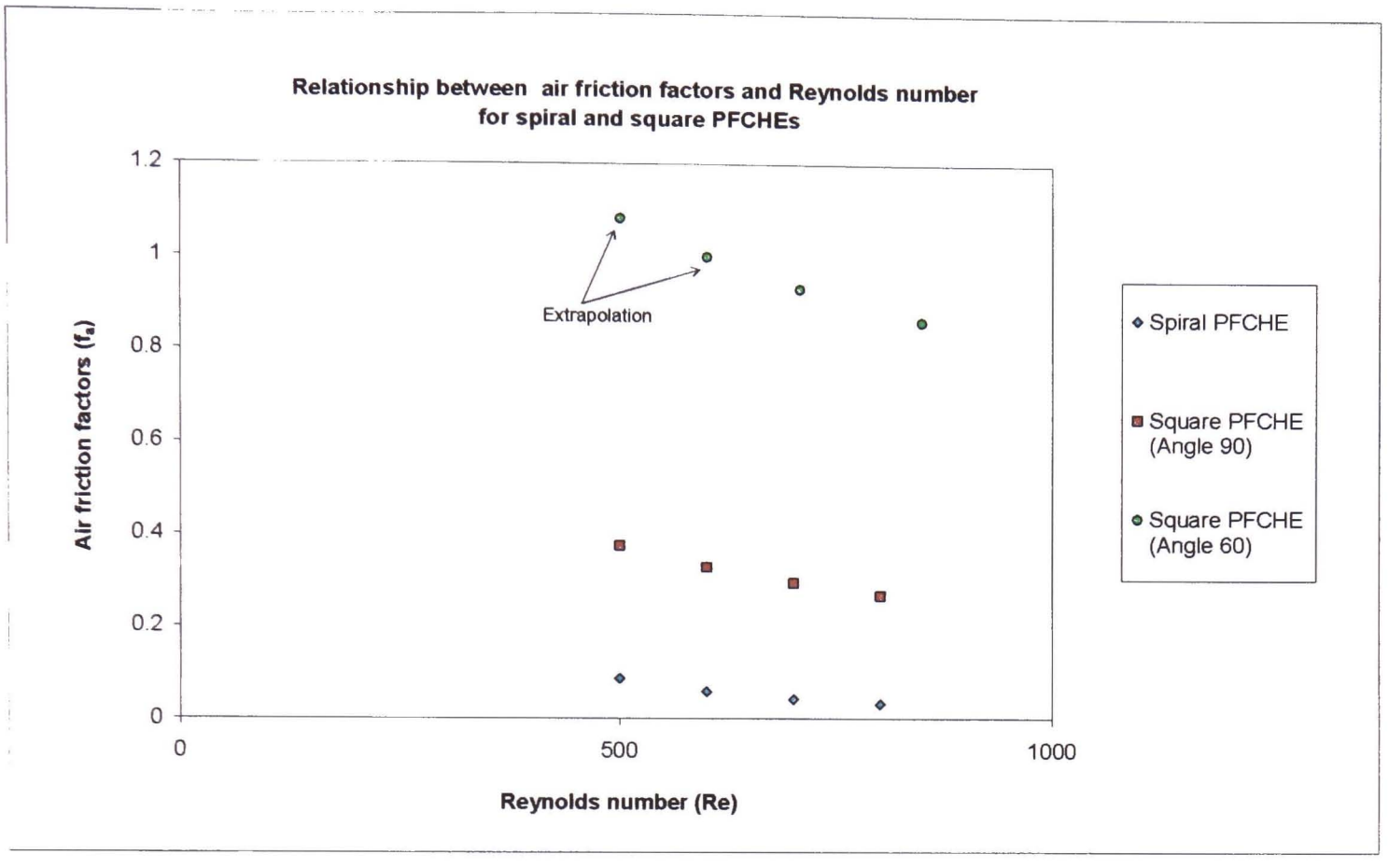


**Figure 5.12 Relationship between friction factor (f) and Reynolds number (Re) for the spiral and square PFCHE**

## 5.6 Conclusion

The Jh correlation (square 90° configuration) for the water/water system was used to calculate the water-side heat transfer coefficients in the spiral PFCHE, although it was impossible to have a 90° corrugation angle for the spiral unit, due to the bending of the polymer sheets around the aluminium core. Nevertheless, this approach was carried out as it was the only set of experimental data available for a water/water system. In performing the spiral calculations, the water-side heat transfer coefficients were found to be much higher than the air-side. This is expected, and therefore it is the air-side which dominates the overall heat transfer coefficient.

From the experimental results, it can be concluded that the square PFCHE achieves higher heat transfer than the spiral PFCHE at the expense of higher pressure drops. Nevertheless, the trends for the spiral PFCHE plots are similar to those observed in the square PFCHE. The difference in the performance observed, can be put down to the difference in the heat exchanger configuration. The air flow in the spiral PFCHE experiences a corrugation angle closer to 60°, as the sheets are bent around the aluminium core. A heat transfer comparison between the spiral and square 60° configuration showed that the former attained 36% of that achieved in the square unit.

In the spiral configuration, the air flow may be flexing the polymer sheets because they were not compressed as rigidly as in the square configuration. The flexing action may have resulted in altering (increasing) the hydraulic diameter and thereby reducing the thermal performance and pressure drop of the unit. This highlights the need of detailed manufacturing issues for the spiral configuration to maintain the physical integrity of the exchanger module. The spiral PFCHE with an air/water system achieved the best experimental results using a 20 $cm^3$/min constant water flow rate with varying air flow rates between 5-15 $m^3$/hr. The spiral design correlations developed based on a 20 $cm^3$/min constant water flow rate and varying air flow rates between 5-15 $m^3$/hr, are shown in the table below. The Jh water-side correlation was developed based on heat transfer results involving 20 $cm^3$/min, 50 $cm^3$/min and 80 $cm^3$/min constant water flow rates.

| System | Jh air | Re air |
|---|---|---|
| air/water | $0.1139\ Re^{-0.8598}$ | 245<Re<744 |
| | Jh water | Re water |
| | $1.4131\ Re^{-0.6504}$ | 2.4<Re<8.4 |
| | f air | Re air |
| | $58098.89\ Re^{-2.16}$ | 245<Re<744 |

**Table 5.2 Design correlations for the spiral PFCHE**

The design details for the spiral and square PFCHE are given in the table below.

| PFCHE configuration | Unit | Square | Spiral |
|---|---|---|---|
| Heat transfer area | $m^2$ | 0.05 | 0.08 |
| Air free flow area | $m^2$ | 0.000135 | 0.000420 |
| Water free flow area | $m^2$ | n/a | 0.000155 |
| Air path length | m | 0.135 | 0.1 |
| Water path length | m | n/a | 0.21 |
| Air flow passages | - | 2 | 4 |
| Water flow passages | - | n/a | 6 |
| Number of sheets | - | 5 | 6 |
| Number of sheets for heat transfer | - | 3 | 4 |
| Air hydraulic diameter | mm | 2 | 2 |
| Water hydraulic diameter | mm | n/a | 1 |

**Table 5.3 Design details for the spiral and square PFCHE**

## 5.7 Summary

This chapter describes the performance testing for the spiral PFCHE under laminar conditions, using an air/water system. The design concept of the unit; along with the experimental and performance calculation procedures are enclosed. Following this, the experimental results are depicted using performance evaluation plots (Jh, f and E) and a performance comparison with the square PFCHE is also included. From the performance evaluation plots, the design correlations (Jh and f) for the spiral unit are then developed.

In the following chapter, the design correlations (Jh and f) developed for the square and spiral PFCHE, are used towards developing alternative units for suitable applications; dominated by metallic heat exchangers. The incentive for this is the huge weight, energy and cost savings that will be generated. We will look into four case studies involving the square PFCHE and one case study for the spiral unit. Three case studies for the square unit involve the water/water system whilst the fourth involves the air/air system. Applications include a cabin air cooler for the aviation industry, fuel cell heat exchangers in transport vehicles and also a car radiator for the automobile industry.

# CHAPTER 6 - CASE STUDIES FOR SQUARE AND SPIRAL PFCHE

## 6.0 Introduction

In Chapter Four, design correlations (Jh and f) for the square PFCHE involving six fluid systems (air/air, water/water and four glycerol-water mixtures/water) have been developed. Following this, a set of spiral design correlations was established in Chapter Five for an air/water system. These correlations for the square and spiral units, are key tools in obtaining alternative designs for applications currently monopolised by metallic heat exchangers. Following the establishment of the design correlations, we now proceed to use them to perform case studies in selected applications; to suit the fluids and the configuration. A case study is simply a feasibility study where an alternative heat exchanger design is produced, to replace a conventional design for a suitable application.

In this chapter, case studies are conducted for the square and spiral polymer film compact heat exchangers. The motivation for adopting the alternative PFCHE design is an increase in heat transfer enhancement, energy efficiency plus weight and cost savings. Indeed performing a case study is the 'tried and tested' route undertaken to test the feasibility of any novel intensified unit, in this case a PFCHE. The main element in performing the case studies is to incorporate the PFCHE heat transfer and pressure drop data, in the form of Jh and f correlations, towards the development of alternative designs. This is achieved by conforming to the conventional design specifications; such as the duty required and pressure drop limitations. The industrial companies involved in disclosing the specifications relevant for the case studies in this chapter are SERCK Aviation, Honeywell SERCK, XCellsis and NISSAN. The case studies were deemed useful by industry in order to generate data for performance, cost, weight reduction and fuel or energy saving comparisons.

For the square PFCHE, design correlations for the air/air and water/water systems are used. An alternative design for cabin air coolers is developed using the air/air system, whilst a filter cooler and two fuel cell heat exchanger designs are developed using the water/water system. The spiral PFCHE design correlations are used in a case study for car radiators. The results of the case studies, which will be explained in the following section, show that the PFCHE design is indeed a suitable alternative to replace its metal counterparts as the weight and cost savings generated are tremendous.

We begin the chapter with a case study for the cabin air cooler in the aviation industry. This is followed by the filter cooler and two fuel cell heat exchangers in transport vehicles. Finally, we consider the case study for the car radiator.

## 6.1 Square PFCHE for cabin air cooler application

Before disclosing the results of the case study, we first provide a general background to highlight the incentive and suitability in choosing the cabin air cooler as a case study for the square PFCHE, in an air/air system.

### *6.1.1 Potential for PFCHE as cabin air coolers*

The convective heat transfer coefficient of gases is usually one to two orders of magnitude lower than that of liquids. For this reason, a large heat transfer area is necessary for realising a high heat transfer rate, especially if one or more fluids are gaseous in a heat exchange unit. To achieve this and to avoid high pressure drops, the heat transfer surface in these units must be compact. By adopting compact units, the heat transfer enhancement will also result in size reduction and thus achieving lower weight and lower investment costs.

It is well known that compact heat exchangers are key components for the development of future aircraft devices. Currently, only compact metallic units are used and the development of the latest technology for such units is quite stagnant. Therefore, new novel designs based on other compatible materials are needed to improve the performance of conventional metallic units, especially in addressing the weight issue, which is of primary importance in the aviation industry.

As the demand for clean and fresh air inside cabin compartments is increasing, there is a strong drive to use energy efficient compact heat exchangers, which are lightweight for achieving such duties. Heat exchangers made from PEEK are an ideal choice, as PEEK is a certified material for use in the aviation industry. Bearing this in mind and the apparent benefits of the PFCHE design, the cabin air cooler is selected as a suitable unit to perform a case study.

The cabin air cooler is a widely used commercial air-conditioning unit in the aviation industry. Air is the heat transfer fluid, whereby it is both heated and cooled by transferring heat from each stream. This is done through a heat transfer surface which is where the design of the PFCHE comes into play, as the ideal surface will maximise the heat transfer between the fluids at a lower expense of energy, weight and cost.

### *6.1.2 Cabin air cooler case study*

The design correlations (Jh and f), for the square PFCHE in an air/air system are used to test the feasibility of the alternative design for an aluminium cabin air cooler. The correlations used are as follows:

$$Jh = 2.0097\ Re^{-0.7644} \qquad \text{for } 510<Re<2540 \qquad (6.1)$$

$$f = 0.5992\ Re^{-0.1698} \qquad \text{for } 510<Re<2540 \qquad (6.2)$$

The design correlations are important tools, as it gives a direct measure of the heat transfer and pressure drop performance of the PFCHE. These correlations are dependent on the Re number involved. Therefore, it should be noted that the current aluminium cabin air coolers involve air flows in the laminar range, which lends support to the use of the square PFCHE design correlations. Due to the low density of air at great altitudes, low Re numbers occur quite often in aircraft applications. Hence, the low Re number range between 500 and 3000 is deemed suitable for the aviation industry.

Data used in this case study, was provided by SERCK Aviation in order to assess the feasibility of using the PFCHE as secondary heat exchangers in cabin air coolers. Table 6.1 below shows the details of an aluminium cabin air cooler currently used by the aviation industry.

| | |
|---|---|
| Length | 0.3 m |
| Width | 0.1m |
| Height | 0.6m |
| No. of sheets | 52 or 53 |
| Duty (kW) | 30 |
| Flow (kg/s) | 0.33 |
| Inlet pressure (kPa) | 350 |
| Inlet temperature (K) | 518 |
| Exit temperature (K) | 433 |
| Pressure Drop (kPa) | 4.1 |

**Table 6.1 Specification for an aluminium cabin air cooler**

The alternative suitable designs of the PFCHE cabin air cooler, complying with the above specification has been presented in Table 6.2 below. Two designs have been presented, each with different dimensions and operating at different Re numbers. It can be seen that the resulting pressure drop is different for both cases but is well below the specified limit, as shown in Table 6.1.

| DESIGN 1 | | DESIGN 2 | |
|---|---|---|---|
| Length, width, height | (0.2 x 0.3 x 0.27)m | Length, width, height | (0.15x 0.25 x 0.47)m |
| Weight | 2.36 kg | Weight | 2.57 kg |
| Number of sheets | 270 | Number of sheets | 470 |
| Re | 582 | Re | 400 |
| Pressure drop | 1.77 kPa | Pressure drop | 0.69 kPa |
| Heat transfer area | 16.1 $m^2$ | Heat transfer area | 17.5 $m^2$ |

**Table 6.2 Alternative designs for metallic cabin air coolers**

From the alternative designs presented in Table 6.2, it can be shown that a significant weight saving resulting in a cost saving of approximately (£8.7M per annum) can be achieved, if the square PFCHE is adopted as a secondary heat exchanger in cabin air coolers. The weight and total cost saving predictions are tabulated in Table 6.4. Prior to this, the total cost evaluated is based on the energy saving and fuel cost information presented in Table 6.3 below. A sample of the calculations involved for the case study is attached in Appendix G.

| | |
|---|---|
| Weight of a 747 plane | 400 tonnes |
| Fuel used during flight | 10 tonnes |
| Total number of aircraft (commercial jet) | 14866 |
| Total fleet flying hours in the last 12 months | 34060073 |
| Cost of 1 tonne of aviation fuel | £296.54 |
| Total fuel saving per year | 29630 tonnes |

**Table 6.3 Fuel cost data provided by SERCK Aviation**

| | |
|---|---|
| Weight of Aluminium Cabin Air Cooler | 40.8 kg |
| Weight of PEEK matrix | 2.7 kg |
| Weight of PEEK manifold | 2.7 kg |
| Weight of PEEK Cabin Air Cooler | 5.4 kg |
| Weight Saving | 88% |
| Total yearly cost saving | £8.7 M |

**Table 6.4 Cost saving predictions for PFCHE cabin air coolers**

The case study clearly suggests that by using PEEK heat exchangers in cabin air coolers, significant cost savings (£8.7M per annum) can be achieved in the aviation industry. The above prediction is a conservative one, as most aircraft employ more than one cabin air cooler. For instance, a typical 747 plane uses at least 3 cabin air coolers.

In the following section, we consider the case studies for a filter cooler and two fuel cell heat exchangers in transport vehicles. These will involve the design correlations for the water/water system in the square PFCHE.

## 6.2 Square PFCHE for fuel cell application

In this section, we consider three case studies for the fuel cell driven transport industry. First we will look into the alternative PFCHE design for a filter cooler, and then for two fuel cell heat exchangers. We begin with a brief background of the units to understand the reasons for employing them as case studies.

### *6.2.1 Potential for PFCHE as fuel cell transport heat exchangers*

Besides the aviation industry, the inherent benefits of the PFCHE have also attracted potential applications in the fuel cell industry for transport vehicles. These fuel cell heat exchangers are apart of several other components that form the engine of a transport vehicle. As shown from literature, by adopting the fuel cells instead of conventional metal units, significant weight and cost savings can be achieved. Nevertheless both of these units are metallic, imposing a limit to the options and advancement in design improvement for the transport industry. This limitation in the freedom of design can be addressed by using polymer film compact heat exchangers.

To widen the scope of improvisation for heat exchangers in transport vehicles, case studies on the polymer film compact heat exchanger (PFCHE) are conducted. Using polymer as the alternative material of construction along with a novel configuration, the PFCHE is believed to bring several benefits over the metallic fuel cell designs in terms of overall performance and energy savings.

In this section, three fuel cell units are discussed as case studies for the PFCHE. The heat transfer fluids involved in these exchangers are de-ionised water and water-ethylene glycol mixtures (WEG). These fluids have similar physical properties to water. Bearing this in mind, the design correlations for the water/water system in a square PFCHE are adopted to develop the alternative designs.

Nevertheless, to increase the accuracy of the case studies performed, the physical properties used for the alternative designs are based on water and water-ethylene glycol mixtures, tabulated in Microsoft Excel. Unlike the cabin air cooler, the design correlations for the PFCHE water/water system need to be extrapolated, as the Re required in the metallic design exceeds the PFCHE correlation range. The design correlations used are as follows:

$$Jh = 1.3886\ Re^{-0.3174} \qquad \text{for } 87<Re<235 \qquad (6.3)$$

$$f = 32.797\ Re^{-0.7192} \qquad \text{for } 87<Re<235 \qquad (6.4)$$

We now proceed to show the results of the three case studies conducted.

*6.2.2 Fuel cell case studies*

Three case studies were carried out in collaboration with Honeywell SERCK and XCellsis. Using the design correlations for a water/water system, prototypes were designed for deionised-water/glycol systems and compared with aluminium and stainless steel units. The designs, which are used in fuel cell driven transport vehicles are as follows:

1. Filter Cooler with duty 14.5 kW
2. Fuel Cell Heat Exchanger with duty 340 kW
3. Fuel Cell Heat Exchanger with duty 260 kW

The specifications for the three heat exchangers, provided by Honeywell SERCK's client XCellsis are presented in Tables 6.5a, b and c below.

Design 1

| | | | | | |
|---|---|---|---|---|---|
| Name | DI-Glycol Filter Cooler | | | | |
| Duty | 14.5 kW | | | | |
| Duty Cycle | 100% | | | | |
| Hot Circuit | Fluid | Deionised water / pure glycol | Cold Circuit | Fluid | WEG |
| | Req'd Outlet Temp (K) | 335 | | Inlet Temp (K) | 330 |
| | Pressure (kPag) | 310 | | Pressure (kPag) | 310 |
| | Pressure Drop (kPad) | <30 | | Pressure Drop (kPad) | <30 |
| | Flow (lpm) | 30 | | Flow (lpm) | 30 |

**Table 6.5a Specification for a Filter Cooler with duty 14.5 kW**

Notes: 1. Materials in contact with DI water limited to 316L or 347 stainless steel, or low copper aluminium (if uncertain contact (XCellsis)
2. WEG flow calculated with a 277K approach. If a tighter approach temperature is possible we will adjust WEG flow to suit.
3. Both water ethylene glycol mixtures are at 50/50

Design 2

| Name | Fuel Cell Heat Exchanger-Option A | | | | |
|---|---|---|---|---|---|
| Duty | 340 kW | | | | |
| Duty Cycle | 100% | | | | |
| Hot Circuit | Fluid-Clean Side | Deionised water/pure glycol | Cold Circuit | Fluid-Dirty Side | WEG |
| | Req'd Outlet Temp (K) | 343 | | Inlet Temp (K) | 338 |
| | Pressure (kPag) | 250 | | Pressure (kPag) | 275 |
| | Pressure Drop (kPad) | <30 | | Pressure Drop (kPad) | <30 |
| | Flow (lpm) | 600 | | Flow (lpm) | 560 |

**Table 6.5b Specification for a Fuel Cell Heat Exchanger with duty 340 kW**

Design 3

| Name | Fuel Cell Heat Exchanger-Option B | | | | |
|---|---|---|---|---|---|
| Duty | 260 kW | | | | |
| Duty Cycle | 100% | | | | |
| Hot Circuit | Fluid-Clean Side | Deionised water/pure glycol | Cold Circuit | Fluid-Dirty Side | WEG |
| | Req'd Outlet Temp (K) | 343 | | Inlet Temp (K) | 338 |
| | Pressure (kPag) | 250 | | Pressure (kPag) | 275 |
| | Pressure Drop (kPad) | <30 | | Pressure Drop (kPad) | <30 |
| | Flow (lpm) | 500 | | Flow (lpm) | 425 |

**Table 6.5c Specification for a Fuel Cell Heat Exchanger with duty 260 kW**

Based on the data provided in Tables 6.5a, b and c, alternative designs for PFCHEs are carried out in order to meet the heat transfer requirement. The results of the case studies are shown in Tables 6.6a, b and c below. The terms (AL) and (SS), refer to aluminium and stainless steel units respectively.

| Design Unit | DI-Glycol Filter Cooler | | | |
|---|---|---|---|---|
| Duty | 14.5 kW | | | |
| Materials | Stainless Steel (SS) | Aluminium (AL) | Polymer (PFCHE) | % Saving wrt SS AL |
| Length (mm) | 110 | 110 | 120 | n/a n/a |
| Width (mm) | 110 | 110 | 120 | n/a n/a |
| Height (mm) | 92 | 73 | 80 | n/a n/a |
| Weight (kg) | 2.96 | 0.77 | 0.12 | 96 84 |
| ΔPdi (kPa) | 23.5 | 8.3 | 1.88 | 92 77 |
| ΔPweg (kPa) | 23.8 | 8.4 | 5.03 | 79 40 |

**Table 6.6a Alternative design and savings for a filter cooler with duty 14.5 kW**

| Design Unit | Fuel Cell Heat Exchanger | | | |
|---|---|---|---|---|
| Duty | 340 kW | | | |
| Materials | Stainless Steel (SS) | Aluminium (AL) | Polymer (PFCHE) | % Saving wrt SS AL |
| Length (mm) | 300 | 300 | 300 | n/a n/a |
| Width (mm) | 300 | 300 | 300 | n/a n/a |
| Height (mm) | 320 | 240 | 180 | n/a n/a |
| Weight (kg) | 65.3 | 18.8 | 2.33 | 96 88 |
| ΔPdi (kPa) | 50.0 | 26.3 | 20.80 | 58 21 |
| ΔPweg (kPa) | 44.6 | 23.5 | 13.90 | 69 41 |

**Table 6.6b Alternative design and savings for a fuel cell heat exchanger with duty 340 kW**

| Design Unit Duty | Fuel Cell Heat Exchanger 260 kW | | | |
|---|---|---|---|---|
| Materials | Stainless Steel (SS) | Aluminium (AL) | Polymer (PFCHE) | % Saving wrt SS AL |
| Length (mm) | 300 | 300 | 300 | n/a n/a |
| Width (mm) | 300 | 300 | 300 | n/a n/a |
| Height (mm) | 285 | 229 | 322 | n/a n/a |
| Weight (kg) | 58.4 | 17.9 | 4.26 | 93 76 |
| ΔPdi (kPa) | 44.1 | 20.8 | 7.05 | 84 66 |
| ΔPweg (kPa) | 33.3 | 15.7 | 5.06 | 85 68 |

**Table 6.6c Alternative design and savings for a fuel cell heat exchanger with duty 260 kW**

It can be concluded that by using the PFCHE as an alternative for fuel cell exchangers, significant weight as well as pressure drop savings can be achieved. In all the case studies performed, the PFCHE design weighs less than a quarter of the fuel cell units. In addition, the average pressure drops of the alternative PFCHE designs are much lower, compared to both the stainless steel and aluminium units. These positive results will consequently translate into considerable fuel and therefore energy savings. We now look at the final case study considered in this chapter, involving the use of the spiral PFCHE design correlations, for a car radiator application.

## 6.3 Spiral PFCHE for car radiator application

In this section, the incentive for adopting polymers in the automobile industry pertaining to the use of spiral PFCHE units, is first disclosed. This is followed with the results of the alternative design for a car radiator.

### *6.3.1 Potential for PFCHE as car radiators*

Following the case studies on fuel cells in transport vehicles, yet another application for the PFCHE in the automobile industry is considered in this section. Unlike the previous case studies which use the square PFCHE design, in this section a spiral PFCHE is adopted for a case study on car radiators.

Conventional diesel engines are associated with three compact heat exchangers namely the radiator, oil-cooler and after-cooler to dissipate the generated heat in the system to the environment. The radiator, oil-cooler and after-coolers are used in the turbo-charged diesel engines for cooling the engine body cooling water, lubricating oil and the turbo-charged air, respectively. Air is the cooling fluid for the radiator and water is the cooling medium for the oil and after-cooler (Charyulu et al. 1999).

In the automobile industry, there are strict and demanding operating requirements that must be met by the exchanger. Here, both the size and weight of the exchanger are important, especially as the automobile manufacturing companies continue to seek to improve fuel efficiency by reducing the weight of automobiles.

One of the means to reduce the weight of heat exchangers is to fabricate the exchanger from polymeric material instead of metal. However, in general, it is not possible to merely substitute polymer for metal. Fabrication techniques that have proven to be quite acceptable using metals (welding at high temperatures) tend to be inapplicable to polymers. This is just the case for the spiral PFCHE, where it incorporates an aluminium core to be able to withstand higher temperatures, as the assembly needs to be baked in an oven as part of the fabrication process. This is conducted after laser welding the PEEK sheets and etching them with acid. Nevertheless, this slight deviation to the normal fabrication techniques is worth the effort, if the polymer units can match the performance requirements of conventional designs, whilst achieving considerable weight and energy savings. The selection of polymers that may be used will depend in particular on the conditions under which the heat exchanger is to be operated. Such conditions include not only the temperatures and pressures that are to be used and the required life of the exchanger, but also the type of fluids that are to be passed through the heat exchanger and around the heat exchanger.

The spiral PFCHE configuration is considered suitable as a car radiator, as it can handle different fluids (air and water) at different flow rates and maintain low pressure drops especially for the gas side whilst maintaining high surface area densities. The polymer of construction, PEEK, can take temperatures up to 220°C and is virtually chemical resistant (apart from concentrated nitric and sulphuric acids). The polymer is also fatigue resistant, has a low creep modulus, impact resistant and provides a sufficiently rigid structure.

In this case study for a car radiator by Nissan, the fluid passed around the heat exchanger is air, whereas the fluid passed through the heat exchanger is usually liquid from the radiator of the vehicle. Such liquid is comprised of water and a so-called anti-freeze (ethylene glycol), but other additives such as anti-rust compounds and the like, may also be present in the liquid. However, the presence of these extra components in the water, do not significantly influence its physical properties. Bearing this in mind, the spiral PFCHE using an air/water

system is deemed appropriate for the alternative design. In the following section, the car radiator case study results are described, following a brief description of the unit.

### *6.3.2 Car radiator case study*

A car radiator is a unit that is familiar to most people. The current favoured design is a metallic flat-tube and fin heat exchanger, which is the most compact and efficient of those available in the motor industry. The restriction on the radiator is one of size and it is usually found at the very front of the engine. This is because, the air is drawn in clean from the atmosphere rather than having passed through the engine first, thus not depositing any oil fouling on the finned surface of the radiator. The temperature of the fluid through a combustion engine must be kept at a fairly constant value. It must be high enough to keep any water as a vapour, but low enough as to not oxidise the lubricating oil. There is no real restriction on the inlet air temperature as this depends on the surrounding atmospheric temperature. It is sensible to look at the worst case, which in a hot country could easily be 38°C.

The main specifications that need to be adhered to are those of the fluid; namely the flow rate, inlet temperature as well as the temperature and pressure drops. The air flow details are not very important, basically as long as the spiral PFCHE can perform the same duty at the same air flow rates, then it has great potential as a car radiator. The table below outlines the specification of a car radiator provided by Nissan European Research Centre Ltd., which is to be used as a case study for the spiral PFCHE.

| | |
|---|---|
| Duty | 20 kW |
| Radiator Size (length, width, height) | 690 ,15 , 360 mm |
| Fin Pitch | 1.1 mm |
| Materials | Aluminium Header, Fins and Tubes, Plastic Tanks |
| Heat Transfer Area | 8.664 $m^2$ |
| Operating Temperature | 383K max |
| Operating Pressure | 90 kPa (typical petrol engine spec.) |
| Fluid Flow Rate | 30-120 l/min |
| Fluid Inlet Temperature | 360-368K |
| Fluid $\Delta T$ | 277-279K |
| Fluid Pressure Drop | approx. 25 kPa |

**Table 6.7 Specification for a car radiator with duty 20 kW**

As mentioned before, the fluid used by Nissan is mainly water with a small amount of anti-freeze added. This apparently does not change the physical properties of the fluid by a significant amount, and so those of water have been used. The water flow chosen was 50 l/min, with an inlet temperature of 360K and a temperature drop of 279K. The air inlet temperature was 311K and from these details, the duty can be obtained. Using all of this data, the case study can now be attempted.

Based on the specification above, an alternative spiral design for the car radiator using the design correlations for an air/water system is attempted. The correlations used are as follows:

$$Jh_{water} = 1.4131\ Re^{-0.6504} \qquad \text{for } 2.4<Re<8.4 \qquad (6.5)$$

$$Jh_{air} = 0.1139\ Re^{-0.8598} \qquad \text{for } 245<Re<744 \qquad (6.6)$$

$$f_{air} = 58098.89\ Re^{-2.16} \qquad \text{for } 245<Re<744 \qquad (6.7)$$

The details of the alternative spiral PFCHE design for a car radiator are shown in the table below.

| Description | PFCHE Design | NISSAN Design |
|---|---|---|
| Length of sheets or unit | 0.7 m | 0.69 m |
| Width of sheets or unit | 0.015 m | 0.015 m |
| Height of sheets or unit | 0.04 m | 0.36 m |
| Number of sheets | 374 | n/a |
| Heat Transfer Volume | 0.0007 $m^3$ | 0.00373 $m^3$ |
| Materials | PEEK , aluminium core, polypropylene casing | Aluminium header, fins and tubes, plastic tanks |
| Heat Transfer Area | 7.7 $m^2$ | 8.664 $m^2$ |
| Operating Temperature | 493K max | 383K max |
| Operating Pressure | 1000 kPa | 90 kPa (typical petrol engine spec.) |
| Fluid Flow Rate | 50 l/min | 30-120 l/min |
| Fluid Inlet Temperature | 360K | 360-368K |
| Fluid $\Delta T$ | 279K | 277-279K |
| Fluid Pressure Drop | 0.3 kPa | (approx. 25 kPa) |
| Weight of sheets | 1.84 kg | 23.4 kg (all aluminium) |

**Table 6.8 Alternative design for a car radiator with duty 20 kW**

Following this, the weight savings achieved when adopting the spiral PFCHE over the NISSAN design, is shown in Table 6.9 below.

| | |
|---|---|
| Weight of aluminium car radiator | 24 kg |
| Weight of PEEK matrix | 2 kg |
| Weight of PEEK manifold | 2 kg |
| Weight of PEEK Cabin Air Cooler | 4 kg |
| Weight Saving | 83% |

**Table 6.9 Weight saving predictions for PFCHE car radiators**

## 6.4 Conclusion

From the case studies conducted, it can be seen that there is a huge incentive for using the square and spiral PFCHEs as an alternative to the conventional metallic units, due to the tremendous energy and cost savings generated. In addition to this, the PFCHE designs are also more compact, require less space, are lightweight and easy to maintain.

The table below shows a summary of the weight savings achieved, when adopting the PFCHE design for the five case studies conducted in this chapter. The terms (AL) and (SS), refer to aluminium and stainless steel units respectively.

| Alternative PFCHE design | Duty (kW) | Weight saving (%) |
|---|---|---|
| Cabin air cooler | 30 | 88 (AL) |
| Filter cooler | 14.5 | 84 (AL) , 96 (SS) |
| Fuel cell heat exchanger | 340 | 88 (AL) , 96 (SS) |
| Fuel cell heat exchanger | 260 | 76 (AL) , 93 (SS) |
| Car radiator | 20 | 83 (AL) |

**Table 6.10 Summary of weight savings for the PFCHE case studies**

It can be seen that in general, the PFCHE designs weigh less than a quarter of the conventional metallic units. This is indeed a huge incentive to adopt the PFCHE as an alternative to conventional metal designs. For the cabin air cooler in particular, an annual cost saving of £8.7M is achieved when incorporating the PFCHE design over metal units.

## 6.5 Summary

Previously in Chapters Four and Five, the square and spiral PFCHEs have been introduced and using the experimental data obtained, the design correlations (Jh and f) are developed for the fluid systems studied in each configuration. Once established, the design correlations are then used in this chapter to perform case studies on conventional metallic heat exchangers for applications in the aviation, fuel cell and automobile industries.

In this chapter, five case studies are conducted to develop alternative PFCHE designs for cabin air coolers, filter coolers, fuel cell heat exchangers and car radiators. The results obtained are very encouraging; involving considerable weight and cost savings.

Following this positive discovery, we proceed to investigate yet another design aspect of the PFCHE (apart from using different fluids and configurations), in order to further extend the potential of the unit. The design aspect next considered in Chapter Seven is the corrugation angle. This study involves the performance testing of three different corrugation angles ($30^{o}$, $60^{o}$ and $90^{o}$), en route to establishing the optimum angle where the best PFCHE performance is achieved. The results obtained will also provide a better understanding of the square and spiral units as both adopt different corrugation angles in their respective designs.

# CHAPTER 7 - THE EFFECTS OF CORRUGATION ANGLE ON HEAT TRANSFER AND PRESSURE DROP IN A SQUARE PFCHE

## 7.0 Introduction

Chapter Four described the square PFCHE and outlined the experimental results for air/air, water/water and four glycerol-water mixtures/water systems. All the fluid systems were tested using a square PFCHE with a 90° corrugation angle. Chapter Five introduced the spiral PFCHE and presented the experimental results for an air/water system. The corrugation angle adopted for the spiral configuration is 20°. Bearing in mind the different corrugation angles adopted in both configurations, it was decided that the next step in research, would be to study the effect of the corrugation angle on the PFCHE performance. The aim was to obtain a better understanding on the impact of the corrugation angle, in order to maximise the potential for both the square and spiral PFCHE units and also extend the knowledge for future designs.

In this chapter an analysis of heat transfer and pressure drop data for different corrugation angles have been carried out. Generic experimental data was obtained from earlier investigations at the Process Intensification and Innovation Centre (Newcastle University).The study involved three corrugation angles (30°, 60° and 90°) in an air/air system over a Re number range of 510-2540. The 30° and 60° corrugation angles were adopted in the same square PFCHE design as explained in Chapter Four, with the only exception being the number of PEEK sheets involved in the heat exchanger matrix. The number of PEEK sheets used and the air flow rates tested, along with the individual Re range for all three corrugation angles are shown in Table 7.1 below.

| Angle (°) | No. of sheets | Air flow rates ($m^3$/hr) | Reynolds range |
|---|---|---|---|
| 30 | 7 | 5-11 | 706-1555 |
| 60 | 7 | 5-17 | 706-2403 |
| 90 | 5 | 3-15 | 510-2540 |

**Table 7.1 Details of the square PFCHE with 30°, 60° and 90° corrugation angles**

Apart from gaining a better understanding of the angles, the main objective of this study is to determine the optimum angle for the square PFCHE, whereby the best overall thermal and hydraulic performance can be achieved. In order to accomplish this, design correlations (Jh and f) are developed to evaluate the performance of each angle. In addition, investigations on the pumping power characteristics (E) and the goodness factor (Jh/f), for each angle are also taken into consideration.

The findings from this study are also expected to contribute towards the future development of the spiral PFCHE for gas/liquid applications. The important feature of the spiral configuration is that low pressure drop for the gas side is essential whilst maintaining high surface area densities. It has been shown that the design correlations developed for the square PFCHE with a 90° corrugation angle, was used to predict the overall performance of the spiral PFCHE. However, the 90° corrugation angle cannot be used on a spiral PFCHE, as it would prove impossible to wrap the polymer film on to a mandrel (aluminium core) due to the stiffness produced by the cross-corrugation.

Therefore in order to predict accurately the performance of the spiral PFCHE, it is essential to understand the effect of the corrugation angle on the heat transfer and pressure drop characteristics of the unit. The results of this study can help in improving the overall performance of the current spiral PFCHE design which has a corrugation angle of 20°.

### 7.1 Experimental apparatus: Design details and test procedure

A schematic diagram showing the square PFCHE is illustrated in Figure 7.1 and a diagram showing the cross-corrugation angles can be seen in Figure 7.2 below. Figure 7.2 shows the angle ($\gamma$) as the angle between the diagonal line of the perspex frame and the corrugation of the sheets. This angle has been chosen as the 'working angle', because of the symmetry of the heat exchanger about its diagonal line. Therefore the corrugations of two adjacent polymer sheets forms an angle of ($2\gamma$) which corresponds to the 30°, 60° and 90° corrugation angles investigated in this study.

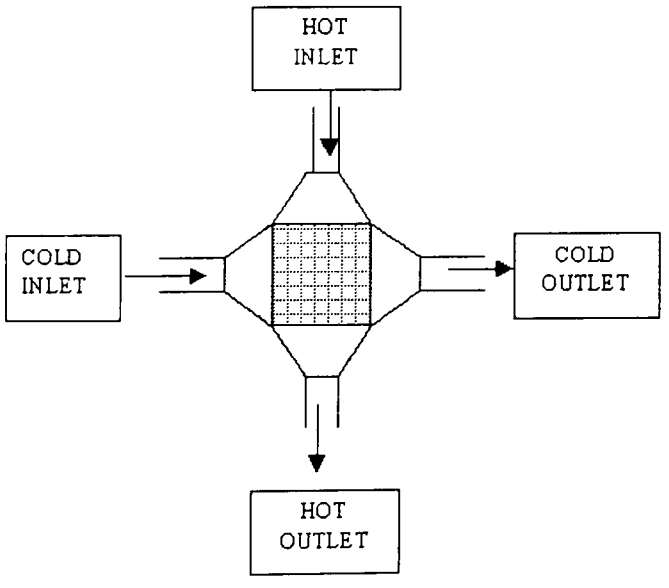


**Figure 7.1 Schematic diagram of the square PFCHE**

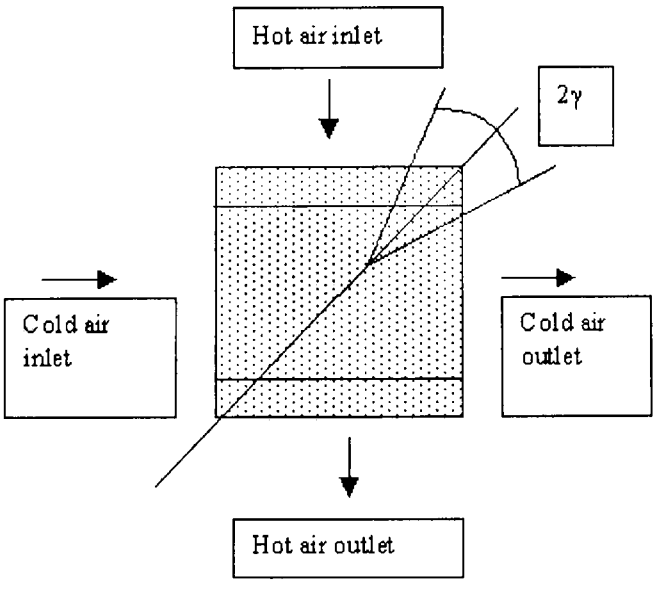


**Figure 7.2 Schematic diagram of the corrugation angle in a square PFCHE**

The procedure for measuring the air flow rates, temperatures and pressure drops across the square PFCHE, is the same as outlined in Chapter Four for the 90° corrugation angle. However, the experimental apparatus used for the 90° corrugation angle, differs slightly from the equipment employed for the 30° and 60° corrugation angles.

For all three angles, volumetric flow rates and temperatures were measured using rotameters and thermocouples respectively. However, different types of rotameters and thermocouples were adopted for the experiments. For the 30° and 60° angles, Fisher Control and 18X type rotameters were used (Menes 1997) whilst for the 90° angle, Nixon rotameters (PVDF floats encapsulated with aluminium) were adopted. The air temperatures were measured at the inlet and outlet compartments of both the hot and cold streams. K-type thermocouples having an accuracy of ±0.1°C were used for the 30° and 60° corrugation angles. On the other hand, the temperatures for the 90° corrugation angle were measured using platinum resistance thermocouples (PRTs) having an accuracy of ±0.05°C.

The pressure drop across the exchanger was measured between the inlet and outlet of each air stream. For the 30° and 60° angles, a tubular manometer that was connected to the exchanger by flexible tubes, was used for pressure drops smaller than 7 kPa. The accuracy of this manometer was ±0.02 kPa when it was measured with water. For higher pressure drops, a digital pressure gauge was used. It had an accuracy of ±0.1 kPa. The pressure drops for the 90° corrugation angle were measured using a digital pressure meter (2000 Series Manometer) having an accuracy of ±0.1 kPa. The heat transfer, friction factor, pumping power and goodness factor calculation procedures used in this chapter, are similar to the ones outlined in Chapter Four.

## 7.2 Effect of corrugation angle on heat transfer

### *7.2.1 Heat balance error (HBE)*

The first step towards the evaluation of the heat transfer performance for the corrugation angles is to calculate the heat loss from the temperature measurements. The heat balance errors calculated over the Re range for the 30°, 60° and 90° corrugation angles are shown below.

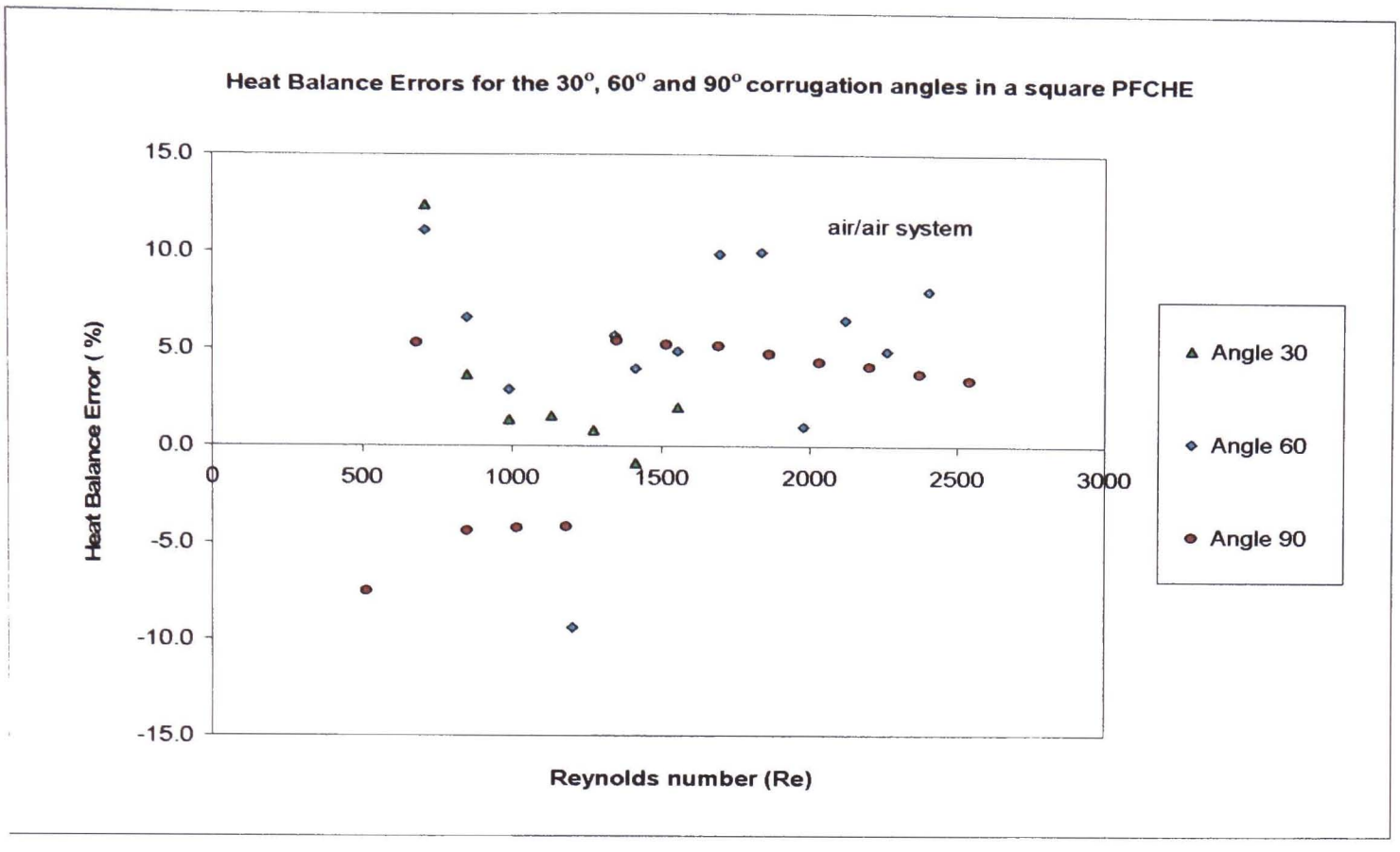


**Figure 7.3 Heat balance errors for the 30°, 60° and 90° corrugation angles of a square PFCHE in an air/air system**

It can be clearly seen that the 90° angle experiences the lowest heat balance errors compared to the 30° and 60° angles, with errors less than 7%. The heat balance errors for the 30° and 60° angles are relatively high but they do improve at higher Re, notably at Re>850, where the errors are within ±10%. Bearing this is mind, the experimental temperature measurements are deemed suitable and are consequently used in determining the Jh factors (dimensionless measure of heat transfer) for the three corrugation angles. This is done to enable a heat transfer performance comparison between the 30°, 60° and 90° angles respectively. We will now investigate the behaviour of the Colburn factors (Jh) in the following section.

### *7.2.2 Colburn factor (Jh)*

Figure 7.4 below, shows the variation of Colburn factor (Jh) with Reynolds number (Re) for the 30°, 60° and 90° corrugation angles in the square PFCHE. Overall, it is apparent that the 30° corrugation angle provides the highest Jh factors over the Re range investigated, followed by the 60° and 90° angles respectively.

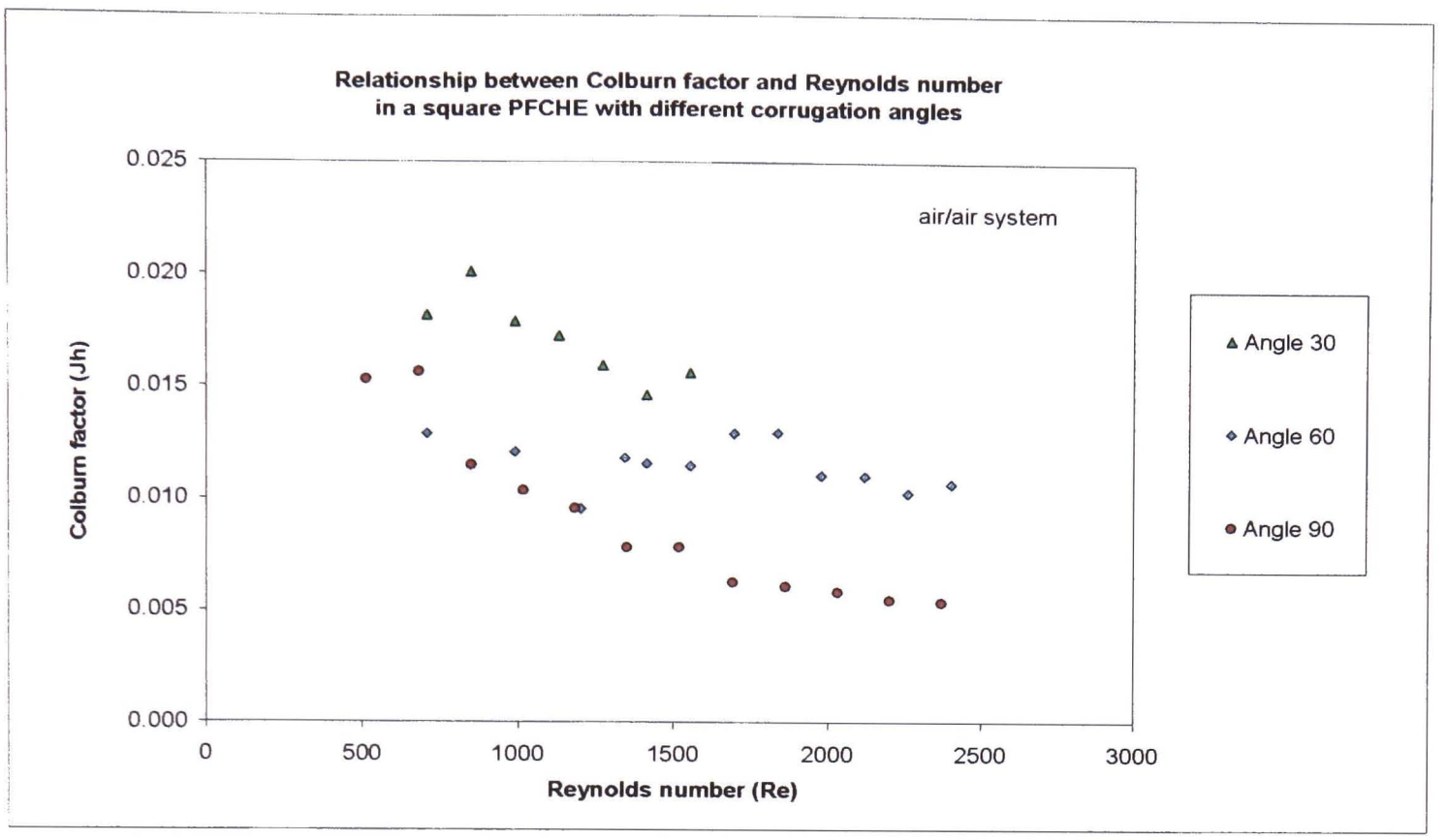


**Figure 7.4 Colburn factor (Jh) plot for the 30°, 60° and 90° corrugation angles of a square PFCHE in an air/air system**

It can be seen that above Re=900, a clear trend exists for the three angles studied. Above Re=900, the Jh value for a given Re is highest for the 30° angle and lowest for the 90° angle. This maybe due to the ability of the channel geometry to disrupt the flow; creating continuous developing flow as the corrugation angle gets smaller. It can also be due to the change in the flow direction along the corrugations from the main cross flow, which will be discussed in Section 7.6.1. At lower Re, there is a clear difference in the thermal behaviour between the 30° angle and the other two angles. However the difference between the 60° and 90° angles is not significant, as the extent of interruption to the flow profile which encourages heat transfer, is similar at lower flow rates. This flow behaviour for the different corrugation angles has been seen visually in earlier tests conducted with water, at the Process Intensification and Innovation Centre (Newcastle University). From Figure 7.4, correlations in the form of $Jh = a\ Re^{b}$ are developed for the three Jh curves using Microsoft Excel as shown below. The parameters 'a' and 'b' are correlation constants depending on the kind of surface and flow character.

Corrugation angle 30°: $Jh = 0.1590\ Re^{-0.3195}$ (7.1)

Corrugation angle 60°: $Jh = 0.0198\ Re^{-0.0751}$ (7.2)

Corrugation angle 90°: $Jh = 2.0097\ Re^{-0.7644}$ (7.3)

A standard method for comparing two heat transfer surfaces (Webb 1994) is to study the ratio of Jh for equal Re. This approach is therefore adopted, to compare the heat transfer characteristics of the 30°, 60° and 90° corrugation angles for the square PFCHE. The Jh value for each corrugation angle at Re=1000 is tabulated below.

| Corrugation angle, 2γ (°) | 30 | 60 | 90 |
|---|---|---|---|
| Reynolds number, Re | 1000 | 1000 | 1000 |
| Colburn factor, Jh | 0.017 | 0.012 | 0.010 |

**Table 7.2 Colburn factors (Jh) for a square PFCHE with different corrugation angles at Re=1000**

Using the values from Table 7.2 above, the ratio of the Colburn factors at Re=1000 are calculated and compared for the three corrugation angles studied.

$$Jh\ 30^\circ / Jh\ 60^\circ = 1.4 \qquad (7.4)$$

$$Jh\ 30^\circ / Jh\ 90^\circ = 1.7 \qquad (7.5)$$

From expressions (7.4) and (7.5), it is clear that the thermal performance of the 30° corrugation angle is better than the 60° and 90° angles, by a factor of 1.4 and 1.7 respectively. However it is well known that for most heat exchangers, the heat transfer enhancement can be achieved at the expense of the pressure drop, due to resistance provided by better mixing. Therefore to get a better understanding of the effect of the corrugation angles on the PFCHE performance, the friction factor characteristics of the 30°, 60° and 90° corrugation angles are investigated in the next section. The friction factors are a dimensionless representation of the pressure drop measurements.

## 7.3 Effect of corrugation angle on pressure drop

### *7.3.1 Friction factor (f)*

The variation of friction factor (f) with Reynolds number (Re) for a square PFCHE with 30°, 60° and 90° corrugation angles, is presented in Figure 7.5 below. As with the Colburn factor, the 30° corrugation angle provides the highest friction factors over the Re range investigated, followed by the 60° and 90° angles respectively. This is as expected since better heat transfer is possible at the expense of a higher pressure drop penalty.

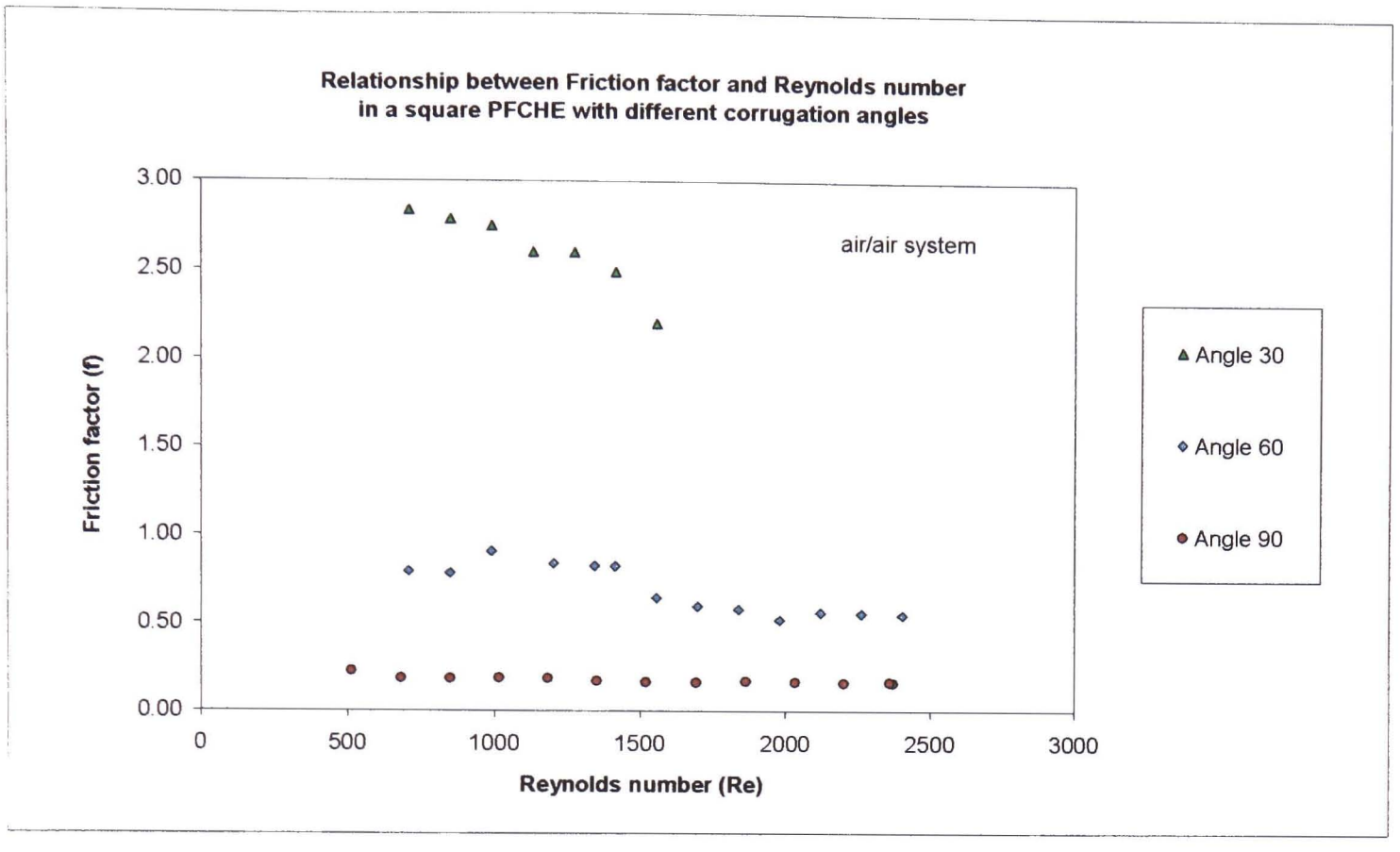


**Figure 7.5 Friction factor (f) plot for the 30°, 60° and 90° corrugation angles of a square PFCHE in an air/air system**

The friction factors calculated for the 30° angle are a lot higher than the 60° and 90° angles. The reason for this occurrence could be due to the 30° angle experiencing a bigger flow deviation from the main cross flow, which generates more resistance to fluid flow. This reasoning is explained further in Section 7.6.1 of this chapter. The 60° angle achieves higher frictions factors than the 90° angle over the entire Re range investigated, which accounts for its superior thermal performance shown earlier in Figure 7.4. Nevertheless at lower Re, the higher pressure drops for the 60° angle is mainly due to frictional losses caused by the flow deviation as it disrupts along the corrugations; lengthening the actual fluid flow length across the heat exchanger. At higher Re, the higher pressure drops noted for the 60° angle contribute more towards its superior thermal performance to the 90° angle. Correlations in the form of $f = a\,Re^{b}$ which were obtained using Microsoft Excel for the three different corrugation angles are as follows:

Corrugation angle 30°: $f = 17.363\,Re^{-0.2713}$ (7.6)

Corrugation angle 60°: $f = 16.158\,Re^{-0.4349}$ (7.7)

Corrugation angle 90°: $f = 0.5992\,Re^{-0.1698}$ (7.8)

As with the previous Colburn ratios, the same method (Webb 1994) is used to study the ratio of f at equal Re. The f value for each corrugation angle at Re=1000 is tabulated in Table 7.3 below.

| Corrugation angle, 2γ (°) | 30 | 60 | 90 |
|---|---|---|---|
| Reynolds number, Re | 1000 | 1000 | 1000 |
| Friction factor, f | 2.6 | 0.8 | 0.2 |

**Table 7.3 Friction factors (f) for a square PFCHE with different corrugation angles at Re=1000**

For Re=1000, the ratios of the friction factors are calculated and compared for the three corrugation angles investigated. The ratios obtained are as follows:

$$f\,30^{\circ} / f\,60^{\circ} = 3.3 \qquad (7.9)$$

$$f\,30^{\circ} / f\,90^{\circ} = 13.0 \qquad (7.10)$$

From expressions (7.9) and (7.10), it can be seen that the friction factor offered by the 30° corrugation angle is higher, than both the 60° and 90° angles. Therefore this means that the 30° corrugation angle, not only provides the highest heat transfer as shown earlier in Figure 7.4, but also achieves the highest friction factors. It achieves higher Jh and f factors at Re=1000, by a factor of 1.7 and 13 respectively, compared to the 90° angle. This outcome is expected as heat transfer enhancement is obtained at the expense of higher pressure drops in most heat exchangers. In addition, the higher pressure drops for the 30° angle also account for the frictional losses caused by the flow deviation along the corrugations, with more disruption and lengthening of the fluid flow path for smaller corrugation angles. Therefore, in order to determine the optimum angle for the PFCHE in this study, a compromise or 'trade off' must be made between the heat transfer and pressure drop characteristics of the unit. In the next section, we consider the effect of the corrugation angle on the overall thermal and hydraulic performance.

## 7.4 Effect of corrugation angle on overall thermal and hydraulic performance

The combined effects of both Jh and f factors can be studied by analysing the goodness factor (Jh/f) and pumping power (E) plots, for the three corrugation angles. These plots take into consideration both the heat transfer and the associated pressure drop characteristics. In the following section, we first consider the goodness factor for the three angles. Experimental data for the 30° angle at higher Re is not available, as it involves high pressure drops which would have compromised the integrity of the matrix.

### *7.4.1 Goodness factor (Jh/f)*

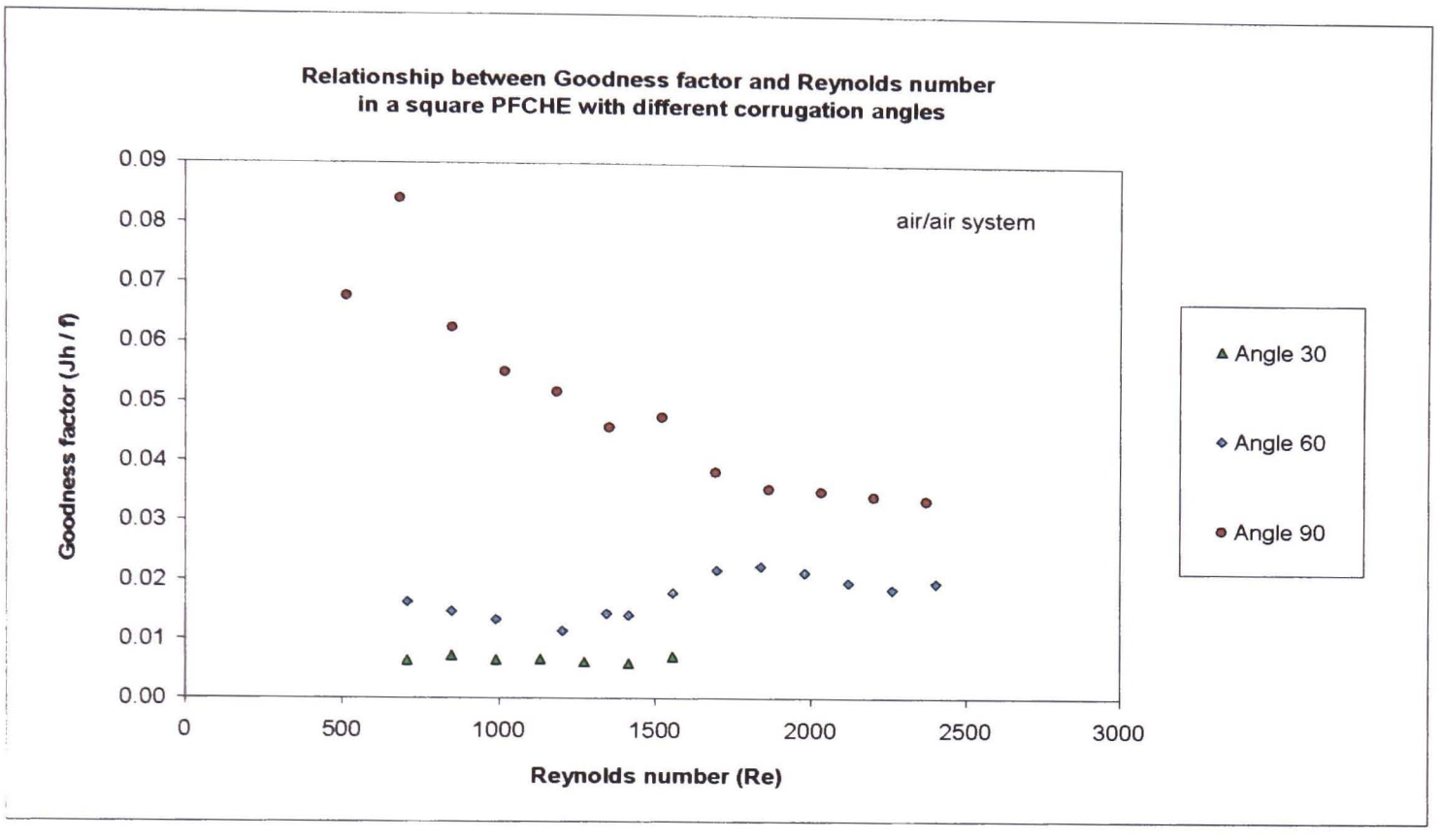


**Figure 7.6 Goodness factor (Jh/f) plot for the 30°, 60° and 90° corrugation angles for a square PFCHE in an air/air system**

Figure 7.6 shows that the 90° angle provides the highest goodness factors compared to the 30° and 60° angles, throughout the Re range investigated. This shows that the thermal efficiency of the 90° angle is superior to that of the other two angles. To get a better grasp of this, the Jh/f ratios for the 30°, 60° and 90° corrugation angles are calculated at equal Re. The Jh/f values at Re=1000 are tabulated in Table 7.4 below.

| Corrugation angle, $2\gamma$ (°) | 30 | 60 | 90 |
|---|---|---|---|
| Reynolds number, Re | 1000 | 1000 | 1000 |
| Goodness factor, Jh/f | 0.007 | 0.018 | 0.055 |

**Table 7.4 Goodness factors (Jh/f) for a square PFCHE with different corrugation angles at Re=1000.**

The ratios of the goodness factors for the three corrugation angles studied are as follows:

$$(Jh/f)\ 90^\circ / (Jh/f)\ 60^\circ = 3.0 \qquad (7.11)$$

$$(Jh/f)\ 90^\circ / (Jh/f)\ 30^\circ = 7.4 \qquad (7.12)$$

From expressions (7.11) and (7.12), it is clearly seen that the 90° angle provides the highest goodness factors followed by the 60° and 30° corrugation angles respectively. Therefore from the goodness factor results, it can be concluded that the 90° corrugation angle provides the highest thermal efficiency over the Re range investigated. This is achieved despite the fact that it has the lowest heat transfer capability compared to the other two angles. The reason for the high thermal efficiency achieved, is mainly due to the relatively low friction factors that it experiences. Since the system investigated is an air/air system, the air pressure drop measurements that lead to the evaluation of the friction factors, play a vital role in the evaluation of the heat exchanger performance. This in turn causes the 90° angle, having the lowest friction factors, to achieve the highest thermal efficiency. To provide support and clarification to these findings, the pumping power is next investigated to finalise the determination of the optimum angle in the square PFCHE. The pumping power plot results are shown in the following section.

*7.4.2 Pumping power, (E)*

The pumping power plot is obtained by plotting the heat transfer coefficient (h) against pumping power loss (E) as shown in Figure 7.7 below. The plot shows that with the same pumping power expended, more heat is transferred using the 90° corrugation angle compared to the 30° and 60° angles. However, this only occurs below a pumping power of 926 W/m$^2$. Above this value, the 60° angle provides the highest heat transfer coefficients.

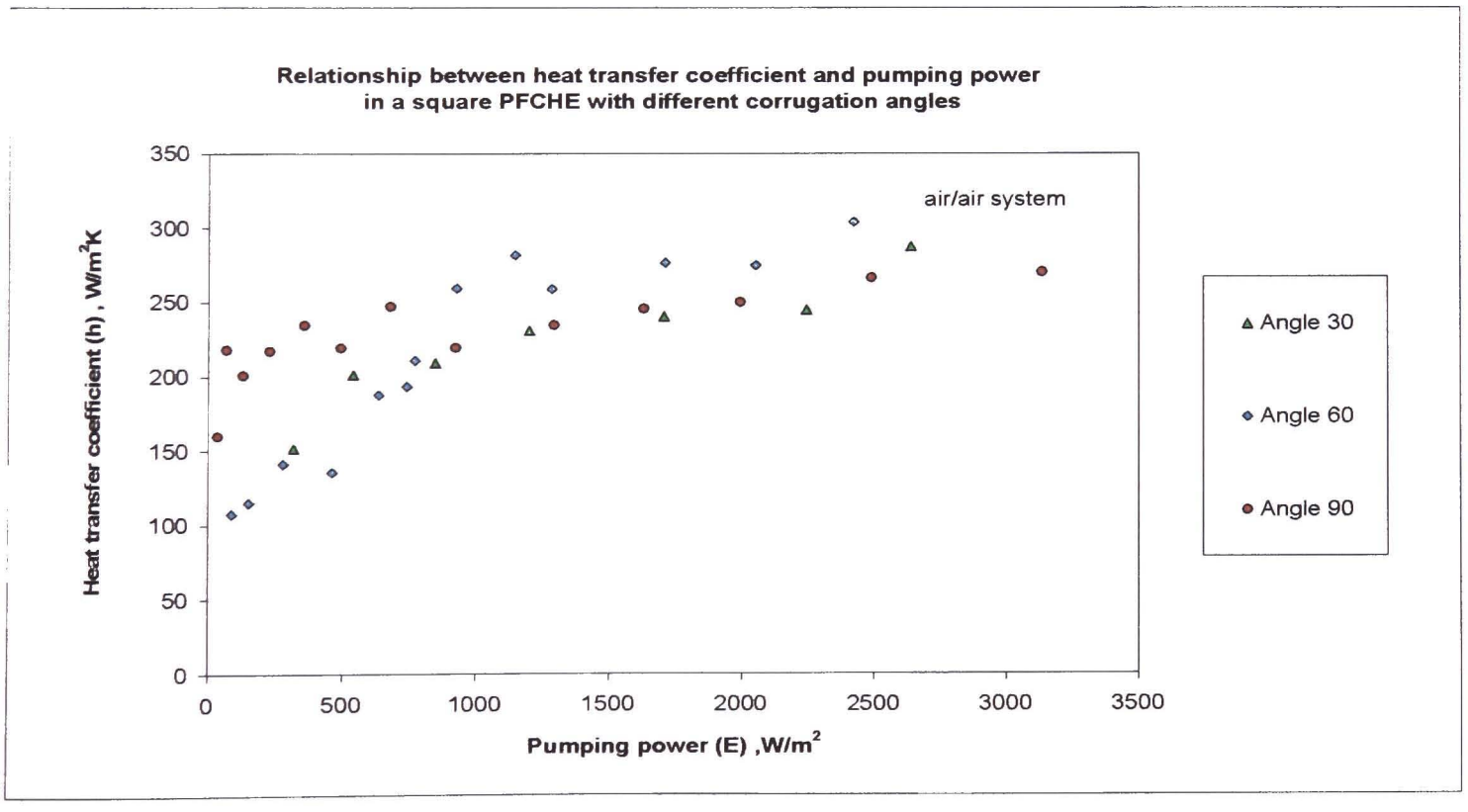


**Figure 7.7 Pumping power (E) plot for the 30°, 60° and 90° corrugation angles for a square PFCHE in an air/air system**

This observation is best illustrated by calculating the h ratios at E=500 W/m$^2$ and E=2000 W/m$^2$, for the three angles investigated. The heat transfer coefficients at these selected points are tabulated in Table 7.5, whilst the h ratios are shown in expressions (7.13) and (7.16).

| Corrugation angle, 2$\gamma$ (°) | Pumping power, E (W/m$^2$) | Heat transfer coefficient, h (W/m$^2$K) | Pumping power, E (W/m$^2$) | Heat transfer coefficient, h (W/m$^2$K) |
|---|---|---|---|---|
| 30 | 500 | 197.14 | 2000 | 257.33 |
| 60 | | 188.45 | | 259.80 |
| 90 | | 226.78 | | 254.78 |

**Table 7.5 Heat transfer coefficients (h) for a square PFCHE with different corrugation angles at E=500 W/m$^2$ and E=2000 W/m$^2$**

From the table above, the ratios of the heat transfer coefficients at the corresponding pumping power values have been calculated and compared for the three different angles.

At E = 500 W/m$^2$

h 90° / h 30° = 1.15 (7.13)

h 90° / h 60° = 1.20 (7.14)

At E = 1000 W/m$^2$

h 60° / h 30° = 1.01 (7.15)

h 60° / h 90° = 1.02 (7.16)

It clearly shows that the 90° corrugation angle gives the best performance at low pumping power values whilst the 60° angle provides superior heat transfer at higher pumping power values. Having considered the results of the performance evaluation plots (Jh, f, Jh/f and E), we proceed to further investigate the trends observed on the plots to provide a better explanation for the results obtained.

## 7.5 Trends in the performance plots for different corrugation angles

The trends observed from the h vs. Re, Jh vs. Re and f vs. Re plots for the 30°, 60° and 90° corrugation angles are studied in the following section. This exercise is conducted to provide a better understanding and reasoning, as to why the observations from the performance plots in the previous section occurred. Overall, it will be shown that there are three operating regions in each performance plot (Regions 1, 2 and 3); with Region 2 displaying the highest scatter from the general trend observed.

### *7.5.1 30° corrugation angle*

| | |
|---|---|
| Working angle, $\gamma$ | = 15° |
| Air flow rates tested | = 5-11 $m^3$/hr |
| Reynolds number range, Re | = 706-1555 |
| Region 2 range, Re | = 848-1413 |

#### 7.5.1.1 Heat transfer coefficient (h)

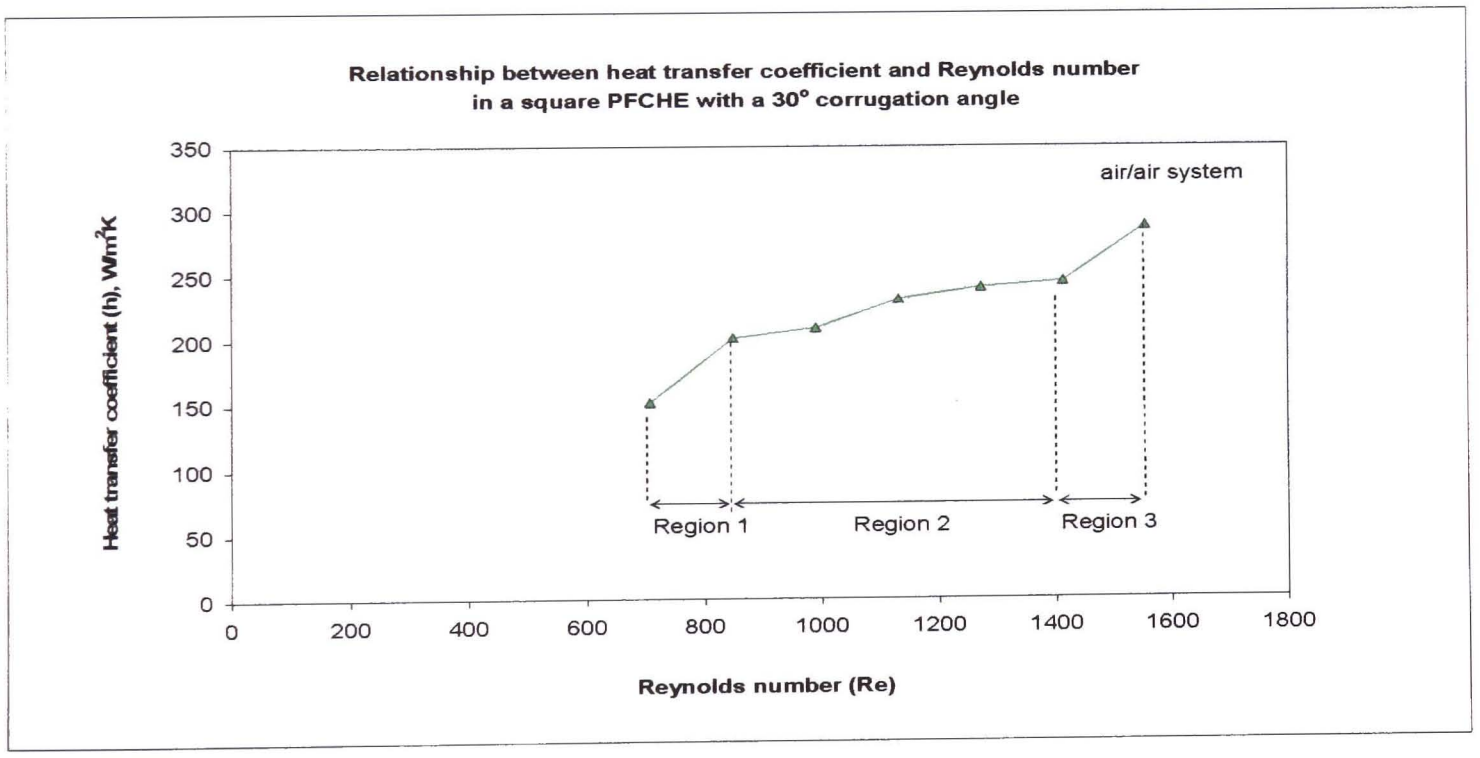


**Figure 7.8a Graph of heat transfer coefficient (h) vs. Reynolds number (Re) for a square PFCHE a with 30° corrugation angle in an air/air system**

There are three regions of operation that can be identified from the results obtained in Figure 7.8a. The general trend is as expected, with the heat transfer coefficient increasing with Re. Region 2 is positioned between 848<Re<1413. In this region, there is a gradual increase in the

heat transfer coefficient values as the Re increases. However in Region 1 and Region 3, there is a much more significant increase in the heat transfer coefficient values with an increase in Re.

7.5.1.2 Colburn factor (Jh)

The overall trend observed is as expected. The Colburn factor decreases as the Re increases with Region 2 positioned between 848<Re<1413. However, Regions 1 and 3, show a deviation to this general trend where the Colburn factors increase with increasing Re.

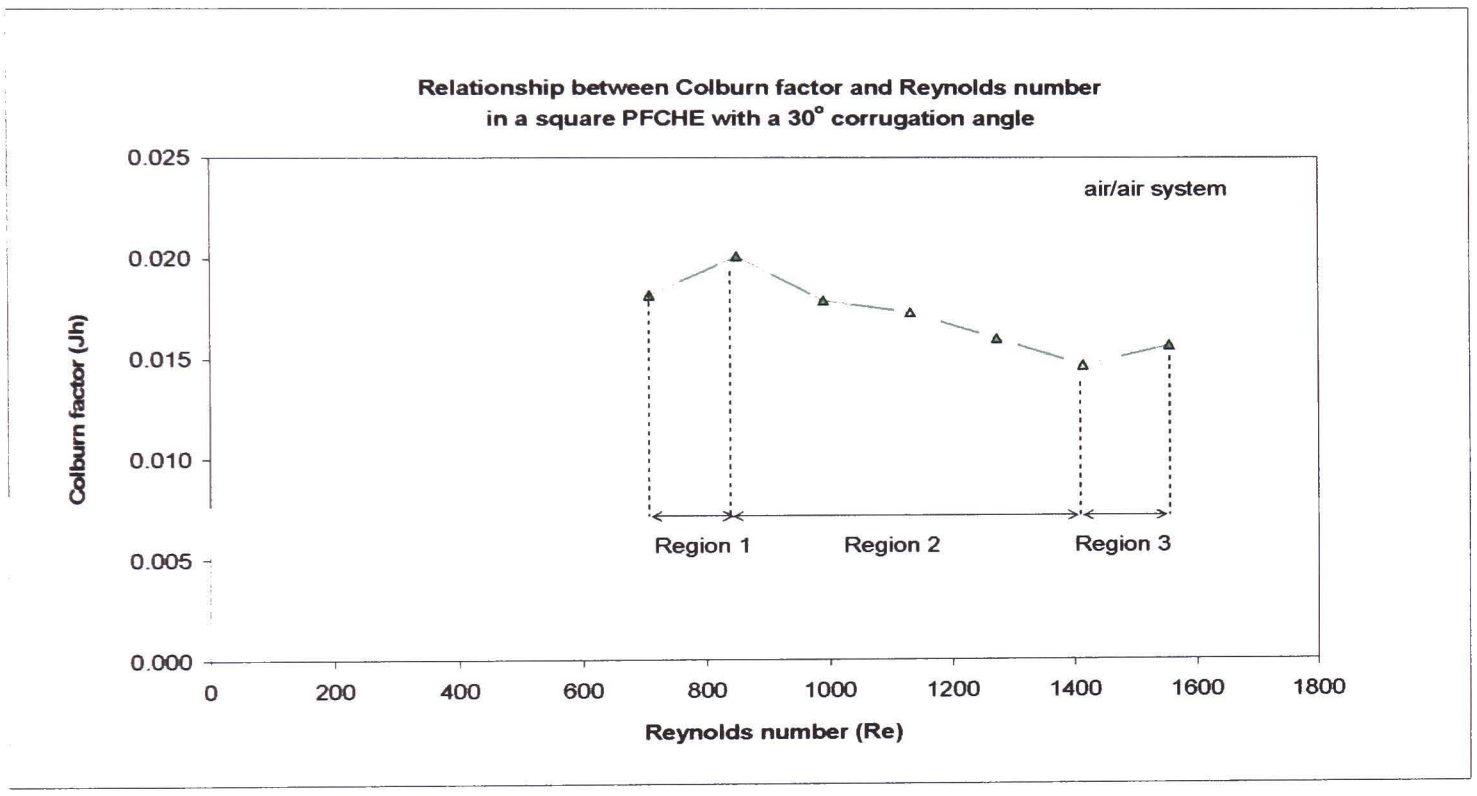


**Figure 7.8b Graph of Colburn factor (Jh) vs. Reynolds number (Re) for a square PFCHE with a 30° corrugation angle in an air/air system**

7.5.1.3 Friction factor (f)

The friction factor graph, depicted in Figure 7.8c below, also shows three regions of operation. The general trend is as expected with the friction factor values decreasing with increasing Re. Region 2 is positioned between 848<Re<1413, which is similar to the Colburn factor plot. In Region 2, a slight fluctuation in the friction factors occur as the Re increases. Regions 1 and 3 both show a steady decline in the friction factors as the Re increases. To fully understand the behaviour of this configuration, further data would be required for higher Re than those that are available at this time.

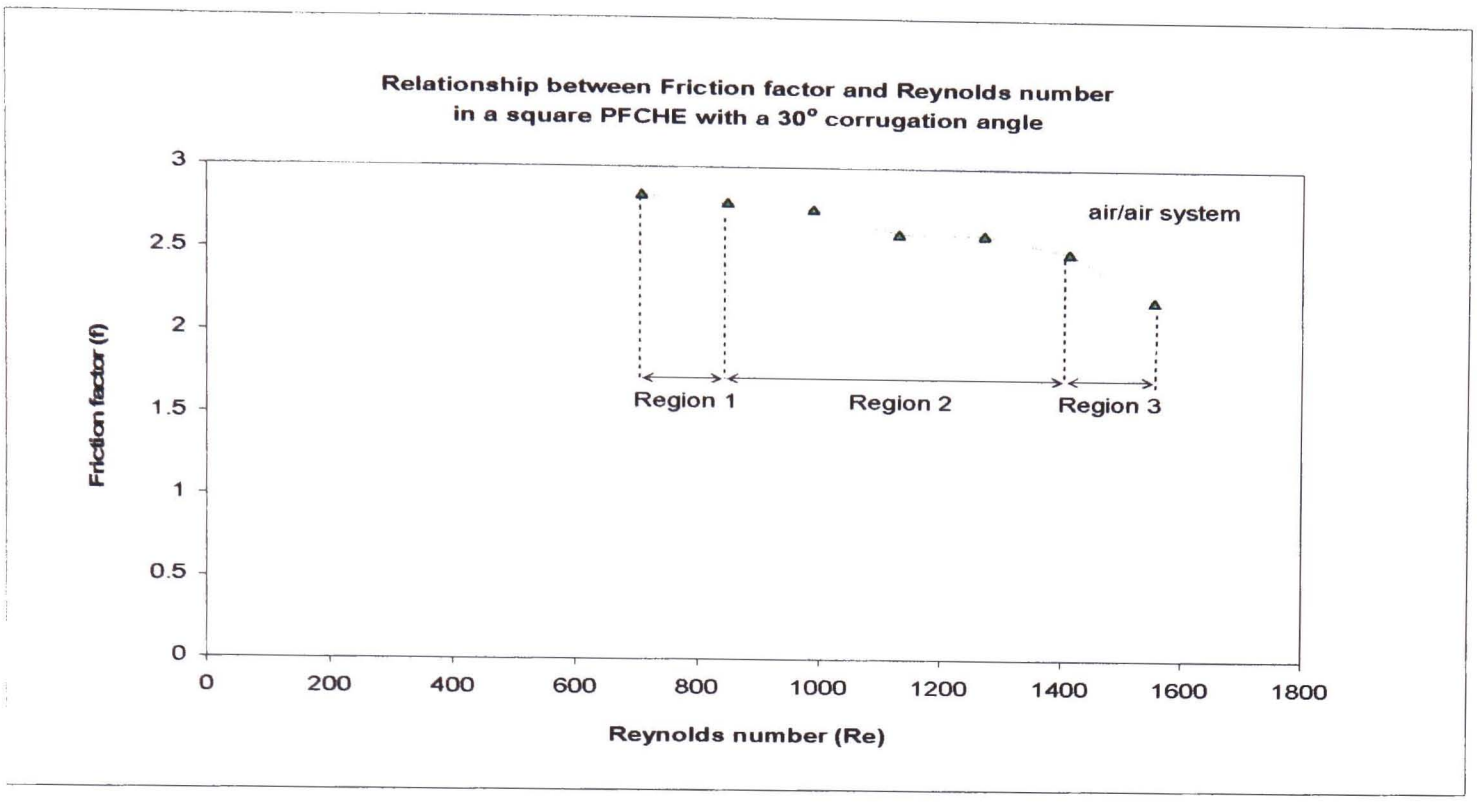


**Figure 7.8c Graph of friction factor (f) vs. Reynolds number (Re) for a square PFCHE with a 30° corrugation angle in an air/air system**

Following the 30° angle, we move on to describe the trends obtained for the 60° corrugation angle in the next section.

*7.5.2 60° corrugation angle*

| | |
|---|---|
| Working angle, $\gamma$ | = 30° |
| Flow rates tested | = 5-17 $m^3$/hr |
| Reynolds number range, Re | = 706-2403 |
| Region 2 range, Re | = 989-1978 |

7.5.2.1 Heat transfer coefficient (h)

For the 60° corrugation angle results, it is more difficult to show the three regions of operation compared to the 30° angle, as there is much more scatter. Nevertheless, from Figure 7.9a below, Region 2 can be deduced to be between 989<Re<1978. This is due to a slight step decrease in the heat transfer coefficients. Region 2 for the 60° angle covers a broader range of Re numbers than the 30° angle. This can be due to the fluctuation in heat transfer caused by a lower degree of mixing since there is less deviation in the fluid flow path. Hence, higher flow rates are needed for the 60° angle to stabilise the heat transfer. Therefore, the initial conclusion that can be drawn is that the corrugation angle has an effect on the range of Region 2 achieved

in the PFCHE performance plots. As mentioned before, Region 2 depicts the range of Re numbers over which the data points experience the highest scatter or instability, from the general trend.

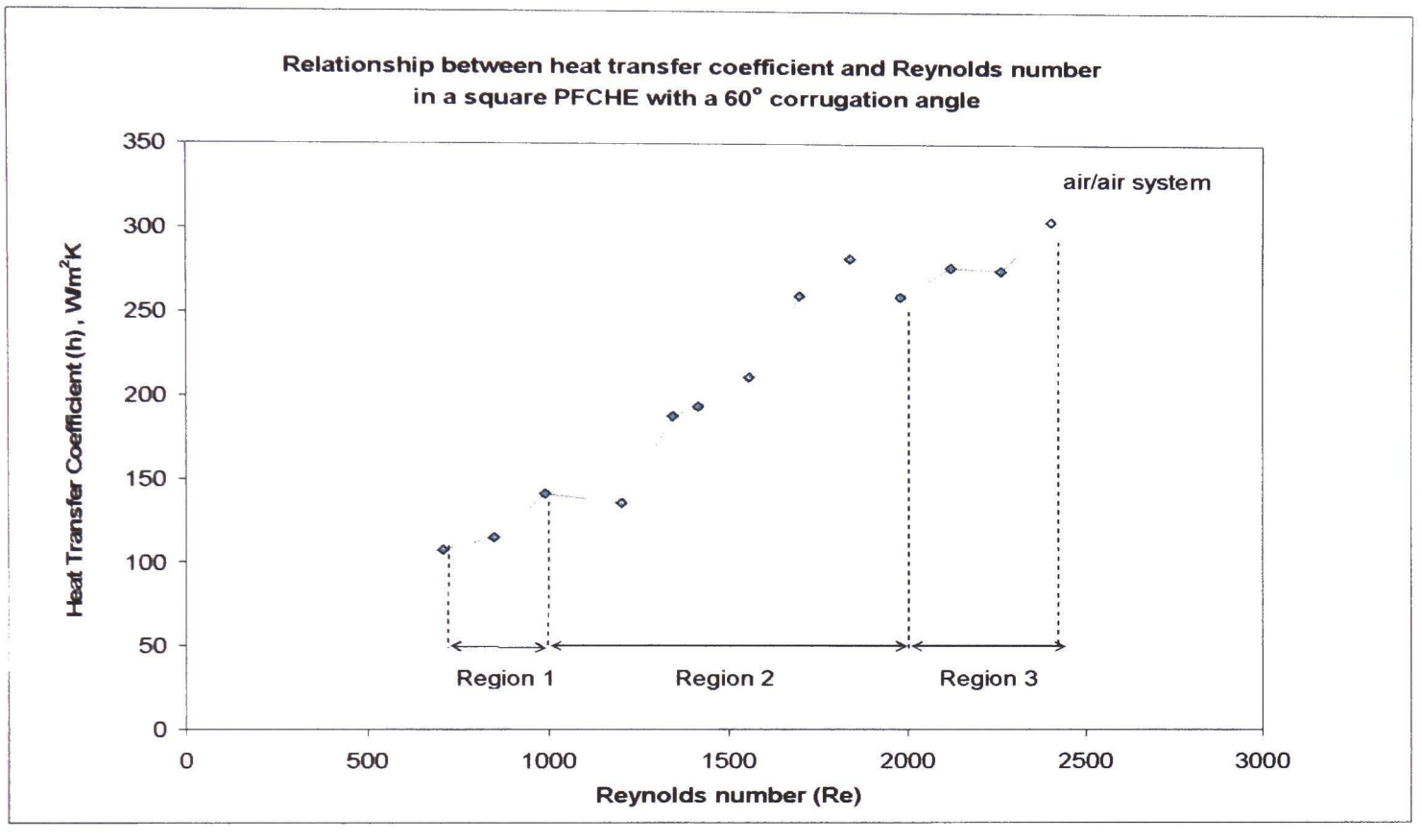


**Figure 7.9a Graph of heat transfer coefficient (h) vs. Reynolds number (Re) for a square PFCHE with a 60° corrugation angle in an air/air system**

7.5.2.2 Colburn factor (Jh)

Figure 7.9b shows the Colburn factor plot for the 60° corrugation angle. The overall trend is as expected with the Colburn factor decreasing with an increase in Re. Region 2 is positioned between 989<Re<1978. In this region, the Colburn factor fluctuates along with Re. Nevertheless in Regions 1 and 3, the general trend is observed. The 60° heat transfer experimental results present a higher degree of scatter compared to the 30° angle, perhaps due to the lower degree of mixing experienced.

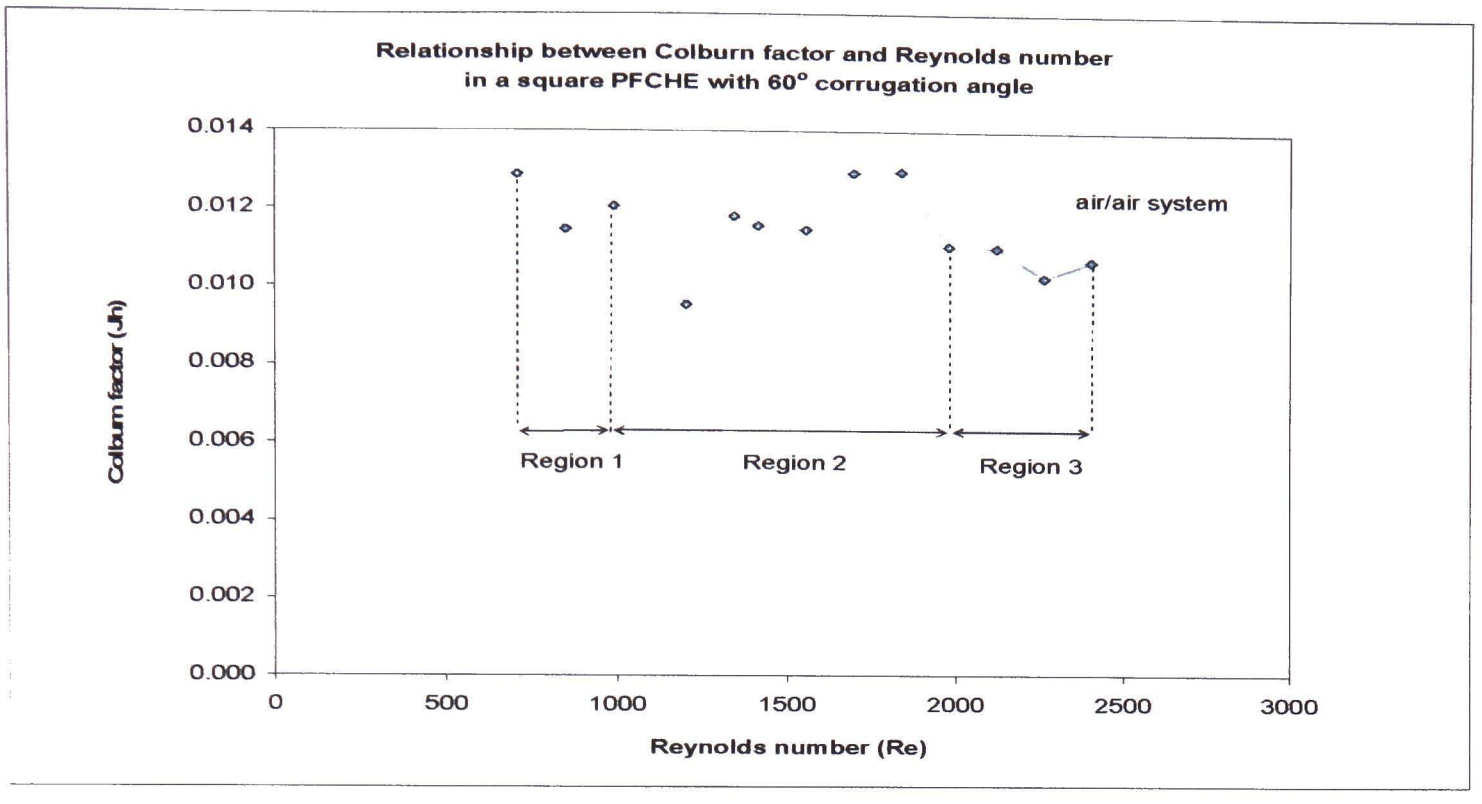


**Figure 7.9b Graph of Colburn factor (Jh) vs. Reynolds number (Re) for a square PFCHE with a 60° corrugation angle in an air/air system**

7.5.2.3 Friction factor (f)

The overall trend observed is as expected with a decrease in friction factor values as Re increases. This can be clearly seen from Figure 7.9c below.

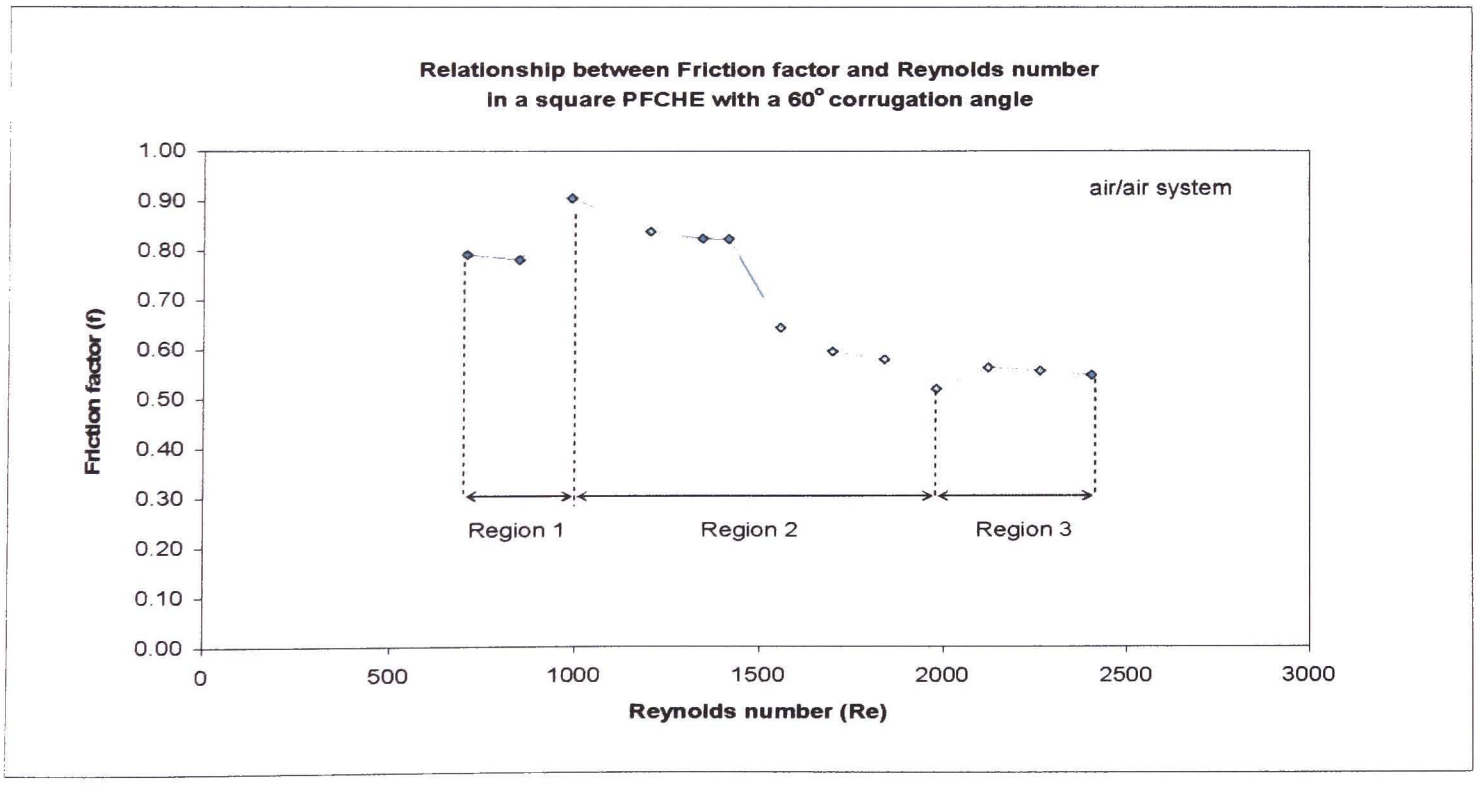


**Figure 7.9c Graph of friction factor (f) vs. Reynolds number (Re) for a square PFCHE with a 60° corrugation angle in an air/air system**

Region 2 is taken to be between 989<Re<1978, which is similar to the Colburn factor plot. Finally in the following section, we investigate the performance trends for the last of the three angles studied in this chapter, namely the 90° corrugation angle.

### *7.5.3 90° corrugation angle*

| | |
|---|---|
| Working angle, $\gamma$ | = 45° |
| Flow rates tested | = 3-15 $m^3$/hr |
| Reynolds number range, Re | = 511-2540 |
| Region 2 range, Re | = 847-1691 |

#### 7.5.3.1 Heat transfer coefficient (h)

From Figure 7.10 below, the general trend observed is that the heat transfer coefficient increases as the Re increases. There are some fluctuations observed between 847<Re<1691 and therefore this is deduced to be Region 2. The increment of the heat transfer coefficient is more uniform at higher Re numbers, which falls within Region 3.

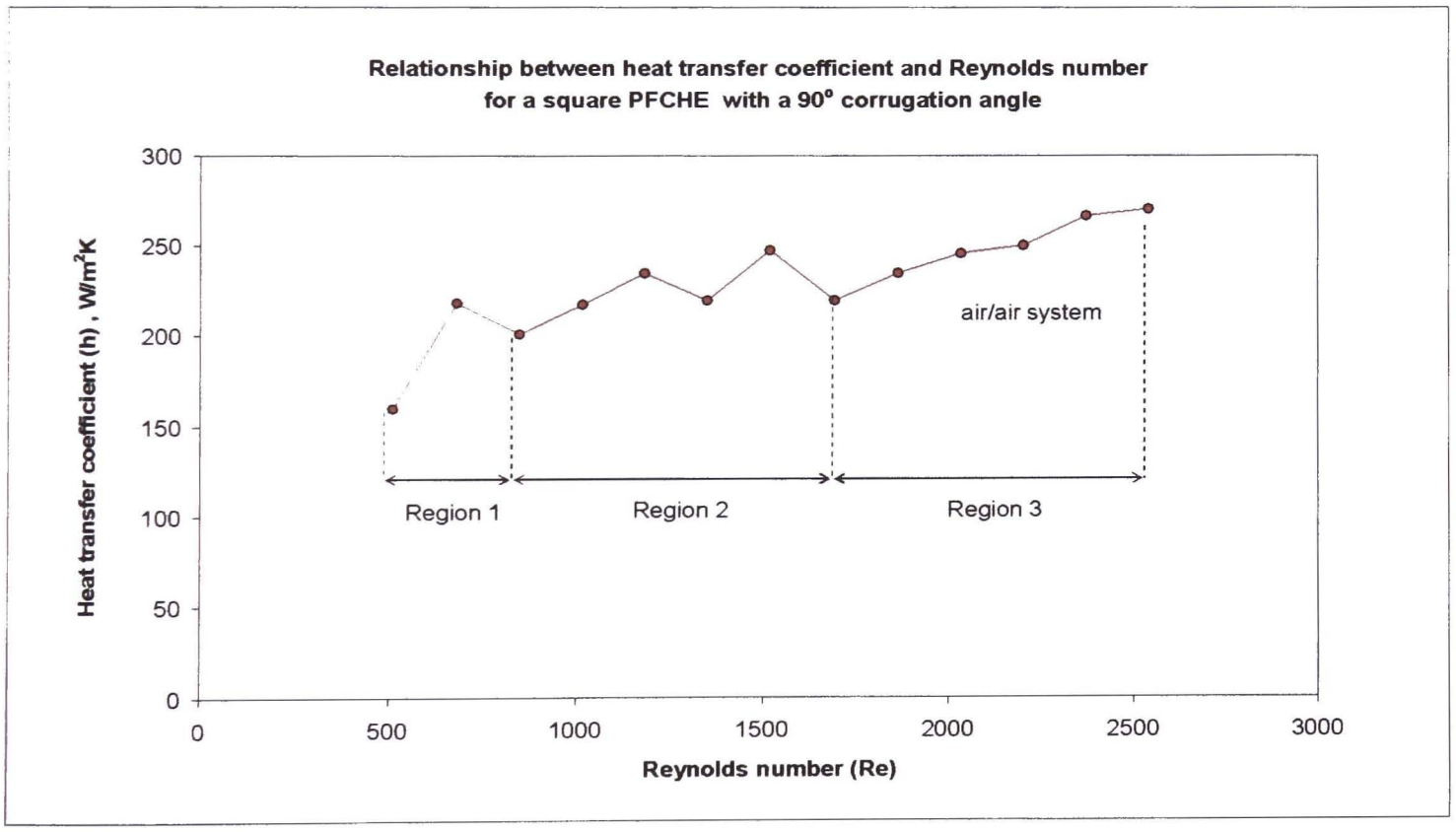


**Figure 7.10a Graph of heat transfer coefficient (h) vs. Reynolds number (Re) for a square PFCHE with a 90° corrugation angle in an air/air system**

7.5.3.2 Colburn factor (Jh)

The results plotted in Figure 7.10b below, show three regions of operation. Region 2 is placed between 847<Re<1691. The general trend observed is a decrease in the Colburn factor as the Re increases, although in each region the degree of decline is different. The decline is much steeper in Region 1 than Regions 2 and 3. There is a gradual decline in Region 3. These differences help illustrate that there are differences in the heat transfer characteristics over the three regions. In Region 1, it can be assumed that there is developing flow and hence an increase in the Re number or more importantly the velocity, will greatly effect the heat transferred. However in Region 3, the flow is perhaps more fully developed. Hence an increase in velocity does not greatly affect the amount of heat transferred.

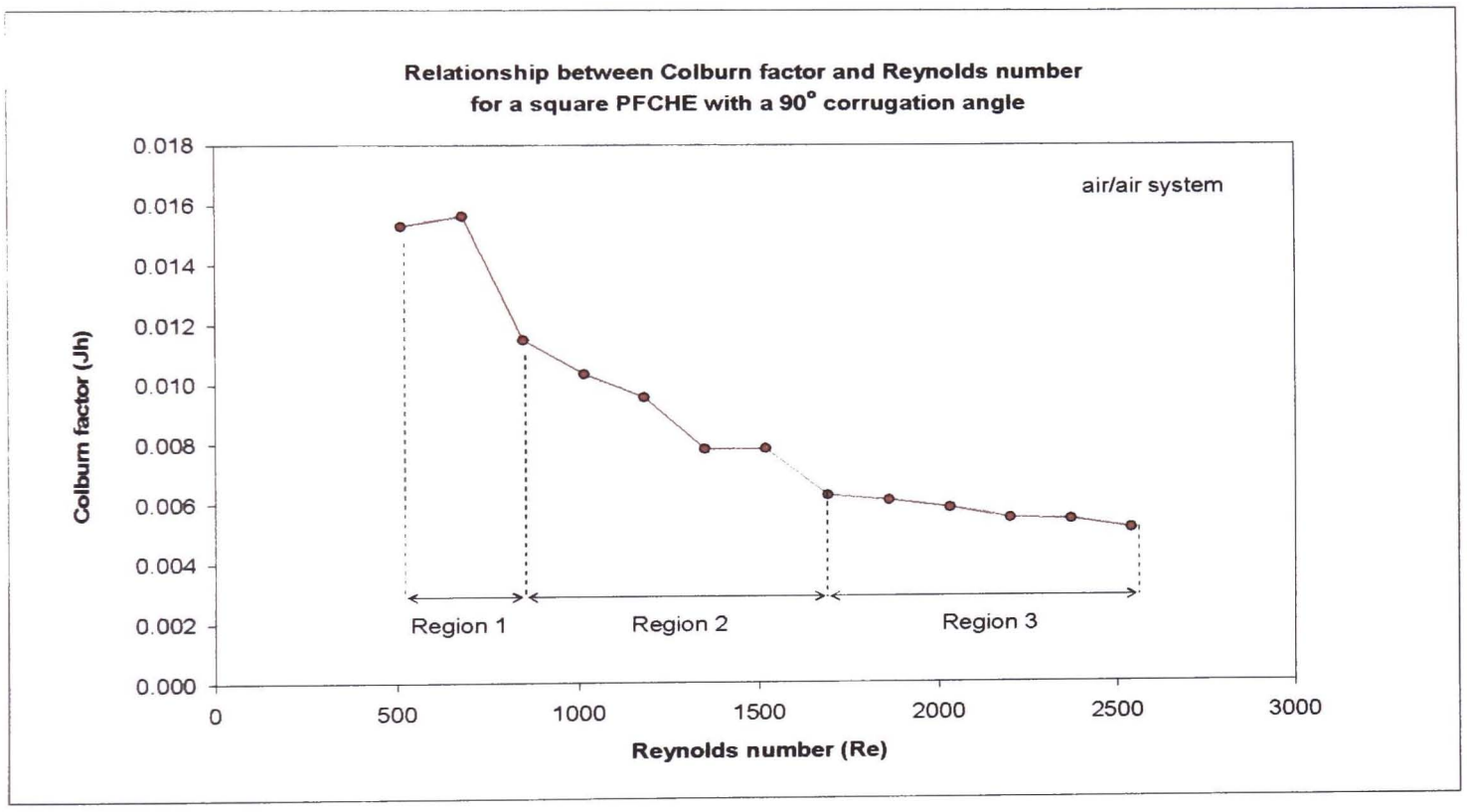


**Figure 7.10b Graph of Colburn factor (Jh) vs. Reynolds number (Re) for a square PFCHE with a 90° corrugation angle in an air/air system**

7.5.3.3 Friction factor (f)

The friction factor plot for the 90° corrugation angle is shown in Figure 7.10c below. The overall trend observed, is as expected with a decrease in friction factor as the Re increases. Region 2 is taken to be between 847<Re<1691.This is coincident with the Colburn factor plot earlier. The friction factor curve for the 90° angle is more uniform compared to the 30° and 60° angles, with less scatter throughout the Re range. This shows that the pressure drop measurements were more accurate for the 90° corrugation angle.

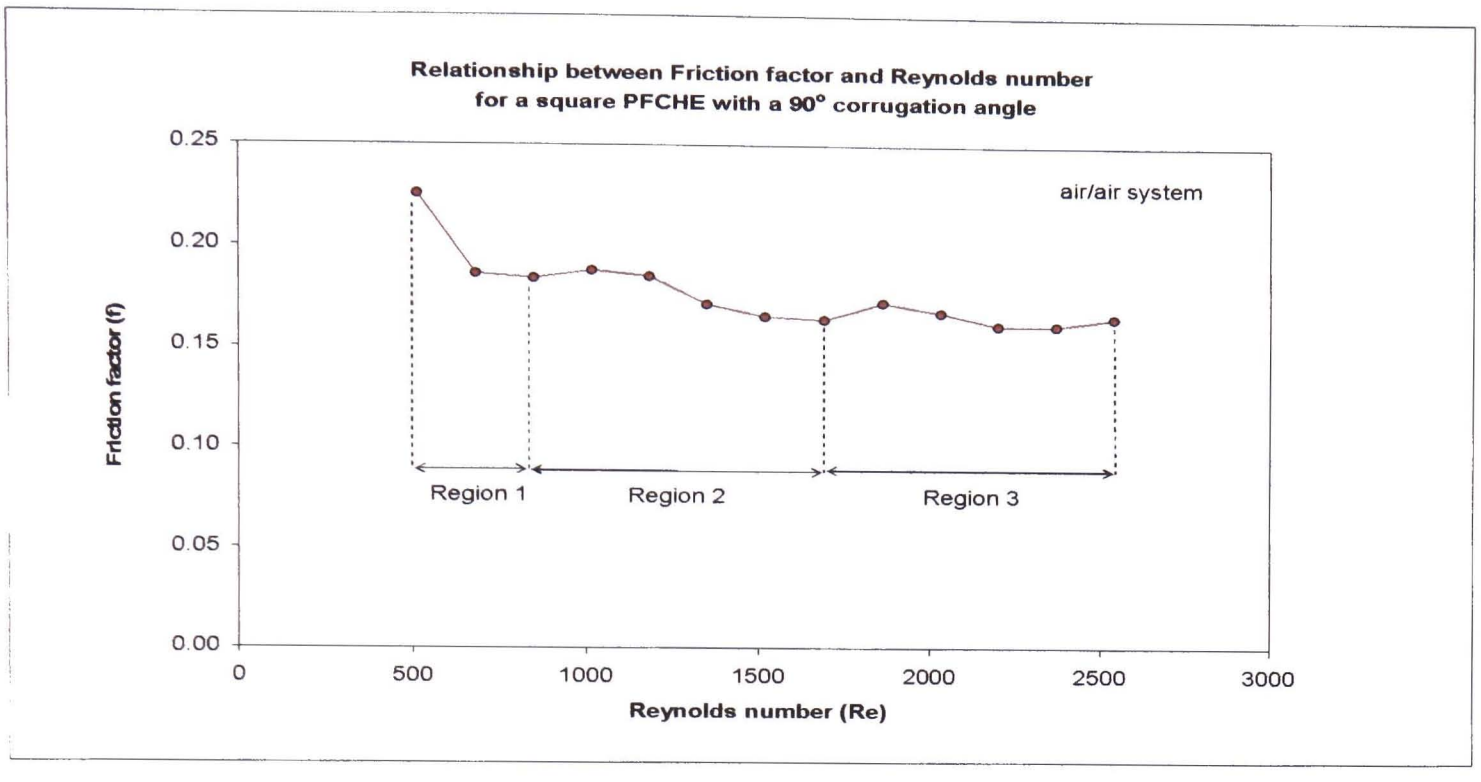


**Figure 7.10c Graph of friction factor (f) vs. Reynolds number (Re) for a square PFCHE with a 90° corrugation angle in an air/air system**

Having seen the experimental results for the three corrugation angles (30°, 60° and 90°), through the performance plots and also the trends observed, we now proceed to provide an explanation and reasoning for the observations noted.

## 7.6 Discussion

In this section, the effects of heat transfer, pressure drop and overall thermal and hydraulic performance for the 30°, 60° and 90° corrugation angles are analysed. The trends of the performance plots are also given a closer look. All this is done to provide a collective explanation concerning the PFCHE performance, covering all the aspects studied in this chapter. We begin with an analysis on the heat transfer characteristics.

### *7.6.1 Analysis of heat transfer characteristics*

The key element in understanding the effect of the corrugation angle on PFCHE heat transfer, is to investigate the relationship between Jh and Re for each corrugation angle. The Colburn factor (Jh) as shown before, is a dimensionless parameter that is proportional to the heat transfer coefficient of a specified fluid system. To simplify the heat transfer investigation, a direct relation can be made between the Colburn factor and the heat transfer achieved for each corrugation angle studied. In other words, the higher the Colburn factor, the higher the heat transfer capability of a system.

The highest heat transfer was achieved by the 30° corrugation angle. This was expected, as the flow path of the fluid into the exchanger would be altered by the largest amount from the main cross flow, to channel the flow through the exchanger. This large alteration of fluid flow leads to a greater deal of mixing as the fluid flow will be interrupted more intensely and therefore breaking down the boundary layers (enhancing the massaging effect), which leads to better heat transfer. The highest heat transfer obtained by the 30° corrugation angle compared to the 60° and 90° angles, would follow the theory that more heat can be transferred in a counter current system than in a co-current or cross current system. As the working angle of the exchanger is decreased, the system approaches a counter-flow system; therefore maximising the heat that that can be transferred in a smaller area. The disadvantage with this arrangement is that the friction factor is much higher due to the high pressure drops across the system. In the following section, we move on to consider the pressure drop characteristics when using different corrugation angles by analysing the results of the friction factor plots.

*7.6.2 Analysis of pressure drop characteristics*

The friction factor as discussed before, is a dimensionless value that is proportional to the pressure drop of a specified fluid system. The results of the friction factor ratio calculations presented in Section 7.3.1, show clearly the effect of varying the corrugation angle on the PFCHE pressure drop.

The 30° angle has the highest friction factor, as would be expected. Nevertheless, the results were notably a lot higher than those of the 60° and 90° corrugation angles. The reason for this was initially accounted to incorrect pressure measurements. Therefore the pressure readings were repeated and the results were found to be consistent to those previously measured, Menes (1997).The conclusion was drawn that the pressure measurements were high due to the change required in the flow path to allow the air into the exchanger. The distinction between the angles confirms what would be expected, that the 90° angle would have the lowest friction factor, as the flow path would not require any alteration to pass through the exchanger. The other angles all required the flow path to be changed to allow the fluid through the exchanger, the greatest change would be for the 30° angle and therefore this would have the highest friction factor.

Further analysis is required at Re numbers above 2000 for the 30° corrugation angle, in order to determine whether the friction factor for this configuration is always higher then the other corrugation angles analysed. In the next section, we proceed to conduct an analysis on the results of the goodness factor and pumping power plots for the three corrugation angles (30°, 60° and 90°) studied. These plots as shown earlier, provide a collective account of the heat

transfer and pressure drop characteristics of the PFCHE, when using the different corrugation angles.

*7.6.3 Analysis on overall thermal and hydraulic performance*

Here the analysis covers two factors namely the goodness factor and the pumping power, whereby the results are shown in Section 7.4.1 and 7.4.2 respectively. Both factors take into account the heat transfer and the pressure drop penalty of the PFCHE performance.

The goodness factor is a direct measure of the thermal efficiency in the PFCHE, as it is the ratio between the Colburn and friction factors. A unit having a high goodness factor value is capable of achieving high heat transfer at the expense of its pressure drop and hence, is deemed thermally efficient. From Figure 7.6 in Section 7.4.1, it can be seen that the 90° corrugation angle has the highest goodness factor values compared to the 30° and 60° angles. Therefore this suggests that when both the heat transfer and friction factor characteristics are considered collectively, the thermal efficiency of the 90° corrugation angle is superior to the 30° and 60° angles, although the thermal performance of the 90° angle is the lowest of all three angles.

In order to support the results of the goodness factor, the pumping power characteristics of each corrugation angle is investigated. Compared to the goodness factor, the pumping power plot is a more in depth measurement of the performance of each corrugation angle as it encompasses a measure of the heat transfer, pressure drop, friction factor, shear stress and the fluid properties of each stream in the exchanger. Therefore, it depicts a better account of the overall performance of the PFCHE. The pumping power is basically the energy required to pump the fluid across the exchanger. In other words, it is the mechanical power expended to overcome fluid friction per unit of surface area. The pumping power plot is an important feature in comparing the performance of different compact heat transfer surfaces, Kays and London (1984).

Apart from using compact surfaces to minimise the friction power, it is apparent from Figure 7.7 in Section 7.4.2, that another way to minimise friction power is to select surfaces that plot high on a pumping power plot. A surface that has a high heat transfer coefficient relative to friction power expenditure is termed a 'high performance' surface. Hence, in this study the corrugation angle that plots high on this plot is the optimum angle of the PFCHE. The pumping power requirements illustrated in Figure 7.7, show that to achieve the same degree of heat transfer, less pumping power is needed for the 90° and 60° angles compared to the 30° angle; at low and high pumping power values respectively. From another perspective this means that at similar pumping powers, the 90° and 60° corrugation angles provide better heat transfer than the 30°

angle. This indicates that although the 30° corrugation angle has the ability to achieve the highest heat transfer compared to the 60° and 90° angles, the higher friction factor and pumping power requirements outweighs its heat transfer merit.

For both the goodness factor and pumping power plots, the 90° corrugation angle achieves the highest values. The only exception to this observation is at higher pumping power values (see Figure 7.7), whereby the 60° angle provides the best heat transfer. Bearing this in mind, it can be implied that when the overall thermal and hydraulic characteristics are considered, the 90° corrugation angle emerges as the optimum corrugation angle for the square PFCHE. To provide further support to this deduction, we go on to analyse the trends of the performance plots in the next section.

*7.6.4 Analysis of trends of performance plots for the different corrugation angles*

From the h vs. Re, Jh vs. Re and f vs. Re plots, three regions of operation can be identified for the 30°, 60° and 90° corrugation angles. They are Regions 1, 2 and 3, respectively. Region 2 is given priority in this study, as it has the highest instability in the fluid flow behaviour. It is well known that instability in fluid flow generates heat transfer enhancement. In addition to this instability, high pressure drops are avoided when there is mixing at lower flow velocities compared to the higher velocities encountered in Region 3. Therefore, the initial conclusion drawn is that Region 2 offers heat enhancement at lower pressure drops (high thermal efficiency), which is the ideal condition sought after in any heat transfer unit. This provides an incentive to investigate the effect of Region 2 on the performance of the PFCHE with 30°, 60° and 90° corrugation angles.

The results in Section 7.5 show that the position and range of Region 2 differs for the 30°, 60° and 90° corrugation angles. From the plots, it can be seen that this region shows fluctuation in heat transfer and friction factor values, over a specified Re range. These fluctuations are often caused by instabilities that might stem from different levels of fluid mixing and deviations in the fluid flow path for each corrugation angle studied. The onset of Region 2 starts when there is a disturbance in the flow in Region 1, whilst it ends when the flow stabilises and regains equilibrium. The range of Region 2 depends on the performance of each corrugation angle to achieve steady state. The instabilities in Region 2 can be associated with the breaking down of the boundary layers in the laminar fluid flow that leads to heat enhancement. When this phenomenon occurs, the fluid flow is termed 'developing flow'. As explained before in Chapter Two, this type of flow occurs in the PFCHE due to the sinusoidal corrugations. In this study, the sinusoidal corrugations of the PFCHE massage the fluid flow through its crests and troughs, and consequently break down the boundary layers. In other words, the corrugation angle that has a

longer Region 2 would experience stronger developing flow and therefore be expected to have a superior thermal performance. The table below shows the range of Region 2 for the 30°, 60° and 90° corrugation angles plots investigated.

| Corrugation angle (°) | Plot | Region 2 (Re) | Region 2 interval ( ΔRe) |
|---|---|---|---|
| 30 | h | 848-1413 | 565 |
| | Jh | 848-1413 | 565 |
| | f | 848-1413 | 565 |
| 60 | h | 989-1978 | 989 |
| | Jh | 989-1978 | 989 |
| | f | 989-1978 | 989 |
| 90 | h | 847-1691 | 844 |
| | Jh | 847-1691 | 844 |
| | f | 847-1691 | 844 |

**Table 7.6 The instability regions (Region 2) for square PFCHE plots (h vs. Re, Jh vs. Re and f vs. Re) with different corrugation angles.**

The results shown in Table 7.6, provides further support to the earlier performance plot analyses, in determining the optimum angle for the PFCHE. The 60° angle has the longest Region 2, followed by the 90° and 30° corrugation angles. This means that the 60° angle experiences fluctuations to heat transfer over a wider range of Re. It achieves developing flow for a broader range of flow rates and should in theory, based on this reasoning alone provide the best performance in the PFCHE. However, this is not the case as the 90° angle achieves the best overall performance from the performance plots. Nevertheless, the outcome of this study on Region 2 does in some way lend support towards the performance plot results, where the 60° angle comes second in the Colburn and goodness factor plots; losing out to the 30° and 90° angles respectively. It also has intermediate friction factors that lie between the 30° and 90° angles.

A direct link between the length of Region 2 for the 60° angle can be made with the performance result noted earlier in Section 7.4.2, where it achieves the highest heat transfer coefficients at high pumping power values compared to the other two angles. This high heat transfer occurrence only happens at high pumping power values because the energy expended for the 60° angle needs to be high, to overcome the fluctuations in friction. More pumping power has to be expended to reap in the heat transfer benefits. When insufficient energy is expended, the

fluctuations in friction outweigh the heat transfer enhancement. This explains the reason why the 60° angle has the lowest heat transfer coefficients at low pumping power values.

Therefore apart from the change in flow direction, which causes disturbance to flow leading to better heat transfer at the expense of higher pressure drops, the length of Region 2 also plays a part in explaining the behaviour of the corrugation angle performance in the PFCHE. The 30° angle has the shortest Region 2; the lowest thermal efficiency and the highest friction factors and pumping power requirements, all of which outweighs the fact that it achieves the highest heat transfer capability.

The 90° angle has the second longest Region 2 and achieves the highest heat transfer coefficients at low pumping power values and comes second at higher pumping power values. It also has the highest thermal efficiency and the lowest friction factors. Taking all this into account, the 90° angle is deemed to give the best overall performance in the PFCHE followed by the 60° and 30° corrugation angles respectively.

*7.6.5 Summary of performance analyses*

Table 7.7 below, shows the summary of the performance plots analysed for the three corrugation angles.

| Order | Highest angle (°) | Mid angle (°) | Lowest angle (°) |
|---|---|---|---|
| Jh plot | 30 | 60 | 90 |
| f plot | 30 | 60 | 90 |
| Goodness factor plot | 90 | 60 | 30 |
| Pumping power plot (E<1000 W/m$^2$) | 90 | 30 | 60 |
| Pumping power plot (E>1000 W/m$^2$) | 60 | 90 | 30 |
| Length of Region 2 | 60 | 90 | 30 |
| Heat balance error | 30 | 60 | 90 |

**Table 7.7 Summary of the performance plots analysed for a square PFCHE with different corrugation angles**

The final results on the overall performance of the corrugation angles in the square PFCHE, is as follows:

| | |
|---|---|
| Optimum angle | 90° |
| 2nd | 60° |
| 3rd | 30° |

**Table 7.8 Order of the optimum angle in the square PFCHE**

To further extend this study on angles, we move on to compare the performance of the square PFCHE having different corrugation angles (30°, 60° and 90°) with metallic heat exchangers.

## 7.7 Comparison with data from literature

In this section, a performance comparison between the PFCHE with different corrugation angles and metallic heat exchangers are carried out. Two metallic heat exchangers are considered in the comparison. They are as follows:

(i) Plate fin heat exchanger (ii) Cross-corrugated plate heat exchanger

Based on the availability of suitable data from literature, further emphasis is placed on the plate fin heat exchanger. We begin the next section with the plate fin before proceeding to touch briefly on the corrugated plate heat exchanger.

### *7.7.1 Plate Fin heat exchanger*

A performance comparison between the square PFCHE with 30°, 60° and 90° corrugation angles was made with an aluminium plate fin (PF) heat exchanger in an air/air system. The basis of the comparison was the hydraulic diameter whereby both units have a similar value of $d_h \approx 2$mm, Kays and London (1984). A description of the plate fin heat exchanger is given in Chapter Nine, whilst further details are attached in Appendix H. The performance comparison will be conducted using four plots, in the order as follows:

(i) Colburn factor (Jh)
(ii) Friction factor (f)
(iii) Pumping power (E)
(iv) Goodness factor (Jh/f)

#### 7.7.1.1 Colburn factor (Jh)

It is clearly shown from Figure 7.11a, that the square PFCHE has a higher thermal performance for all three angles than the plate fin heat exchanger (PF).

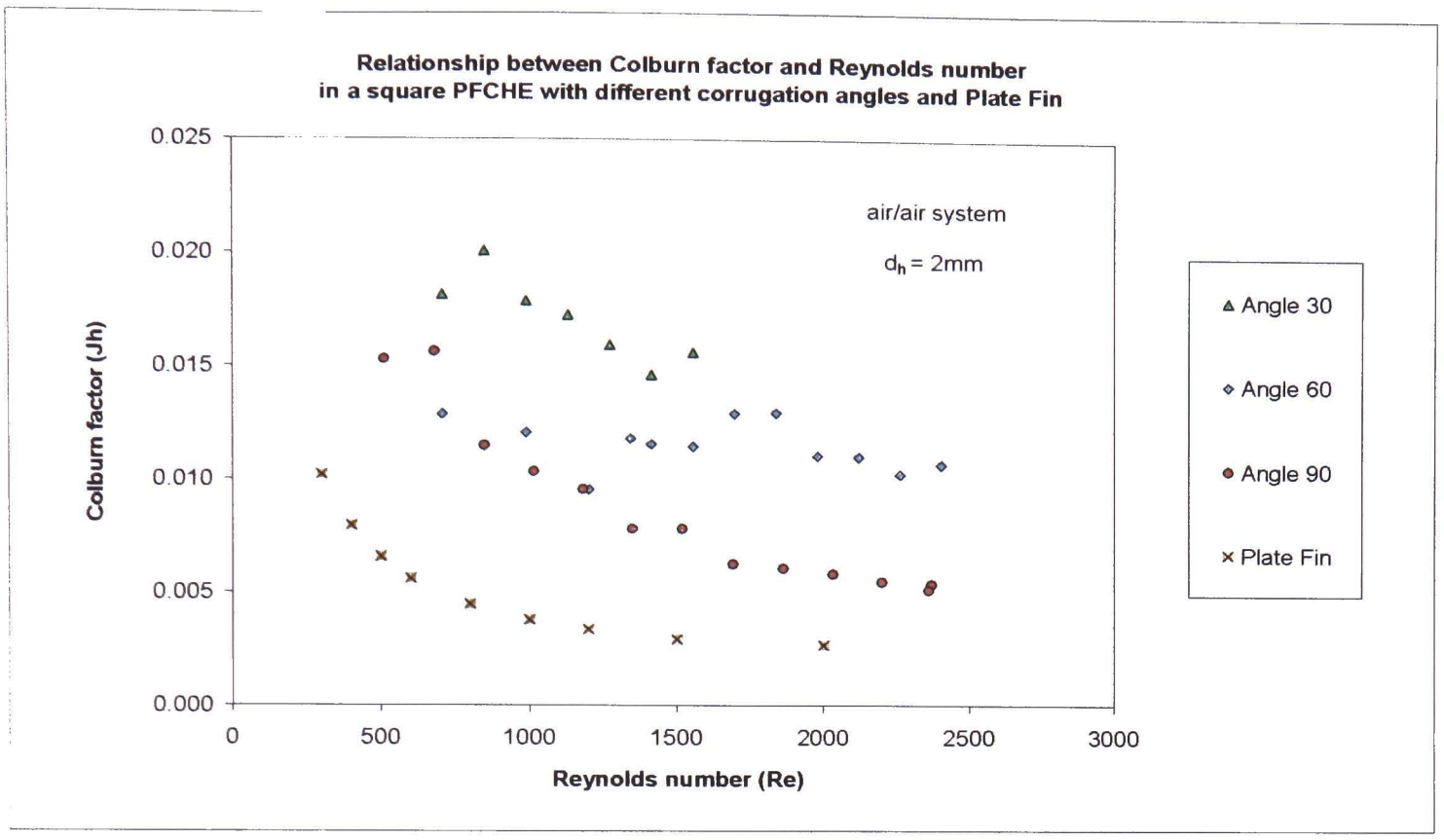


**Figure 7.11a Graph of Colburn factor (Jh) vs. Reynolds number (Re) for a square PFCHE with 30°, 60° and 90° corrugation angles and Plate Fin in an air/air system**

For a better quantitative comparison, the Jh ratios calculated at Re=1000 are shown below.

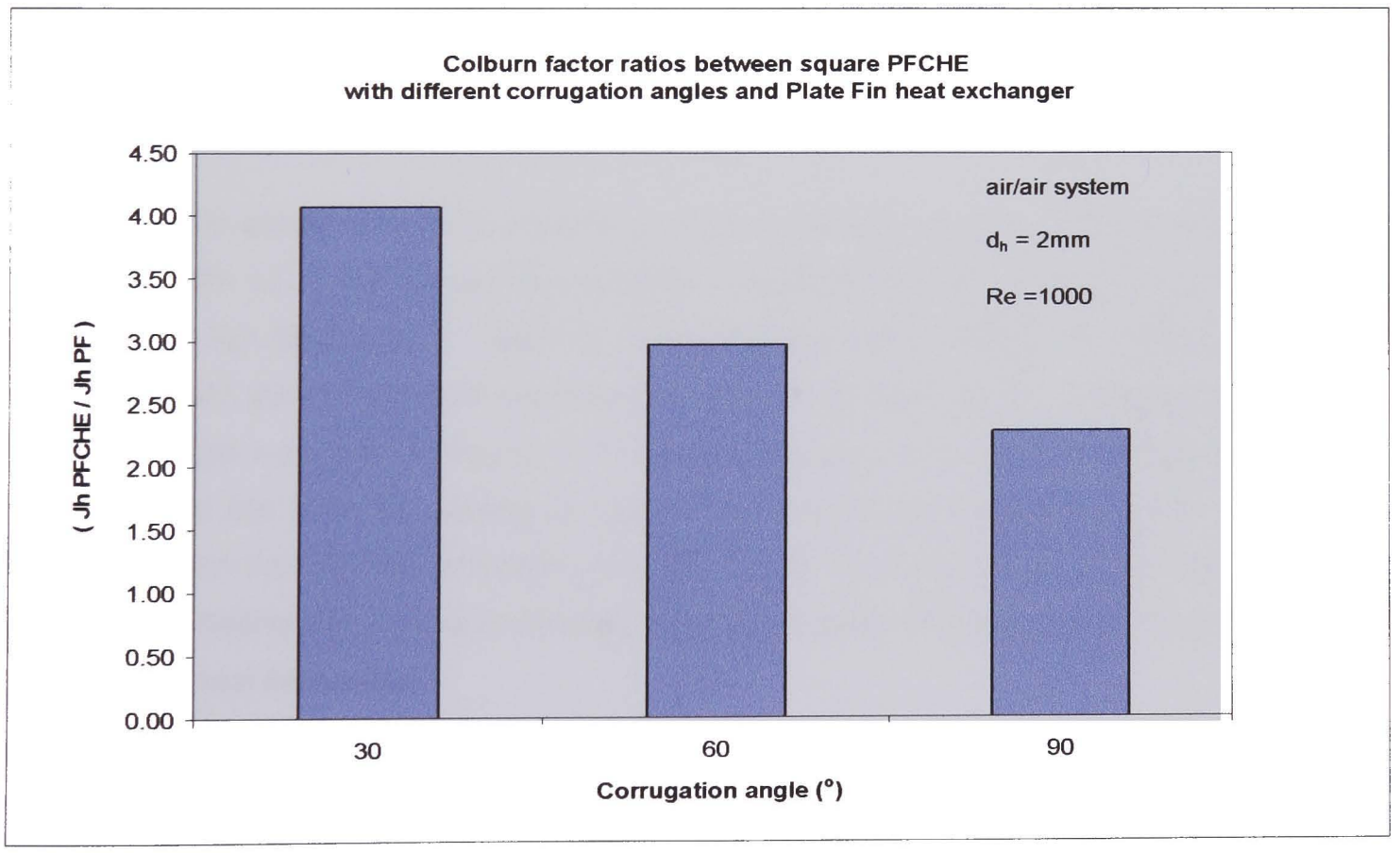


**Figure 7.11b Colburn factor (Jh) ratios between a square PFCHE with 30°,60° and 90° corrugation angles and Plate fin in an air/air system**

Figure 7.11b shows a close up of the ratios calculated at Re=1000,

Jh $30^{o}$/ Jh $_{PF}$ = 4.1
Jh $60^{o}$/ Jh $_{PF}$ = 3.0
Jh $90^{o}$/ Jh $_{PF}$ = 2.3

The PFCHE with a $30^{o}$ corrugation angle has a higher heat transfer capacity by up to a factor of 4, compared to the plate fin heat exchanger. This can be due to the smaller $L/d_h$ value ($L/d_h$=1) for the PFCHE, which translates into the fluid having developing flow. The term (L) is the length of uninterrupted flow, which for the PFCHE is 2 mm. The $L/d_h$ value for the plate fin, is relatively much higher at about 74. This means that in the PFCHE, the fluid uninterrupted flow length (L) is shorter and frequently interrupted which leads to the onset of developing flow, where the boundary layers are constantly broken and rebuilt. Hence due to this 'massaging effect' on the fluid flow, the heat transfer in the PFCHE is enhanced.

The plate fin heat exchanger which has a higher $L/d_h$ value, (L/dh=73.84) experiences fully developed heat transfer which is less effective than developing heat transfer in generating high heat transfer coefficients. This is due to the heat transfer resistance provided by the boundary layers of the fully developed flow. From the definition of the hydraulic diameter, $d_h=(4A_{ff}L/A)$, it is interesting to note that the expression $4L/d_h$ is equivalent to the ratio between the total heat transfer area (A), and the free flow area ($A_{ff}$) of the exchanger. Therefore it follows that the $A/A_{ff}$ ratio for the PFCHE is lower than that of the plate fin.

From the NTU expression ($NTU = UA/C_{min}$), it can be concluded that U is inversely proportional to A. The term (U) is the overall heat transfer coefficient. Therefore a smaller A, (but relatively higher than $A_{ff}$) generates a higher U. Consequently with a higher U, higher heat transfer coefficients are generated which explains the higher Jh for the PFCHE, compared to the plate fin heat exchanger as shown in Figure 7.11a above. Moreover a smaller Aff, brings about a larger A/Aff ratio for the plate fin, leading to higher velocities and consequently higher Re numbers. Therefore from the Colburn definition ($Jh = Nu/ Re\ Pr^{0.33}$), lower Jh values are obtained for the plate fin. Following this, we next compare the friction factor characteristics for the PFCHE and the plate fin heat exchanger.

7.7.1.2 Friction factor (f)

Figure 7.12a below, shows that the PFCHE has a higher friction factor for all three angles compared to the plate fin heat exchanger (PF). This can be seen by the f ratios calculated at Re=1000.The PFCHE has a higher friction factor by up to a factor of 138 compared to the plate fin heat exchanger.

An illustration of the ratios calculated at Re=1000, is shown in Figure 7.12b.

$f\ 30^{\circ}/\ f_{PF} = 137.8$

$f\ 60^{\circ}/\ f_{PF} = 41.1$

$f\ 90^{\circ}/\ f_{PF} = 10.4$

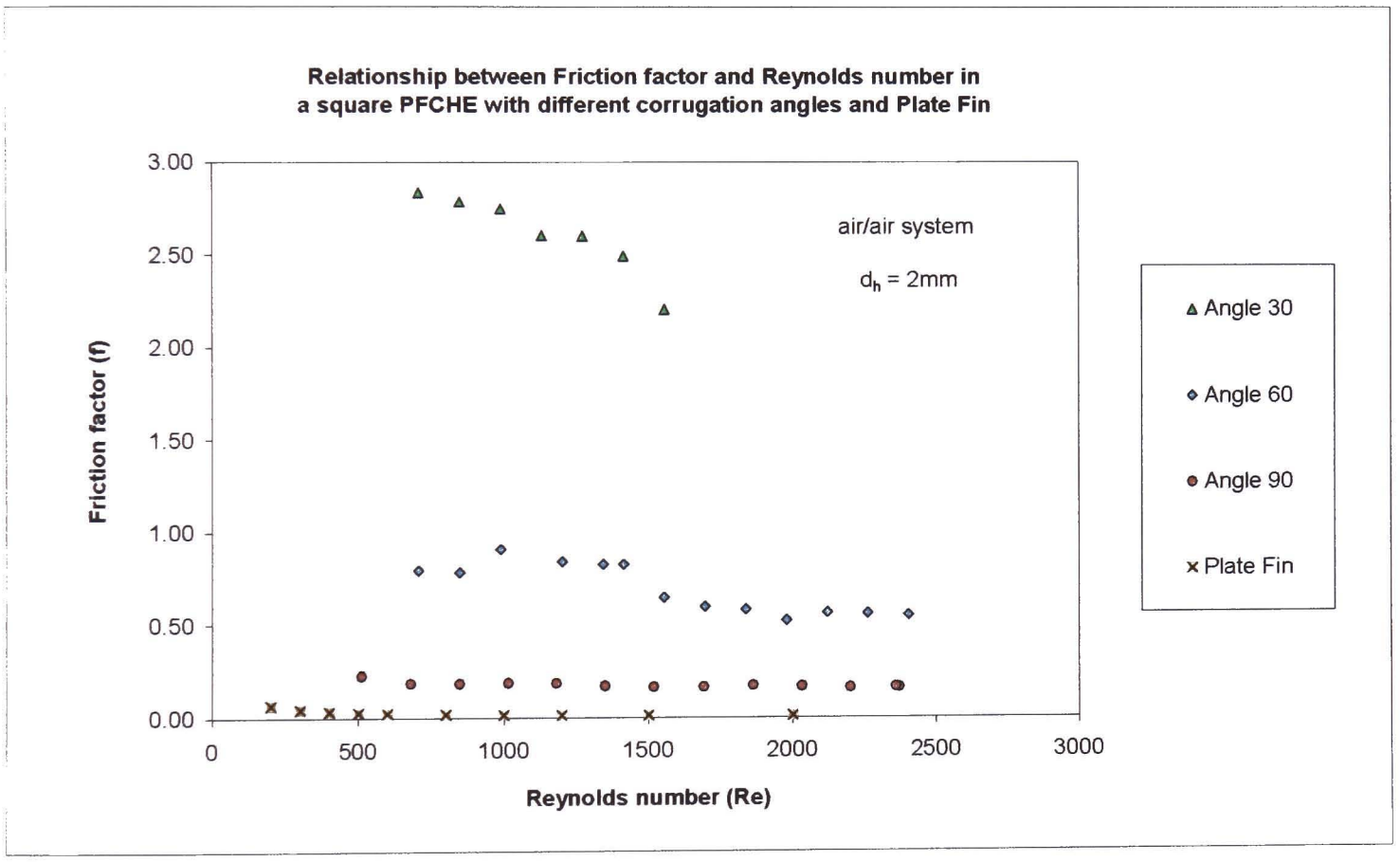


**Figure 7.12a Graph of friction factor (f) vs. Reynolds number (Re) for a square PFCHE with 30°, 60° and 90° corrugation angles and Plate Fin in an air/air system**

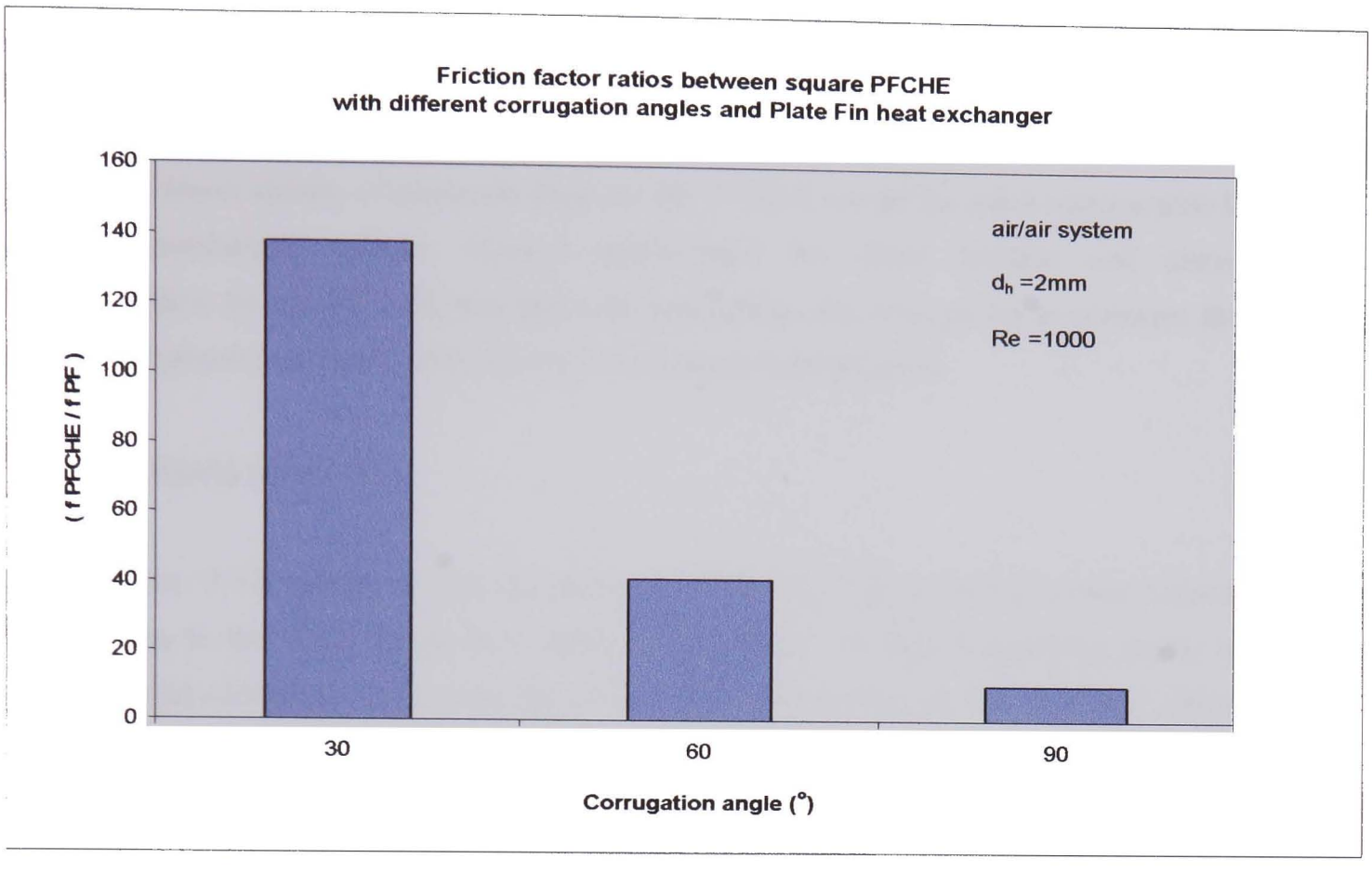


**Figure 7.12b Friction factor (f) ratios between a square PFCHE with 30°,60° and 90° corrugation angles and Plate fin in an air/air system**

The PFCHE friction factors for all the three angles are much higher than the plate fin. The pressure drops for both heat exchangers measured over a similar Re range, are shown in the table below. The pressure drops for the PFCHE are found to be much higher than the plate fin.

| Unit | L (mm) | ΔP (kPa) | Re range | ($\Delta P_{PFCHE}/\Delta P_{PF}$) min | ($\Delta P_{PFCHE}/\Delta P_{PF}$) max | ($\Delta P_{PFCHE}/\Delta P_{PF}$) average |
|---|---|---|---|---|---|---|
| PFCHE (over all angles) | 135 | 0.3-14.50 | 700-2500 | 5.0 | 12.2 | 11.8 |
| PF | 127 | 0.06-1.22 | 700-2500 | | | |

**Table 7.9 Pressure drops for a square PFCHE and Plate Fin over similar Re**

This could be due to the different length definitions (L) used in measuring the pressure drops for both units. For the PFCHE, (L) refers to the flow length of the total heat exchanger. On the other hand for the plate fin, it is the uninterrupted flow length. The actual plate fin heat exchanger flow length may involve several flow lengths of fin material placed end to end, Kays and London (1984). This causes a big difference in the pressure drops measured and consequently the friction factors calculated. In view of this, it can be inferred that the pressure drops measured for

the PFCHE will be much lower, if the uninterrupted flow length of 2 mm was used. The factor difference between the total flow length of the PFCHE and the uninterrupted flow length is 67.5 (135/2 mm). Therefore the pressure drops should be reduced by a factor of 67.5. These theoretical lower values of pressure drop for the PFCHE would be more comparable to the plate fin heat exchanger values. Having appreciated the heat transfer and pressure drop characteristics for the PFCHE and plate fin separately, we now go on to consider the pumping power and goodness factor plots which incorporates both aspects.

7.7.1.3 Pumping power (E)

From Figure 7.13 below, it can be seen that the PFCHE pumping power values are only comparable to the plate fin up to a value of 500 W/m$^2$. At higher pumping power values, the plate fin heat exchanger cannot be included in the comparison as the data from literature is not sufficient, Kays and London (1984). The plate fin offers a similar heat transfer capability to the 60° angle but loses out to the 30° and 90° angles. As shown before, the 90° angle achieves the best heat transfer at low pumping power values.

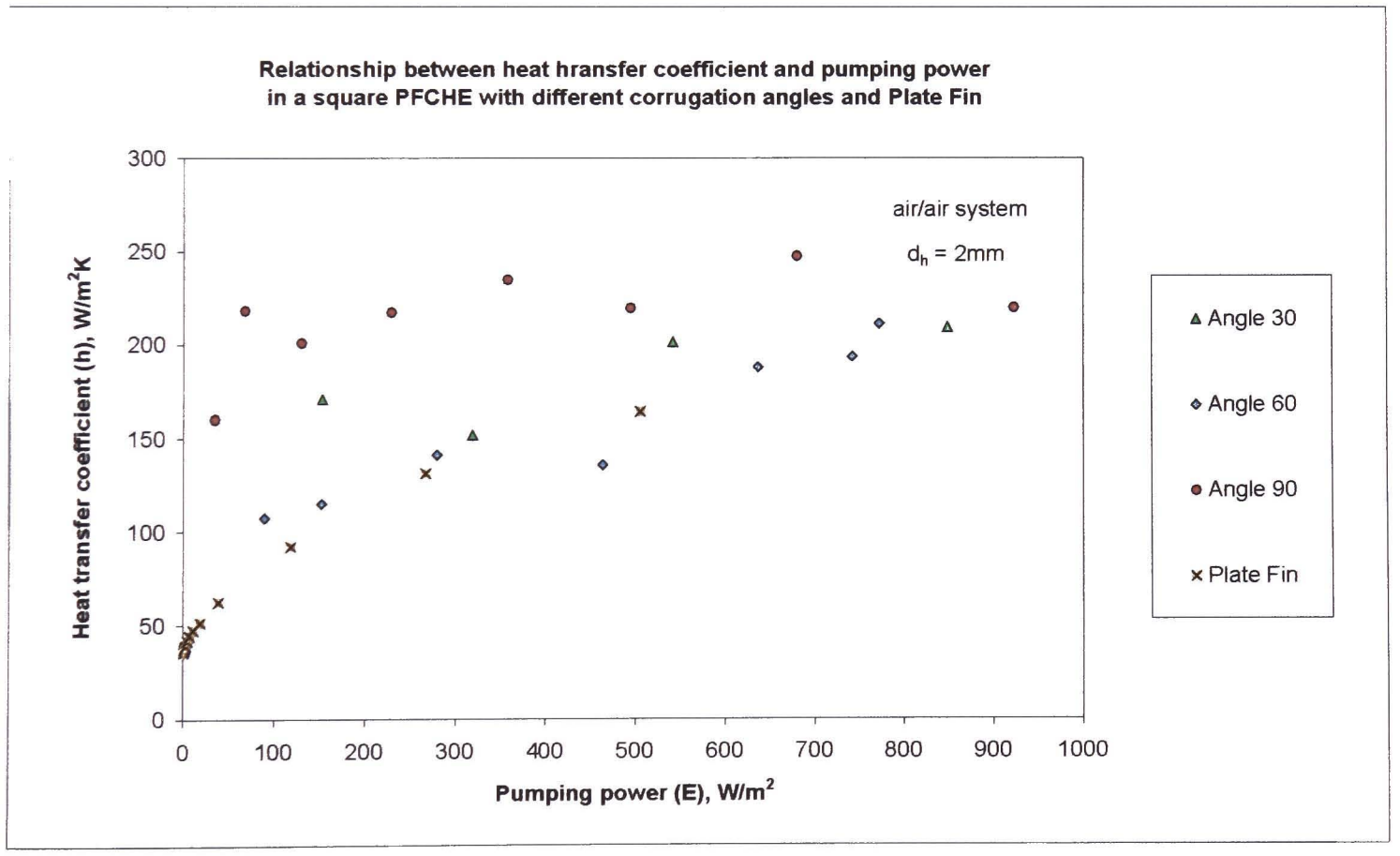


**Figure 7.13 Graph of heat transfer coefficient (h) vs. pumping power (E) for a square PFCHE with 30°, 60° and 90$^0$ corrugation angles and Plate Fin in an air/air system**

The heat transfer coefficient ratios calculated at E=200 W/m$^2$ are as follows:

$h\ 30^{\circ}/ h_{PF} = 1.4$

$h\ 60^{\circ}/ h_{PF} = 1.1$

$h\ 90^{\circ}/ h_{PF} = 1.7$

From the ratios calculated, it can be seen that the PFCHE achieves higher heat transfer coefficients than the plate fin when expending the same pumping power. The 90° angle provides the best performance in the comparison. In other words, even though the PFCHE has higher friction factors than the plate fin, it outperforms the latter, when both the heat transfer and pressure drop characteristics are taken into consideration. It should noted that the heat transfer coefficient ratios, would be more in favour to the PFCHE, if the pressure drops were measured over similar lengths for both units.

7.7.1.4 Goodness factor (Jh/f)

Figure 7.14 below shows the goodness factors for the plate fin heat exchanger and the PFCHE with different corrugation angles (30°, 60° and 90°). It can be seen that the goodness factor for the plate fin is far superior to the PFCHEs, despite the latter having better heat transfer capabilities. This is again due to the high friction factors of the PFCHE compared to the plate fin, which can be seen earlier in Figure 7.12a.

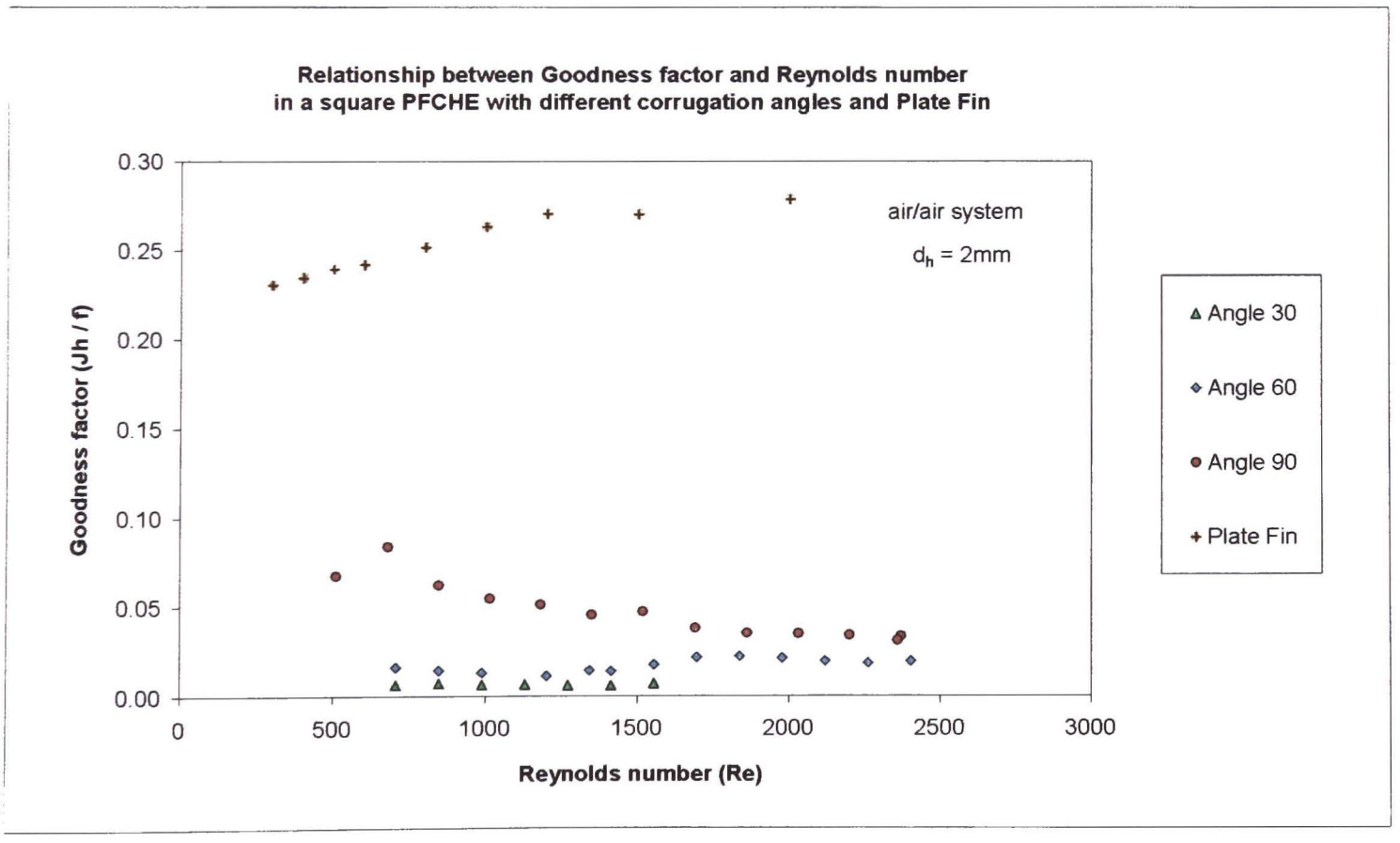


**Figure 7.14 Graph of goodness factor (Jh/f) vs. Reynolds number (Re) for a square PFCHE with 30°, 60° and 90° corrugation angles and Plate Fin in an air/air system**

The Jh/f ratios calculated at Re=1000 are as follows:

$(Jh/f\ 30^{o}/\ (Jh/f)_{PF} = 0.03$
$(Jh/f)\ 60^{o}/\ (Jh/f)_{PF} = 0.07$
$(Jh/f)\ 90^{o}/\ (Jh/f)_{PF} = 0.22$

The reason for the large difference in the goodness factors calculated for both units is the length parameter (L) used in measuring the pressure drops. As explained before for the friction factor plot in Section 7.7.1.2, the length used for the PFCHE is the total flow length of the exchanger whereas the plate fin uses the uninterrupted flow length, which is much shorter. This difference in the length definition causes the measured pressure drop of the PFCHE to be much higher compared to the plate fin, which consequently leads to a higher friction factor. For instance, consider the 90° angle whereby the pressure drop of this unit is higher than the plate fin by a factor of 10, whilst the heat transfer is higher than the plate fin by a factor of 2. Hence the high pressure drops measured, outweighs the heat transfer capability of the PFCHE compared to the plate fin. If the length definition for both units were the same, the PFCHE will experience relatively lower pressure drops that will lead to lower friction factors. Therefore in this case, the PFCHE will be deemed more thermally efficient and be comparable to the plate fin. This conclusion would lend support to the results of the pumping power comparison earlier, where the PFCHE performance is superior. In the next section, we consider another metallic heat exchanger for the performance comparison with the PFCHE. The unit chosen is the cross-corrugated plate heat exchanger.

### *7.7.2 Cross- corrugated plate heat exchanger (CPHE)*

CPHEs are made of a large number of corrugated plates placed against each other such that the herringbone pattern of the corrugation on adjacent plates is pointing at opposite directions. The heat exchanging fluids are pumped in a counter flow direction through alternate channels, created by each pair of plates. The size of the heat exchanger is directly dependant on the number of plates used in its assembly. Two variables of importance in the design of cross-corrugated plate heat exchangers are the size of the corrugation; the height (H) and pitch (P), and the orientation of the corrugation with respect to the main counter-flow direction which is also known as the angle of inclination ($\gamma$). The use of the angle of inclination can also be adopted for the PFCHE design, although in this case the main flow is in the cross-flow direction.

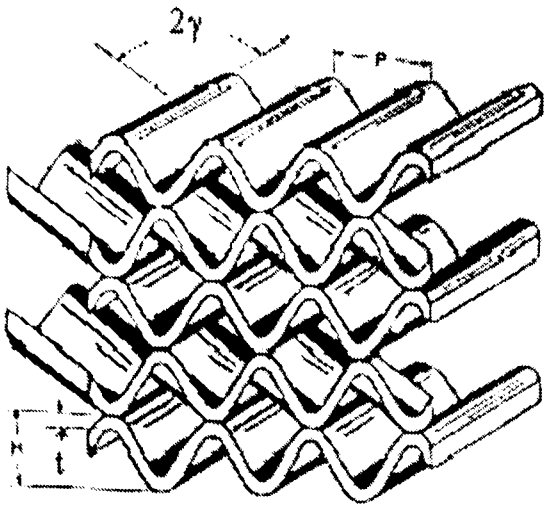


**Figure 7.15 Diagram of cross-corrugation between plates**

It should be noted though, that the symbol ($\gamma$) for the PFCHE, is used to indicate the working angle, which is the angle between the diagonal line of the perspex frame and the corrugation of the sheets. This angle has been chosen as the 'working angle', because of the symmetry of the heat exchanger about its diagonal line, as shown in Figure 7.2. Therefore, ($\gamma$) is not the inclination angle for the PFCHE, as it does not represent the orientation of the corrugation with respect to the main cross-flow direction. Instead, the angle of inclination is represented by (90-$2\gamma$).

For the CPHE, the effects of the corrugation angle ($2\gamma$) on the thermal and hydraulic performance in the exchanger, have been investigated through laboratory experimentations for a single-phase application using water (Hessami 1999).Two test heat exchangers with $2\gamma = 90^{o}$ and $120^{o}$, especially designed for this purpose were tested. The results showed that the $120^{o}$ channel compared to the $90^{o}$ sample, has a better thermal performance for Re<1500. However, a cross-over takes place at higher values of Re, where the $90^{o}$ test sample was found to be superior. This is contrary to the general understanding of heat transfer in such geometries, since the $120^{o}$ angle has a higher angle of inclination; ($60^{o}$) as opposed to only ($45^{o}$), for the $90^{o}$ corrugation angle. Intuitively, as the angle of inclination increases, flow should become more turbulent and therefore the heat transfer should increase (Focke and Zachariades 1985). It is known that the transition to turbulence for flow in such geometries (CPHEs) occurs at approximately Re=200. Commercial heat exchangers normally operate under turbulent conditions and therefore high Re regions. Hence, the pressure drops in conventional CPHEs increase substantially with an increase in the angle of inclination. Additionally, the pressure drop in the $90^{o}$ channel was about half of that for the $120^{o}$ channel, for nearly all flow rates (Hessami 1999). These unexpected findings indicate that the $90^{o}$ channel should be preferred for commercial heat exchangers (contrary to the commonly used $120^{o}$ channel), because the flow

through commercial units are mostly at Re>1500. Therefore, the results show that under normal operating conditions, the 90° channel should be preferred over the 120° channel in cross-corrugated plate heat exchangers (CPHEs). These findings for the CPHE support the PFCHE results earlier, where the 90° corrugation angle is the optimum angle for the PFCHE; despite having the lowest heat transfer, as it provides the best overall performance (highest goodness factors) compared to the other angles studied.

In order to be able to compare the present experimental PFCHE data with more CPHE data from literature, it is essential to ensure that there is a similar basis for comparison (similar variables which affect the heat transfer). However, not many authors provide the necessary information in their papers to facilitate this comparison. Keeping this in mind, experimental data from a number of sources have been gathered and combined with the PFCHE experimental results. Since most of the data from literature have been provided as plots of $Nu/Pr^{0.33}$ vs. Re, this convention is also used for the PFCHE, as shown in Figure 7.16 below, to represent the heat transfer achieved. The list in Table 7.10, describes the labels for each series of plots by identifying the reference, as well as providing the heat transfer variables involved for the studies from literature.

| Reference | Corrugation angle or angle between the plates, $2\gamma$ (°) | P/H | $d_h$ (mm) | Pr |
|---|---|---|---|---|
| Focke and Zachariades (1985) | 120 | 2.0 | 5.0 | 5.8 |
| Luo and Yu (1988) | 120 | 3.45 | 11.6 | 5.5 |
| Okada et al. (1972) | 120 | 4.55 | 5.7 | 5.7 |
| Hessami (1999) | 90 | 4.55 | 11.0 | 4.1 |
| Hessami (1999) | 120 | 4.55 | 11.0 | 3.4 |
| Stasiek et al. (1996) | 60 | 4.0 | 13.8 | 0.7 |
| Stasiek et al. (1996) | 95 | 4.0 | 11.0 | 0.7 |
| Present study | 30 | 2.0 | 2.0 | 0.7 |
| Present study | 60 | 2.0 | 2.0 | 0.7 |
| Present study | 90 | 2.0 | 2.0 | 0.7 |

**Table 7.10 Details for the heat transfer plot involving different corrugation angles for the PFCHE and cross-corrugated plate heat exchangers**

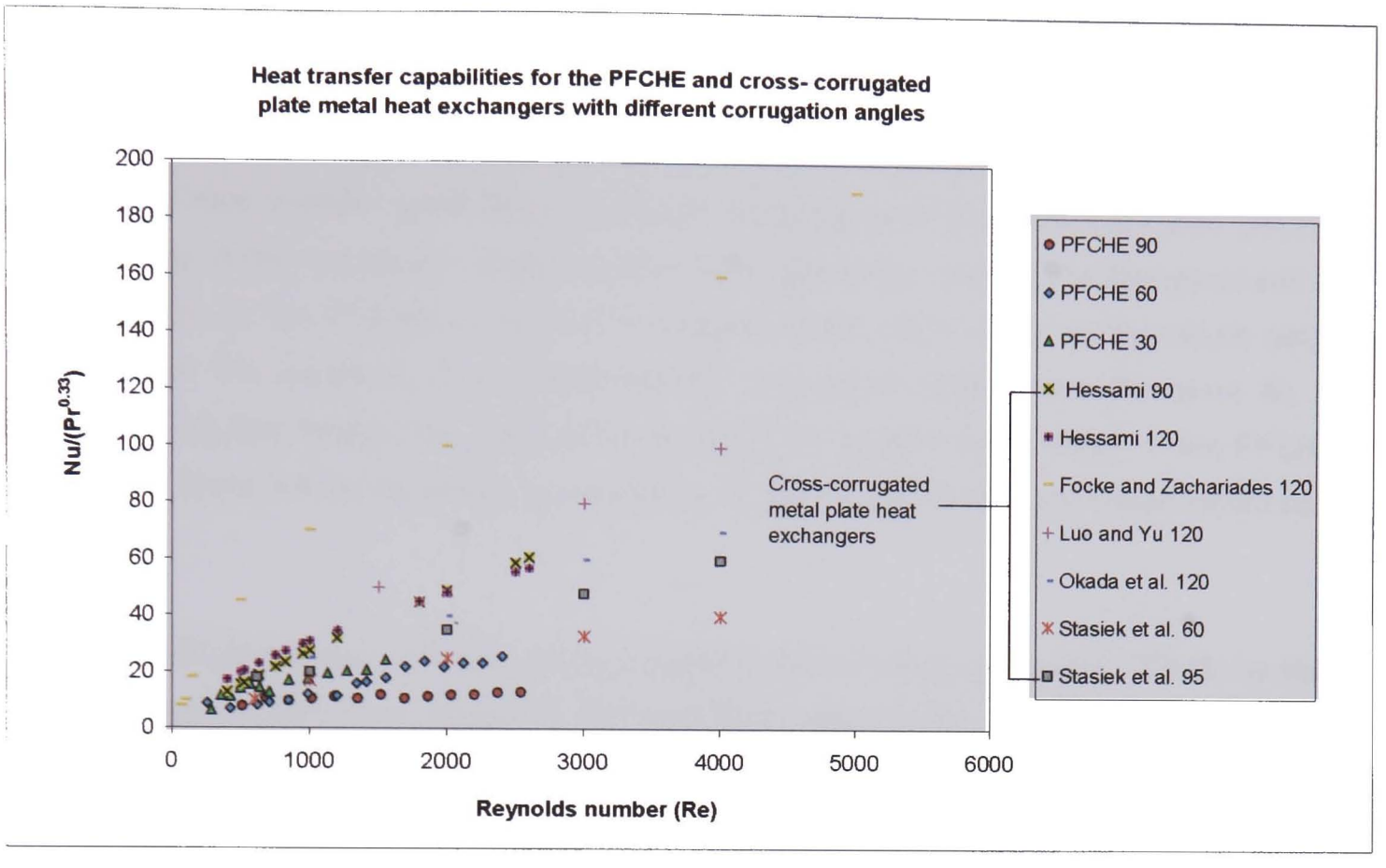


**Figure 7.16 Heat transfer capabilities for the PFCHE and cross-corrugated plate heat exchangers with different corrugation angles**

The series of plots in Figure 7.16, show that there is a relatively large scatter between the literature data for the CPHEs. For example, for the 120° corrugation angle, the difference in the heat transfer value at Re=4000, reported in Focke and Zachariades (1985) is nearly 50% higher than that published in Okada et al. (1972). However, the trend appears to be that the heat transfer is higher, for higher values of the corrugation angle (higher values of inclination angle). The data from Hessami (1999) falls between the wide scatter of the literature data, and agrees fairly well with the data from Okada et al. (1972) and Luo and Yu (1988).

For the PFCHE, it can be seen that the lower corrugation angle; 30° as opposed to the 60° and 90° angles, achieves better heat transfer. In this case, as the corrugation angle ($2\gamma$) decreases, the inclination angle ($90-2\gamma$) increases. Therefore, there is higher deviation from the main cross flow, which promotes better mixing. The data for the PFCHE 60° corrugation angle agrees well with the 60° corrugation angle, reported in Stasiek et al. (1996). In the following section, we summarise the findings for the PFCHE performance comparison with the plate fin and cross-corrugated plate heat exchangers.

*7.7.3 Conclusion of PFCHE comparison with data from literature*

From the comparison between the PFCHE and the aluminium plate fin heat exchanger, it can be concluded that in an air/air system, the PFCHE has superior overall performance. The PFCHE has better heat transfer capabilities and lower pumping power requirements than the plate fin irrespective of the corrugation angle adopted. The high friction factors and low goodness factors experienced by the PFCHE, is not a true account of the unit's ability as the length definitions over which the pressure drop measurements are taken differs from the plate fin. If the uninterrupted flow length was used as for the plate fin, instead of the length of the PFCHE, the goodness factor will be increased considerably as the friction factors calculated would be much lower.

The PFCHE comparison with the cross-corrugated plate fin heat exchanger (CPHE) by Hessami (1999), supports the result where the 90° corrugation angle is the optimum angle in the PFCHE. The CPHE study shows that the 90° angle is superior compared to the conventionally used 120° angle in process industries. However, it should be noted that the 30° and 60° angles studied for the PFCHE, have not been investigated in this CPHE study. This therefore prevents a direct comparison for the two angles. Nevertheless, the data for the PFCHE 60° corrugation angle, agrees well with the 60° corrugation angle reported in Stasiek et al. (1996).

## 7.8 Conclusion

In this chapter, the Colburn factor results for the 30°, 60° and 90° corrugation angles, show that the heat transfer achieved in the PFCHE, is very much dependant on the corrugation angle. Smaller angles achieve higher heat transfer due to the larger deviation in the flow path from the main cross flow, which promotes better mixing. Nevertheless the 30° angle, which offers the highest heat transfer, exhibits the shortest instability region (Region 2) from the Jh trends observed. This implies that the 30° angle experiences the least developing flow; less breaking down of the boundary layers. Therefore in this case, the high heat transfer achieved for the 30° angle is more due to the change in path flow, rather than the presence of developing flow. The highest heat transfer obtained by the 30° corrugation angle compared to the 60° and 90° angles, would follow the theory that more heat can be transferred in a counter-current system than in a co-current or cross current system. As the working angle of the exchanger is decreased, the system approaches a counter-flow system; therefore maximising the heat that that can be transferred in a smaller area. The disadvantage with this arrangement is that the friction factor is much higher due to the high pressure drops across the system.

The PFCHE friction factor results also show a dependence on the corrugation angle. As expected, the 30° angle is found to have the highest friction factors, as its superior heat transfer ability is achieved at the expense of high pressure drops, due to the largest deviation from the main cross flow. Next in line are the 60° and 90° angles respectively. The 90° angle has the highest thermal efficiency and the lowest pumping power requirements. It also has an intermediate Region 2 length, which translates into a strong presence of developing flow. All of this outweighs the fact that it has the lowest heat transfer capability. In view of the overall thermal and hydraulic performance, the 90° corrugation angle is deduced to be the optimum angle and should be preferred over the 30° and 60° angles, for applications in the square PFCHE. The summary of the results obtained in this chapter, are shown in Table 7.11 below. The first part of the results is a replicate of Table 7.7, shown earlier.

Perhaps in a gas/liquid or liquid/liquid application where the pumping power expended is not a major concern or when the 90° angle is not possible, the 60° angle would be the next best choice based on this study. An example of this application is in the spiral PFCHE where it is impossible to have a 90° angle, as the polymer films have to be bent around the aluminium core. The findings from this PFCHE angle study also support the literature results performed by Hessami (1999), whereby the 90° angle gives the best performance in cross-corrugated aluminium plate heat exchangers (CPHEs). In addition it was found that the square PFCHE; irrespective of the angle employed, outperforms the plate fin heat exchanger in an air/air system between 500<Re<2000.

| Order | Highest angle (°) | Mid angle (°) | Lowest angle (°) |
|---|---|---|---|
| Jh plot | 30 | 60 | 90 |
| f plot | 30 | 60 | 90 |
| Goodness factor plot | 90 | 60 | 30 |
| Pumping power plot (E<1000 W/m$^2$) | 90 | 30 | 60 |
| Pumping power plot (E>1000 W/m$^2$) | 60 | 90 | 30 |
| Length of Region 2 | 60 | 90 | 30 |
| Heat balance error | 30 | 60 | 90 |

| Angle | Jh | f | Re | Region 2 (Re) | Region 2 interval (ΔRe) |
|---|---|---|---|---|---|
| 90 | $2.0097\ Re^{-0.7644}$ | $0.5992\ Re^{-0.1698}$ | 510<Re<2540 | 847-1691 | 844 |
| 60 | $0.0198\ Re^{-0.0751}$ | $16.158\ Re^{-0.4349}$ | 706<Re<2403 | 989-1978 | 989 |
| 30 | $0.1590\ Re^{-0.3195}$ | $17.363\ Re^{-0.2713}$ | 706<Re<1555 | 848-1413 | 283 |

*Region 2 depicts the instability region on the PFCHE performance data plots.

**Table 7.11 Summary of the PFCHE corrugation angle study**

## 7.9 Summary

In this chapter, the effects of the corrugation angle on the square PFCHE performance, was investigated. This study was a follow up from the work done in Chapters Four and Five, involving the use of different fluid systems and configurations for the PFCHE. The aim of this investigation was to determine the optimum angle for the unit, whereby the best overall performance can be achieved. In addition to this, the results obtained will contribute towards the development of the spiral PFCHE, currently employing a 20° angle and also other future designs.

Three corrugation angles are tested in the square PFCHE, namely the 30°, 60° and 90° angles; the latter obtained from Chapter Four. Experimental results for all the three angles are then presented collectively using performance evaluation plots (Jh, f, Jh/f and E). Following the analysis of results obtained, it is concluded that the optimum angle is 90°. We then proceeded to conduct a performance comparison between the PFCHE and two metallic heat exchangers (plate fin and the cross-corrugated plate heat exchanger). Results showed that the PFCHE performance surpasses the plate fin irrespective of the angle adopted, whilst the 90° optimum angle deduced, is also the optimum angle for the cross-corrugated plate heat exchanger based on a study by Hessami (1999).

In the next chapter, we will look at the effect of Prandtl (Pr) number on the square PFCHE performance. This chapter will have a direct link with Chapter Four, since the Pr number is a representation of the different fluids systems that have been tested. The experimental results will be validated collectively using the performance evaluation plots (Jh, Nu, f, Jh/f and E), en route to developing a design model using regression analysis, that will be a function of both Re and Pr numbers. This will enable the use of standard PFCHE design correlations for a range of fluid systems.

# CHAPTER 8 - THE EFFECTS OF PRANDTL NUMBER ON HEAT TRANSFER AND PRESSURE DROP IN A SQUARE PFCHE

## 8.0 Introduction

In Chapter Seven, the effects of the corrugation angle on the square PFCHE performance were investigated. Three corrugation angles (30°, 60° and 90°) were studied, and it was shown that the 90° corrugation angle gave the best overall performance. To add another branch to the studies conducted on the square PFCHE, further analysis is conducted on the performance results for the different fluid systems; described in Chapter Four. This is conducted by studying the effect of Pr numbers. The incentive for this further work is to enable an understanding of yet another aspect of the unit, whereby these dimensionless numbers can represent the physical properties of the different fluid systems.

The Pr number can be defined as follows:

$$\mathrm{Pr} = \frac{cp\,\mu}{k} = \frac{\left(\frac{\mu}{\rho}\right)}{\left(\frac{k}{cp\rho\mu}\right)} = \frac{momentum\ difussion\ coefficient}{thermal\ diffusion\ coefficient} \qquad (8.1)$$

The expression for momentum transfer for a fully developed flow in a tube is shown below, Knudsen and Katz (1958).

$$\frac{\tau}{\rho\, v^2} = A\,\mathrm{Re}^{-0.2} \qquad (8.2)$$

where A is a constant and $\tau$ is the turbulent shear stress.

The expression for heat transfer for a fully developed flow in a tube is as follows:

$$St = B\,Re^{-0.2}\,Pr^{-2/3} \qquad (8.3)$$

where B is a constant

The switch from momentum transfer to heat transfer under these conditions is accounted for by the (diffusivity ratio)$^{-2/3}$, which is essentially $Pr^{-2/3}$. A similar form of expression for heat transfer; but with a different Pr exponent, can be extended to developing laminar flow in the PFCHE. This is because the performance achieved in the PFCHE; shown later in plots using the experimental results, can be proved to be comparable to that achieved in the fully developed tube.

The PFCHE heat transfer expression; incorporating the Pr number, can be developed and compared to a study on laminar flows in smooth tubes by Obot et al. (1997). The basis for the comparison is the use of laminar flows in both units. In addition, based on the plot below, it can be seen that the laminar flow heat transfer in smooth tubes is comparable to that achieved in the PFCHE. This is because the smooth tube heat transfer data; plotted as a function of the distance from the beginning of the heat transfer section, lies within the scatter for the PFCHE heat transfer data. Figure 8.1 shows that similar trends for the Nu numbers are generated, using the PFCHE experimental data and the Graetz expression from literature. The Graetz expression has been developed for laminar flow heat transfer in circular tubes, where the velocity profile is fully developed.

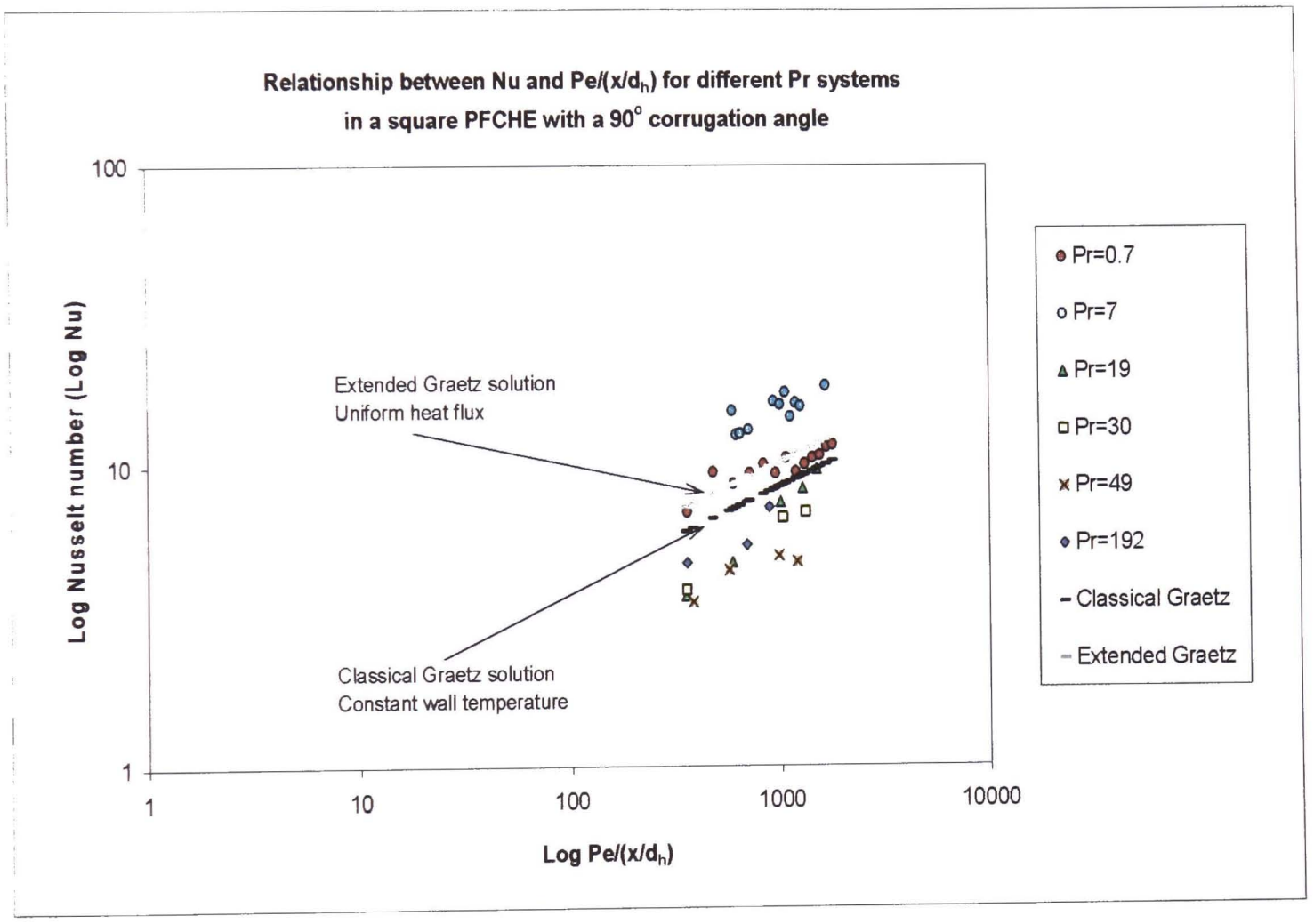


**Figure 8.1 Nusselt number for laminar flow in a square PFCHE and smooth tubes**

The classical Graetz solution, Knudsen and Katz (1958), for constant wall temperature and parabolic velocity distribution is shown below. This equation represents the mean Nu number over a length of tube (x).

$$Nu = 3.66 + \frac{0.0688\left[\left(x/d_h\right)/Pe\right]^{-1}}{1+0.04\left[\left(x/d_h\right)/Pe\right]^{-2/3}} \qquad (8.4)$$

where Pe = Peclet number = RePr

Simplifying the equation above, the expression for the Nu number when the $(x/r_h)/Pe$ term is small; as in the case for the PFCHE, is as follows:

$$Nu = 1.357\left(\frac{x/r_h}{Pe}\right)^{-1/3} \qquad \frac{x/r_h}{Pe} \leq 0.01 \qquad (8.5)$$

A useful extension of the classical Graetz solution using a boundary condition other than constant wall temperature, is shown below for constant heat flux and is plotted in Figure 8.1.

$$Nu = 1.639\left(\frac{x/r_h}{Pe}\right)^{-1/3} \qquad \frac{x/r_h}{Pe} \angle 0.01 \qquad (8.6)$$

In the study by Obot et al. (1997), the smooth tube heat transfer expression involving the Pr number, was developed using the Nusselt number (Nu) and Reynolds number (Re), instead of the Colburn factor (Jh). Therefore in order to be consistent, the PFCHE heat transfer expression is also developed using the Nu and Re numbers to develop the PFCHE heat transfer expression of the form, $Nu = x\, Re^y\, Pr^z$.

However, it should be noted that although the tube experiences laminar flows, the experiment involved using a tube of 181 diameters, causing the flow and temperature profiles to be nearly fully developed. On the other hand, the flow in the PFCHE is repeatedly disturbed over a length of L=2 mm, since $(L/d_h=1)$. Hence, the flow is perpetually disturbed and developing. Nevertheless, although the flow characteristic differs for both units, it can be shown that the heat transfer achieved in the developing flow is higher than that obtained in the nearly developed or fully developed flow. This can be explained using the schematic diagrams below, showing the development of the velocity (v) and temperature (T) profiles in a smooth tube, with respect to the flow length (x) from the entrance of the tube.

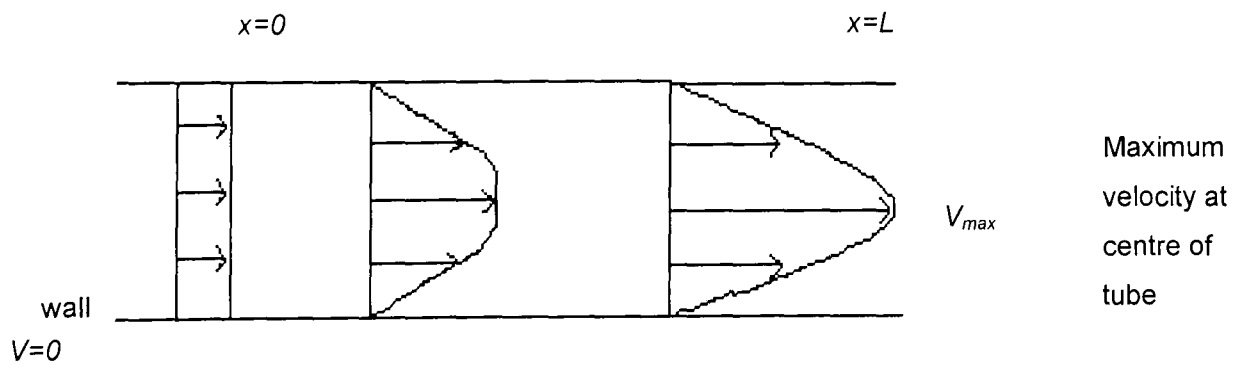

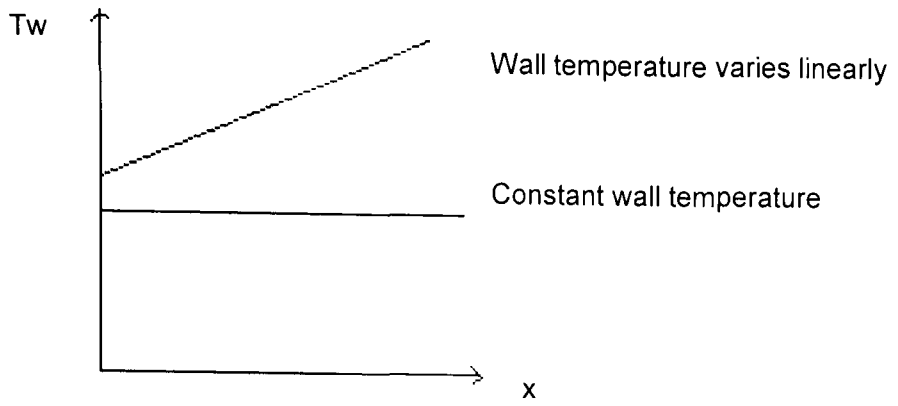


**Figure 8.2 Velocity and temperature profiles in a smooth tube**

For the temperature profile, there is a uniform wall temperature along the tube and also a uniform rate of heat transfer along the length of the tube. The velocity and thermal boundary layers may develop simultaneously. However, the velocity and thermal boundary layers coincide only if the Pr number is unity, implying equal values for the momentum and thermal diffusivity. The larger velocity and temperature gradients achieved in developing flow enhances the heat transfer performance of such flows, compared to fully developed flows. A fully developed velocity profile, transfers less heat from a duct wall because of the convective influence of the velocity profile on the temperature profile. In addition, a fully developed temperature profile transfers less heat from a duct wall because the gradient of the temperature at the wall is reduced due to the adiabatic centreline boundary condition. Therefore to maximise heat transfer, the developing flow is preferred as the thermal and velocity boundary layers are repeatedly broken down.

Apart from heat transfer, a smooth tube friction factor expression involving the Pr number was also developed. As with the heat transfer, the friction factor expression is also compared to the study by Obot et al. (1997). The PFCHE friction factor expression takes the form of, $f = a\,Re^{b}\,Pr^{c}$.

This chapter investigates the effects of Pr number on the square PFCHE performance by compiling the results of six different fluid systems established in Chapter Four. The working fluids considered for the study are air (Pr=0.7), water (Pr=7) and four glycerol-water mixtures (Pr=19, 30, 49 and 192). This can be seen from the table below, which shows the details of the different fluid systems tested in the square PFCHE.

| System | Pr number | Re range | Flow rate ($m^3$/hr) |
|---|---|---|---|
| air/air | 0.7 | 510<Re<2540 | 3-15 |
| water/water | 7 | 87<Re<235 | 0.44-1.17 |
| (30% glycerol + water mixture/water) | 19 | 19<Re<78 | 0.22-0.90 |
| (50% glycerol + water mixture/water) | 30 | 12<Re<44 | 0.20-0.76 |
| (60% glycerol + water mixture/water) | 49 | 8<Re<24 | 0.21-0.66 |
| (70% glycerol + water mixture/water) | 192 | 2<Re<5 | 0.18-0.44 |

**Table 8.1 Details of the different fluid systems tested on the square PFCHE**

The experimental tests covered a Re range of 2-2540, over all six Pr systems investigated. The present work involves compiling the performance data for the six Pr systems (air/air, water/water and four glycerol-water mixtures/water) and then studying the overall effect of the Pr numbers on performance plots (Jh, Nu, f, Jh/f and E). Once the performance plots are established, the unique design correlations incorporating both the Re and Pr numbers, are developed using regression analysis in Microsoft Excel. These take into account, either the heat transfer or pressure drop characteristics of the Pr systems investigated. Further details will be provided in context, later in the chapter.

By using these unique correlations, a standard approach for predicting the performance of the square PFCHE for a range of Pr numbers, can be achieved. More importantly, this will allow alternative designs to be developed; by using just one set of design correlations for a range of different fluids. We conclude this chapter with a comparison between the PFCHE design correlations developed, with those from literature. In the following section, we proceed to investigate the effects of Pr number on the square PFCHE performance. We begin with an investigation on the heat transfer aspect of the unit.

## 8.1 Effects of Prandtl number on heat transfer

Using the heat transfer results for the different fluid systems in Chapter Four, two graphs are plotted in this section to investigate the effect of Pr number on heat transfer in a square PFCHE. The two graphs plotted are as follows and will be discussed in the order shown below.

(i) Colburn factor (Jh) vs. Reynolds number (Re)

(ii) Nusselt number (Nu) vs. Reynolds number (Re)

The Jh vs. Re graph as used in Chapter Four, is the standard and most widely used method for evaluating heat transfer data for industrial heat exchangers. Nevertheless, in this chapter the Nu number is used to represent the PFCHE heat transfer data, as this dimensionless factor is used to represent heat transfer data in most correlations from literature. In addition, the Nu number also plays a major role towards the development of the PFCHE heat transfer expression involving the Pr number. The Nu vs. Re graph is plotted as a basis to compare the PFCHE heat transfer data with relevant correlations from literature. Using the results from the Nu plot, a regression analysis is conducted to obtain the PFCHE heat transfer expression as a function of Re and Pr numbers. This is to done to enable a more specific comparison between the PFCHE; featuring sinusoidal corrugations, with heat transfer in smooth tubes.

*8.1.1 Colburn factor (Jh)*

The general trend observed from Figure 8.3 below, shows that the Jh decreases with increasing Re number for all six Pr systems. The Jh correlations developed for the six Pr systems (Pr = 0.7,7,19,30,49 and 192) using Microsoft Excel, are shown in Table 8.2 below. It was difficult to carry out a Re based comparison, as each system had a different Re range due to the different flow rates used. Nevertheless from Figure 8.3, it was found that the Pr=192 system has the highest heat transfer, whilst the Pr=0.7 system has the lowest heat transfer.

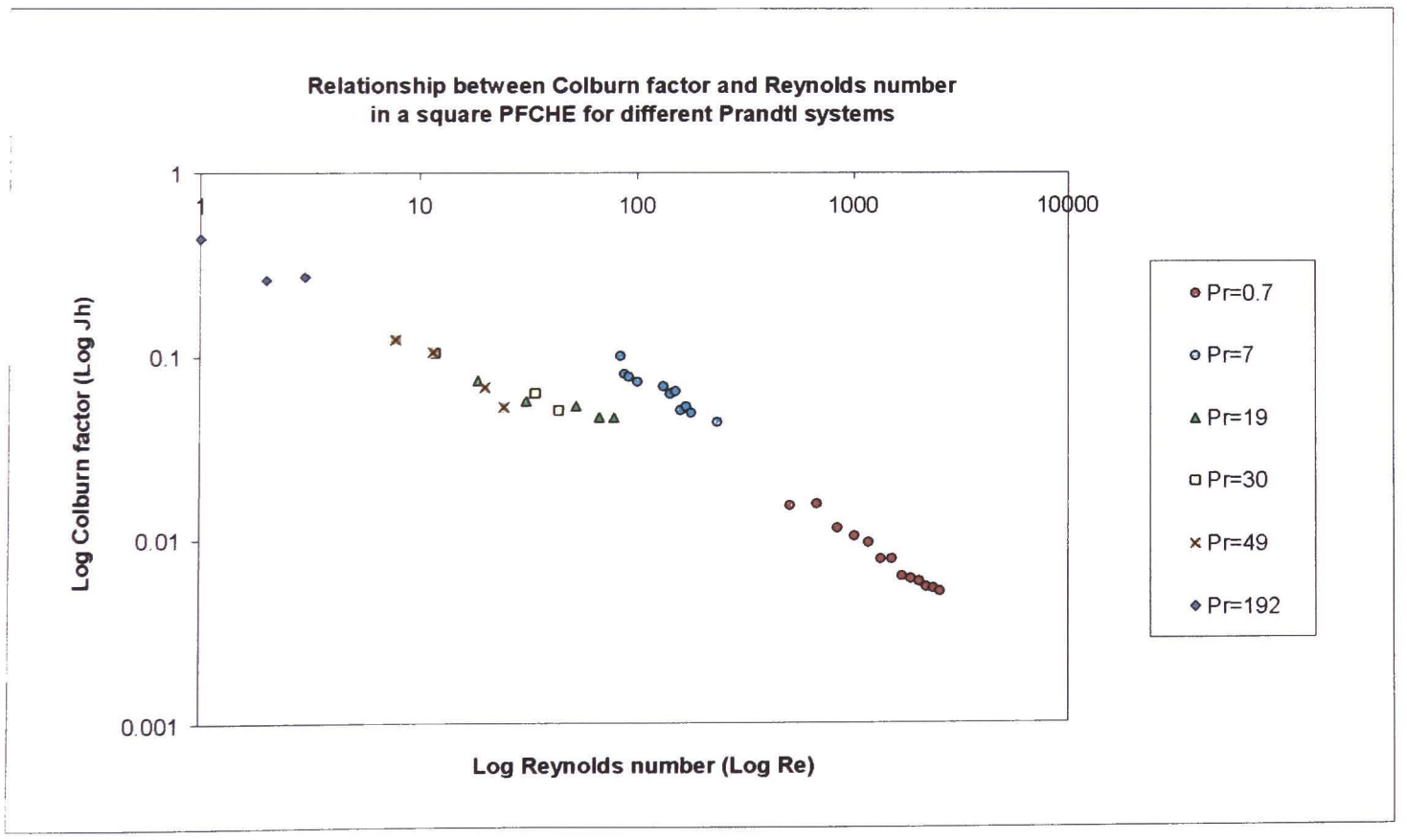


**Figure 8.3 Relationship between Colburn factor (Jh) and Reynolds number (Re) for a square PFCHE with different Pr systems (0.7<Pr<192)**

| Pr | Jh Correlation | Re range |
|---|---|---|
| 0.7 | $2.0097\ Re^{-0.7644}$ | 510<Re<2540 |
| 7 | $1.3886\ Re^{-0.6337}$ | 87<Re<235 |
| 19 | $0.1816\ Re^{-0.3174}$ | 19<Re<78 |
| 30 | $0.3916\ Re^{-0.5282}$ | 12<Re<44 |
| 49 | $0.5868\ Re^{-0.7314}$ | 8<Re<24 |
| 192 | $0.6157\ Re^{-0.5838}$ | 2<Re<5 |

**Table 8.2 Colburn factor (Jh) correlations for different Pr systems in a square PFCHE**

At low Re numbers (Re=20), the Pr=19 and Pr=49 systems can be compared. Pr =19 has a slightly higher Jh value than the Pr=49 system. This observation abides to the Colburn factor definition as shown in equation (8.7) below, whereby a lower Pr would give a higher Jh at the same Re and Nu numbers, if Nu were independent of Pr. To check the latter, the results on the effect of Nu number on Pr number in a square PFCHE, will be shown in Section 8.1.2.

$$Jh = Nu/Re\ Pr^{0.33} \qquad (8.7)$$

At a higher Re number (Re=80), two comparable Pr systems are Pr=7 and Pr=19. From the graph, it can be seen that the Pr=7 system has the higher Jh value, hence abiding once again to the Colburn definition. In the following section, we investigate the effect of Nusselt number (Nu) on the different Pr systems investigated in the square PFCHE.

*8.1.2 Nusselt number (Nu)*

From Figure 8.4, it can be seen that there is a general trend for the six Pr systems investigated. The Nu number increases with Re number for air (Pr=0.7), water (Pr=7) and for the glycerol-water mixtures (Pr=19, 30, 49 and 192). This observation is expected, based on the Colburn definition mentioned earlier. Rearranging the equation gives ($Nu = Jh\ Re\ Pr^{0.33}$), which shows that the Nu number is directly proportional to the Re number. The Nu correlations developed using Microsoft Excel for the different Pr systems are shown in Table 8.3 below.

The Pr=192 system only has three data points on the plot; over a small range of Re numbers, as experimental data was not available for higher Pr systems due to the limitations in the test rig facility involving higher pressure drops. The gap between the Pr=0.7 system and the Pr=7, 19, 30 and 49 systems can be due to the fact that the Pr=0.7 system has a lower thermal conductivity, resulting in lower heat transfer. Taking this into account, a better trend for the thermal performance can be seen in Figure 8.8 under Section 8.5.1.1, where the effect of both the Pr and Re numbers on the thermal performance is considered.

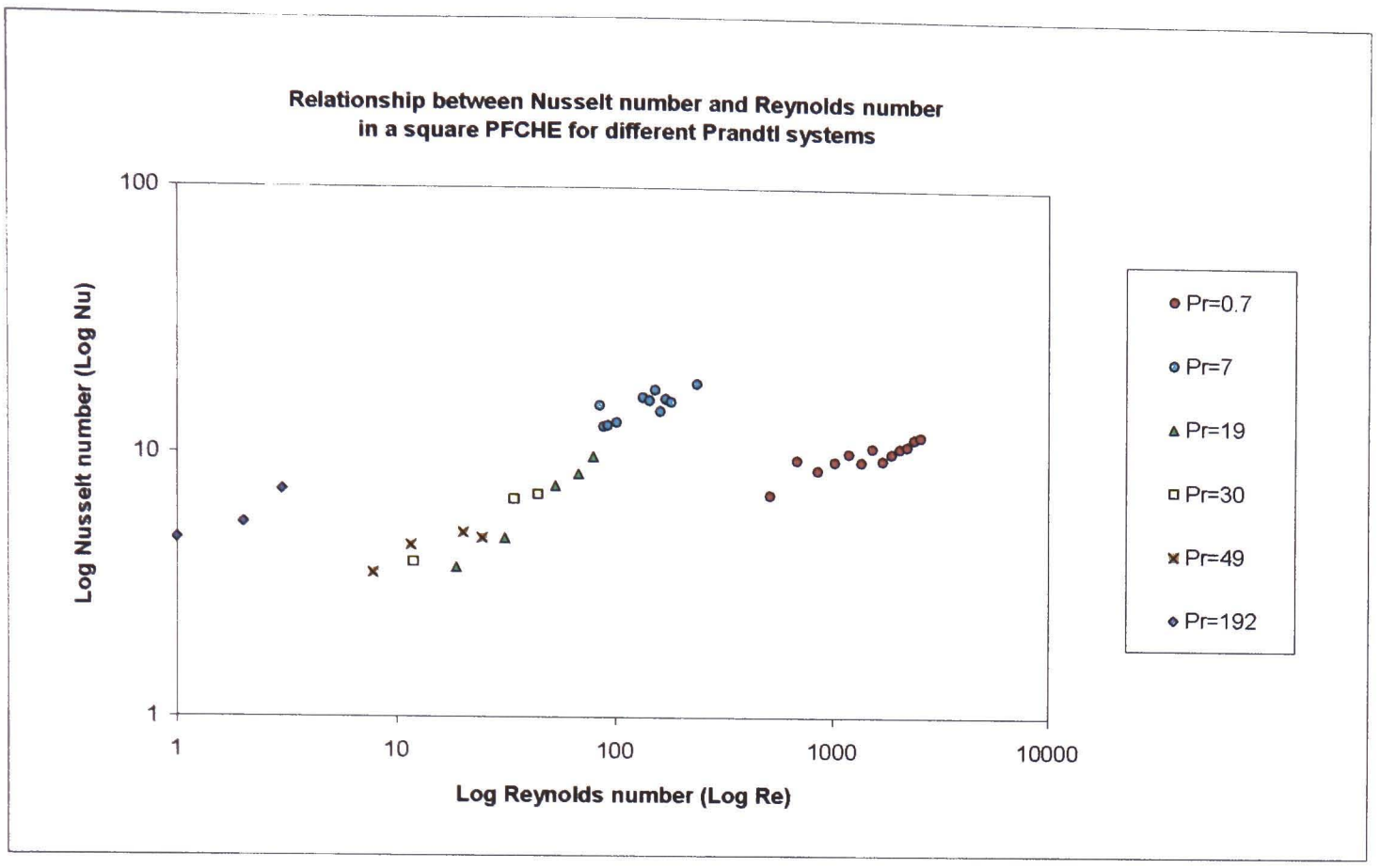


**Figure 8.4 Relationship between Nusselt number (Nu) and Reynolds number (Re) for a square PFCHE with different Pr systems (0.7<Pr<192)**

| Pr | Nu correlation | Re range |
|---|---|---|
| 0.7 | $Nu = 1.8225\ Re^{0.2334}$ | 510< Re<2540 |
| 7 | $Nu = 3.6538\ Re^{0.2919}$ | 87<Re<235 |
| 19 | $Nu = 0.4864\ Re^{0.6823}$ | 19<Re<78 |
| 30 | $Nu = 1.2150\ Re^{0.4720}$ | 12<Re<44 |
| 49 | $Nu = 2.1470\ Re^{0.2690}$ | 8<Re<24 |
| 192 | $Nu = 4.5936\ Re^{0.3666}$ | 2<Re<5 |

**Table 8.3 Nusselt number (Nu) correlations for different Pr systems in a square PFCHE**

A regression analysis using Microsoft Excel was carried out see the effect on Nu when Pr and Re are varied, en route to developing the Nu correlation of the form, $Nu = x\ Re^{y}\ Pr^{z}$. The 'x' and 'y' and 'z' terms are the Nu correlation constants. The heat transfer correlation developed is as follows:

$$Nu = 0.356\ Re^{0.51}\ Pr^{0.42} \qquad (0.7<Pr<192) \qquad (8.8)$$

The 0.42 Pr exponent for the Nu correlation, is higher than the value of 0.4 recommended in the literature, for smooth tube turbulent flow heat transfer calculations using the Dittus-Boelter correlation. This comparison will be explained further in Section 8.5 of this chapter.

Ideally for future work, experimental data for systems between Pr=49 and Pr=192, as well as above and below the current Pr range, are needed to obtain a more accurate Nu correlation. This will then enable a better comparison with the smooth tube results. Next, we move on to consider how the friction factors are affected when using different Pr systems in the square PFCHE.

## 8.2 Effects of Prandtl number on friction factor

The non-dimensional pressure drop characteristics of the square PFCHE are presented in terms of friction factors (f), and are plotted over a range of Re numbers for different fluid systems. As with the heat transfer, six fluid systems corresponding to (Pr= 0.7, 7, 19, 30, 49 and 192) are investigated. The acquisition of the experimental data was obtained by measuring the pressure drops at different flow rates for each system, as shown in Chapter Four. The friction factor plot is needed to develop the PFCHE friction factor correlation as a function of Re and Pr numbers, using regression analysis in Microsoft Excel.

### *8.2.1 Friction factor (f)*

The trend observed in Figure 8.5 below, shows that as the Re number increases, the friction factor decreases for all six Pr systems investigated. The f correlations developed for each Pr system using Microsoft Excel, are tabulated in Table 8.4 below.

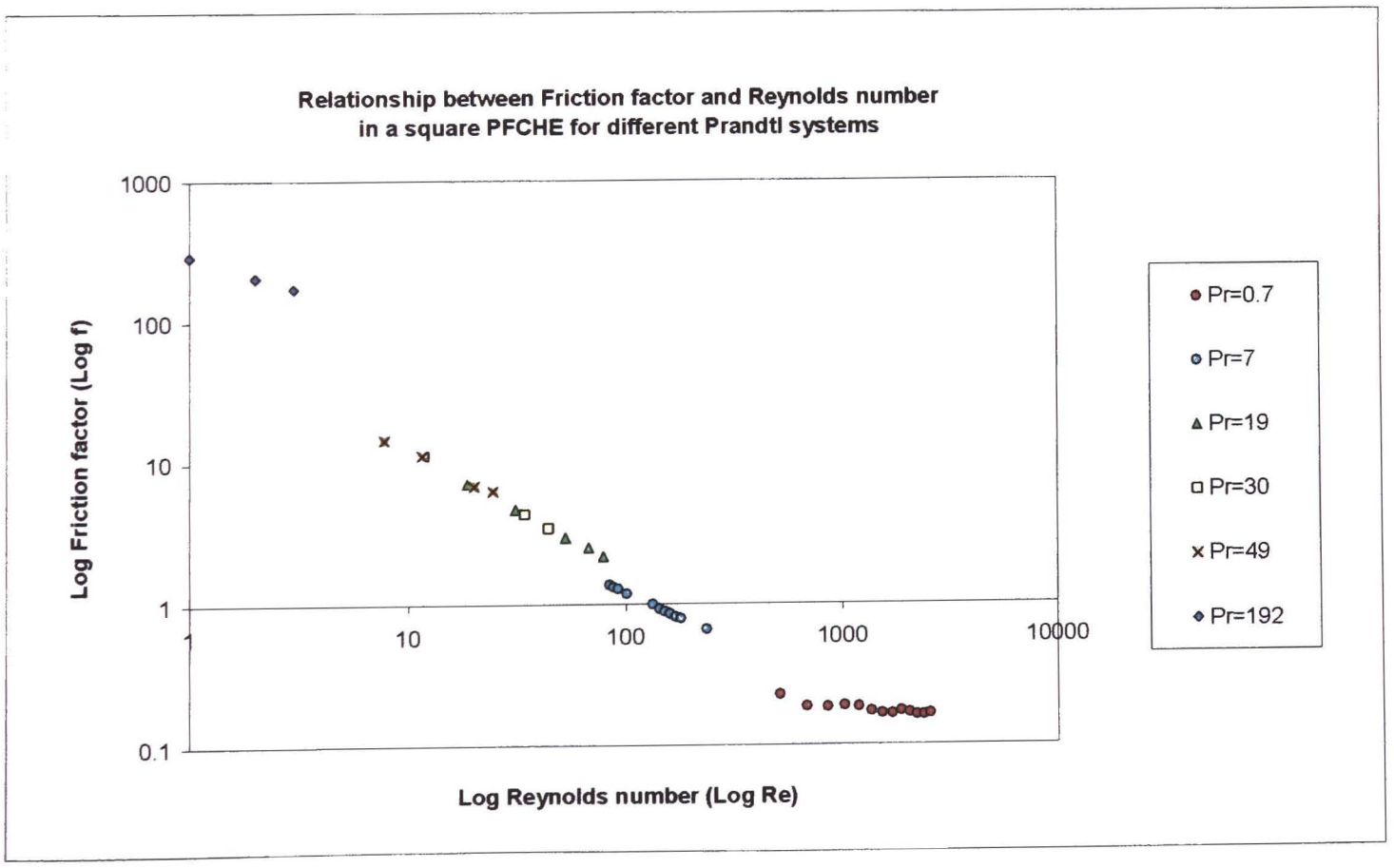


**Figure 8.5 Relationship between friction factor (f) and Reynolds number (Re) for a square PFCHE with different Pr systems ( 0.7<Pr<192 )**

| Pr | f correlation | Re range |
|---|---|---|
| 0.7 | $0.5992\ Re^{-0.1698}$ | 510<Re<2540 |
| 7 | $32.797\ Re^{-0.7192}$ | 87<Re<235 |
| 19 | $83.501\ Re^{-0.8361}$ | 19<Re<78 |
| 30 | $276.79\ Re^{-0.4636}$ | 12<Re<44 |
| 49 | $70.811\ Re^{-0.7701}$ | 8<Re<24 |
| 192 | $412.66\ Re^{-0.5361}$ | 2<Re<5 |

**Table 8.4 Friction factor (f) correlations for different Pr systems in a square PFCHE**

The Pr=192 system has relatively high friction factors compared to the other systems, whilst the Pr=0.7 system has the lowest friction factors. The general trend observed for all systems is that the friction factor decreases with an increase in Re number. At a low Re number (Re=12), two comparable systems are Pr=30 and Pr=49. The Pr=49 system achieves higher friction factors as it is more viscous and therefore experiences a larger pressure drop.

At a higher Re number (Re=80), the Pr=19 system has higher friction factors than the Pr=7 system. This is due to the fact that glycerol-water mixtures are more viscous than water and thus impose more restriction to flow. Having considered the friction factors for all six systems, we now proceed to develop the friction factor correlation of the form, $f = a\ Re^{b}\ Pr^{c}$, using regression analysis. A regression analysis using Microsoft Excel was carried out to study the effect on f when Pr and Re are varied. The PFCHE friction factor correlation developed for the selected range of Pr numbers is as follows:

$$f = 18.91\ Re^{0.67}\ Pr^{-0.36} \qquad (0.7<Pr<192) \qquad (8.9)$$

For the smooth tube, the friction factor is independent of Pr number over the range of 0.7<Pr<125 in the laminar region. The PFCHE comparison with the smooth tube friction factor performance is explained further in Section 8.5.1.3 of this chapter. Having developed the design correlations for the square PFCHE, we now move on to consider the goodness factors for the six Pr systems investigated in the unit.

## 8.3 Effects of Prandtl number on goodness factor

The term 'goodness factor' (Jh/f), is used to highlight the thermal efficiency of a heat exchanger, whereby the higher the value, the better the thermal efficiency. The goodness factor plot is not depicted here as experimental data was not available for high Pr systems due to the limitations in the test rig facility involving high pressure drops. The goodness factor plots for the Pr=0.7 and Pr=7 systems have been shown earlier in Figure 4.11 and Figure 4.18 respectively. Nevertheless, it can be assumed that as the Pr number increases,

the thermal efficiency of the PFCHE decreases. This is expected, because higher Pr numbers signify higher viscosities and as the channel dimensions of the PFCHE remain unchanged (2 mm), the pressure drop plays a dominating role in determining the thermal efficiency. Following this, we next consider the effect of Pr number on pumping power in the square PFCHE. This plot incidentally, is the final performance evaluation plot performed for the six Pr systems in the square PFCHE.

### 8.4 Effect of Prandtl number on pumping power

Apart from the heat transfer, pressure drop and thermal efficiency characteristics studied in previous sections, the pumping power behaviour for the different Pr systems is also investigated. Figure 8.6 below, shows the pumping power characteristics for the six Pr systems in the square PFCHE.

A system that plotted 'high' on this diagram, would be able to transfer a given amount of heat for less friction power and therefore smaller pressure drop, which is the condition sought after in any exchanger unit. The heat transfer coefficients were determined by using the same method as outlined in Chapter Four. However, since the hot and cold fluids are different in the glycerol-water mixtures/water systems compared to the water/water systems, the water heat transfer coefficients need to be determined first. This was done by using the correlation developed for the water/water system, which relates the heat transfer coefficient (h) for a range of Re numbers in the square PFCHE. The h correlation used is as follows:

$$h = 754.35\ Re^{0.3663} \qquad \text{for } 87<Re<235 \qquad (8.10)$$

Once the water heat transfer coefficients are determined, the heat transfer coefficients for the glycerol-water mixtures having Pr=19, 30, 49 and 192, can be determined using the equation below.

$$1/U = 1/h_{water} + 1/h_{gly\text{-}water} + t/k_{film} \qquad (8.11)$$

The pumping power plot for the six Pr systems investigated is shown below.

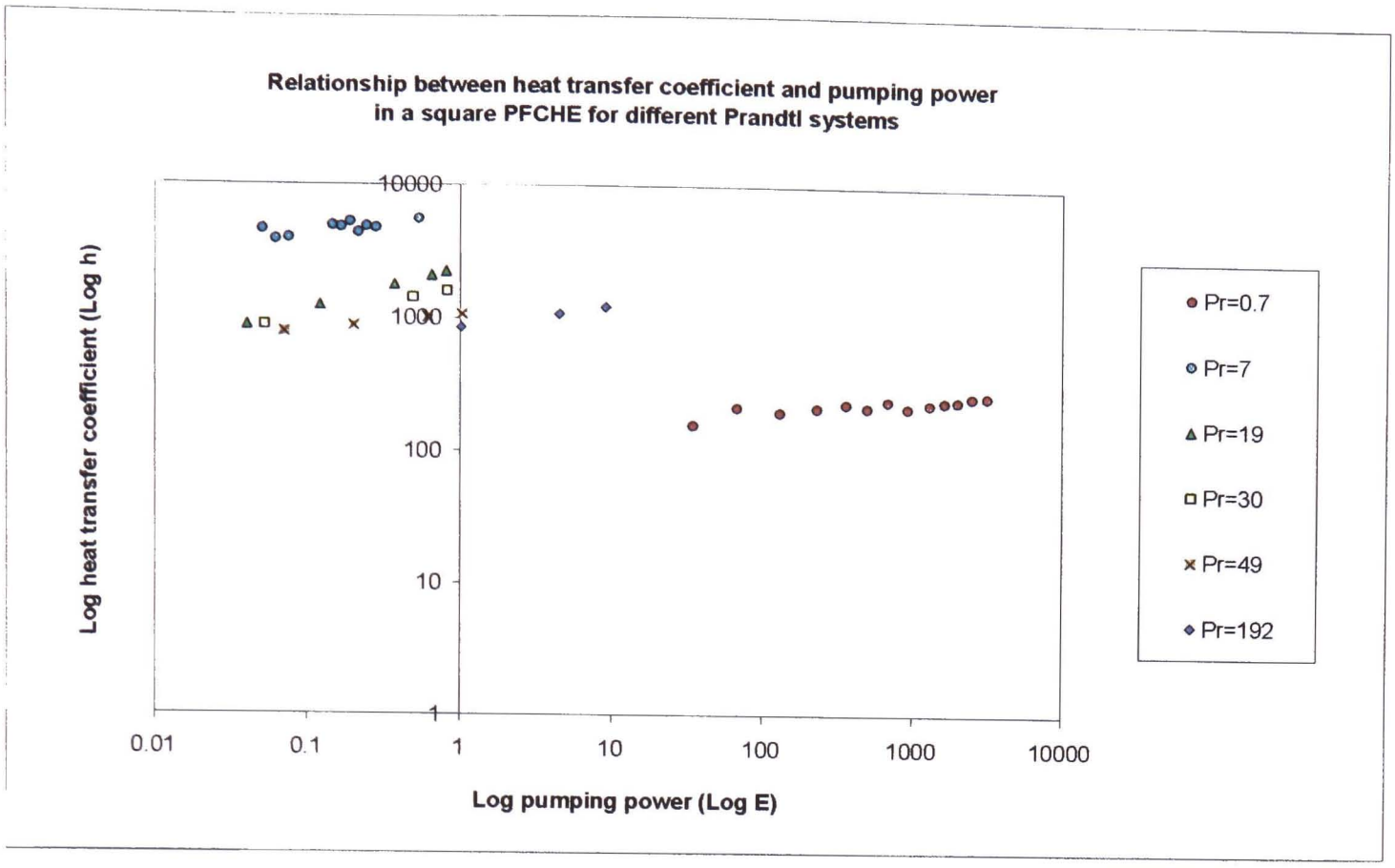


**Figure 8.6 Relationship between heat transfer coefficient (h) and pumping power (E) for a square PFCHE with different Pr systems (0.7<Pr<192)**

It can be seen that for all six systems, the heat transfer coefficient (h) increases along with pumping power (E). The water/water system (Pr=7) gives the highest operating points compared to the four glycerol-water mixtures, at similar pumping power values. This is due to the lower viscosity of the water/water system, which provides less restriction to fluid flow. The air/air system has the lowest operating points due its much lower density value, compared to the other systems. For the glycerol-water mixtures, the Pr=19 system has the highest operating points whilst the Pr=192 system achieves the lowest. This occurrence supports the viscosity reasoning earlier, where fluids having higher viscosity need more pumping power to overcome the resistance to flow. The pumping power correlations developed using Microsoft Excel for each system is tabulated in Table 8.5 below.

| Pr | Pumping power correlation | E range |
|---|---|---|
| 0.7 | $134.5\ E^{0.0840}$ | 34<E<3132 |
| 7 | $5794.8\ E^{0.1152}$ | 0.05<E<0.5 |
| 19 | $2400.7\ E^{0.3148}$ | 0.04<E<0.8 |
| 30 | $1665.3\ E^{0.2197}$ | 0.05<E<0.8 |
| 49 | $1063.4\ E^{0.1194}$ | 0.07<E<1.0 |
| 192 | $843.1\ E^{0.1704}$ | 1.0<E<9.1 |

**Table 8.5 Pumping power correlations for different Pr systems in a square PFCHE**

The pumping power trends observed for the six systems in the square PFCHE, can be further analysed using the smooth tube pumping power relation. All the systems tested abide to the smooth tube pumping power relation, where h is proportional to E. However for the PFCHE, the degree of proportionality differs from system to system as shown in Table 8.5 above. The smooth tube relation will be explained further in Section 8.5.1 of this chapter.

To obtain a better understanding of the PFCHE pumping power behaviour, the fluid properties of each system are investigated. The fluid properties, Perry and Green (1997) at the highest operating points for each system, are tabulated in Table 8.6 below.

| Pr | k (W/mK) | cp (J/kgK) | ρ ($kg/m^3$) | μ ($Ns/m^2$) | h ($W/m^2K$) | E ($W/m^2$) |
|---|---|---|---|---|---|---|
| 0.7 | 0.05 | 1047 | 1.29 | 0.0000315 | 270 | 3132 |
| 7 | 0.603 | 4184 | 1000 | 0.001 | 5561 | 0.53 |
| 19 | 0.487 | 3724 | 1071 | 0.0025 | 1598 | 0.82 |
| 30 | 0.452 | 3561 | 1098 | 0.0038 | 2240 | 0.81 |
| 49 | 0.420 | 3381 | 1125 | 0.0061 | 1065 | 1.03 |
| 192 | 0.358 | 3002 | 1181 | 0.0229 | 1233 | 9.1 |

**Table 8.6 Fluid properties for different Pr systems in a square PFCHE**

From the table above, the fluid properties of the glycerol-water systems can be directly compared to the water/water system using the density (ρ), as a basis of comparison. However, the density of air is much lower than the other fluids, by up to a factor of 1000. The densities of the glycerol-water mixtures (Pr=19, 30, 49 and 192) and water (Pr=7) are almost similar. However, the viscosity (μ) of the mixtures are higher, whilst the thermal conductivity (k) and specific heat capacity (cp) values are lower. It is assumed that a combination of these effects causes the degree of proportionality of h to E, to be different for the systems investigated. To obtain a better illustration of the effect of fluid properties on the pumping power plot for the different Pr systems investigated, the heat transfer coefficients are plotted against the different fluid properties. These plots are shown in Figures 8.7a, b and c and d below.

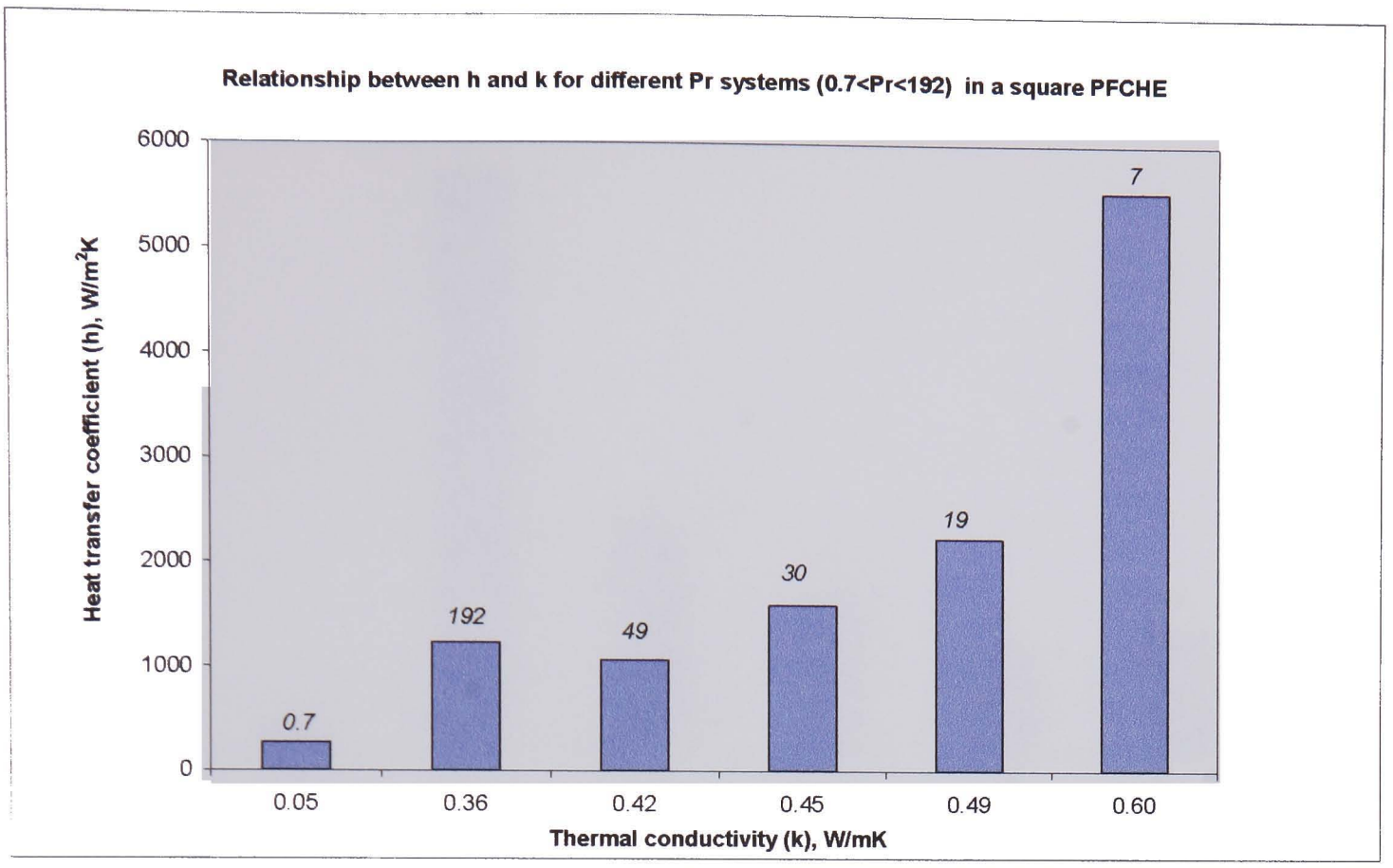


**Figure 8.7a Relationship between heat transfer coefficient (h) and thermal conductivity (k) for different Pr systems in a square PFCHE**

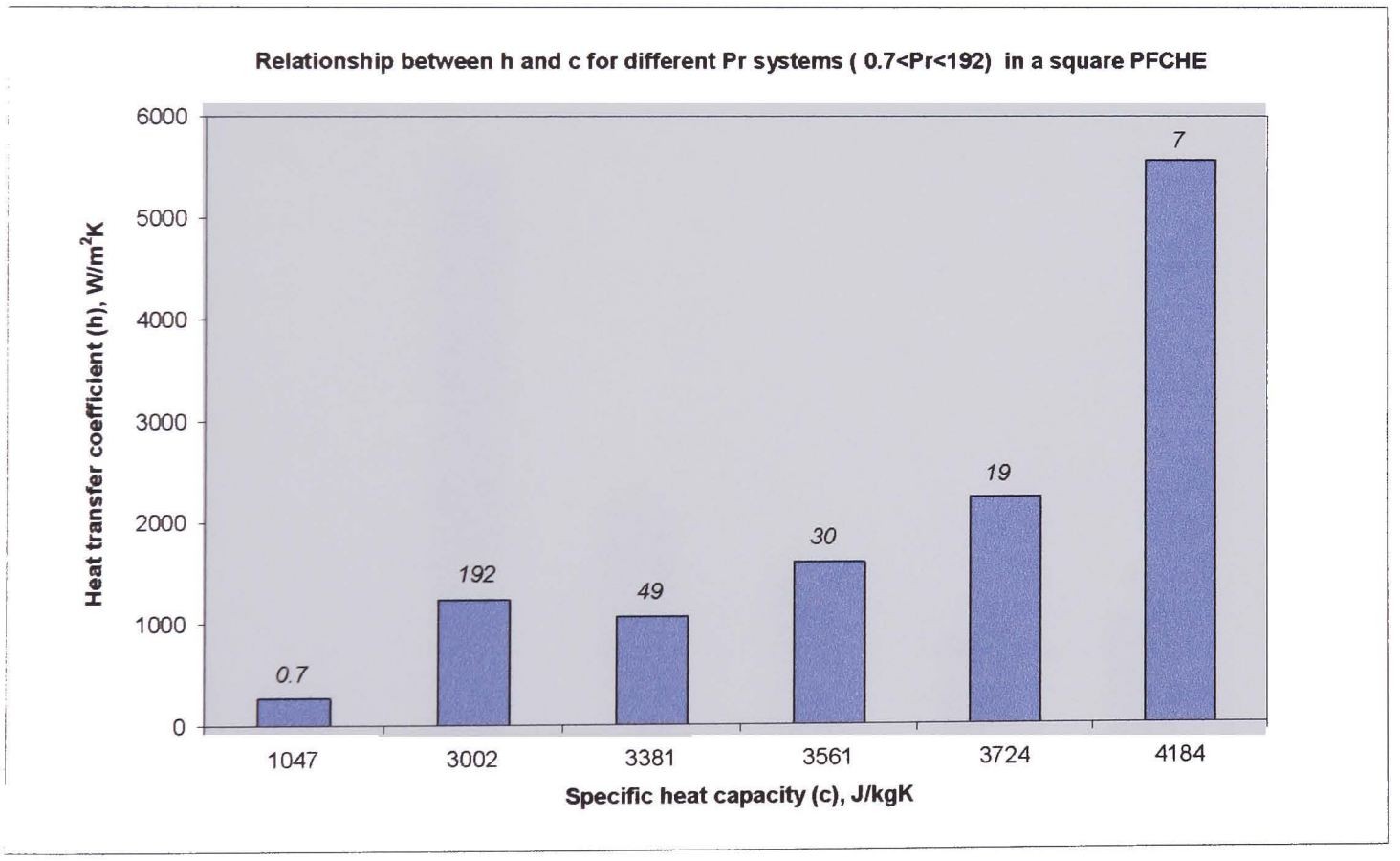


**Figure 8.7b Relationship between heat transfer coefficient (h) and specific heat capacity (cp) for different Pr systems in a square PFCHE**

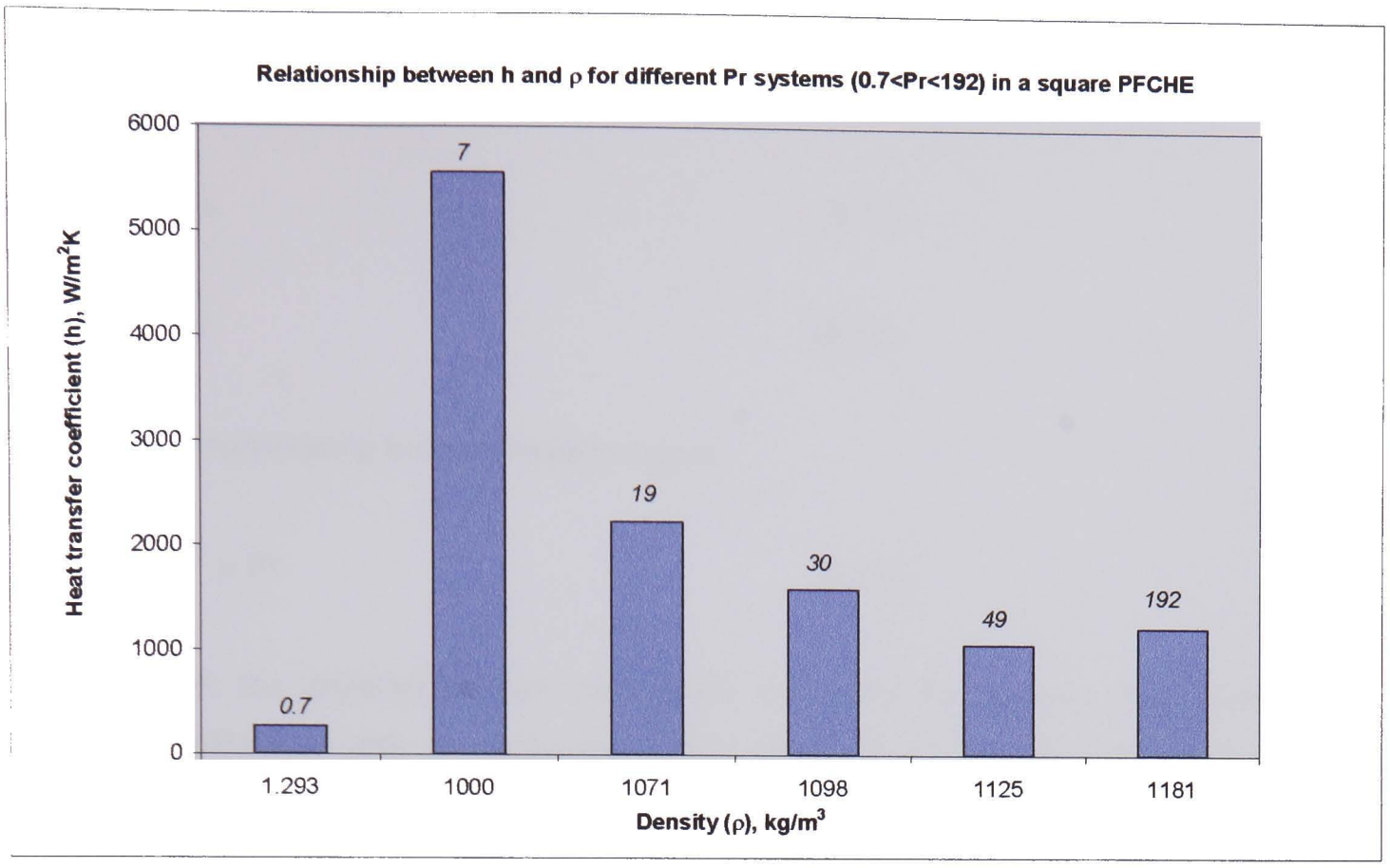


**Figure 8.7c Relationship between heat transfer coefficient (h) and density (ρ) for different Pr systems in a square PFCHE**

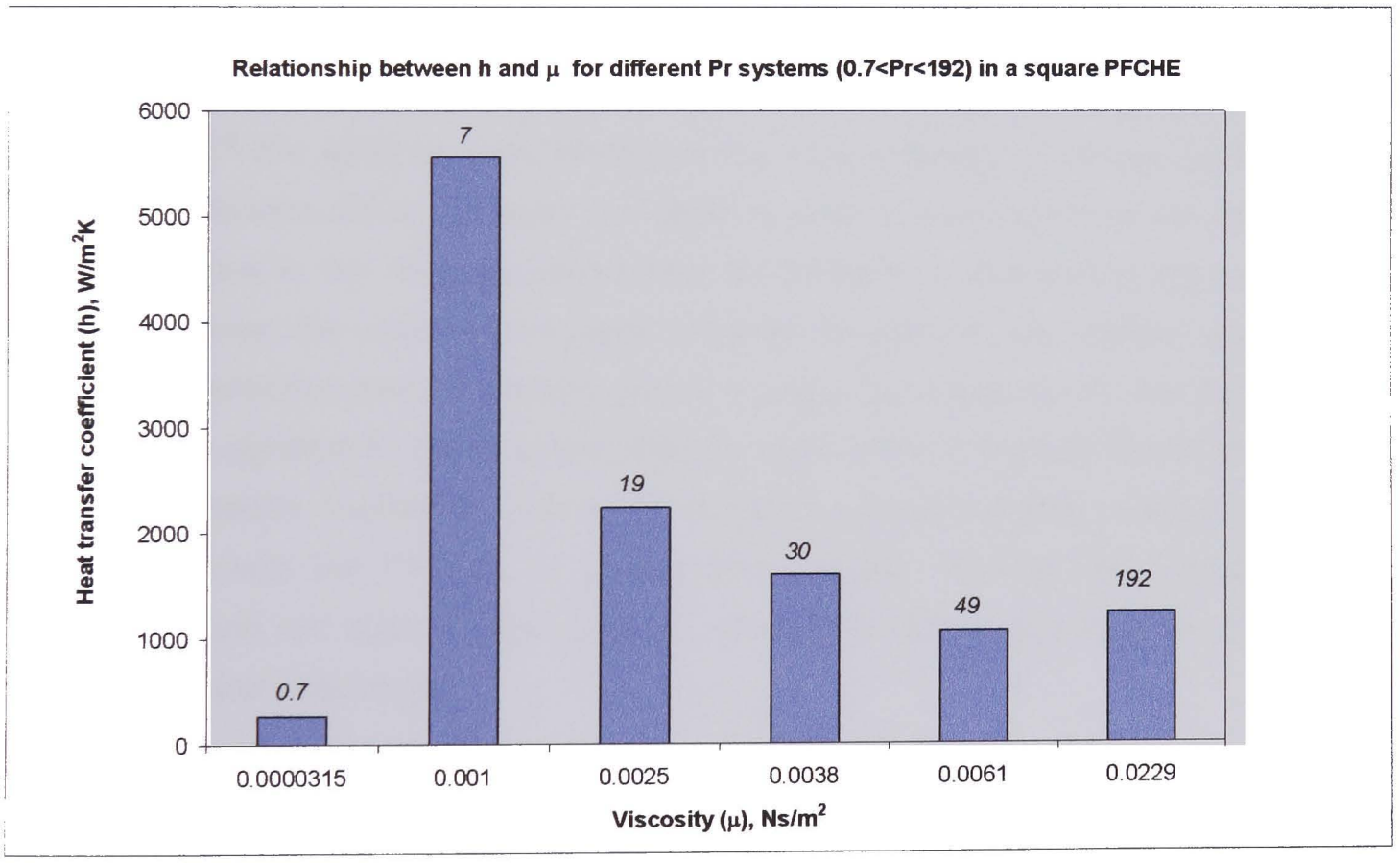


**Figure 8.7d Relationship between heat transfer coefficient (h) and viscosity (μ) for different Pr systems in a square PFCHE**

From the graphs above, the overall relations for both the heat transfer coefficients and Pr systems, with the specified fluid properties in the square PFCHE, are as follows:

$$h \alpha k\, cp\, \rho / \mu \qquad (8.12)$$

$$Pr \alpha cp\, \mu / k \qquad (8.13)$$

Therefore incorporating both expressions give

$$h \alpha k\, cp\, \rho / \mu\, Pr \qquad (8.14)$$

In a nutshell, the physical property plots show that lower Pr systems achieve higher heat transfer coefficients (with an exception to air), due to the higher thermal conductivity and specific heat capacity values of such systems. In addition to this, lower Pr systems also have lower viscosities, which generate less restriction to fluid flow. The results of this investigation involving the physical property values of each Pr system, ties in nicely with the earlier observation in the pumping power plot (Figure 8.6), where the lowest Pr system investigated (excluding air), achieves the highest heat transfer coefficients at similar pumping power requirements.

The Pr systems compared in this study ($0.7<Pr<192$), have densities ranging from 1.3 kg/m$^3$ to 1181 kg/m$^3$.The air/air system, which has the lowest density, achieves the lowest heat transfer coefficients. Since the water and glycerol-water mixtures have similar densities, the wider difference in the viscosity values take precedence in determining the heat transfer achieved. Hence, the water/water system achieves the highest heat transfer coefficients. It should be mentioned that the density carries a higher consequence for the air/air system, since it has a significantly lower density than the other fluids, and therefore achieves a much lower heat transfer coefficient. Due to its low density, more pumping power is required to pump air through the PFCHE, to enable heat transfer. Besides that, its low thermal conductivity and low specific heat capacity values also play a part towards the low heat transfer coefficients achieved.

The pumping power plot supports this reasoning as shown earlier in Figure 8.6, whereby the maximum air heat transfer coefficient of 270 W/m$^2$K (approximately a factor of 10 less than the other fluids), is achieved by using a pumping power value of $\approx$3000 W/m$^2$, which is up to 1000 greater than that used in the other fluid systems. Following the development of the PFCHE design correlations, along with the investigation on goodness factor and pumping power, we now move on to carry out a comparison between the PFCHE results with literature.

## 8.5 Comparison between PFCHE experimental data with literature

In this section, the performance characteristics involving the Pr number for the PFCHE, smooth tube, offset fin heat exchangers and rectangular ducts in the laminar region are compared. These will be discussed in the order below:

(i) Smooth tube
(ii) Offset fin heat exchangers
(iii) Rectangular ducts

A quantitative comparison between the PFCHE and smooth tube is carried out using the Dittus-Boelter correlation, Coulson (1996), laminar design correlations, Obot et al. (1997), as well as the smooth tube pumping power relation, Kays and Crawford (1993). However for the offset fin, Hu and Herold (1995), only a qualitative comparison can be conducted since there are no suitable design correlations available in the literature. Nevertheless, the surface geometry of the offset fin is similar to the sinusoidal corrugations in the PFCHE, where the flow through the channels is repeatedly disturbed. Therefore the observations and reasoning used for the fluid flow behaviour in the offset fin, can be adopted to help explain the PFCHE heat transfer behaviour. In addition, the fluid flow behaviour in a rectangular duct is also investigated for a qualitative comparison with the PFCHE. The aim of conducting a comparison with literature, is to gain a better understanding of the PFCHE heat transfer and pressure drop characteristics involving the Pr number. We begin the next section with the smooth tube comparison.

### *8.5.1 Smooth tube*

The comparison between the performance of the smooth tube and the PFCHE is discussed in this section, covering four sub-sections. The heat transfer characteristics are compared in the Dittus-Boelter and Nu correlations whilst the pressure drop effects are compared in the f correlation and pumping power sub-sections. These will be discussed in the order below.

(i) Dittus-Boelter correlation
(ii) Nu correlation
(iii) f correlation
(iv) Pumping power relation

#### 8.5.1.1 Dittus-Boelter correlation

The Pr exponent in the PFCHE Nu correlation ($Pr^{0.42}$), is similar to the value for turbulent flow heat transfer calculations in a smooth tube. The Pr exponent for the smooth tube is expressed in the Dittus-Boelter correlation, Coulson (1996).The PFCHE and Dittus-Boelter correlations are tabulated in Table 8.7 below.

| Unit | Re range | Pr range | Nu correlation |
|---|---|---|---|
| Smooth tube | >10 000 | 0.7<Pr<160 | (Dittus-Boelter) $0.023\ Re^{0.8}\ Pr^{0.4}$ |
| PFCHE | 2<Re<2540 | 0.7<Pr<192 | $0.356\ Re^{0.51}\ Pr^{0.42}$ |

**Table 8.7 PFCHE and Dittus-Boelter heat transfer correlations**

The Pr exponent for the PFCHE correlation is 0.42, compared to 0.4 for the Dittus-Boelter correlation. This means that although the flow is laminar in the PFCHE, the heat transfer achieved is comparable if not higher, to that of turbulent flow in smooth tubes. This is an encouraging and positive result for the square PFCHE. In order to get a better illustration of the differences between the correlations above, a ($Nu/Pr^{0.4}$ vs. Re) graph is plotted as shown in Figure 8.8 below. The plot clearly shows that the PFCHE achieves superior heat transfer than the smooth tube, irrespective of the Pr system. In fact, it should be noted that if the $Pr^{0.42}$ exponent is used for the PFCHE; instead of the $Pr^{0.4}$ exponent, the heat transfer achieved would be even higher. However, it should be noted that the Dittus-Boelter correlation is valid for Re higher than 10,000 and therefore the representation below is not entirely accurate. Nevertheless, it provides a simple illustrative approach in comparing the PFCHE correlations developed, with the literature available.

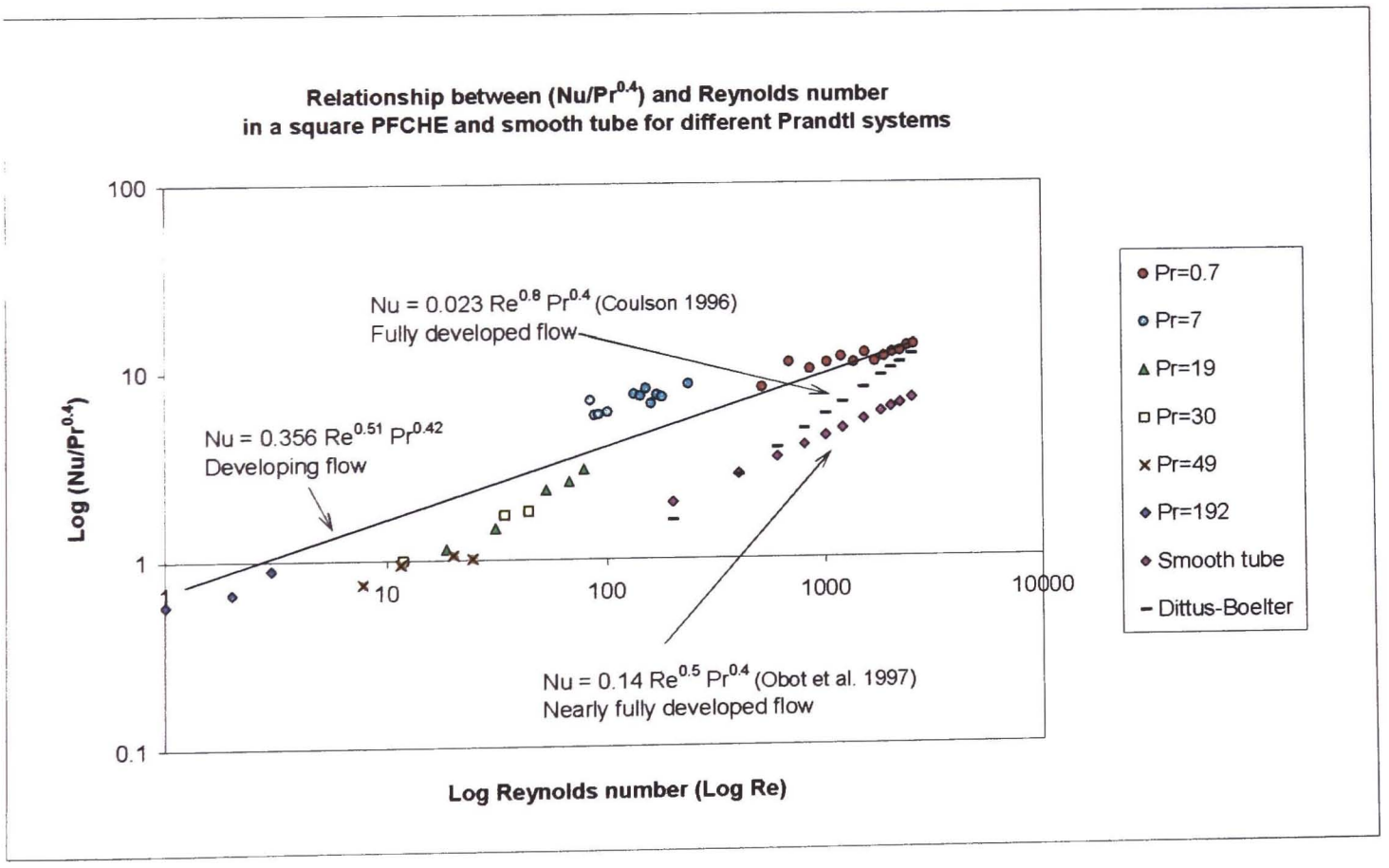


**Figure 8.8 Relationship between $Nu/Pr^{0.4}$ and Reynolds number (Re) for a smooth tube and a square PFCHE with different Pr systems**

In the next section, we move on to investigate the Nu correlation by Obot et al. (1997), to further compare the heat transfer characteristics between the PFCHE and the smooth tube in the laminar region.

8.5.1.2 Nu correlation

In the previous section, a comparison was made between the heat transfer achieved in the laminar region for the PFCHE with the turbulent region in a smooth tube, using the Dittus-Boelter correlation. This was performed to show the advantage of laminar flow heat transfer in the PFCHE, over turbulent flow in a smooth tube. In this section, a heat transfer comparison in the laminar region for both units is conducted using the Nu correlation by Obot et al. (1997). The heat transfer correlations for the smooth tube and the PFCHE in the laminar region, is as follows:

| Unit | Re range | Pr range | Nu correlation |
|---|---|---|---|
| Smooth tube | 200<Re<2500 | 0.7<Pr<125 | $0.14\ Re^{0.5}\ Pr^{0.4}$ |
| PFCHE | 2<Re<2540 | 0.7<Pr<192 | $0.356\ Re^{0.51}\ Pr^{0.42}$ |

**Table 8.8 PFCHE and smooth tube heat transfer correlations**

The 0.4 Pr exponent for the smooth tube, is slightly lower than the value of 0.42 for the square PFCHE. The 0.4 exponent also corresponds to the Dittus-Boelter correlation as shown in Table 8.7 previously. This shows that the heat transfer achieved by the PFCHE, is better than the smooth tube in either turbulent or laminar regions (see Figure 8.8).

To further illustrate the heat transfer enhancement achieved when adopting developing flow in the PFCHE, we consider a sample case at Re=300 and Pr=0.7. Using the Nu correlations in Table 8.7 and Table 8.8 earlier, we find that the PFCHE attained a Nu value of 5.6 compared to 2.1 and 1.9 respectively, for the nearly fully developed (Obot 1997) and fully developed flows (Coulson 1996) in the smooth tubes. This observation supports the heat transfer benefits of adopting developing flow. For a more accurate comparison, a PFCHE correlation covering a wider range of Re in the laminar region; over all the Pr systems investigated, needs to be developed. In the next section, we go on to consider the friction factor characteristics for the smooth tube and the square PFCHE.

8.5.1.3 f correlation

For the smooth tube, the friction factor is independent of Pr number in the laminar region. The friction factor correlations for the smooth tube and the PFCHE, is as follows:

| Unit | Re range | Pr range | f correlation |
|---|---|---|---|
| Smooth tube | Re<2500 | 0.7<Pr<125 | $16\ Re^{-1}$ |
| PFCHE | 2<Re<2540 | 0.7<Pr<192 | $18.91\ Re^{-0.67}\ Pr^{-0.36}$ |

**Table 8.9 PFCHE and smooth tube friction factor correlations**

For a better illustration of the friction factors for both units, a plot showing the friction factor curves for all the Pr systems in the PFCHE, and the (f=16/Re) curve for the smooth tube is generated. This is illustrated in Figure 8.9 below. It can be seen that the friction factors for the PFCHE are higher than the smooth tube, especially at higher Pr systems. This is expected as higher Pr systems involve higher viscosity values. However, it should be noted that the Pr=7 system approaches he smooth tube as the Re increases and for the Pr=0.7 system the friction factors level out. Perhaps from this observation, it can be inferred that even for higher Pr systems, the friction factors will eventually level out as the Re increases. Further tests at higher Re for the glycerol mixture systems, need to be carried out to confirm this deduction. Friction factor comparisons with other compact geometries have been presented in Chapter Seven and Chapter Nine (see Figure 7.12 and Figure 9.3 respectively).

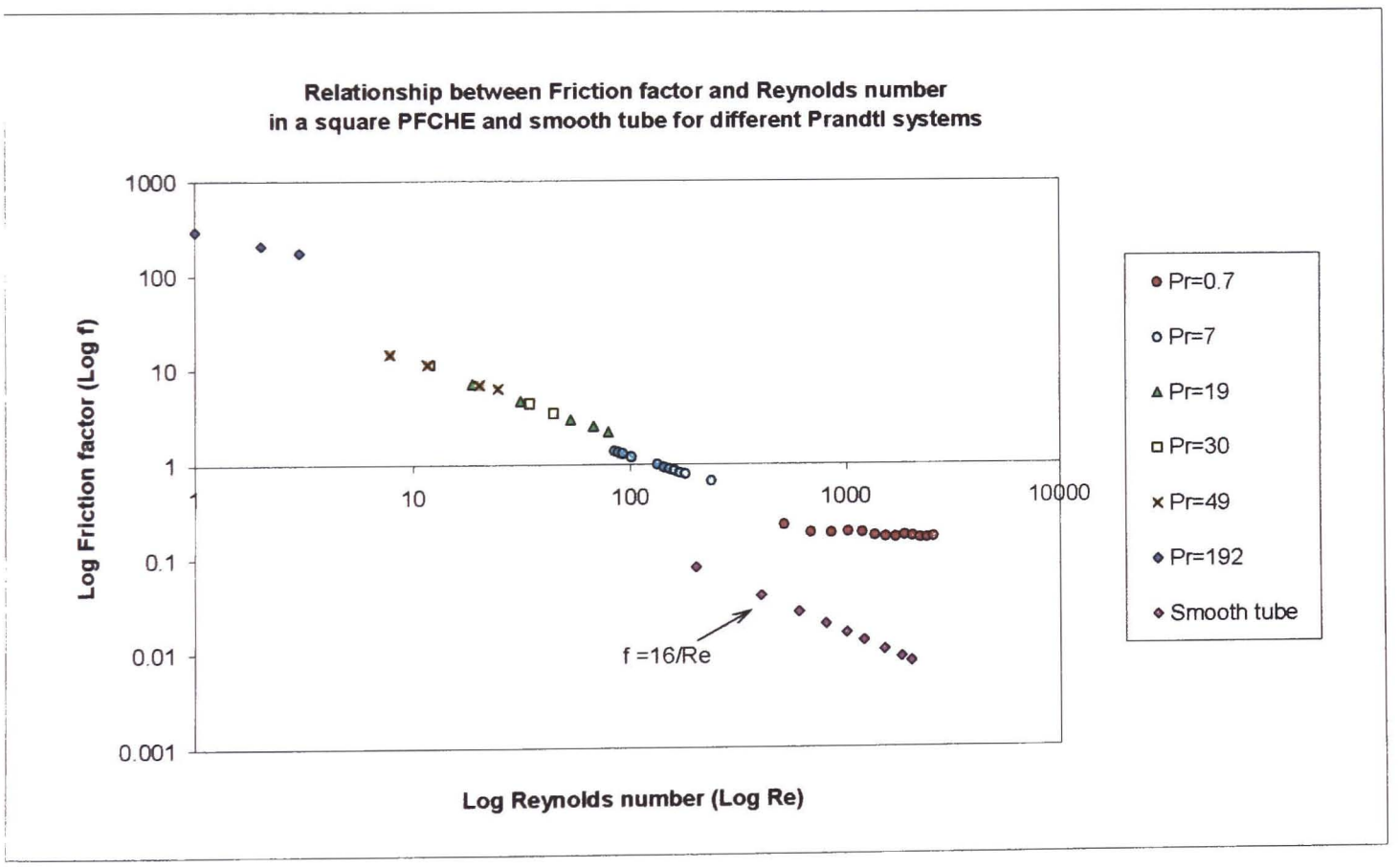


**Figure 8.9 Relationship between friction factor (f) and Reynolds number (Re) for a smooth tube and a square PFCHE with different Pr systems (0.7<Pr<192)**

In the following section, we proceed to investigate the pumping power characteristics between the PFCHE and the smooth tube, to further understand the performance differences between the two units.

8.5.1.4 Pumping power relation

The trends of the PFCHE pumping power plot can be explained using equation (8.19) below. This equation considers a fully developed turbulent flow in a long smooth-walled tube of any cross sectional shape (circular, rectangular etc.), Kays and Crawford (1993). Prior to this, the relationship between the pumping power and the heat transfer coefficient for a long smooth tube, is derived from the following expressions (8.15) to (8.18).

$$h = \frac{\mu\ cp}{\mathrm{Pr}^{2/3}} \frac{1}{4r_h} \mathrm{Re}\ Jh \qquad (8.15)$$

$$E = \frac{1}{2} \frac{\mu^3}{\rho^2} \left( \frac{1}{4r_h} \right)^3 \mathrm{Re}^3\ f \qquad (8.16)$$

Expressions (8.15) and (8.16) provide a rational basis for comparing the performance of one surface configuration against another.

$$Jh = 0.023\ \mathrm{Re}^{-0.2} \qquad (8.17)$$

$$f = 0.046\ \mathrm{Re}^{-0.2} \qquad (8.18)$$

Expressions (8.17) and (8.18) are reasonable approximations for Jh and f over a range of Pr numbers from the gases to the very viscous liquids (virtually all fluids except the liquid metals). We substitute expressions (8.17) and (8.18) into expressions (8.15) and (8.16) and combine them to get the smooth tube pumping power relation as follows:

$$E = \frac{12465\ h^{3.5}\ \mu^{1.83}\ (4r_h)^{0.5}}{k^{2.33}\ cp^{1.77}\ \rho^2} \qquad (8.19)$$

Therefore from equation (8.21) the following smooth tube relation can be deduced.

$$h\ \alpha\ \frac{k\ cp\ \rho\ E}{\mu} \qquad (8.20)$$

The smooth tube pumping power relation demonstrates that mechanical energy must be expanded in order to transfer heat, and that this expenditure is a very strong function of the heat transfer rate. It also shows that the amount of mechanical energy expanded, is heavily dependent upon the fluid properties. In the case of the PFCHE, the 4rh term in equation

(8.19) is equivalent to 2 mm for all the Pr systems. The development of the PFCHE pumping power relation is explained in Section 8.4 earlier. Both the smooth tube and the PFCHE have the same relationship between the heat transfer coefficient and the fluid properties, as shown below.

$$\text{PFCHE: } h \alpha k\, cp\, \rho\, E/\mu \qquad \text{Smooth tube: } h \alpha k\, cp\, \rho\, E/\mu \qquad (8.21)$$

Following this, we proceed to consider the PFCHE comparison with the offset fin heat exchanger.

*8.5.2 Offset fin heat exchanger*

After considering the smooth tube, we will now briefly look at the performance comparison between the PFCHE and the offset fin heat exchanger. A quantitative comparison between the two is not possible, due to the unavailability of suitable offset fin correlations in the laminar region from literature. Nevertheless, the explanations for the fluid flow behaviour in the offset fin can be used for the PFCHE, as the sinusoidal corrugations and the offset fin surface geometry are similar, where both promote developing flow. The Nu number increases with Pr number for (3<Pr<150), in the laminar region for the offset fin, Hu and Herold (1995). From the Colburn definition, whereby $Jh= Nu/(Re\ Pr^{0.33})$, Jh increases as Pr decreases, if the Nu is independent of Pr. For the offset fin, the Nu increases with Pr, but at a rate less than $Pr^{0.33}$. Therefore, the Colburn definition still holds.

The effects on heat transfer in the offset fin can be divided into two categories: fin and array. The fin effect shows the dependence of developing Nu number on Pr number, whilst the array effect shows the dependence on thermal entry length. Due to the periodic interruptions on the fins, the heat transfer is influenced by both the Re and Pr numbers. High Re and Pr numbers are desirable for the fin perspective. Longer thermal developing regions on each fin exist at high Pr, which achieves a higher average heat transfer over the fin. A larger Re, extends the Nu region on each fin by reducing the boundary layer thickness, causing a higher developing Nu number. Both of these effects translate to better heat transfer performance. For the array perspective, high Re and Pr numbers give longer thermal entry lengths, which correspond to higher Nu numbers. Hence, with longer thermal entry lengths better heat transfer is achieved.

This reasoning lends support to the PFCHE results obtained, where the Pr=192 system achieves the highest heat transfer over the other six systems. Nevertheless, this occurs at a very low Re number (2<Re<5), and cannot be compared with any other system for the same Re range. Therefore this reasoning cannot be taken entirely, but is interesting to note. For fluids with large Pr numbers, the velocity boundary layer is much thicker, and so the

hydraulic length is much shorter than the corresponding thermal characteristics (i.e. the thermal boundary layer is much thinner, which leads to a longer thermal entry length). It is well known that for a high Pr fluid, the thermal boundary layer develops much slower than the hydrodynamic boundary layer, because the thermal diffusivity is relatively low compared to the momentum diffusivity. All of these observations, contribute towards explaining why higher Pr systems obtain higher heat transfer in the offset fin heat exchanger; subject to having high Re numbers as well.

As with the smooth tube, the friction factor is independent of Pr number for the offset fin in the laminar region. Due to the lack of friction factor correlations, a direct comparison with the PFCHE is not possible. The observations and explanations for the offset fin, can be used in helping to explain some of the trends in the PFCHE graphs; particularly the exceptional case at low Re in the Jh plot (Figure 8.3), where high heat transfer is achieved for the Pr=192 system. In the next section, we go on to investigate yet another comparison involving the Pr number, which is between the PFCHE and the rectangular duct.

*8.5.3 Rectangular duct*

In a continuous rectangular duct, the Nu number is independent of the Pr number, as the flow is fully developed. Normally, when a fluid flows into a continuous duct, there is a developing region near the entrance of the duct, where a higher heat transfer coefficient is attained than that of the fully developed flow, Hu and Herold (1995). Such a developing region is what we refer to as the developing flow in the PFCHE, which accounts for its high heat transfer capability. The energy transfers in the entrance region of the duct are similar to the boundary layer development on a plate. The transition to a fully developed condition occurs after the boundary layers forming on the walls meet in the centre of the duct and the velocity and temperature profiles become invariant in the flow direction. A fully developed velocity profile, transfers less heat from a duct wall due to the convective influence of the velocity profile, on the temperature profile. A fully developed temperature profile, transfers less heat from a duct wall because the gradient of the temperature at the wall is reduced, due to the adiabatic centreline boundary condition.

Nevertheless, the Pr number has a strong influence on developing heat transfer in a rectangular duct at the entrance. Fluids with a large Pr number have longer thermal development sections and therefore better heat transfer. At the same Re, the flow with higher Pr, has a larger Nu in the entrance region and therefore better heat transfer. This again provides an explanation to the isolated case in the Jh plot at low Re (Figure 8.3), where the Pr=192 system in the PFCHE, has the highest heat transfer. However, in the thermally fully developed section for laminar flow in a rectangular duct, the Pr number has no

effect on the heat transfer. Therefore, the PFCHE fluid flow behaviour is only similar to the rectangular duct fluid flow characteristics, at the entrance of the duct.

Having considered the PFCHE experimental results and the performance comparisons with data from literature involving the Pr number, we now move on to provide further explanations and reasoning for the observations noted in both sections.

## 8.6 Discussion

The discussion section of this chapter is divided into two parts as shown below, whereby both incorporate the PFCHE experimental results and the comparison with literature.

(i) Analysis of the heat transfer characteristics
(ii) Analysis of the pressure drop characteristics

In the following section, we begin with an analysis on the heat transfer results for the different Pr systems in the PFCHE, along with the comparison conducted with literature.

### *8.6.1 Analysis of heat transfer characteristics*

In this section, three sub-sections are included to cover the heat transfer analysis on the effect of Pr number in the square PFCHE. These sub-sections will be discussed in the following order:

(i) Developing heat transfer
(ii) Colburn factor (Jh)
(iii) Goodness factor (Jh/f)

#### 8.6.1.1 Developing heat transfer

The design concept of the sinusoidal corrugations in the PFCHE, is to ensure that each corrugation has a uniform temperature and velocity field, so that the heat transfer characteristics approximate those of that at the entrance region of a duct. However in practice, the crests and troughs of each corrugation are closely spaced. Therefore although the boundary layers that form on each corrugation are still present, these layers are altered by diffusion and convection effects, when the next corrugation is encountered. Nevertheless, it is this non-uniformity, also known as the massaging effect, which leads to the heat enhancement of the unit. Due to the interruptions to the thermal boundary layer development by the sinusoidal corrugations, the developing heat transfer is higher than that of the fully developed flow obtained in a comparable rectangular duct.

The Pr number shows an influence on developing heat transfer in a PFCHE, whereby in general, lower Pr systems achieve higher heat transfer which abides to the Colburn definition. Nevertheless, the highest heat transfer values are achieved by the Pr=192 system at low Re. Perhaps this isolated occurrence could mean; as with the offset fin, that the thermal development length is longer for higher Pr systems and therefore there is more developing flow. However for the offset fin, this is only true at higher Re. Hence, further tests at higher Re for the Pr=192 system, are needed to confirm this deduction.

Different from rectangular ducts or smooth tubes, the PFCHE is influenced by both Re and Pr numbers for developing laminar flow heat transfer. This can be seen from the Nu heat transfer correlation developed in Section 8.1.2. The Nu numbers for both the rectangular ducts and smooth tubes are influenced by the Re numbers as the flow is fully developed. However, the offset fin follows the PFCHE behaviour, whereby both the Re and Pr numbers affect the developing heat transfer.

### 8.6.1.2 Colburn factor (Jh)

The heat transfer behaviour for a PFCHE can best be described using the Colburn factor plot. From the Colburn definition ($Jh= Nu/(Re\ Pr^{0.33})$), Jh increases as Pr decreases if the Nu is independent of Pr. However for the square PFCHE application, it was found that the Nu number is not entirely independent of Pr number, but increases on an average rate of $Pr^{0.42}$. This is shown in the PFCHE heat transfer correlation developed in Section 8.1.2.Therefore the Colburn definition, is not strictly speaking fully applicable in the PFCHE. This needs to be further investigated by performing more tests in the PFCHE, covering a wider range of Pr systems.

Nevertheless from the Jh plot, it can be seen that the Colburn definition still holds true for the most part, where higher Jh values are achieved by lower Pr systems such as water (Pr=7), compared to the glycerol-water mixtures (Pr=19 and 30). It should be noted however, that a direct comparison between all the systems, cannot be made as the Re ranges do not coincide. Further tests need to be conducted to extend the Re range applicable to all systems investigated, for a more valid comparison. It is observed that the Pr=192 system, achieves the highest Jh values from the Jh plot, contrary to the Colburn definition. Apart from the offset fin behaviour, this occurrence can also be explained using the analogy with the flow through a rectangular duct. As mentioned before, the flow in a higher Pr system has a larger Nu number in the entrance region, due to a longer thermal entry length which enhances heat transfer.

A larger Pr number implies a longer distance to achieve a fully developed thermal field. Longer developing heat transfer means higher heat transfer coefficients, which leads to an increase in Jh. Therefore, this theory supports the finding where the Pr=192 system has the highest heat transfer at low Re (Re=2). At higher Re numbers such as Re=80, the PFCHE results do not support the thermal entry length effects, as the Pr=7 system achieves better heat transfer than the Pr=19 system. Instead this observation abides to the Colburn definition. If using the thermal entry length effects, the Pr=7 system should give a lower Jh value, due to a shorter thermal developing region. However this does not happen. Therefore, it can be initially inferred that the Colburn definition holds true for the PFCHE at higher Re numbers, with the lower Pr systems achieving higher heat transfer. On the other hand, the thermal entry length effects are significant at lower Re numbers, where the higher Pr systems achieve better heat transfer. It should be noted that the Pr=192 system cannot be compared with any other system at such low Re numbers (Re=2), due to the lack of experimental data. In accordance to this, further tests need to be conducted at higher Re numbers (Re>100) for the Pr=192 system and the other glycerol-water mixtures, in order to make a direct performance comparison over the same Re range. This will lead to a better understanding of the Pr effects, on the PFCHE heat transfer performance.

#### 8.6.1.3 Goodness factor (Jh/f)

The thermal efficiency decreases with an increase in Pr number due to the higher viscosities involved, which subsequently leads to higher pressure losses. The issue can be addressed by using polymer films with increased corrugation height (2-5 mm) as opposed to the current height of 1 mm. A larger corrugation height will give a higher hydraulic diameter ($d_h$) and therefore a lower pressure loss. This can be shown by rearranging the friction factor equation to give the formula, ($\Delta P = 4\ \rho\ v^2 L / 2d_h$).

The water/water system achieves higher goodness factors than the glycerol-water mixtures/water systems. The higher thermal efficiency achieved, may be due to the fact that water has a higher thermal conductivity and lower viscosity than the glycerol mixtures. This contributes towards its higher heat transfer capabilities at the expense of lower pressure drops. The water/water system also has higher goodness factors than the air/air system, although the Re ranges are not the same. The reason that gases yield lower heat transfer coefficients is related to the mechanical power necessary to pump a gas through a heat exchanger. The energy required is influenced by its lower thermal conductivity and density compared to liquids. In gas flow, the pressure drop calculations are just as important as the heat transfer calculations. In fact if care is not taken, it is very easy to expend in mechanical power, as much as is gained by the heat transfer function of the heat exchanger. The situation is different for liquids, where the pressure drop is seldom of controlling influence in

the design. In this sense, the design of gas flow heat exchangers is a more complex problem than that of liquid flow heat exchangers.

Next, we move on to consider the analysis of the pressure drop characteristics for the square PFCHE using the different fluid systems, and also the relevant comparisons with literature.

*8.6.2 Analysis of pressure drop characteristics*

The analysis of the effect of Pr number on the PFCHE pressure drop characteristics can be explained using the friction factor and the pumping power results. These will be discussed in the order shown below.

(i) Friction factor (f)
(ii) Pumping power (E)

8.6.2.1 Friction factor (f)

Unlike the smooth tube and offset fin, the friction factor in the PFCHE is not independent of the Pr number in the laminar region. The friction factor decreases at higher Re and increases with Pr, which is expected as higher Pr systems are more viscous, and hence provide more restriction to flow. This can be seen from the friction factor plot (Figure 8.5) and the PFCHE friction factor correlation developed in Section 8.2.1 earlier.

8.6.2.2 Pumping power (E)

The PFCHE pumping power plot shows that the air/air, water/water and glycerol-water mixtures/water systems, obey the smooth tube relation, where the heat transfer coefficient is proportional to the pumping power expended. Lower Pr systems (with an exception to air), achieve higher heat transfer coefficients. This is due to the higher thermal conductivity and lower viscosity values of such systems; the latter causing less resistance to flow. The air/air system achieves the lowest heat transfer coefficients due to its lower density and thermal conductivity values, causing a high pumping power requirement to enable heat transfer. The trends of the fluid properties (k, cp, $\rho$, $\mu$) involved in the pumping power relation for the six Pr systems are also investigated. The behaviour of the fluid properties for both the PFCHE and smooth tube relations, are similar. The relations obtained are shown below and have been previously explained, in Sections 8.4 and 8.5.1.4 respectively.

PFCHE: $h \alpha k\, cp\, \rho\, E / \mu$ Smooth tube: $h \alpha k\, cp\, \rho\, E / \mu$

## 8.7 Conclusion

The PFCHE heat transfer and friction factor characteristics, are dependent on the Re and Pr numbers in laminar flow over the range of 0.7<Pr<192. The general trend observed is that the heat transfer decreases, whilst the friction factor increases with an increase in Pr number. For the heat transfer, the lower Pr systems achieve better heat transfer, which abides to the Colburn definition. Lower Pr systems achieve higher heat transfer coefficients due to the higher thermal conductivity and specific heat capacity of such systems. In addition to this, lower Pr systems also have lower viscosities that generate less restriction to fluid flow. Both the thermal efficiency and pumping power capability decrease at higher Pr numbers. Nevertheless, only two to three Pr systems can be compared at any chosen point on the performance plots, as the Re range is not the same for all the systems investigated. This reduces the accuracy of the observations noted, and therefore further tests need to be conducted to obtain a similar Re range, for all the fluid systems investigated.

For the PFCHE, the Nu number is proportional to $Pr^{0.42}$ in the development of the laminar heat transfer correlation. The 0.42 exponential value is similar to the well-known Dittus-Boelter correlation, Coulson (1996), for turbulent flow in smooth tubes and the Nu correlation, Obot et al. (1997), for laminar flows. This shows that the PFCHE laminar flow heat transfer is comparable to that of smooth tubes in either turbulent or laminar regions. The friction factor correlation is proportional to $Pr^{-0.36}$, when developing the expression using regression analysis. The design correlations developed from this study are shown in Table 8.10 below.

To obtain more accurate and useful PFCHE design correlations, further studies are needed to fill in the gap between the Pr=49 and Pr=192 systems, and also extend the range at lower and higher Pr systems. Furthermore, when using regression analysis in Microsoft Excel, the design correlations (Nu and f) achieved $R^2$ values of 0.6 and 0.9 respectively. The $R^2$ value (coefficient of determination) is an indicator from 0 to 1 that reveals how closely the estimated values for the correlation correspond to the actual data. A correlation is most reliable when its $R^2$ value is close to 1. Therefore, more experimental data is needed to obtain a better PFCHE model and hence achieve design correlations having $R^2$ values closer to 1.

The correlations developed in this study along with those obtained from literature are shown in the table below.

| Unit | Fluids | Re range | Pr range | Nu correlation |
|---|---|---|---|---|
| Smooth tube | air<br>water<br>ethylene glycol<br>ethylene glycol/water | 600<Re<2500<br>600<Re<2500<br>200<Re<2500<br>200<Re<2500 | 0.7<Pr<126 | $0.14\ Re^{0.5}\ Pr^{0.4}$ |
| Smooth tube (Dittus-Boelter) | air<br>water<br>acetone<br>kerosene<br>benzene | >10 000 | 0.7< Pr<160 | $0.023\ Re^{0.8}\ Pr^{0.4}$ |
| Offset fin | water<br>polyalphaolefin | 10<Re<2000 | 3<Pr< 150 | (not available) |
| PFCHE | air<br>water<br>glycerol-water mixtures/water | 510<Re<2540<br>87<Re<235<br>2<Re<78 | 0.7<Pr<192 | $0.356\ Re^{0.51}\ Pr^{0.42}$ |
| Unit | Fluids | Re range | Pr range | f correlation |
| Smooth tube | air<br>water<br>ethylene glycol<br>ethylene glycol/water | 600<Re<2500<br>600<Re<2500<br>200<Re<2500<br>200<Re<2500 | 0.7<Pr<126 | $16\ Re^{-1}$ |
| PFCHE | air<br>water<br>glycerol-water mixtures/water | 510<Re<2540<br>87<Re<235<br>2<Re<78 | 0.7<Pr<192 | $18.91\ Re^{-0.67}\ Pr^{-0.36}$ |

**Table 8.10 PFCHE and literature heat transfer and friction factor correlations**

## 8.8 Summary

In this chapter, the effects of using different fluid systems in the square PFCHE are investigated using the Pr number. The experimental results for the individual systems obtained from Chapter Four, are grouped together and the performance characteristics (Jh, Nu, f, Jh/f and E) are studied collectively in this chapter. A regression analysis using Microsoft Excel is performed on the Nu and f plots to develop unique design correlations, incorporating both the Re and Pr numbers for the square PFCHE.

Apart from the smooth tube, PFCHE comparisons are also conducted with the offset fin heat exchangers and rectangular ducts, to gain a better understanding of the effect of Pr number on the overall performance in the square PFCHE. It is shown, that the PFCHE laminar heat transfer achieved for all the Pr systems investigated, is superior to the smooth tube in either laminar or turbulent conditions. The fluid flow behaviour involving the Pr number for the offset fin exchanger and the rectangular duct, lend support to the benefits of developing laminar flow in the PFCHE, which enhances heat transfer.

In the next chapter, a PFCHE surface geometry comparison with literature; involving six plate fin geometries is conducted. This is followed by a performance investigation on the effect of using a different polymer; PVDF instead of PEEK, as a material of construction for the unit.

# CHAPTER 9 - PFCHE COMPARISON STUDIES: SURFACE GEOMETRY AND MATERIAL OF CONSTRUCTION

## 9.0 Introduction

In the last two chapters, the effects of using different corrugation angles and also Pr numbers on the square PFCHE performance have been investigated. Chapter Seven showed that the 90° corrugation angle is the optimum angle in the square PFCHE, and results from Chapter Eight proved that the overall performance for the unit is better at lower Pr systems. In addition, the design correlations for the unit as a function of both the Re and Pr numbers, have also been developed. As a follow up to these investigations, we now consider the effect of surface geometry and the material of construction on the performance of the square PFCHE. In this chapter, we conduct a performance comparison between the sinusoidal corrugations of the PFCHE, with various plate fin geometries, before moving on to investigate the effect of using another polymer for the unit, as opposed to PEEK (poly ether ether ketone).

Basically, this chapter is divided into two parts. In the first section, the performance of the sinusoidal corrugations is compared to that of six plate fin surface geometries, in air/air systems. We conduct the performance comparison by using four performance evaluation plots (Jh, f, Jh/f and E). The aim of this surface geometry study is to achieve a better understanding of the sinusoidal corrugations; investigating its advantages over the plate fin geometries and its impact towards the overall performance of the square PFCHE. The second part of this chapter deals with the use of PVDF (polyvinylidene fluoride), as a material of construction for the PFCHE. All the previous chapters in this thesis have involved units made from PEEK, since its high chemical, thermal and mechanical stability has made it the primary choice for the manufacture of the square PFCHE. Nevertheless, other polymers need to be considered as an alternative to PEEK in the square PFCHE.

In accordance to this, PVDF performance evaluation plots in an air/air system are compared against PEEK to highlight the strengths of each polymer. The findings from this comparison could aid in potential applications where PEEK is unsuitable, for example, in environments involving concentrated sulphuric and nitric acids. In the following section, we will look at the surface geometry comparison study between the sinusoidal corrugations of the PFCHE and the plate fin surface geometries. We begin with a brief introduction describing the basis of the comparison, before proceeding with the details of the sinusoidal corrugations and the plate fin surface geometries.

## 9.1 Surface geometry comparison: sinusoidal corrugations (PFCHE) and Plate Fin

The plate fin heat exchanger (PF) is selected for this comparison as it has several different geometries to consider, thus enabling a wider comparison to be made with the PFCHE. Furthermore, the plate fin surface geometries, Kays and London (1984) have similar hydraulic diameters to that of the PFCHE, at approximately 2 mm. It is this similarity that forms the basis for the surface geometry comparison study. In total, six plate fin surface geometries are compared with the sinusoidal corrugations of the PFCHE. They are the plain, wavy, strip, louvered, pin and perforated fins respectively.

Although all the geometries have similar hydraulic diameters, the definition of the length parameters (L) used in the heat transfer and pressure drop calculations, differ for both units. The PFCHE interprets (L) as the total length of the exchanger, that is the total summation of all the sinusoidal corrugation lengths along one side of the exchanger. This is the length over which the experimental temperature and pressure drop measurements are taken. On the other hand, the plate fin heat exchangers define (L) as the uninterrupted flow length, which is essentially the length of one fin, wavelength or spacing depending on the surface geometry. In other words, the Jh and f factors presented in the literature for the plate fin are calculated based on the uninterrupted flow length whereas for the PFCHE, the total length of the exchanger is used.

Even so, the basis of using the hydraulic diameter is still acceptable. This is because the heat transfer and free flow area involved in the determination of the hydraulic diameter for both units, accounts for the different length definitions adopted. In the PFCHE, both heat transfer and free flow areas are calculated over the exchanger length whereas in the plate fin, the areas are calculated over a single fin length. This implies that the use of the length definitions is consistent in determining the hydraulic diameter for both units. The equation for the hydraulic diameter used for both units, is shown below.

$$d_h = ( 4 A_{ff} L)/A \qquad (9.1)$$

The hydraulic diameters calculated for the seven geometries investigated, are shown in the table below.

| Surface geometry | Hydraulic diameter ($d_h$),mm |
|---|---|
| PFCHE | 2.00 |
| Plain Fin | 1.72 |
| Wavy Fin | 2.12 |
| Strip Fin | 2.07 |
| Louvered Fin | 3.08 |
| Perforated Fin | 2.50 |
| Pin Fin | 1.64 |

**Table 9.1 Hydraulic diameters for PFCHE and Plate Fin surface geometries**

Having understood the basis of the comparison study, we now move on to consider the details of the sinusoidal corrugations and the six plate fin surface geometries.

*9.1.1 Sinusoidal corrugations of the PFCHE*

The PFCHE has continuous sinusoidal corrugations on the polymer film, extending from edge to edge. The highest point of each corrugation is called the crest and the lowest point is known as the trough. The wavelength or channel length (L), of each corrugation is defined as the distance between two subsequent crests or two subsequent troughs. The amplitude or height of the channel (h), is the distance between the crests and troughs. This is clearly illustrated in the surface diagram below.

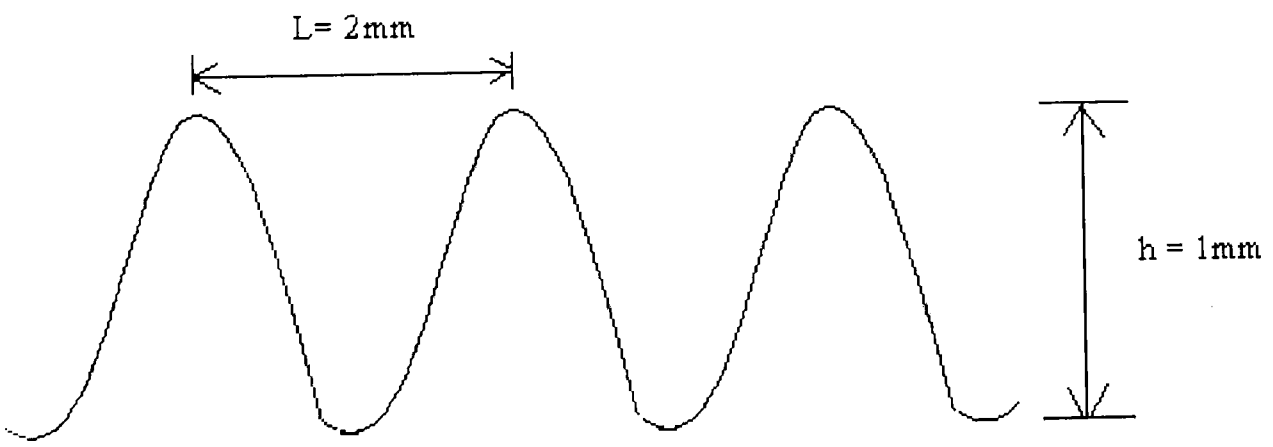


**Figure 9.1 PFCHE sinusoidal corrugation surface diagram**

The length to diameter ratio ($L/d_h$) for the PFCHE is 1 mm. This low value shows that the fluid flow is interrupted frequently, as it moves through the crests and troughs of the corrugations. The fluid experiences 'developing flow' which gives rise to enhanced heat transfer as the boundary layers, which forms the barrier to heat transfer are broken down repeatedly. This 'massaging effect' of the flow encourages mixing which leads to improved heat transfer.

9.1.1.1 Details of the PFCHE sinusoidal corrugation

| | |
|---|---|
| Corrugation angle | = 90° |
| Flow passage hydraulic diameter, $d_h$ | = 2 mm |
| Channel width, $L_w$ | = 2 mm |
| Flow length of sheet, $L_s$ | = 135 mm |
| ($L_w$ /dh) | = 1 |
| Film thickness, t | = 0.1 mm |
| Channel height, h | = 1 mm |

In the following section, we will look at the details of the plate fin surface geometries.

*9.1.2 Surface geometries of the Plate Fin heat exchanger*

In compact gas-to-gas heat exchangers, large area density is desirable on both fluid sides, and a method for accomplishing this objective with fins, is achieved by the plate fin arrangement. The plate fin heat exchanger is built up as a sandwich of flat plates bonded to inter-connecting fins. The two fluids are carried between alternate pairs of plates and can be arranged in either counter flow or cross flow, which provides an added degree of flexibility in this arrangement.

The plate fin surfaces that will be discussed in this chapter are the plain, wavy, louvered, strip, pin and perforated fin types respectively. The length (L), used in the performance calculations as mentioned before, is not necessarily the flow length of the total heat exchanger, but is rather the flow length of uninterrupted fin; the actual heat exchanger flow length may involve several flow lengths of fin material placed end to end. Unless absolute perfect alignment is obtained, the surface will behave as if there were a new hydrodynamic and thermal entry length. In commercial heat exchangers, no attempt is usually made to obtain perfect alignment. A brief description of the six plate fin surface geometries discussed in this chapter is outlined below. Further details, along with the surface diagrams of the geometries are attached in Appendix H.

9.1.2.1 Plain Fin

In general, the plain fin surfaces include rectangular passages, triangular passages and passages with rounded and re-entry corners. The semi-descriptive method of designating plain fin surfaces refers to the number of fins per inch transverse to the flow direction. Thus surface 16.96, has 668 fins per metre. The 16.96T plain fin surface type has been chosen for this study. The additional letter T, indicates that the surfaces have definite triangular passages. This surface is selected due to its hydraulic diameter, which is similar to the

PFCHE and also because it is assumed that triangular passages give the closest match to the sinusoidal corrugations.

9.1.2.2. Wavy Fin

The wavy fin surfaces are also high-performance surfaces. These surfaces are designated by two figures, giving the number of fins per inch and the wavelength, followed by the letter W. Thus the chosen wavy fin surface for this study (17.8-3/8W), has 701 fins per metre and a complete wave every 0.01 m. This surface is selected as its hydraulic diameter is the most comparable to the PFCHE. The wavy fin surfaces are quite similar to the louvered and strip fin surfaces, both of which will be explained later. In this wavy fin geometry, the change in the flow direction induced by the fins, causes boundary layer separation with effects that are similar to complete fin interruption.

9.1.2.3 Louvered Fin

The louvered fin surfaces are characterised by fins that have been cut and bent out into the flow stream at frequent intervals. The purpose of louvering is to break up the boundary layer, so as to yield higher heat transfer coefficients than are possible with plain fins, under the same flow conditions. As a general rule, the more frequent the interruption, the higher the conductance, although the friction factor is also increased. The louvered fin surface is grouped using the louver spacing followed by the fin pitch parameter. For the purpose of this study, the chosen louvered fin based on a similar hydraulic diameter to the PFCHE, is the designated type 3/16-11.1. It has a louver spacing of 0.005 m and accommodates 437 fins per metre.

9.1.2.4 Strip Fin

The strip fin surfaces are similar in principle to the louvered fin surfaces, the only difference being that the short sections of the fins are aligned entirely with the flow direction. With the strip fin configuration, it is feasible to have very short flow lengths and thus very high heat transfer coefficients. Nevertheless, the experimental uncertainty for the strip fin surfaces is probably somewhat greater than for any of the other surfaces, because of its friction performance that is primarily affected by the thickness and character of the fin leading edge. Fins of this type are generally constructed by a machine-cutting process that inevitably leaves a slightly bent and scarfed fin edge, which differs depending upon the fin material and the character of the cutting tool. The designation scheme for the strip fin surfaces is essentially the same as that used for the louvered surfaces. Based on a similar hydraulic diameter to the PFCHE, the 1/7-15.75(D) strip fin type is chosen for this study.

9.1.2.5 Pin Fin

Pin fin surfaces are another example of the plate fin system, where the purpose is to achieve very high heat transfer coefficients by maintaining thin boundary layers on the fins. By constructing the fins from small diameter wire, the effective flow length of the fins can be very small indeed. The pin fin surfaces are, however, characterised by quite high friction factors; attributable primarily to form drag associated with the boundary layer separation that occurs on the pins. Nevertheless, the very high heat transfer coefficients attainable, often more than offsets the high friction factors when the final heat exchanger design is considered. The designation scheme for the pin fin surface chosen, PF-3, is not descriptive.

9.1.2.6 Perforated Fin

The perforated fin surface is designated simply by the number of fins per inch, transverse to the flow and the letter P. The perforated fin surface chosen is the type 13.95(P). Holes cut out of the fins again provide boundary layer interruption. The friction factors for this surface are quite low, suggesting that there is very little form drag induced. Unfortunately, there is insufficient data on this kind of surface to draw much in the way of general conclusions.

Having understood the basis of the comparison study, along with the respective geometry details, we now proceed to consider the results of the study between the sinusoidal corrugations of the PFCHE and the plate fin surface geometries. The results will be depicted in four performance evaluation plots (Jh, f, Jh/f and E) to incorporate the heat transfer, pressure drop and the overall performance of the surface geometries investigated. In the next section, we will first look at the heat transfer characteristics before moving on to the pressure drop and overall performance results.

*9.1.3 Effect of surface geometry on heat transfer*

The heat transfer behaviour of the surface geometries is depicted on a Colburn factor (Jh) plot and the observations are discussed below. This study is conducted to aid in the understanding of the effect of sinusoidal corrugations on the PFCHE heat transfer.

9.1.3.1 Investigation on the Colburn factor (Jh)

From Figure 9.2, the PFCHE gives very encouraging heat transfer results compared to the plate fin surface geometries. It can be seen that at low Re (Re<500), the highest Jh are achieved by the PFCHE, with close competition given by the strip, louvered and wavy fins. However at higher Re, the PFCHE is overtaken by these fin geometries.

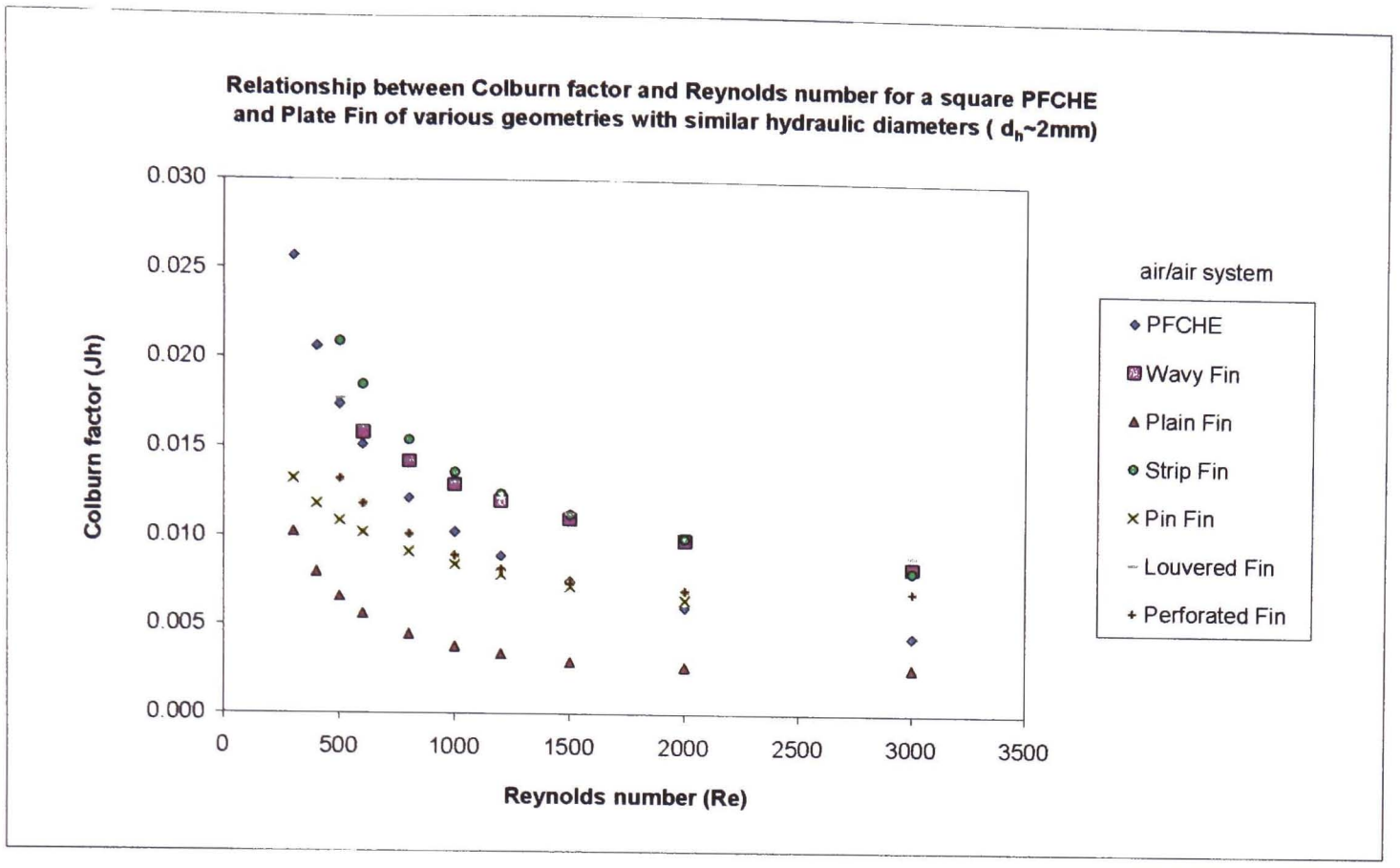


**Figure 9.2 Relationship between Colburn factor (Jh) and Reynolds number (Re) for a square PFCHE and Plate Fin of various geometries**

Between 500<Re<1500, the strip fin provides the highest heat transfer, followed by the wavy and louvered fins respectively. Above Re=1500, the heat transfer capabilities of the strip, louvered and wavy fins are similar. The pin and perforated fin geometries have intermediate heat transfer capabilities over the entire Re range (200<Re<3000) investigated, whilst the plain fin provides the lowest heat transfer.

At low Re, the sinusoidal corrugations on the PEEK polymer film achieve better heat transfer than the aluminium fin surface geometries. This shows that the developing heat transfer that exists in the sinusoidal corrugations are much more significant at lower Re. The high heat transfer achieved by the PFCHE is due to the developing flow, caused by the breakdown of the boundary layers as the fluid moves through the crests and troughs of the sinusoidal corrugations. Destruction and restarting of the boundary layer causes an increase in heat transfer by producing a boundary layer that is thinner on average than the uninterrupted boundary layer. The mixing benefits associated with this self-sustained unsteadiness, contributes towards its heat transfer augmentation.

However at higher Re, the PFCHE heat transfer loses out to the strip, louvered and wavy fin geometries as the flow becomes more fully developed. For instance, the heat transfer decreases gradually as the Re increases between 500<Re<3000. Over this range, the difference in the heat transferred between the PFCHE and the fin geometries increases gradually up to a point, where the heat transfer rate for the strip, louvered and wavy fins, are almost double than that of the PFCHE. Perhaps, this could be due to the change in the flow

direction that is induced by the fins, at higher Re. This change causes boundary layer separation with effects similar to complete fin interruption, which gives the fin geometries an extra edge towards achieving better heat transfer than the PFCHE.

The factor of difference between the PFCHE Colburn factor and the other geometries at Re=1000 are shown below.

| Ratio of PFCHE Colburn factor to Plate Fin at Re=1000 | Ratio Value | Sequence from geometry with highest Jh | L (mm) | $d_h$ (mm) | $L/d_h$ |
|---|---|---|---|---|---|
| Jh PFCHE / Jh strip fin | 0.75 | strip | 3.6 | 2.07 | 1.75 |
| Jh PFCHE / Jh wavy fin | 0.78 | wavy | 9.0 | 2.12 | 4.24 |
| Jh PFCHE / Jh louvered fin | 0.78 | louvered | 4.8 | 3.08 | 1.55 |
| Jh PFCHE / Jh PFCHE | 1.00 | PFCHE | 135.0 | 2.00 | 67.50 |
| Jh PFCHE / Jh perforated fin | 1.15 | perforated | 2.0 | 2.50 | 0.80 |
| Jh PFCHE / Jh pin fin | 1.21 | pin | 1.5 | 1.64 | 0.93 |
| Jh PFCHE / Jh plain fin | 2.68 | plain | 127.0 | 1.72 | 73.84 |

**Table 9.2 Table showing the interpretation of the Colburn factor plot for different surface geometries**

From Table 9.2 above, it can be seen that the PFCHE has superior heat transfer than the plain fin by up to a factor of 3. This can be due to the smaller $L/d_h$ value of the PFCHE, although as mentioned earlier, the length definition differs for both units. The length adopted for the PFCHE is the exchanger flow length, whereas the plate fin uses the uninterrupted flow length. For argument sake, it should be noted that if the uninterrupted flow length for the PFCHE were adopted, the $L/d_h$ value would be even smaller, leading to perhaps even better heat transfer. This is because the length involved will be much shorter at L=2 mm, as opposed to L=135 mm. Hence, the L/dh value will be much smaller at $L/d_h$=1, which is 74 times less than the plain fin. Currently from Table 9.2 above, the difference is only a factor of 1.1. The PFCHE flow length (using either definition) is shorter than the plain fin. The flow

length is frequently interrupted which leads to the onset of developing flow, where the boundary layers are broken and hence the heat transfer is enhanced. On the other hand, the plain fin which has a higher $L/d_h$ value, experiences more fully developed heat transfer, which is less effective than developing heat transfer in generating high heat transfer coefficients.

From the Jh plot, it can be seen that the strip fin gives the best heat transfer performance of all the surface geometries investigated. From Table 9.2, the $L/d_h$ value is approximately 38 times lower than the PFCHE, which suggests that due to the shorter flow length of the strip fin, the boundary layers of the flow are broken down more frequently leading to better heat transfer. Compared to the PFCHE, its heat transfer is higher by a factor of 1.3. This means that the developing flow in the strip fin, is more prominent compared to the PFCHE, which explains its higher heat transfer capability. However, as mentioned before, this happens when both units adopt different length definitions. If the L=2mm were adopted for the PFCHE, it will cause the $L/d_h$ value for the strip fin to be higher. This suggests that if the temperature measurements were made over one sinusoidal corrugation instead of an entire row, the PFCHE would probably give the best heat transfer performance, as it will have the lowest $L/d_h$ value ($L/d_h$=1) compared to the other surface geometries.

The plain fin achieves the lowest heat transfer as the fluid flow does not experience sufficient interruption. The surface is characterised by long uninterrupted flow passages, with performance similar to that obtained inside long circular tubes. Hence, the boundary layers are intact, and this creates an obstruction to rapid heat transfer. Moreover, the plain fin does not have extra features on its fins such as waves or louvers that act as turbulence promoters, to help break up the boundary layers of the flow and enhance mixing.

The pin and perforated fins have similar heat transfer capabilities to the PFCHE, especially at higher Re. There is only a slight advantage in using the PFCHE over these two surfaces. This implies that the geometry of the units provide a similar degree of heat enhancement by ensuring boundary layer interruption of the flow. The pin and perforated surfaces outperform the plain fin but they still lose out to the other fin geometries, as well as the PFCHE.

### *9.1.4 Effect of surface geometry on pressure drop*

Having considered the heat transfer characteristics of the surface geometries, we now move on to consider the pressure drop characteristics by using the friction factor plot.

### 9.1.4.1 Investigation on the friction factor (f)

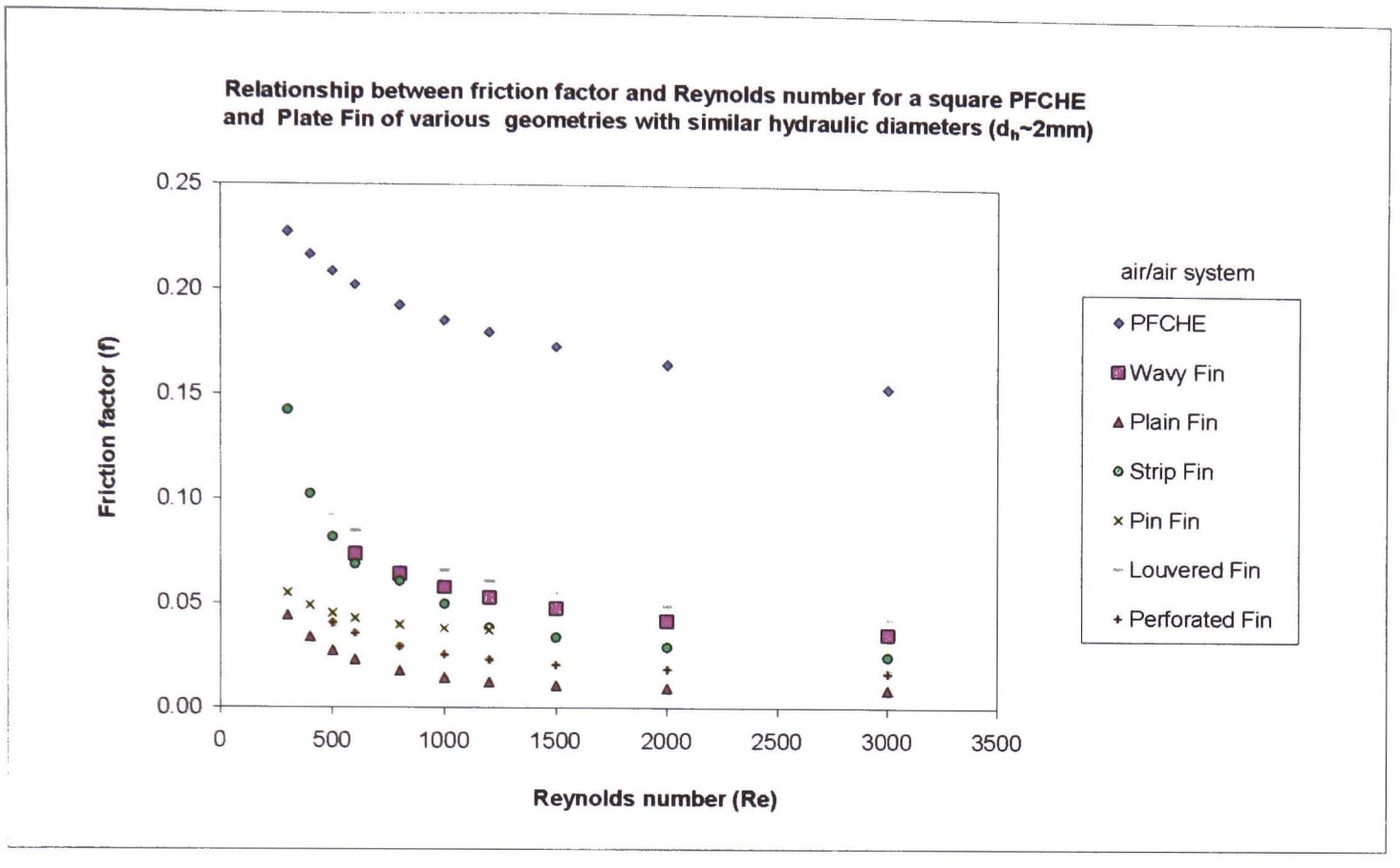


**Figure 9.3 Relationship between friction factor (f) and Reynolds number (Re) for a square PFCHE and Plate Fin of various geometries**

As expected, the PFCHE has the highest friction factor of all the surface geometries investigated. This is due to its length definition, which accounts for the entire length of the exchanger, instead of the uninterrupted flow length used for the plate fin geometries. The pressure drop for the PFCHE is measured over a length of 135 mm instead of 2 mm, which leads to high pressure drop readings. Consequently, this leads to higher friction factors.

Following the PFCHE; the louvered, wavy and strip fins have the next highest friction factors. As with the Colburn factor plot, the pin and perforated fin geometries have intermediate friction factors over the entire Re range investigated, whilst the plain fin achieves the lowest friction factors. The details of the graph interpretation are shown in the table below.

| Ratio of PFCHE friction factor to plate fin at Re=1000 | Ratio Value | Sequence of geometry from highest f | L (mm) | $d_h$ (mm) | $L/d_h$ | Pressure drop (kPa) |
|---|---|---|---|---|---|---|
| f PFCHE / f PFCHE | 1.00 | PFCHE | 135.0 | 2.00 | 67.50 | 0.21-14.50 |
| f PFCHE / f louvered fin | 2.80 | louvered | 4.8 | 3.08 | 1.55 | 0.003-0.04 |
| f PFCHE / f wavy fin | 3.20 | wavy | 9.0 | 2.12 | 4.25 | 0.016-0.19 |
| f PFCHE / f strip fin | 3.71 | strip | 3.6 | 2.07 | 1.75 | 0.003-0.06 |
| f PFCHE / f pin fin | 4.84 | pin | 1.5 | 1.64 | 0.93 | 0.001-0.01 |
| f PFCHE / f perforated fin | 7.21 | perforated | 2.0 | 2.50 | 0.80 | 0.001-0.01 |
| f PFCHE / f plain fin | 12.87 | plain | 127.0 | 1.72 | 73.80 | 0.06-1.22 |

**Table 9.3 Table showing the interpretation of the friction factor plot for different surface geometries**

From Table 9.3, it can be seen that the length of the extended fin geometries are much shorter in comparison to the PFCHE, which generates a lower pressure drop and hence a lower friction factor.

The plain fin has the lowest friction factors among all the geometries investigated, even though it experiences higher pressure drops; with exception to the PFCHE. The reason for this occurrence could be due to the fact that it has a longer flow length, and a lower hydraulic diameter compared to the other extended fin surfaces. Therefore, its $L/d_h$ values are much higher than the other fin surfaces, which give rise to lower friction factors. This is because the friction factor is inversely proportional to the $L/d_h$ term. This is shown in the friction factor equation, where $f = (2 \Delta P d_h / 4 \rho v^2 L)$. Looking closely at the plain fin and the PFCHE, it can be seen that their $L/d_h$ values are similar. Nevertheless, there is a significant difference in the pressure drops measured. This is again due to the different length definitions adopted in both units. The pressure drops noted for the PFCHE would be lot less, if measurements were taken across just one corrugation, instead of the exchanger flow length.

From Table 9.3, it is shown that the pressure drops for the PFCHE are higher than the plain plate fin by approximately a factor of 10. This difference corresponds to the f ratio value of 12.87, whereby the PFCHE has the higher friction factor.

Having seen the effects of heat transfer and pressure drop separately, we now consider both factors collectively by investigating the pumping power and goodness factor characteristics in the PFCHE and plate fin geometries. We begin with the pumping power, followed by the goodness factor.

### *9.1.5 Effect of surface geometry on overall thermal and hydraulic performance*

In this section, we consider the overall performance comparison between the PFCHE and the plate fin geometries by using two plots; pumping power and goodness factor. We begin the following section with the pumping power plot.

#### 9.1.5.1 Investigation on pumping power (E)

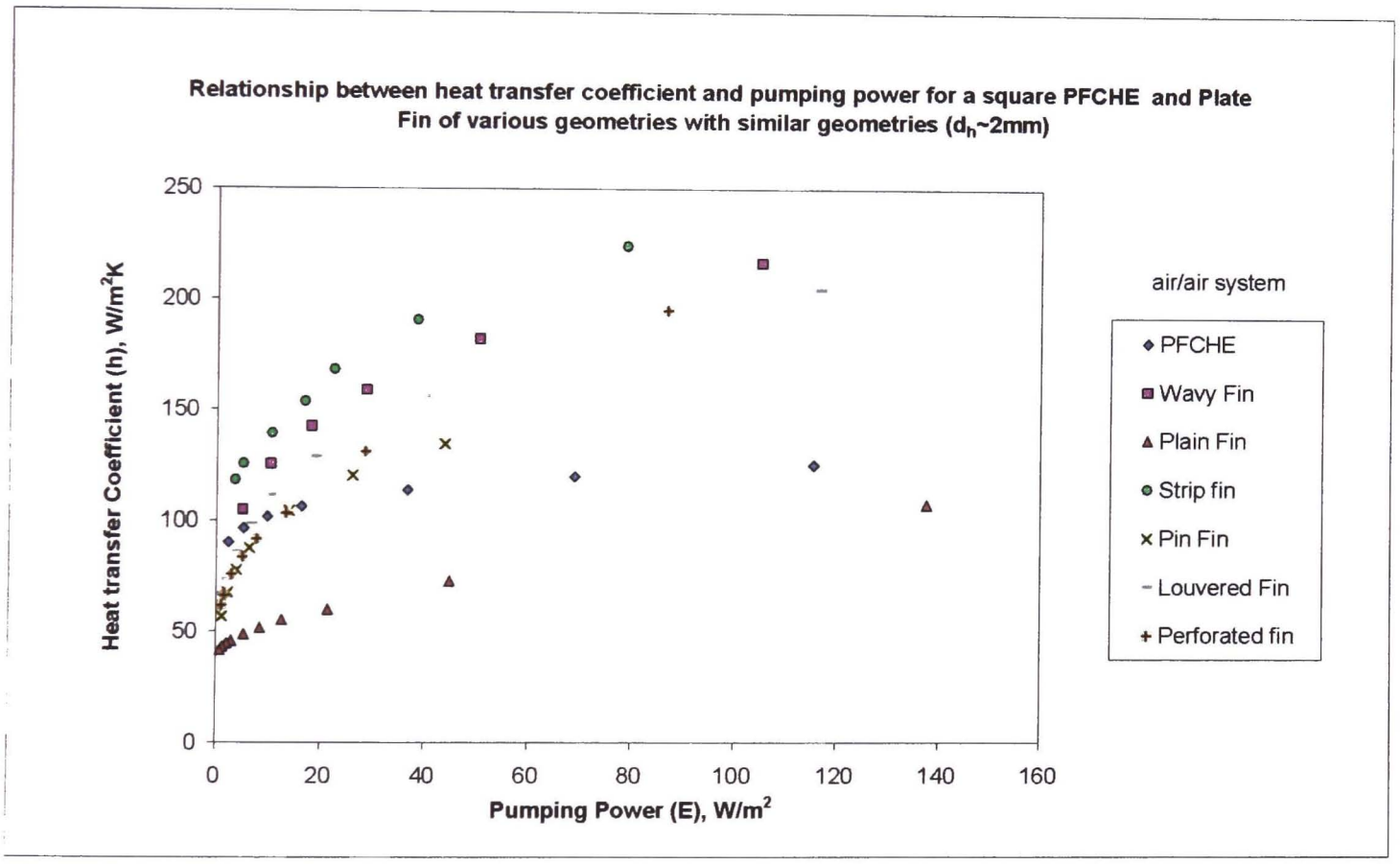


**Figure 9.4 Relationship between heat transfer coefficient (h) and pumping power (E) for a square PFCHE and Plate Fin of various geometries**

To incorporate the combined effect of the heat transfer and pressure drop characteristics on the surface geometries, the pumping power for each surface is evaluated. The pumping power and heat transfer coefficients for the surface geometries are calculated and plotted as shown in Figure 9.4 above.

The factor of difference between the PFCHE heat transfer coefficient and the other geometries at E=30 W/m$^2$ are shown below. This pumping power value is chosen, as a wider comparison can be made, whereby at higher values only a few geometries can be studied.

| Ratio of PFCHE heat transfer coefficient to plate fin at E=30 W/m$^2$ | Ratio Value | Sequence of geometry with highest h | L (mm) | $d_h$ (mm) | $L/d_h$ | h (W/m$^2$K) |
|---|---|---|---|---|---|---|
| h PFCHE / h strip fin | 0.63 | strip | 3.6 | 2.07 | 1.75 | 173.50 |
| h PFCHE / h wavy fin | 0.68 | wavy | 9.0 | 2.12 | 4.25 | 158.81 |
| h PFCHE / h louvered fin | 0.77 | perforated | 4.8 | 3.08 | 1.55 | 130.93 |
| h PFCHE / h perforated fin | 0.84 | louvered | 2.0 | 2.50 | 0.80 | 142.32 |
| h PFCHE / h pin fin | 0.87 | pin | 1.5 | 1.64 | 0.93 | 123.50 |
| h PFCHE / h PFCHE | 1.00 | PFCHE | 135.0 | 2.00 | 67.5 | 109.50 |
| h PFCHE / h plain fin | 1.67 | plain | 127.0 | 1.72 | 73.8 | 65.50 |

**Table 9.4 Table showing the interpretation of the pumping power plot for different surface geometries**

The results show that the strip fin gives the best overall performance compared to the other surface geometries. At a glance, the pumping power results echo the heat transfer results with the strip fin at the highest, wavy fin a close second and the plain fin occupying the lowest position. However looking closely, the position of the perforated, louvered and pin fins; as well as the PFCHE, shifts up and down a little. The louvered fin, which falls third in the heat transfer results, now lies in fourth position between the perforated and the pin fins for its pumping power capacity. This means that in order to achieve the same amount of heat transfer, the louvered fin needs to expend more energy than the perforated fin but less than the pin fin.

The PFCHE moves down two steps from fourth to sixth position, between the heat transfer and pumping power results. This can be due to the high friction factors it experiences, as shown in Figure 9.3. The pin and perforated fins, move one and two steps up respectively, which shows that their overall thermal and hydraulic performance outweighs their lower heat transfer capabilities. Following the pumping power results, we now move on to consider the goodness factors for the surface geometries investigated.

### 9.1.5.2 Investigation on goodness factor (Jh/f)

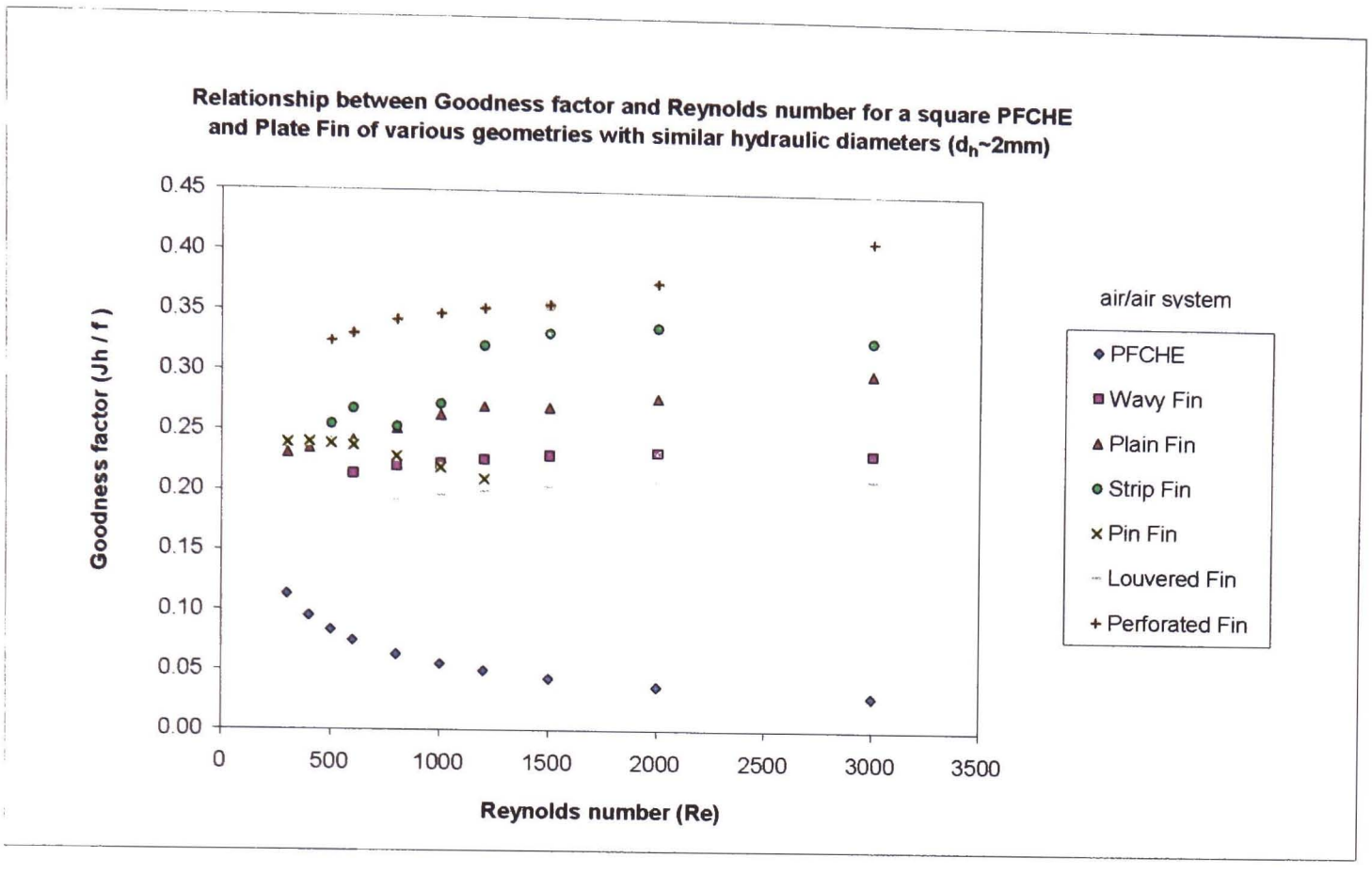


**Figure 9.5 Relationship between goodness factor (Jh/f) and Reynolds number (Re) for a square PFCHE and Plate Fin of various geometries**

The perforated fin has the highest goodness factors compared to the other surface geometries. As expected, the PFCHE has the lowest goodness factors as it experiences the highest friction factors, as shown in Figure 9.3 earlier. The strip fin, which achieves the highest heat transfer and the lowest pumping power requirements, comes in second on the goodness factor plot. The plain fin, which has the lowest heat transfer, friction factor and pumping power performance, comes in third ahead of the wavy and louvered fin geometries.

From Figure 9.5 above, the perforated pin gives the best Jh/f ratios, and therefore it is deemed the most thermally efficient surface in this study. This shows that the perforated fin is able to transfer more heat, at the expense of friction that it experiences. The perforated fin achieves this, despite the fact that it does not provide the highest heat transfer or the lowest friction factors compared to the other geometries. Hence, the results prove that the goodness factor plot depicts the thermal efficiency of each surface geometry, relative to its heat transfer capability and friction factor penalty. The plot enables a comparison between the Jh/f ratios achieved for each geometry, and not the two factors separately.

For instance, a high goodness factor on the plot does not mean that a certain geometry has the highest Jh factor and the lowest f factor, compared to the other geometries. Instead, the higher the goodness factor ratio, the more thermally effective the geometry or in other words

'higher goodness' is achieved. The factor of difference between the PFCHE goodness factor and the other geometries at Re=1000 are shown below.

| Ratio of PFCHE Goodness factor at Re=1000 | Ratio Value | Sequence of geometry with highest (Jh/f) | L (mm) | $d_h$ (mm) | $L/d_h$ | (Jh/f) |
|---|---|---|---|---|---|---|
| (Jh/f) PFCHE / (Jh/f) perforated fin | 0.16 | perforated | 4.8 | 3.08 | 1.55 | 0.3475 |
| (Jh/f) PFCHE / (Jh/f) strip fin | 0.20 | strip | 3.6 | 2.07 | 1.75 | 0.2726 |
| (Jh/f) PFCHE / (Jh/f) plain fin | 0.21 | plain | 127.0 | 1.72 | 73.80 | 0.2632 |
| (Jh/f) PFCHE / (Jh/f) wavy fin | 0.24 | wavy | 9.0 | 2.12 | 4.25 | 0.2280 |
| (Jh/f) PFCHE / (Jh/f) pin fin | 0.25 | pin | 1.5 | 1.64 | 0.93 | 0.2193 |
| (Jh/f) PFCHE / (Jh/f) louvered fin | 0.28 | louvered | 2.0 | 2.50 | 0.80 | 0.1964 |
| (Jh/f) PFCHE / (Jh/f) PFCHE | 1.00 | PFCHE | 135.0 | 2.00 | 67.50 | 0.0552 |

**Table 9.5 Table showing the interpretation of the goodness factor plot for different surface geometries**

*9.1.6 Conclusion*

The PFCHE, represented by its sinusoidal corrugations comes in at fourth position out of the seven geometries investigated, for its heat transfer capability. This result is somewhat encouraging. However, it also achieves the highest friction factors and due to this obtains the lowest goodness factors and exhibits mediocre pumping power ability. Nevertheless, this is by no means an accurate prediction of the PFCHE performance, as different length (L) definitions were used for the PFCHE and plate fin geometries in taking the experimental temperature and pressure drop measurements. The length used in the PFCHE is the flow length of the exchanger (summation of several corrugation wavelengths), whereas the uninterrupted flow length (one corrugation wavelength) is used for the plate fin geometries, Kays and London (1984). Once incorporated into the performance calculations, this difference in the length definition decreases the PFCHE's overall performance tremendously, due to its huge pressure drop penalty.

Bearing this length difference in mind, a performance comparison is still conducted based on the basis of a similar hydraulic diameter of 2 mm for the seven geometries investigated. These are the wavy, strip, louvered, perforated, pin and plain fins along with the sinusoidal corrugations of the PFCHE. The strip fin gives the best overall performance of all the seven surface geometries, as it achieves the highest points on the heat transfer and pumping power plots. In addition, it also has the second highest goodness factors. This is achieved despite having the second highest friction factors. The plain fin, however, is on the other end of the scale, generating the lowest heat transfer and highest pumping power requirements. Nevertheless, it does as a consolation achieve the lowest friction factors, which enables it to claim third place on the goodness factor plot.

From these results, the initial conclusion obtained is that the PFCHE outperforms the plain fin, but on the whole loses out to the other variations of the plate fin (strip, wavy, louvered, pin and perforated fins). It loses out by a margin of less than a factor of 2, which means that with slight modifications; such that will introduce more interruption to flow, the possibility of achieving higher heat transfer is bright. Moreover it should be noted, that the PFCHE has a slightly higher heat transfer capability than the pin and perforated fins. This positive outlook is supported by the fact that the PFCHE provides the highest heat transfer compared to the other geometries, at low Re (Re<500). This high heat transfer capability is due to the occurrence of strong developing flow along the sinusoidal corrugations at low Re numbers. However, at higher Re, the flow in the PFCHE becomes more fully developed and hence loses the benefits of developing flow heat transfer enhancement. The massaging effect provided by the sinusoidal corrugations is less significant, as the fluid flow velocities are higher. These higher flow velocities race through the sinusoidal corrugations, and so the flow through the PFCHE becomes more fully developed. In addition, the rigidity of the polymer film is not sufficient enough to ensure that the fluid flow follows the crests and troughs of the film length, at higher velocities. Nevertheless, for applications where low fluid flow rates are essential; such that it experiences a truly laminar flow, the PFCHE provides an alternative to metallic units.

Furthermore, the PFCHE sinusoidal corrugations are easy to manufacture compared to the complexities of the extended plate fin geometries. A simple method of manufacture, involving thin polymer sheets being placed on a spring loaded mould is all that is required. Therefore there are no non-uniformity issues raised in the corrugations formed, which occurs in the plate fin manufacture. Also other problems such as the scarfing of fins and varying fin thickness do not occur. This is not the case for the plate fin, where for instance, the strip fin has a high degree of uncertainty towards its performance and is also more tedious to manufacture.

The table below shows a summary of the performance evaluation plots for the PFCHE and the plate fin geometries investigated.

| Performance plot | Highest position | Lowest position | PFCHE position |
|---|---|---|---|
| Colburn factor (Jh) for Re<500 | PFCHE | plain fin | n/a |
| for Re>500 | strip fin | plain fin | 4th |
| Friction factor (f) | PFCHE | plain fin | n/a |
| Goodness factor (Jh/f) | perforated fin | PFCHE | n/a |
| Pumping power (E) | strip fin | plain fin | 5th |

**Table 9.6 Summary of the performance plots for the PFCHE and Plate Fin surface geometries**

In the following section, we go on to consider the effect of using two types of polymers (PVDF and PEEK), as a material of construction for the PFCHE. The results for the PEEK exchangers are taken from Chapter Four of this thesis.

## 9.2 PFCHE material of construction comparison: PEEK and PVDF

As mentioned before, traditionally polymers were not used within the field of heat transfer, due to their extremely poor thermal conductivity compared with that of available metals. Typically metals have thermal conductivity values up to as much as 390 W/mK for copper, whereas PVDF and PEEK have thermal conductivities of 0.17 and 0.24 W/mK respectively. This illustrates that polymers are not at first glance, an ideal choice for the construction of heat transfer equipment. Nevertheless, as mentioned before, when using thin polymer films, the film resistance (t/k), becomes negligible towards the evaluation of the overall heat transfer coefficient. In this section, we will highlight the incentive of using PVDF as a material of construction for the PFCHE.

Following PEEK, PVDF has also many properties, which make it an ideal material for use within the process industries, especially in areas where PEEK is considered unsuitable such as in concentrated sulphuric and nitric acid environments. PVDF is chemically inert as it is resistant to most acids, aliphatic and aromatic compounds, chlorinated solvents and alcohols. PVDF also exhibits excellent mechanical properties over a wide range of temperatures. An example of this, is that it has a tensile yield strength of up to 55 MPa at 296 K and up to 10 MPa at 423 K. This allows PVDF to be used for low temperature heat transfer duties. In addition, it also has high reliability during long-term use. This has been illustrated by studying the field in which PVDF is presently used, where in most cases the equipment has not required replacement for the period of use. An example of this, is the Channelplate heat exchanger constructed by *Serendip*, which is guaranteed for fifteen years.

The tensile yield strength after 25,000 hours usage at 165°C is still greater than 90%, again illustrating its resistance to thermal ageing. The relatively easy processing of PVDF also enables easy fabrication of equipment. This provides in some cases, especially with aggressive media; cheaper alternatives to the metal equivalent. PVDF also has excellent fouling resistance properties, which makes it ideal for the use with highly fouling chemicals. For further details, the property data sheets for PVDF and PEEK are attached in Appendix I.

### *9.2.1 Construction of the PVDF Polymer Film Compact Heat Exchanger (PFCHE)*

The construction of the PVDF heat exchanger is similar to the PEEK heat exchanger, as outlined in Chapter Four, apart from the thickness of the PVDF polymer films, which are 200 μm thick, as opposed to 100 μm for PEEK. The experimental procedures involved are also the same, involving flow rate, temperature and pressure drop measurements. The equipment used for these experimental measurements are outlined in Table 9.7 below. The raw data for the PVDF heat exchanger is provided based on work by Walker (1997).

| Experimental Measurements | Equipment |
|---|---|
| Flow rate | Low: Fisher 18X rotameters fitted with Duralamin floats<br>High: Nixon rotameters |
| Temperature | K-type thermocouples |
| Pressure Drop | Digital pressure gauge |

**Table 9.7 Experimental equipment for the PVDF heat exchanger**

In the following section, we show the results of the performance comparison between the PVDF and PEEK heat exchangers.

### *9.2.2 Comparison between PVDF and PEEK PFCHEs*

In this section, we compare the heat transfer, pressure drop and the overall thermal and hydraulic characteristics between the PEEK and PVDF exchangers, in an air/air system. We begin with the effects of heat transfer, which will be depicted using a number of graphs. These will be shown in the order below.

(i) Heat balance error (HBE) vs. Reynolds number (Re)
(ii) Heat transfer coefficient (h) vs. Reynolds number (Re)
(iii) Effectiveness (E) vs. Reynolds number (Re)

The pressure drop characteristics will then be shown through the friction factor plot and finally, the overall thermal and hydraulic characteristics for both polymers, will be described using the pumping power plot.

### 9.2.2.1 Effects of heat transfer

Prior to viewing the heat transfer results for the PVDF and PEEK heat exchangers, we first investigate the degree of heat loss involved in both units, using the heat balance plot shown below.

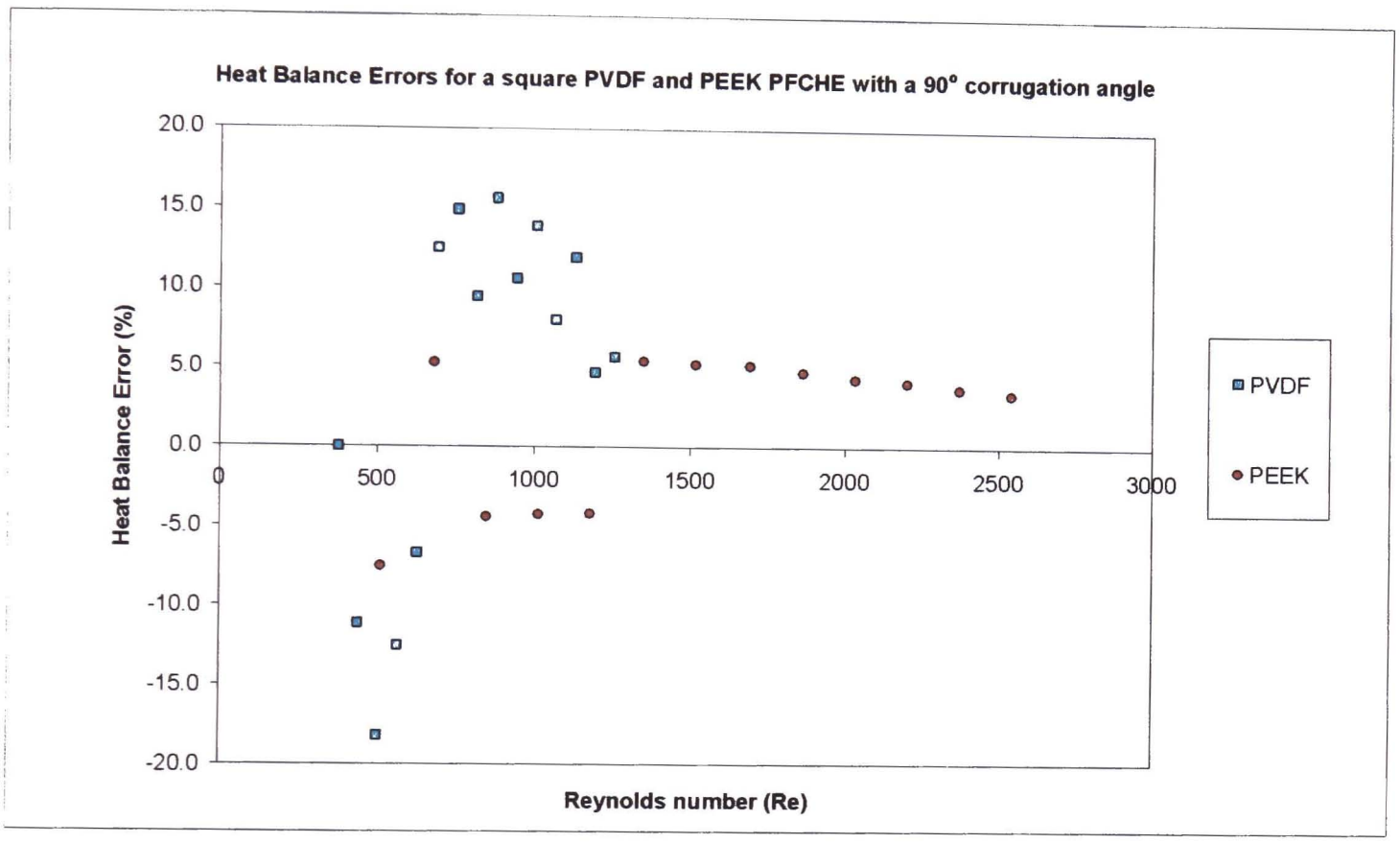


**Figure 9.6 Comparison of heat balance errors between PVDF and PEEK square PFCHEs with a 90° corrugation angle in an air/air system**

There is less heat loss for the PEEK heat exchanger, with a maximum error of 7.5%. For the PVDF, there are errors exceeding 10%, which are deemed unacceptable for design correlations. Nevertheless for the purpose of this study, the PVDF heat transfer experimental data is accepted for the determination of the heat transfer coefficients (h), as this will provide an estimate of the heat transfer performance for the PVDF PFCHE. Consequently, using the h values, a performance comparison with the PEEK exchanger can be conducted. The heat loss of the PVDF exchanger could be due to the plastic tubing at the inlet and outlet streams and also the exchanger housing, rather than the PVDF exchanger core itself. To overcome this, the design of the test facility needs to be addressed with emphasis on insulation and lagging. However, in this study the main aim is to generate preliminary experimental data for the unit. Once this is established, the results obtained will serve as a stepping-stone towards future work on PDVF PFCHEs, with more emphasis on accuracy and detail. For a numeric

account of the heat transfer achieved by the two polymer heat exchangers, the heat transfer coefficient plot is shown in Figure 9.7 below.

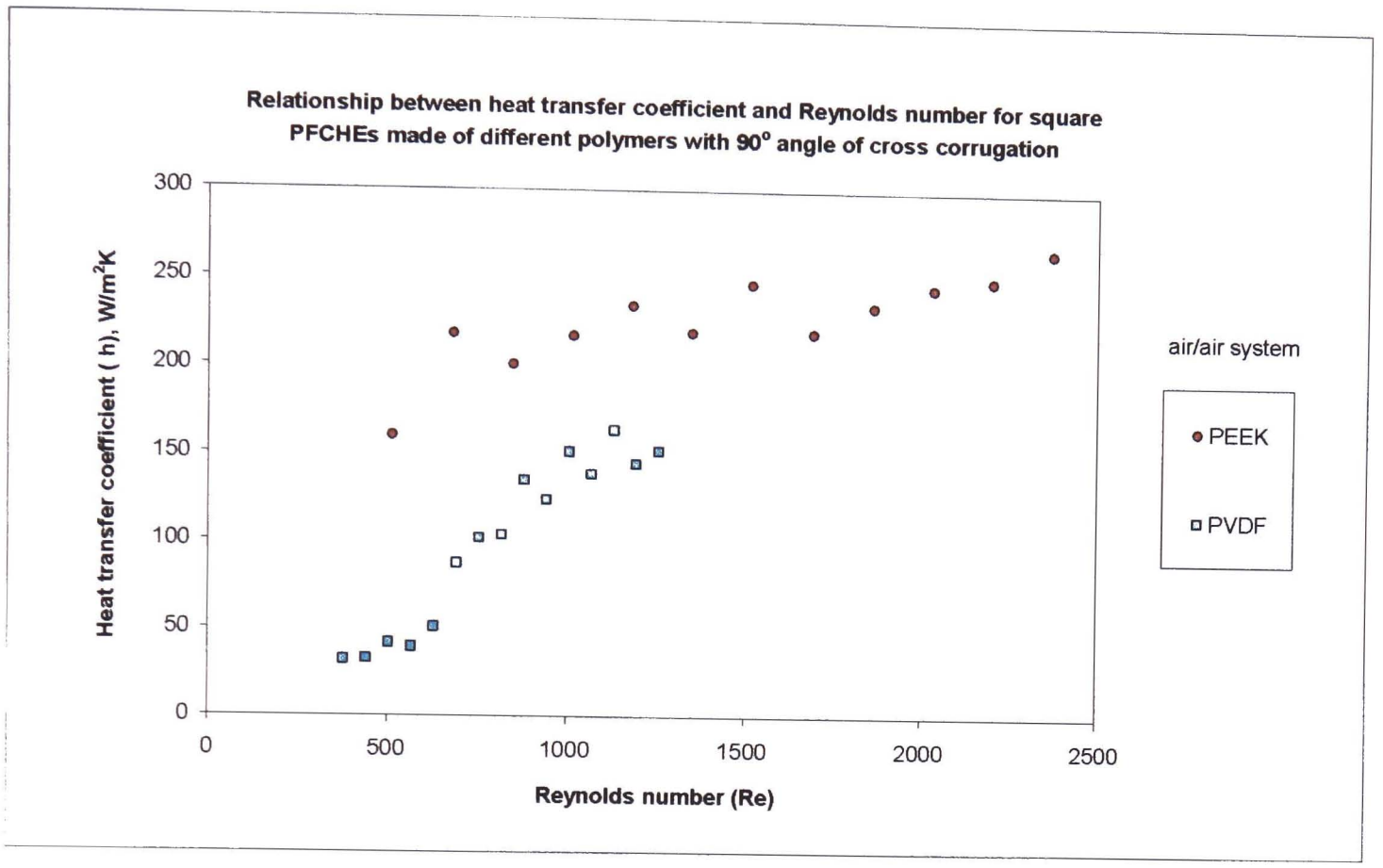


**Figure 9.7 Comparison of heat transfer coefficient plots between PEEK and PVDF square PFCHEs with a 90° corrugation angle**

Both the polymers show similar trends, whereby the heat transfer coefficient increases with Re number. The heat transfer achieved by the PVDF exchanger is lower than the PEEK exchanger, over the entire Re range. Nevertheless at higher Re, the PVDF heat transfer coefficients do get closer to that achieved by the PEEK heat exchanger. Further tests at higher Re for the PVDF heat exchanger, are needed to obtain a more accurate comparison between the two units. Higher heat transfer coefficients are obtained for the PEEK heat exchanger, due to a combination of several factors such as the heat transfer area (A), film resistance (t/k), number of transfer units (NTU) and heat exchanger effectiveness (E). The first two factors are consistent throughout each heat exchanger system, whilst the latter two vary with temperature and flow rate of air. The values of the first two factors for both heat exchangers are shown in the table below.

| Polymer | Heat transfer area (A), $m^2$ | Film resistance (t/k), $m^2K/W$ |
|---|---|---|
| PVDF | 0.09 | 0.0011 |
| PEEK | 0.05 | 0.0004 |

**Table 9.8 Heat transfer area and film resistance values for the PVDF and PEEK PFCHEs**

The heat transfer area (A) comes into play in the determination of the overall heat transfer coefficient (U), whilst the film resistance (t/k) is directly involved in the evaluation of the individual heat transfer coefficient (h). The overall heat transfer coefficient is determined using the following equation:

$$U = (NTU\ C_{min})/A \qquad (9.2)$$

The individual heat transfer coefficient values are determined using the following equation.

$$1/U = 2/h + t/k \qquad (9.3)$$

The PVDF heat exchanger has a higher heat transfer area and film resistance compared to PEEK, which causes its heat transfer coefficient to be much lower. To obtain a better understanding of this, we next investigate the effectiveness of both polymer heat exchangers.

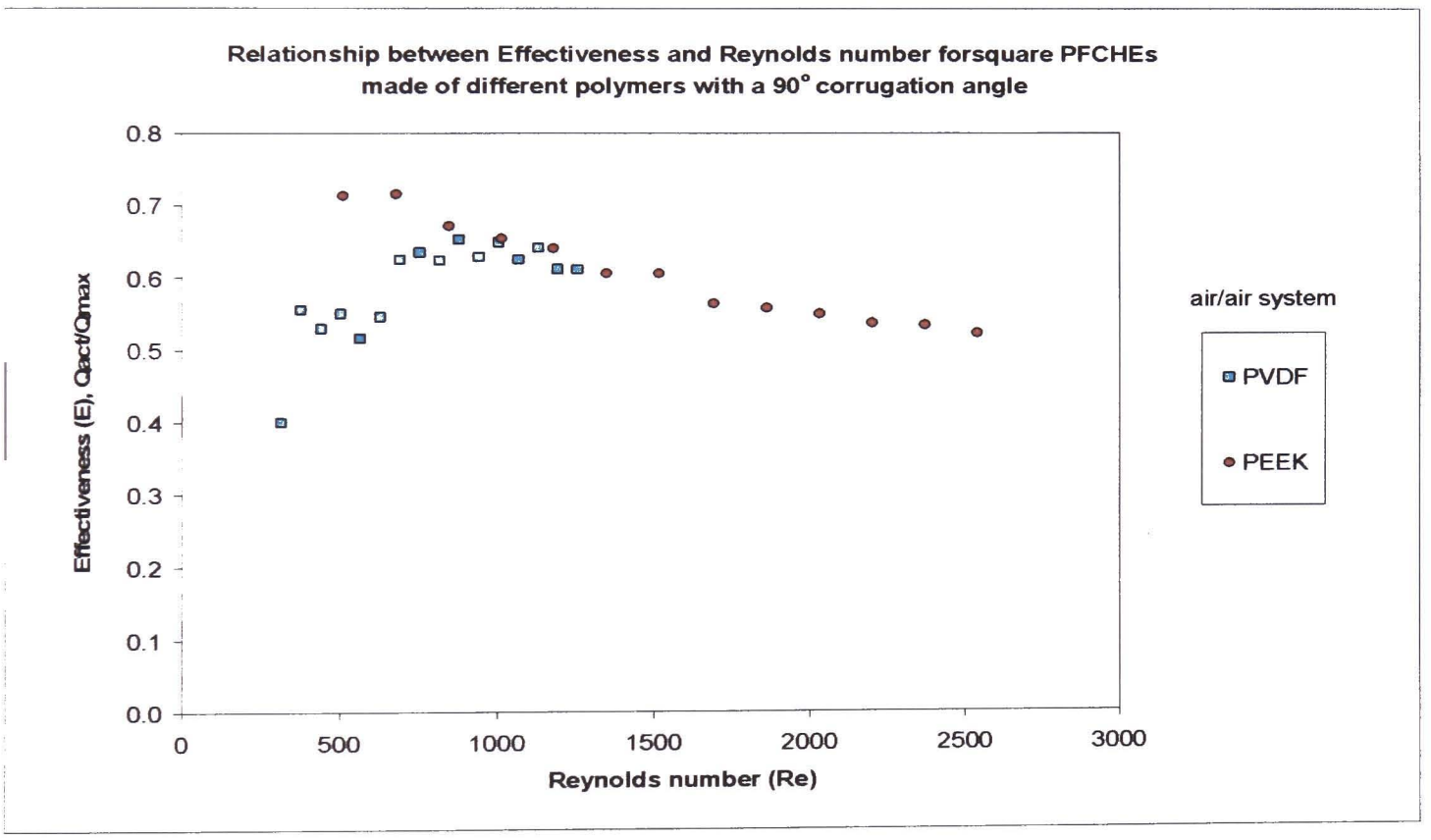


**Figure 9.8 Comparison of effectiveness plots between PEEK and PVDF square PFCHEs with a 90° corrugation angle**

Due to its higher heat balance errors, the PVDF heat exchanger has a lower effectiveness compared to the PEEK heat exchanger. This is shown in the graph above. Using the E-NTU Bessel function as shown in Chapter Four, the lower effectiveness achieved by the PVDF exchanger, leads to lower NTU values. Hence from equation (9.2), it can be seen that a combination of two effects (high heat transfer area and low NTU values), will lead to lower overall heat transfer coefficients (U) for the PVDF heat exchanger, compared to its PEEK counterpart. Consequently, this will bring about lower individual heat transfer coefficients (h)

for the PVDF heat exchanger, as shown in Figure 9.7. In the following section, we consider the friction factor characteristics of both polymer heat exchangers.

9.2.2 2 Effects of pressure drop

It can be seen from Figure 9.9 below, that the general trend observed for both friction factor curves, is that the friction factor decreases as the Re number increases. The PEEK friction factor curve experiences less scatter of data points compared to the PVDF curve. This means that the pressure drop measurements taken for PEEK, are more accurate, since a gradual decrease of friction factor values over the Re range is observed. Nevertheless, the PEEK exchanger has higher friction factor values throughout the entire Re range compared to the PVDF exchanger. This means that there is slightly more resistance to flow in the PEEK exchanger, than in the PVDF unit.

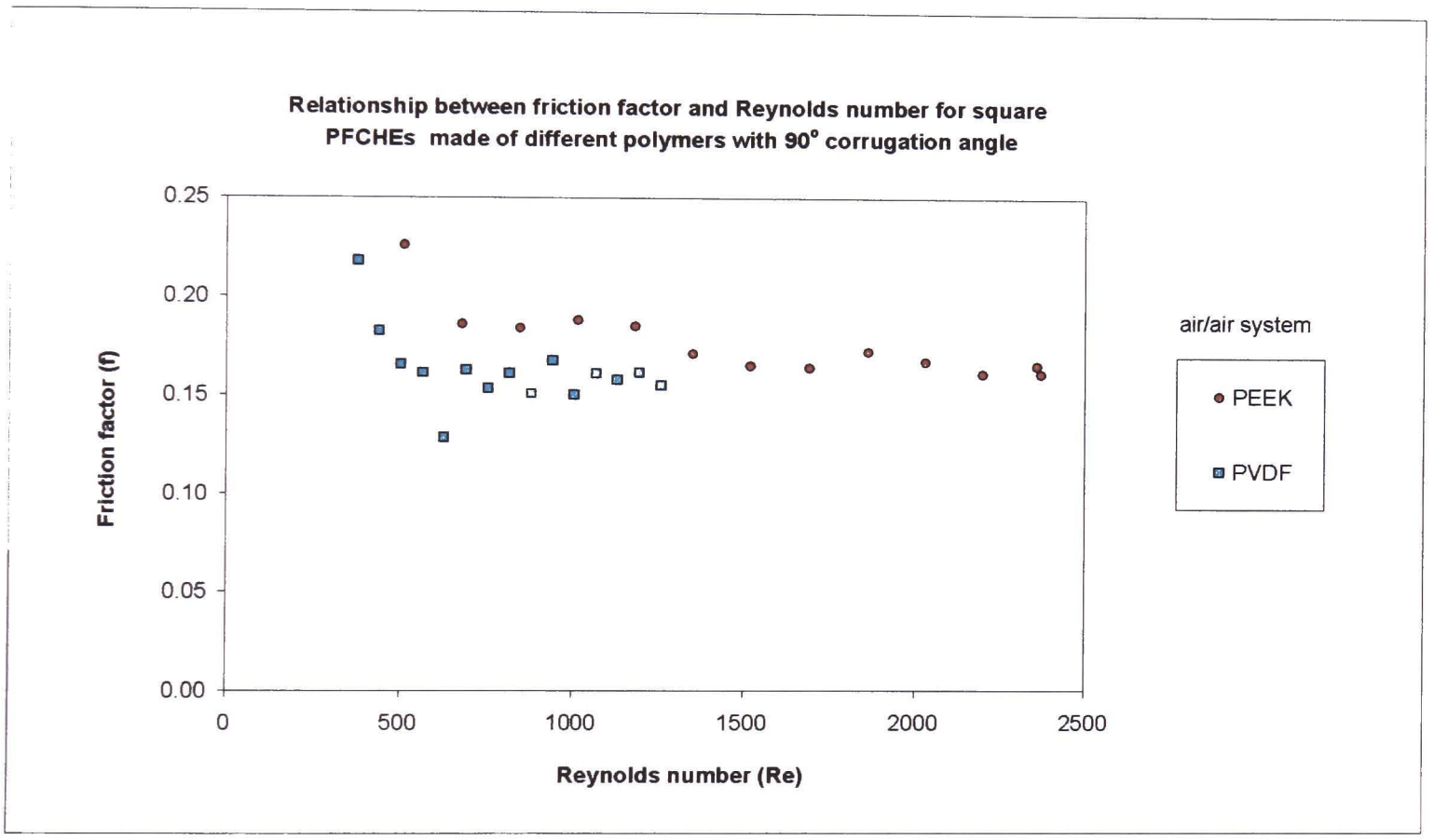


**Figure 9.9 Comparison of friction factor plots between PEEK and PVDF square PFCHEs with a 90° corrugation angle**

Having considered the heat transfer and pressure drop characteristics for both polymer units, we now go on to investigate the overall performance through the pumping power plot.

9.2.2.3 Effects of overall thermal and hydraulic performance

The pumping power results in Figure 9.10, illustrate the main difference between the PVDF and PEEK polymers, when used in this type of exchanger. Using similar pumping power requirements, the PEEK heat exchanger can achieve a higher degree of heat transfer

compared to the PVDF heat exchanger. In other words to achieve a similar degree of heat transfer, less pumping power is needed by the PEEK heat exchanger.

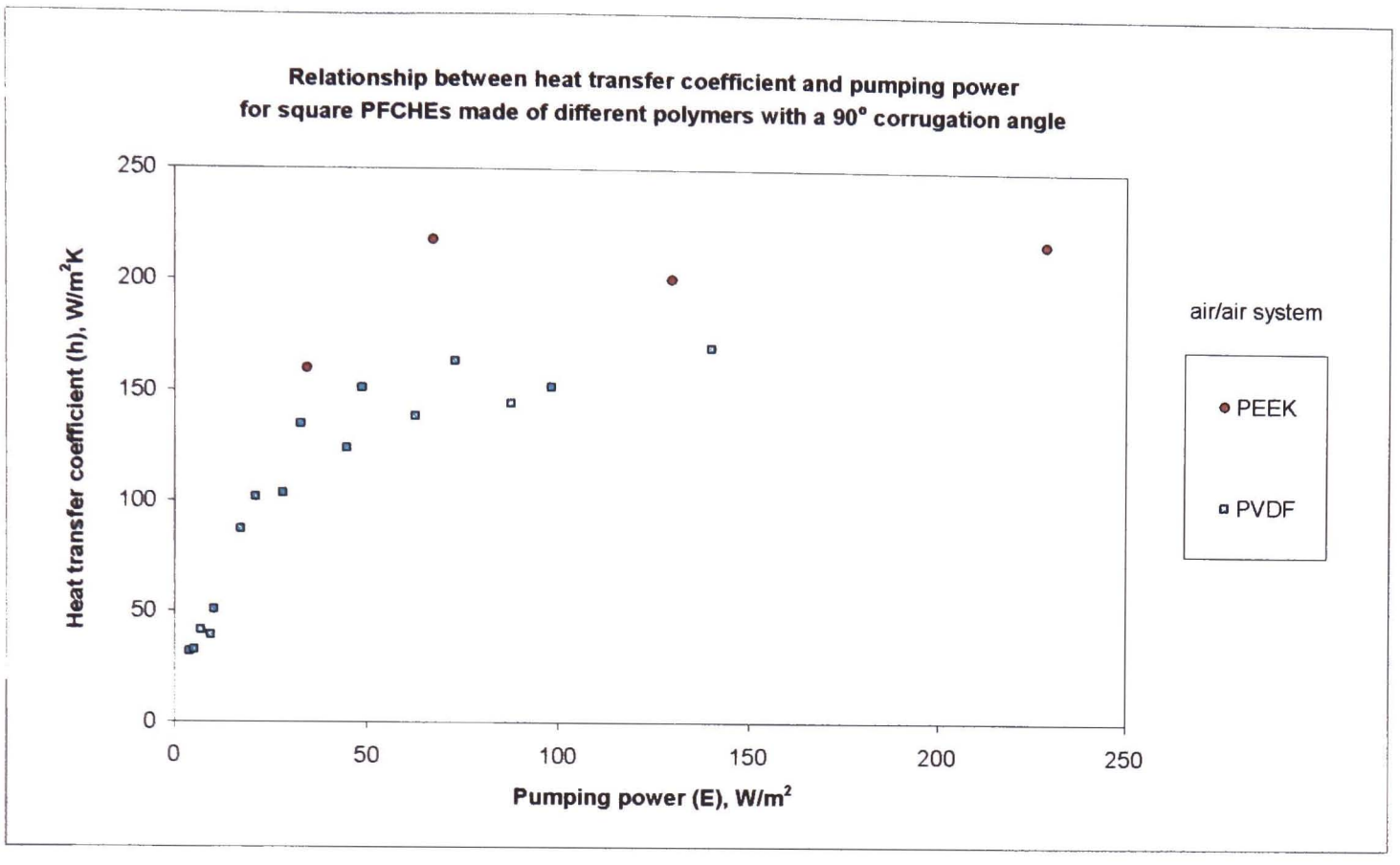


**Figure 9.10 Comparison of pumping power plots between PEEK and PVDF square PFCHEs with a 90° corrugation angle**

This is clearly depicted by the values tabulated in Table 9.9 below. Further tests at higher pumping power values for the PVDF exchanger, could be conducted for a better comparison with the PEEK PFCHE.

| Polymer | Heat transfer coefficients (h), $W/m^2K$ | Pumping power (E), $W/m^2$ |
|---|---|---|
| PEEK | 160 (similar h values) | 34 |
| PVDF | 164 | 73 |
| | | |
| PEEK | 218 | 67 (similar E values) |
| PVDF | 164 | 73 |

**Table 9.9 Comparable operating points on the pumping power plot for a PVDF and PEEK square PFCHE**

*9.2.3 Conclusion*

Apart from PEEK, PVDF is a suitable material to construct polymer film compact heat exchangers (PFCHE), especially in applications where PEEK is deemed unsuitable such as in concentrated sulphuric and nitric acid environments. An example of this, is in flue gas

applications where PVDF is a cheaper alternative to some exotic metals such as Ni-Cr-Mo alloy. A summary of the results obtained is shown in the table below.

| Performance plot | Higher polymer |
|---|---|
| Heat transfer coefficient (h) | PEEK |
| Friction factor (f) | PEEK |
| Pumping power (E) (lower requirement) | PEEK |

**Table 9.10 Summary of PFCHE material of construction comparison study**

Therefore from the results shown, it can be concluded that PEEK is definitely the primary choice as the material of construction in the PFCHE, whilst PVDF can be used in applications where PEEK is deemed unsuitable.

## 9.3 Summary

In this chapter, we looked at the effect of surface geometry and the material of construction on the square PFCHE performance. In the first part of the chapter, a comparison between the sinusoidal corrugations of the PFCHE and six plate fin geometries (strip, wavy, louvered, perforated, pin and plain) was conducted by using four performance evaluation plots (Jh, f, Jh/f and E). The basis of this comparison was that the hydraulic diameter of all the geometries investigated, were similar at $d_h \approx 2mm$. The length used in the PFCHE is the flow length of the exchanger (summation of several corrugation wavelengths), whereas the uninterrupted flow length (one corrugation wavelength) is used for the plate fin geometries. Overall, the PFCHE gave encouraging results by outperforming the plain fin, but losing out in particular, to the strip fin. Nevertheless, it should be noted that if similar flow length definitions were used in both units, the overall PFCHE performance could improve tremendously.

In the second part of the chapter, we compared the performance of PEEK and PVDF PFCHEs adopting the same design. Thinner PEEK films (100 μm) were used compared to the 200 μm thick PVDF films employed, which gave the PVDF unit a higher film resistance, (t/k). Results show that the PEEK exchanger achieved better heat balances, higher heat transfer and lower pumping power requirements than the PVDF exchanger, which makes it a much better choice as a material of construction in the PFCHE. However, the performance of the PVDF exchanger does show improvement at higher Re numbers. Therefore, more data involving higher Re numbers are needed for the PVDF exchanger, for a better comparison and to support its use as an alternative polymer to PEEK in the square PFCHE. In the following chapter, we draw together the results and conclusions of all the studies in the previous chapters. Recommendations for future research are also outlined.

# CHAPTER 10 - CONCLUSIONS AND RECOMMENDATIONS

## 10.0 Introduction

This chapter presents a summary of the results and conclusions of the research contained in the preceding chapters, and also highlights areas where further research is required. We first review the motivation for this research, involving the merits of the PFCHE design as an alternative to metallic heat exchangers; particularly for applications where weight and cost savings are a major concern.

Following this, the aims of the research are reviewed and a summary of the work conducted is outlined to show that the aims have been fulfilled in this thesis. To summarise the work in previous chapters, key features of the PFCHE which affect the performance of the unit, such as the use of different fluid systems, configurations, corrugation angles, surface geometry and material of construction; along with the design correlations developed are briefly described in turn. A list of contributions of this thesis is then drawn up, and finally areas requiring further research are identified.

## 10.1 Summary of the main findings of the thesis

Here, the reasons behind adopting the current PFCHE design are first considered. We then move on to a summary of the main findings in previous chapters, to illustrate that the aims of this research have indeed been met.

### *10.1.1 Reasoning/Argument for the PFCHE design*

The reasons for adopting the current PFCHE design have been briefly explained, highlighting issues such as the use of polymers; in particular PEEK, plus the adoption of thin polymer films, sinusoidal corrugations, narrow channels and developing laminar flow. Further details are given in Chapter Two.

(a) Polymers are chosen as an alternative material of construction for heat exchangers, in order to address the disadvantages posed by conventional metal units. Among the disadvantages of using metals that can be overcome by using the PFCHE, are:

- metallic heat exchangers are heavy, bulky and costly

- although metals are good conductors of heat, the atmosphere surrounding the heat exchanger provides either a source of unwanted heat to a coolant fluid, or an unwanted extractor of heat from a heating fluid used in the heat exchanger
- when processing corrosive fluids, specialised expensive metals or alloys are needed
- most metals are easily wet with liquids such as aqueous liquids, which in turn promote their interaction with the liquid such as chemical reactions and fouling of the metal

The PFCHE is developed to help overcome these shortcomings, particularly in applications where weight and cost savings are of primary concern. Apart from the novel design of the unit, the PFCHE can address these shortcomings due to the properties of the polymer used.

(b) PEEK (poly ether ether ketone) is selected as the polymer of construction for the PFCHE, due to its outstanding properties. These are listed below.

- Excellent chemical and fatigue resistance. It is resistant to a wide range of organic and inorganic liquids and is only susceptible to concentrated nitric or sulphuric acids (>50% concentration).

- Exhibits good thermal stability and has a working temperature of about 220°C.

- The PFCHE matrix, constructed in corrugated 100 μm PEEK films, is remarkably robust and can withstand a differential pressure of about 1000 kPa at ambient temperatures. The matrix is made up of many sheets stacked on top of one another, so that the turbulence in the headers can be efficient enough to homogenise the temperature within.

- The PEEK films have hydrophobic super-smooth surfaces, which allow the fouling characteristics of polymer films to be intrinsically superior to those of metal.

- The PEEK films have a high coefficient of thermal expansion which can assist in the 'self-cleaning' capability of the unit, although considerations should be given to the level of expansion when installing the unit.

(c) The use of thin polymer films overcomes the low thermal conductivity of polymers by reducing the film's thermal resistance (t/k), to give higher overall heat transfer coefficients. A film thickness of 100 μm appears to be appropriate; on cost (£15/$m^2$) as well as fabrication grounds. Thinner films do not have the required mechanical strength for supporting corrugations, which are a key feature of the heat exchanger developed and are also more expensive to extrude. A

thickness value of 100 μm is not possible for metals, where the minimum thickness is approximately 0.7 mm for aluminium.

(d) The sinusoidal corrugations on the polymer films provide heat transfer enhancement, as the flow is repeatedly mixed and redeveloped over the crests and troughs of the corrugations. This massaging effect encourages more mixing which leads to better heat transfer, as the corrugations interrupt the flow periodically, causing a thermal boundary layer to develop on each corrugation. In addition, the corrugations on the polymer films also offer support and rigidity to the unit as a whole.

(e) Narrow channels are employed in the PFCHE, to enable higher heat transfer coefficients to be achieved. This can be seen from the definition of the Nusselt number (Nu).The Nu number can be expressed as the ratio between the observed convection and conduction heat flux. The latter is generated by conduction over the chosen characteristic length (L). Therefore large channels, which lead to large Nu numbers, do not necessarily imply good heat transfer performance. On the other hand, narrow channels appear attractive since the heat transfer coefficient increases with a decrease in the length dimension.

(f) Laminar flow as opposed to turbulent flow is experienced in the PFCHE, leading to better thermal and hydraulic performances. Instead of adopting high velocities, the heat transfer can be increased by employing narrow channels. Low velocities are adequate to achieve good fluid mixing in the unit. This was proven in the flow visualisation study in Chapter Four under Section 4.3.1.6, whereby a good degree of mixing was achieved at laminar flow conditions comparable to that in turbulent flow. Therefore for the PFCHE, heat transfer enhancement is achieved at the expense of lower pressure drops. Due to low-pressure losses, low pumping power requirements are also achieved using laminar flow.

(g) The developing flow in the PFCHE generates better heat transfer than the fully developed flow experienced in turbulent systems. In the developing flow, the boundary layers that resist heat transfer are broken down along the sinusoidal corrugations. This action creates better mixing which leads to heat transfer enhancement. In the case of fully developed flow, the boundary layers are intact, hence obstructing heat transfer.

Having understood the reasons for adopting the PFCHE design, we move on to check if the aims of this thesis have been fulfilled.

*10.1.2 Have the research objectives been achieved?*

The objectives set forth at the beginning of this research were as follows:

- To establish credibility for the technology
- To perform testing of the PFCHEs (different configurations) using different fluid systems under industrial conditions and to develop design correlations for each fluid system
- To present industrial case studies for evaluating the PFCHE technology
- To develop unique design correlations involving Pr numbers, that will enable the evaluation of the PFCHE performance for a wide range of fluid systems
- To investigate different aspects of the PFCHE (corrugation angle, surface geometry and material of construction) and its effect on exchanger performance

We now attempt to show briefly, how they have been achieved by providing a summary of the work done in previous chapters.

(a) Chapter One shows that despite having lower thermal conductivities, the PFCHE has better heat transfer capabilities than its metal counterparts. This is due to the use of thin polymer films (100 μm). Not only does the PFCHE outperform conventional metallic heat exchangers such as the plate frame and the shell and tube by a huge margin, its performance also surpasses those of current compact metallic heat exchangers, such as the plate fin. The results for the latter are shown in Chapter Seven. The benefits of laminar flow heat transfer in the PFCHE are supported by the flow visualisation work in Chapter Four, which shows that even at low Re numbers, a good degree of mixing is achieved; comparable to that of metallic heat exchangers in turbulent flow.

(b) Two PFCHE configurations have been tested using different fluid systems under industrial conditions. They are the square and spiral configurations. Air/air, water/water and four glycerol-water mixtures/water systems were tested in the square PFCHE, whilst an air/water system was studied using the spiral configuration. A general uncertainty analysis was conducted in Chapter Three to show the reliability of the experimental data. The experimental procedures and performance plots are detailed in Chapters Four and Five, for the square and spiral units respectively. The details of the design for both units are tabulated in Table 5.3. Apart from the performance testing, design correlations (Jh and f) have been developed for the different fluid systems in both units. The design correlations developed for the square and spiral units are shown in Tables 4.2 and 5.2. These correlations are the main tools for developing alternative PFCHE designs for suitable applications dominated by metallic heat exchangers.

(c) Using the design correlations developed, five case studies were carried out to provide alternative PFCHE designs to conventional metallic heat exchangers; for applications in the aviation, fuel cells and automobile industries. Four case studies adopted the square configuration (cabin air cooler, filter cooler and two types of fuel cell heat exchangers), whilst the fifth case study used the spiral configuration (car radiator). Details of the alternative designs are provided in Chapter Six. A summary of the weight savings achieved by the alternative PFCHE designs, with respect to metallic units, are shown in Table 6.10. It was shown that the associated cost saving achieved by using the PFCHE cabin air cooler design, is approximately £8.7M per annum. This is indeed a huge incentive to adopt the technology in the aviation industry.

(d) Apart from performance testing, developing design correlations and performing case studies, different design aspects of the PFCHE were also investigated to gain a better understanding of the unit, and to improve on the current design. We begin this with an investigation on the effect of the corrugation angle on the PFCHE performance in an air/air system. Up to this point (Chapters One to Six), all of the performance testing for the square PFCHE have been conducted using a $90^{\circ}$ corrugation angle. In Chapter Seven, its performance with corrugation angles of $30^{\circ}$ and $60^{\circ}$ were studied and compared against the $90^{\circ}$ corrugation angle case.

The results showed that the PFCHE performance is dependent on the corrugation angle. Smaller angles achieve higher heat transfer and friction factors due to the larger deviation in the flow path from the main cross flow, as this promotes better mixing at the expense of higher pressure drops. The instability regions (Region 2) on the performance plots (Jh and f) were also determined, as they give good indications of the degree of developing flow present for each angle. A summary of all the performance plots analysed for the three corrugation angles, is shown in Table 7.11. In view of the overall thermal and hydraulic performance, it was concluded that the $90^{\circ}$ corrugation angle is the optimum angle, and should be preferred over the $30^{\circ}$ and $60^{\circ}$ angles for applications in the square PFCHE. The findings from this study support the literature results performed by Hessami (1999), where the $90^{\circ}$ angle configuration has shown to give the optimum performance in a cross-corrugated aluminium plate heat exchanger (CPHE). In addition, it was also found that the square PFCHE outperformed the plate fin heat exchanger, irrespective of the corrugation angle used.

(e) Chapter Eight is a progression of the work done on the square PFCHE in Chapter Four, and focuses on further analysis of the experimental results obtained. Here, the results of the different fluid systems tested in the square PFCHE, are grouped together and analysed collectively. The different fluid systems are represented by the Pr number, which accounts for each system's specific heat capacity, viscosity and thermal conductivity. The range of the Pr numbers studied is between $0.7<Pr<192$.

In general, lower Pr systems achieve better heat transfer in the square PFCHE, thus adhering to the Colburn definition. Nevertheless, the Pr=192 system achieves the highest heat transfer but it cannot be compared with any other system, since different Re ranges are employed. The thermal efficiency and pumping power capability decrease at higher Pr systems due to the high friction factors experienced. This is expected because high Pr numbers indicate high viscosities, and as the channel dimensions of the PFCHE remain unchanged, the pressure drop plays a dominant role in determining thermal efficiency and pumping power. This issue can be addressed by using polymer films with increased corrugation height (2-5 mm) as opposed to the current height of 1 mm. A larger corrugation height will give a higher hydraulic diameter and therefore a lower pressure loss.

In Chapter Four, the individual design correlations for each fluid system were established. Chapter Eight progresses this by developing unique design correlations that will incorporate all the different fluid systems tested in the square PFCHE. This will make it far easier than using the separate correlations developed for each fluid system, when attempting alternative designs. The unique design correlations are functions of Re and Pr numbers, and were developed using regression analysis (see Table 8.10). It was found that the Pr exponential value ($Pr^{0.42}$), for the PFCHE Nu correlation is slightly higher than the Pr exponential value ($Pr^{0.4}$), for both laminar, Obot et al. (1997) and turbulent heat transfer correlations (Dittus-Boelter equation) in a smooth tube. This observation is encouraging, showing that even at low Re (laminar flow), the square PFCHE can achieve good heat transfer.

(f) Following the investigation on corrugations angles, the surface geometry aspect of the PFCHE is then looked into, whereby the sinusoidal corrugations are compared with six plate fin surface geometries. The summary of the performance comparison study, based on a similar hydraulic diameter (2 mm) for the six surface geometries (wavy, strip, louvered, perforated, pin and plain fins), are shown in Table 9.6. The PFCHE has the highest heat transfer at low Re ($Re<500$) compared to the plate fin geometries. This high heat transfer capability is due to the occurrence of developing flow along the sinusoidal corrugations, which promotes better mixing and therefore leads to heat transfer enhancement. At higher Re, the PFCHE surpasses the pin, perforated and plain fins but loses out to the strip, wavy and louvered fins. The latter is perhaps due to better fluid mixing achieved in the strip, wavy and louvered fins at higher Re numbers. Therefore, it can be concluded that the developing flow in the PFCHE is less effective for heat transfer at higher Re numbers.

It should also be noted that the PFCHE's relatively high friction factors and low goodness factors, as shown in Table 9.6, is not an accurate account of its true potential. This inaccuracy is caused by the different length definitions adopted. The length used in the PFCHE is the flow

length of the exchanger (summation of several corrugation wavelengths), whereas the uninterrupted flow length (one corrugation wavelength) is used for the plate fin geometries, Kays and London (1984). If similar length definitions are adopted, there is a high probability that the overall performance of the PFCHE would vastly improve; to be comparable or even surpass those offered by the plate fin geometries.

g) Acknowledging that the PFCHEs with sinusoidal corrugations are capable of competing with the performance of the plate fin surface geometries, we considered yet another aspect of the PFCHE design, which is the material of construction. All previous chapters in this thesis involve polymer film heat exchangers made from PEEK (poly ether ether ketone). Therefore to investigate the effect of the material of construction, PFCHE performance results using a different type of polymer was compared with the PEEK PFCHE. Due to its impressive properties, PVDF (polyvinylidene fluoride) was selected and compared with PEEK, in an air/air system. Both heat exchangers showed similar trends in the performance plots studied. A summary of the results obtained is shown in Table 9.10. Despite having similar thermal conductivity values, the results show that the overall performance of PEEK is better than the PVDF polymer, by up to a factor of 2. This is mainly due to the use of thinner films for the PEEK exchanger, which lowers the film resistance (t/k). Nevertheless, PVDF can be used as an alternative in applications where PEEK is deemed unsuitable, such as in concentrated sulphuric and nitric acid environments. In the following section, we briefly outline the contributions of this thesis towards the development of the PFCHE technology.

## 10.2 A list of contributions of the work

- Performed a general uncertainty analysis on all PFCHE experiments mentioned in this thesis; covering ten different systems, to show the reliability of the experimental data

- Developed six individual design correlations (Jh and f) for the square PFCHE, involving six fluid systems (air/air, water/water and four glycerol-water mixtures/water) in laminar flow conditions

- Illustrated experimentally through flow visualisation work, that a good degree of mixing is achieved in laminar flows for the PFCHE. The degree of mixing is comparable to the mixing obtained in turbulent conditions

- Developed another set of design correlations (Jh and f) for the spiral PFCHE, involving an air/water system in laminar flow conditions

- Conducted five successful case studies (cabin air cooler, three fuel cell heat exchangers and a car radiator) for the PFCHE, as an alternative design to metallic units used in the aviation, fuel cell transport and automobiles industries

- Showed that the $90^{o}$ corrugation angle is the optimum angle in the square PFCHE, compared to the $30^{o}$ and $60^{o}$ angles

- Developed a set of unique design correlations involving Re and Pr numbers for different fluid systems in the square PFCHE, to enable performance prediction of the PFCHE over a range of fluid systems, ($0.7<Pr<192$)

- Demonstrated that the PFCHE surface geometry (sinusoidal corrugations), outperforms the plain plate fin and is comparable to other plate fin surface geometries (strip, wavy, louvered, pin and perforated fins) having similar hydraulic diameters

- Demonstrated that PEEK films achieve better overall performance than PVDF films, when adopted in the PFCHE design at low Re numbers

Thus, the research objectives for this thesis have indeed been met. However, as is always the case with research, there is room for improvement and certain issues can be addressed to enable a better evaluation of the results obtained, and to further develop the technology. Some recommendations for future work involving the PFCHE are outlined next.

### 10.3 Directions for further research

- The design correlations for the water/water system and the four glycerol-water mixtures/water systems in the square PFCHE, need to be extended over higher Re numbers; at least in the region of $Re\approx2000$ as opposed to the current $100<Re<200$ region. This is important to increase accuracy and avoid extrapolation in future case studies involving similar fluid systems. A higher Re range can be achieved by conducting performance testing at higher flow rates. The Re range for the air/air system at $510<Re<2540$, is considered to be sufficient by representative of the range of laminar flows in the PFCHE.

- For the spiral design correlations, a higher Re range for the water-side needs to be developed, as the current Re range ($2.4<Re<8.4$) is too low. As with the square PFCHE, this extension needs to be looked into to avoid extrapolation for future use in industrial

case studies. In addition, the spiral design for an air/water system needs to address the leaks caused by laser burns on the PEEK films.

- An air/water system can be tested in the square PFCHE, in order to enable a direct PFCHE configuration comparison with the spiral PFCHE, having similar fluid systems. By doing this, the strengths of each design can be established and hence lead to potential improvements.

- On the Pr study, experimental data between the Pr=49 and the Pr=192 systems, need to be obtained to improve the accuracy of the existing design correlations developed in this thesis. Further experimental data involving different Pr systems could produce a better model, and consequently increase the accuracy of the correlations developed.

- For the flow visualisation work, the experimental results obtained can be supported by using computational fluid dynamics (CFD), for a better understanding of the flow behaviour in the polymer matrix.

- More industrial case studies need to be conducted, to demonstrate the ability of the PFCHE as an alternative unit in applications currently dominated by metallic heat exchangers. Apart from heat transfer applications, the possibility of using the PFCHE as a chemical reactor also needs to be investigated.

- Different surface geometries subject to fabrication issues, need to be tested to encourage more flow interruption and heat transfer enhancement in the PFCHE. Perhaps as a starting point, a design similar to that of the strip fin can be tested. In addition, a detailed mechanical testing of the prototype needs to be considered.

- A study on the dynamics and control of a PFCHE could also be looked into, to enable integration into existing chemical plants. As of yet there are no plants built entirely from intensified components due to the lack of knowledge on how the equipment will integrate. Besides the design data, the dynamic responses on intensified equipment are important in plant operation. For instance if the conditions within one unit change, how will this effect the performance of the other units in the plant? Will the existing control methods be sufficient or appropriate with perhaps minor adjustments or will there be new control problems to overcome? Questions like this need to be addressed before operators can install compact equipment with confidence.

## Appendix A-Compact heat exchangers and principal applications

| Type of heat exchanger<br>Features | Plate-and-frame (Gasket) | Partially welded plate | Fully welded Plate (alfaRex) | Brazed plate | Bavex plate | Platular plate | Compabloc plate | Packinox plate | Spiral | Brazed plate fin | Diffusion bonded plate fin | Printed circuit | Polymer (e.g. channel plate) | Plate and shell | Marbond |
|---|---|---|---|---|---|---|---|---|---|---|---|---|---|---|---|
| Compactness ($m^2/m^3$) | → 200 | → 200 | → 200 | → 200 | 200-300 | 200 | → 300 | → 300 | → 200 | 800-1500 | 700-800 | 200-5000 | 450 | - | → 10000 |
| Stream types[1] | liquid-liquid gas-liquid 2-phase | liquid-liquid gas-liquid 2-phase | liquid-liquid gas-liquid 2-phase | liquid-liquid 2-phase | gases liquids 2-phase | gases liquids 2-phase | liquids | gases liquids 2-phase | liquid-liquid 2-phase | gases liquids 2-phase | gases liquids 2-phase | gases liquids 2-phase | gas-liquid (14) | liquids | gases liquids 2-phase |
| Materials[2] | s/s, Ti, Incoloy Hastelloy graphite polymer | s/s Ti Incoloy Hastelloy | s/s Ti Ni alloys | s/s | s/s, Ni, Cu,Ti, special steels | s/s Hastelloy Ni alloys | s/s Ti Incoloy | s/s, Ti Hastelloy Inconel | c/s ,s/s Ti, Incoloy Hastelloy | Al, s/s Ni alloy | Ti s/s | s/s, Ni, Ni alloys Ti | PVDF[20] PP[21] | s/s, Ti (shell also in c/s) [15] | s/s, Ni, Ni alloys, Ti |
| Temperature Range (°C) | -35 to +200 | -35 to +200 | -50 to +350 | -195 to +220 | -200 to +900 | → 700 | → 300 | -200 to +700 | → 400 | Cryogenic t0 +250 | → 550 | -200 to +900 | → 15018 | → 350 | -200 to +900 |
| Maximum Pressure (bar)[3] | 25 | 25 | 40 | 30 | 60 | 40 | 32 | 300 | 25 | 90 | >200 | >400 | 6 | 70 | >400 |
| Cleaning methods | Mech.[19] | Mech.[4,19] Chem.[6] | Chemical | Chem.[5] | Mech.[11,19] Chemical | Mech.[12,19] | Mech.[19] | Mech.[16,19] | Mech.[19] | Chemical | Chemical | Chemical | Water wash | Mech.[16,19] Chem.[17] | Chemical |
| Corrosion resistance | Good[7] | Good[7] | Excellent | Good[8] | Good | Good | Good | Good | Good | Good | Excellent | Excellent | Excellent | Good | Excellent |
| Multi-stream capability | Yes[9] | No | No | No | In principle | Yes[13] | Not usually | Yes[9] | No | Yes | Yes | Yes | No | No | Yes |
| Multi-pass capability | Yes | Yes | Yes | No[10] | Yes | Yes | Yes | Yes | No | Yes | Yes | Yes | Not usually | Yes | Yes |

**Table A.1 Summary of the principle features of several types of compact heat exchangers** (Reay 1999)

s/s =stainless steel,c/s= carbon steel, Ti=titanium,Ni= nickel, Cu=copper, Chem.=chemical, Mech.=mechanical

Notes
1 Two-phase includes boiling and condensing duties
2 Outer special alloys are frequently available
3 The maximum pressure capability is unlikely to occur at the higher operating temperatures, and assumes no pressure/stress-related corrosion
4 On the gasket side
5 Ensure compatibility with copper braze
6 On welded side
7 Function of gasket as well as plate material
8 Function of braze as well as plate material
9 Not common
10 Not in a single unit
11 On tube side
12 Only when flanged access provided, otherwise chemical cleaning
13 Five fluids maximum
14 Condensing on gas side
15 Shell may be composed of polymeric material
16 On shell side
17 On plate side
18 PEEK ( polyetheretherketone) can go to 250°C
19 Can be dismantled
20 Polyvinylidene difluoride
21 Polypropylene

| Heat Exchanger Type | Sector and Application |
|---|---|
| Plate and frame heat exchanger | Chemicals & petrochemicals<br>Food & drink<br>Paper & board<br>Textiles & fabric care<br>Oil & gas processing<br>Prime movers<br>General applications:<br>Refrigeration<br>Air compressors<br>MVR<br>Hazardous stream separation |
| Brazed plate heat exchanger | Chemicals & petrochemicals<br>Food & drink<br>Oil & gas processing<br>Prime movers<br>General applications:<br>Air compressors<br>MVR<br>Refrigeration<br>Hazardous stream separation |
| Welded plate heat exchangers | Chemicals & petrochemicals<br>Food & drink<br>Oil & gas processing |
| Spiral heat exchanger | Chemicals & petrochemicals<br>Paper & board<br>Effluent treatment<br>Generic application:<br>Hazardous stream separation |
| Plate fin heat exchanger | Chemicals & petrochemicals<br>Cryogenics<br>Oil & gas processing<br>Prime movers<br>Generic applications:<br>Refrigeration<br>Hazardous stream separation |
| Printed circuit heat exchanger | Chemicals & petrochemicals<br>Cryogenics<br>Oil & gas processing<br>Prime movers<br>Generic applications:<br>Refrigeration<br>Hazardous stream separation |
| Marbond™ heat exchangers<br>(1. Heat exchangers)<br>(2. Heat exchanger/ reactors) | Chemicals & petrochemicals (1,2)<br>Prime movers (1,2)<br>Process intensification (1,2)<br>Absorption refrigeration (1) |
| Compact shell and tube heat exchangers | Chemicals & petrochemicals<br>Prime movers |
| Compact types retaining a shell | Chemicals & petrochemicals<br>Cryogenics<br>Food & drink |

(Reay 1999)

**Table A.2 Summary of principal application areas of compact heat exchangers**

## Appendix B-Details of the Shell and Tube and the Plate Frame heat exchangers

a) Shell and Tube

| Mechanical design data | | | | |
|---|---|---|---|---|
| Item | | Units | | |
| Tubes: o.d..i.d..thk..pitch, angle | | mm | 19.05 x 14.83 x 2.11 x 25.4 x 90° | |
| Tube material | | - | Carbon steel | |
| No. of tubes per shell | No. of passes | - | 744 | 4 |
| Tube length: overall | effective | m | 5 | 4.764 |
| No. shells in unit | | - | 1 | |
| Arrangement :series | parallel | - | 1S | 1P |
| Surface [1] : one shell | unit | $m^2$ | 212.1 | 212.1 |
| Nozzle i.d. (in/out): shell [2] | tubes | mm | 254.5 / 254.5 | 202.7 / 202.7 |
| Shell i.d. | | mm | 889 | |
| Exchanger type | | - | Split backing ring floating head | |
| TEMA designation | | - | AES | |

(Saunders 1988)

**Table B.1 Details of Shell and Tube heat exchanger**

Notes:

(1) Surface based on tube o.d.

(2) Imping. baffle at inlet.

b) Plate Frame

Constructional Data-The constructional data given below are not related to a particular maker's standard model, but are sufficiently realistic to demonstrate the calculations required.

| | |
|---|---|
| Overall plate size (mm x mm) | 1740 x 550 |
| Effective surface area per plate ($m^2$) | 0.752 |
| Chevron angle ( degrees) | 45 |
| Plate pitch ( m) | 0.0035 |
| Plate thickness (m) | 0.0006 |
| Enlargement factor ($\mu$ ) | 1.17 |
| Total number of plates | 321 |
| Total surface area ($m^2$) | 240 |
| Flow arrangement | Two pass / two pass |
| All port diameters (mm) | 150 |
| Effective channel width (m) | 0.5 |
| Flow length in one pass (m) | 1.5 |

(Saunders 1988)

**Table B.2 Details of Plate Frame heat exchanger**

## Appendix C-Sample calculations of extension factor and hydraulic diameter

Calculation of the extension factor, (F)

The extension factor is the ratio between the real and projected heat transfer area.

(i) Calculation of the effective projected area

The polymer film, which has been used in the square PFCHE, is a corrugated PEEK sheet and is square in shape. The length of each side of the sheet is 13.5 cm.

Each sheet has 66 corrugations (wavelengths)
Therefore one wavelength = 13.5/66 = 2.06 mm

Projected area of one sheet = (13.5 x 13.5) $cm^2$
= 182.25 $cm^2$

As sealant (Araldite 119) is used to seal two sheets at their edges, the occluded area has to be taken into consideration.

Area covered by sealant = (1.5 x 13.5 x 2) $cm^2$
= 40.5 $cm^2$

Therefore the effective projected area of one sheet = (182.25 – 40.5) $cm^2$
= 141.75 $cm^2$

Total effective projected area for heat exchanger having 5 sheets = (141.74 x 3)
(The top and bottom sheets in the matrix are excluded) = 425.22 $cm^2$
= 0.0425 $m^2$

(ii) Calculation of the real heat transfer area

From above it can be concluded that the effective projected area dimension for each polymer sheet is 10.5 cm x 13.5 cm.

Number of corrugation (wavelengths) in 10.5 cm = 10.5/0.2
= 51

Real length of one corrugation = 4 mm

Therefore real width of one sheet = (51 x 4/10) cm
= 20.4 cm

Real dimension of one sheet is 20.4 x 13.5 cm

Real area of one sheet = (20.4 x 13.5) $cm^2$

= 275.4 $cm^2$

Real area of the heat exchanger = (275.4 x 3)

= 826.2 $cm^2$

= 0.08262 $m^2$

Therefore the extension factor (F) = real area/ projected area

= 0.08262/0.0425

= 1.9

The extension factor (F) is equal to 1.9

Calculation of hydraulic diameter, ($d_h$)

$d_h = (4\ A_{ff}\ L)/\ A$

where Aff = minimum free flow area ($m^2$)

L = length of polymer sheet (m)

A = heat transfer area for one sheet ($m^2$)

Minimum free flow area = 0.5 x channel height x length of sheet

= 0.5 x 0.001 x 0.135

= 0.0000675 $m^2$

Heat transfer area = Length of sheet x width of sheet

= 0.135 x 0.135

= 0.0182 $m^2$

Hydraulic diameter = (4 x 0.0000675 x 0.135) / 0.0182

= 2 mm

## Appendix D-Table of results for Square PFCHE

| $F_{hin}$ | $F_{cin}$ | $T_{hin}$ | $T_{hout}$ | $T_{cin}$ | $T_{cout}$ | $\Delta T_h$ | $\Delta T_c$ | HBE | $\Delta P_h$ | $\Delta P_c$ | Re |
|---|---|---|---|---|---|---|---|---|---|---|---|
| $m^3/hr$ | $m^3/hr$ | C | C | C | C | C | C | % | kPa | kPa | |
| 3 | 3 | 23.02 | 21.34 | 20.67 | 22.48 | 1.68 | 1.81 | 7.51 | 1.5 | 0.3 | 511 |
| 4 | 4 | 25.24 | 22.22 | 21.01 | 23.88 | 3.03 | 2.87 | 5.31 | 2.2 | 0.1 | 679 |
| 5 | 5 | 30.27 | 24.18 | 21.20 | 27.56 | 6.08 | 6.37 | 4.39 | 3.4 | 1.0 | 847 |
| 6 | 6 | 32.04 | 26.00 | 22.8 | 29.12 | 6.04 | 6.32 | 4.23 | 5.0 | 2.0 | 1014 |
| 7 | 7 | 36.02 | 28.30 | 23.96 | 32.02 | 7.72 | 8.06 | 4.17 | 6.7 | 2.5 | 1179 |
| 8 | 8 | 37.25 | 28.72 | 23.15 | 31.23 | 8.53 | 8.08 | 5.44 | 8.1 | 3.9 | 1349 |
| 9 | 9 | 37.28 | 29.00 | 23.58 | 31.44 | 8.28 | 7.86 | 5.25 | 9.9 | 4.3 | 1516 |
| 10 | 10 | 34.34 | 25.26 | 18.21 | 26.83 | 9.08 | 8.62 | 5.19 | 12.1 | 5.1 | 1691 |
| 11 | 11 | 32.63 | 24.48 | 17.99 | 25.76 | 8.15 | 7.77 | 4.77 | 15.4 | 8.3 | 1862 |
| 12 | 12 | 31.92 | 24.69 | 18.74 | 25.66 | 7.23 | 6.92 | 4.35 | 17.8 | 10.0 | 2031 |
| 13 | 13 | 32.29 | 25.47 | 19.56 | 26.10 | 6.82 | 6.55 | 4.13 | 20.1 | 11.0 | 2200 |
| 14 | 14 | 31.28 | 25.19 | 19.85 | 25.72 | 6.08 | 5.86 | 3.74 | 23.3 | 13.1 | 2370 |
| 15 | 15 | 31.18 | 25.45 | 20.19 | 25.73 | 5.73 | 5.54 | 3.41 | 27.4 | 15.0 | 2539 |

**Table D.1 Results for the air/air system in a square PFCHE with a 90° corrugation angle**

(continued on next page)

| $F_{hin}$ | $F_{cin}$ | $T_{hin}$ | $T_{hout}$ | $T_{cin}$ | $T_{cout}$ | $\Delta T_h$ | $\Delta T_c$ | HBE | $\Delta P$ | Re |
|---|---|---|---|---|---|---|---|---|---|---|
| $m^3/hr$ | $m^3/hr$ | C | C | C | C | C | C | % | kPa | |
| 0.44 | 0.44 | 25.90 | 18.40 | 13.60 | 21.30 | 7.50 | 7.70 | 2.67 | n/a | 87.44 |
| 0.46 | 0.46 | 25.70 | 18.80 | 13.70 | 20.10 | 6.90 | 6.40 | 7.25 | 0.36 | 91.54 |
| 0.48 | 0.48 | 26.90 | 20.50 | 15.10 | 21.10 | 6.40 | 6.00 | 6.25 | n/a | 96.12 |
| 0.50 | 0.50 | 26.70 | 20.30 | 14.70 | 20.80 | 6.40 | 6.10 | 4.69 | 0.40 | 100.45 |
| 0.52 | 0.52 | 25.90 | 19.80 | 15.00 | 20.70 | 6.10 | 5.70 | 6.56 | n/a | 103.58 |
| 0.54 | 0.54 | 25.20 | 19.00 | 13.60 | 19.60 | 6.20 | 6.00 | 3.23 | 0.44 | 108.40 |
| 0.56 | 0.56 | 25.20 | 20.00 | 15.20 | 20.30 | 5.20 | 5.10 | 1.92 | n/a | 112.01 |
| 0.58 | 0.58 | 25.30 | 20.10 | 15.50 | 20.60 | 5.20 | 5.10 | 1.92 | 0.50 | 115.63 |
| 0.62 | 0.62 | 24.40 | 19.80 | 15.20 | 19.70 | 4.60 | 4.50 | 2.17 | 0.55 | 124.06 |
| 0.66 | 0.66 | 22.80 | 18.20 | 13.60 | 18.00 | 4.60 | 4.40 | 4.35 | 0.59 | 132.49 |
| 0.71 | 0.71 | 22.90 | 18.80 | 14.50 | 18.50 | 4.10 | 4.00 | 2.44 | 0.63 | 142.13 |
| 0.75 | 0.75 | 22.00 | 18.00 | 13.50 | 17.40 | 4.00 | 3.90 | 2.50 | 0.68 | 150.56 |
| 0.79 | 0.79 | 21.80 | 18.00 | 13.50 | 17.20 | 3.80 | 3.70 | 2.63 | 0.73 | 158.99 |
| 0.84 | 0.84 | 22.10 | 18.70 | 14.30 | 17.70 | 3.40 | 3.40 | 0.00 | 0.77 | 168.62 |
| 0.89 | 0.89 | 21.80 | 18.60 | 14.20 | 17.50 | 3.20 | 3.30 | 3.13 | 0.84 | 178.26 |
| 0.93 | 0.93 | 21.10 | 18.10 | 13.70 | 16.80 | 3.00 | 3.10 | 3.33 | 0.90 | 186.69 |
| 0.97 | 0.97 | 24.90 | 20.40 | 13.50 | 18.10 | 4.50 | 4.60 | 2.22 | 0.96 | 195.12 |
| 1.02 | 1.02 | 23.30 | 18.80 | 12.50 | 16.90 | 4.50 | 4.40 | 2.22 | 1.03 | 204.76 |
| 1.07 | 1.07 | 22.80 | 18.40 | 12.20 | 16.50 | 4.40 | 4.30 | 2.27 | 1.09 | 214.39 |

| $F_{hin}$ | $F_{cin}$ | $T_{hin}$ | $T_{hout}$ | $T_{cin}$ | $T_{cout}$ | $\Delta T_h$ | $\Delta T_c$ | HBE | $\Delta P$ | Re |
|---|---|---|---|---|---|---|---|---|---|---|
| $m^3/hr$ | $m^3/hr$ | C | C | C | C | C | C | % | kPa | |
| 1.12 | 1.12 | 23.00 | 18.90 | 12.60 | 16.80 | 4.10 | 4.20 | 2.44 | 1.16 | 224.03 |
| 1.17 | 1.17 | 22.40 | 18.40 | 12.00 | 16.10 | 4.00 | 4.10 | 2.50 | 1.23 | 234.87 |

(continued from previous page)

**Table D.2 Results for the water/water system in a square PFCHE with a 90° corrugation angle**

| $F_{hin}$ | $F_{cin}$ | $T_{hin}$ | $T_{hout}$ | $T_{cin}$ | $T_{cout}$ | $\Delta T_h$ | $\Delta T_c$ | HBE | $\Delta P$ | Re |
|---|---|---|---|---|---|---|---|---|---|---|
| $m^3/hr$ | $m^3/hr$ | C | C | C | C | C | C | % | kPa | |
| 0.22 | 0.22 | 39.70 | 18.30 | 10.50 | 20.10 | 21.40 | 9.60 | 6.65 | 0.48 | 18.59 |
| 0.37 | 0.37 | 33.10 | 19.90 | 10.00 | 19.90 | 13.20 | 9.90 | 6.94 | 0.88 | 30.98 |
| 0.49 | 0.49 | 31.40 | 21.00 | 11.00 | 21.00 | 10.40 | 10.00 | 3.22 | 1.34 | 44.40 |
| 0.63 | 0.63 | 29.70 | 21.50 | 10.70 | 20.60 | 8.20 | 9.90 | 1.72 | 1.61 | 52.67 |
| 0.80 | 0.80 | 27.90 | 21.50 | 10.40 | 20.20 | 6.40 | 9.80 | 1.24 | 2.23 | 67.12 |
| 0.94 | 0.94 | 26.70 | 21.20 | 10.10 | 19.40 | 5.50 | 9.30 | 4.37 | 2.98 | 82.61 |

Pr=19

**Table D.3 Results for the glycerol 30% + water/water system in a square PFCHE with a 90° corrugation angle**

| $F_{hin}$ | $F_{cin}$ | $T_{hin}$ | $T_{hout}$ | $T_{cin}$ | $T_{cout}$ | $\Delta T_h$ | $\Delta T_c$ | HBE | $\Delta P$ | Re |
|---|---|---|---|---|---|---|---|---|---|---|
| $m^3/hr$ | $m^3/hr$ | C | C | C | C | C | C | % | kPa | |
| 0.20 | 0.20 | 41.70 | 17.70 | 10.00 | 20.10 | 24.00 | 10.10 | 7.90 | 0.70 | 11.84 |
| 0.34 | 0.34 | 34.50 | 18.60 | 9.70 | 19.80 | 15.90 | 10.10 | 0.50 | 1.24 | 19.50 |
| 0.47 | 0.47 | 31.70 | 20.10 | 10.30 | 20.40 | 11.60 | 10.10 | 2.08 | 1.82 | 29.24 |
| 0.59 | 0.59 | 30.00 | 21.40 | 10.10 | 19.70 | 8.60 | 9.60 | 0.08 | 2.24 | 34.12 |
| 0.76 | 0.76 | 27.90 | 21.30 | 9.60 | 19.00 | 6.60 | 9.40 | 0.85 | 2.93 | 43.87 |

Pr=30

**Table D.4 Results for the glycerol 40% + water/water system in a square PFCHE with a 90° corrugation angle**

| $F_{hin}$ | $F_{cin}$ | $T_{hin}$ | $T_{hout}$ | $T_{cin}$ | $T_{cout}$ | $\Delta T_h$ | $\Delta T_c$ | HBE | $\Delta P$ | Re |
|---|---|---|---|---|---|---|---|---|---|---|
| $m^3/hr$ | $m^3/hr$ | C | C | C | C | C | C | % | kPa | |
| 0.21 | 0.21 | 28.00 | 14.90 | 10.00 | 15.10 | 13.10 | 5.10 | 0.30 | 0.88 | 7.56 |
| 0.31 | 0.31 | 23.50 | 16.30 | 10.60 | 15.10 | 7.20 | 4.50 | 7.73 | 1.70 | 11.56 |
| 0.43 | 0.43 | 21.30 | 16.00 | 9.90 | 14.40 | 5.30 | 4.50 | 6.00 | 1.85 | 16.00 |
| 0.54 | 0.54 | 20.00 | 15.70 | 9.90 | 14.10 | 4.30 | 4.20 | 2.20 | 3.06 | 20.00 |
| 0.66 | 0.66 | 19.30 | 15.40 | 10.00 | 14.50 | 3.90 | 4.50 | 5.73 | 4.20 | 24.44 |

Pr=49

**Table D.5 Results for the glycerol 50% + water/water system in a square PFCHE with a 90° corrugation angle**

| $F_{hin}$ | $F_{cin}$ | $T_{hin}$ | $T_{hout}$ | $T_{cin}$ | $T_{cout}$ | $\Delta T_h$ | $\Delta T_c$ | HBE | $\Delta P$ | Re |
|---|---|---|---|---|---|---|---|---|---|---|
| $m^3/hr$ | $m^3/hr$ | C | C | C | C | C | C | % | kPa | |
| 0.18 | 0.18 | 31.50 | 13.20 | 9.40 | 15.00 | 18.30 | 5.60 | 1.29 | 15.2 | 1.86 |
| 0.31 | 0.31 | 39.30 | 21.10 | 9.60 | 19.80 | 18.20 | 10.20 | 4.12 | 32.4 | 3.11 |
| 0.35 | 0.35 | 35.20 | 20.00 | 10.10 | 19.40 | 15.20 | 9.30 | 2.04 | 46.3 | 3.85 |
| 0.44 | 0.44 | 31.00 | 18.50 | 8.30 | 17.80 | 12.50 | 9.50 | 0.61 | 55.0 | 4.60 |

Pr=192

**Table D.6 Results for the glycerol 70% + water/water system in a square PFCHE with a 90° corrugation angle**

| $F_{hin}$ | $F_{cin}$ | $T_{hin}$ | $T_{hout}$ | $T_{cin}$ | $T_{cout}$ | $\Delta T_h$ | $\Delta T_c$ | HBE | $\Delta P$ | Re |
|---|---|---|---|---|---|---|---|---|---|---|
| $m^3/hr$ | $m^3/hr$ | C | C | C | C | C | C | % | kPa | |
| 5.0 | 5.0 | 35.7 | 24.5 | 18.6 | 28.4 | 11.2 | 9.8 | 12.4 | 13.2 | 706.6 |
| 6.0 | 6.0 | 37.0 | 23.3 | 17.7 | 30.9 | 13.7 | 13.2 | 3.6 | 18.7 | 848.0 |
| 7.0 | 7.0 | 39.2 | 24.5 | 18.0 | 32.5 | 14.7 | 14.5 | 1.4 | 25.1 | 989.3 |
| 8.0 | 8.0 | 37.1 | 24.1 | 18.2 | 31.0 | 13.0 | 12.8 | 1.5 | 31.1 | 1130.6 |
| 9.0 | 9.0 | 37.1 | 24.6 | 18.6 | 31.0 | 12.5 | 12.4 | 0.8 | 39.2 | 1271.9 |
| 10.0 | 10.0 | 35.8 | 24.5 | 18.7 | 30.1 | 11.3 | 11.4 | 0.9 | 16.4 | 1413.3 |
| 11.0 | 11.0 | 34.2 | 24.0 | 19.0 | 29.0 | 10.2 | 10.0 | 2.0 | 49.7 | 1554.6 |

**Table D.7 Results for the air/air system in a square PFCHE with a 30° corrugation angle**

| $F_{hin}$ | $F_{cin}$ | $T_{hin}$ | $T_{hout}$ | $T_{cin}$ | $T_{cout}$ | $\Delta T_h$ | $\Delta T_c$ | HBE | $\Delta P$ | Re |
|---|---|---|---|---|---|---|---|---|---|---|
| $m^3/hr$ | $m^3/hr$ | C | C | C | C | C | C | % | kPa | |
| 5.0 | 5.0 | 38.8 | 28.0 | 22.0 | 31.6 | 10.8 | 9.6 | 11.1 | 3.7 | 706.6 |
| 6.0 | 6.0 | 36.8 | 27.7 | 22.2 | 30.7 | 9.1 | 8.5 | 6.6 | 5.2 | 848.0 |
| 7.0 | 7.0 | 37.6 | 27.3 | 21.3 | 31.3 | 10.3 | 10.0 | 2.9 | 8.3 | 989.3 |
| 8.5 | 8.5 | 36.9 | 28.4 | 22.5 | 31.8 | 8.5 | 9.3 | 9.4 | 11.3 | 1201.3 |
| 9.5 | 9.5 | 40.0 | 29.4 | 23.1 | 33.1 | 10.6 | 10.0 | 5.7 | 13.9 | 1342.6 |
| 10.0 | 10.0 | 39.5 | 29.4 | 23.3 | 33.0 | 10.1 | 9.7 | 4.0 | 15.4 | 1413.3 |
| 11.0 | 11.0 | 38.1 | 27.9 | 21.7 | 31.4 | 10.2 | 9.7 | 4.9 | 14.5 | 1554.6 |
| 12.0 | 12.0 | 40.6 | 28.8 | 22.0 | 32.6 | 11.8 | 10.6 | 9.9 | 16.0 | 1695.9 |
| 13.0 | 13.0 | 39.5 | 28.6 | 22.4 | 32.2 | 10.9 | 9.8 | 10.0 | 18.2 | 1837.2 |
| 14.0 | 14.0 | 38.2 | 28.5 | 22.4 | 32.0 | 9.7 | 9.6 | 1.0 | 19.0 | 1978.6 |
| 15.0 | 15.0 | 37.7 | 28.5 | 22.7 | 31.3 | 9.2 | 8.6 | 6.5 | 23.6 | 2119.9 |
| 16.0 | 16.0 | 39.6 | 29.4 | 22.6 | 32.3 | 10.2 | 9.7 | 4.9 | 26.6 | 2261.2 |
| 17.0 | 17.0 | 39.5 | 29.5 | 23.0 | 32.2 | 10.0 | 9.2 | 8.0 | 29.5 | 2402.5 |

**Table D.8 Results for the air/air system in a square PFCHE with a 60° corrugation angle**

| $F_{hin}$ | $F_{cin}$ | $T_{hin}$ | $T_{hout}$ | $T_{cin}$ | $T_{cout}$ | $\Delta T_h$ | $\Delta T_c$ | HBE | $\Delta P$ | Re |
|---|---|---|---|---|---|---|---|---|---|---|
| $m^3/hr$ | $m^3/hr$ | C | C | C | C | C | C | % | kPa | |
| 3.0 | 3.0 | 21.1 | 20.6 | 20.2 | 20.7 | 0.5 | 0.5 | 0.0 | 0.32 | 377 |
| 3.5 | 3.5 | 21.8 | 20.9 | 20.1 | 21.1 | 0.9 | 1.0 | -11.1 | 0.37 | 440 |
| 4.0 | 4.0 | 21.8 | 20.7 | 19.8 | 21.1 | 1.1 | 1.3 | -18.2 | 0.44 | 502 |
| 4.5 | 4.5 | 23.1 | 21.5 | 20.0 | 21.8 | 1.6 | 1.8 | -12.5 | 0.54 | 565 |
| 5.0 | 5.0 | 27.4 | 24.4 | 21.9 | 25.1 | 3.0 | 3.2 | -6.7 | 0.53 | 628 |
| 5.5 | 5.5 | 28.8 | 24.8 | 22.4 | 25.9 | 4.0 | 3.5 | 12.5 | 0.82 | 691 |
| 6.0 | 6.0 | 29.8 | 25.1 | 22.4 | 26.4 | 4.7 | 4.0 | 14.9 | 0.92 | 754 |
| 6.5 | 6.5 | 30.9 | 25.6 | 22.4 | 27.2 | 5.3 | 4.8 | 9.4 | 1.12 | 817 |
| 7.0 | 7.0 | 31.3 | 24.9 | 21.5 | 26.9 | 6.4 | 5.4 | 15.6 | 1.22 | 879 |
| 7.5 | 7.5 | 33.1 | 26.5 | 22.6 | 28.5 | 6.6 | 5.9 | 10.6 | 1.56 | 942 |
| 8.0 | 8.0 | 32.9 | 25.7 | 21.8 | 28.0 | 7.2 | 6.2 | 13.9 | 1.59 | 1005 |
| 8.5 | 8.5 | 34.8 | 27.3 | 22.8 | 29.7 | 7.5 | 6.9 | 8.0 | 1.93 | 1068 |
| 9.0 | 9.0 | 35.5 | 27.1 | 22.4 | 29.8 | 8.4 | 7.4 | 11.9 | 2.12 | 1131 |
| 9.5 | 9.5 | 36.6 | 28.1 | 22.7 | 30.8 | 8.5 | 8.1 | 4.7 | 2.41 | 1193 |
| 10.0 | 10.0 | 37.2 | 28.4 | 22.8 | 31.1 | 8.8 | 8.3 | 5.7 | 2.57 | 1256 |

**Table D.9 Results for the air/air system in a square PVDF PFCHE with a 90° corrugation angle**

## Appendix E-Table of results for the Spiral PFCHE

| $F_h$ (air) | $F_c$ (water) | $Th_{in}$ | $Th_{out}$ | $Tc_{in}$ | $Tc_{out}$ | $\Delta T_h$ | $\Delta T_c$ | HBE | $\Delta P_h$ | Re air |
|---|---|---|---|---|---|---|---|---|---|---|
| $m^3/hr$ | $cm^3/min$ | C | C | C | C | C | C | % | kPa | |
| 5 | 20 | 28.26 | 25.23 | 21.55 | 25.48 | 3.03 | 3.92 | 6.12 | 0.5 | 244.77 |
| 6 | 20 | 27.56 | 24.56 | 20.89 | 25.08 | 3.00 | 4.20 | 4.38 | 0.7 | 294.56 |
| 7 | 20 | 28.18 | 26.28 | 22.78 | 26.18 | 1.89 | 3.40 | 5.45 | 0.4 | 341.99 |
| 8 | 20 | 26.17 | 24.28 | 20.94 | 24.28 | 1.89 | 3.00 | 9.37 | 0.5 | 394.12 |
| 9 | 20 | 25.40 | 24.10 | 20.49 | 23.48 | 1.30 | 3.41 | 4.44 | 0.3 | 444.28 |
| 10 | 20 | 26.85 | 25.43 | 22.22 | 25.63 | 1.42 | 3.48 | 1.04 | 0.5 | 490.78 |
| 11 | 20 | 26.48 | 25.30 | 22.05 | 25.52 | 1.18 | 3.22 | 9.32 | 0.5 | 540.21 |
| 12 | 20 | 26.17 | 25.15 | 22.08 | 25.30 | 1.02 | 2.35 | 7.31 | 0.5 | 590.12 |
| 13 | 20 | 25.76 | 24.98 | 22.27 | 24.62 | 0.79 | 2.65 | 5.11 | 0.4 | 640.08 |
| 14 | 20 | 24.77 | 23.95 | 20.38 | 23.03 | 0.82 | 3.65 | 5.25 | 0.4 | 692.23 |
| 15 | 20 | 24.01 | 23.25 | 20.24 | 23.27 | 0.76 | 3.03 | 7.81 | 0.5 | 743.96 |

**Table E.1 Results for the constant water flow rate at 20 $cm^3/min$ in a spiral PFCHE**

| $F_h$ (air) | $F_c$ (water) | $Th_{in}$ | $Th_{out}$ | $Tc_{in}$ | $Tc_{out}$ | $\Delta T_h$ | $\Delta T_c$ | HBE | $\Delta P_h$ | Re air |
|---|---|---|---|---|---|---|---|---|---|---|
| $m^3/hr$ | $cm^3/min$ | C | C | C | C | C | C | % | kPa | |
| 5 | 50 | 25.18 | 22.26 | 19.92 | 21.60 | 2.92 | 1.67 | 14.55 | 0.1 | 247.89 |
| 6 | 50 | 25.45 | 22.62 | 19.42 | 21.19 | 2.83 | 1.78 | 6.21 | 0.1 | 297.07 |
| 7 | 50 | 25.43 | 23.21 | 20.15 | 21.84 | 2.22 | 1.68 | 9.93 | 0.1 | 346.17 |
| 8 | 50 | 23.66 | 23.62 | 21.85 | 21.88 | 0.04 | 0.03 | 1.98 | 0.5 | 396.76 |
| 9 | 50 | 22.97 | 22.91 | 21.37 | 21.42 | 0.06 | 0.06 | 5.30 | 0.8 | 447.67 |
| 10 | 50 | 25.68 | 24.03 | 20.94 | 22.67 | 1.64 | 1.73 | 7.32 | 1.1 | 493.42 |
| 11 | 50 | 22.58 | 22.52 | 21.77 | 21.83 | 0.06 | 0.06 | 7.57 | 1.0 | 548.05 |
| 12 | 50 | 23.00 | 21.77 | 19.02 | 20.51 | 1.22 | 1.48 | 2.61 | 0.9 | 598.30 |
| 13 | 50 | 22.52 | 21.36 | 18.91 | 20.35 | 1.16 | 1.44 | 3.43 | 1.3 | 649.38 |
| 14 | 50 | 22.60 | 21.44 | 18.95 | 20.68 | 1.16 | 1.73 | 7.11 | 1.5 | 699.08 |
| 15 | 50 | 23.47 | 22.21 | 19.39 | 21.34 | 1.26 | 1.95 | 4.67 | 1.3 | 746.42 |

**Table E.2 Results for the constant water flow rate at 50 $cm^3/min$ in a spiral PFCHE**

| $F_h$ (air) | $F_c$ (water) | $Th_{in}$ | $Th_{out}$ | $Tc_{in}$ | $Tc_{out}$ | $\Delta T_h$ | $\Delta T_c$ | HBE | $\Delta P_h$ | Re air |
|---|---|---|---|---|---|---|---|---|---|---|
| $m^3/hr$ | $cm^3/min$ | C | C | C | C | C | C | % | kPa | |
| 5 | 80 | 21.47 | 21.00 | 17.74 | 17.99 | 0.47 | 0.25 | 41.32 | 1.0 | 250.51 |
| 6 | 80 | 19.36 | 18.79 | 17.32 | 17.15 | 0.57 | 0.17 | 18.69 | 1.2 | 303.38 |
| 7 | 80 | 20.62 | 20.24 | 17.89 | 18.04 | 0.38 | 0.14 | 13.35 | 0.9 | 351.91 |

| $F_h$ (air) | $F_c$ (water) | $Th_{in}$ | $Th_{out}$ | $Tc_{in}$ | $Tc_{out}$ | $\Delta T_h$ | $\Delta T_c$ | HBE | $\Delta P_h$ | Re air |
|---|---|---|---|---|---|---|---|---|---|---|
| $m^3/hr$ | $cm^3/min$ | C | C | C | C | C | C | % | kPa | |
| 8 | 50 | 18.91 | 18.62 | 17.29 | 17.43 | 0.29 | 0.14 | 5.00 | 1.2 | 405.05 |
| 9 | 50 | 19.88 | 19.44 | 16.67 | 16.94 | 0.43 | 0.27 | 10.64 | 1.2 | 453.94 |
| 10 | 50 | 19.68 | 19.21 | 16.94 | 17.21 | 0.47 | 0.27 | 6.25 | 1.2 | 504.84 |
| 11 | 50 | 17.55 | 17.03 | 14.65 | 14.99 | 0.52 | 0.34 | 3.56 | 1.4 | 560.48 |
| 12 | 50 | 19.85 | 19.40 | 17.56 | 17.90 | 0.44 | 0.34 | 2.88 | 0.9 | 605.34 |
| 13 | 50 | 21.04 | 20.46 | 18.56 | 19.02 | 0.58 | 0.46 | 1.25 | 1.2 | 652.65 |
| 14 | 50 | 22.37 | 22.03 | 18.47 | 18.77 | 0.34 | 0.30 | 2.27 | 1.0 | 698.55 |
| 15 | 50 | 22.46 | 21.97 | 20.03 | 20.50 | 0.49 | 0.47 | 3.79 | 0.9 | 748.39 |

**Table E.3 Results for the constant water flow rate at 80 $cm^3$/min in a spiral PFCHE**

## Appendix F-Sample calculations of PFCHE performance evaluation

This section contains the numerical procedure that needs to be carried out on the raw experimental data in order to be able to obtain the overall and individual heat transfer coefficients, and the Colburn and friction factors. This procedure has also been made into spreadsheet, for ease of computation. This spreadsheet has not been attached as part of this thesis. The following shows a performance calculation for the actual $4m^3$/hr run (air/air system) conducted in the square PFCHE.

### Heat transfer characteristics

#### Input data

| The following data is required: | | Cold stream inlet temperature | 21.01°C |
|---|---|---|---|
| Hot stream inlet temperature | 25.24°C | Cold stream outlet temperature | 23.88°C |
| Hot stream outlet temperature | 22.22°C | Flow rate | 4 $m^3$/hr |

#### Effectiveness

Effectiveness is given by the ratio of the actual heat transfer transferred between the fluids and the maximum heat transfer that can be achieved.

$$E = Q_{act}/Q_{max} \qquad (F.1)$$

= m cp $\Delta$T of either the hot or cold fluid stream / $(m\ cp)_{min}\ (\Delta T)_{max}$

where m = mass flow rate = 0.0014 kg/s

cp = specific heat transfer capacity = 1045.96 J/kgK

$Q_{act}$ = 0.0014 x 1045.96 x (25.24-22.22)

= 4.55 W

$Q_{max}$ = 0.0014 x 1045.96 x (25.24-21.01)

= 6.357

E = 4.55/6.357 = 0.7157

#### Number of transfer units

The NTU can be found using the expression below by iteration.

$$E = 1-\exp(-2\ NTU)\ [I_o(2\ NTU)+I_1(2\ NTU)] \qquad (F.2)$$

where $I_n$ = nth order modified Bessel function

NTU = 3.7968

Overall heat transfer coefficient

The overall heat transfer is calculated from the following expression

$$NTU = UA/C_{min} \qquad (F.3)$$

Where U = overall heat transfer coefficient ($W/m^2K$)

A = free flow area ($m^2$)

$C_{min}$ = minimum value of (m cp)

$U = (3.7968 \times 1.5022)/0.05$

$= 104.32\ W/m^2K$

Individual heat transfer coefficient

The individual heat transfer coefficient can be determined from the equation:

$$1/U = 2/h + t/k \qquad (F.4)$$

$$h = 2/ ((1/U) - (t/k)) \qquad (F.5)$$

where t = thickness of PEEK film (m)

k = thermal conductivity of PEEK film (W/mK)

$h = 2/ ((1/104.32) - (0.0001/0.237))$

$= 218.25\ W/m^2K$

Colburn factor

The Colburn factor is given by $Jh = St\ Pr^{2/3}$

Where St = Stanton number = Nu/(Re Pr) (F.6)

Nu = Nusselt number = $(h\ d_h)/k$ (F.7)

$= (218.2 \times 0.002)/ 0.046 = 9.5$

Re = Reynolds number = $(\rho\ v\ d_h)/\mu$ (F.8)

$= (1.293 \times 8.2 \times 0.002)/0.0000135 = 680$

Pr = Prandtl number = $(cp\ \mu)/k = 0.7$ (F.9)

v = velocity = flowrate/ free flow area (F.10)

= 0.0011/0.000135 = 8.2 m/s

Hence $Jh = (Nu/Re\ Pr)\ Pr^{2/3}$ (F.11)

$= (Nu/Re\ Pr^{1/3})$

$= 0.01564$

## Pressure drop characteristics

### Input data

Hot fluid stream pressure drop = 2.2 kPa

### Friction factor

The friction factor is given by:

$f = (2\ \Delta P\ d_h)/(4\ \rho\ v^2\ L)$ (F.12)

$= (2 \times 2200 \times 0.002)/(4 \times 1.293 \times 8.2^2 \times 0.135)$

$= 0.186$

## Pumping power characteristics

The pumping power is calculated using the expression below:

$E = \tau\ v$ (F.13)

where $E$ = pumping power ($W/m^2$)

$\tau$ = wall shear stress ($N/m^2$) = $0.5\ f\ \rho\ v^2 = 8.148$

$E = 8.148 \times 8.2$

$= 67.06\ W/m^2$

## Goodness factor

The goodness factor is the ratio between the Colburn and friction factors.

$Jh/f = 0.01564/0.186 \quad = 0.084$ (F.14)

## Appendix G-Sample calculations of PFCHE case study

This section contains the numerical procedure that needs to be carried out to produce an alternative PFCHE design for a selected application, based on the specifications given for a conventional design. The case study is deemed successful when the alternative design can match the specifications; in particular the duty required and pressure drop limitations, whilst achieving considerable weight and cost savings.

The parameters that decide the heat transfer credibility of the study are *Areq* and *Ageo* respectively. *Areq* is the heat transfer area required to match the specified duty and *Ageo* is the alternative design's heat transfer area. If (*Ageo>Areq)*, then the design is suitable as long as the pressure drop limitations are adhered to. This can be checked using the friction factor calculated.

The procedure has also been made into a spreadsheet, for ease of computation. This spreadsheet has not been attached as part of this thesis. The following shows a case study calculation for the cabin air cooler using the design correlations (Jh and f) for a square PFCHE in an air/air system.

Specification

Hot stream inlet temperature = 518K Flow rate = 0.33 kg/s

Hot stream outlet temperature = 433K Pressure drop = 4.1 kPa

Cold stream inlet temperature = 398K

Cold stream outlet temperature = 478K

The physical properties of each stream are determined using the physical property formula for air as the function of its inlet and outlet temperatures.

$$cp(t) = 0.0004 \times ((t_1 + t_2)/2)^2 + 0.0163 \times ((t_1+t_2)/2) + 1005.9 \quad (J/kgK) \quad (G.1)$$

$$\mu(t) = -4 \times 10^{-11} \times ((t_1+t_2/2)^2 + 5 \times 10^{-8} \times ((t_1+t_2)/2) + 0.00002 \quad (Ns/m^2) \quad (G.2)$$

$$k(t) = -0.00000002 \times ((t_1+t_2)/2)^2 + 0.00008 \times ((t_1+t_2)/2) + 0.024 \quad (W/mK) \quad (G.3)$$

$$\rho(p,t) = p \text{ in (atm)} \times 10^5/(287 \times (273.15 + t)) \quad (kg/m^3) \quad (G.4)$$

Duty

Q hot stream = 28.921 kW

Q cold stream = 27.057 kW

Heat balance error generated is 6.4%

Colburn factor

Using the Jh correlation for an air/air system,

$Jh = 2.0097\ Re^{-0.7644}$ (G.5)

| Hot air stream | Cold air stream |
|---|---|
| Re = 581.62 | Re = 609.97 |
| Jh = 0.0152 | Jh = 0.0149 |

Heat transfer coefficient

Using $h = Jh\ k\ Re / dh\ Pr^{-0.33}$ (G.6)

| Hot air stream | Cold air stream |
|---|---|
| $h = 160.524\ W/m^2K$ | $h = 152.017\ W/m^2K$ |

Overall heat transfer coefficient

Using $U = 1/((\ 1/h_1)+(1/h_2)\ +(t/k))$ (G.7)

$U = 77.165\ W/m^2K$

t = thickness of PEEK film = 0.0001m

k = thermal conductivity of PEEK = 0.2W/mK

Effectiveness

$E=Q_{act} / Q_{max} = 0.71$ (G.8)

$Q_{act} = (mcp)_h \times \Delta T_h$ or $(mcp)_c \times \Delta T_c$

$Q_{max} = \min ((mcp)_h,(\ mcp)_c) \times \Delta T_{max}$

$\Delta T_{max} = Th_{in} - Tc_{in}$

subscripts h and c refer to hot and cold streams respectively

Number of transfer units

NTU first determined iteratively using E-Bessel function.

$E = 1\text{-}exp\ (-2\ NTU)\ [I_o(2\ NTU)+I_1(2\ NTU)]$ (G.9)

$= 3.66$

Heat transfer area

Using $A = (C_{min}\ NTU)/U$ (G.10)

***Areq* = 16.046 $m^2$**

$C_{min} = \min ((mcp)_h,(\ mcp)_c)$ (G.11)

This is also known as *Areq* or the heat transfer area required, adhering to the specifications.

Geometry Calculations

Here the alternative design begins by selecting arbitrary values for the following:

Length of sheet = 0.2 m

Width of sheet = 0.3 m

Number of sheets= 270

Number of sheets for heat transfer = 268

Number of flow passages = 267

Free flow area

$A_{ff}$ = 0.5 x 0.3 x height of channel (0.001) x 267 (G.12)

= 0.04 $m^2$ (used to determine the velocity and Re used above)

Heat transfer area

A = 0.2 x 0.3 x 268 (G.13)

***Ageo* = 16.08$m^2$**

This is also known as *Ageo* or the heat transfer achieved with respect to the alternative design geometry. **Since *Ageo* > *Areq*, the design is deemed suitable.** Next we have to check the pressure drop to ensure that it falls within the specification.

Pressure drop calculations

Using $f = 0.5992\ Re^{-0.1698}$ (G.14)

$\Delta P = (4\ f\ \rho\ v^2\ L)/(2\ d_h)$ (G.15)

= 1.78 kPa

**The pressure drop calculated is less than the specification value of 4.1 kPa, therefore the design is accepted**.

Weight calculations

Volume of PEEK unit = *Ageo* x thickness of PEEK film (G.16)

= 0.001608 $m^3$

Weight of PEEK unit = Volume of unit x density of PEEK (1250 kg/$m^3$) (G.17)

= 2.01 kg

Weight saving = Weight of aluminium unit – (G.18)

2(weight of PEEK unit) to account for manifold

= 40- 2(2.01)

= 35.98 kg

Percentage weight saving = 100- [(40 – 2(2.36)) /40) x 100] (G.19)

= 88%

Cost calculations

Weight of a 747 plane = 400 tonnes or 40543 kg

Fuel used during flight = 10 tonnes or 10136 kg

Total fleet flying hours in the last 12 months (Year 2000) = 34060073

Cost of one tonne of aviation fuel = £294.54

Fuel used to lift 1 kg in 1 hr = 10/400 = 0.025 (G.20)

Total fuel saving per year = 34060073 x 0.025 x 35.27 (weight saving in kg) (G.21)

= 30037593.79 kg

= 29632 tonnes

Total yearly saving = 29632 x 296.54 (G.22)

= **£8.7M**

## Appendix H-Surface diagrams and details of Plate Fin heat exchangers

Surface Diagrams for the Plate Fin heat exchangers

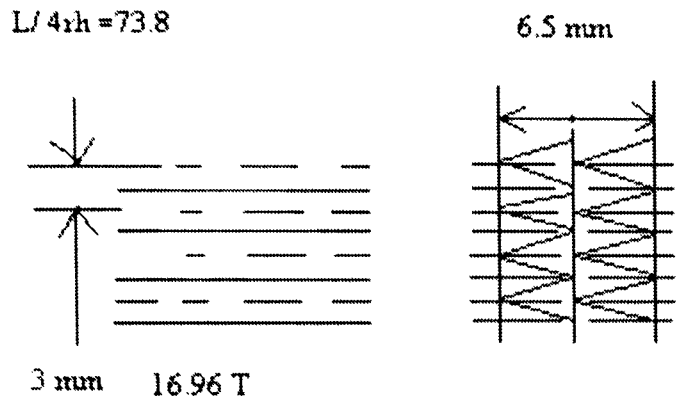


**Figure H1. Plain Fin surface diagram**

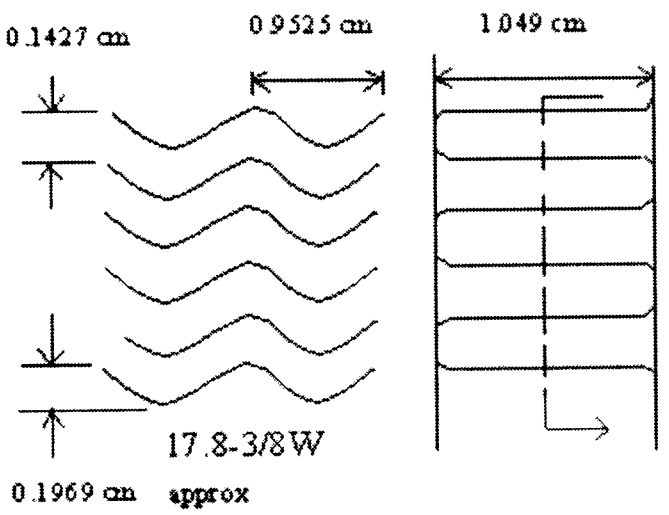


**Figure H2. Wavy fin surface diagram**

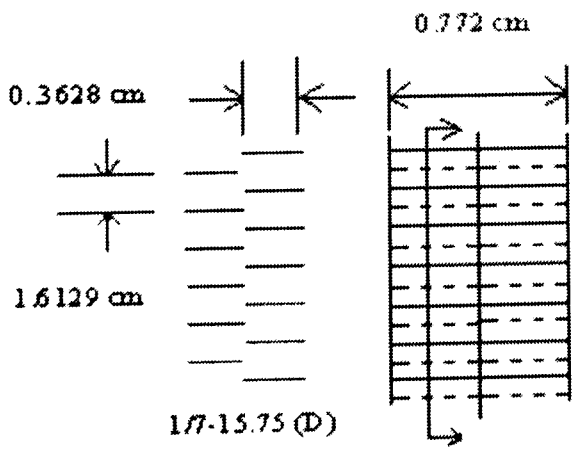


**Figure H3. Strip fin surface diagram**

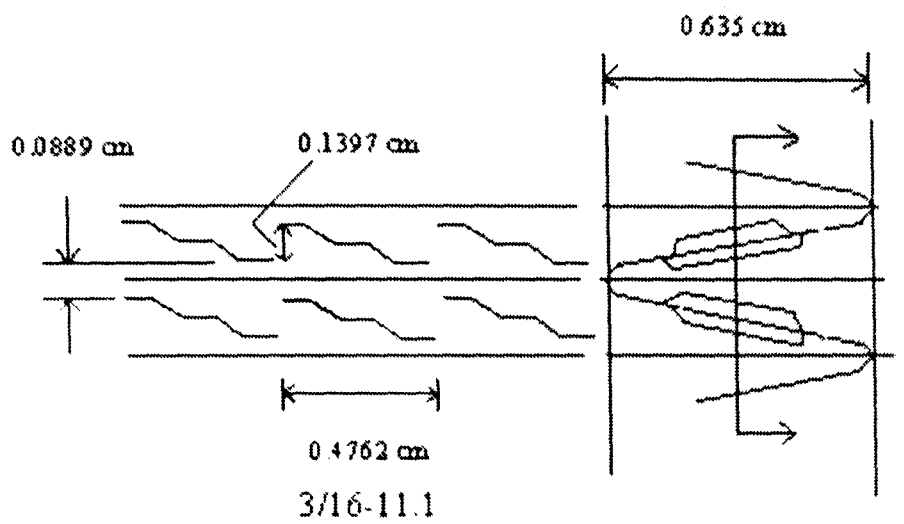


**Figure H4. Louvered fin surface diagram**

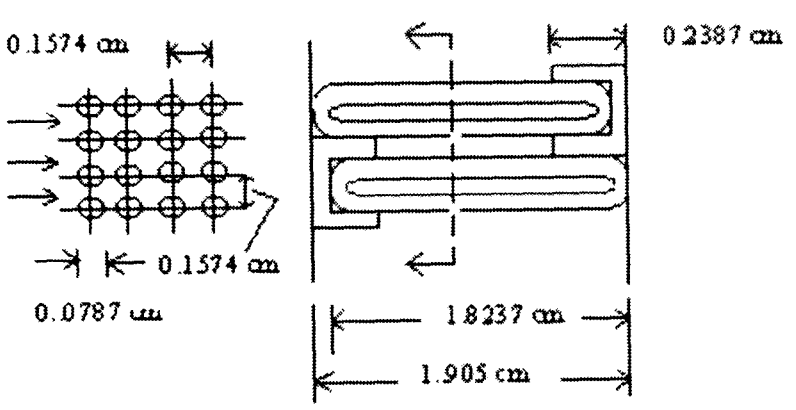


**Figure H5. Pin fin surface diagram**

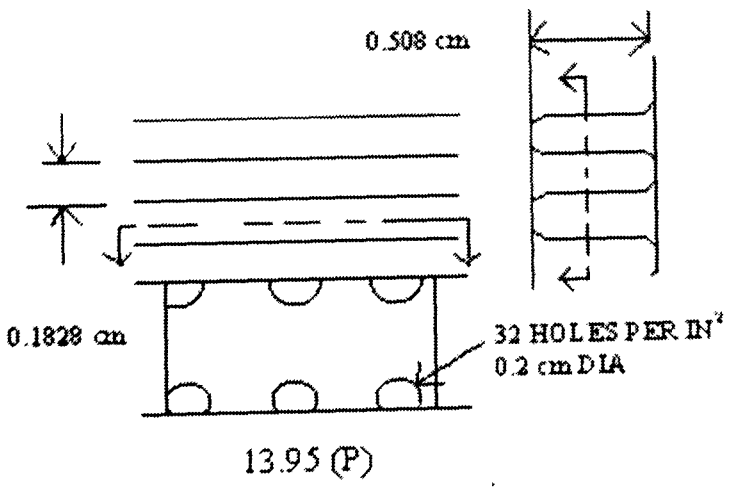


**Figure H6. Perforated fin surface diagram**

Details of the Plate Fin surface geometries

Plain Fin (with triangular flow passages) 16.96T

Fin pitch = 16.96 per in. = 676.7 per m

Plate spacing, b = 0.256 in. = 6.5 mm

Fin length flow direction, L = 127 mm

Flow passage hydraulic diameter,4rh = 1.722 mm

(L /4rh) = 73.8

Fin aluminium metal thickness = 0.152 mm

Total heat transfer area/volume between plates, $\beta$ = 1994 $m^2/m^3$

Fin area/ total area = 0.861

Wavy Fin 17.8-3/8W

Fin pitch = 17.8 per in. = 701 per m

Plate spacing, b = 1.413 in. = 10.49 mm

Flow passage hydraulic diameter,4rh = 2.123 mm

Fin aluminium metal thickness = 0.152 mm

Total heat transfer area/volume between plates, $\beta$ = 1686 $m^2/m^3$

Channel width or wavelength = 3/8 in. = 9 mm

Fin area/ total area = 0.892

Louvered Fin 3/16-11.1

Fin pitch = 11.1 per in. = 437 per m

Plate spacing, b = 0.250 in. = 6.35 mm

Louver spacing = 0.1875 in. = 4.763 mm

Fin gap = 0.035 in. = 0.89 mm

Louver gap = 0.055 in. = 1.4 mm

Flow passage hydraulic diameter, 4rh = 3.084 mm

Fin aluminium metal thickness = 0.152 mm

Total heat transfer area/ volume between plates, $\beta$ = 1204 $m^2/m^3$

Fin area/ total area = 0.756

Strip Fin 1/7-15.75(D)

Fin pitch = 15.75 per in. = 620 per m

Plate spacing, b = 0.304 in. = 7.72 mm

Splitter symmetrically located

Fin length flow direction = 1/7 in. = 3.63 mm

Flow passage hydraulic diameter, 4rh = 2.07 mm

Fin aluminium metal thickness = 0.102 mm

Splitter thickness = 0.152 mm

Total heat transfer area/ volume between plates, $\beta$ = 1726 $m^2/m^3$

Fin area (including splitter)/total = 0.859

Pin- Fin PF-3

Pin aluminium diameter = 0.79 mm

Pin pitch parallel to flow = 0.062 in. = 1.53 mm

Pin pitch perpendicular to flow = 0.062 in. = 1.53 mm

Plate spacing, b = 0.750 in. = 1.91 mm

Flow passage hydraulic diameter, 4rh =1.636 mm

Total heat transfer area/ volume between plates, $\beta$ =1112 $m^2/m^3$

Fin area/total area = 0.843

Perforated Fin 13.95(P)

Fin pitch = 13.95 per in. = 510 per m

Plate spacing, b = 0.200 in. = 5.08 mm

Fin centre material perforated with 0.079 in. = (2 mm) diameter holes spaced 32 per $in^2$ (4.96 $X10^6$ per $m^2$) on square pattern (16% open)

Flow passage hydraulic diameter, 4rh = 2.504 mm

Fin aluminium metal thickness = 0.305 mm

Total heat transfer area/ volume between plates, $\beta$ = 1250 $m^2/m^3$

Fin area/ total area = 0.705

Area in rim of holes in fin area

## Appendix I-PEEK and PVDF property data sheets

### 'STABAR' K200 POLYETHERTHERKETONE (PEEK)

| PROPERTY | | ASTM TEST METHOD | UNITS | | VALUE |
|---|---|---|---|---|---|
| GENERAL | | | | | |
| Haze | | D1003-61 | % | | 3.0 |
| Total luminous transmission | | D1003-61 | % | | 86 |
| Density | | D1505 | $kg/m^3$ | | 1250 |
| | | | gm/cc | | 1.25 |
| Crystalline melting point | | | °C | | 340 |
| MECHANICAL | | | | | |
| 1% Secant modulus | 23°C | D882-67 | MPa | MD/TD | 2500/2500 |
| | | | $kg/cm^3$ | | 25500/25500 |
| | | | psi | | 37000/37000 |
| Ultimate tensile strength | 23°C | D882-67 | MPa | MD/TD | 120/120 |
| | | | $kg/cm^3$ | | 1220/1220 |
| | | | psi | | 17400/17400 |
| Elongation at break | 23°C | D882-67 | % | MD/TD | 240/240 |
| Initial tear resistance | 23°C | D1004 | kg/cm | MD/TD | 450/450 |
| | | | g/25 microns | | 1120/1120 |
| | | | g/mil | | 1120/1120 |
| Tear propagation resistance | 23°C | ICI method | kg/cm | MD/TD | 14/14 |
| | | | g/25 microns | | 35/35 |
| | | | g/mil | | 35/35 |
| THERMAL | | | | | |
| Long term resistance | | | °C | | 250 |
| Coefficient of thermal expansion | | | cm/cm/°C | | $4 \times 10^{-3}$ |
| ( between 0°C and 110°C) | | | | | |
| Specific heat | | | J/kg/°C | | 1450 |
| | | | J/g/°C | | 1.45 |
| | | | cal/g/°C | | 0.35 |
| Shrinkage (150°C, 30sec) | | | % | | 0.5/0.5 |
| Oxygen index | | D2863-77 | % | | 25 |
| Maximum specific optical density | | E562-79 | | | 1 |
| (NBS chamber, flaming code) | | | | | |
| Flammability | | UL94 VTM | | | VTM-1(100micron) |
| ELECTRICAL | | | | | |
| Permittivity, 50 Hz | 25°C | D150 | - | | 3.3 |
| Dissipation Factor, 50 Hz | 25°C | D150 | - | | 0.0018 |
| Dissipation Factor, 50 Hz | 100°C | D150 | - | | 0.0016 |
| Dissipation Factor, 10 Hz | 25°C | D150 | - | | 0.0025 |
| Volume resistivity | 25°C | D257 | Ohm m | | 1013 |
| | | | Ohm cm | | 1017 |
| Dielectric strength | 25°C | D149-64 | KV/mm | | 128 |
| | | | V/micron | | 128 |
| | | | V/mη | | 3200 |
| Miscellaneous | | | | | |
| Water absorption | | | % | | 0.4 |
| (24 hr immersion at 23°C) | | | | | |
| Coefficient of hygroscopic expansion | | | cm/cm/% RH | | $5.0 \times 10^{-6}$ |
| ( between 20% and 70% RH) | | | | | |
| Water vapour permeability | | E96 | $g/m^2/atm/24$ hr | | 13 |
| (at 38°C and 90% RH) | | | $g/100\ in^2/m\eta/atm/24$ hr | | 3.4 |
| Oxygen permeability | | D1434 | $cc/m^2/atm/24hr$ | | 90 |
| (at 25°C and 45% Rh) | | | cc/100 in2/mη/atm/24 hr | | 23 |

Data have been measured on 100 microns (4 mη) film samples using standard test procedures on defined specimens. The results should therefore be regarded as a general guide to material properties and not as design data.

POLYVINYLIDENE FLUORIDE (PVDF)

| Property | Standard | Unit | Value |
|---|---|---|---|
| Density | ASTM D 792 | $kg/dm^3$ | 1.78 |
| Yield Strength | ASTM D 638 | MPa | 55 to 60 |
| Tensile Strength | id | MPa | 55 to 60 |
| Elongation at break | id | % | 20 |
| Tensile modulus | id | MPa | 2000 |
| Compressive modulus | ASTM D 695 | MPa | 1300 |
| Flexural modulus | ASTM D 790 | MPa | 2250 |
| Torsion modulus | ASTM D 1043 | MPa | 800 |
| Izod impact strength (notched test) | ASTM D 256 | J/m | 100 to 200 |
| Rockwell hardness | ASTM D 785 | - | R 110 |
| Friction coefficient<br>• static<br>• dynamic | ASTM D 1894 | <br>-<br>- | <br>0.4<br>0.3 |
| Abrasion | Taber CS 10 load 1 kg | mg/1000 cycles | 5 to 10 |
| Melting point | | $^{o}C$ | 178 |
| Vicat softening point | ASTM D 1525 | $^{o}C$ | 145 to 151 |
| Heat distortion temperature ( 0.46 MPa) | ASTM D 648 | $^{o}C$ | 148 to 150 |
| Linear thermal expansion coefficient (average between 20 and 150°C) | ASTM D 696 | $^{o}C^{-1}$ | $12.10^{-5}$ |
| Thermal conductivity | ASTM C 177 | W/m °C | 0.17 |

## Appendix J-Schematic diagrams of the manifolds for the Square and Spiral PFCHE

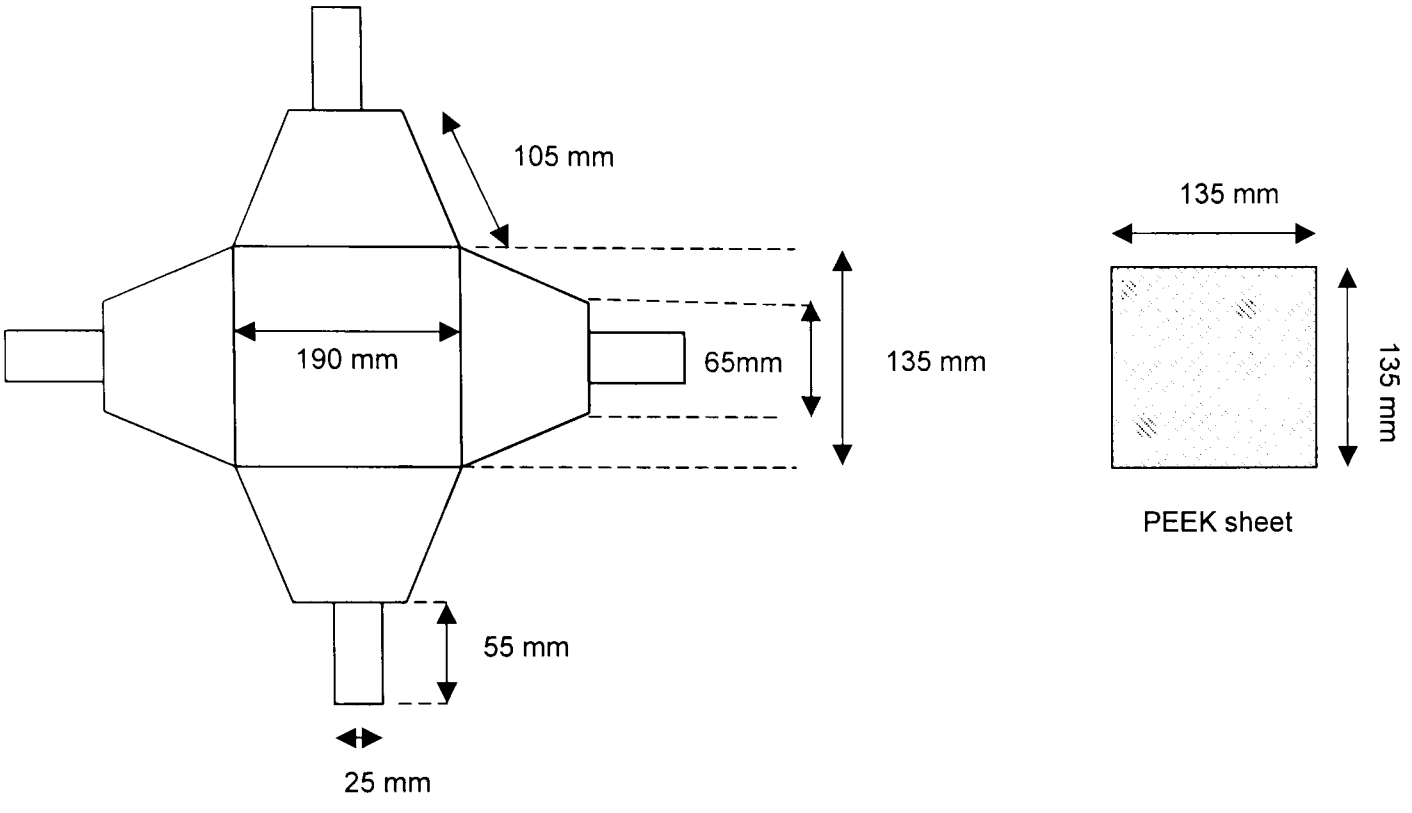


**Figure J.1 Details of the square PFCHE manifold**

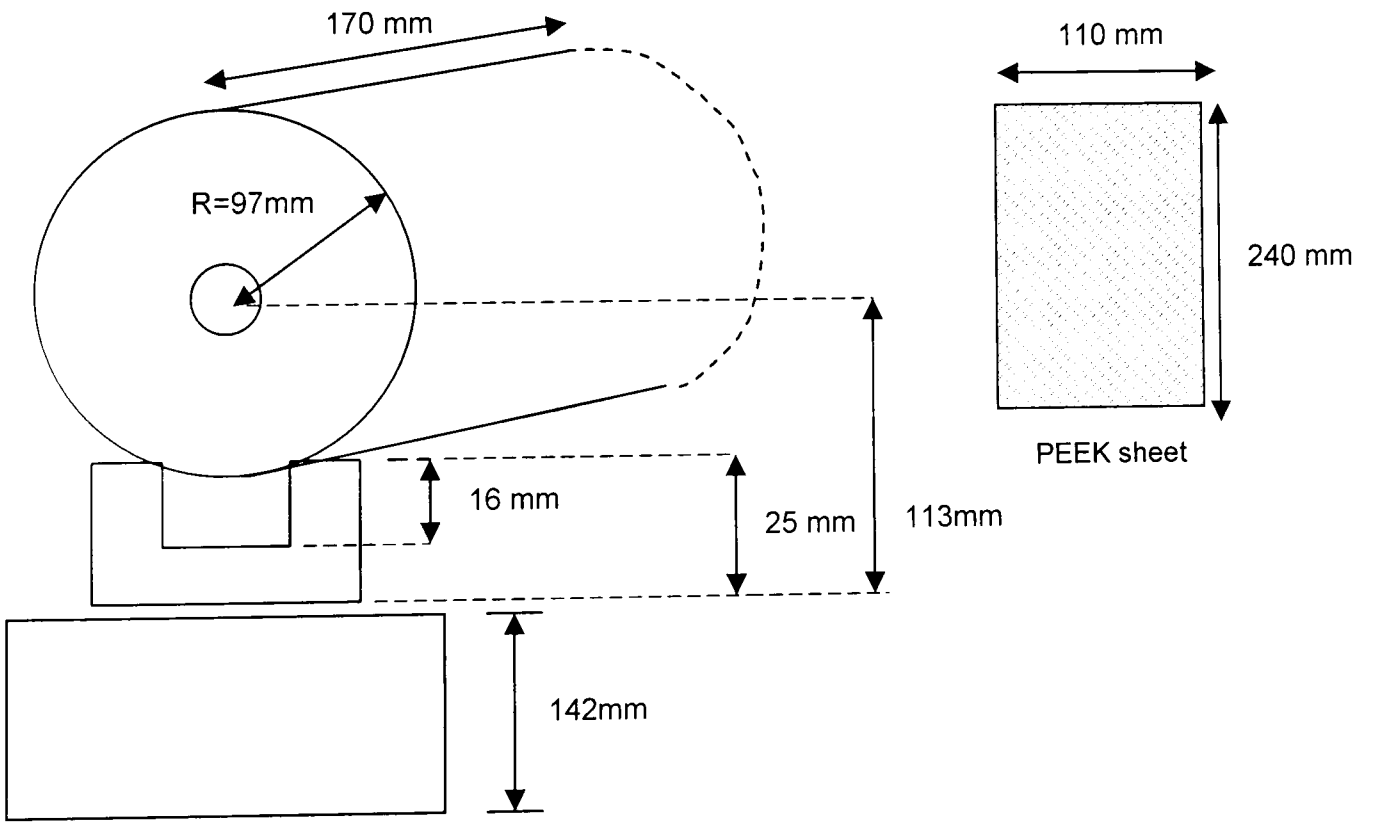


**Figure J.2 Details of the spiral PFCHE manifold**

## References


Alander, J.H. (1995). Method for Manufacturing Heat Exchangers, US Patent No. 5474639.

AMETEK, (1988). *AMETEK Brochure, Heat exchangers of Teflon,* US.

AMETEK, (1990). *AMETEK Brochure, Heat exchangers of Teflon, Case History*, US.

Aoune, A. and Ramshaw, C. (1999). Process intensification: Heat and mass transfer characteristics of liquid films on rotating discs, International Journal of Heat and Mass Transfer, 42, 14, pp 2543-2556.

Australian Energy News, (1998). Air-conditioners, http://www.isr.gov.au/resources/netenergy/aen.html, 14 September 1998.

Baclic, B.S. (1978). Journal of Heat Transfer, ASME, 100, pp 746-747.

Boman, A. and Doty, D. (2001). Design and manufacture of ultra-low-mass, cryogenic heat exchangers, Cryogenics, 41, 11-12, pp 797-803.

Cesaroni, A.J. (1996). Multi-Panelled Heat Exchanger, US Patent No. 5499676.

Charyulu, D.G., Singh, G. and Sharma J.K. (1999). Performance evaluation of a radiator in a diesel engine – a case study, Applied Thermal Engineering, 19, 6, pp 625-639.

Chem-Resist, (1990). *Chem Resist Thermoplastic Shell and Tube Heat Exchangers, Technical Bulletin,* UK.

Coleman, H.W. (1999). *Experimentation and uncertainty analysis for engineers,* 2nd edition, Wiley, New York.

Coulson, J.M. and Richardson, J.F. (1996). *Chemical Engineering- Fluid flow, Heat transfer and Mass Transfer,* Vol.1., Bath, Butterworth and Heinmann, UK.

Cross, W.T. and Ramshaw, C. (1986). Process Intensification: Laminar Heat Flow Transfer, Chemical Engineering Research and Design, 64, pp 293-301.

Deronzier, J.C. and Bertolini, G. (1997). Plate heat exchangers in liquid-crystal polymers, Applied Thermal Engineering, 17, 8-10, pp 799-808.

Doshi, S. (2000). Method of Making a Dimensionally Stable Tube Plastic Heat Exchangers, E.I Du Pont de Nemours and Company, Wilmington, US Patent No. 6094816.

Du Pont, (1988). *Teflon Heat Exchangers, Product Bulletin,* US.

Du Pont, (1990). *Du Pont Heat Exchangers with non-corroding Tubes of Teflon, Case Studies,* US.

Eberhard, P.D. (2000). Plastic heat exchanger, Holland, European Patent No. DE19853526.

ECOPOL. (1999). Polymer Heat Exchangers, http://www.ecopol.com/Imgles/PresentacionI.htm, 13 October 1999.

El-Bourawi, M.S. and Ramshaw, C. (1998). *Fouling Mitigation in Polymer Film Compact Heat Exchangers,* University of Newcastle Upon Tyne, UK.

Emmerich (1990). Plastic Crosscurrent Heat Exchanger, Germany, European Patent No. 4907648.

Ferreira, C.A.I. (2000). Compact Air-Refrigerant Evaporator, http://www-pe.wbmt.tudelft.nl/kk/comair.htm, 11 October 1999.

Fletcher, E.L. (1991). Panel heat exchangers formed from thermoplastic polymers, Du Pont Canada Inc., Mississauga, US Patent No. 5050671.

Fletcher, E.L. (1992). Method for the manufacture of a comfort heat exchanger, Du Pont Canada Inc., Mississauga, US Patent No. 5078946.

Fluorotherm, (1999). Polymer Heat Exchangers, http://www.fluorotherm.com/index.htm, 11 October 1999.

Focke, W.W and Zachariades, J. (1985). The effect of the corrugations angle on the thermohydraulic performance of plate heat exchangers, International Journal of Heat and Mass Transfer, 28, 8, pp 1469-1479.

Georg, P., Dittman, B., Golbis, K., Stastna, J., Hohmann, M., Oberbeck, S., Schwalbe, T. (2001). Miniturised reaction apparatus, Cellular Process Chemistry Inc., European Patent No. EP1123734.

George Fischer, (1999). Tube plate heat exchanger, http://www.us.piping.georgefischer.com/html/nr_heat_exchange.htm, 8 October 1999.

Go, J.S., Kim, S.J., Lim, G., Yun, H., Lee, J., Song, I. and Pak, Y. (2001). Heat transfer enhancement using flow-induced vibration of a microfin array, Sensors and Actuators: Physical, 90, 3, pp 232-239.

Green, A. and Wood, S. (1997). Methodologies for process intensification, 2nd International Conference on Process Intensification in Practice, Antwerp, Belgium, Mechanical Engineering Publications Limited, 11, pp 25-36.

Gschwind, P.K., Regele, A., Kottke, V. (1999). Heat and mass transfer of free-flow arrangements with corresponding pressure drop, International Conference on Compact Heat Exchangers and Enhancement Technology for the Process industries, Banff Centre for Conferences, Banff, Canada, Begell House Inc., 4, pp 199-203.

Gush, H.P. (1991). A compact low thermal conductivity support for cryogenic use, Review of Scientific Instruments, 62, 4, pp 1106-1108.

Hall, D.W., Scott, K. and Jachuck, R.J.J. (2001). Determination of mass transfer coefficient of a cross-corrugated memebrane reactor by the limiting-current technique, International Journal of Heat and Mass Transfer, 44, 6, pp 2201-2207.

Hessami, M.A. (1999). The effects of corrugation angle on heat transfer and pressure loss in a cross-corrugated passage, International Conference on Compact Heat Exchangers and Enhancement Technology for the Process Industries, Banff Centre for Conferences, Banff, Canada, Begell House Inc., 9, pp 149-157.

Holowczak, E.A. (1997), Polymeric heat exchanger with ceramic material insert, US Patent No. 5623988.

Hu, S and Herold, K.E. (1995). Prandtl number effect on offset fin heat exchanger performance: predictive model for heat transfer and pressure drop, International Journal of Heat and Mass Transfer, 38, 6, pp 1043-1051.

Hu, S and Herold, K.E. (1995). Prandtl number effect on offset fin heat exchanger performance: experimental results, International Journal of Heat and Mass Transfer, 38, 6, pp 1053-1061.

Huebner (1988). Plastic Heat Exchanger, Plascore, Inc., Zeeland, Michigan, US Patent No. 4735261.

IndhexAB, (2000), Polymer plate heat exchanger, http://www.indhex.com, 18 October 1999.

Jachuck, R.J.J. (1999). Opportunities presented by cross-corrugated polymer film compact heat exchangers. International Conference on Compact Heat Exchangers and Enhancement Technology for the Process industries, Banff, Canada, Begell House Inc., 8, pp 243-250.

Jachuck, R.J.J. and Ramshaw, C. (1992). *Process Intensification: The Acquisition of Design Data for Compact Polymer Heat Exchangers*, Process Intensification & Innovation Centre, Dept. of Chemical & Process Engineering, University of Newcastle Upon Tyne, UK.

Jachuck, R.J.J. and Ramshaw, C (1995). Process Intensification: Polymer film compact heat exchanger, Trans IChemE, 72, 7, pp 255-262.

Jachuck, R.J.J. and Ramshaw, C (1995). Process Intensification: Compact spiral polymer film compact heat exchanger, 1st International Conference on Process Intensification for the Chemical Industry, BHR Group Conference series, 7, pp 19-26.

Jacobi, A.M. and Shah, R.K. (1998). Air-side flow and heat transfer in compact heat exchangers: A discussion of enhancement mechanisms, Heat Transfer Engineering, 19, 4, pp 29-41.

Jayanti, S. and Hewitt, G.F. (1997).Hydrodynamics and heat transfer of wavy thin film flow, International Journal of Heat and Mass Transfer, 40, 1, pp 179-190.

Karlson, K.E., Massimino, R., Singh, A.K., Cooper, G.N. and Moran, J.M. (1987). Initial clinical experience with a more efficient hollow fiber oxygenator of unique design, The Journal of Cardiovascular Surgery, 28, 4, pp 384-387.

Kays, W.M. and London, A.L. (1984). *Compact Heat Exchangers*, 3rd edition, Krieger Publishing Company, Florida, US.

Kays, W.M. and Crawford, M.E. (1993). *Convective Heat and Mass Transfer,* 3rd edition, McGraw Hill Publications, Singapore.

Kern, D.Q. (1950). *Process Heat Transfer*, McGraw Hill, New York.

Kletz, T.A. (1991). *Plant Design for Safety*, 2nd edition, Hemisphere Pub. Corp., New York.

Knudsen, J.G. and Katz, D.L. (1958). *Fluid Dynamics and Heat Transfer,* McGraw Hill, New York.

Kordelin, T.T. (1997). Heat exchanger element, US Patent No. 5671804.

Lowenstein (1999). Thin Plastic Film for Absoprtion Chillers, US Patent No. 5992508.

Lu, T.J. (1998). Heat transfer efficiency of metal honeycombs, International Journal of Heat and Mass Transfer, 42,11, pp 2301-2040.

Luo Di-an and Yu Yunlin (1988). Heat transfer, pressure drop and flow visualisation in two corrugated ducts of different corrugation patterns, Proc. ASME National Heat Transfer Conference, Houston, Texas, 24-27 July, 1988, pp 483-488.

Lyon, H. (1995). *Spiral Polymer Film Heat Exchangers*. MEng Dissertation, Dept. of Chemical and Process Engineering, University of Newcastle Upon Tyne, UK.

Maquet, N.L. (1988). *PVDF-A True Versatile Engineering Thermoplastic Designed for Highly Demanding Service Conditions Involved in Heat Transfer Process*, Laboratoire Central de Solvay & Cie S.A, Brussels.

Melendo, M.H. (1996). *Effect of Prandtl Number on the Heat Transfer Characteristics of PFCHE,* MEng Dissertation, Dept. of Chemical & Process Engineering, University of Newcastle Upon Tyne.

Menes, R. (1997). Process intensification: Effect of corrugation angle in a cross-corrugated polymer film compact heat exchanger. International Conference on Compact Heat Exchangers for the Process Industries, Cliff Lodge and Conference Centre, Snowbird, Utah, Begell House Inc., 8, pp 149-157.

Metwally, M.N., AbouZiyan, H.Z. and ElLeathy, A.M. (1997). Performance of advanced corrugated duct solar air collector compared with five conventional designs, Renewable Energy, 10, 4, pp 519-537.

Moore (2000). Molded Heat Exchanger Structure for Portable Computer, Compaq Computer Corporation, Houston, Tex, US Patent No. 6026888.

Obot, N.T., Das, L., Vakili, D.E. and Green, R.A. (1997). Effect of Prandtl number on smooth tube heat transfer and pressure drop, International Communications in Heat and Mass Transfer, 24, 6, pp 889-896.

Okada, K., Ono, M., Torimura, T., Okuma, T., Konno, H., Ohtani, S. (1972). Design and heat transfer characteristics of new plate heat exchanger, Heat Transfer-Japanese Research, 1, 5, pp 90-95.

Osizik, M.N. (1985). *Heat Transfer: A Basic Approach*, McGraw Hill Publications, Singapore.

Patel, A.B. and Brisson, J.G. (1998). Experimental performance of a single stage superfluid Stirling refrigerator using a small plastic recuperator, Journal of Low Temperature Physics, 111, 1-2, pp 210-212.

Perry, C.R. and Dietz, L.H.S. and Shannon, R.L. (1983). Heat exchange apparatus having thin film flexible Sheets, The Boeing Company, Seattle, US Patent No. 4411310.

Perry, R.H. and Green, D.W. (1997). *Perry's Chemical Engineers' Handbook*, 7th edition, McGraw Hill, US.

Pfahler, J., Harley, J., Bau, H. and Zemel, J.N. (1991). Gas and liquid flow in small Channels. Micromechanical Sensors, Actuators, and Systems; American Society of Mechanical Engineers, Dynamic Systems and Control division (Publication), 32, pp 49-60.

Placon (1996). *Placon brochure, Plastic Construction: The Professionals in Plastics,* UK.

Ramshaw, C. (1995). The incentive for process intensification, 1st International Conference on Process Intensification, Antwerp, Belgium, BHR Group Conference Series, Mechanical Engineering Publications Limited, pp 1-2.

Ramshaw, C. (1997) Process intensification: Opportunities for exploiting compact heat Exchangers, International Conference on Compact Heat Exchangers for the Process Industries, Cliff Lodge and Conference Centre, Snowbird, Utah, Begell House, 11, pp 29-40.

Reay, D.A. (1999). *Learning from Experiences with Compact Heat Exchangers,* Caddet Analyses Series No.25, Sittard, Netherlands.

Reay, D. A. (2000). Polymer *Heat Exchangers: Exploitation of the Technology-A discussion of some options,* David Reay & Associates, Newcastle, UK.

Redman, J. (1988).Compact Future for Heat Exchangers, The Chemical Engineer, pp 12-16.

Rousse, D.R., Martin, D.Y., Theriault, R., Leveillee, F. and Boily, R. (2000). Heat recovery in greenhouses: a practical solution, Applied Thermal Engineering, 20, 8, pp 680-706.

Saji, N., Nagai, S., Tsucjiya, K., Asakura, H. and Obata, M. (2001). Development of a compact laminar flow heat exchanger with stainless steel micro-tubes, Physica C: Superconductivity, 354, 1-4, pp 148-151.

Salamon, T.R., Rogers, J.A., Eggleton, B.J. (2001). Analysis of heat flow in optical fiber devices that use micro fabricated thin film heaters, Sensors and Actuators A: Physica, 95, 1, pp 8-16.

Saunders, E.A.D. (1988). *Heat Exchangers-Selection, Design & Construction*, Longman Group, UK.

Schnon, S.G. (1988). Plastic Film Plate Type Heat Exchanger, US Patent No. 4744414.

Semel, J. (1997). Process Intensification in practice, 2nd International Conference on Process Intensification, Antwerp, Belgium, BHR Conference Group Series, Mechanical Engineering Publications Limited, pp 1-2.

Shah, R.K. Compact Heat Exchanger Technology and Applications, In: *Compact Heat Exchangers: Techniques for Size Reduction*, Heat Exchange Engineering 2, Ellis Horwood Series, 26, pp 1-27.

Shah, R.K and Mashelkar, R.A. (1988). *Heat Transfer Equipment Design,* Hemisphere Publishing Corp, New York.

Shuster, J. and Cesaroni, A.J. (1990). Heat Exchanger Fabricated from Polymer Compositions, US Patent No. 4955435.

Smith, W.F. (1988). Solar energy absorber, US Patent No. 4763641.

Stasiek, J., Collins, M.W., Ciofalo, M. and Chew, P.E. (1996). Investigation of flow and heat transfer in corrugated passages: experimental results, International Journal of Heat and Mass Transfer, 29, 15, pp 149-164.

Stevens, M.P (1999). *Polymer Chemistry: An Introduction*, 3rd Edition, Oxford University Press, UK.

Takada, M. and Drake, J.C. (1983).An application of improved high performance Evaporator, Desalination, 45, 1-3, pp 3-12.

Tan, Z. M. and Yang, W.J. (1997). Heat transfer during asymmetrical collision of thermal waves in a thin film, International Journal of Heat and Mass Transfer, 40, 17, pp 3999-4006.

Tayler, C. (1988). *Think 'plastics' for more effective heat transfer, Process Engineering Supplement,* UK.

Therme-America, (1988). *Process Coils in Solef PVDF, Technical Bulletin*, US.

Thomas, P.T. (1992). Apparatus for concentrating bleed-off water for evaporating Coolers, Munters Corporation, Fort Myers, US Patent No. 5112538.

Thonon, B.M and Mercier, P. (1997). Compact to very compact heat exchangers for the process industry, 2nd International Conference on Process Intensification in Practice, Antwerp, Belgium, BHR Conference Group series, Mechanical Engineering Publications Limited, pp 49-62.

Tsilingiris, P.T. (2000). Heat transfer analysis of low thermal conductivity solar energy absorbers, Applied thermal Engineering, 20, 14, pp 1297-1314.

Verschaeve, R.C. (1987). *Heat Exchangers of Polyvinylidene Fluoride for treatment of Aggressive Media*, Solvay, Brussels.

Wagner, R. and Frossati, G. (1990). A small plastic dilution refrigerator, Physica B, 165-166, 1, pp 43-44.

Walker, A. (1997). *The Effect of the Angle of Cross-Corrugation on the Heat Transfer and Pressure Characteristics of a Polymer Film Compact Heat Exchanger*, MEng Dissertation, Dept. of Chemical and Process Engineering, University of Newcastle Upon Tyne, UK.

Walker, G. (1990). *Industrial Heat Exchanger: A Basic Approach*, 2nd edition, UK.

Wang, G.V. and Vanka, S.P. (1995). Convective heat transfer in periodic wavy passages, International Journal of Heat and Mass Transfer, 38, 17, pp 3129-3230.

Webb, R.L. (1994). *Principles of Enhanced Heat Transfer*, Wiley, New York.

Welles, C.G. (2000). Portable heat generating device, US Patent No. 6062210.

Zeng, J.S., Stevens, P.C., Hunt, A.J., Grief, R. and Daehee, L. (1996). Thin-film heater thermal conductivity apparatus and measurement of thermal conductivity of silica aerogel, International Journal of Heat and Mass Transfer, 39, 11, pp 2311-2317.